frontiers | Research Topics

Pathogenesis, immune escape, prognosis and novel management of lymphoid proliferative disorders

Edited by
Wei Sang, Weili Zhao, Ken Young and Mingzhi Zhang

Published in
Frontiers in Immunology

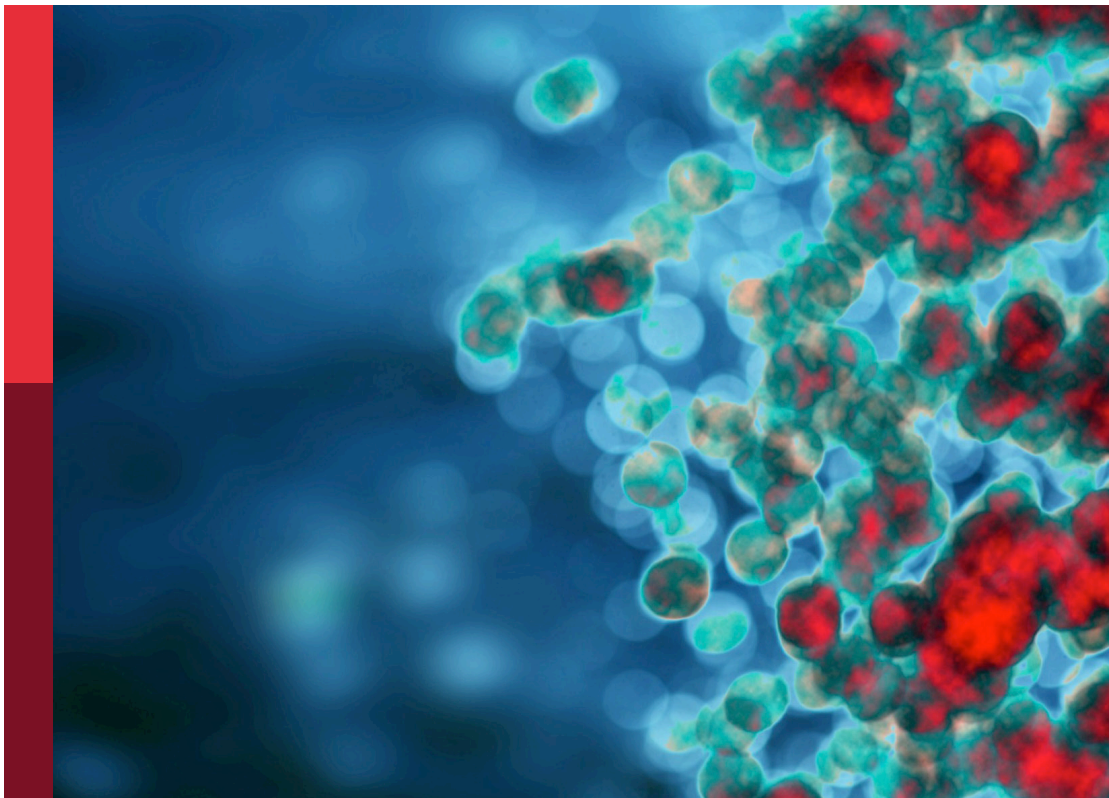

ISSN 1664-8714
ISBN 978-2-83250-964-7
DOI 10.3389/978-2-83250-964-7

About Frontiers

Frontiers is more than just an open access publisher of scholarly articles: it is a pioneering approach to the world of academia, radically improving the way scholarly research is managed. The grand vision of Frontiers is a world where all people have an equal opportunity to seek, share and generate knowledge. Frontiers provides immediate and permanent online open access to all its publications, but this alone is not enough to realize our grand goals.

Frontiers journal series

The Frontiers journal series is a multi-tier and interdisciplinary set of open-access, online journals, promising a paradigm shift from the current review, selection and dissemination processes in academic publishing. All Frontiers journals are driven by researchers for researchers; therefore, they constitute a service to the scholarly community. At the same time, the *Frontiers journal series* operates on a revolutionary invention, the tiered publishing system, initially addressing specific communities of scholars, and gradually climbing up to broader public understanding, thus serving the interests of the lay society, too.

Dedication to quality

Each Frontiers article is a landmark of the highest quality, thanks to genuinely collaborative interactions between authors and review editors, who include some of the world's best academicians. Research must be certified by peers before entering a stream of knowledge that may eventually reach the public - and shape society; therefore, Frontiers only applies the most rigorous and unbiased reviews. Frontiers revolutionizes research publishing by freely delivering the most outstanding research, evaluated with no bias from both the academic and social point of view. By applying the most advanced information technologies, Frontiers is catapulting scholarly publishing into a new generation.

What are Frontiers Research Topics?

Frontiers Research Topics are very popular trademarks of the *Frontiers journals series*: they are collections of at least ten articles, all centered on a particular subject. With their unique mix of varied contributions from Original Research to Review Articles, Frontiers Research Topics unify the most influential researchers, the latest key findings and historical advances in a hot research area.

Find out more on how to host your own Frontiers Research Topic or contribute to one as an author by contacting the Frontiers editorial office: frontiersin.org/about/contact

Pathogenesis, immune escape, prognosis and novel management of lymphoid proliferative disorders

Topic editors

Wei Sang — The Affiliated Hospital of Xuzhou Medical University, China
Weili Zhao — Shanghai Jiao Tong University, China
Ken Young — Duke University, United States
Mingzhi Zhang — First Affiliated Hospital of Zhengzhou University, China

Citation

Sang, W., Zhao, W., Young, K., Zhang, M., eds. (2022). *Pathogenesis, immune escape, prognosis and novel management of lymphoid proliferative disorders*. Lausanne: Frontiers Media SA. doi: 10.3389/978-2-83250-964-7

The author declares that the research was conducted in the absence of any commercial or financial relationships that could be construed as a potential conflict of interest.

Table of contents

06 Editorial: Pathogenesis, immune escape, prognosis, and novel management of lymphoid proliferative disorders

Wei Sang

09 Comparison of Chemotherapy Combined With Chidamide Versus Chemotherapy in the Frontline Treatment for Peripheral T-Cell Lymphoma

Jinni Wang, Ning Su, Yu Fang, Shuyun Ma, Yuchen Zhang, Jun Cai, Qihua Zou, Xiaopeng Tian, Yi Xia, Panpan Liu, Zhiming Li, He Huang, Huiqiang Huang and Qingqing Cai

18 A Novel Prognostic Index Model for Adult Hemophagocytic Lymphohistiocytosis: A Multicenter Retrospective Analysis in China

Ziyuan Shen, Yingliang Jin, Qian Sun, Shuo Zhang, Xi Chen, Lingling Hu, Chenlu He, Ying Wang, Qinhua Liu, Hao Zhang, Xin Liu, Ling Wang, Jun Jiao, Yuqing Miao, Weiying Gu, Fei Wang, Chunling Wang, Yuye Shi, Jingjing Ye, Taigang Zhu, Cai Sun, Xuguang Song, Linyan Xu, Dongmei Yan, Haiying Sun, Jiang Cao, Depeng Li, Zhenyu Li, Zhao Wang, Shuiping Huang, Kailin Xu, and Wei Sang on behalf of HHLWG

28 CD56-Negative Extranodal Natural Killer/T-Cell Lymphoma: A Retrospective Study in 443 Patients Treated by Chemotherapy With or Without Asparaginase

Jing Yang, Pengfei Li, Yingshi Piao, Xindi Liu, Liqiang Wei, Wei Sang, Luo Zhang and Liang Wang

41 Identification of the Predictive Models for the Treatment Response of Refractory/Relapsed B-Cell ALL Patients Receiving CAR-T Therapy

Jingxian Gu, Sining Liu, Wei Cui, Haiping Dai, Qingya Cui, Jia Yin, Zheng Li, Liqing Kang, Huiying Qiu, Yue Han, Miao Miao, Suning Chen, Shengli Xue, Ying Wang, Zhengming Jin, Xiaming Zhu, Lei Yu, Depei Wu and Xiaowen Tang

54 Oncogenic Mutations and Tumor Microenvironment Alterations of Older Patients With Diffuse Large B-Cell Lymphoma

Yue Zhu, Di Fu, Qing Shi, Ziyang Shi, Lei Dong, Hongmei Yi, Zhenhua Liu, Yan Feng, Qian Liu, Hai Fang, Shu Cheng, Li Wang, Qiang Tian, Pengpeng Xu and Weili Zhao

67 Anti-PD-1 Therapy Enhances the Efficacy of CD30-Directed Chimeric Antigen Receptor T Cell Therapy in Patients With Relapsed/Refractory CD30+ Lymphoma

Wei Sang, Xiangmin Wang, Hongzhi Geng, Tianci Li, Dashan Li, Bingpei Zhang, Yi Zhou, Xuguang Song, Cai Sun, Dongmei Yan, Depeng Li, Zhenyu Li, Caixia Li and Kailin Xu

75 Epstein-Barr Virus-Positive Lymphoma-Associated Hemophagocytic Syndrome: A Retrospective, Single-Center Study of 51 Patients
Ailin Zhao, Jinrong Yang, Meng Li, Linfeng Li, Xinai Gan, Jie Wang, He Li, Kai Shen, Yunfan Yang and Ting Niu

85 T Cell Defects: New Insights Into the Primary Resistance Factor to CD19/CD22 Cocktail CAR T-Cell Immunotherapy in Diffuse Large B-Cell Lymphoma
Jiachen Wang, Kefeng Shen, Wei Mu, Weigang Li, Meilan Zhang, Wei Zhang, Zhe Li, Tong Ge, Zhoujie Zhu, Shangkun Zhang, Caixia Chen, Shugang Xing, Li Zhu, Liting Chen, Na Wang, Liang Huang, Dengju Li, Min Xiao and Jianfeng Zhou

99 Aberrantly Activated APOBEC3B Is Associated With Mutant p53-Driven Refractory/Relapsed Diffuse Large B-Cell Lymphoma
Xuzhao Zhang, Zhaoxing Wu, Yuanyuan Hao, Teng Yu, Xian Li, Yun Liang, Jinfan Li, Liansheng Huang, Yang Xu, Xiuzhen Li, Xiaohua Xu, Weiqin Wang, Genbo Xu, Xiaohong Zhang, Qinghua Lv, Yongming Fang, Rongzhen Xu and Wenbin Qian

112 Clinical and Molecular Characteristics of 60 Patients With Human Immunodeficiency Virus-Negative Castleman Disease
Siyu Qian, Mengjie Ding, Huting Hou, Zeyuan Wang, Jieming Zhang, Yue Zhang, Meng Dong, Linan Zhu, Guannan Wang, Wencai Li and Xudong Zhang

120 Machine Learning Models for the Diagnosis and Prognosis Prediction of High-Grade B-Cell Lymphoma
Hui Kong, Haojie Zhu, Xiaoyun Zheng, Meichen Jiang, Lushan Chen, Lingqiong Lan, Jinhua Ren, Xiaofeng Luo, Jing Zheng, Zhihong Zheng, Zhizhe Chen, Jianda Hu and Ting Yang

131 m6A-Regulator Expression Signatures Identify a Subset of Follicular Lymphoma Harboring an Exhausted Tumor Microenvironment
Tingting Zhang, Hengqi Liu, Fenghua Gao, Wenchen Gong, Yaoli Cui, Jin He, Lanfang Li, Lihua Qiu, Zhengzi Qian, Shiyong Zhou, Bin Meng, Xiubao Ren, Huilai Zhang and Xianhuo Wang

143 Fucosylation Promotes Cytolytic Function and Accumulation of NK Cells in B Cell Lymphoma
Xing Tong, Yuhua Ru, Jianhong Fu, Ying Wang, Jinjin Zhu, Yiyang Ding, Fulian Lv, Menglu Yang, Xiya Wei, Chenchen Liu, Xin Liu, Lei Lei, Xiaojin Wu, Lingchuan Guo, Yang Xu, Jie Li, Peng Wu, Huanle Gong, Jia Chen and Depei Wu

154 Case Report: Primary Cardiac T-Cell Lymphoma With Complete Atrio-Ventricular Block Diagnosed by Endomyocardial Biopsy
Panpan Chen, Yuanyuan Hao, Xi Qiu, Xibin Xiao, Wei Zhu, Yang Xu and Wenbin Qian

159 Timing of Tocilizumab Administration Under the Guidance of IL-6 in CAR-T Therapy for R/R Acute Lymphoblastic Leukemia

Yinqiang Zhang, Fen Zhou, Zhuolin Wu, Yingnan Li, Chenggong Li, Mengyi Du, Wenjing Luo, Haiming Kou, Cong Lu and Heng Mei

169 The Outcome of Induction Therapy for EBV-Related Hemophagocytic Lymphohistiocytosis: A Model for Risk Stratification

Tingting Cui, Jingshi Wang and Zhao Wang

179 Oncogenic signaling pathway-related long non-coding RNAs for predicting prognosis and immunotherapy response in breast cancer

Huamei Li, Hongjia Liu, Qiongyu Hao, Xianglin Liu, Yongzhong Yao and Meng Cao

frontiers | Frontiers in Immunology

TYPE Editorial
PUBLISHED 21 November 2022
DOI 10.3389/fimmu.2022.1063418

OPEN ACCESS

EDITED AND REVIEWED BY
Katy Rezvani,
University of Texas MD Anderson Cancer Center, United States

*CORRESPONDENCE
Wei Sang
sw1981726@126.com

SPECIALTY SECTION
This article was submitted to Cancer Immunity and Immunotherapy, a section of the journal Frontiers in Immunology

RECEIVED 07 October 2022
ACCEPTED 28 October 2022
PUBLISHED 21 November 2022

CITATION
Sang W (2022) Editorial: Pathogenesis, immune escape, prognosis, and novel management of lymphoid proliferative disorders. *Front. Immunol.* 13:1063418. doi: 10.3389/fimmu.2022.1063418

Editorial: Pathogenesis, immune escape, prognosis, and novel management of lymphoid proliferative disorders

Wei Sang*

Department of Hematology, The Affiliated Hospital of Xuzhou Medical University, Xuzhou, Jiangsu, China

KEYWORDS

immune escape, prognosis, lymphoid proliferative disorders, pathogenesis, lymphoproliferative disease

Editorial on the Research Topic

Pathogenesis, immune escape, prognosis, and novel management of lymphoid proliferative disorders

This Research Topic examines lymphoproliferative diseases (LPD), focusing on the pathological microenvironment, immune escape, prognosis, and the processes involved with seeking novel treatment methods. Including four editors who worked with invited reviewers, for this collection we invited potential contributors and accepted online contributions. Based on the comprehensive evaluation of the theme fit and the quality of those manuscripts, 17 contributions were accepted. These manuscripts include different types of LPD, such as hemophagocytic lymphohistiocytosis (HLH), follicular cell lymphoma (FL), peripheral T cell lymphoma (PTCL), diffuse large B cell lymphoma (DLBCL), Castleman disease (CD), extranodal natural killer/T cell lymphoma (NK/TCL), Hodgkin lymphoma (HL), and other subtypes of non-Hodgkin lymphoma (NHL).

LPDs are often driven by different causes and have great differences in pathogenesis, pathology, and genetic characteristics. Clarifying these potential cloning and transformation mechanisms and regulatory mechanisms will help us better understand these kinds of diseases. The prognosis of DLBCL in the elderly is often poor. Zhu et al. found that the elderly DLBCL is accompanied by undesirable clinical and molecular features, represented by the accumulation of oncogenic mutations and with the MYD88-like genetic subtype and immunosuppressive tumor microenvironment alterations. It is proposed that, in the future, elderly DLBCL patients need to explore new treatment methods based on these characteristics. Tumor protein 53 (*TP53*) mutation predicts an unfavorable prognosis in DLBCL. Zhang et al. demonstrated that aberrantly activated APOBEC3B can induce TP53 G/C-to-A/T mutations in DLBCL, which may lead to

proliferation and drug resistance and may contribute to R/R DLBCL, providing insight into the mechanism underlying TP53 mutation in DLBCL as well as a potential target for overcoming drug resistance in this disease. Xianhuo Wang et al. explored the role of m6A regulator expression in FL. Through the analysis of the database and the verification in the clinical cohort, it was confirmed that the patients with a low level of m6A scores had poor survival, accompanied by specific gene characteristics and a high expression of PDL1, which also had certain significance for guiding the treatment of PD1 inhibitor. CD is a rare LPD. Qian et al. demonstrated that thrombocytopenia and hypoalbuminemia are independent poor diagnostic factors for CD. In addition, they also confirmed that mTOR activation was higher in CD compared to reactive lymphoid hyperplasia. It is helpful to better understand CD and explain the molecular basis of targeted mTOR therapy.

Many studies focused on the prognostic characteristics of LPD. The prognosis of CD56-negative extranodal NKT cell lymphoma is poor, especially suitable for early-stage NK/TCL. In a large retrospective study, Yang et al. proved that combined chemotherapy based on asparaginase can overcome its disadvantage, but it needs to be confirmed in future prospective clinical studies. HLH is a clinical syndrome with the clinical manifestation of immune overreaction caused by many factors. The clinical manifestations are heterogeneous. At present, there is a lack of a standardized prognosis evaluation system to guide clinical individualized treatment. Shen et al. established a novel prognosis score system (HHLWG-NPI) through multi-center data in China, which effectively distinguishes the prognosis of patients. It is valuable to guide the accurate stratification and individual treatment in adult HLH. The limitation of the study is that more complex variables such as gene mutation, sCD25, and pro-inflammatory markers were not included. Further prospective multicenter studies are urgently needed to validate the model. In another study on Epstein–Barr virus (EBV)-related HLH, Zhao Cui et al. explored the risk factors leading to the failure of induction therapy, and based on these variables, established a nomogram prognosis model. The model can better distinguish the risk and help to guide the individualized treatment of patients. In this study, VP16 is recommended as the treatment choice for high-risk patients. EBV infection is one of the main causes of HLH. EBV-associated lymphomas are more likely to be accompanied by HLH. Zhao et al. retrospectively analyzed the clinical characteristics and prognostic factors of 51 patients in a single center. They found that patients with lymphoma accompanied by HLH could obtain a better objective response rate and overall survival (OS) by anti-lymphoma treatment as soon as possible after anti-HLH was controlled. In addition, they also proved that the increase of alanine aminotransferase is a bad prognostic factor for EBV-related lymphoma with HLH. High-grade LBCL (HGBL) is a highly invasive NHL. Kong et al. explored some clinical features of HGBL through machine learning. They found that cardiovascular appearance, Ann Arbor stage, lactate dehydrogenase (LDH), and International Progressive Index (IPI) were independent risk factors for HGBL patients. In addition, in the high-IPI-risk group, CD10 expression, extranodal involvement, a high level of LDH, a high level of white blood cell (WBC), bone marrow involvement, old age, advanced Ann Arbor stage, and high SUVmax had a higher risk of death within 1 year. This research is helpful for a more accurate and high-level individualized evaluation and treatment selection.

In terms of innovative treatment, several studies were focused on chimeric antigen receptor T cells (CAR-T) treatment. In the PD1 inhibitor and BV era, there is still an unmet need for the treatment of r/r cHL. Sang et al. explored the feasibility of targeting CD30 CAR-T cell treatment and the optimized combination therapy strategy in r/r cHL. They proved that the PD1 inhibitor combination could enhance the efficacy of anti-CD30 CAR-T cell therapy. In this study, a 50% CR rate was obtained in general, while the combination of PD1 inhibitors can reach an 80% CR rate, and the 5-year OS reached 70%. It provides a new choice for the treatment of r/r cHL. CAR-T cell treatment is important for r/r B-ALL, but there are still treatment failures and relapses after CAR-T cell treatment. In a prospective study, Gu et al. developed and validated the predictive models for CAR-T clinical responses in r/r B-ALL patients and further confirmed the diagnostic value of the risk model, which helps to screen more suitable patients and provide some reference for solving the problem of CART cell therapy failure in the future. Wang et al. explored the causes of the primary failure of CAR-T cell treatment. Through clinical variable analysis, they proved that a higher LDH level and a lower cytokine release syndrome (CRS) were independent prognostic factors for T cell dysfunction. In addition, they also explored the genetic characteristics of patients with treatment failure through full exon sequencing. This study is helpful to explain the potential mechanism of primary failure of CAR-T cell therapy and has certain significance for solving the problem of failure of CAR-T cell therapy in the future. CRS and ICANS are the main complications of CAR-T cell therapy. At present, the use of tocilizumab mainly refers to the CRS level, but some patients still progress to severe CRS. The research of Zhang et al. proved that patients with less than four increases in IL-6 levels had a higher incidence of severe CRS after receiving tocilizumab (37.5% *versus* 0%, $p = 0.0125$), which provided a basis for referring the CRS intervention strategies under the guidance of IL-6 level. It is helpful to assist patients in obtaining safer CAR-T cell therapy. NK cell therapy is also an important strategy of immune cell therapy, but there are many bottlenecks and limitations. Zhang et al. tried to explore the synergistic NK cell therapy, and the experimental results proved that fucosymulation helped promote NK cell infiltration in the B-

cell tumor microenvironment and improve the function of NK cells. It has important reference value for the future exploration of NK cell therapy. The treatment of peripheral T cell lymphoma is facing challenges. HDAC has achieved good efficacy in the treatment of refractory and relapsed PTCL. Wang et al. (Front Immunol. 2022 Feb 2;13:835103.) explored the feasibility of first-line treatment of PTCL with chidamide combined with chemotherapy. The results show that the combination of chidamide can improve the progression-free survival of patients with peripheral T cell lymphoma, and the safety is controllable.

On the whole, this special issue brings together high-quality manuscripts, exploring some unresolved clinical problems of LPD, with value for accurate diagnosis, prognosis, and innovative treatments in the future.

Author contributions

The author confirms being the sole contributor to this work and has approved it for publication.

Acknowledgments

We sincerely thank all the contributing authors to this collection.

Conflict of interest

The author declares that the research was conducted in the absence of any commercial or financial relationships that could be construed as a potential conflict of interest.

Publisher's note

frontiers in Immunology

ORIGINAL RESEARCH
published: 02 February 2022
doi: 10.3389/fimmu.2022.835103

Comparison of Chemotherapy Combined With Chidamide Versus Chemotherapy in the Frontline Treatment for Peripheral T-Cell Lymphoma

Jinni Wang[1,2†], Ning Su[3†], Yu Fang[1,2†], Shuyun Ma[1,2], Yuchen Zhang[1,2], Jun Cai[1,2], Qihua Zou[1,2], Xiaopeng Tian[1,2], Yi Xia[1,2], Panpan Liu[1,2], Zhiming Li[1,2], He Huang[1,2], Huiqiang Huang[1,2] and Qingqing Cai[1,2]*

[1] State Key Laboratory of Oncology in South China, Collaborative Innovation Center of Cancer Medicine, Sun Yat-sen University Cancer Center, Guangzhou, China, [2] Department of Medical Oncology, Sun Yat-sen University Cancer Center, Guangzhou, China, [3] Department of Oncology, Guangzhou Chest Hospital, Guangzhou, China

OPEN ACCESS

Edited by:
Wei Sang,
The Affiliated Hospital of Xuzhou Medical University, China

Reviewed by:
Dong-Hua Yang,
St. John's University, United States
Xudong Zhang,
Zhengzhou University, China

***Correspondence:**
Qingqing Cai
caiqq@sysucc.org.cn

[†]These authors have contributed equally to this work

Specialty section:
This article was submitted to Cancer Immunity and Immunotherapy, a section of the journal Frontiers in Immunology

Received: 14 December 2021
Accepted: 12 January 2022
Published: 02 February 2022

Citation:
Wang J, Su N, Fang Y, Ma S, Zhang Y, Cai J, Zou Q, Tian X, Xia Y, Liu P, Li Z, Huang H, Huang H and Cai Q (2022) Comparison of Chemotherapy Combined With Chidamide Versus Chemotherapy in the Frontline Treatment for Peripheral T-Cell Lymphoma. Front. Immunol. 13:835103. doi: 10.3389/fimmu.2022.835103

Background: Peripheral T-cell lymphoma (PTCL) is featured with a poor survival outcome. China has approved chidamide, an oral novel histone deacetylase inhibitor, for patients diagnosed with relapsed or refractory PTCL.

Objective: We compared the benefit of traditional chemotherapy alone and a combination of chidamide and traditional chemotherapy against newly diagnosed PTCL. Prognostic factors related to progression and survival in patients diagnosed with untreated PTCL were also investigated.

Methods: 104 patients with newly diagnosed PTCL were enrolled and divided into chemotherapy (ChT) group and chemotherapy combined with chidamide (ChT+C) group. Survival curves were plotted by the Kaplan-Meier method. Univariate and multivariate analysis were conducted with Log-rank test and Cox's proportional hazard regression. Subgroup analysis and interaction tests were conducted to evaluate factors associated with prognostic differences between ChT and ChT+C groups.

Results: Compared with patients in ChT group, those in ChT+C group had superior progression-free survival (PFS) (p=0.047). However, there was no significantly statistical difference observed between the two groups in overall survival (OS) (p=0.212). High IPI scores have a negative relationship with survival. Multivariate analysis revealed that the type of frontline treatment regimen is an independent factor associated with PFS of PTCL patients (p=0.045). In the subgroup of patients with high international prognostic index scores (3-5), the HR value for PFS comparing ChT with ChT+C was 4.675. A test of interaction between IPI and treatment showed statistical significance (p = 0.037), implying that the benefits of ChT+C are higher for patients with high IPI scores.

Conclusions: In summary, the combination of ChT and chidamide may provide a promising prospect for patients with newly diagnosed PTCL.

Keywords: peripheral T-cell lymphoma, HDAC inhibitor, chidamide, chemotherapy, frontline

INTRODUCTION

Peripheral T-cell lymphomas (PTCL) comprise a group of rare lymphoid malignancies with distinct phenotypes and clinical presentations (1). In Western countries, these aggressive lymphomas account for 10–12% of non-Hodgkin lymphomas (NHL), but in Eastern Asian for 20% (2, 3).

Frontline treatment of PTCL is mainly supplied from the experience in treatment of B-cell counterparts. Unfortunately, compared with B-cell NHL, PTCLs have a poorer prognosis under conventional treatment. Except for anaplastic lymphoma kinase (ALK)–positive anaplastic large cell lymphoma (ALCL), complete and durable response rates are disappointingly low with most commonly employed anthracycline-based regimens (4, 5). Even though the intensive-dose induction therapy consolidated with autologous stem-cell transplantation (ASCT) in first remission was applied, 18% patients with PTCL still suffered from disease relapses and progressions within 2 years (6). The ECHELON-2 trial displayed the efficacy and safety of brentuximab vedotin in the frontline setting, but only for CD30-positive peripheral T-cell lymphomas (7). Thus, there is an urgent practical necessity for innovative treatment strategies that are highly effective and tolerable for patients with PTCL.

Globally, HDAC inhibitors (HDACi) belinostat, romidepsin and chidamide, with the overall response rate (ORR) ranging from 25% to 28%, have been approved for relapsed or refractory PTCL (8–10). These inhibitors promote differentiation, growth arrest, and apoptosis in neoplastic cells *in vitro* (11). The efficacy of HDACi may be attributed to the epigenetic dysregulation in PTCL (12). China has approved chidamide, an oral novel histone deacetylase inhibitor, for patients with relapsed or refractory PTCL, based on a small phase II trial showing a high ORR of 28%. However, there is still a lack of consensus on the application of chidamide in the frontline setting. Furthermore, with modest effectiveness, HDACi monotherapy is not capable to completely overcome the poor prognosis of PTCL. Thus, the optimal therapeutic approach for patients with PTCL need to be further investigated.

In the present research, we compared the efficacy of traditional chemotherapy alone and traditional chemotherapy combined with chidamide against newly diagnosed PTCL. Prognostic factors having an impact on progression and survival of patients diagnosed with untreated PTCL were also explored.

MATERIALS AND METHODS

Patients

421 PTCL patients managed in Sun Yat-sen University Cancer Center from January 2014 to July 2020 were reviewed, in which 104 patients were diagnosed with newly diagnosed PTCL and retrospectively analyzed in our study, as shown in **Figure 1**. Except for T-cell prolymphocytic leukemia, Sézary syndrome, mycosis fungoides and extranodal NK/T cell lymphoma, nasal type, other subtypes of untreated PTCL patients were enrolled. This study was approved by the institutional ethical review board of Sun Yat-sen University Cancer Center.

Study Design

Our study retrospectively analyzed the efficacy of chemotherapy (ChT) and chemotherapy +chidamide (ChT+C) among patients with newly diagnosed PTCL. According to the frontline treatment they received, patients were divided into two treatment groups, one was ChT group, the other one was ChT+C group. The primary endpoint was progression-free survival (PFS). The overall survival (OS), objective response rate (ORR) and complete remission (CR) rate were secondary endpoints. PFS was calculated from the initiation of frontline treatment to the time point of relapse, progression, start of second-line treatment, death, or the last follow-up. OS was estimated as the time period from diagnosis to death or last follow-up. EBER *in situ* hybridization was applied to detection EBV infection. Computed tomography, magnetic resonance imaging and positron emission computed tomography were repeated every two or three cycles in order to evaluate the disease response, which was performed according to 2016 Lugano Classification lymphoma response criteria. The toxicity grading was conducted based on the National Cancer Institute Common Toxicity Criteria.

Statistical Analysis

The differences in clinicopathological characteristics between the two groups were analyzed by $\chi 2$ test or Fisher' s exact test. Survival curves were generated using the Kaplan-Meier method. A univariate analysis of survival was conducted using the log-rank test. The variables included for the univariate analyses were as follows: treatment group, International Prognosis Index (IPI), age, Ann Arbor stage, serum lactic dehydrogenase (LDH), Eastern Cooperative Oncology Group (ECOG) performance status, extranodal sites and EBER. Multivariate Cox's regression analysis was performed for significant variables identified by using univariate analysis to determine independent prognostic factors.

To further evaluate factors associated with prognostic differences between ChT and ChT+C group, subgroup analysis was performed to assess survival outcomes of treatment groups in subgroups defined according to IPI (high scores of 0–2 and low scores of 3-5), LDH (normal and elevated), age (≤60 and >60 years), stage (I-II and III-IV), gender (male and female) and EBER (positive and negative). Interaction tests were performed on the patients enrolled in our study. Results are presented using

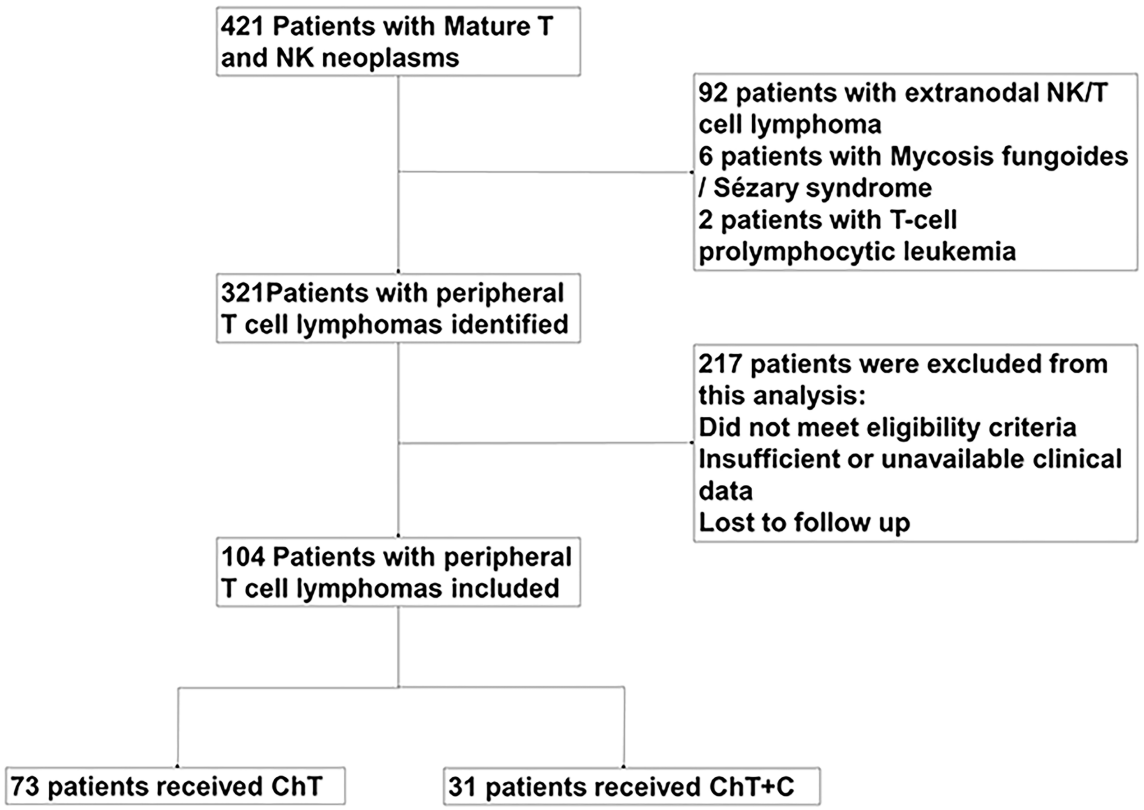

FIGURE 1 | The process of patients inclusion.

forest plot with *p* values for the interaction effects and hazard ratios.

Since baseline imbalance and chemotherapy regimen may generate discrepancies in treatment outcome between groups, we conducted a 1:1 matched case-control analysis with the propensity score matching method. A total of 16 patients treated with CHOP-C and 16 patients treated with CHOP were included in further analysis. In the matched groups, IPI were matched between groups. Based on the matched population, survival analysis was conducted using the Kaplan–Meier method.

Statistical analysis was conducted with IBM SPSS Statistics 20.0 software. A p-value less than 0.05 was considered statistically significant.

RESULTS

Baseline Characteristics

Included in our analysis were 104 patients with newly diagnosed PTCL. The baseline characteristics of the patients was shown in **Table 1**. The median age was 59.5 years (range 24–87 years). Of the 104 patients, 37 were males (35.6%), whereas 67 (64.4%) were females. The ChT group comprised 73, whereas 31 patients were included in the ChT+C group. The mean IPI in both groups was 2. Compared with ChT+C group, the ChT group comprised of more PTCL-NOS (54.8% vs 22.6%), and less AITL (13.7% vs 51.6%) patients. The two treatment groups did not differ in other characteristics. A total of 52 (71.2%) and 17 (54.8%) in ChT group and ChT+C group, respectively, received doxorubicin-based regimens as frontline chemotherapy. Meanwhile, 9 (12.3%) and 12 (38.7%) in ChT group and ChT+ C group, respectively, received etoposide-based regimens as frontline chemotherapy. Only two of patients included in this study underwent ASCT in the frontline setting. 17 patients received maintenance treatment with HDACi. In ChT group, 33 patients had available salvage treatment information, including 20 patients receiving chemotherapy, 7 patients receiving chidamide-contained treatment, 4 patients enrolled in clinical trials and 2 patients receiving other targeted treatment. In ChT+C group, 6 patients had available salvage treatment information, including 2 patients receiving chemotherapy, 2 patients receiving chidamide-contained treatment, 1 patient receiving lenalidomide and 1 patient receiving radiotherapy.

Outcomes of Treatment

The ORR for ChT group and ChT+C group were 72.6% and 77.4%, respectively (p=0.608), with the CR rate of 47.9% and 54.8% (p=0.520). Among patients achieving CR/PR in both two groups, the median time to best response was 1.5 months. After

TABLE 1 | Baseline characteristics of 104 PTCL patients.

Characteristics	Overall n = 104	ChT n = 73	Chidamide+ChT n = 31	*p*
Age, years				0.562
median	59.5	59	60	
range	(24-87)	(24-87)	(27-84)	
Gender				0.377
Male	37 (35.6%)	24 (32.9%)	13 (41.9%)	
Female	67 (64.4%)	49 (67.1%)	18 (58.1%)	
LDH				0.084
Normal	57 (54.8%)	36 (49.3%)	21 (67.7%)	
Elevated	47 (45.2%)	37 (50.7%)	10 (32.3%)	
ECOG				0.103
0-1	92 (88.5%)	62 (84.9%)	30 (96.8%)	
≥2	12 (11.5%)	11 (15.1%)	1 (3.2%)	
Stage				0.770
I-II	22 (21.2%)	16 (21.9%)	6 (19.4%)	
III-IV	82 (78.8%)	57 (78.1%)	25 (80.6%)	
Extranodal sites				0.382
0-1	88 (84.6%)	60 (82.2%)	28 (90.3%)	
≥2	16 (15.4%)	13 (17.8%)	3 (9.7%)	
IPI				0.561
0	8 (7.7%)	6 (8.2%)	2 (6.5%)	
1	25 (24.0%)	14 (19.2%)	11 (35.5%)	
2	36 (34.6%)	25 (34.2%)	11 (35.5%)	
3	28 (26.9%)	22 (30.1%)	6 (19.4%)	
4	5 (4.8%)	4 (5.5%)	1 (3.2%)	
5	2 (1.9%)	2 (2.7%)	0	
Histopathology				<0.001
PTCL-NOS	47 (45.2%)	40 (54.8%)	7 (22.6%)	
AITL	26 (25.0%)	10 (13.7%)	16 (51.6%)	
Others	31 (29.8%)	23 (31.5%)	8 (25.8%)	
EBER				0.500
Positive	37 (35.6%)	24 (32.9%)	13 (41.9%)	
Negative	64 (61.5%)	46 (63.0%)	18 (58.1%)	
Unknown	3 (2.9%)	3 (4.1%)	0	

PTCL-NOS, peripheral T-cell lymphoma, not otherwise specified; AITL, angioimmunoblastic T-cell lymphoma; ChT, chemotherapy; LDH, lactate dehydrogenase; IPI, international prognostic index.

the median follow-up of 16.8 months (range 2.0-132.0 months), the median duration of response (CR+PR) in ChT group and ChT+C group were 10.0 months and 14.0 months, with no significant difference (p=0.135). The median PFS was 8.5 months (range 1.0-84.0 months) and 12.4 months (range 3.4-47.3 months) in ChT group and ChT+C group, respectively. The median OS were 16.5 months (range 2.0-132.0 months) versus 17.1 months (range 8.0-48.5 months), for ChT and ChT+C group, respectively. The one-year PFS rate and OS rate were 44.6%, and 67.7% in ChT group, respectively, whereas 54.1% and 85.1% in ChT+C group, respectively. Compared with patients who received ChT, those who received ChT+C displayed significantly longer PFS (p=0.047, **Figure 2A**). However, there was no significantly statistical difference observed between the two groups in OS (p=0.212, **Figure 2B**).

Prognostic Factor Analysis

High IPI scores have a negative relationship with PFS and OS (p=0.028 and 0.003, respectively) (**Figures 3A, B**). The prognostic significance of EBER and the components of the IPI, including age, ECOG performance status, LDH, Ann Arbor stage and number of extranodal sites, were analyzed by univariate analysis. Patients older than sixty years tended to have inferior PFS and OS (p = 0.064 and 0.060, respectively) (**Figure 4** and **Supplementary Figure 1**). Patients with poor performance status tended to have a worse overall survival (p=0.053, **Supplementary Figure 1**).

Multivariate analysis was done by Cox's proportional hazards regression model, including frontline treatment regimen and prognostic factors identified by above univariate survival analysis. Frontline treatment regimen was an independent prognostic factor affecting PFS, with the HR of 1.881 (95%CI 1.015 to 3.487, p=0.045).

Subgroup Analysis

A forest plot of HRs illustrating the subgroup analyses was shown in **Figure 5**. For patients with high IPI scores (3-5), the HR value for PFS comparing ChT with ChT+C was 4.675 (95% CI 1.079 to 20.258). For patients with advanced disease, the HR value was 2.676 (95%CI 1.294 to 5.534). A test of interaction between IPI and frontline treatment regimen was statistically significant (p = 0.037), indicating longer PFS for patients treated with ChT+C in the high-IPI subgroup. There was no evidence of heterogeneity in the effect of chidamide in subgroups defined according to histopathology, EBER, gender, stage, age and LDH.

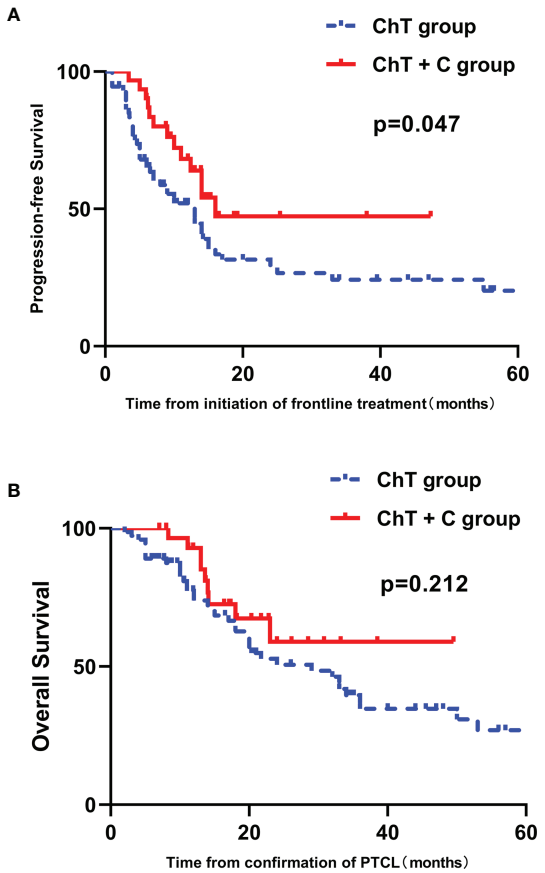

FIGURE 2 | Survival outcomes in patients with untreated PTCL stratified by type of therapy. **(A)** PFS curves in patients stratified by treatment group. **(B)** OS curves in patients stratified by treatment group.

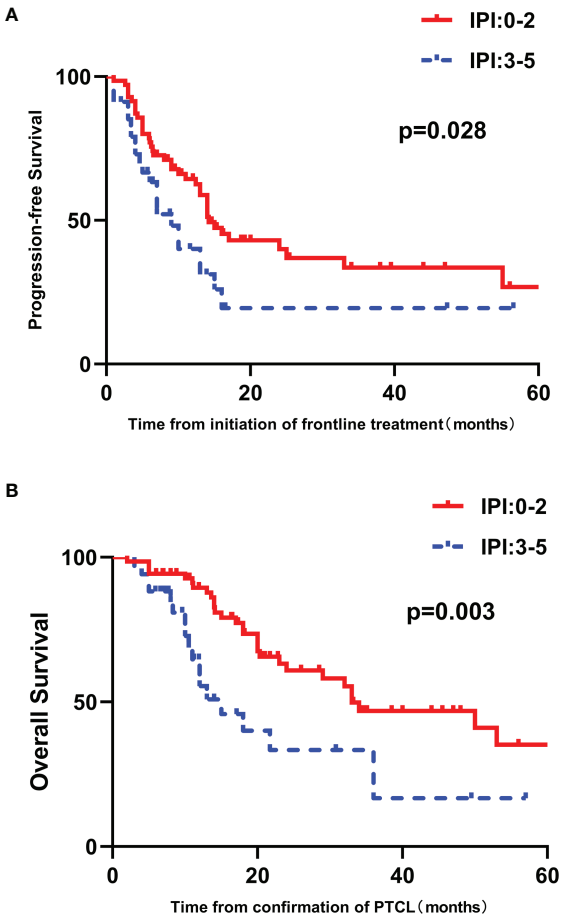

FIGURE 3 | Survival outcomes in patients with untreated PTCL stratified by IPI score. **(A)** PFS curves in patients stratified by IPI score. **(B)** OS curves in patients stratified by IPI score.

Case-Control Analysis

After matching, 9 female patients (56.3%) and 7 female patients (43.7%) were enrolled in CHOP and CHOP+C group, respectively. Patients with high IPI scores (3-5) and low IPI scores (0-2) accounted for 18.8% (3/16) and 81.2% (13/16) in the two groups, respectively. No statistical difference was found in baseline characteristics between these two groups (p>0.05, **Supplementary Table 1**). After a median follow-up of 18.0 months (range 5.0-53.0 months), median PFS was 8.5 months (range, 4.0-40.0 months) in CHOP group versus 14.5 months (range 5.0-47.0 months) in CHOP+C group. The median OS for patients treated with CHOP and CHOP+C was 17.5 months (range 5.0-53.0 months) and 18.0 months (range 7.0-50.0 months), respectively. Median PFS in CHOP+C group was obviously longer compared with CHOP group, but no significant difference was observed in PFS and OS (p = 0.134 and 0.319, respectively) (**Figures 6A, B**).

Toxicity Profiles

Hematological adverse events (AEs) were the most frequent treatment-related AEs. In the ChT and ChT+C group, the incidence of grade 3/4 anemia was 17.8% and 16.1% (p=0.836), the incidence of grade 3/4 leukocytopenia was 24.7% and 17.6% (p=0.557), and the incidence of grade 3/4 thrombocytopenia was 23.3%, and 16.1% patients (p=0.414), respectively. Frequency of AEs did not appear to be significantly different between the two groups. None of the adverse reactions resulted to death.

DISCUSSION

In this study, we examined whether adding chidamide to traditional chemotherapy can potentiate the antitumor activities and improve survival, in the frontline setting of PTCL. Compared with patients treated with ChT, those treated with ChT+C group superior PFS. However, there was no significantly statistical difference observed between the two groups in OS. High IPI scores were associated with poor PFS and OS, consistent with previous data (13). Among patient with untreated PTCL, frontline treatment regimen was considered as an independent prognostic factor for PFS. Severe treatment-related AEs were infrequent. The incidence of hematological toxicity is highest in both two groups, without significant difference. The results of our study indicated the

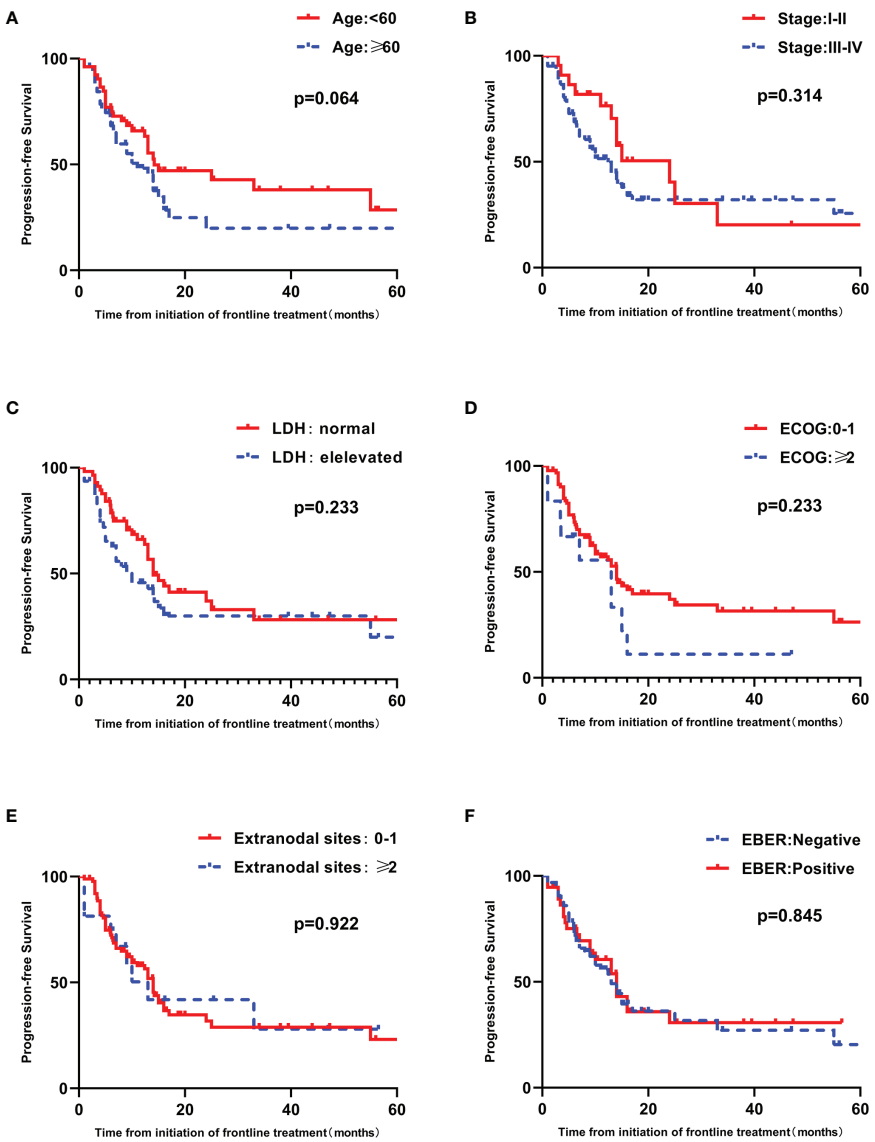

FIGURE 4 | Univariate analyses of PFS in patients with untreated PTCL. **(A)** PFS curves in patients stratified by age. **(B)** PFS curves in patients stratified by Ann Arbor stage. **(C)** PFS curves in patients stratified by LDH. **(D)** PFS curves in patients stratified by ECOG. **(E)** PFS curves in patients stratified by extranodal sites. **(F)** PFS curves in patients stratified by EBER.

combination of ChT and chidamide confers better prognosis to untreated PTCL patients with acceptable toxicity.

In the era of traditional chemotherapy, a large proportion of PTCL patients suffered frequent relapse and unfavorable outcome (14). Chidamide, as a kind of HACDi, may bring us a promising future. HDACis promote apoptosis and inhibit angiogenesis through acetylation of both histone and non-histone proteins (15, 16). However, HDACi monotherapy demonstrated modest and short-lived effectiveness, without complete and durable responses (10). Thus, in order to improve the prognosis, more optimal combination therapeutic approach for PTCL should be optimized further. In addition, previous researches have proven that the synergy between HDAC inhibitors and cytotoxic agents *in vitro* (17–19). Given the potential synergistic effect, for patients with untreated PTCL, it is reasonable to explore the integration of chidamide into standard chemotherapy.

Subgroup analyses revealed that remarkable differences in PFS among subgroups as defined by IPI. Within the ChT+C group, more PFS benefit was observed in the high-IPI subgroup. In contrast, chidamide had no noticeable impact on PFS in the low-IPI subgroup. A nominally significant interaction between IPI and frontline treatment was observed, which indicates IPI as a prognostic indicator should be taken into consideration in clinical settings. Based on the results of our study, IPI was an independent risk factor for poor prognosis. Therefore, one reasonable explanation for PFS benefit in the subgroup of patients with high

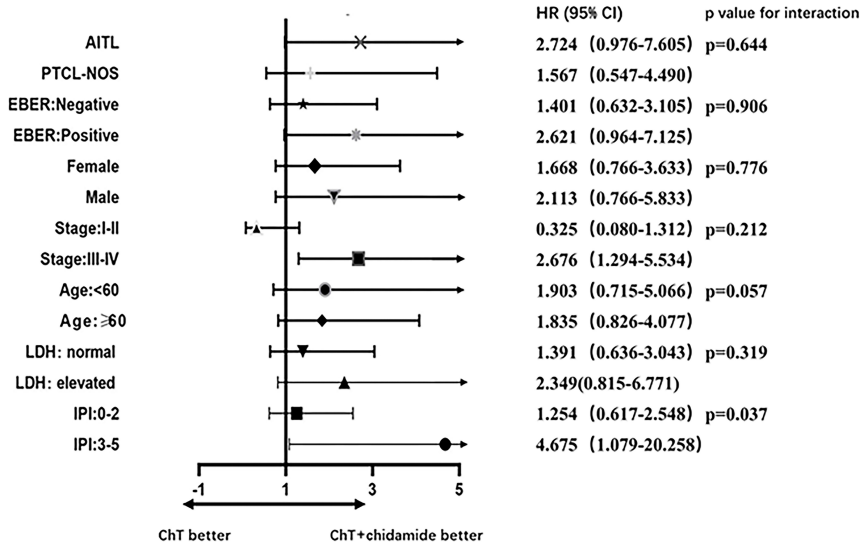

FIGURE 5 | Prespecified subgroup analyses of patients with untreated PTCL.

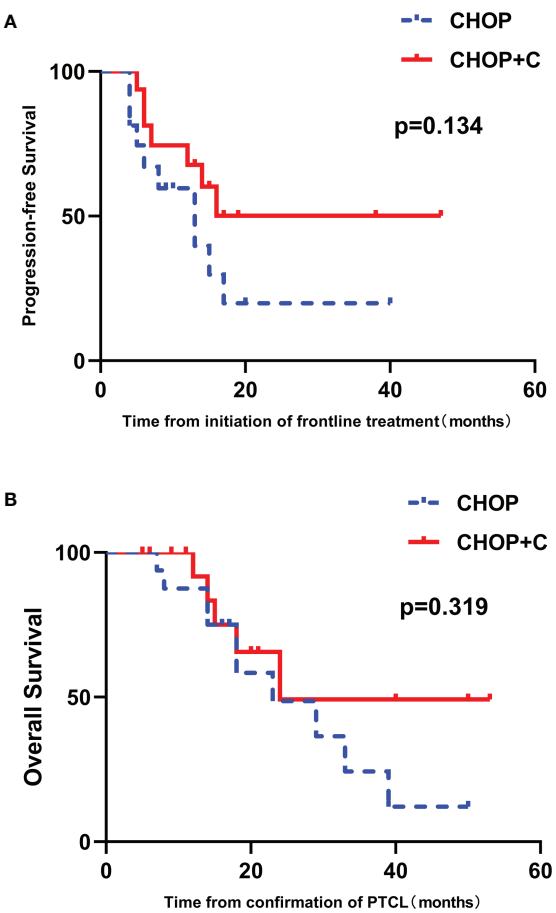

FIGURE 6 | The 1:1 matched case-control analysis of patients with untreated PTCL. **(A)** PFS curves in patients stratified by treatment group. **(B)** OS curves in patients stratified by treatment group.

IPI scores is that risk factor can be overcome by chidamide to a certain extent. Patients with low IPI scores tended to have better survival outcome and derive less benefit from chidamide, so ChT alone might be an appropriate treatment option for this cohort. These findings suggested that baseline characteristics of patients could guide individualized treatment selection.

According to the survival analysis in our study, IPI was found to have prognostic significance in the survival of the patients with newly diagnosed PTCL, which are consistent with previous studies. Additionally, the choice of chemotherapy regimen may make a difference to the survival outcome. There was the potential baseline imbalance in IPI and chemotherapy regimen between the two groups. Hence, a 1:1 (low IPI scores: high IPI scores) matched case-control analysis was conducted, selecting IPI as the matching conditions and using the propensity score matching method in the patients receiving CHOP or CHOP+C. The results indicated that median PFS in CHOP+C group was obviously longer compared with CHOP group, but there was no significant difference observed. Given that most patients included in case-control analysis had low IPI scores (81.2%), the non-significantly different survival outcome may be attributed to the less benefit of ChT+C in patients with low IPI, which was consistent with the subgroup analysis.

The toxicity profile was generally featured with the predictable and manageable hematological events. The AEs following frontline treatment was analogous, regardless of whether chidamide was utilized.

In fact, there were several restrictions in our study. Firstly, there is growing evidence that ASCT as the frontline consolidation therapy can improve survival (6). However, most of patients included in this study did not undergo ASCT because of their inadequate understanding of ASCT and poor economic conditions. Secondly, due to the lack of an effective treatment regimen, physician and patient preferences as confounding variables might have influenced the outcome. Thirdly, this observational study with small sample size has a limitation towards conducting further analysis. Taken together, studies with larger randomized design are necessary to validate our findings.

CONCLUSIONS

To sum up, traditional chemotherapy combined with chidamide may prolong the PFS in patients with newly diagnosed PTCL, especially for patients with high IPI scores. Treatment-related toxicities characterized by hematological events were manageable and reversible. It is attractive to explore further with a larger and randomized study in order to identify the more excellent strategy.

DATA AVAILABILITY STATEMENT

The raw data supporting the conclusions of this article will be made available by the authors, without undue reservation.

ETHICS STATEMENT

The studies involving human participants were reviewed and approved by the review board of Sun Yat-sen University Cancer Center. The patients/participants provided their written informed consent to participate in this study.

AUTHOR CONTRIBUTIONS

All authors contributed to the study conception and design. Material preparation, data collection and analysis were performed by JW and NS. The first draft of the manuscript was written by JW, and all authors commented on previous versions of the manuscript. All authors read and approved the final manuscript.

FUNDING

This study was supported by grants from the Special Support Program of Sun Yat-sen University Cancer Center (PT19020401, QC), the Science and Technology Planning Project of Guangzhou, China (202002030205, QC), and the Clinical Oncology Foundation of Chinese Society of Clinical Oncology (Y-XD2019-124, QC). The open access publication fees were paid by the Science and Technology Planning Project of Guangzhou, China (202002030205, QC).

SUPPLEMENTARY MATERIAL

The Supplementary Material for this article can be found online at: https://www.frontiersin.org/articles/10.3389/fimmu.2022.835103/full#supplementary-material

Supplementary Figure 1 | Univariate analyses of OS in patients with untreated PTCL. **(A)** OS curves in patients stratified by age. **(B)** OS curves in patients stratified by Ann Arbor stage. **(C)** OS curves in patients stratified by LDH. **(D)** OS curves in patients stratified by ECOG. **(E)** OS curves in patients stratified by extranodal sites. **(F)** OS curves in patients stratified by EBER.

REFERENCES

1. A clinical evaluation of the International Lymphoma Study Group. Classification of Non-Hodgkin's Lymphoma. The Non-Hodgkin's Lymphoma Classification Project. *Blood* (1997) 89(11):3909–18. doi: 10.1182/blood.V89.11.3909
2. Vose J, Armitage J, Weisenburger D, International TCLP. International Peripheral T-Cell and Natural Killer/T-Cell Lymphoma Study: Pathology Findings and Clinical Outcomes. *J Clin Oncol* (2008) 26(25):4124–30. doi: 10.1200/JCO.2008.16.4558
3. Au WY, Ma SY, Chim CS, Choy C, Loong F, Lie AK, et al. Clinicopathologic Features and Treatment Outcome of Mature T-Cell and Natural Killer-Cell Lymphomas Diagnosed According to the World Health Organization Classification Scheme: A Single Center Experience of 10 Years. *Ann Oncol* (2005) 16(2):206–14. doi: 10.1093/annonc/mdi037
4. Rudiger T, Weisenburger DD, Anderson JR, Armitage JO, Diebold J, MacLennan KA, et al. Peripheral T-Cell Lymphoma (Excluding Anaplastic Large-Cell Lymphoma): Results From the Non-Hodgkin's Lymphoma

Classification Project. *Ann Oncol* (2002) 13(1):140–9. doi: 10.1093/annonc/mdf033
5. Melnyk A, Rodriguez A, Pugh WC, Cabannillas F. Evaluation of the Revised European-American Lymphoma Classification Confirms the Clinical Relevance of Immunophenotype in 560 Cases of Aggressive Non-Hodgkin's Lymphoma. *Blood* (1997) 89(12):4514–20. doi: 10.1182/blood.V89.12.4514
6. d'Amore F, Relander T, Lauritzsen GF, Jantunen E, Hagberg H, Anderson H. Up-Front Autologous Stem-Cell Transplantation in Peripheral T-Cell Lymphoma: NLG-T-01. *J Clin Oncol* (2012) 30(25):3093–9. doi: 10.1200/JCO.2011.40.2719
7. Horwitz S, O'Connor OA, Pro B, Illidge T, Fanale M, Advani R, et al. Brentuximab Vedotin With Chemotherapy for CD30-Positive Peripheral T-Cell Lymphoma (ECHELON-2): A Global, Double-Blind, Randomised, Phase 3 Trial. *Lancet* (2019) 393(10168):229–40. doi: 10.1016/S0140-6736(18)32984-2
8. Coiffier B, Pro B, Prince HM, Foss F, Sokol L, Greenwood M, et al. Romidepsin for the Treatment of Relapsed/Refractory Peripheral T-Cell Lymphoma: Pivotal Study Update Demonstrates Durable Responses. *J Hematol Oncol* (2014) 7:11. doi: 10.1186/1756-8722-7-11
9. O'Connor OA, Horwitz S, Masszi T, Van Hoof A, Brown P, Doorduijn J, et al. Belinostat in Patients With Relapsed or Refractory Peripheral T-Cell Lymphoma: Results of the Pivotal Phase II BELIEF (CLN-19) Study. *J Clin Oncol* (2015) 33(23):2492–9. doi: 10.1200/JCO.2014.59.2782
10. Shi Y, Dong M, Hong X, Zhang W, Feng J, Zhu J, et al. Results From a Multicenter, Open-Label, Pivotal Phase II Study of Chidamide in Relapsed or Refractory Peripheral T-Cell Lymphoma. *Ann Oncol* (2015) 26(8):1766–71. doi: 10.1093/annonc/mdv237
11. Bose P, Dai Y, Grant S. Histone Deacetylase Inhibitor (HDACI) Mechanisms of Action: Emerging Insights. *Pharmacol Ther* (2014) 143(3):323–36. doi: 10.1016/j.pharmthera.2014.04.004
12. Iqbal J, Wright G, Wang C, Rosenwald A, Gascoyne RD, Weisenburger DD, et al. Gene Expression Signatures Delineate Biological and Prognostic Subgroups in Peripheral T-Cell Lymphoma. *Blood* (2014) 123(19):2915–23. doi: 10.1182/blood-2013-11-536359
13. Piccaluga PP, Agostinelli C, Gazzola A, Mannu C, Bacci F, Sabattini E, et al. Prognostic Markers in Peripheral T-Cell Lymphoma. *Curr Hematol Malig Rep* (2010) 5(4):222–8. doi: 10.1007/s11899-010-0062-x
14. Savage KJ, Chhanabhai M, Gascoyne RD, Connors JM. Characterization of Peripheral T-Cell Lymphomas in a Single North American Institution by the WHO Classification. *Ann Oncol* (2004) 15(10):1467–75. doi: 10.1093/annonc/mdh392
15. Ning ZQ, Li ZB, Newman MJ, Shan S, Wang XH, Pan DS, et al. Chidamide (CS055/HBI-8000): A New Histone Deacetylase Inhibitor of the Benzamide Class With Antitumor Activity and the Ability to Enhance Immune Cell-Mediated Tumor Cell Cytotoxicity. *Cancer Chemother Pharmacol* (2012) 69(4):901–9. doi: 10.1007/s00280-011-1766-x
16. Minucci S, Pelicci PG. Histone Deacetylase Inhibitors and the Promise of Epigenetic (and More) Treatments for Cancer. *Nat Rev Cancer* (2006) 6(1):38–51. doi: 10.1038/nrc1779
17. Marchion DC, Bicaku E, Turner JG, Daud AI, Sullivan DM, Munster PN. Synergistic Interaction Between Histone Deacetylase and Topoisomerase II Inhibitors Is Mediated Through Topoisomerase IIbeta. *Clin Cancer Res* (2005) 11(23):8467–75. doi: 10.1158/1078-0432.CCR-05-1073
18. Cheriyath V, Kuhns MA, Kalaycio ME, Borden EC. Potentiation of Apoptosis by Histone Deacetylase Inhibitors and Doxorubicin Combination: Cytoplasmic Cathepsin B as a Mediator of Apoptosis in Multiple Myeloma. *Br J Cancer* (2011) 104(6):957–67. doi: 10.1038/bjc.2011.42
19. Lopez G, Liu J, Ren W, Wei W, Wang S, Lahat G, et al. Combining PCI-24781, a Novel Histone Deacetylase Inhibitor, With Chemotherapy for the Treatment of Soft Tissue Sarcoma. *Clin Cancer Res* (2009) 15(10):3472–83. doi: 10.1158/1078-0432.CCR-08-2714

Conflict of Interest: The authors declare that the research was conducted in the absence of any commercial or financial relationships that could be construed as a potential conflict of interest.

The handling editor declared a past co-authorship with the authors NS, SM, XT, HuH, and QC.

frontiers in Immunology

ORIGINAL RESEARCH
published: 18 February 2022
doi: 10.3389/fimmu.2022.829878

OPEN ACCESS

Edited by:
Katy Rezvani,
University of Texas MD Anderson Cancer Center, United States

Reviewed by:
Xiao-Dong Mo,
Peking University People's Hospital, China
Hirokazu Kanegane,
Tokyo Medical and Dental University, Japan
Ting Niu,
Sichuan University, China

***Correspondence:**
Wei Sang
xyfylbl515@xzhmu.edu.cn
Kailin Xu
lihmd@163.com
Shuiping Huang
hsp@xzhmu.edu.cn

†These authors have contributed equally to this work and share first authorship

Specialty section:
This article was submitted to Cancer Immunity and Immunotherapy, a section of the journal Frontiers in Immunology

Received: 06 December 2021
Accepted: 28 January 2022
Published: 18 February 2022

Citation:
Shen Z, Jin Y, Sun Q, Zhang S, Chen X, Hu L, He C, Wang Y, Liu Q, Zhang H, Liu X, Wang L, Jiao J, Miao Y, Gu W, Wang F, Wang C, Shi Y, Ye J, Zhu T, Sun C, Song X, Xu L, Yan D, Sun H, Cao J, Li D, Li Z, Wang Z, Huang S, Xu K and Sang W (2022) A Novel Prognostic Index Model for Adult Hemophagocytic Lymphohistiocytosis: A Multicenter Retrospective Analysis in China. Front. Immunol. 13:829878. doi: 10.3389/fimmu.2022.829878

A Novel Prognostic Index Model for Adult Hemophagocytic Lymphohistiocytosis: A Multicenter Retrospective Analysis in China

Ziyuan Shen[1†], Yingliang Jin[2†], Qian Sun[3†], Shuo Zhang[3], Xi Chen[1], Lingling Hu[3], Chenlu He[1], Ying Wang[4], Qinhua Liu[5], Hao Zhang[6], Xin Liu[6], Ling Wang[7], Jun Jiao[7], Yuqing Miao[8], Weiying Gu[9], Fei Wang[9], Chunling Wang[10], Yuye Shi[10], Jingjing Ye[11], Taigang Zhu[12], Cai Sun[3], Xuguang Song[3], Linyan Xu[3], Dongmei Yan[3], Haiying Sun[3], Jiang Cao[3], Depeng Li[3], Zhenyu Li[3], Zhao Wang[13], Shuiping Huang[2], Kailin Xu[3*] and Wei Sang[3*] on behalf of HHLWG[14]*

[1] Department of Epidemiology and Biostatistics, School of Public Health, Xuzhou Medical University, Xuzhou, China, [2] Center for Medical Statistics and Data Analysis, School of Public Health, Xuzhou Medical University, Xuzhou, China, [3] Department of Hematology, Affiliated Hospital of Xuzhou Medical University, Xuzhou, China, [4] Department of Personnel, Suqian First Hospital, Suqian, China, [5] Department of Hematology, The First Affiliated Hospital of Anhui Medical University, Hefei, China, [6] Department of Hematology, The Affiliated Hospital of Jining Medical University, Jining, China, [7] Department of Hematology, Taian Central Hospital, Taian, China, [8] Department of Hematology, Yancheng First People's Hospital, Yancheng, China, [9] Department of Hematology, The First People's Hospital of Changzhou, Changzhou, China, [10] Department of Hematology, Huai'an First People's Hospital, Huai'an, China, [11] Department of Hematology, Qilu Hospital of Shandong University, Jinan, China, [12] Department of Hematology, The General Hospital of Wanbei Coal-Electric Group, Suzhou, China, [13] Department of Hematology, Beijing Friendship Hospital, Capital Medical University, Beijing, China, [14] Huaihai Lymphoma Working Group: The Huaihai Lymphoma Working Group (HHLWG) was a non-governmental group established in November 2017 and included 18 medical centers in Huaihai Economic Zone of China, Xuzhou, China*

Hemophagocytic lymphohistiocytosis (HLH) is an immune disorder with rapid progression and poor survival. Individual treatment strategy is restricted, due to the absence of precise stratification criteria. In this multicenter retrospective study, we aimed to develop a feasible prognostic model for adult HLH in China. A total of 270 newly diagnosed patients of adult HLH were retrieved from the Huaihai Lymphoma Working Group (HHLWG), of whom 184 from 5 medical centers served as derivation cohort, and 86 cases from 3 other centers served as validation cohort. X-Tile program and Maxstat analysis were used to identify optimal cutoff points of continuous variables; univariate and multivariate Cox analyses were used for variable selection, and the Kaplan–Meier curve was used to analyze the value of variables on prognosis. The C-index, Brier Score, and calibration curve were used for model validation. Multivariate analysis showed that age, creatinine, albumin, platelet, lymphocyte ratio, and alanine aminotransferase were independent prognostic factors. By rounding up the hazard ratios from 6 significant variables, a maximum of 9 points was assigned. The final scoring model of HHLWG-HPI was identified with four risk groups: low risk (≤3 pts), low-intermediate risk (4 pts), high-

intermediate risk (5-6 pts), and high risk (≥7 pts), with 5-year overall survival rates of 68.5%, 35.2%, 21.3%, and 10.8%, respectively. The C-indexes were 0.796 and 0.758 in the derivation and validation cohorts by using a bootstrap resampling program. In conclusion, the HHLWG-HPI model provides a feasible and accurate stratification system for individualized treatment strategy in adult HLH.

Keywords: hemophagocytic lymphohistiocytosis, adult, multicenter, prognostic model, stratification

INTRODUCTION

Hemophagocytic lymphohistiocytosis (HLH) is a severe hyperinflammatory syndrome characterized by excessive activation of T cells and macrophages and is classified into primary/hereditary (pHLH) and secondary/acquired (sHLH). Primary HLH is a fatal disease and usually develops in infancy or early childhood with a median survival of 2 months if without hematopoietic stem cell transplantation (1). Secondary HLH can be initiated by a large variety of inducements that activate the immune system, such as infections, autoimmune diseases, and tumors (2). Epstein–Barr virus is a common pathogenic factor of HLH, accounting for about 70% of infection-associated HLH (3, 4), and the most common cause of tumor-associated HLH is non-Hodgkin's lymphoma (5, 6).

The widely used diagnostic criteria for HLH are HLH-2004 and HScore (7, 8). Currently, the recommended initial therapeutic regimens are HLH-94 and HLH-2004 (8, 9). Wang et al. proposed the DEP regimen as a salvage therapy, which showed an encouraging overall response rate (76.2%) in adult refractory and relapsed HLH (10). Due to the complexity of etiology and the heterogeneity of clinical manifestations, there is a lack of precise prognostic stratification and unified individualized treatment criteria in adult HLH.

In recent years, numerous studies have explored the prognostic factors of HLH in pediatric patients. Q. et al. proposed that the lymphocyte subset was essential for prognosis (11), and Pan et al. revealed that a higher disseminated intravascular coagulation (DIC) score and lower albumin, hemoglobin, and platelet levels were negative prognostic factors in malignancy-associated HLH (12). Schram et al. confirmed that platelets and alanine aminotransferase were independent factors for overall survival (OS) in adult HLH (13). Zhou et al. confirmed that high ferritin levels (>1,050 μg/l) were associated with poor survival (14). However, other studies revealed that ferritin was not an independent prognostic indicator for adult HLH. So, the value of ferritin on the prognosis of HLH was still controversial (15, 16). Furthermore, the heterogeneity and genetic abnormalities of HLH increase the difficulty of individualized treatment for adult HLH (5, 17, 18). Therefore, there is an urgent need to establish a prognostic stratification system for adult HLH.

Based on multicenter data from the Huaihai Lymphoma Working Group (HHLWG) in China, we carried out this retrospective study to explore the prognosis of adult HLH and attempted to establish a novel prognostic model to guide precise stratification for individualized treatment.

MATERIALS AND METHODS

Patient Cohort

Data From Five Medical Centers of HHLWG for Prognostic Index Development

Data from five centers of HHLWG in this study served as the derivation cohort. The five centers are (1) Affiliated Hospital of Xuzhou Medical University (n = 75) (2), the Affiliated Hospital of Jining Medical University (n = 38) (3), Yancheng First People's Hospital (n = 37) (4), Huai'an First People's Hospital (n = 22), and (5) Taian Central Hospital (n = 12).

Data From Three Medical Centers of HHLWG for External Validation

Data from three centers of HHLWG in this study served as the external validation cohort. The three centers are (1) The First Affiliated Hospital of Anhui Medical University (n = 40) (2), The First People's Hospital of Changzhou (n = 30), and (3) Qilu Hospital of Shandong University (n = 16). Study approval was obtained from the independent Ethics Committees of each participating center in HHLWG and met the Helsinki Declaration. Patients over 18 years old with newly diagnosed HLH retrieved from the above centers between January 1, 2013, and August 19, 2020, were included. Median follow-up was 30.6 months [95% *CI* (22.2–38.9)] in the derivation cohort and 54.8 months [95% *CI* (25.3–84.3)] in the validation cohort. **Figure 1** shows the flowchart of the inclusion and exclusion processes in this study.

Baseline Characteristics of Patients

At admission, the following variables were collected: age, gender, etiologies, ferritin, triglycerides (TG), fibrinogen (FIB), lactate dehydrogenase (LDH), creatinine (Cr), alanine aminotransferase (ALT), hemoglobin (Hb), platelet (PLT), lymphocyte ratio (LYR), albumin (ALB), fever, EBV infection, presence or absence of splenomegaly, and therapeutic regimens.

Diagnosis of HLH

The diagnosis of HLH was established according to HLH-2004 diagnostic guidelines (8). Five of eight criteria are required to make a diagnosis of HLH (1): fever (2); splenomegaly (3); cytopenias (affecting ≥2 of 3 lineages in the peripheral blood: hemoglobin <90 g/l (in infants: hemoglobin < 100 g/l), platelets $< 100 \times 10^9$/l, neutrophils $< 1.0 \times 10^9$/ (4); hypofibrinogenemia and/or hypertriglyceridemia: fasting triglycerides ≥ 3.0 mmol/l; fibrinogen ≤1.5 g/l) (5); hemophagocytosis in bone marrow, spleen, or lymph nodes (6); low or absent NK-cell activity

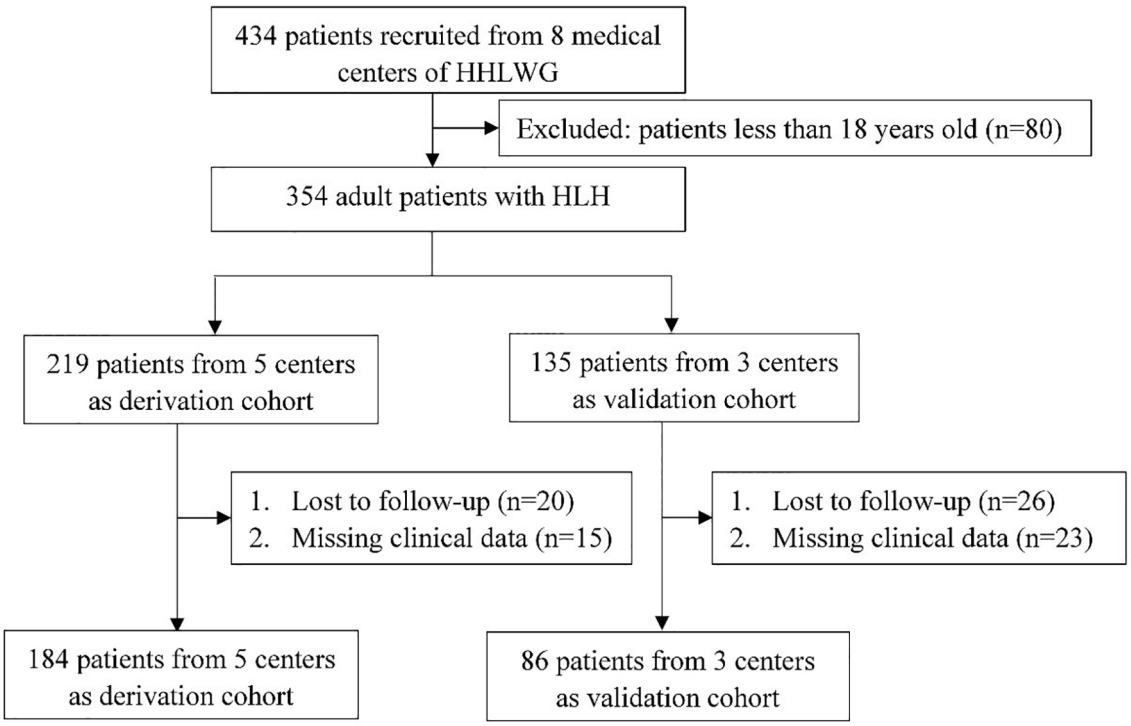

FIGURE 1 | Flow chart of screening patients with HLH.

(according to local laboratory reference) (7); ferritin ≥ 500 μg/l; and (8) soluble CD25 (soluble IL-2 receptor) ≥ 2,400 U/ml. All pathological biopsies were double blinded reviewed by at least two pathologists.

Follow-Up and Endpoints

Follow-up was conducted by consulting inpatient medical records and making phone calls. We followed up all the patients until February 19, 2021, or the death of patients. Overall survival (OS) was calculated as the interval between the time of diagnosis and death from any cause or the last follow-up. The survival status of all patients was confirmed with death records or a telephone call to next of kin (if patient died during the follow-up) or to the patients themselves.

Statistical Analysis

Development of HHLWG-HPI

Based on the data from HHLWG, we attempted to develop a prognostic index model for adult HLH, the HHLWG-HPI. Data were presented as numbers (percentages) for categorical variables and median (interquartile range, IQR) for all continuous variables. Outliers were verified by the hospital medical record system. All cases were required to have complete clinical information in order to avoid unnecessary bias. The Shapiro–Wilk test was used to test the normality of numerical variables. Differences in clinical factors between etiology groups were analyzed by using the Kruskal–Wallis test and analysis of variance (ANOVA) test. Continuous variables were transformed into categorical variables by X-Tile program (Yale University, New Haven, CT, USA) (19) and Maxstat analysis (titled as Maximally Selected Rank Statistics). The X-Tile program can help divide patients into subgroups by determining the optimal cutoff points of a continuous or ordinal categorical variable based on the maximum χ^2 statistic value on the log-rank test (20). The Cox proportional hazard model was used to analyze the univariate association between prognostic factors and OS. All variables with $p<0.1$ in univariate analysis were kept in the multivariate analysis by using backward selection for the best predictor set, and Akaike information criteria (AIC) was used to evaluate the model. All statistical tests were two-sided, and the statistical significance was set at $p < 0.05$.

The prognostic index (HHLWG-HPI) was derived from the prognostic model that was identified using the Cox proportional hazards model. Index scores were assigned proportionally to the estimates of the relative contribution of the independent factors in the HHLWG-HPI model. The proximity of Kaplan–Meier was used to stratify patients into risk strata based on each score value.

Validation of HHLWG-HPI

The model was internally validated using a bootstrap resampling procedure (1,000 iterations) with a relatively corrected Harrell's C-statistics (C-index). A C-index score around 0.70 indicates a good model (21). Brier Score is another score function that measures the accuracy of probabilistic prediction. In survival analysis, the Brier Score measures the mean of the difference

between the observed and the estimated survival beyond a certain time. The score value ranges from 0 to 1, and a higher score indicates higher inaccuracy (22, 23). The calibration curve for probability of survival was used to show optimal agreement between prediction and actual observation. External validation of the HHLWG-HPI was performed using data from 3 medical centers of HHLWG. The C-index and calibration curve were based on the basis of the regression analysis. The statistical analysis was performed by SPSS statistics for Windows, Version 19.0 (Armonk, NY: IBM Corp.), and R software (version 4.0.3; http://www.Rproject.org).

RESULTS

Cohort Characteristics

There were 434 HLH patients retrieved from HHLWG, of whom 354 were older than 18 years. Eighty-four patients were ineligible for inclusion, so 270 patients were eventually included in the whole cohort. The derivation cohort consisted of 184 cases, and the external validation cohort consisted of 86 patients. The characteristics of patients in both cohorts were compared, as shown in **Table 1**. The median age was 56 (IQR, 46–66) years, and 53.6% patients were male in the derivation cohort. Noticeably, patients in the derivation cohort were younger compared with the validation cohort (median age 56 vs. 61 years). Of the 184 patients, infections (n = 88) and tumor (n = 64) were the most frequent underlying etiologies, accounting for 83%. The results of the Kruskal–Wallis test showed that the lymphocyte ratio was significantly different among etiology groups, with the highest value in the infection-associated group.

Clinical Survival Analysis

In the whole cohort (n = 270), infection (n = 119) and tumor (n = 97) were the most frequent underlying etiologies, accounting for 80%. There was no significant difference among different etiology groups ($p = 0.092$, **Figure 2A**). The survival curves of different etiologies groups were examined by KM analysis, and the results showed that the OS of patients in the infection-associated group was significantly higher than that in the tumor-associated group ($\chi^2 = 6.400$, $p = 0.011$), and there was no significant difference between the OS of patients in the infection-associated group and that in the autoimmunity-associated group ($\chi^2 = 0.895$, $p = 0.344$). The results showed that the 5-year survival rates were significantly different in infection-associated, autoimmunity-associated, other etiologies, and tumor-associated groups ($p < 0.01$).

EBV-DNA data were available in 163 evaluable patients, of whom 82 exceeded 1,000 copies/ml. KM analysis showed that high EBV-DNA level was associated with poor outcome, with only 39% of 5-year OS. Maxstat analysis was performed in 105 cases with explicit value, and the optimal cutoff value of EBV-DNA was 1,520 copies/ml. The influence of different etiologies on the prognosis of adult HLH was further explored. According to KM analysis results, we found that there were no significant differences between EBV infection and other groups in prognosis ($p > 0.05$). In addition, we explored the prognostic value of ferritin in adult HLH. Of the 270 patients, the ferritin levels of 230 were above 500 ng/ml, and there was no survival difference between them and those with ferritin levels below 500 ($p = 0.99$). Of the 173 patients with explicit values that could be evaluated, an optimal cutoff value could not be obtained.

In this study, patients received regimens of HLH-94 (n = 39), HLH-2004 (n = 26), DEP regimen (n = 6), steroid (n = 50), antiviral (n = 60), CHOP/CHOP-like (n = 22), and supportive

TABLE 1 | Basic clinical information of adult HLH.

Characteristics	Derivation cohort n (%)	Validation cohort n (%)	*p*
Age[a]	56 (46,66)	61 (47.75,70.00)	0.148
ALT[a]	72.5 (35.475,146.00)	77.5 (38.25,168.25)	0.736
Cr[a]	58.8 (45.15,77.75)	63.5 (50.00,80.00)	0.135
TG[a]	1.835 (1.418,2.455)	2.235 (1.795,3.050)	<0.050
Gender			0.088
Male	106 (57.60)	40 (46.51)	
Female	78 (42.40)	46 (53.49)	
Hb (g/L)			0.429
<120	156 (84.78)	76 (88.37)	
≥120	28 (15.22)	10 (11.63)	
PLT ($\times 10^9$/L)			0.166
<100	138 (75.00)	71 (82.56)	
≥100	46 (25.00)	15 (17.44)	
		0)	
FIB (g/L)			0.115
<1.5	51 (27.72)	32 (37.21)	
≥1.5	133 (72.28)	54 (62.79)	
Splenomegaly			0.537
absence	67 (36.50)	28 (32.56)	
presence	117 (63.50)	58 (67.44)	

[a]*Variables were presented using median and interquartile range.*

ALT, alanine aminotransferase; Cr, creatinine; TG, triglycerides; Hb, hemoglobin; PLT, platelet; FIB, fibrinogen.

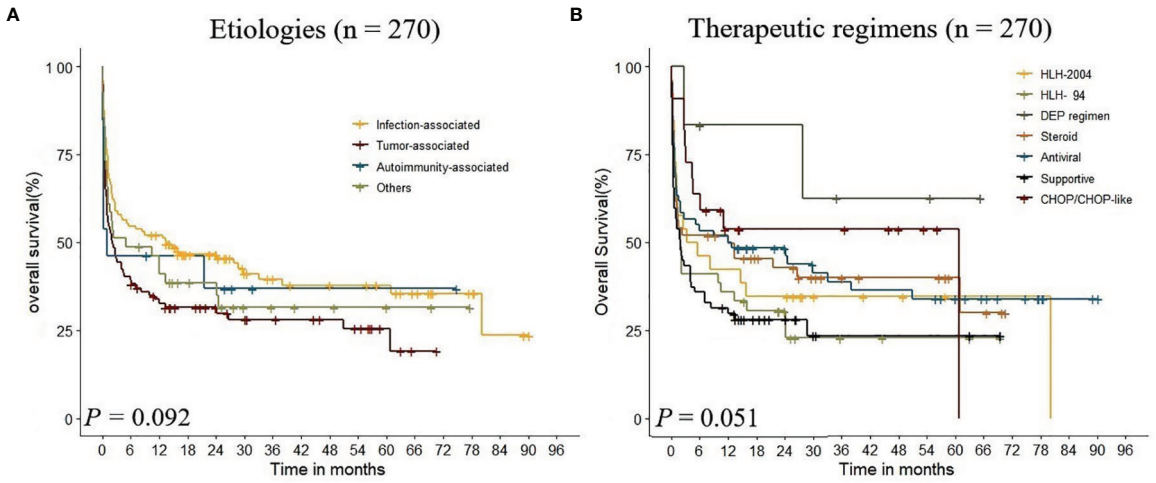

FIGURE 2 | Kaplan–Meier analysis estimate of survival rate in adult HLH according to the underlying etiologies and therapeutic regimens.

treatment (n = 67). The 1-year OS of each treatment group was 42.3%, 35.9%, 83.3%, 52.0%, 51.7%, 31.3%, and 53.7%, respectively. KM analysis indicated that there was no significant difference in therapeutic regimens on the prognosis of adult HLH (p = 0.051, **Figure 2B**). The results showed that the 5-year survival rates were significantly different among DEP regimen, HLH-94 regimen, HLH-2004 regimen, and steroid regimen groups ($p < 0.01$).

Correlation Analysis of Immune Status and Survival

In patients with evaluable immune globulin (IgA, IgG, and IgM) and lymphocyte subset data, the correlations between immune status and survival were analyzed. The linear association of all immune factors was measured by Pearson's correlation. The results suggested that CD8 had a significant positive linear association with IgG (r = 0.334, p = 0.015) and CD3 was negatively correlated with IgM (r = -0.383, p = 0.004).

KM analysis indicated that there was no significant difference in immune globulin and lymphocyte subsets according to reference ranges (**Figure 3**). By Maxstat analysis, the optimal cutoff points for CD4+, CD8+ proportion, and CD4+/CD8+ ratio were 20.13, 19, and 3.24, respectively. Based on those cutoff points above, the survival of patients could be stratified.

Cutoff Point Identification of Variables in the Derivation Cohort

In this study, continuous variables included in this study were age, lactate dehydrogenase (LDH), hemoglobin (Hb), platelet (PLT), fibrinogen (FIB), lymphocyte ratio (LYR), albumin (ALB), triglycerides (TG), creatinine (Cr), and alanine aminotransferase (ALT). The optimal cutoff values of TG, FIB, and ALT obtained by maximally selected rank statistics (**Figure 4A**) were 1.41, 1.2, and 40, respectively. Based on these cutoff values, we divided patients into higher group and lower group. X-Tile software was used to determine the optimal cutoff points for age, ALB, Hb, PLT, Cr, and LYR (**Figure 4B**). The best cutoff values for age were 50 and 65, for ALB 29.8 and 35.2, for Hb 68 and 104, for PLT 25 and 72, for Cr 53 and 66, and for LYR 21.1 and 45.8.

Univariate and Multivariate Analyses of HLH Patients

The univariate analysis showed that age, Cr, ALB, PLT, LYR, Hb, FIB, ALT, etiologies, and gender significantly affected survival in the derivation cohort, whereas hepatosplenomegaly did not. Age, Cr, and ALB appeared to be stronger predictors ($p < 0.001$). The correlations between the clinical characteristics at diagnosis and OS are shown in **Table 2**.

Development of HHLWG-HPI and Internal Validation

In the multivariate Cox regression model, age was stratified into three groups (18–49, 50–65, and > 65 years); albumin in three groups (<29.8, 29.8–35.2, and >35.2 g/l); creatinine in three groups (<53, 53–66, and >66 μmol/l); lymphocyte ratio in two groups (≤45.8 and >45.8%); alanine aminotransferase in two groups (≤40 and >40), and platelet in two groups (≤72 and >72 × 10^9/l). After rounding up the hazard ratios of the significant variables, the current HHLWG-HPI used 6 factors with a maximum of 9 scoring points (**Table 3**). Additionally, we assessed the accuracy using C-index and we also calculated the error of the model fitting on survival data using Brier Score in the internal validation. On average, the derivation cohort generated a high C-index (0.796) and a low brier score (0.184). The calibration curve for the probability of 5-year OS showed a good correlation between the actual observed outcome and the prediction by HHLWG-HPI

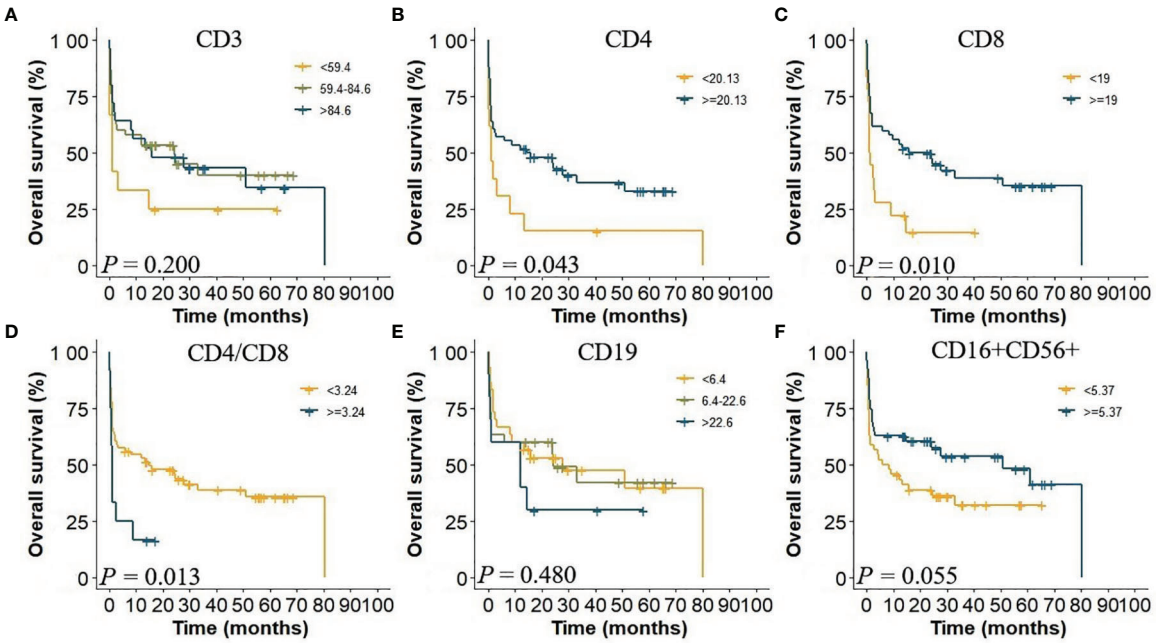

FIGURE 3 | Kaplan–Meier analysis of lymphocyte subsets.

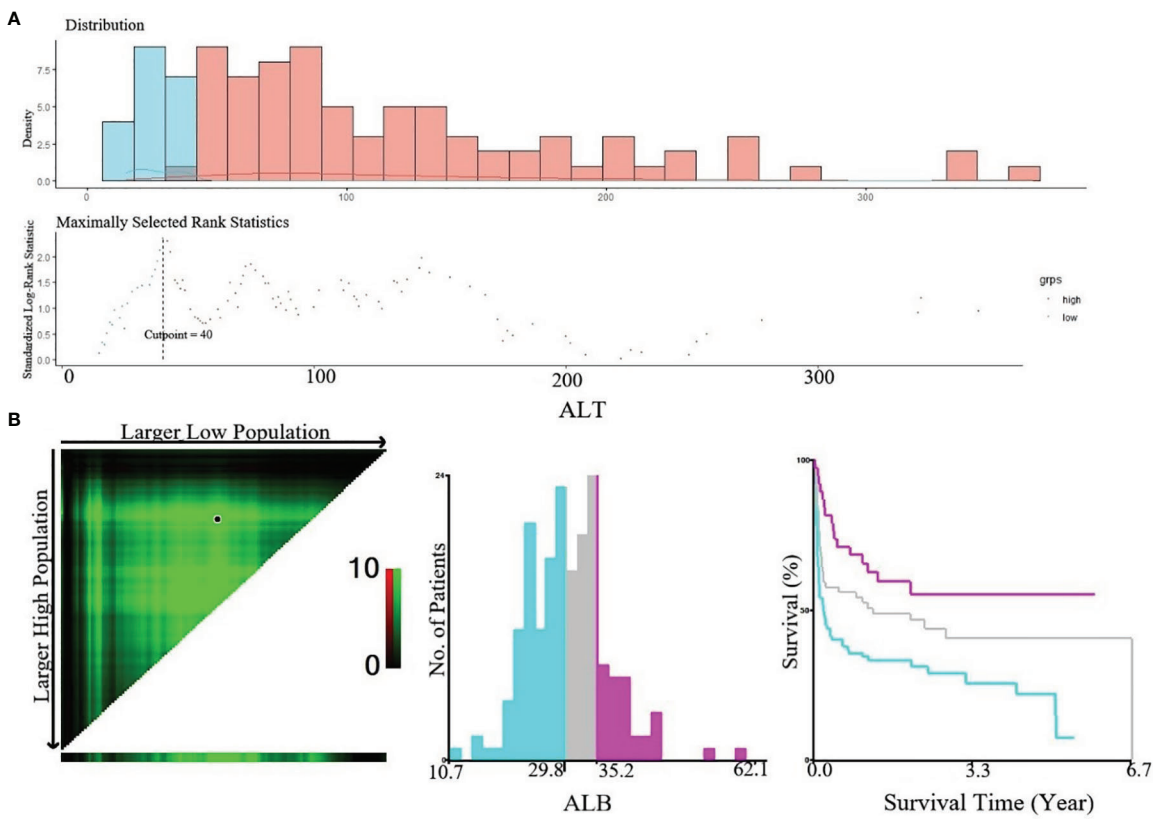

FIGURE 4 | **(A)** Cut-off point of ALT defined by using maximally selected log-rank statistics. The estimated optimal cut-off point of ALT was 40 U/L; **(B)** X-Tile analysis of OS according to Alb. The black circles highlighted the optimal cut-off values which were presented in histograms.

TABLE 2 | Univariate and multivariate analyses in the derivation cohort.

	Univariate analysis		Multivariate analysis		
Variables	***p***	**95% *CI***	***HR***	***p***	**95% *CI***
Age	<0.001	(1.338–2.187)	1.535	0.001	(1.188–1.983)
Cr	<0.001	(1.288–2.051)	1.401	0.006	(1.102–1.783)
ALB	<0.001	(0.472–0.789)	0.654	0.002	(0.499–0.857)
PLT	0.001	(0.518–0.850)	0.779	0.049	(0.606–0.960)
LYR	0.087	(0.966–1.650)	1.325	0.037	(1.017–1.725)
ALT	0.025	(1.065–2.593)	1.716	0.019	(1.092–2.696)
Etiologies	0.061	(0.993–1.371)	1.144	0.132	(0.960–1.364)
FIB	0.010	(0.369–0.871)			
Hb	0.003	(0.501–0.865)			
Gender	0.078	(0.487–1.039)			

Cr, creatinine; ALB, albumin; PLT, platelet; LYR, lymphocyte ratio; Hb, hemoglobin; FIB, fibrinogen; ALT, alanine aminotransferase.

(**Figure 5A**). Using this index, four risk groups were formed: low risk (LR, ≤3 pts), low-intermediate risk (LIR, 4 pts), high-intermediate risk (HIR, 5–6 pts), and high risk (HR, ≥7 pts) (**Figure 6A**). There was clearly a difference in OS between each of these risk groups (global comparison $p < 0.001$; LR vs. LIR $p = 0.012$; LIR vs. HIR $p = 0.024$; HIR vs. HR $p = 0.014$). This model showed precise stratification of outcomes with 5-year OS of 68.5%, 35.2%, 21.3%, and 10.8%, respectively.

External Validation of HHLWG-HPI

We further validated the HHLWG-HPI externally by the calibration curve and by computing the C-index and Brier Score in an independent validation cohort of 86 patients. The C-index was 0.758, and the Brier Score was 0.176 (**Figure 5B**). Noticeably, 25.58% of patients were classified as high risk. KM analysis also showed that there were significant differences in OS between the four groups, confirming the reproducibility of the HHLWG-HPI (**Figure 6B**).

TABLE 3 | The HHLWG-HPI.

HHLWG-HPI	**Score**
Age (year)	
<50	0
50–65	1
>65	2
ALB (g/L)	
>35.2	0
29.8–35.2	1
<29.8	2
Cr (μmol/L)	
<53	0
53–66	1
>66	2
PLT (×10^9/L)	
≥72	0
<72	1
ALT (U/L)	
<40	0
≥40	1
LYR (%)	
<45.8	0
≥45.8	1

Alb, albumin; Cr, creatinine; PLT, platelet; ALT, alanine aminotransferase; LYR, lymphocyte ratio.

Validation in Retrospective Regimens With HHLWG-HPI

In this retrospective study, multiple regimens were adopted for adult HLH, and patients in the DEP regimen group had the best 5-year OS (62.5%). However, it was confusing that patients in the HLH-94 regimen group had poor survival (5-year OS 22.9%), even worse than that in steroid regimen group (5-y OS 30%), which was probably a consequence of improper individual treatment strategies. Thus, we used the HHLWG-HPI model to verify the whole cohort. Chi-square analysis results suggested that the proportion of HIR/HR patients in the HLH-94 regimen was significantly higher than that in the CHOP/CHOP-like regimen ($\chi^2 = 6.608$, $p = 0.010$). Similarly, the proportion of HIR/HR patients in the supportive treatment group was higher than that in the HLH-2004 regimen ($\chi^2 = 5.955$, $p = 0.015$) and CHOP/CHOP-like regimen ($\chi^2 = 17.161$, $p < 0.001$). Due to the lack of accurate risk stratification, the individual therapeutic regimen could not be reasonably selected, resulting in the confusing survival data in different groups.

DISCUSSION

Hemophagocytic lymphohistiocytosis is a rare, life-threatening disorder with excessive immune activation. The therapeutic regimens available for the treatment of adult HLH vary widely in intensity (24, 25). Due to the lack of an accurate prognostic stratification system, there are no individualized therapeutic criteria for adult HLH (26, 27). Therefore, based on feasible clinical variables, we first established the HHLWG-HPI model, providing a novel stratification system for adult HLH.

Several studies have shown that albumin, age, and alanine aminotransferase can be independent prognostic factors for HLH (13, 28). Based on the results of this cohort study, KM analysis showed that etiologies were not independent factors for the prognosis of adult HLH. However, further analysis between subgroups found that the survival rate of patients in the infection-associated group was significantly higher than that in the tumor-associated group. Of 270 cases, EBV-DNA data were available in 163 evaluable patients, and KM analysis showed that a high EBV-DNA

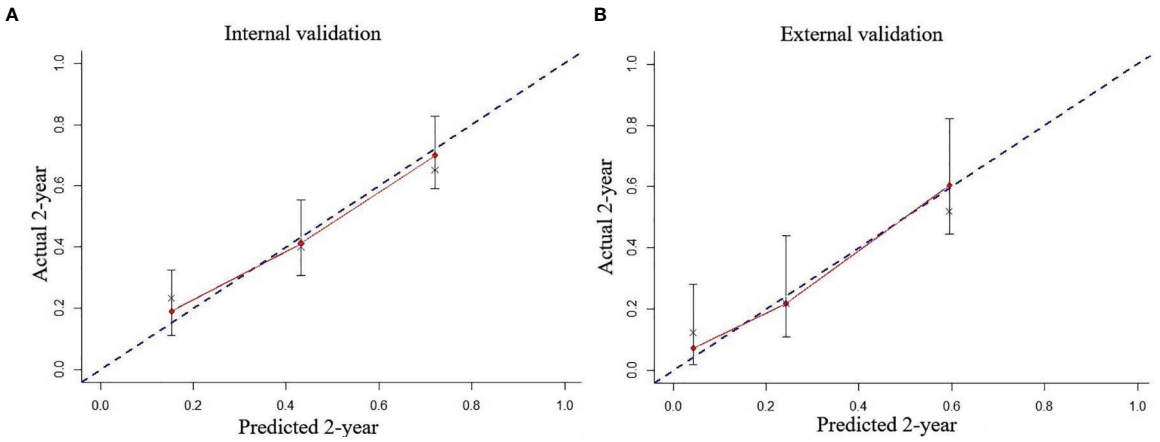

FIGURE 5 | The predicted probability of 2-year OS by HHLWG-HPI was plotted on the x-axis, and the actual 2-year OS was plotted on the y-axis in internal **(A)** and external **(B)** validation.

level was associated with poor outcome. We also attempted to explore the effect of ferritin on the prognosis of adult HLH, but approximately 36% data were missing, and there was no correlation between ferritin level and the prognosis of adult HLH. Although therapeutic regimens were not independent factors for the prognosis, the 5-year survival rate of the patients in the DEP regimen was higher than that in the HLH-94 regimen, HLH-04 regimen, and steroid regimen in this study. In addition, we proved that the levels of immune globulin were not associated with survival. However, patients with a low ratio of CD4/CD8 were with better prognosis.

Multivariate analysis showed that age, albumin, creatinine, alanine transaminase, lymphocyte ratio, and platelet were independent prognostic factors for adult HLH, and these variables were grouped by respective optimal cutoff points. X-Tile program results suggested that platelet >72 × 10^9/l could predict a better outcome and older age at onset, and ALT ≥ 40 U/l and Cr>66 μmol/l were positively associated with poor survival, which were consistent with previous reports (26, 29). After the model iterations of multivariate analysis, we developed the HHLWG-HPI model with a maximum of score of 9 and 4 risk groups. The 5-year OS of the high-risk group in the derivation cohort was higher than that in the validation cohort (10.8% vs. 4.5%), and we found that the median age of patients in the validation population was higher, which may offer an explanation of a lower OS in the validation cohort. In addition, the derivation cohort generated a high C-index (0.703) and a low Brier Score (0.189), and the C-index and Brier Score were 0.721 and 0.169, respectively. It is worth noting that both cohorts are unselected and from real-world settings.

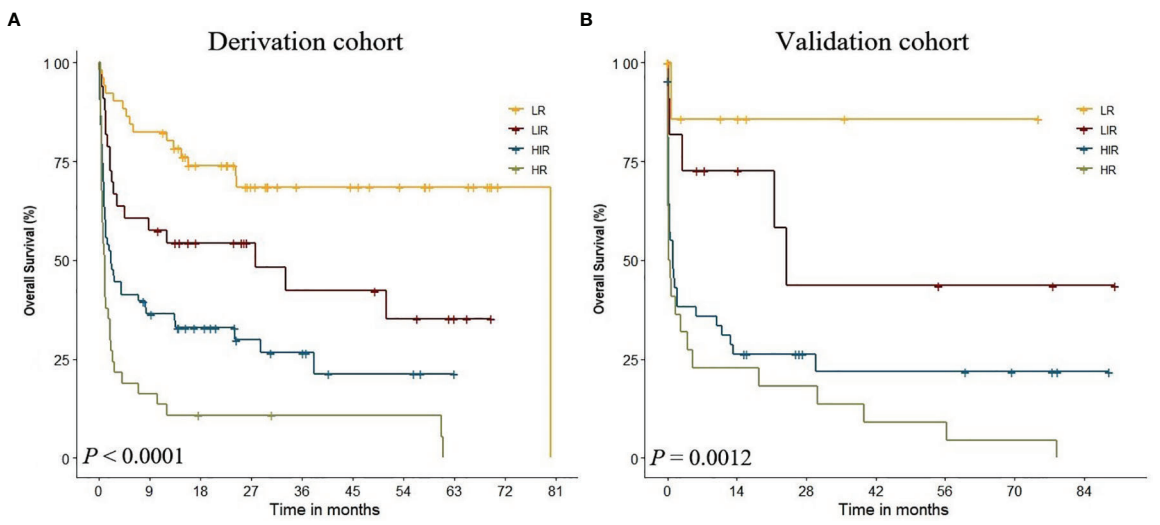

FIGURE 6 | KM analysis of four risk groups in derivation **(A)** and validation **(B)** cohort by HHLWG-HPI.

TABLE 4 | Distribution of patients in different therapeutic regimens groups.

Therapeutic regimens	Distinct risk groups				Total (%)
	LR (%)	LIR (%)	HIR (%)	HR (%)	
DEP regimen	1 (16.67)	5 (83.33)			6 (2.22)
CHOP/CHOP-like	9 (40.91)	7 (31.82)	2 (9.09)	4 (18.18)	22 (8.15)
Steroid	12 (24.00)	6 (12.00)	24 (48.00)	8 (16.00)	50 (18.52)
Antiviral	10 (16.67)	10 (16.67)	29 (48.33)	11 (18.33)	60 (22.22)
HLH-2004	8 (30.77)	5 (19.23)	10 (38.46)	3 (11.54)	26 (9.63)
HLH-94	9 (23.08)	6 (15.38)	17 (43.59)	7 (17.95)	39 (14.45)
Supportive treatment	11 (16.42)	5 (7.46)	25 (37.31)	26 (38.81)	67 (24.81)

The HLH-94 regimen and the HLH-2004 regimen are still the current first-line treatments for HLH. Wang et al. showed that the DEP regimen was an optimal salvage therapy for adult HLH with an overall response of 76.2% (10), which is worth noting. In this real-world retrospective study, the DEP regimen showed the best clinical response, but HLH-94, HLH-2004 regimen, and supportive treatment groups showed poor clinical response. The differences in clinical response among treatment groups may be due to different risks of patients, so the HHLWG-IPI model was used to validate the whole cohort, and the results suggested that the proportion of HIR/HR patients in the HLH-94 regimen was significantly higher than that in the CHOP/CHOP-like regimen (**Table 4**). There were also a high proportion of HIR/HR patients in steroid regimen and antiviral regimen groups, but the 5-year OS of patients was even higher than that in the HLH-94 regimen group, which was worth further discussion in the following studies. In this study, all patients in the DEP regimen were classified into low-risk and low-intermediate-risk groups, indicating that the DEP regimen could also be used for the treatment of patients at low-risk and low-intermediate-risk groups. However, due to the limited sample size, further studies are needed.

In conclusion, based on multicenter data of HHLWG, we developed the HHLWG-HPI model, which will potentially provide criteria for accurate stratification and individual treatment strategy in adult HLH. However, in this retrospective study, we did not collect the data of genetic measurements, sCD25, and pro-inflammatory markers, which may reduce model sensitivity and specificity. Further prospective multicenter studies are urgently needed to validate the model.

DATA AVAILABILITY STATEMENT

The raw data supporting the conclusions of this article will be made available by the authors, without undue reservation.

ETHICS STATEMENT

Study approval was obtained from the independent Ethics Committees of each participating center in HHLWG. The patients/participants provided their written informed consent to participate in this study.

AUTHOR CONTRIBUTIONS

WS, SH, and KX: designed this study. ZS and CH: analysis and interpretation. ZS, YJ, QS, SZ, XC, LH, YW, QL, HZ, XL, LW, JJ, YM, WG, FW, CW, YS, JY, TZ, CS, XS, LX, DY, HS, JC, DL, ZL, and ZW: acquisition of data. JC, DL, ZL, and ZW provided the advices of this study. All authors contributed to the article and approved the submitted version.

FUNDING

This study was funded by the Natural Science Foundation of Jiangsu Province, Grant/Award Number: BK20171181; Jiangsu Key Research and Development Project of Social Development, Grant/Award Number: BE2019638; and Young Medical Talents of Jiangsu Science and Education Health Project, Grant/Award Number: QNRC2016791.

ACKNOWLEDGMENTS

Thanks are given to the Huaihai Lymphoma Working Group (HHLWG) for its participation in this study.

REFERENCES

1. Pachlopnik Schmid J, Cote M, Menager MM, Burgess A, Nehme N, Menasche G, et al. Inherited Defects in Lymphocyte Cytotoxic Activity. *Immunol Rev* (2010) 235:10–23. doi: 10.1111/j.0105-2896.2010.00890.x
2. Jing-Shi W, Yi-Ni W, Lin W, Zhao W. Splenectomy as a Treatment for Adults With Relapsed Hemophagocytic Lymphohistiocytosis of Unknown Cause. *Ann Hematol* (2015) 94:753–60. doi: 10.1007/s00277-014-2276-9
3. Maakaroun NR, Moanna A, Jacob JT, Albrecht H. Viral Infections Associated With Haemophagocytic Syndrome. *Rev Med Virol* (2010) 20:93–105. doi: 10.1002/rmv.638
4. Lai W, Wang Y, Wang J, Wu L, Jin Z, Wang Z. Epstein-Barr Virus-Associated Hemophagocytic Lymphohistiocytosis in Adults and Adolescents-A Life-Threatening Disease: Analysis of 133 Cases From a Single Center. *Hematology* (2018) 23:810–6. doi: 10.1080/10245332.2018.1491093
5. Riviere S, Galicier L, Coppo P, Marzac C, Aumont C, Lambotte O, et al. Reactive Hemophagocytic Syndrome in Adults: A Retrospective Analysis of 162 Patients. *Am J Med* (2014) 127:1118–25. doi: 10.1016/j.amjmed.2014.04.034
6. Parikh SA, Kapoor P, Letendre L, Kumar S, Wolanskyj AP. Prognostic Factors and Outcomes of Adults With Hemophagocytic Lymphohistiocytosis. *Mayo Clin Proc* (2014) 89:484–92. doi: 10.1016/j.mayocp.2013.12.012
7. Fardet L, Galicier L, Lambotte O, Marzac C, Aumont C, Chahwan D, et al. Development and Validation of the HScore, A Score for the Diagnosis of Reactive Hemophagocytic Syndrome. *Arthritis Rheumatol* (2014) 66:2613–20. doi: 10.1002/art.38690

8. Henter JI, Horne A, Arico M, Egeler RM, Filipovich AH, Imashuku S, et al. HLH-2004: Diagnostic and Therapeutic Guidelines for Hemophagocytic Lymphohistiocytosis. *Pediatr Blood Cancer* (2007) 48:124–31. doi: 10.1002/pbc.21039
9. Henter J. HLH-94: A Treatment Protocol for Hemophagocytic Lymphohistiocytosis. *Med Pediatr Oncol* (1997) 28:342–7. doi: 10.1002/(SICI)1096-911X(199705)28:5<342::AID-MPO3>3.0.CO;2-H
10. Wang Y, Huang W, Hu L, Cen X, Li L, Wang J, et al. Multicenter Study of Combination DEP Regimen as a Salvage Therapy for Adult Refractory Hemophagocytic Lymphohistiocytosis. *Blood* (2015) 126:2186–92. doi: 10.1182/blood-2015-05-644914
11. An Q, Fang DH, Xuan CM, Xu SM, Jin MW, Ji Q. Lymphocyte Subsets in Children With Hemophagocytic Lymphohistiocytosis (HLH) and Its Clinical Significance. *Eur Rev Med Pharmacol Sci* (2018) 22:2000–4. doi: 10.26355/eurrev_201804_14728
12. Pan H, Huo Y, Sun L. Comparison Between Clinical Features and Prognosis of Malignancy- and Non-Malignancy-Associated Pediatric Hemophagocytic Lymphohistiocytosis. *BMC Pediatr* (2019) 19:468. doi: 10.1186/s12887-019-1702-5
13. Zhou J, Zhou J, Wu ZQ, Goyal H, Xu HG. A Novel Prognostic Model for Adult Patients With Hemophagocytic Lymphohistiocytosis. *Orphanet J Rare Dis* (2020) 15:215. doi: 10.1186/s13023-020-01496-4
14. Zhou J, Zhou J, Shen DT, Goyal H, Wu ZQ, Xu HG. Development and Validation of the Prognostic Value of Ferritin in Adult Patients With Hemophagocytic Lymphohistiocytosis. *Orphanet J Rare Dis* (2020) 15:71. doi: 10.1186/s13023-020-1336-6
15. Lin TF, Ferlic-Stark LL, Allen CE, Kozinetz CA, McClain KL. Rate of Decline of Ferritin in Patients With Hemophagocytic Lymphohistiocytosis as a Prognostic Variable for Mortality. *Pediatr Blood Cancer* (2011) 56:154–5. doi: 10.1002/pbc.22774
16. Schram AM, Campigotto F, Mullally A, Fogerty A, Massarotti E, Neuberg D, et al. Marked Hyperferritinemia Does Not Predict for HLH in the Adult Population. *Blood* (2015) 125:1548–52. doi: 10.1182/blood-2014-10-602607
17. Hayden A, Park S, Giustini D, Lee AY, Chen LY. Hemophagocytic Syndromes (HPSs) Including Hemophagocytic Lymphohistiocytosis (HLH) in Adults: A Systematic Scoping Review. *Blood Rev* (2016) 30:411–20. doi: 10.1016/j.blre.2016.05.001
18. Miao Y, Zhu HY, Qiao C, Xia Y, Kong Y, Zou YX, et al. Pathogenic Gene Mutations or Variants Identified by Targeted Gene Sequencing in Adults With Hemophagocytic Lymphohistiocytosis. *Front Immunol* (2019) 10:395. doi: 10.3389/fimmu.2019.00395
19. Camp RL, Dolled-Filhart M, Rimm DL. X-Tile: A New Bio-Informatics Tool for Biomarker Assessment and Outcome-Based Cut-Point Optimization. *Clin Cancer Res* (2004) 10:7252–9. doi: 10.1158/1078-0432.CCR-04-0713
20. Kano K, Yamada T, Yamamoto K, Komori K, Watanabe H, Hara K, et al. Association Between Lymph Node Ratio and Survival in Patients With Pathological Stage II/III Gastric Cancer. *Ann Surg Oncol* (2020) 27:4235–47. doi: 10.1245/s10434-020-08616-1
21. Harrell FE Jr, Lee KL, Mark DB. Multivariable Prognostic Models: Issues in Developing Models, Evaluating Assumptions and Adequacy, and Measuring and Reducing Errors. *Stat Med* (1996) 15:361–87. doi: 10.1002/(SICI)1097-0258(19960229)15:4<361::AID-SIM168>3.0.CO;2-4
22. Chaudhary K, Poirion OB, Lu L, Garmire LX. Deep Learning-Based Multi-Omics Integration Robustly Predicts Survival in Liver Cancer. *Clin Cancer Res* (2018) 24:1248–59. doi: 10.1158/1078-0432.CCR-17-0853
23. Zhang X, Li Y, Akinyemiju T, Ojesina AI, Buckhaults P, Liu N, et al. Pathway-Structured Predictive Model for Cancer Survival Prediction: A Two-Stage Approach. *Genetics* (2017) 205:89–100. doi: 10.1534/genetics.116.189191
24. Ambruso DR, Hays T, Zwartjes WJ, Tubergen DG, Favara BE. Successful Treatment of Lymphohistiocytic Reticulosis With Phagocytosis With Epipodophyllotoxin VP 16-213. *Cancer* (1980) 45:2516–20. doi: 10.1002/1097-0142(19800515)45:10<2516::aid-cncr2820451008>3.0.co;2-v
25. Henter JI, Elinder G, Finkel Y, Soder O. Successful Induction With Chemotherapy Including Teniposide in Familial Erythrophagocytic Lymphohistiocytosis. *Lancet* (1986) 2:1402. doi: 10.1016/s0140-6736(86)92047-7
26. Arca M, Fardet L, Galicier L, Riviere S, Marzac C, Aumont C, et al. Prognostic Factors of Early Death in a Cohort of 162 Adult Haemophagocytic Syndrome: Impact of Triggering Disease and Early Treatment With Etoposide. *Br J Haematol* (2015) 168:63–8. doi: 10.1111/bjh.13102
27. Zhou M, Li L, Zhang Q, Ma S, Sun J, Zhu L, et al. Clinical Features and Outcomes in Secondary Adult Hemophagocytic Lymphohistiocytosis. *QJM* (2018) 111:23–31. doi: 10.1093/qjmed/hcx183
28. Huang J, Yin G, Duan L, Tian T, Xu J, Wang J, et al. Prognostic Value of Blood-Based Inflammatory Biomarkers in Secondary Hemophagocytic Lymphohistiocytosis. *J Clin Immunol* (2020) 40:718–28. doi: 10.1007/s10875-020-00801-x
29. Guo Y, Bai Y, Gu L. Clinical Features and Prognostic Factors of Adult Secondary Hemophagocytic Syndrome: Analysis of 47 Cases. *Med (Baltimore)* (2017) 96:e6935. doi: 10.1097/MD.0000000000006935

Conflict of Interest: The authors declare that the research was conducted in the absence of any commercial or financial relationships that could be construed as a potential conflict of interest.

Publisher's Note: All claims expressed in this article are solely those of the authors and do not necessarily represent those of their affiliated organizations, or those of the publisher, the editors and the reviewers. Any product that may be evaluated in this article, or claim that may be made by its manufacturer, is not guaranteed or endorsed by the publisher.

frontiers in Immunology

ORIGINAL RESEARCH
published: 17 March 2022
doi: 10.3389/fimmu.2022.829366

CD56-Negative Extranodal Natural Killer/T-Cell Lymphoma: A Retrospective Study in 443 Patients Treated by Chemotherapy With or Without Asparaginase

Jing Yang[1†], Pengfei Li[2,3,4†], Yingshi Piao[5,6], Xindi Liu[1], Liqiang Wei[1], Wei Sang[7], Luo Zhang[8,9*] and Liang Wang[1,10*]*

[1] Department of Hematology, Beijing TongRen Hospital, Capital Medical University, Beijing, China, [2] Department of Medical Oncology, Sun Yat-sen University Cancer Center, Guangzhou, China, [3] Department of Hematology and Oncology, Southern Medical University Cancer Center, Guangzhou, China, [4] Hospital of Integrated Traditional Chinese and Western Medicine, Southern Medical University, Guangzhou, China, [5] Department of Pathology, Beijing TongRen Hospital, Capital Medical University, Beijing, China, [6] Beijing Key Laboratory of Head and Neck Molecular Diagnostic Pathology, Beijing TongRen Hospital, Capital Medical University, Beijing, China, [7] Department of Hematology, Affiliated Hospital of Xuzhou Medical University, Xuzhou, China, [8] Department of Otolaryngology Head and Neck Surgery, Beijing TongRen Hospital, Capital Medical University, Beijing, China, [9] Beijing Key Laboratory of Nasal Disease, Beijing Institute of Otolaryngology, Beijing, China, [10] Beijing Advanced Innovation Center for Big Data-Based Precision Medicine, Beihang University & Capital Medical University, Beijing TongRen Hospital, Beijing, China

Objective: Extranodal natural killer/T cell lymphoma (NKTCL) is an aggressive EBV-related lymphoma, originating from NK cells or T cells. Previous study demonstrated that CD56 negative NKTCL should be recognized as a distinct subtype. In this study, the value of CD56 in NKTCL is validated in the era of asparaginase, and genomic analysis was done to dissect the differences between CD56-negative and positive NKTCL.

Methods: 443 patients with newly diagnosed NKTCL were enrolled in this retrospective study, and correlation between CD56 positivity and survival outcomes was analyzed. The gene sequencing data was downloaded (http://www.biosino.org/node/project/detail/OEP000498), and bioinformatics analysis was done to delineate the tumor microenvironment and differentially expressed genes.

Results: CD56 was expressed in 337 patients (76.1%). Within a median follow-up time of 51 months, the 5-year overall survival (OS) and progression free survival (PFS) rates were 63.8% and 51.9%, respectively. For the whole cohort, patients who were CD56-positive had superior OS (5-year OS, 86.2% vs. 51.9%, p=0.019) and PFS (5-year PFS, 55.9% vs. 40.1%, p=0.016). For patients in early stage disease, CD56 positivity was associated with superior OS and PFS (p=0.008 and 0.005, respectively). In patients who received non-asparaginase-based chemotherapy, CD56-negative was associated with shorter OS and PFS (p<0.001), and in patients who received asparaginase-based chemotherapy, CD56-negative was not related to inferior OS and PFS (p=0.093 and p=0.829, respectively). The genomic analysis demonstrated that CD56 positive NKTCL probably originated from NK cells and CD56 negative NKTCL originated from T cells. CD56 positive NKTCL had

OPEN ACCESS

Edited by:
Catherine Sautes-Fridman,
INSERM U1138 Centre de Recherche des Cordeliers (CRC), France

Reviewed by:
Meng Lv,
Peking University People's Hospital, China
Peng Liu,
Fudan University, China
Choon Kiat Ong,
National Cancer Centre Singapore, Singapore
Yong Yang,
Fujian Medical University Union Hospital, China

***Correspondence:**
Liang Wang
wangliangtrhos@126.com
Luo Zhang
dr.luozhang@139.com
Wei Sang
xyfylbl515@xzhmu.edu.cn

[†]These authors have contributed equally to this work

Specialty section:
This article was submitted to Cancer Immunity and Immunotherapy, a section of the journal Frontiers in Immunology

Received: 05 December 2021
Accepted: 24 February 2022
Published: 17 March 2022

Citation:
Yang J, Li P, Piao Y, Liu X, Wei L, Sang W, Zhang L and Wang L (2022) CD56-Negative Extranodal Natural Killer/T-Cell Lymphoma: A Retrospective Study in 443 Patients Treated by Chemotherapy With or Without Asparaginase. Front. Immunol. 13:829366. doi: 10.3389/fimmu.2022.829366

significantly higher proportion of resting NK cells, activated NK cells, and activated CD8+ and CD4+ T cells in the tumor microenvironment.

Conclusions: CD56 negative NKTCL differs from CD56 positive NKTCL in both the tumor microenvironment and survival outcomes, and asparaginase-based treatment may overcome the poor prognosis brought by CD56 negativity.

Keywords: extranodal natural killer/T cell lymphoma, tumor microenvironment, prognosis, asparaginase, bioinformatics analysis

INTRODUCTION

Extranodal natural killer/T cell lymphoma (NKTCL), nasal type, is a distinct entity of non-Hodgkin's lymphoma (NHL) with unique epidemiologic, clinical, histologic and etiologic features. NKTCL is rare in the Western countries, but is more prevalent in East Asia and Latin America (1). Although the standard therapy for NKTCL is not well established, radiotherapy plays a key role in the treatment of early-stage disease (2), and increasing studies have demonstrated the value of systemic chemotherapy in localized disease as reducing the distant relapses (3, 4). Due to the high expression of multi-drug resistance (MDR) gene in NKTCL cells (5), anthracycline-based chemotherapy regimens are no longer recommended in the treatment of NKTCL. Recently, increasing asparaginase-based regimens have proven highly efficacious in the treatment of NKTCL (4, 6–10).

NKTCL is featured by frequent necrosis and angioinvasion. The tumor cells usually express cytoplasmic CD3 and CD56, and have a cytotoxic immunophenotype, expressing perforin, granzyme B (gzm B), and T cell-restricted intracellular antigen (TIA-1) (11). Most cases derive from NK cells that express CD3ϵ and CD56, and lack T-cell receptor (TCR) gene rearrangement, while a very small proportion of cases originate from T cells, with expression of cCD3ϵ and/or sCD3, cytotoxic molecules, and Epstein-Barr virus (EBV) but are negative for CD56 (12–15). Previous studies reported that CD56-negative NKTCL should be regarded as a distinct lymphoma subtype (16, 17). In a large cohort of patients with early-stage NKTCL, CD56-negative NKTCL showed a significantly poorer survival outcome than CD56-positive NKTCL, regardless of the treatment strategies (16). To explore a more effective therapeutic strategy for CD56-negative NKTCL, it is important to examine the response and failure rate of chemotherapy with asparaginase-based regimens in a large number of CD56-negative NKTCL cases.

Hence, we conducted a retrospective study in a large cohort of 443 patients, to identify if patients of CD56-negative NKTCL had a worse outcome than patients of CD56-positive NKTCL, especially who received chemotherapy with or without asparaginase-based regimens. Furthermore, a genomic analysis was done to dissect the differences between CD56-negative and positive NKTCL.

MATERIALS AND METHODS

Patients

Between January 2000 and December 2020, 443 patients with newly diagnosed NKTCL, for whom both detailed pathologic and clinical information were available, were treated in Beijing Tongren Hospital and Sun Yat-sen University Cancer Center, and included in this retrospective analysis. The criteria for case inclusion were as follows: pathologically confirmed diagnosis of NKTCL according to the criteria of the World Health Organization (WHO) classification (15); no previous malignancy; no previous treatment for NKTCL; received at least two cycles of chemotherapy or radiotherapy; adequate pathologic and clinical information. Patients who were negative for EBV-encoded RNA (EBER) were excluded from our study. This study was approved by the Ethic Committee of Beijing Tongren Hospital and Sun Yat-sen University Cancer Center. The need for informed consent was waived because all patients had been de-identified in our datasets.

Pathological Evaluation

Patient pathological records and original histopathologic slides were reviewed by one lymphoma pathologist (YSP) to confirm the diagnosis again. A standard panel of immunohistochemistry staining, including CD20, cCD3ϵ, CD16, CD56, Ki-67, TIA-1, perforin, granzyme B, and *in situ* hybridization for EBER, was performed. As previously reported (18), CD56-positive NKTCL is defined as expression of NK/T cell antigens, including either CD56+, cCD3ϵ+, and positive for cytotoxic molecules, while CD56-negative NKTCL is defined as cCD3ϵ+ and CD56-, but positive for both cytotoxic molecules and EBER. Staining for CD56 was considered positive when 10% or more of the abnormal lymphoid cells showed positive immunoreactivity.

Clinical Information

All available clinical information including survival outcomes was collected for analysis. Patients were staged based on the Ann-Arbor staging system (Both MRI and CT scan were more commonly used to stage patients diagnosed before 2010, and PET-CT dominated after 2010, with a total of 320 patients having PET-CT staging).

All patients enrolled in the study received treatment. One of the following initial treatment strategies was delivered: (1) chemotherapy followed by involved field radiotherapy (IFRT); (2) sandwich protocols (IFRT after an initial 2 to 4 cycles of chemotherapy, followed by 2 to 4 cycles of chemotherapy as consolidation); (3) chemotherapy alone; (4) IFRT alone.

The initial chemotherapy regimens included the following: (1) Anthracycline-based regimens (or non-Asparaginase-based regimens) were CHOP (cyclophosphamide, doxorubicin, vincristine, and prednisone) or CHOP-like regimens, and

EPOCH (etoposide, doxorubicin, vincristine, cyclophosphamide, and prednisone); (2) Asparaginase-based regimens were CHOP-L (CHOP plus L-asparaginase), EPOCHL (EPOCH plus L-asparaginase), GELOX/P-GEMOX (gemcitabine, oxaliplatin, and L-asparaginase or Pegaspargase), and SVILE (dexamethasone, vindesine, ifosfamide, L-asparaginase, etoposide). After at least 2 cycles of chemotherapy, patients with early stage disease received IFRT at a total dose of 50Gy to 68 Gy. CT scan, MRI scan, or PET/CT scan was performed to evaluate the treatment responses every two courses of chemotherapy (19, 20). After completion of treatment, patients were followed up every three months for the first two years, every six months for the next three years, and yearly thereafter or whenever clinically indicated. Patients who received auto-HSCT or other clinical trials were not censored in our study.

NKTCL Dataset and Preprocessing

The sequencing data (WGS, WES, and RNA-seq) of NKTCL used in this study can be viewed and downloaded in NODE (http://www.biosino.org/node) using the accession No. OEP000498 (21). The detailed mutation calls, CNV, and RNA-seq expression data can be downloaded from the Mendeley Dataset, accessible through https://data.mendeley.com/datasets/7gwtb7mgrr/draft?a=85eac518-0f19-41f8-aa58-69ed36b66e41. All NKTCL samples were sorted by CD56 expression level from low to high, and they were divided into the high expression group and the low expression group (in our study, CD56 was positive in 76.1% patients of NKTCL, thus, we arbitrarily assigned the top 75% samples as high expression group and the bottom 25% samples as low expression group).

To quantify the proportions of immune cells in the NKTCL samples, we used the CIBERSORT method with the LM22 gene signature from CIBERSORT website, which allows for sensitive and specific discrimination of 22 human immune cell phenotypes, including B cells, T cells, natural killer cells, macrophages, DCs, and myeloid subsets. CIBERSORT is a deconvolution algorithm and it uses a set of reference gene-expression values (a signature with 547 genes) considered a minimal representation for each cell type and, based on these values, infers cell type proportions in data from many kinds of tumor samples or other samples with mixed cell types using support vector regression. The gene expression profile was prepared according to the standard annotation file samples provided by CIBERSORT web portal, and the data were analysed by CIBERSORT.R, which is downloaded from the CIBERSORT web portal (http://cibersort.stanford.edu/), with the algorithm run using the LM22 signature file and 1000 permutations. Proportions of stromal cells were estimated by applying the Microenvironment Cell Populations-counter method, which allows for robust quantification of the absolute abundance of eight immune and two stromal cell populations in heterogeneous tissues from transcriptomic data.

To identify different genes associated with the expression of CD56, we grouped all patients into groups based on the expression of CD56. Differentially expressed genes among these groups were determined using the R package limma, which implements an empirical Bayesian approach to estimate gene-expression changes using moderated t tests. The differentially expressed genes among groups were determined by significance criteria (abs(log2FC)>1 and adjusted P value<0.05) as implemented in the R package limma. The heatmap was drawn by pheatmap R package according to the differentially expressed genes. Then we performed unsupervised analyzing and hierarchical clustering of common differentially expressed genes based on expression data.

The signature genes were annotated and enriched by clusterProfiler R package. Then in order to have further insight into the function of genes and their interactions, we used the pathway enrichment analysis of DEGs to those signature genes. ClusterProfiler R package was applied to the analysis of KEGG pathways to present the top 10 pathways.

Statistical Analysis

Treatment responses were evaluated as previously reported (19, 20). Due to the relatively large time span of our study, two different criteria were adopted. For patients who used CT and MRI for response evaluation, the criteria reported by Cheson et al. in 1999 was used (20). For patients who used PET-CT for response evaluation, the criteria reported by Cheson et al. in 2007 was used (19). Overall survival (OS) was calculated from the date of diagnosis to the date of death or the last date of follow-up visit, whichever came first. Progression-free survival (PFS) was measured from the date of diagnosis to the date of confirmed disease progression, relapse, death, or the date of the last follow-up visit, whichever came first. The correlation between CD56 expression and clinicopathologic features of the NKTCL patients was evaluated by the chi-squared test. The Kaplan-Meier product-limit method was used to estimate the probability of OS and PFS, and survival curves were compared for statistical differences by using the log-rank test. Both univariate and multivariate analyses were done using the forward selection method in the stepwise Cox proportional hazard model. Two-sided P values less than 0.05 was considered statistically significant. All statistical analysis was conducted using SPSS software (SPSS Standard Version 20.0, SPSS Inc., Chicago, IL, USA).

RESULTS

Patient Characteristics

A total of 443 patients fulfilled the inclusion criteria, and the clinical characteristics are presented in **Table 1**. The median age was 44 years (range 18–79). Three hundred and forty-nine patients (78.8%) had a good performance status (Eastern Cooperative Oncology Group 0-1). The majority of patients initially presented with early stage disease (n=389, 87.7%) or upper aerodigestive tract (UAT) tumors (n=309, 69.8%). 75.6% of patients were categorized as low risk according to international prognostic index (IPI), and 60.3% were in group 1 or 2 according to Korean prognostic index (KPI).

TABLE 1 | Clinical characteristics and CD56 expression status of 443 patients at diagnosis with NKTCL.

Characteristics	All cases (n=443,100%)	CD56-positive Group (n=337, 76.1%)	CD56-negative Group (n=106, 23.9%)	*P* value
Gender				0.230
Male	299 (67.5%)	233 (69.1%)	66 (62.3%)	
Female	144 (32.5%)	104 (30.9%)	40 (37.7%)	
Age at diagnosis >60 (years)	64 (14.4%)	44 (13.1%)	20 (18.9%)	0.185
ECOG PS score ≥2	94 (21.2%)	61 (18.1%)	33 (31.1%)	0.006*
Subtypes				0.974
Nasal cavity	309 (69.8%)	236 (70.0%)	73 (68.9%)	
Extranasal UAT	93 (21.0%)	70 (20.8%)	23 (21.7%)	
Extra UAT	41 (9.2%)	31 (9.2%)	10 (9.4%)	
B-symptoms	205 (46.3%)	148 (43.9%)	57 (53.8%)	0.096
Primary tumor invasion	268 (60.5%)	198 (58.8%)	70 (66.0%)	0.221
Extranodal sites ≥ 2	87 (19.6%)	67 (19.9%)	20 (18.9%)	0.929
Regional lymphadenopathy	191 (43.1%)	143 (42.4%)	48 (45.3%)	0.686
Elevated serum LDH level	120 (27.1%)	92 (27.3%)	28 (26.4%)	0.957
Ann Arbor Stage				0.886
I, II	389 (87.8%)	295 (87.5%)	94 (88.7%)	
III, IV	54 (12.2%)	42 (12.5%)	12 (11.3%)	
IPI score				0.047*
0, 1	335 (75.6%)	263 (78.0%)	72 (67.9%)	
≥ 2	108 (24.4%)	74 (22.0%)	34 (32.1%)	
KPI score				0.318
0, 1	267 (60.5%)	208 (61.7%)	59 (55.7%)	
≥ 2	176 (39.5%)	129 (38.3%)	47 (44.3%)	

ECOG PS, Eastern Cooperative Oncology Group performance status; Extranasal UAT, Extranasal upper aerodigestive tract; Extra UAT, extraupper aerodigestive tract; LDH, lactate dehydrogenase; IPI, International Prognostic Index; KPI, Korean Prognostic Index.
**Indicates statistically significant.*

Association of CD56 With Pathologic and Clinical Characteristics

Figures 1A, B represented the typical CD56 negative and positive NKTCL cases. As is shown in **Figure 1C**, about half patients with CD56 positive NKTCL had CD56 expression in more than 80% of lymphoma cells. Categorical associations between CD56 expression and main clinical features are summarized in **Table 1**. CD56 was expressed in 337 patients (76.1%). The CD56-negative group showed statistically significant increase in cases with poor ECOG score and IPI score compared with the CD56-positive group (p=0.006 and p=0.047, respectively). No categorical association was observed with other clinical features, such as gender, age, primary tumor invasion, number of extranodal sites, serum LDH level, and Ann-Arbor stage.

Treatment Modalities and Responses

The initial treatment modalities were as follows: (1) for early stage disease, 293 (75.3%) patients received chemotherapy followed by radiotherapy, 80 (20.6%) patients received chemotherapy alone, and 11 patients received radiotherapy alone; Two hundred and nineteen (57.9%) patients received asparaginase-based chemotherapy and the other 159 (42.1%) patients received non-asparaginase-based chemotherapy. (2) For advanced stage disease, 54 (100%) patients received chemotherapy, and eight (14.8%) patients with local residual disease received radiotherapy after induction chemotherapy; Twenty-six (48.1%) patients received asparaginase-based chemotherapy and the other 28 (51.9%) patients received non-asparaginase-based chemotherapy. No significant difference was found in the treatment modalities as well as chemotherapy regimens between patients with different CD56 expression status (p=0.543 and p=0.113, respectively). The treatment responses were evaluated in 422 (95.2%) patients. 304 (72.0%) patients and 68 (16.1%) patients achieved complete response (CR) and partial response (PR), respectively, thus the overall response rate (ORR) was 88.1%. The CR rate was significantly higher in patients who were treated with asparaginase-based therapy (75.8 vs. 64.1%, p = 0.006). ORR of patients with CD56-positive and CD56-negative expression were 89.3% and 82.1%, respectively (p = 0.609).

Prognostic Role of CD56 in Patients With NKTCL

Within a median follow-up time of 51 months (range, 1 to 180 months), 196 patients experienced disease progression or relapse and 145 patients died. The 5-year OS and PFS rates for all 443 patients were 63.8% (95% CI, 58.7–68.9%) and 51.9% (95% CI, 46.6–57.2%), respectively (**Figures 2A, B**). Patients who were CD56-positive had significantly superior OS (5-year OS, 86.2% vs. 51.9%, p = 0.019, **Figure 2C**) and PFS (5-year PFS, 55.9% vs. 40.1%, p =0.016, **Figure 2D**). For patients in the early stage disease, CD56 positivity was associated with superior OS and PFS (p=0.008, **Figure 3A** and p=0.005, **Figure 3B**, respectively). However, for patients in the advanced stage disease, CD56 positivity was not related to OS and PFS (p=0.857 and p=0.856, respectively. **Supplementary Figures 1A, B**). In patients who received non-asparaginase-based chemotherapy, CD56-negative was associated with inferior OS and PFS (both p<0.001), while in patients who received asparaginase-based chemotherapy, CD56-negative was not related to OS and PFS (p=0.093 and p=0.829, respectively). Asparaginase-based

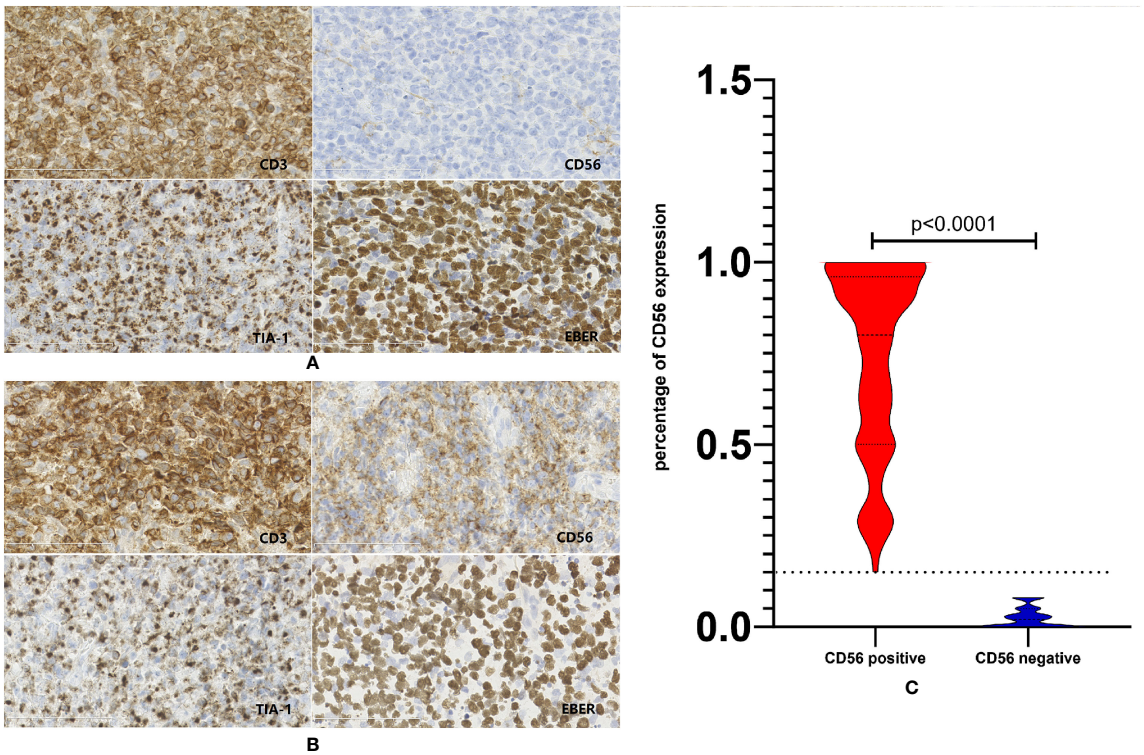

FIGURE 1 | Expression status of CD56 in patients with NKTCL. **(A)** Representative case of NKTCL defined as CD56 negative. **(B)** Representative case of NKTCL defined as CD56 positive. **(C)** Violin plot of CD56 expression status in the whole cohort of NKTCL.

chemotherapy significantly improved the prognosis compared with non-asparaginase-based regimens in the whole cohort (5-year OS, 75.0% vs. 55.0%, p<0.001, **Figure 4A**; 5-year PFS, 63.2% vs. 42.5%, p<0.001, **Figure 4B**), and in patients with early stage disease (5-year OS, 80.6% vs. 59.5%, p<0.001; 5-year PFS, 68.2% vs. 45.8%, p<0.001). Subgroup analysis showed that CD56-negative was associated with inferior OS and PFS (p=0.029, **Figure 4C** and p=0.017, **Figure 4D**, respectively) in patients with early stage disease who received non-asparaginase-based chemotherapy, but not related to OS and PFS (p=0.626, **Figure 4E** and p=0.731, **Figure 4F**, respectively) in early stage patients treated with asparaginase-based regimens. Compared with non-asparaginase-based chemotherapy, asparaginase-based chemotherapy obviously improved OS and PFS (5-year OS, 80.6% vs. 46.4%, p<0.001 and 5-year PFS, 66.8% vs. 31.4%, p<0.001) for patients with CD56-negative early stage disease (**Table 2**).

As is shown in **Table 2**, univariate analysis revealed that age, ECOG PS, Subtype, B symptoms, primary tumor invasion, number of extranodal sites, regional lymphadenopathy invasion, LDH level, Ann-Arbor stage, expression status of CD56, IPI score and KPI score correlated significantly with both OS and PFS. Clinical factors that were statistically significant predictors of OS and PFS were included in the multivariate analysis (see **Table 3**), which showed that age, ECOG PS, primary tumor invasion and Ann-Arbor stage were independent prognostic factors for both OS and PFS. KPI score was also an independent prognostic factor for PFS, but failed to be prognostic for OS. The expression status of CD56 had a trend towards independent prognostic factors for OS and PFS (p=0.188 and 0.146, respectively). Next, we performed both univariate and multivariate analysis in patients with early stage disease. As is shown in **Table 4**, age, ECOG PS, primary tumor invasion, regional lymphadenopathy, and CD56 expression status were found to be independent prognostic factors for PFS.

Bioinformatic Analysis Favored CD56 Negative NKTCL to Be a Distinct Entity

Using CIBERSORT algorithm and the LM22 gene signature, we can evaluate the proportion of various immune cells in the tumor microenvironment of NKTCL. As is shown in **Figure 5**, both resting and activated NK cells, $CD8^+$ T cells and activated $CD4^+$ memory T cells were significantly elevated in high CD56 expression group. As the heatmap shows in **Figure 6A**, numerous genes were differentially expressed between CD56 high and low expression group. According to the KEGG analysis shown in **Figure 6B**, those differentially expressed genes mainly involve in Cytokine-cytokine receptor interaction (map04060), Chemokine signaling pathway(map04062), Viral protein interaction with cytokine and cytokine receptor (map04061), Natural killer cell mediated cytotoxicity (map04650), and Wnt signaling pathway(map04310).

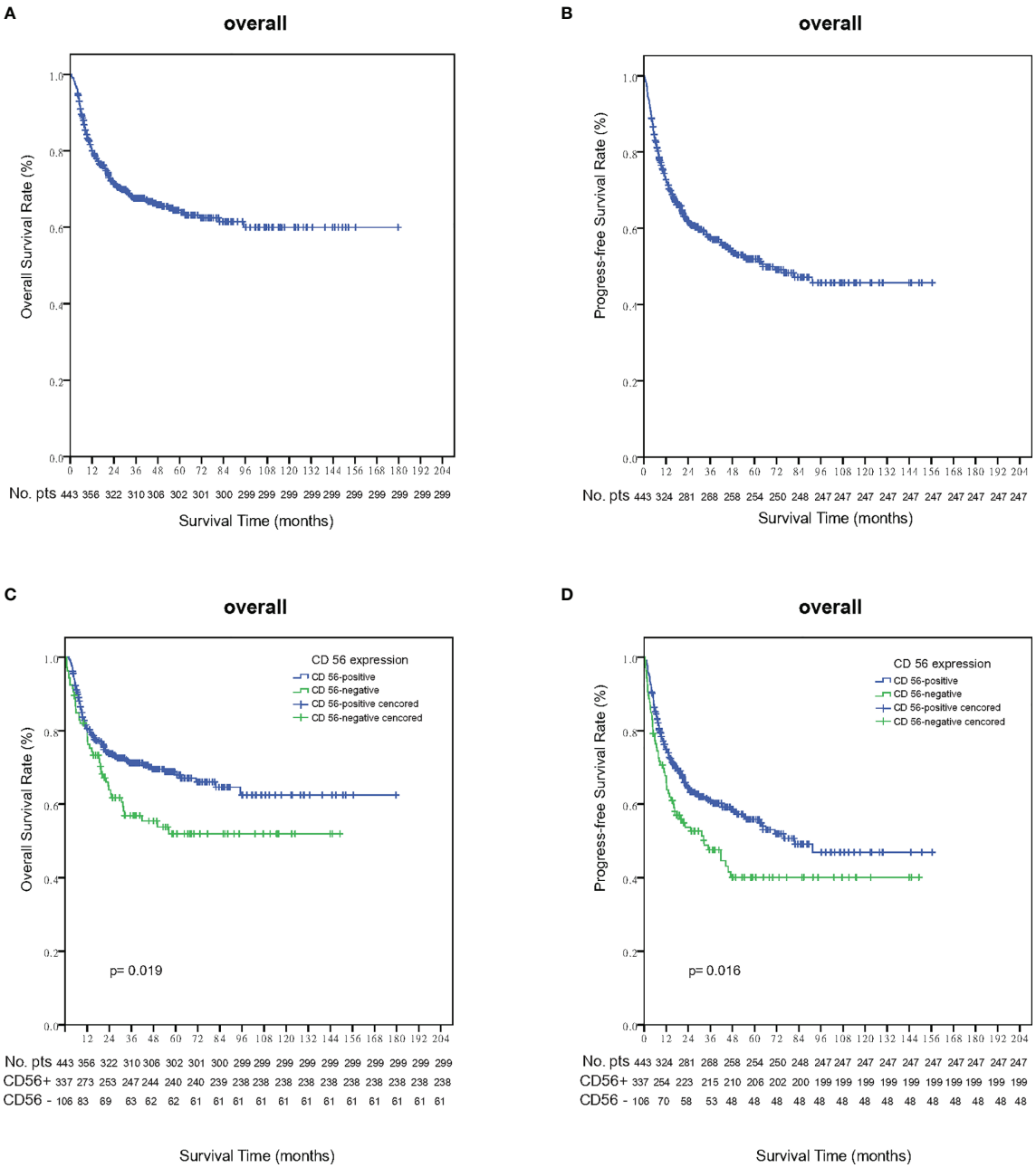

FIGURE 2 | Survival outcomes in the whole cohort of NKTCL. **(A)** Overall survival (OS); **(B)** Progression-free survival (PFS); **(C)** Overall survival (OS) analysis according to the expression status of CD56 in the whole cohort of NKTCL; **(D)** Progression-free survival (PFS) analysis according to the expression status of CD56 in the whole cohort of NKTCL.

DISCUSSION

Most cases of NKTCL are derived from NK cells, which are generally featured by CD56+, surface CD3−, and cytoplasmicCD3ϵ+ (14).However, NKTCL originated from T cells can be less commonly seen, usually with TCR rearrangement (12, 22, 23). CD56 expression is not specific for NKTCL and the diagnosis of NKTCL can still be confirmed for patients with typical morphology and expression of CD3ϵ, cytotoxic proteins and EBER (15). A previous study showed that patients with CD56-negative NKTCL had significantly dismal outcomes, indicating a distinct entity of NKTCL (16).

In the present study, 443 patients with NKTCL were assessed for the expression of CD56, with 76% positivity. Our findings were consistent with previous studies, in which the percentage of CD56 expression ranged from 74-97% (16–18). Our data

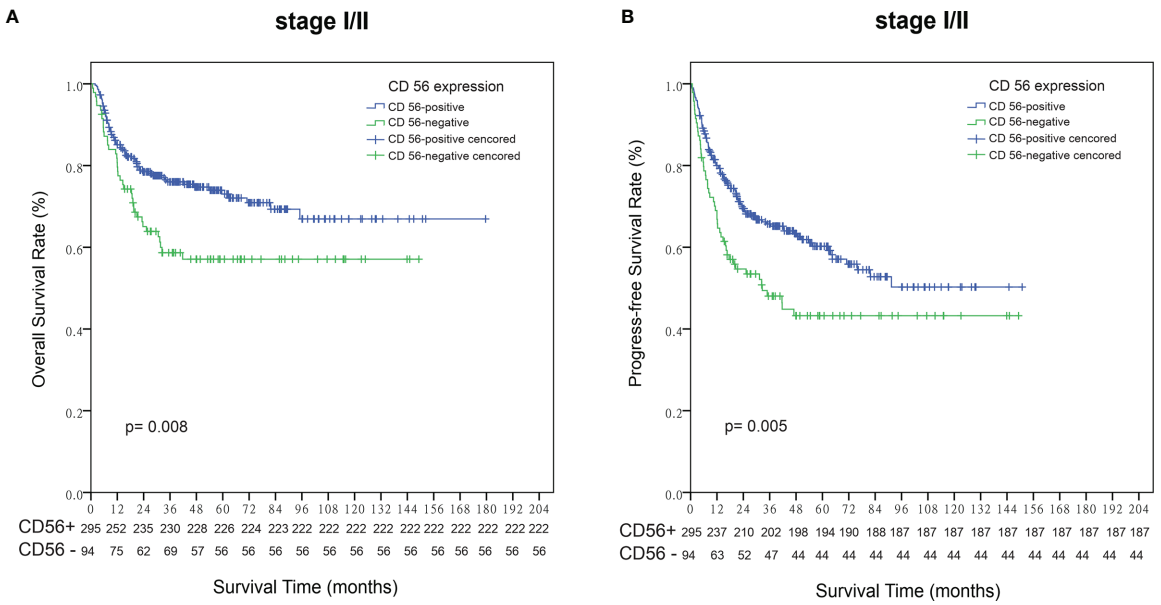

FIGURE 3 | Survival analysis according to the expression status of CD56 in patients with early stage NKTCL. **(A)** Overall survival (OS); **(B)** Progression-free survival (PFS).

demonstrated a notable difference in several clinical behaviors between the CD56-positive and CD56-negative groups. There were more patients with poor ECOG PS and higher IPI score in CD56-negative group. Although CD56 expression status did not influence the responses to initial treatment modalities as ORR did not differ between CD56 positive and negative groups, it was found to be a prognostic factor for PFS and OS in both the whole cohort and patients with early stage disease. Meanwhile, CD56 expression status was demonstrated to be an independent prognostic factor for PFS in patients with early stage disease, but failed to show an independent role for predicting OS in those patients. Our findings were consistent with a previous retrospective study, which identified CD56-negative expression was an independent adverse prognostic factor for PFS in early stage disease (16). Only 12 patients with advanced stage disease were CD56 negative, which may explain the failure to reveal independent role for predicting survival outcomes in patients with stage III/IV disease. Moreover, diverse salvage treatment regimens may impact the true value of CD56 expression status in predicting OS.

Currently, combined chemotherapy and radiotherapy is recommended for early-stage NKTCL (2, 6, 7, 24). Anthracycline-based chemotherapy regimens (e.g., CHOP or CHOP-like) were proven unfit for NKTCL, partially due to overexpression of MDR in NKTCL cells (5). Asparaginase-containing regimens have been recognized as standard of care treatment for both early and advanced disease (6, 7, 24–26). Our study showed that CD56-negative expression resulted in reduced PFS and OS rate of early-stage patients who received non-asparaginase-based chemotherapy, while this phenomena was not seen in patients who received asparaginase-based chemotherapy. These findings suggest that asparaginase-based treatment strategies might overcome the poor prognosis of CD56-negative NKTCL.

Xiong et al. successfully proposed the molecular subtypes of NKTCL using multi-omics analysis (21). In their cohort, 24 out of 99 patients had TCR rearrangement, who were defined as true T cells origin. Using a novel algorithm developed by Xiong et al. (based on quantitative gene expression metrics of NK-cell and T-cell associated genes), they divided 102 patients into NK-cell origin (n = 53) and T-cell origin (n = 49). The discrepancy between this novel algorithm and TCR results have not been fully understood (21). However, according to the findings reported by Xiong et al, the genes used for construction of this algorithm were not robustly specific for either T cell or NK cell. Thus, this algorithm needs to be validated further.

In our study, we arbitrarily defined patients with the top 75% expression level of CD56 as high expression group and the bottom 25% as low expression group to explore the differences between different CD56 expression status. As the heatmap shows in **Figure 5**, there was a distinct gene expression mode, indicating a possible different cell origin. The KEGG analysis showed that differentially expressed genes mainly involved in Natural killer cell mediated cytotoxicity and so on, which inferred that NKTCL with high CD56 expression may originate from NK cells. This conclusion was confirmed in the tumor microenvironment analysis of NKTCL, which showed that patients with high CD56 expression had significantly higher proportion of both resting and activated NK cells. Moreover, the activated $CD8^+$ and $CD4^+$ T cells were significantly higher in patients with high CD56 expression, and these cells could promote the immune attack towards tumors cells and result in

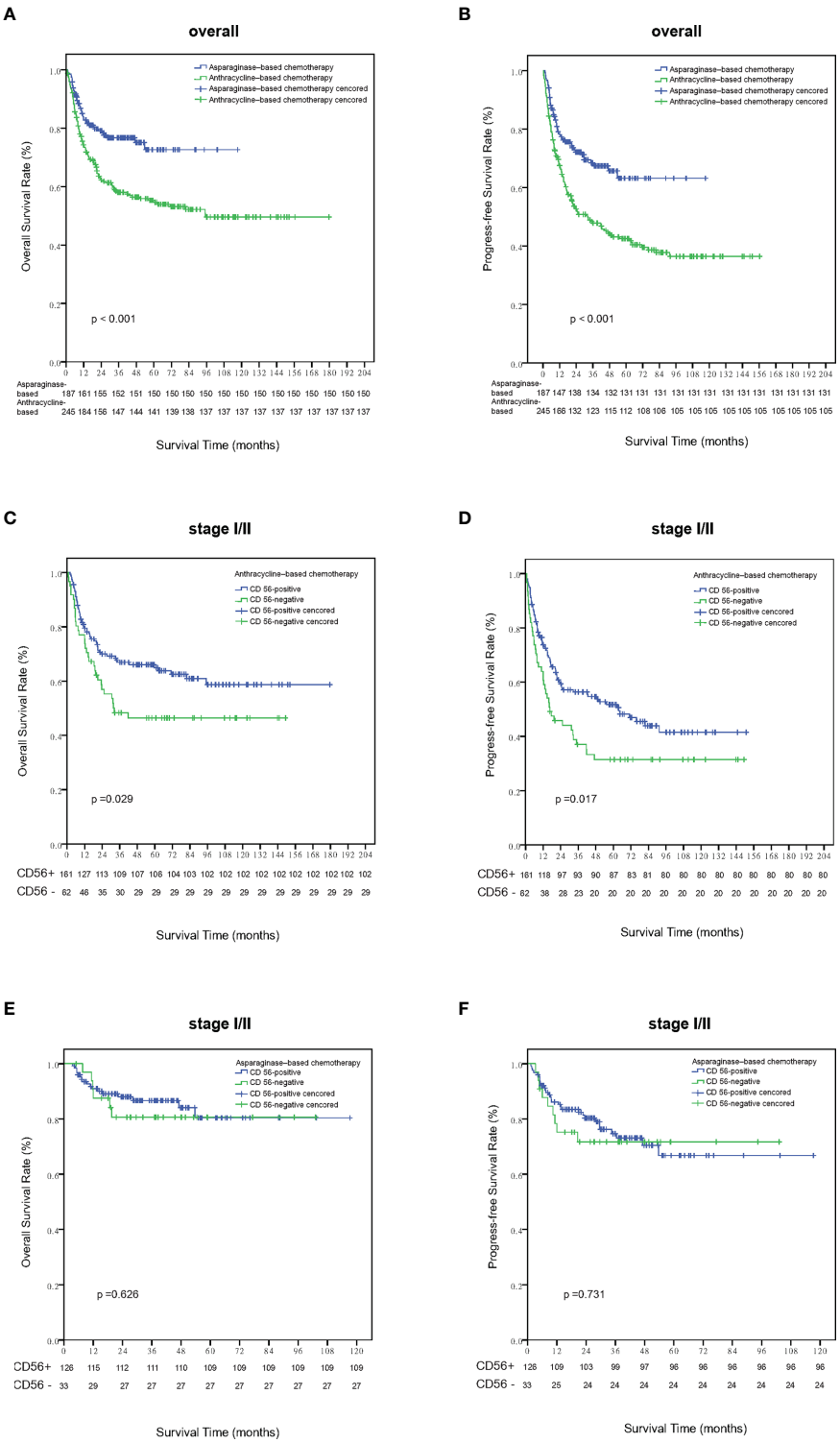

FIGURE 4 | Survival analysis according to different treatment strategies. Patients treated with asparaginase-based chemotherapy had significantly better overall survival **(A)** and progression-free survival **(B)** than those treated with anthracycline-based regimens. Out of patients with stage I-II disease who were treated with anthracyline-based chemotherapy, patients who were CD56 negative had significantly inferior overall survival **(C)** and progression-free survival **(D)** than those CD56 positive ones. Out of patients with stage I-II disease who were treated with asparaginase–based chemotherapy, the expression status of CD56 was not related with overall survival **(E)** and progression-free survival **(F)**.

TABLE 2 | Treatment outcomes of patients with CD56-positive vs. CD56-negative NKTCL.

Characteristics		5-year OS (%)			5-year PFS (%)		
		CD56-positive group (%) (n=337)	CD56-negative group (%) (n=106)	P value	CD56-positive group (%) (n=337)	CD56-negative group (%) (n=106)	P value
Gender	Male	64.6	45.8	0.017*	54.9	35.4	0.002*
	Female	75.0	61.4	0.314	57.8	47.6	0.867
Age at diagnosis (years)	≤60	69.1	60.7	0.364	56.6	45.5	0.245
	>60	61.3	15.9	0.004*	50.2	16.2	0.002*
ECOG PS score	0,1	72.7	55.3	0.012*	59.6	46.3	0.052
	≥2	46.2	45.1	0.649	38.9	27.5	0.081
Subtypes	Nasal cavity	71.7	61.2	0.178	58.2	49.5	0.191
	Extranasal UAT	68.5	40.3	0.030*	56.3	20.1	0.009*
	Extra UAT	41.0	0.0	0.337	34.4	0.0	0.574
B-symptoms	Prestent	65.7	39.5	0.018*	54.4	30.7	0.017*
	Absent	69.7	67.3	0.652	57.0	51.4	0.463
Serum LDH level	Elevated	53.8	37.1	0.247	43.7	24.6	0.064
	Normal	73.2	57.3	0.034*	60.4	45.8	0.080
Ann Arbor Stage	I, II	73.0	57.1	0.008*	60.2	43.2	0.005*
	III, IV	30.8	20.0	0.857	25.1	21.9	0.856
IPI score	0,1	74.6	60.4	0.015*	62.5	47.2	0.028*
	≥2	44.1	32.2	0.644	32.4	24.2	0.918
KPI score	0,1	76.6	53.4	0.079	65.0	52.1	0.143
	≥2	54.0	36.6	0.250	40.9	24.5	0.112
Treatment	Chemotherapy	42.2	33,6	0.601	28.8	22.1	0.402
	Chemotherapy and radiotherapy	75.9	61.9	0.108	62.6	49.9	0.175
Chemotherapy regimens	Asparaginase-based	74.3	77.2	0.963	61.2	70.5	0.829
	Non-asparaginase-based	60.6	41.6	0.027*	48.4	28.3	0.017*

ECOG PS, Eastern Cooperative Oncology Group performance status; Extranasal UAT, Extranasal upper aerodigestive tract; Extra UAT, extraupper aerodigestive tract; LDH, lactate dehydrogenase; IPI, International Prognostic Index; KPI, Korean Prognostic Index.
**Indicates statistically significant.*

good prognosis, which was confirmed by our survival analysis. Intriguingly, resting NK cells dominated in tumor microenvironment of NKTCL with high expression of CD56. Our results were derived from CIBERSORT algorithm, which reflects both the tumoral cells and tumor microenvironment cells. According to the algorithm Xiong et al. conceived to categorize cell origin (21), we reproduced their findings (Please see **Supplementary Figure 2**). Firstly, we compared the RNA

TABLE 3 | Results of univariate and multivariate analyses of prognostic factors for OS and PFS in all patients.

Parameter	OS			PFS		
	Univariate analysis	Multivariate analysis		Univariate analysis	Multivariate analysis	
	P-value	HR (95% CI)	*P*-value	*P*-value	HR (95% CI)	*P*-value
Age > 60 years	< 0.0001*	2.976(1.876–4.717)	< 0.0001*	0.020*	1.776(1.166-2.710)	0.008*
Gender, male	0.055			0.546		
ECOG PS ≥ 2	< 0.0001*	2.169(1.429-3.289)	< 0.0001*	< 0.0001*	1.770(1.232-2.545)	0.002*
Subtype, Extra UAT	< 0.0001*			< 0.0001*		
B symptoms	0.013*			0.012*		
Primary tumor invasion	< 0.0001*	1.761(1.167-2.653)	0.007*	< 0.0001*	1.595(1.134-2.242)	0.007*
Extranodal sites ≥ 2	0.001*			0.008*		
Regional lymphadenopathy	0.002*			< 0.0001*		
Elevated serum LDH	< 0.0001*			< 0.0001*		
CD 56- negative	0.019*	1.285 (0.885–1.866)	0.188	0.016*	1.269 (0.920–1.751)	0.146
Stage III, IV	< 0.0001*	2.688 (1.447–4.975)	0.002*	< 0.0001*	1.757 (1.002–3.086)	0.049*
IPI score ≥ 2	< 0.0001*			< 0.0001*		
KPI score ≥ 2	< 0.0001*			< 0.0001*	1.767(1.109-2.817)	0.017*

OS, overall survival; PFS, progression-free survival; RR, relative risk; CI, confidence interval; ECOG PS, Eastern Cooperative Oncology Group performance status; Extra UAT, extraupper aerodigestive tract; LDH, lactate dehydrogenase; IPI, International Prognostic Index; KPI, Korean Prognostic Index.
**Indicates statistically significant.*

TABLE 4 | Results of univariate and multivariate analyses of prognostic factors for OS and PFS in patients with Stage I/II.

Parameter	OS			PFS		
	Univariate analysis	Multivariate analysis		Univariate analysis	Multivariate analysis	
	P-value	RR (95% CI)	*P*-value	*P*-value	RR (95% CI)	*P*-value
Age > 60 years	< 0.0001*	2.604(1.675–4.065)	< 0.000*	0.005*	1.812(1.217-2.695)	0.003*
Gender, male	0.024*			0.491		
ECOG PS ≥ 2	< 0.0001*	1.672(1.092-2.564)	0.018*	< 0.0001*	1.730(1.200-2.494)	0.003*
Subtype, Extra UAT	0.471			0.292		
B symptoms	0.146			0.341		
Priamry tumor invasion	< 0.0001*	1.761(1.167-2.653)	0.002*	< 0.0001*	1.595(1.134-2.242)	0.001*
Extranodal sites ≥ 2	0.681			0.823		
Regional lymphadenopathy	0.042*	1.437(0.953-2.165)	0.083	0.002*	1.543(1.092-2.183)	0.014*
Elevated serum LDH	0.038*			0.026*		
CD 56- negative	0.008*	1.451(0.975–2.160)	0.067	0.005*	1.786 (1.250–2.551)	0.024*

OS, overall survival; PFS, progression-free survival; RR, relative risk; CI, confidence interval; ECOG PS, Eastern Cooperative Oncology Group performance status; Extra UAT, extraupper aerodigestive tract; LDH, lactate dehydrogenase; IPI, International Prognostic Index; KPI, Korean Prognostic Index.
**Indicates statistically significant.*

level of CD56 in different cell origins, and found that CD56 was significantly elevated in NK-cell origin samples (Please see **Supplemental Figure 3**, $p=3.2\times10^{-6}$). Subsequently, we compared the tumor microenvironment status between patients with NK-cell origin and T-cell origin (Please see **Supplemental Figure 4**) using CIBERSORT algorithm. In

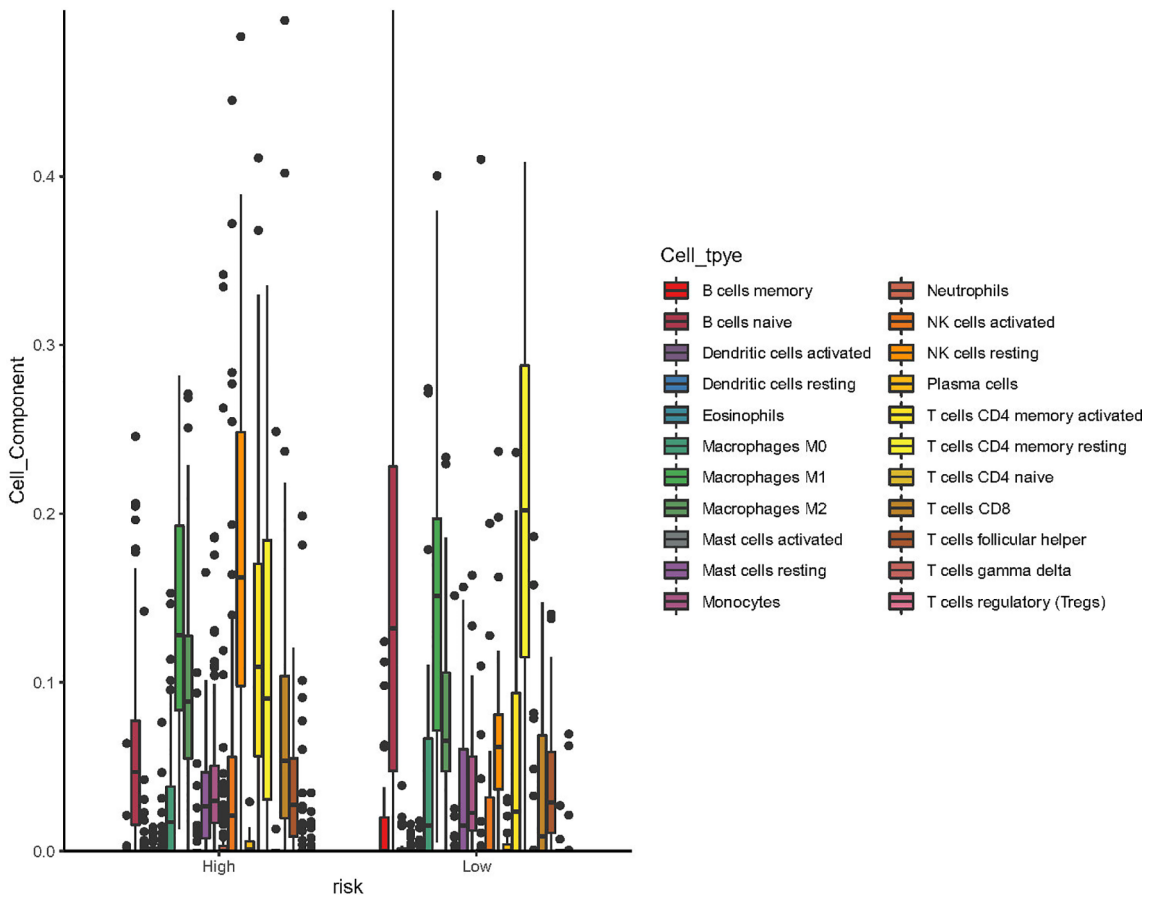

FIGURE 5 | Box plot of the processed data according to their CIBERSORT results (using ggboxplot from ggpubr R package). The figure showed that resting NK cells, activated NK cells, $CD8^+$ T cells and activated $CD4^+$ T memory cells was significantly higher in patients with high expression of CD56.

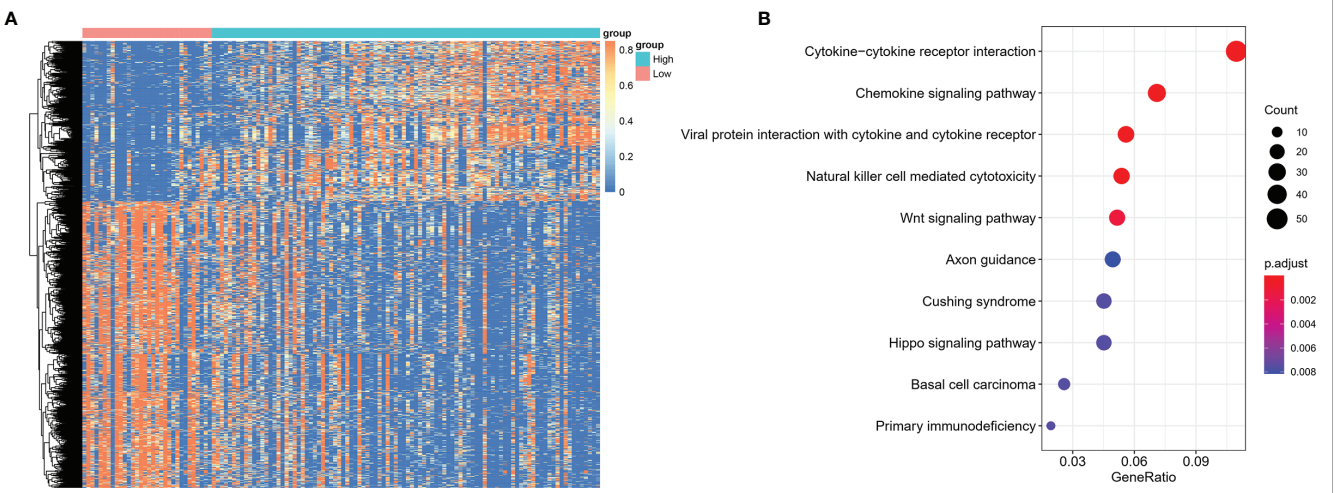

FIGURE 6 | Differentially expressed genes between NKTCL patients with high and low expression of CD56. **(A)** Heatmap shows the differentially expressed genes among groups, which were determined by significance criteria (abs(log2FC)>1 and adjusted P value<0.05) as implemented in the R package limma. The heatmap was drawn by pheatmap R package according to the differentially expressed genes. Unsupervised analyzing and hierarchical clustering of common differentially expressed genes based on expression data. **(B)** Gene annotation enrichment analysis using the clusterProfiler R package was performed on signature genes. The top five pathways with the greatest enrichment were Cytokine-cytokine receptor interaction, Chemokine signaling pathway, Viral protein interaction with cytokine and cytokine receptor, Natural killer cell mediated cytotoxicity, Wnt signaling pathway.

consistence with our findings, resting NK cells dominated in NK-cell origin group, and we can see the proportion of activated NK cells were much higher in patients with NK-cell origin. Thus, although we know that tumoral NK cells are more likely to be activated ones, the CIBERSORT algorithm has limitations to reflect the whole picture of tumor microenvironment accurately, and maybe sing-cell RNA sequencing data could help better define the NK cells status.

In conclusion, we found that CD56-negative NKTCL significantly correlated with poor outcomes and can further discriminate the prognosis of patients with early stage. The use of asparaginase-based regimens could overcome the dismal impact brought by CD56-negative NKTCL. Moreover, CD56 expression status may infer the cell origin of NKTCL. However, this is a retrospective study, and these results need to be validated in prospective trials.

DATA AVAILABILITY STATEMENT

The analyzed data sets generated during the study are available from the corresponding author, on reasonable request. The sequencing data (WGS, WES, and RNA-seq) of NKTCL used in this study can be viewed and downloaded in NODE (http://www.biosino.org/node) using the accession No. OEP000498 through the URL: http://www.biosino.org/node/project/detail/OEP000498. The detailed mutation calls, CNV, and RNA-seq expression data can be downloaded from the Mendeley Dataset, accessible through the following link: https://data.mendeley.com/datasets/7gwtb7mgrr/draft?a=85eac518-0f19-41f8-aa58-69ed36b66e41.

ETHICS STATEMENT

This study was approved by the Ethic Committee of Beijing Tongren Hospital and Sun Yat-sen University Cancer Center. The need for informed consent was waived because all patients had been de-identified in our datasets. Written informed consent for participation was not required for this study in accordance with the national legislation and the institutional requirements.

AUTHOR CONTRIBUTIONS

LW, LZ, and WS designed this study. JY and PL collected all clinical data and analyzed the data. YP reviewed the pathology reports and evaluated the expression of CD56. XL did the bioinformatics analysis. LQW, PL, WS, LZ, and LW contributed to patient selection and treatment. LW, JY, WS, and PL wrote the paper. All authors read and approved the submission of this paper.

FUNDING

This work was supported by grants from the National Natural Science Foundation of China (grant No. 81873450 and 82170181), the Open Research Fund from Beijing Advanced Innovation Center for Big Data-Based Precision Medicine, Beijing Tongren Hospital, Beihang University, and Capital Medical University (grant No. BHTR-KFJJ-202009), and Beijing Hospitals Authority Youth Programme (code: QML20200201) to LW.

SUPPLEMENTARY MATERIAL

The Supplementary Material for this article can be found online at: https://www.frontiersin.org/articles/10.3389/fimmu.2022.829366/full#supplementary-material

Supplementary Figure 1 | Survival analysis according to the expression status of CD56 in patients with advanced stage NKTCL. **(A)** Overall survival (OS); **(B)** Progression-free survival (PFS).

Supplementary Figure 2 | According to the algorithm conceived by Xiong et al. (reported in Cancer Cell. 2020), we reproduced the categorization of NKTCL according to NK-cell or T-cell origin.

Supplementary Figure 3 | Using data reported by Xiong et al. (reported in Cancer Cell. 2020), CD56 was significantly elevated in patients with NK-cell origin.

Supplementary Figure 4 | CIBERSORT analysis in groups with different cell origins, which were categorized using the algorithm conceived by Xiong et al. (reported in Cancer Cell. 2020).

REFERENCES

1. Vose J, Armitage J, Weisenburger D, International TCLP. International Peripheral T-Cell and Natural Killer/T-Cell Lymphoma Study: Pathology Findings and Clinical Outcomes. *J Clin Oncol* (2008) 26(25):4124–30. doi: 10.1200/JCO.2008.16.4558
2. Kwong YL. Natural Killer-Cell Malignancies: Diagnosis and Treatment. *Leukemia* (2005) 19(12):2186–94. doi: 10.1038/sj.leu.2403955
3. Li CC, Tien HF, Tang JL, Yao M, Chen YC, Su IJ, et al. Treatment Outcome and Pattern of Failure in 77 Patients With Sinonasal Natural Killer/T-Cell or T-Cell Lymphoma. *Cancer* (2004) 100(2):366–75. doi: 10.1002/cncr.11908
4. Wang L, Wang JW. Extranodal Natural-Killer T-Cell Lymphoma: Experience From China. *Lancet Haematol* (2020) 7(6):e441. doi: 10.1016/S2352-3026(20)30103-4
5. Wang B, Li XQ, Ma X, Hong X, Lu H, Guo Y. Immunohistochemical Expression and Clinical Significance of P-Glycoprotein in Previously Untreated Extranodal NK/T-Cell Lymphoma, Nasal Type. *Am J Hematol* (2008) 83(10):795–9. doi: 10.1002/ajh.21256
6. Jiang M, Zhang H, Jiang Y, Yang Q, Xie L, Liu W, et al. Phase 2 Trial of "Sandwich" L-Asparaginase, Vincristine, and Prednisone Chemotherapy With Radiotherapy in Newly Diagnosed, Stage IE to IIE, Nasal Type, Extranodal Natural Killer/T-Cell Lymphoma. *Cancer* (2012) 118(13):3294–301. doi: 10.1002/cncr.26629
7. Wang L, Wang ZH, Chen XQ, Li YJ, Wang KF, Xia YF, et al. First-Line Combination of Gemcitabine, Oxaliplatin, and L-Asparaginase (GELOX) Followed by Involved-Field Radiation Therapy for Patients With Stage IE/IIE Extranodal Natural Killer/T-Cell Lymphoma. *Cancer* (2013) 119(2):348–55. doi: 10.1002/cncr.27752
8. Wang H, Wang L, Li C, Wuxiao Z, Chen G, Luo W, et al. Pegaspargase Combined With Concurrent Radiotherapy for Early-Stage Extranodal Natural Killer/T-Cell Lymphoma, Nasal Type: A Two-Center Phase II Study. *Oncologist* (2020) 25(11):e1725–e31. doi: 10.1634/theoncologist.2020-0144
9. Wang L, Wang ZH, Chen XQ, Wang KF, Huang HQ, Xia ZJ. First-Line Combination of GELOX Followed by Radiation Therapy for Patients With Stage IE/IIE ENKTL: An Updated Analysis With Long-Term Follow-Up. *Oncol Lett* (2015) 10(2):1036–40. doi: 10.3892/ol.2015.3327
10. Wang L, Wang WD, Xia ZJ, Zhang YJ, Xiang J, Lu Y. Combination of Gemcitabine, L-Asparaginase, and Oxaliplatin (GELOX) Is Superior to EPOCH or CHOP in the Treatment of Patients With Stage IE/IIE Extranodal Natural Killer/T Cell Lymphoma: A Retrospective Study in a Cohort of 227 Patients With Long-Term Follow-Up. *Med Oncol* (2014) 31 (3):860. doi: 10.1007/s12032-014-0860-4
11. Jaffe ES, Krenacs L, Raffeld M. Classification of Cytotoxic T-Cell and Natural Killer Cell Lymphomas. *Semin Hematol* (2003) 40(3):175–84. doi: 10.1016/S0037-1963(03)00132-X
12. Yoon TY, Lee HT, Chang SH. Nasal-Type T/natural Killer Cell Angiocentric Lymphoma, Epstein-Barr Virus-Associated, and Showing Clonal T-Cell Receptor Gamma Gene Rearrangement. *Br J Dermatol* (1999) 140(3):505–8. doi: 10.1046/j.1365-2133.1999.02718.x
13. Ohsawa M, Nakatsuka S, Kanno H, Miwa H, Kojya S, Harabuchi Y, et al. Immunophenotypic and Genotypic Characterization of Nasal Lymphoma With Polymorphic Reticulosis Morphology. *Int J Cancer* (1999) 81(6):865–70. doi: 10.1002/(SICI)1097-0215(19990611)81:6<865::AID-IJC5>3.0.CO;2-S
14. Harabuchi Y, Takahara M, Kishibe K, Moriai S, Nagato T, Ishii H. Nasal Natural Killer (NK)/T-Cell Lymphoma: Clinical, Histological, Virological, and Genetic Features. *Int J Clin Oncol* (2009) 14(3):181–90. doi: 10.1007/s10147-009-0882-7
15. Cazzola M. Introduction to a Review Series: The 2016 Revision of the WHO Classification of Tumors of Hematopoietic and Lymphoid Tissues. *Blood* (2016) 127(20):2361–4. doi: 10.1182/blood-2016-03-657379
16. Wang L, Wang Z, Xia ZJ, Lu Y, Huang HQ, Zhang YJ. CD56-Negative Extranodal NK/T Cell Lymphoma Should Be Regarded as a Distinct Subtype With Poor Prognosis. *Tumour Biol* (2015) 36(10):7717–23. doi: 10.1007/s13277-015-3485-0
17. Li YX, Wang H, Feng XL, Liu QF, Wang WH, Lv N, et al. Immunophenotypic Characteristics and Clinical Relevance of CD56+ and CD56- Extranodal Nasal-Type Natural Killer/T-Cell Lymphoma. *Leuk Lymphoma* (2011) 52 (3):417–24. doi: 10.3109/10428194.2010.543718
18. Ng SB, Lai KW, Murugaya S, Lee KM, Loong SL, Fook-Chong S, et al. Nasal-Type Extranodal Natural Killer/T-Cell Lymphomas: A Clinicopathologic and Genotypic Study of 42 Cases in Singapore. *Mod Pathol* (2004) 17(9):1097–107. doi: 10.1038/modpathol.3800157
19. Cheson BD, Pfistner B, Juweid ME, Gascoyne RD, Specht L, Horning SJ, et al. Revised Response Criteria for Malignant Lymphoma. *J Clin Oncol* (2007) 25 (5):579–86. doi: 10.1200/JCO.2006.09.2403
20. Cheson BD, Horning SJ, Coiffier B, Shipp MA, Fisher RI, Connors JM, et al. Report of an International Workshop to Standardize Response Criteria for Non-Hodgkin's Lymphomas. NCI Sponsored International Working Group. *J Clin Oncol* (1999) 17(4):1244. doi: 10.1200/JCO.1999.17.4.1244
21. Xiong J, Cui BW, Wang N, Dai YT, Zhang H, Wang CF, et al. Genomic and Transcriptomic Characterization of Natural Killer T Cell Lymphoma. *Cancer Cell* (2020) 37(3):403–19.e6. doi: 10.1016/j.ccell.2020.02.005
22. Ohshima K, Liu Q, Koga T, Suzumiya J, Kikuchi M. Classification of Cell Lineage and Anatomical Site, and Prognosis of Extranodal T-Cell Lymphoma – Natural Killer Cell, Cytotoxic T Lymphocyte, and Non-NK/CTL Types. *Virchows Arch* (2002) 440(4):425–35. doi: 10.1007/s00428-001-0545-1
23. Harabuchi Y, Imai S, Wakashima J, Hirao M, Kataura A, Osato T, et al. Nasal T-Cell Lymphoma Causally Associated With Epstein-Barr Virus: Clinicopathologic, Phenotypic, and Genotypic Studies. *Cancer* (1996) 77(10):2137–49. doi: 10.1002/(SICI)1097-0142(19960515)77:10<2137::AID-CNCR27>3.0.CO;2-V
24. Wei W, Wu P, Li L, Zhang ZH. Effectiveness of Pegaspargase, Gemcitabine, and Oxaliplatin (P-GEMOX) Chemotherapy Combined With Radiotherapy in Newly Diagnosed, Stage IE to IIE, Nasal-Type, Extranodal Natural Killer/T-Cell Lymphoma. *Hematology* (2017) 22(6):320–9. doi: 10.1080/10245332.2016.1264163
25. Yamaguchi M, Kwong YL, Kim WS, Maeda Y, Hashimoto C, Suh C, et al. Phase II Study of SMILE Chemotherapy for Newly Diagnosed Stage IV, Relapsed, or Refractory Extranodal Natural Killer (NK)/T-Cell Lymphoma, Nasal Type: The NK-Cell Tumor Study Group Study. *J Clin Oncol* (2011) 29 (33):4410–6. doi: 10.1200/JCO.2011.35.6287
26. Jaccard A, Gachard N, Marin B, Rogez S, Audrain M, Suarez F, et al. Efficacy of L-Asparaginase With Methotrexate and Dexamethasone (AspaMetDex Regimen) in Patients With Refractory or Relapsing Extranodal NK/T-Cell Lymphoma, a Phase 2 Study. *Blood* (2011) 117(6):1834–9. doi: 10.1182/blood-2010-09-307454

Conflict of Interest: The authors declare that the research was conducted in the absence of any commercial or financial relationships that could be construed as a potential conflict of interest.

this article, or claim that may be made by its manufacturer, is not guaranteed or endorsed by the publisher.

frontiers in Immunology

ORIGINAL RESEARCH
published: 17 March 2022
doi: 10.3389/fimmu.2022.858590

Identification of the Predictive Models for the Treatment Response of Refractory/Relapsed B-Cell ALL Patients Receiving CAR-T Therapy

Jingxian Gu[1,2,3†], Sining Liu[1,2,3†], Wei Cui[1,2,3†], Haiping Dai[1,2,3], Qingya Cui[1,2,3], Jia Yin[1,2,3], Zheng Li[1,2,3], Liqing Kang[4], Huiying Qiu[1,2,3], Yue Han[1,2,3], Miao Miao[1,2,3], Suning Chen[1,2,3], Shengli Xue[1,2,3], Ying Wang[1,2,3], Zhengming Jin[1,2,3], Xiaming Zhu[1,2,3], Lei Yu[4], Depei Wu[1,2,3] and Xiaowen Tang[1,2,3*]*

[1] National Clinical Research Center for Hematologic Diseases, Jiangsu Institute of Hematology, The First Affiliated Hospital of Soochow University, Suzhou, China, [2] Institute of Blood and Marrow Transplantation, Collaborative Innovation Center of Hematology, Soochow University, Suzhou, China, [3] Key Laboratory of Thrombosis and Hemostasis of Ministry of Health, Institute of Blood and Marrow Transplantation, Suzhou, China, [4] Research and Development Department, Shanghai Unicar-Therapy Bio-Medicine Technology Co., Ltd., Shanghai, China

Background/Aims: Chimeric antigen receptor (CAR) T cells for refractory or relapsed (r/r) B-cell acute lymphoblastic leukemia (ALL) patients have shown promising clinical effectiveness. However, the factors impacting the clinical response of CAR-T therapy have not been fully elucidated. We here aimed to identify the independent factors of CAR-T treatment response and construct the models for predicting the complete remission (CR) and minimal residual disease (MRD)-negative CR in r/r B-ALL patients after CAR-T cell infusion.

Methods: Univariate and multivariate logistic regression analyses were conducted to identify the independent factors of CR and MRD-negative CR. The predictive models for the probability of remission were constructed based on the identified independent factors. Discrimination and calibration of the established models were assessed by receiver operating characteristic (ROC) curves and calibration plots, respectively. The predictive models were further integrated and validated in the internal series. Moreover, the prognostic value of the integration risk model was also confirmed.

Results: The predictive model for CR was formulated by the number of white blood cells (WBC), central neural system (CNS) leukemia, *TP53* mutation, bone marrow blasts, and CAR-T cell generation while the model for MRD-negative CR was formulated by disease status, bone marrow blasts, and infusion strategy. The ROC curves and calibration plots of the two models displayed great discrimination and calibration ability. Patients and infusions were divided into different risk groups according to the integration model. High-risk groups showed significant lower CR and MRD-negative CR rates in both the training and validation sets ($p < 0.01$). Furthermore, low-risk patients exhibited improved overall survival (OS) (log-rank $p < 0.01$), higher 6-month event-free survival (EFS) rate ($p < 0.01$),

OPEN ACCESS

Edited by:
Wei Sang,
The Affiliated Hospital of Xuzhou Medical University, China

Reviewed by:
Kourong Miao,
Nanjing Medical University, China
Xiao-Dong Mo,
Peking University People's Hospital, China
Heng Mei,
Huazhong University of Science and Technology, China

***Correspondence:**
Xiaowen Tang
xwtang1020@163.com
Depei Wu
drwudepei@163.com;
wudepei@suda.edu.cn

†These authors share first authorship

Specialty section:
This article was submitted to Cancer Immunity and Immunotherapy, a section of the journal Frontiers in Immunology

Received: *20 January 2022*
Accepted: *21 February 2022*
Published: *17 March 2022*

Citation:
Gu J, Liu S, Cui W, Dai H, Cui Q, Yin J, Li Z, Kang L, Qiu H, Han Y, Miao M, Chen S, Xue S, Wang Y, Jin Z, Zhu X, Yu L, Wu D and Tang X (2022) Identification of the Predictive Models for the Treatment Response of Refractory/Relapsed B-Cell ALL Patients Receiving CAR-T Therapy. Front. Immunol. 13:858590. doi: 10.3389/fimmu.2022.858590

and lower relapse rate after the allogeneic hematopoietic stem cell transplantation (allo-HSCT) following CAR-T cell infusion ($p = 0.06$).

Conclusions: We have established predictive models for treatment response estimation of CAR-T therapy. Our models also provided new clinical insights for the accurate diagnosis and targeted treatment of r/r B-ALL.

Keywords: chimeric antigen receptor T cells, refractory or relapsed B-cell acute lymphoblastic leukemia, predictive models, complete remission, MRD-negative complete remission

INTRODUCTION

Refractory or relapsed (r/r) B-cell acute lymphoblastic leukemia (ALL) remains one of the most fatal hematological malignancies with the reported median overall survival (OS) ranging from 3.0 to 8.4 months even after salvage chemotherapy or transplantation (1–4). Chimeric antigen receptor (CAR) T-cell therapy emerges as a new cellular immunotherapeutic strategy these years showing impressive efficacy in r/r B-ALL (5, 6). Published clinical trials have indicated a high complete remission (CR) rate of 67% to 93% in r/r B-ALL patients who received CAR-T cell infusion (7–13). However, there are still approximately 10% to 30% patients who had no response to the treatment and a large proportion of patients who relapsed soon after achieving CR (7–13). This is mainly because engineered T-cell therapy is an immensely individualized treatment due to the high heterogeneity of the malignancies, patients, and these functional T cells, which was originally collected from each patient (6, 14). Hence, to further improve therapeutic response, it is imperative for effective predictive tools to select the most benefited patients before infusion. In addition, on account of the considerable costs of CAR-T therapy, pretreatment evaluation is also of great significance to improve the cost-effectiveness as the application of this therapy is increasingly broadened (15, 16).

The influence factors of CAR-T therapeutic effect remain unclear. The results of several studies trying to identify these clinical factors varied (17–19). Besides, previous studies mainly centered on the resistance of cancer cells to the modified T cells and the lack of the persistence of CAR-T cells, irrespective of the clinical characteristics of the patients themselves (20, 21). Therefore, studies investigating the baseline characteristics as the potential predictive or prognostic factors of this novel therapy are warranted to help facilitate clinical prediction and guide personalized treatment. Here, we enrolled a large cohort of r/r B-ALL patients treated with CAR-T cells from three clinical trials and performed analyses to screen the independent factors of CAR-T treatment response. Also ultimately, in this study we first established the simple-to-use models for predicting the clinical outcome of these patients.

MATERIALS AND METHODS

Patients and Data Collection

A total of 286 consecutive r/r B-ALL patients who received CAR-T cells enrolled on three clinical trials (www.clinicaltrials.gov, identifiers: NCT03919240, NCT03614858, and NCT03275493) from December 2015 to September 2021 were included in this study. The major inclusion criteria were as follows: (1) diagnosed as refractory/relapsed B-ALL; (2) Karnofsky performance status score ≥ 60 or Eastern Cooperative Oncology Group performance score ≤ 2; (3) estimated survival time ≥3 months; and (4) ineligible for or refusal to allogeneic hemopoietic stem cell transplantation (allo-HSCT). Relapsed disease was defined as >5% bone marrow blasts, reappearance of circulating blasts, or development of extramedullary disease. Refractory disease was defined as those patients who did not achieve CR after 2 courses of intensive induction chemotherapy (13, 22). All three clinical trials and this study were approved by the Institutional Ethics Committees of the First Affiliated Hospital of Soochow University and conformed to the provisions of the Declaration of Helsinki. Written informed consent was obtained from the patients or their legal guardians. Clinical data including the clinical characteristics of every subject and the baseline information of the CAR-T cells used for each time of infusion for each patient were collected. All the data were extracted from the electronic medical record system of the patients.

Study Design

The overall design of this study is as summarized in **Figure 1**. Herein, two main phases including constructing and validating the predictive models for r/r B-ALL patients after CAR-T therapy were conducted. Out of all the 286 subjects, 204 patients enrolled on the above three clinical trials from December 2015 to March 2020 were treated as the discovery dataset. Another 82 patients from April 2020 to September 2021 were taken as the independent validation set. During the discovery phase, the first time of CAR-T cell infusion of each subject from the discovery set was included for the model construction. Firstly, the univariate and multivariate logistic regression analyses were applied to screen and identify the independent CR- and minimal residual disease (MRD)-negative CR-related factors. Except binary variables, all the variables were transformed into categorical ones before putting into logistic models. Moreover, the cutoff values adopted for the transformed covariates were as shown in **Table 1**. In the meantime, the predictive models were generated from the forward stepwise multivariate analysis (likelihood ratio). Then, for model evaluation, receiver operating characteristic (ROC) curves, along with the corresponding area under the curve (AUC), were used to assess the discrimination ability. The calibration curves for estimation of the consistency between the actual observation and the model-predicted value, and the

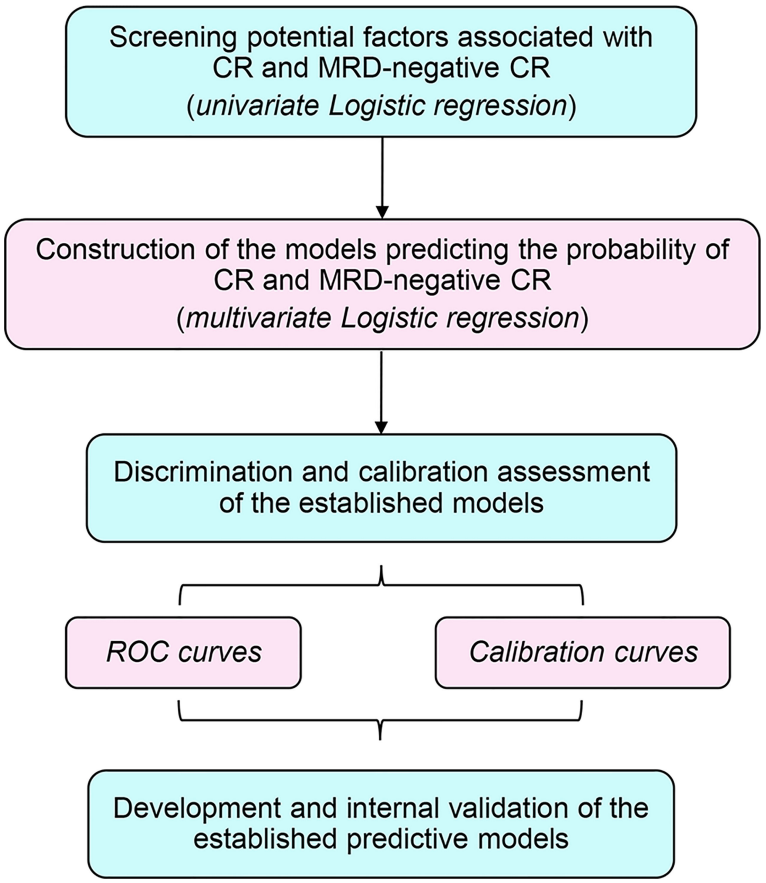

FIGURE 1 | Flowchart of the analytic process of this study.

Hosmer–Lemeshow chi-square (χ^2) test were carried out simultaneously for evaluating the accuracy and goodness of fit (23). In the validation analyses, the two models predicting CR and MRD-negative CR were integrated into one risk model for better prediction. First of all, we used all the infusions of 204 patients in the discovery set (some patients received more than one time of CAR-T cell infusion) as the training set to preliminarily validate the risk model. Furthermore, we also followed up the 204 participants for their survival status, 6-month event-free survival (EFS) status, subsequent treatments including transplantation, etc. The OS, 6-month EFS rate, and relapse rate of those who received allo-HSCT after CAR-T therapy were compared between different risk groups, respectively, to confirm the prognostic value of the modified model. Eventually, all the infusions of an independent patient cohort were used to further validate our risk model.

CAR-T Therapy

CAR-T cells were produced by Shanghai UniCAR Technology Co., Ltd. (UCT, Shanghai, China) (24, 25). Briefly, mononuclear cells for CAR-T cell production were obtained from the peripheral blood of the patients, transplant, or healthy donors by leukapheresis. Then, these cells were purified and transduced with lentiviral vector encoding chimeric T-cell antigen receptors. The CAR was finally composed of targeted single-chain variable fragment (scFv), intracellular domain including 4-1BB or CD28 as a co-stimulation signal, and a cytoplasmic signaling sequence, CD3ζ. Antigen receptors of these CAR-T cells contain CD19, CD22, and dual target, CD19+CD22.

Patients received fludarabine and cyclophosphamide (FC)-based lymphodepletion regimen prior to CAR-T cell infusion. Bridging chemotherapy before lymphodepletion included decitabine, rituximab, or other cytotoxic chemotherapy, such as MVP regimen (MVP: mitoxantrone, vincristine and prednisone). For one single time of infusion, CAR-T cells were infused on 3 consecutive days with 10%, 30%, and 60% of the total dose, respectively, or on 2 days, 40% for day +1 and 60% for day +2. The median cell dose of the infused cells was 0.5×10^7/kg (range, 0.05–67 $\times 10^7$/kg). Philadelphia chromosome (Ph)-positive B-ALL patients were given tyrosine kinase inhibitors (TKI).

Response Assessment and Follow-Up

CR was defined as <5% blasts in bone marrow and absence of extramedullary disease. MRD-negative CR was defined as <0.01% blasts in bone marrow detected by multicolor flow cytometry and, also, no evidence of extramedullary disease (13, 19).

TABLE 1 | Patient covariates (N = 204).

Covariates	n*
Baseline characteristics	
Gender (female/male)	105/99
Age (years)	30 (6–65)
WBC[a] ($\times 10^9$/L) (<20/20–100/≥100)	110/52/42
Extramedullary disease[#] (yes/no)	62/142
CNS leukemia (yes/no)	14/190
High cytogenetic risk	
Ph+ (yes/no)	63/141
Ph-like (yes/no)	14/190
TP53 mutation (yes/no)	16/188
T315I mutation (yes/no)	28/176
Del (7) (yes/no)	8/196
Complex karyotype (yes/no)	48/156
MLL aberrations (yes/no)	12/192
WT1 (positive/negative [b])	65/139
EVI1 (positive/negative [b])	36/168
IgH rearrangement (yes/no)	8/196
TCR rearrangement (yes/no)	5/199
Switched from CML lymphoblastic crisis (yes/no)	10/194
Disease status (relapsed/refractory)	159/45
Response after first chemotherapy (CR/PR/NR)	159/16/29
Previous allo-HSCT (yes/no)	44/160
Number of relapses (0/1/>1)	42/113/49
Number of previous therapies (<3/3–4/>4)	56/76/72
CAR-T therapy	
Bone marrow blasts (%)[c] (<5/5–25/25–50/>50)	99/39/31/35
Lymphodepletion regimen (FC/without FC)	193/11
Decitabine (yes/no)	12/192
Rituximab (yes/no)	12/192
MVP (yes/no)	19/185
Infusion strategy (single target/dual-target/sequential infusion)	152/42/10
IL-6 knockdown (yes/no)	11/193
Generation (2nd/3rd or 4th)	151/53
Interferon (yes/no)	9/195
Glucocorticoid (yes/no)	45/159
Tocilizumab (yes/no)	26/178
CRS after CAR-T	
CRS grade (0–2/>2)	153/51
CRES (0–2/>2)	187/17
Hemophagocytic histiocytosis (yes/no)	4/200
Tumor lysis syndrome (yes/no)	3/201

WBC, white blood cells; CNS, central nervous system; Ph, Philadelphia chromosome; CML, chronic myeloid leukemia; CR, complete remission; PR, partial remission; NR, no response; allo-HSCT, allogeneic hematopoietic stem cell transplantation; CAR-T, chimeric antigen receptor T-cell immunotherapy; FC, fludarabine and cyclophosphamide; MVP, mitoxantrone, vincristine and prednisone; CRS, cytokine release syndrome; CRES, CAR-T cell-related encephalopathy syndrome.

**Median and range for age, absolute patient numbers for other covariates.*

[#]EMD other than CNS involvement.

[a]The numbers of WBC in peripheral blood were detected when newly diagnosed.

[b]Positive: copy number>10/10,000abl copies, otherwise negative.

[c]Bone marrow blasts detected before lymphodepletion or CAR-T cell infusion (for those without lymphodepletion).

Bone marrow examination was performed at least 28 days after CAR-T cell infusion for evaluation of treatment response. Cytokine release syndrome (CRS) including CAR-T cell-related encephalopathy syndrome (CRES) was graded according to the criteria proposed by Lee et al. (26, 27). The last follow-up of the long-term survival of the patients from the discovery group was on December 31, 2020. OS was defined as the interval between the date of the first infusion and the date of death of any cause, allotransplant, or the last follow-up. EFS was calculated from the date of the first infusion to the date of relapse, death, or the last follow-up. If a patient had no response to CAR-T therapy, EFS status was also defined as 1 (28).

Statistical Considerations

To prevent missing more clinically significant indexes, the p values less than 0.2 from univariate analysis were considered as the threshold for inclusion in multivariate analysis. The univariate and multivariate logistic regression analyses were carried out *via* SPSS 23.0 for Windows (SPSS, Chicago, IL). The ROC curves with AUC calculation, Kaplan–Meier curves, and log-rank tests were performed in GraphPad Prism, version 7.0. The Hosmer–Lemeshow test was conducted by SPSS software (version 23.0), and its p value more than 0.05 indicated that the difference between the expected and actually observed values was insignificant. For each infusion, the patient could obtain a probability score of CR or MRD-negative CR generated from the constructed models. The clinical outcome of each infusion was then evaluated as high probability of CR (X^{high}) or low probability of CR (X^{low}), and high probability of MRD-negative CR (Y^{high}) or low probability of MRD-negative CR (Y^{low}) based on the cutoff values generated from ROC curves when Youden's indexes achieved maximum. The proportions of CR, MRD-CR, event-free, and relapse patients among different groups were compared by χ^2 test or Fisher's exact test using absolute numbers of subjects in SPSS software as well. $p < 0.05$ in this study was considered statistically significant, otherwise indicated.

RESULTS

Clinical Characteristics of the Study Population

The baseline characteristics of 204 participants in the discovery set and the CAR-T cells they initially received are presented in **Table 1**. Out of them, 10 (4.9%) r/r B-ALL patients were switched from CML and 44 (21.6%) had at least one allo-HSCT before CAR-T therapy. The Philadelphia chromosome was detected positive in 63 (30.9%) samples. 42 (20.6%) participants had extremely high tumor burden with white blood cells (WBC) in peripheral blood more than 100×10^9/l when newly diagnosed, while nearly half of the patients (N = 99) had relatively low (<5% of blasts) tumor burden before lymphodepletion, because most of the patients were heavily treated before CAR-T infusion with a median previous therapy number of 4, leading to varying degrees of bone marrow hypocellularity. Extramedullary disease other than CNS involvement was found in 62 (30.4%) subjects at enrollment. 14 patients were diagnosed with central neural system (CNS) leukemia. CRS occurred in 155 (76.0%) patients including 51 (25.0%) with severe symptoms (grade ≥3). 17 (8.3%) patients developed CRES of grade 3 or higher. In all, 176 (86.3%) patients achieved CR after CAR-T therapy and among them, 145 (71.1%) achieved MRD-negative CR. The 1-year probability of survival was 71.8% with the median follow-up time of 16.2 months (range: 1.3–52.1 months).

Searching for the Factors Associated With CR and MRD-Negative CR in r/r B-ALL Patients After CAR-T Therapy

To search for the possible factors of r/r B-ALL patients receiving CAR-T treatment, we first conducted univariate logistic regression analysis on clinical characteristics of the patients (**Table 2**) and the CAR-T cells infused for the first time (**Table 3**). The univariate analytic results revealed that the number of WBC in peripheral blood detected at diagnosis, CNS leukemia, *TP53* mutation, number of relapses, and bone marrow blasts detected before lymphodepletion or CAR-T cell infusion (for those without lymphodepletion) were significantly associated with CR after CAR-T cell infusion ($p < 0.05$, **Tables 2**, **3**). Also, two factors, number of relapses and CRS grade, were shown to have significant relations to MRD-negative CR ($p < 0.05$, **Tables 2**, **3**), while the relation between CRS grade and CR was marginally significant ($p = 0.06$, **Table 3**). The following factors, the number of WBC in peripheral blood detected at diagnosis ($p = 0.09$, **Table 2**) and bone marrow blasts detected before lymphodepletion or CAR-T cell infusion ($p = 0.08$, **Table 3**), were found to have marginally significant correlations with MRD-negative CR despite their statistically significant relations to CR.

Identification of the Independent Factors Impacting CAR-T Therapeutic Response

In order to further identify the independent factors of the remission after CAR-T therapy, the possible influence factors (univariate logistic $p < 0.2$) from the above univariate analyses were incorporated into the following multivariate logistic regression analyses. The multivariate analytic results showed that the number of WBC in peripheral blood detected at diagnosis, CNS leukemia, *TP53* mutation, bone marrow blasts detected before lymphodepletion, or CAR-T cell infusion and CAR-T cell generation were significant independent factors of CR ($p < 0.05$, **Supplementary Table 1**), while for MRD-negative CR, the independent factors were as follows: disease status (refractory or relapsed disease), bone marrow blasts detected before lymphodepletion, or CAR-T cell infusion and infusion strategy which referred to the choice of the infusion of single- or dual-target CAR-T cells or sequential infusion of two single-specific CAR-T cells ($p < 0.05$, **Supplementary Table 2**).

Construction of the Predictive Models for the Treatment Response of r/r B-ALL Patients Receiving CAR-T Cell Infusion

The models for predicting the probability of CR and MRD-negative CR of r/r B-ALL patients after CAR-T therapy were constructed based on the above stepwise multivariate logistic regression analysis. The predictive model for CR was as follows:

$$\mathbf{P^{CR}=1/(1+e^{-X})}$$

$$\mathbf{X=2.04-0.68\times WBC-1.40\times CNS-1.82\times TP53-0.44\times Blast+1.68\times Generation}$$

Definition and value:

P^{CR} = the probability of CR;

X = the probability score of CR;

WBC: the number of WBC in peripheral blood detected at diagnosis; the value of WBC ($\times 10^9$/L): <20:1; 20–100:2; ≥100:3;

CNS leukemia: no:0; yes = 1;

TP53 mutation: no:0; yes = 1;

Blast: bone marrow blasts detected before lymphodepletion or CAR-T cell infusion (for those without lymphodepletion); the value of blast: <5:0; 5–25:1; 25–50:2; ≥50:3;

Generation: CAR-T cell generation used for this infusion; the value of generation: 2nd:1; 3rd or 4th:2.

The predictive model for MRD-negative CR was as follows:

$$\mathbf{P^{MRD-CR}=1/(1+e^{-Y})}$$

$$\mathbf{Y=0.56-0.77\times Disease\_status-0.47\times Blast+0.83\times Infusion\_strategy}$$

Definition and value:

$P^{MRD\text{-}CR}$ = the probability of MRD-negative CR;

Y = the probability score of MRD-negative CR;

Disease_status: relapsed:0; refractory:1;

Blast: bone marrow blasts detected before lymphodepletion or CAR-T cell infusion (for those without lymphodepletion); the value of Blast: <5:0; 5–25:1; 25–50:2; ≥50:3;

Infusion_strategy: infusion of single- or dual-target CAR-T cells or sequential infusion of two single-specific CAR-T cells; single target:1; dual-target:2; sequential infusion: 3.

The discrimination ability of the established models was assessed by ROC curves. The CR-predicting model exhibited great performance in distinguishing CR patients from those not achieving CR with the AUC reaching 0.79 (95% CI: 0.69–0.89) (**Figure 2A**). The AUC of the ROC curves plotted based on the predictive model for MRD-negative CR was 0.66 (95% CI: 0.58–0.74) (**Figure 2B**). The accuracy of the two models was evaluated by calibration curves. The calibration plots showed good agreement when comparing the expected values generated from the constructed models and the observed values. The Hosmer–Lemeshow tests of the two models showed great goodness of fit with the *p* values, 0.62 and 0.68, respectively (**Figures 2C, D**).

Development and Preliminary Validation of the Constructed Predictive Models

To better predict the treatment response of r/r B-ALL patients after CAR-T therapy, the above two predictive models were further modified and integrated as one risk model. In the validation analyses, the training group was composed of the 242 infusions which 204 patients had altogether. A total of 242 infusions were divided into X^{high} and X^{low} groups, Y^{high} and Y^{low} groups, by the cutoff value, 1.8 and 1.0, respectively. The treatment outcome of an infusion evaluated as X^{high} and Y^{high} simultaneously was defined as the low-risk infusion while an infusion assessed as X^{low} and Y^{low} was defined as high-risk, otherwise intermediate-risk (**Figure 3A**). The CR and MRD-negative CR rates were compared among three subgroups (high-risk, intermediate-risk, and low-risk groups).

TABLE 2 | Univariate logistic regression analyses of the clinical characteristics of r/r B-ALL patients associated with CR and MRD-negative CR.

Variables	CR		MRD-negative CR	
	OR (95% CI)	*p* value	OR (95% CI)	*p* value
Gender				
Female	1.00 (reference)		1.00 (reference)	
Male	0.56 (0.25–1.27)	0.17*	1.17 (0.64–2.14)	0.61
Age (years)		0.39		0.62
<20	1.00 (reference)		1.00 (reference)	
20–40	0.36 (0.10–1.33)	0.13*	0.69 (0.31–1.56)	0.38
40–60	0.35 (0.09–1.34)	0.12*	0.67 (0.28–1.60)	0.37
≥60	0.20 (0.02–2.55)	0.22	0.30 (0.04–2.36)	0.25
WBC[a] (×10^9/L)		0.01*		0.09*
<20	1.00 (reference)		1.00 (reference)	
20–100	0.77 (0.26–2.24)	0.63	1.02 (0.48–2.19)	0.95
≥100	0.25 (0.10–0.64)	<0.01*	0.46 (0.22–0.96)	0.04*
Extramedullary disease[#]				
No	1.00 (reference)		1.00 (reference)	
Yes	1.71 (0.66–4.46)	0.27	1.41 (0.71–2.78)	0.32
CNS leukemia				
No	1.00 (reference)		1.00 (reference)	
Yes	0.25 (0.08–0.80)	0.02*	0.72 (0.23–2.23)	0.56
Ph+				
No	1.00 (reference)		1.00 (reference)	
Yes	1.14 (0.47–2.74)	0.78	1.15 (0.59–2.23)	0.68
Ph-like				
No	1.00 (reference)		1.00 (reference)	
Yes	2.15 (0.27–17.14)	0.47	1.76 (0.57–5.45)	0.32
TP53 mutation				
No	1.00 (reference)		1.00 (reference)	
Yes	0.22 (0.07–0.67)	0.01*	0.49 (0.17–1.39)	0.18*
T315I mutation				
No	1.00 (reference)		1.00 (reference)	
Yes	0.69 (0.24–2.00)	0.50	0.69 (0.30–1.61)	0.40
Del (7)				
No	1.00 (reference)		1.00 (reference)	
Yes	1.12 (0.13–9.45)	0.92	1.23 (0.24–6.28)	0.80
Complex karyotype				
No	1.00 (reference)		1.00 (reference)	
Yes	0.60 (0.25–1.43)	0.25	0.98 (0.48–2.01)	0.97
MLL aberrations				
No	1.00 (reference)		1.00 (reference)	
Yes	1.80 (0.22–14.51)	0.58	1.24 (0.32–4.73)	0.76
WT1 [b]				
Negative	1.00 (reference)		1.00 (reference)	
Positive	1.48 (0.59–3.67)	0.40	1.22 (0.63–2.37)	0.55
EVI1 [b]				
Negative	1.00 (reference)		1.00 (reference)	
Positive	3.11 (0.70–13.76)	0.13*	1.27 (0.56–2.90)	0.57
IgH rearrangement				
No	1.00 (reference)		1.00 (reference)	
Yes	1.12 (0.13–9.45)	0.92	0.67 (0.15–2.88)	0.59
TCR rearrangement				
No	1.00 (reference)		1.00 (reference)	
Yes	0.63 (0.07–5.83)	0.68	1.65 (0.18–15.04)	0.66
Switched from CML lymphoblastic crisis				
No	1.00 (reference)		1.00 (reference)	
Yes	0.62 (0.12–3.08)	0.56	0.95 (0.24–3.79)	0.94
Disease status				
Relapsed	1.00 (reference)		1.00 (reference)	
Refractory	1.82 (0.60–5.56)	0.29	0.59 (0.29–1.19)	0.14*
Response after first chemotherapy		0.99		0.13*
CR	1.00 (reference)		1.00 (reference)	
PR	1.12 (0.24–5.29)	0.88	2.76 (0.60–12.65)	0.19*
NR	1.00 (0.32–3.16)	1.00	0.56 (0.25–1.26)	0.16*

(Continued)

TABLE 2 | Continued

Variables	CR		MRD-negative CR	
	OR (95% CI)	*p* value	OR (95% CI)	*p* value
Previous allo-HSCT				
No	1.00 (reference)		1.00 (reference)	
Yes	0.64 (0.26–1.58)	0.34	1.50 (0.69–3.28)	0.31
Number of relapses		0.04*		0.03*
0	1.00 (reference)		1.00 (reference)	
1	0.59 (0.16–2.19)	0.43	2.28 (1.06–4.92)	0.04*
>1	0.24 (0.06–0.91)	0.04*	0.97 (0.42–2.27)	0.95
Number of previous therapies		0.85		0.57
<3	1.00 (reference)		1.00 (reference)	
3–4	0.89 (0.32–2.51)	0.83	0.70 (0.33–1.49)	0.35
≥5	0.75 (0.27–2.07)	0.58	0.96 (0.44–2.10)	0.91

r/r B-ALL, refractory or relapsed B-cell acute lymphoblastic leukemia; CR, complete remission; MRD, minimal residual disease; OR, odds ratio; 95% CI, 95% confidence interval; WBC, white blood cells; CNS, central nervous system; Ph, Philadelphia chromosome; CML, chronic myeloid leukemia; PR, partial remission; NR, no response; allo-HSCT, allogeneic hematopoietic stem cell transplantation.

**Statistically significant (p < 0.2 for univariate analysis).*

#EMD other than CNS involvement.

[a]The numbers of WBC in peripheral blood were detected when newly diagnosed.

[b]Positive: copy number>10/10,000abl copies, otherwise negative.

The results showed that three risk groups had significantly different remission proportions ($p < 0.01$, **Figures 3B, C**).

To further explore the prognostic value of the predictive models, the long-term survival was compared among three risk groups. As seen from the Kaplan–Meier curves, low-risk patients had significantly better OS than high-risk and intermediate-risk patients (log-rank $p < 0.01$, **Figure 4A**). The 6-month EFS rate was also compared and significantly differed among three subgroups ($p < 0.01$, **Figure 4B**). In addition, the prognosis of the patients who received allo-HSCT after CAR-T cell infusion was assessed. 25 high-risk patients and 43 low-risk patients underwent allotransplant following CAR-T therapy altogether. The relapse rate in high-risk patients was higher than that in low-risk ones ($p = 0.06$, p value was insignificant probably because of the limited number of samples) (**Figure 4C**).

Further Validation of the Risk Model Using the Independent Patient Group

The independent validation cohort consisted of 82 r/r B-ALL patients enrolled during a subsequent period of time. 82 patients had 84 infusions altogether (2 patients had twice). The baseline characteristics of the validation group are shown in **Supplementary Table 3**. According to the established predictive models for CR and MRD-negative CR, each time of CAR-T cell infusion could get an X and Y value. Then, based on the final risk model, all the 84 infusions (as the final validation dataset) could be stratified into high-risk, intermediate-risk, and low-risk groups (**Figure 5A**). The lower risk series showed higher CR and MRD-negative rates after CAR-T therapy, and the p value was statistically significant ($p < 0.01$, **Figures 5B, C**).

DISCUSSION

In this study, we constructed the risk model of both predictive and prognostic values in r/r B-ALL patients receiving CAR-T therapy. Our final model integrated two independent predicting models for CR and MRD-negative CR as a second modification which can be expected of better predictive efficiency. Whether the integration model or the independent models were easy to use because all used variables could be conveniently obtained before the treatment, as they were all routine tests and baseline clinical data. Moreover, the contribution of each variable to the whole model could be quickly calculated according to their coefficients in the formulas which greatly increased its clinical applicability as well. Using the models, r/r B-ALL patients could be stratified into different risk groups, predicted of the treatment response in advance of CAR-T cell infusion, and provided with personalized therapeutic advice.

Consistent with the previous studies, our results also showed that high tumor burden especially marrow disease burden was related to poor treatment response of CAR-T therapy in r/r B-ALL patients (17, 19, 29). Multivariate analytic results demonstrated that the number of bone marrow blasts before lymphodepletion or CAR-T cell infusion was the independent factor of both CR and MRD-negative CR. The other direct marker of tumor burden, the number of WBC in peripheral blood when newly diagnosed, was an independent factor of CR. From univariate analysis, WBC $\geq 100 \times 10^9$/l was a significant risk factor ($p = 0.04$) of MRD-negative CR although it was not independently associated with MRD-negative CR. Therefore, pretreatment to lower leukemia burden particularly for those high-risk patients before infusion with CAR-T cells might be a cardinal approach to improve CAR-T therapeutic effects.

In terms of the other baseline characteristics of r/r B-ALL patients, our findings showed that *TP53* mutation and CNS leukemia were the independent risk factors of CR. It has been demonstrated by numerous studies that *TP53* mutation was associated with unfavorable outcome of patients with various cancers including hematological malignancies (30, 31). A recent large-cohort retrospective study by Zhang et al. also reported that *TP53* mutation was independently correlated with the CR rate in B-ALL patients receiving CD19 CAR-T therapy (17). A non-

TABLE 3 | Univariate logistic regression analyses of the baseline information of CAR-T therapy and CAR-T cells associated with CR and MRD-negative CR.

Variables	CR		MRD-negative CR	
	OR (95% CI)	*p* value	OR (95% CI)	*p* value
Bone marrow blasts (%) [a]		0.01*		0.08*
<5	1.00 (reference)		1.00 (reference)	
5–25	0.48 (0.16–1.50)	0.21	0.73 (0.32–1.69)	0.46
25–50	0.82 (0.20–3.30)	0.78	0.60 (0.25–1.46)	0.26
≥50	0.19 (0.07–0.53)	<0.01*	0.34 (0.15–0.77)	0.01*
Lymphodepletion regimen				
Without FC	1.00 (reference)		1.00 (reference)	
FC	1.43 (0.29–6.98)	0.66	2.14 (0.63–7.32)	0.22
Decitabine				
No	1.00 (reference)		1.00 (reference)	
Yes	0.78 (0.16–3.78)	0.76	2.11 (0.45–9.94)	0.34
Rituximab				
No	1.00 (reference)		1.00 (reference)	
Yes	0.45 (0.11–1.77)	0.25	1.24 (0.32–4.74)	0.32
MVP				
No	1.00 (reference)		1.00 (reference)	
Yes	0.56 (0.17–1.82)	0.34	0.67 (0.25–1.80)	0.43
Infusion strategy		0.18*		0.18*
Single target	1.00 (reference)		1.00 (reference)	
Dual-target	3.94 (0.89–17.36)	0.07*	1.74 (0.78–3.93)	0.18*
Sequential infusion	1.77 (0.22–14.61)	0.60	4.28 (0.53–34.75)	0.17*
IL-6 knockdown				
No	1.00 (reference)		1.00 (reference)	
Yes	0.70 (0.14–3.42)	0.66	0.70 (0.20–2.48)	0.58
Generation				
2nd	1.00 (reference)		1.00 (reference)	
3rd or 4th	3.31 (0.96–11.44)	0.06*	2.01 (0.96–4.45)	0.06*
Glucocorticoid				
No	1.00 (reference)		1.00 (reference)	
Yes	0.66 (0.27–1.63)	0.37	0.59 (0.29–1.19)	0.14*
Tocilizumab				
No	1.00 (reference)		1.00 (reference)	
Yes	0.62 (0.21–1.82)	0.39	0.50 (0.22–1.17)	0.11*
CRS grade				
0–2	1.00 (reference)		1.00 (reference)	
>2	0.46 (0.20–1.05)	0.06*	0.42 (0.22–0.82)	0.01*
CRES				
0–2	1.00 (reference)		1.00 (reference)	
>2	0.34 (0.11–1.04)	0.06*	0.42 (0.15–21.15)	0.09*
Hemophagocytic histiocytosis				
No	1.00 (reference)		1.00 (reference)	
Yes	0.47 (0.05–4.67)	0.52	1.22 (0.12–12.02)	0.86
Tumor lysis syndrome				
No	1.00 (reference)		1.00 (reference)	
Yes	0.31 (0.03–3.54)	0.35	0.20 (0.02–2.23)	0.19*

CAR-T, chimeric antigen receptor T-cell immunotherapy; CR, complete remission; MRD, minimal residual disease; OR, odds ratio; 95% CI, 95% confidence interval; allo-HSCT, allogeneic hematopoietic stem cell transplantation; FC, fludarabine and cyclophosphamide; MVP, mitoxantrone, vincristine and prednisone; CRS, cytokine release syndrome; CRES, CAR-T cell-related encephalopathy syndrome.

**Statistically significant ($p < 0.2$ for univariate analysis).*

[a]Bone marrow blasts detected before lymphodepletion or CAR-T cell infusion (for those without lymphodepletion).

randomized clinical trial involving 51 r/r B-ALL participants receiving CD19 CAR-T cells showed that extramedullary disease (EMD) other than CNS leukemia was independently associated with the poor survival of B-ALL patients after CAR-T therapy (18). However, in our study, we did not find significant relations between EMD and CR or MRD-negative CR, which was in accord with the results of Professor Zhang and her colleagues' study (17). Anyway, these risk factors might greatly influence CAR-T treatment response and r/r B-ALL patients harboring these factors were probably not the appropriate candidates for the therapy.

Interestingly, we found that disease status (relapsed or refractory) right before infusion was the independent factor of MRD-negative CR in r/r B-ALL patients. Relapsed patients had a higher probability of MRD-CR remission after CAR-T therapy than refractory ones. To the best of our knowledge, clinical and experimental evidence is lacking in comparing the treatment response of these two subgroups at present. Our findings in this study led to speculation that relapsed patients might be more sensitive to antitumor therapy while refractory patients were more easily resistant to the treatment. However,

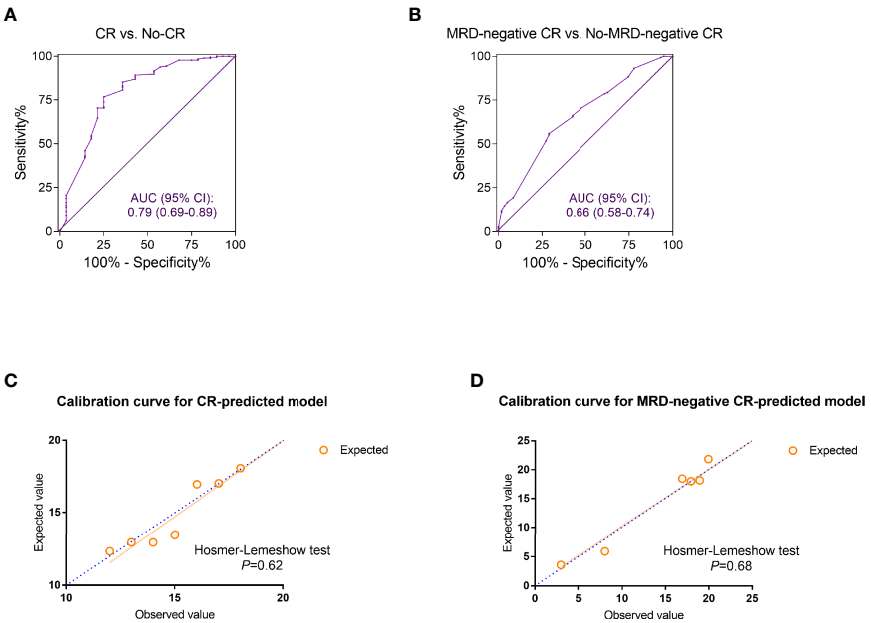

FIGURE 2 | The discrimination and calibration evaluation of the complete remission (CR) and minimal residual disease (MRD)-negative CR predicted models. **(A, B)** The receiver operating characteristic (ROC) curves discriminating the refractory or relapsed (r/r) B-cell acute lymphoblastic leukemia (ALL) patients who achieved CR **(A)** or MRD-negative CR **(B)** from those who did not. The area under the curve (AUC) of ROC was calculated for evaluation. **(C, D)** Calibration curves for the estimation of CR **(C)** and MRD-negative CR **(D)**. The observed and the model-expected numbers of events (CR and MRD-negative CR) were plotted on the x- and y-axes, respectively. *p* values generated from Hosmer–Lemeshow tests were also calculated for assessing the goodness of fit of the constructed models.

more studies are needed to validate our results and reveal molecular biological mechanisms.

With respect to the characteristics of CAR-T cells used for each infusion, our study revealed that the third and fourth generations of CAR-T cells were associated with higher probability of remission compared to the second generation. Besides, for target recognition, either dual-target infusions or sequential infusions of two single-specific CAR-T cells demonstrated better clinical response than single-target infusions. At present, dual-target infusion is considered as a promising and effective strategy for the antigen-loss relapse after single-target CAR-T cells (32). A previous meeting abstract and a case report showed that sequential infusions could significantly improve the clinical outcome of r/r B-ALL patients as well (33, 34). Recently, sequential infusion of two single-specific CAR-T cells was proposed as a cocktail therapy in r/r B-ALL patients for its proved superior efficacy and safety in the clinical trial (35), while thus far, few clinical trials comparing the efficacy of dual-target and sequential infusions have been reported. In our study, we found that patients who received sequential infusions were more likely to achieve MRD-negative CR compared to those after dual-target infusions. However, more targets or latest generation indicated higher cost of this therapy. Accordingly, in order to reduce treatment expenses of patients, prioritize medical resources, and meanwhile, improve individual prognosis, based on our models, low-risk patients are highly recommended for latest and dual-targeting or sequential infusion of CAR-T cells.

Our study has several limitations. Firstly, selection bias of the retrospective study was inevitable. Secondly, although the patients were from three clinical trials, they were treated in one similar medical center and were all Chinese. Therefore, larger patient groups, especially non-Chinese populations, from different medical centers are needed to further validate our models. Moreover, the application of our risk model was finally extended to each time of CAR-T cell infusion. However, the sample size of other infusions (not first-time infusion) was limited in this study. Thus, more real-world data of multiple CAR-T cell infusions of one single patient are need for validation as well. Besides, our models were constructed based on several common types of CAR-T cells. To further broaden the application of these models, more data of patients receiving the CAR-T cells of different targets, structures, and origins are needed to test and validate the models. Lastly, before putting into analyses, all the continuous variables were transformed into categorical ones to facilitate the application, which might simultaneously decrease the robustness of the constructed models. In spite of all the limitations, the predictive models for r/r B-ALL patients after CAR-T therapy, hereon we attempted to establish for the first time, displayed excellent clinical efficacy even in prognosis estimation.

In summary, we here developed and validated the predictive models for CAR-T therapeutic responses in r/r B-ALL patients and further confirmed the prognostic value of the risk model. The combined application of the two independent models for CR and MRD-negative CR estimation and the modified risk model can provide credible advice on the selection of the most benefited r/r B-ALL patients from this novel therapy and on the prevention treatment of these patients for clinicians and hematologists.

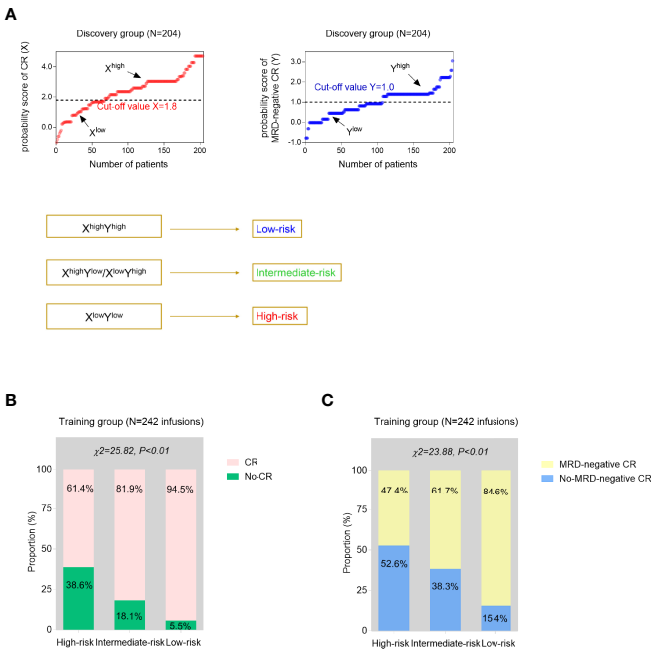

FIGURE 3 | Development and validation analyses of the established models. **(A)** Using the CR-predicted and MRD-negative CR-predicted models, each time of CAR-T cell infusion could be evaluated as high probability of CR (X^{high}) or low probability of CR (X^{low}), high probability of MRD-negative CR (Y^{high}), or low probability of MRD-negative CR (Y^{low}) with the cutoff values generated from the discovery cohort. Then, two independent predictive models were further integrated as one risk stratification model based on the simultaneous estimation of the probability of CR and MRD-negative CR. **(B, C)** The proportions of CR **(B)** and MRD-negative CR **(C)** infusions were compared among three risk groups from the training group. *p* values were calculated *via* the chi-square (χ^2) test.

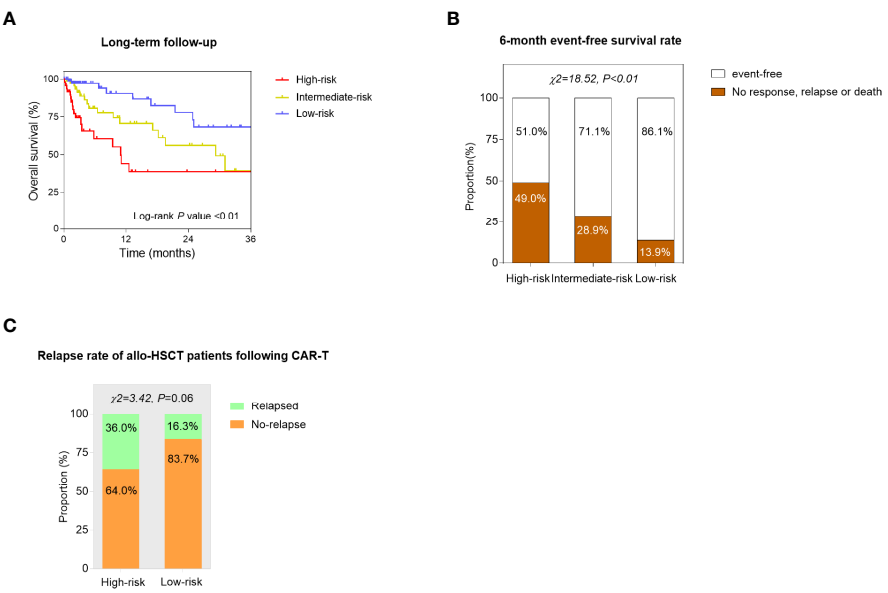

FIGURE 4 | Confirmation of the prognostic value of the constructed models. **(A)** Kaplan–Meier curves of the high-risk, intermediate-risk, and low-risk r/r B-ALL patients. The overall survival (OS) was compared by the log-rank test. **(B)** The 6-month event-free survival (EFS) rate was compared among high-risk, intermediate-risk, and low-risk groups using the chi-square (χ^2) test. **(C)** The relapse rate of the patients who received allogeneic hemopoietic stem cell transplantation (allo-HSCT) following CAR-T therapy was compared between high-risk and low-risk subgroups. *p* values were generated from the χ^2 test.

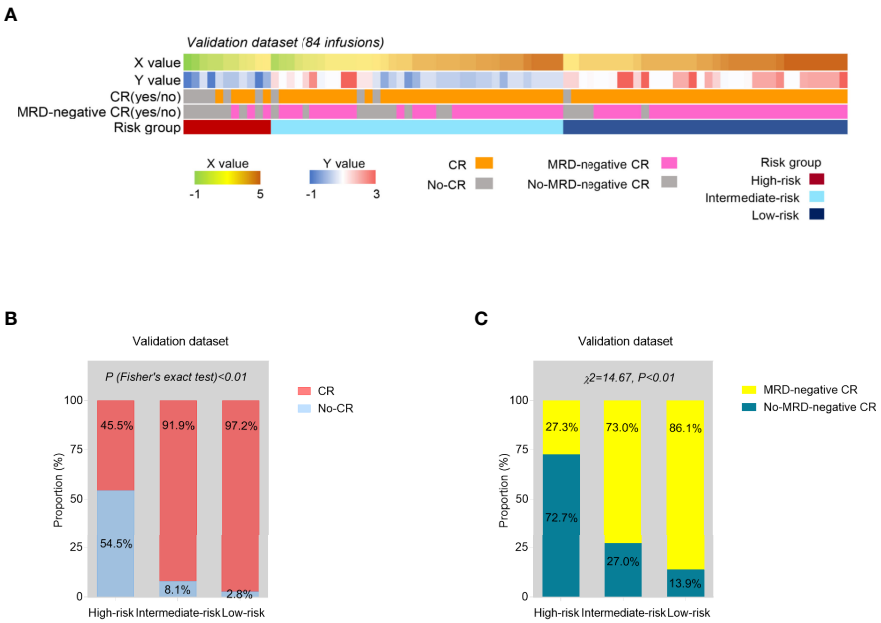

FIGURE 5 | Internal validation of the risk model. **(A)** The predicted probability score of CR (X) and MRD-negative CR (Y) and risk group based on the constructed models, and the actual treatment response of each time of CAR-T cell infusion in the validation series (N = 84). **(B, C)** The proportions of CR **(B)** and MRD-negative CR **(C)** infusions were compared among three risk groups from the validation set. *p* values were calculated *via* Fisher's exact test **(B)** and chi-square (χ^2) test **(C)**.

What is more, as commercial products of CAR-T cells are increasingly reported these years, our models need to be tested and improved based on these multicenter real-world data. Nevertheless, our findings may also give clinical implications in improving CAR-T therapeutic effectiveness.

DATA AVAILABILITY STATEMENT

The raw data supporting the conclusions of this article will be made available by the authors, without undue reservation.

ETHICS STATEMENT

The studies involving human participants were reviewed and approved by the Institutional Ethics Committees of the First Affiliated Hospital of Soochow University. Written informed consent to participate in this study was provided by the participants' legal guardian/next of kin.

AUTHOR CONTRIBUTIONS

XT, DW, and JG designed the research. JG, SL, HD, QC, JY, ZL, LK, HQ, YH, MM, SC, SX, YW, ZJ, XZ, and LY cared for the enrolled patients and conducted the medical visits. LK and LY were also responsible for the production of CAR-T cells. JG, WC, and SL collected and analyzed the patients' data. HD, QC, JY, and ZL constructed the figures. JG and WC drafted the manuscript. XT and DW revised the manuscript. All authors contributed to the article and approved the submitted version.

FUNDING

This work was supported by research grants from the National Natural Science Foundation of China (81873443, 82070162, 81900175, 81400155, 81700139), Major Natural Science Research Projects in institutions of higher education of Jiangsu Province (19KJA210002), The Key Science Research Project of Jiangsu Commission of Health (K2019022), Translational Research Grant of NCRCH (2020ZKZC04), Natural Science Foundation of Jiangsu Province (BK20190181, BK20201169, BK20170360), the Frontier Clinical Technical Project of the Science and Technology Department of Jiangsu Province (BE2018652), and the Priority Academic Program Development of Jiangsu Higher Education Institutions (PAPD).

ACKNOWLEDGMENTS

The authors thank the patients and their families, Uni CAR Technology Co., Ltd., Shanghai, China, and the First Affiliated Hospital of Soochow University for their strong support and close cooperation when performing this study.

SUPPLEMENTARY MATERIAL

The Supplementary Material for this article can be found online at: https://www.frontiersin.org/articles/10.3389/fimmu.2022.858590/full#supplementary-material

REFERENCES

1. Gökbuget N, Stanze D, Beck J, Diedrich H, Horst HA, Hüttmann A, et al. Outcome of Relapsed Adult Lymphoblastic Leukemia Depends on Response to Salvage Chemotherapy, Prognostic Factors, and Performance of Stem Cell Transplantation. *Blood* (2012) 120:2032–41. doi: 10.1182/blood-2011-12-399287
2. Forman SJ, Rowe JM. The Myth of the Second Remission of Acute Leukemia in the Adult. *Blood* (2013) 121:1077–82. doi: 10.1182/blood-2012-08-234492
3. Kantarjian H, Stein A, Gökbuget N, Fielding AK, Schuh AC, Ribera JM, et al. Blinatumomab Versus Chemotherapy for Advanced Acute Lymphoblastic Leukemia. *N Engl J Med* (2017) 376:836–47. doi: 10.1056/NEJMoa1609783
4. O'Brien S, Thomas D, Ravandi F, Faderl S, Cortes J, Borthakur G, et al. Outcome of Adults With Acute Lymphocytic Leukemia After Second Salvage Therapy. *Cancer* (2008) 113:3186–91. doi: 10.1002/cncr.23919
5. Brentjens RJ, Rivière I, Park JH, Davila ML, Wang X, Stefanski J, et al. Safety and Persistence of Adoptively Transferred Autologous CD19-Targeted T Cells in Patients With Relapsed or Chemotherapy Refractory B-Cell Leukemias. *Blood* (2011) 118:4817–28. doi: 10.1182/blood-2011-04-348540
6. Lee DW, Barrett DM, Mackall C, Orentas R, Grupp SA. The Future Is Now: Chimeric Antigen Receptors as New Targeted Therapies for Childhood Cancer. *Clin Cancer Res* (2012) 18:2780–90. doi: 10.1158/1078-0432.ccr-11-1920
7. Lee DW, Kochenderfer JN, Stetler-Stevenson M, Cui YK, Delbrook C, Feldman SA, et al. T Cells Expressing CD19 Chimeric Antigen Receptors for Acute Lymphoblastic Leukaemia in Children and Young Adults: A Phase 1 Dose-Escalation Trial. *Lancet* (2015) 385:517–28. doi: 10.1016/s0140-6736(14)61403-3
8. Davila ML, Riviere I, Wang X, Bartido S, Park J, Curran K, et al. Efficacy and Toxicity Management of 19-28z CAR T Cell Therapy in B Cell Acute Lymphoblastic Leukemia. *Sci Transl Med* (2014) 6:224ra25. doi: 10.1126/scitranslmed.3008226
9. Maude SL, Frey N, Shaw PA, Aplenc R, Barrett DM, Bunin NJ, et al. Chimeric Antigen Receptor T Cells for Sustained Remissions in Leukemia. *N Engl J Med* (2014) 371:1507–17. doi: 10.1056/NEJMoa1407222
10. Turtle CJ, Hanafi LA, Berger C, Gooley TA, Cherian S, Hudecek M, et al. CD19 CAR-T Cells of Defined CD4+:CD8+ Composition in Adult B Cell ALL Patients. *J Clin Invest* (2016) 126:2123–38. doi: 10.1172/jci85309
11. Gardner RA, Finney O, Annesley C, Brakke H, Summers C, Leger K, et al. Intent-To-Treat Leukemia Remission by CD19 CAR T Cells of Defined Formulation and Dose in Children and Young Adults. *Blood* (2017) 129:3322–31. doi: 10.1182/blood-2017-02-769208
12. Maude SL, Laetsch TW, Buechner J, Rives S, Boyer M, Bittencourt H, et al. Tisagenlecleucel in Children and Young Adults With B-Cell Lymphoblastic Leukemia. *N Engl J Med* (2018) 378:439–48. doi: 10.1056/NEJMoa1709866
13. Park JH, Rivière I, Gonen M, Wang X, Sénéchal B, Curran KJ, et al. Long-Term Follow-Up of CD19 CAR Therapy in Acute Lymphoblastic Leukemia. *N Engl J Med* (2018) 378:449–59. doi: 10.1056/NEJMoa1709919
14. Hong M, Clubb JD, Chen YY. Engineering CAR-T Cells for Next-Generation Cancer Therapy. *Cancer Cell* (2020) 38:473–88. doi: 10.1016/j.ccell.2020.07.005
15. Singh AK, McGuirk JP. CAR T Cells: Continuation in a Revolution of Immunotherapy. *Lancet Oncol* (2020) 21:e168–78. doi: 10.1016/s1470-2045(19)30823-x
16. Lin JK, Muffly LS, Spinner MA, Barnes JI, Owens DK, Goldhaber-Fiebert JD. Cost Effectiveness of Chimeric Antigen Receptor T-Cell Therapy in Multiply Relapsed or Refractory Adult Large B-Cell Lymphoma. *J Clin Oncol* (2019) 71:689–703. doi: 10.1200/jco.18.02079
17. Zhang X, Yang J, Li J, Li W, Song D, Lu XA, et al. Factors Associated With Treatment Response to CD19 CAR-T Therapy Among a Large Cohort of B Cell Acute Lymphoblastic Leukemia. *Cancer Immunol Immunother* (2021). doi: 10.1007/s00262-021-03009-z
18. An F, Wang H, Liu Z, Wu F, Zhang J, Tao Q, et al. Influence of Patient Characteristics on Chimeric Antigen Receptor T Cell Therapy in B-Cell Acute Lymphoblastic Leukemia. *Nat Commun* (2020) 11:5928. doi: 10.1038/s41467-020-19774-x
19. Hay KA, Gauthier J, Hirayama AV, Voutsinas JM, Wu Q, Li D, et al. Factors Associated With Durable EFS in Adult B-Cell ALL Patients Achieving MRD-Negative CR After CD19 CAR T-Cell Therapy. *Blood* (2019) 133:1652–63. doi: 10.1182/blood-2018-11-883710
20. Shah NN, Fry TJ. Mechanisms of Resistance to CAR T Cell Therapy. *Nat Rev Clin Oncol* (2019) 16:372–85. doi: 10.1038/s41571-019-0184-6
21. Mueller KT, Maude SL, Porter DL, Frey N, Wood P, Han X, et al. Cellular Kinetics of CTL019 in Relapsed/Refractory B-Cell Acute Lymphoblastic Leukemia and Chronic Lymphocytic Leukemia. *Blood* (2017) 130:2317–25. doi: 10.1182/blood-2017-06-786129
22. Döhner H, Estey E, Grimwade D, Amadori S, Appelbaum FR, Büchner T, et al. Diagnosis and Management of AML in Adults: 2017 ELN Recommendations From an International Expert Panel. *Blood* (2017) 129:424–47. doi: 10.1182/blood-2016-08-733196
23. Tessler MJ, Charland L, Wang NN, Correa JA. The Association of Time of Emergency Surgery - Day, Evening or Night - With Postoperative 30-Day Hospital Mortality. *Anaesthesia* (2018) 73:1368–71. doi: 10.1111/anae.14329
24. Hua J, Zhang J, Zhang X, Wu X, Zhou L, Bao X, et al. Donor-Derived Anti-CD19 CAR T Cells Compared With Donor Lymphocyte Infusion for Recurrent B-ALL After Allogeneic Hematopoietic Stem Cell Transplantation. *Bone Marrow Transplant* (2021) 56:1056–64. doi: 10.1038/s41409-020-01140-6
25. Yang X, Dai H, Kang L, Qu C, Li Z, Yin J, et al. Donor Origin CAR19 T Cell Infusion for B-ALL Relapsed After Allogeneic Hematopoietic Stem Cell Transplantation. *Hematol Oncol* (2019) 37:655–8. doi: 10.1002/hon.2682
26. Lee DW, Gardner R, Porter DL, Louis CU, Ahmed N, Jensen M, et al. Current Concepts in the Diagnosis and Management of Cytokine Release Syndrome. *Blood* (2014) 124:188–95. doi: 10.1182/blood-2014-05-552729
27. Lee DW, Santomasso BD, Locke FL, Ghobadi A, Turtle CJ, Brudno JN, et al. ASTCT Consensus Grading for Cytokine Release Syndrome and Neurologic Toxicity Associated With Immune Effector Cells. *Biol Blood Marrow Transplant* (2019) 25:625–38. doi: 10.1016/j.bbmt.2018.12.758
28. Zhang C, Wang XQ, Zhang RL, Liu F, Wang Y, Yan ZL, et al. Donor-Derived CD19 CAR-T Cell Therapy of Relapse of CD19-Positive B-ALL Post Allotransplant. *Leukemia* (2021) 35:1563–70. doi: 10.1038/s41375-020-01056-6
29. Zhang X, Lu XA, Yang J, Zhang G, Li J, Song L, et al. Efficacy and Safety of Anti-CD19 CAR T-Cell Therapy in 110 Patients With B-Cell Acute Lymphoblastic Leukemia With High-Risk Features. *Blood Adv* (2020) 4:2325–38. doi: 10.1182/bloodadvances.2020001466
30. Stengel A, Kern W, Haferlach T, Meggendorfer M, Fasan A, Haferlach C. The Impact of TP53 Mutations and TP53 Deletions on Survival Varies Between AML, ALL, MDS and CLL: An Analysis of 3307 Cases. *Leukemia* (2017) 31:705–11. doi: 10.1038/leu.2016.263
31. Stengel A, Schnittger S, Weissmann S, Kuznia S, Kern W, Kohlmann A, et al. TP53 Mutations Occur in 15.7% of ALL and Are Associated With MYC-Rearrangement, Low Hypodiploidy, and a Poor Prognosis. *Blood* (2014) 124:251–8. doi: 10.1182/blood-2014-02-558833
32. Ruella M, Barrett DM, Kenderian SS, Shestova O, Hofmann TJ, Perazzelli J, et al. Dual CD19 and CD123 Targeting Prevents Antigen-Loss Relapses After CD19-Directed Immunotherapies. *J Clin Invest* (2016) 126:3814–26. doi: 10.1172/jci87366
33. Liu SY, Deng BP, Lin YH, Yin ZC, Pan J, Wu T, et al. Sequential CD19-And CD22-CART Cell Therapies for Relapsed B-Cell Acute Lymphoblastic Leukemia After Allogeneic Hematopoietic Stem Cell Transplantation. *Blood* (2018) 132(Supplement 1):2126–2126. doi: 10.1182/blood-2018-99-111856
34. Hua J, Qian W, Wu X, Zhou L, Yu L, Chen S, et al. Sequential Infusion of Anti-CD22 and Anti-CD19 Chimeric Antigen Receptor T Cells for a Pediatric Ph-Like B-ALL Patient That Relapsed After CART-Cell and Haplo-HSCT Therapy: A Case Report and Review of Literature. *Onco Targets Ther* (2020) 13:2311–7. doi: 10.2147/ott.s235882
35. Wang N, Hu X, Cao W, Li C, Xiao Y, Cao Y, et al. Efficacy and Safety of CAR19/22 T-Cell Cocktail Therapy in Patients With Refractory/Relapsed B-Cell Malignancies. *Blood* (2020) 135:17–27. doi: 10.1182/blood.2019000017

Conflict of Interest: Authors LK and LY are employed by Shanghai Unicar-Therapy Bio-Medicine Technology Co., Ltd.

The remaining authors declare that the research was conducted in the absence of any commercial or financial relationships that could be construed as a potential conflict of interest.

the publisher, the editors and the reviewers. Any product that may be evaluated in this article, or claim that may be made by its manufacturer, is not guaranteed or endorsed by the publisher.

frontiers in Immunology

ORIGINAL RESEARCH
published: 25 March 2022
doi: 10.3389/fimmu.2022.842439

Oncogenic Mutations and Tumor Microenvironment Alterations of Older Patients With Diffuse Large B-Cell Lymphoma

Yue Zhu[1†], Di Fu[1†], Qing Shi[1†], Ziyang Shi[1†], Lei Dong[2], Hongmei Yi[2], Zhenhua Liu[3], Yan Feng[4], Qian Liu[4], Hai Fang[1], Shu Cheng[1], Li Wang[1,5], Qiang Tian[1], Pengpeng Xu[1] and Weili Zhao[1,5*]*

[1] Shanghai Institute of Hematology, State Key Laboratory of Medical Genomics, National Research Center for Translational Medicine at Shanghai, Ruijin Hospital, Shanghai Jiao Tong University School of Medicine, Shanghai, China, [2] Department of Pathology, Ruijin Hospital, Shanghai Jiao Tong University School of Medicine, Shanghai, China, [3] Department of Ultrasound, Ruijin Hospital, Shanghai Jiao Tong University School of Medicine, Shanghai, China, [4] State Key Laboratory of Microbial Metabolism, School of Life Sciences and Biotechnology, Shanghai Jiao Tong University, Shanghai, China, [5] Laboratory of Molecular Pathology, Pôle de Recherches Sino-Français en Science du Vivant et Génomique, Shanghai, China

The incidence of diffuse large B-cell lymphoma (DLBCL) increases by age and older DLBCL are commonly related to poor prognosis. However, the clinical and biological features of older DLBCL patients remain to be determined. A total of 2,445 patients with newly diagnosed DLBCL were enrolled for clinical data analysis according to age at diagnosis, with tumor samples of 1,150 patients assessed by DNA sequencing and 385 patients by RNA sequencing. Older DLBCL presented advanced disease stage, elevated serum lactate dehydrogenase, poor performance status, multiple extranodal involvement, high percentage of double expressor subtype, and adverse clinical outcome. According to molecular features, age was positively correlated with the oncogenic mutations of *PIM1*, *MYD88*, *BTG2*, *CD79B*, *TET2*, *BTG1*, *CREBBP*, *TBL1XR1*, and with the MYD88-like genetic subtype. These oncogenic mutations were involved in B-cell receptor/NF-κB signaling, B-cell differentiation, and histone acetylation based on biological functions. Older DLBCL also manifested reduction in $CD4^+$ naïve T and $CD8^+$ naïve T cells, and also increased recruitment of exhausted T cells and macrophages, leading to immunosuppressive tumor microenvironment. Our work thus contributes to the understanding of aging-related oncogenic mutations and tumor microenvironment alterations in lymphoma progression, and may provide new insights to mechanism-based targeted therapy in DLBCL.

Keywords: diffuse large B-cell lymphoma, aging, oncogenic mutations, tumor microenvironment, B-cell receptor, histone acetylation

OPEN ACCESS

Edited by:
Rachel Maurie Gerstein, University of Massachusetts Medical School, United States

Reviewed by:
Reuben Matthew Tooze, University of Leeds, United Kingdom
Michael Green, University of Texas MD Anderson Cancer Center, United States

***Correspondence:**
Weili Zhao
zhao.weili@yahoo.com
Pengpeng Xu
pengpeng_xu@126.com

[†]These authors have contributed equally to this work

Specialty section:
This article was submitted to Cancer Immunity and Immunotherapy, a section of the journal Frontiers in Immunology

Received: *23 December 2021*
Accepted: *24 February 2022*
Published: *25 March 2022*

Citation:
Zhu Y, Fu D, Shi Q, Shi Z, Dong L, Yi H, Liu Z, Feng Y, Liu Q, Fang H, Cheng S, Wang L, Tian Q, Xu P and Zhao W (2022) Oncogenic Mutations and Tumor Microenvironment Alterations of Older Patients With Diffuse Large B-Cell Lymphoma. Front. Immunol. 13:842439. doi: 10.3389/fimmu.2022.842439

INTRODUCTION

Diffuse large B-cell lymphoma (DLBCL) is the most common aggressive non-Hodgkin lymphoma, with the incidence increased by age. Age >60 at diagnosis is an important risk factor of the International Prognostic Index (IPI), indicating unfavorable clinical outcomes of patients treated by rituximab in combination with cyclophosphamide, doxorubicin, vincristine, and prednisone (R-CHOP) (1). More recently, the National Comprehensive Cancer Network database (NCCN)-IPI has further categorized DLBCL patients into 4 age groups (≤40 years, 41–60 years, 61–75 years, and >75 years) with increasing hazard ratio for inferior overall survival (2). As older DLBCL often present poor baseline health status and intolerance to immunochemotherapy, personalized therapy for older patients remain unmet clinical needs, which may rely on specific molecular features associated with age, especially oncogenic mutations and tumor microenvironment.

As reported, somatic mutations accumulate with age and may be related to tumor progression (3). In DLBCL, *MYD88*, *PIM1*, and *CD79B* mutations were more frequently observed in older patients (4, 5). Although less often occurred in lymphoid malignancies, *TET2* mutations were reported as age-related in other hematological malignancies (6, 7). In addition, immunosenescence contributes to reduced functioning of the immune system with aging (8). As an important feature of immunosenescence, the output of naïve T cells decreases after thymic involution, thereby altering the distribution of $CD4^+$ and $CD8^+$ naïve T cells in peripheral blood and immune organ (9). Within the tumors, T-cell exhaustion is regulated by immunosuppressive cytokines such as IL-10, and immune cells like macrophages, manifested by loss of effector functions and overexpression of inhibitory receptors like programmed cell death protein-1 (PD-1) (10). Particularly, immunosuppressive M2 macrophages accumulate in older lymphoid tissues and regulate T-cell functions by secreting immunosuppressive cytokines and expressing ligands to inhibitory receptors, and promoting tumor growth and metastasis (11). However, the clinical and biological features of older DLBCL patients remain to be determined.

In this study, we investigated the clinical characteristics and prognostic significance linked to age at diagnosis in a large cohort of 2,445 patients with newly diagnosed DLBCL, and performed genomic and transcriptomic analyses to illustrate the oncogenic mutations and tumor microenvironment alterations associated with older patients.

METHODS

Patients

A flow chart is outlined in **Figure 1** to summarize the patient selection. From September 2002 to April 2021, a total of 2,445 patients with newly diagnosed DLBCL were included, with the last

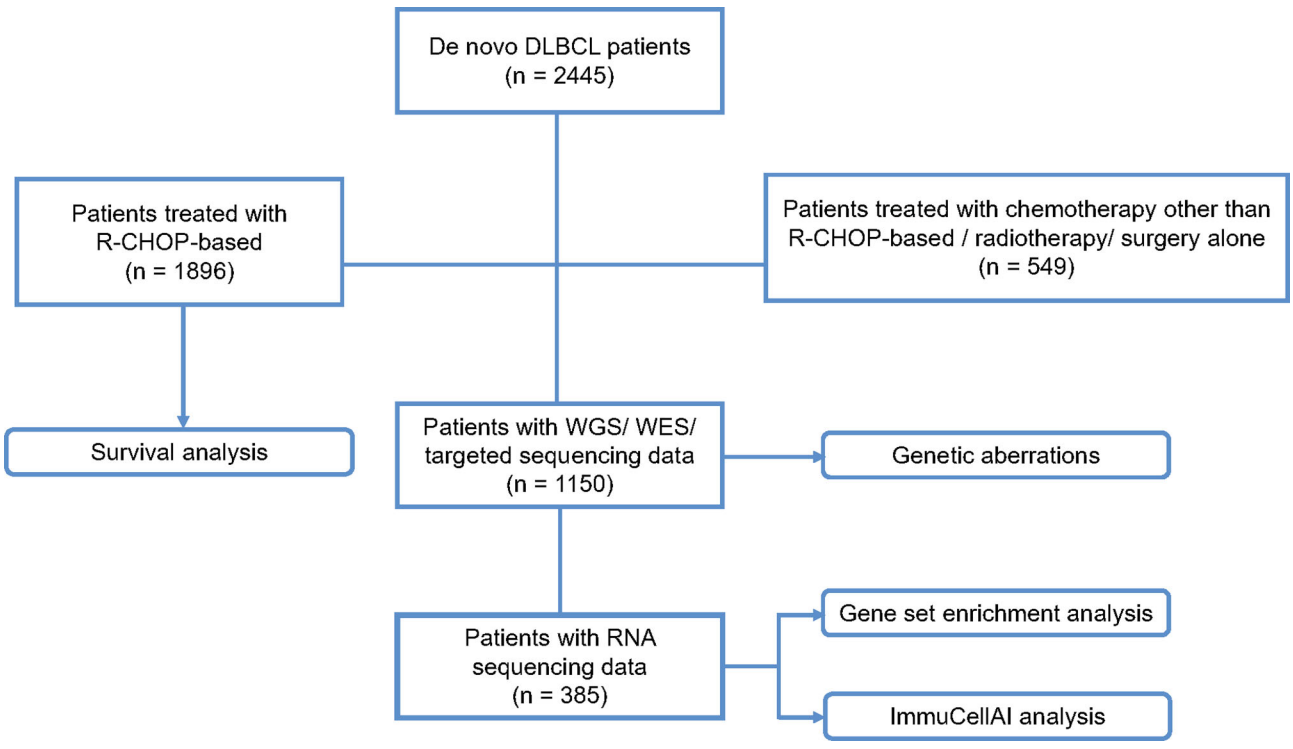

FIGURE 1 | Flow chart of the patient selection and methods. DLBCL, diffuse large B-cell lymphoma; R-CHOP, rituximab, cyclophosphamide, doxorubicin, vincristine and prednisone; WGS, whole genome sequencing; WES, whole exome sequencing.

follow-up through August 31, 2021. Histological diagnosis was established based on the World Health Organization (WHO) classification reviewed by two experienced pathologists, LD and HY (12). Survival analysis was performed on 1,896 patients receiving R-CHOP-based immunochemotherapy. DNA and RNA sequencing were performed on 1,150 and 385 patients with available tumor and blood samples, respectively, for detection of genetic aberrations, tumor microenvironmental analysis, and gene set enrichment analysis (GSEA). This study was approved by the Shanghai Rui Jin Hospital Review Board with informed consent obtained in accordance with the Declaration of Helsinki.

DNA Sequencing

DNA sequencing of 340 patients by whole-genome sequencing (WGS, n = 117) and whole-exome sequencing (WES, n = 223) were performed on available frozen or quality controlled FFPE tumor samples, as reported by our previous studies, along with detailed procedures for DNA sequencing (13–15). Targeted sequencing of 55 lymphoma associated genes were performed among 810 patients with available FFPE tumor samples based on the criteria as previously described (13–15). The mean depth of samples sequenced by WES and WGS was 120.25× (range 50–200×), with an average 97.65% (range 82.64–99.06%) of the target sequence being covered sufficiently deep for variant calling (≥10× coverage). The mean depth of samples sequenced by targeted sequencing was 1,351× (range 505–3,224×), with an average 88.57% (range 59.56–98.26%) of the target sequence being covered sufficiently deep for variant calling (200× coverage). Single nucleotide variations (SNVs) and indels were called by Genome Analysis Toolkit (GATK, v3.4) Haplotype Caller, and GATK Unified Genotyper and mapped to the genome location using the UCSC Genome Browser (http://genome.ucsc.edu) for annotation. The filtration of SNVs and indels was carried out by homemade pipeline with the software mentioned above. Variant allele frequency of mutations included should be over 5%. Mutations were filtered according to the rules listed below. Mutations were preserved if they met the following conditions: 1) sites reported as somatic mutations in our previous studies (13–15); 2) sites verified as somatic mutations by sequencing on paired blood samples; 3) sites commonly considered as hotspot mutations like *MYD88L265P*; 4) sites categorized into tier I and II variants according to the Guideline for Evidence-Based Categorization of Somatic Variants (16); 5) sites not included in the SNP database, or related to hematological malignancies (N >5) as reported in the COSMIC (the Catalogue of Somatic Mutations in Cancer). Mutations were excluded if they met the following conditions: 1) sites verified as germline mutations by sequencing on paired blood samples; 2) sites categorized into tier IV variants according to the Guideline for Evidence-Based Categorization of Somatic Variants; and 3) sites with extraordinarily high frequencies but never reported in previous studies. The mutation data among the 55 genes are listed in **Supplementary Table 1**. Clinical and pathological features of patients with WGS/WES/targeted sequencing data are shown in **Supplementary Table 2**. No statistically significant difference was found in the frequencies of mutations detected by WGS/WES/targeted sequencing called in the components of the cohort after balancing the baseline of clinical and pathological characteristics using propensity score matching, except *DDX3X* (**Supplementary Tables 3, 4**).

Based on the Gene Ontology database, 55 mutated genes were assigned to biological processes, namely, chromatin organization, immune response, cell-cycle/p53, and also oncogenic signaling pathways B-cell receptor (BCR)/NF-κB, JAK-STAT, PI3K-AKT, and Wnt. The list of genes involved in biological function is shown in **Supplementary Table 5**.

RNA Sequencing, ImmuCellAI Analysis and GSEA Analysis

RNA sequencing was performed on 385 patients with available frozen tumor samples. A total of 361 patients of them were from our previous studies (13–15) and 24 patients were newly analyzed, namely, 98 patients with WGS, 98 with WES, and 189 with targeted sequencing data, respectively. Clinical and pathological features of patients with RNA sequencing data are shown in **Supplementary Tables 6–8**. RNA was extracted by Trizol and an RNeasy Mini Kit (Qiagen) from available qualified frozen tumor samples of 385 patients. RNA was purified by Ribo-Zero rRNA Removal Kits (Illumina). RNA concentration was assessed on NanoDrop and integrity by an Agilent 2100 Bioanalyzer. RNA libraries were generated with a TruSeq RNA Library Preparation Kit (Illumina) based on instructions of the manufacturer. The concentration and the quality of RNA libraries were controlled by Qubit and BioAnalyzer 2100 system. Paired-end sequencing was performed on Illumina HiSeq sequencer following Illumina-provided protocols. The read pairs were aligned to Refseq hg19 through Burrows-Wheeler Aligner version 0.7.13-r1126. The transcript counts table files were generated by the HTSeq (17). Potential false positive results were excluded by visual inspection. R package "sva" was applied to remove batch effect by r 4.0.3. The expressional data related are shown in **Supplementary Table 9**. Cell of origin classification based on gene expression was performed using Lymph2Cx assay (18). Based on raw counts data of RNA sequencing, the infiltration of immune cells including 24 immune cell types were estimated by ImmuCellAI algorithm, a website tool (http://bioinfo.life.hust.edu.cn/web/ImmuCellAI/) (19). Pathway enrichment analysis was performed using GSEA v4.0.1 software as recommended by the GSEA team (http://www.broadinstitute.org/gsea). Pathways were considered of statistical significance with a P-value <0.05 and a false discovery rate <0.25.

Immunohistochemistry

Immunohistochemistry was performed on paraffin sections using antibodies against CD10, BCL6, MUM1, BCL2, and MYC by indirect immunoperoxidase method. Germinal center B-cell-like (GCB) and non-GCB phenotypes were determined with 30% cutoff values of CD10, BCL6, and MUM1, according to Han's algorithm (20). BCL2/MYC double-expressors were defined by BCL-2 and MYC with cutoff values of 50 and 40%, respectively (12).

Fluorescence *In-Situ* Hybridization

Fluorescence *in-situ* hybridization of BCL2, BCL6, and MYC rearrangements was performed on paraffin sections with 10% cutoff values. The results in detail are listed in **Supplementary Table 10**.

Molecular Classification

DLBCL genotypes were identified as described by Lacy et al. using the 47 genes available among 1,150 patients with DNA sequencing data (R code version, https://github.com/ecsg-uoy/DLBCLGenomicSubtyping) (21).

Statistical Analysis

Pearson's χ^2 test or Fisher's exact test was used to analyze baseline characteristics of patients. Progression-free survival (PFS) was calculated from the date of diagnosis to the date when disease progression or relapse was recognized or the date of last follow-up. Overall survival (OS) was measured from the date of diagnosis to the date of death or the date of last follow-up. Survival functions were analyzed using the Kaplan–Meier method and compared by the log-rank test. Univariate hazard was analyzed using the Cox regression method and the significant variables were then kept in multivariate set. Normalized gene expression in two groups was analyzed using Mann–Whitney *U* test. All statistical analysis was performed by Statistical Package for the Social Sciences (SPSS) 26.0 software. All tests were two-sided, with statistical significance defined as $P < 0.05$.

RESULTS

Clinical and Pathological Characteristics of DLBCL Patients Based on Age at Diagnosis

Among 2,445 patients with newly diagnosed DLBCL, 1,140 patients were >60 years old and 1,305 patients were ≤60 years old at diagnosis. The clinical characteristics of the patients are listed in **Table 1**. Patients diagnosed at age >60 years were associated with advanced Ann Arbor stage ($P < 0.001$), elevated serum lactate dehydrogenase (LDH) ($P < 0.001$), poor performance status ($P < 0.001$), multiple extranodal involvement ($P = 0.001$), high percentage of double expressor subtype ($P = 0.012$), as compared to those at age ≤60 years. No significant difference was observed between the two age groups, according to gender, cell of origin (Hans), cell of origin (Lymph2Cx), or double/triple-hit.

TABLE 1 | Clinical and pathological characteristics of DLBCL patients (n = 2,445).

Characteristics	Age		*P*-value
	≤60 y (n = 1,305)	>60 y (n = 1,140)	
Gender			0.500
Male	708 (54.25%)	634 (55.61%)	
Female	597 (45.75%)	506 (44.39%)	
Ann Arbor stage			<0.001
I–II	694 (53.18%)	516 (45.26%)	
III–IV	611 (46.82%)	624 (54.74%)	
LDH			<0.001
Normal	722 (55.33%)	533 (46.75%)	
Elevated	583 (44.67%)	607 (53.25%)	
ECOG score			<0.001
0–1	1,179 (90.34%)	949 (83.25%)	
≥2	126 (9.66%)	191 (16.75%)	
Extranodal involvement			0.001
0–1	993 (76.09%)	797 (69.91%)	
≥2	312 (23.91%)	343 (30.09%)	
Cell of origin (Hans)			0.199
GCB	395/999 (39.54%)	342/932 (36.70%)	
Non-GCB	604/999 (60.46%)	590/932 (63.30%)	
cell-of-origin (Lymph2Cx)			
ABC	94/202 (46.53%)	98/183 (53.55%)	0.129
GCB	65/202 (32.18%)	42/183 (22.95%)	
unclassified	43/202 (21.29%)	43/183 (23.50%)	
Double expressor			0.012
Yes	180/785 (22.93%)	201/702 (28.63%)	
No	605/785 (77.07%)	501/702 (71.37%)	
Double-hit/triple-hit			0.386
Yes	31/529 (5.86%)	25/535 (4.67%)	
No	498/529 (94.14%)	510/535 (95.33%)	

P-value indicated difference between DLBCL ≤60 years (y) and >60 y.

DLBCL, diffuse large B-cell lymphoma; LDH, lactate dehydrogenase; ECOG, Eastern Cooperative Oncology Group; GCB, germinal center B-cell; ABC, activated B-cell.

Survival Analysis and Prognostic Significance of DLBCL Patients Based on Age at Diagnosis

Among 1,896 patients receiving R-CHOP-based immunochemotherapy, the median follow-up time was 55.0 months (0.2–224.2 months). The 3-year PFS and OS rates of patients diagnosed at age >60 years were 60.8 and 71.0%, significantly lower than those of patients at age ≤60 years (72.1%, P <0.001; 83.2%, P <0.001, respectively) (**Figures 2A, B**). Using univariate analysis, the 5 factors of IPI were of great significance and were included in the multivariate analysis. In the Cox proportional-hazards model, independent prognostic factors of inferior PFS and OS were age (P both <0.001), along with Ann Arbor stage (P both <0.001), serum LDH (P both <0.001), performance status (P both <0.001), and multiple extranodal involvement (P both <0.05) (**Table 2**). Similar results were observed based on age factor according to NCCN-IPI. The 3-year PFS and OS rates of patients >75 years were 51.2 and 57.6%, significantly lower than those of patients 61–75 years (62.0 and 72.8%), 41–60 years (72.5 and 83.4%), and ≤40 years (71.4 and 82.8%) (**Figures 2C, D**).

Oncogenic Mutation Alterations Related to Age at Diagnosis

Oncogenic mutations closely related to age at diagnosis were analyzed in 1,150 patients, namely, 117 cases by WGS, 223 cases by WES, and 810 cases by targeted sequencing. A total of 55 genes related to the tumorigenesis of DLBCL were analyzed (**Figure 3A**). The association of oncogenic mutations and age at diagnosis among the patients were assessed by univariate logistic regression. Eight genes were significantly correlated with age (**Figure 3B**), namely, *PIM1* (OR = 1.015, 95% CI = 1.005–1.026, P = 0.002), *MYD88* (OR = 1.022, 95% CI = 1.011–1.033, P <0.001), *BTG2* (OR = 1.014, 95% CI = 1.003–1.025, P = 0.015), *CD79B* (OR = 1.030, 95% CI = 1.016–1.044, P <0.001), TET2 (OR = 1.016, 95% CI = 1.003-1.030, P = 0.014), *BTG1* (OR = 1.014, 95% CI = 1.001–1.028, P = 0.037), *CREBBP* (OR = 1.016, 95% CI = 1.002–1.031, P = 0.025), and *TBL1XR1* (OR = 1.019, 95% CI = 1.002–1.036, P = 0.025). Meanwhile, the same results were observed on $MYD88^{L265P}$ mutation alone (OR = 1.024, 95% CI = 1.011–1.037, P <0.001), or with *CD79B* mutation (OR = 1.038, 95% CI = 1.013–1.064, P = 0.002) (**Figure 3C**).

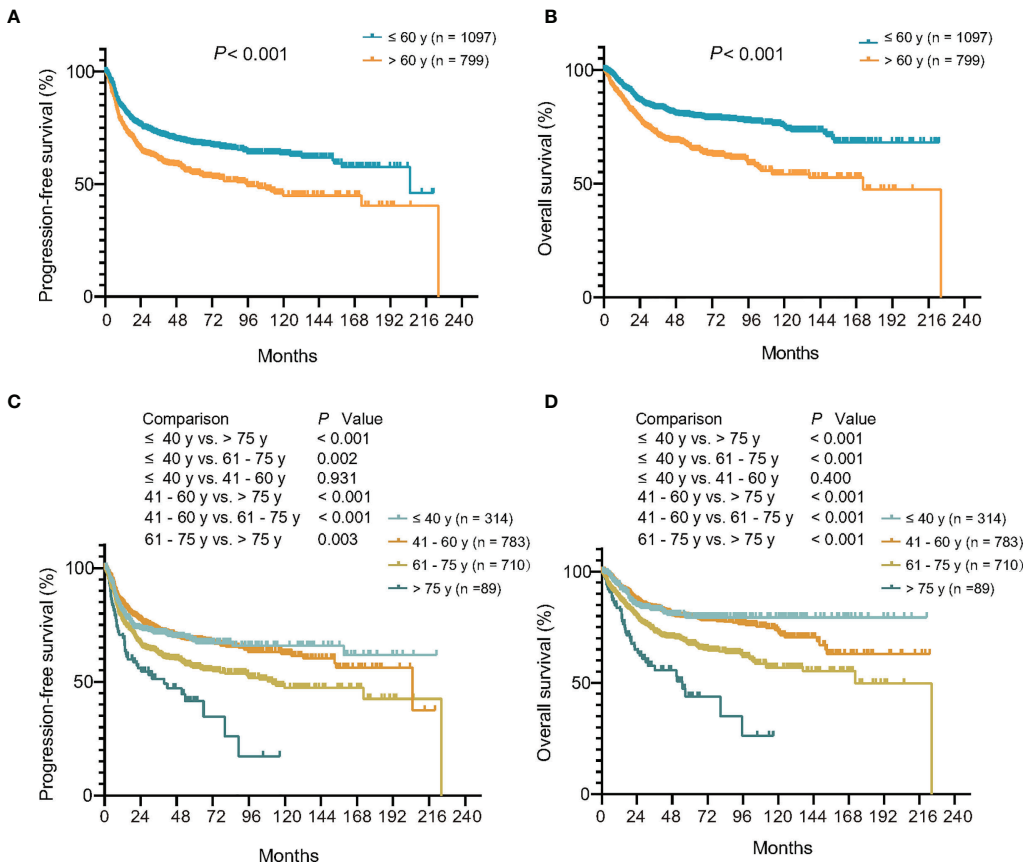

FIGURE 2 | Relationship between age at diagnosis and clinical outcome upon R-CHOP-based immunochemotherapy. **(A, B)** Kaplan–Meier models of progression-free survival **(A)** and overall survival **(B)** according to age at diagnosis of IPI. **(C, D)** Kaplan–Meier models of progression-free survival **(C)** and overall survival **(D)** according to age at diagnosis of NCCN-IPI. R-CHOP, rituximab, cyclophosphamide, doxorubicin, vincristine, and prednisone; IPI, International Prognostic Index; NCCN, National Comprehensive Cancer Network database.

TABLE 2 | Univariate and multivariate analysis for PFS and OS of DLBCL patients (n = 1,896).

	PFS				OS			
	Univariate analysis		Multivariate analysis		Univariate analysis		Multivariate analysis	
	P-value	HR (95% CI)	*P*-value	HR (95% CI)	*P*-value	HR (95% CI)	*P*-value	HR (95% CI)
Age, >60 year	<0.001	1.555 (1.333–1.813)	<0.001	1.394 (1.194–1.628)	<0.001	1.898 (1.577–2.284)	<0.001	1.710 (1.419–2.060)
AA stage, III–IV	<0.001	3.175 (2.693–3.743)	<0.001	2.090 (1.728–2.529)	<0.001	3.506 (2.860–4.297)	<0.001	2.062 (1.634–2.602)
Serum LDH	<0.001	2.994 (2.551–3.513)	<0.001	2.038 (1.714–2.424)	<0.001	3.946 (3.225–4.829)	<0.001	2.652 (2.135–3.294)
ECOG score, ≥2	<0.001	2.772 (2.261–3.399)	<0.001	1.732 (1.404–2.136)	<0.001	3.184 (2.530–4.007)	<0.001	1.887 (1.490–2.390)
ENI, ≥2	<0.001	2.369 (2.015–2.785)	0.018	1.244 (1.039–1.491)	<0.001	2.523 (2.086–3.052)	0.030	1.262 (1.023–1.557)

DLBCL, diffuse large B-cell lymphoma; PFS, progression-free survival; OS, overall survival; HR, hazard ratio; AA, Ann Arbor; LDH, lactate dehydrogenase; ECOG, Eastern Cooperative Oncology Group; ENI, extranodal involvement.

All 1,150 patients were genetically classified (21), namely, MYD88-like (191, 16.6%), SOCS1/SGK1-like (148, 12.9%), BCL2-like (222, 19.3%), and NEC-like subtype (589, 51.2%). MYD88-like subtype was significantly associated with age (OR = 1.024, 95% CI = 1.012–1.036, P <0.001) (**Figure 3D**). Based on biological functions, mutations involving BCR/NF-κB signaling (OR = 1.017, 95% CI = 1.009–1.026, *P* <0.001), B-cell differentiation (OR = 1.012, 95% CI = 1.003–1.020, *P* = 0.009), and histone acetylation (OR = 1.012, 95% CI = 1.002–1.023, *P* = 0.018) were significantly associated with age (**Figure 3E**). The total mutation load in the coding genome also showed positive correlation with age in 340 patients with WGS or WES data (*P* = 0.005, r = 0.152) (**Figure 3F**).

Tumor Microenvironment Alterations Related to Age at Diagnosis

The abundance of immune cells in tumor microenvironment was evaluated using RNA sequencing data. The association between the abundance of immune cells and age was estimated using Spearman's rank correlation. With abundance of $CD4^+$ naïve T and $CD8^+$ naïve T cells decreased at age (*P* = 0.006 and *P* = 0.006), and abundance of exhausted T cells and macrophages increased with age (*P* = 0.002 and *P* = 0.046) (**Figure 4A**).

As exhausted T cells and macrophages play essential roles in immune evasion, their relations with age-associated mutations and effects on tumor progression were further assessed. All the patients were subsequently divided into two groups according to the median of abundance of the two immune cells, respectively. *CD79B* mutations were found more frequently mutated in the exhausted T-high group and macrophage-high group (*P* = 0.009 and *P* = 0.030) (**Figure 4B**). As revealed by GSEA, BCR signaling pathway was upregulated according to *CD79B* mutations (**Supplementary Figure 1A**). *IL10*, one of the key cytokines associated with T-cell exhaustion and macrophage M2 polarization, was found significantly higher in *CD79B* mutation patients (*P* = 0.001) (**Supplementary Figure 1B**). The abundance of macrophages showed positive linear correlations with the abundance of exhausted T cells (*P* <0.001) (**Figure 4C**).

Correspondingly, GSEA analysis revealed negative regulation of T-cell immunity (T-cell differentiation, lymphocyte activation, and T-cell proliferation, and IL-2 production), upregulation of PD-1 signaling, inhibitory cytokines production and signaling, and also the recruitment of the inhibitory immune cells in exhausted T-high group, as compared to exhausted T-low patients (**Figure 4D**). *IL10*, but not *TGFB1* (TGFβ), showed positive linear correlations with the abundance of exhausted T-cells (*P* <0.001) (**Supplementary Figure 2A**). When analyzing the expression levels of inhibitory receptors and their ligands and the abundance of exhausted T cells, inhibitory receptors, namely, *LAG3*, *PDCD1* (PD-1), *CD244* (2B4), *HAVCR2* (TIM3), *CTLA4*, *TIGIT*, *CD160*, and *BTLA*, and ligands to inhibitory receptors, namely, *TNFRSF14* (HVEM), *LGALS9*, *PDCD1LG2* (PDL2), *CD48*, and *CD274* (PDL1) showed positive linear correlations with the abundance of exhausted T cells (all *P* <0.05) (**Figure 4E** and **Supplementary Figure 2B**). Among them, the expression of *CD244* and *PDCD1* was increased with age (*P* = 0.016 and *P* = 0.031) (**Supplementary Figure 2C**).

According to the abundance of macrophages, GSEA analysis indicated that upregulation of macrophage recruitment and activation, immunoregulatory interactions of lymphoid and non-lymphoid cells, inflammation, collagen degradation, PD-1 signaling, angiogenesis, aging, and also inhibitory cytokine production and signaling in macrophage-high group, as compared to macrophage-low group (**Figure 5A**). Markers of macrophage M1 and M2 were further compared, showing that M2 markers, namely, *CD163* (log_2foldchange = 2.693, *P* <0.001), *MSR1* (log_2foldchange = 2.785, *P* <0.001), and *MRC1* (log_2foldchange = 1.807, *P* <0.001) were significantly upregulated in macrophage-high group (**Figure 5B**). Meanwhile, cytokines *IL10*, *CSF1*, *IL1B*, *IL6*, and *TGFB1*, which were involved in M2 polarization, showed positive linear correlations with the abundance of macrophages (all *P* <0.001) (**Supplementary Figure 3A**). Since macrophages may contribute to T-cell exhaustion through the expression of ligands to inhibitory receptors, the relationships between the expression levels of inhibitory receptors and their ligands with the abundance of macrophages were analyzed. Among them, ligands to inhibitory receptors, namely, *PDCD1LG2*, *CD274*, *LGALS9*, *TNFRSF14*, *PVR*, and *CD48*, and also inhibitory receptors, namely, *HAVCR2*, *CD244*, *LAG3*, *VSIR* (VISTA), *PDCD1*, *CTLA4*, *CD160*, and *ENTPD1* (CD39), showed positive linear correlations with the abundance of macrophages (all P <0.05) (**Figure 5C** and **Supplementary Figure 3B**). When analyzing the expression levels of chemokines and the abundance of macrophage, chemokines related to macrophage recruitment *CCL8*, *CXCL16*, *CCL2*, *CCL18*, *CCL3*, *CCL4*, *CCL5*, *CXCL12*, *CXCL8*, *CX3CL1*, *CCL14*, and *CCL26* showed positive linear correlations with the abundance of macrophages (all *P* <0.05) (**Figure 5D**). Among these chemokines, the expression of *CCL3* and *CCL5* was increased with age (*P* = 0.024 and *P* = 0.045) (**Supplementary Figure 3C**).

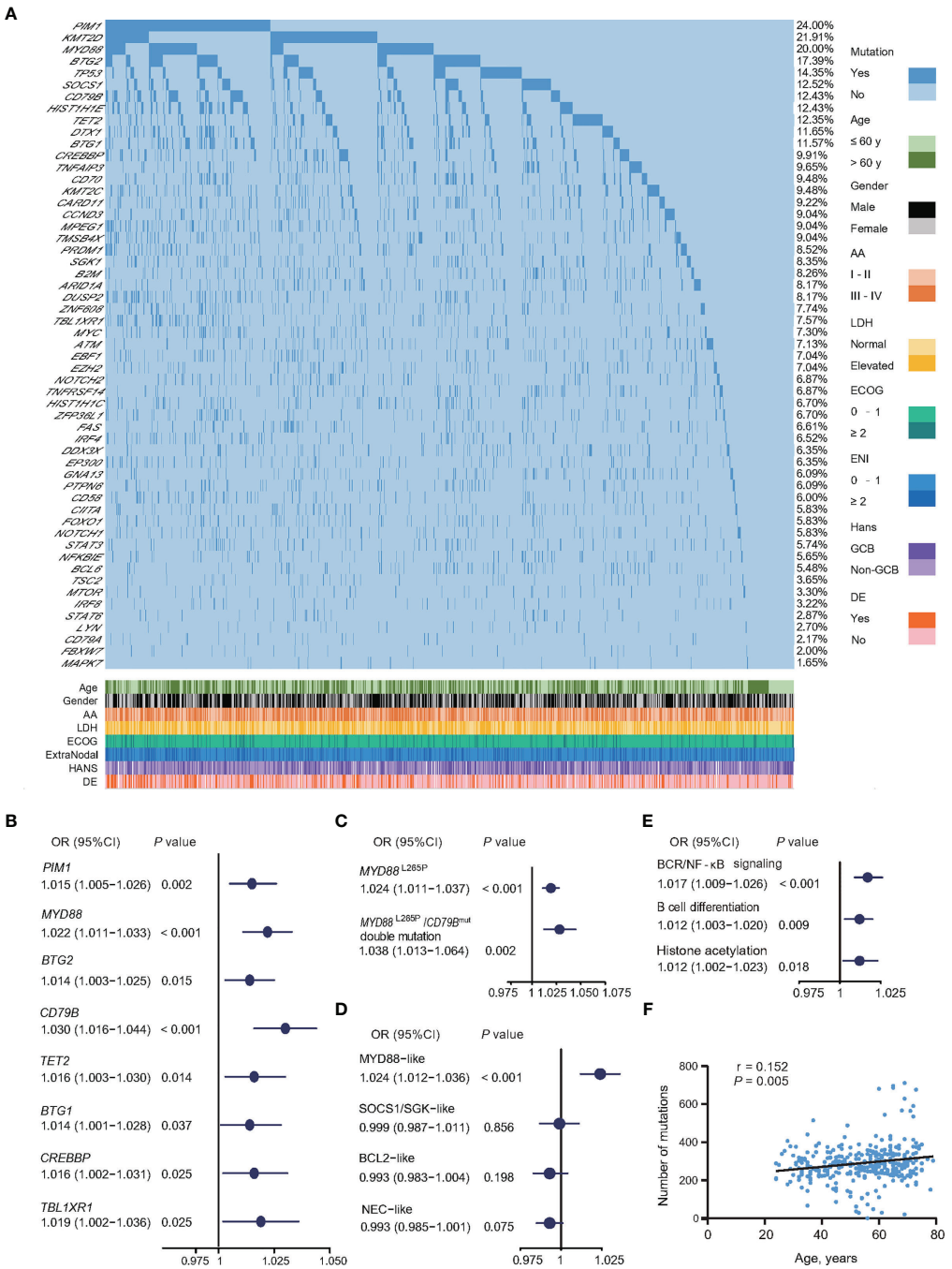

FIGURE 3 | Relationship between oncogenic mutations and age at diagnosis in DLBCL. **(A)** Oncogenic mutations identified by WGS/WES/targeted sequencing in DLBCL patients. **(B)** Univariate logistic regression analysis of oncogenic mutations according to age at diagnosis. **(C)** Univariate logistic regression analysis of *MYD88*^{L265P} mutations alone or with *CD79B* mutations according to age at diagnosis. **(D)** Univariate logistic regression analysis of genetic subtypes according to age at diagnosis. **(E)** Univariate logistic regression analysis of oncogenic pathways according to age at diagnosis. **(F)** Correlation between the number of oncogenic mutations sequenced by WGS/WES and age at diagnosis in DLBCL. **(B–E)** Odd ratios (OR), 95% confidence intervals (95% CI), and *P*-values are indicated on the left of each forest plot. DLBCL, diffuse large B-cell lymphoma; WGS, whole genome sequencing; WES, whole exome sequencing; AA, Ann Arbor; LDH, lactate dehydrogenase; ECOG, Eastern Cooperative Oncology Group; ENI, extranodal involvement; DE, double expressor; GCB, germinal center B-cell.

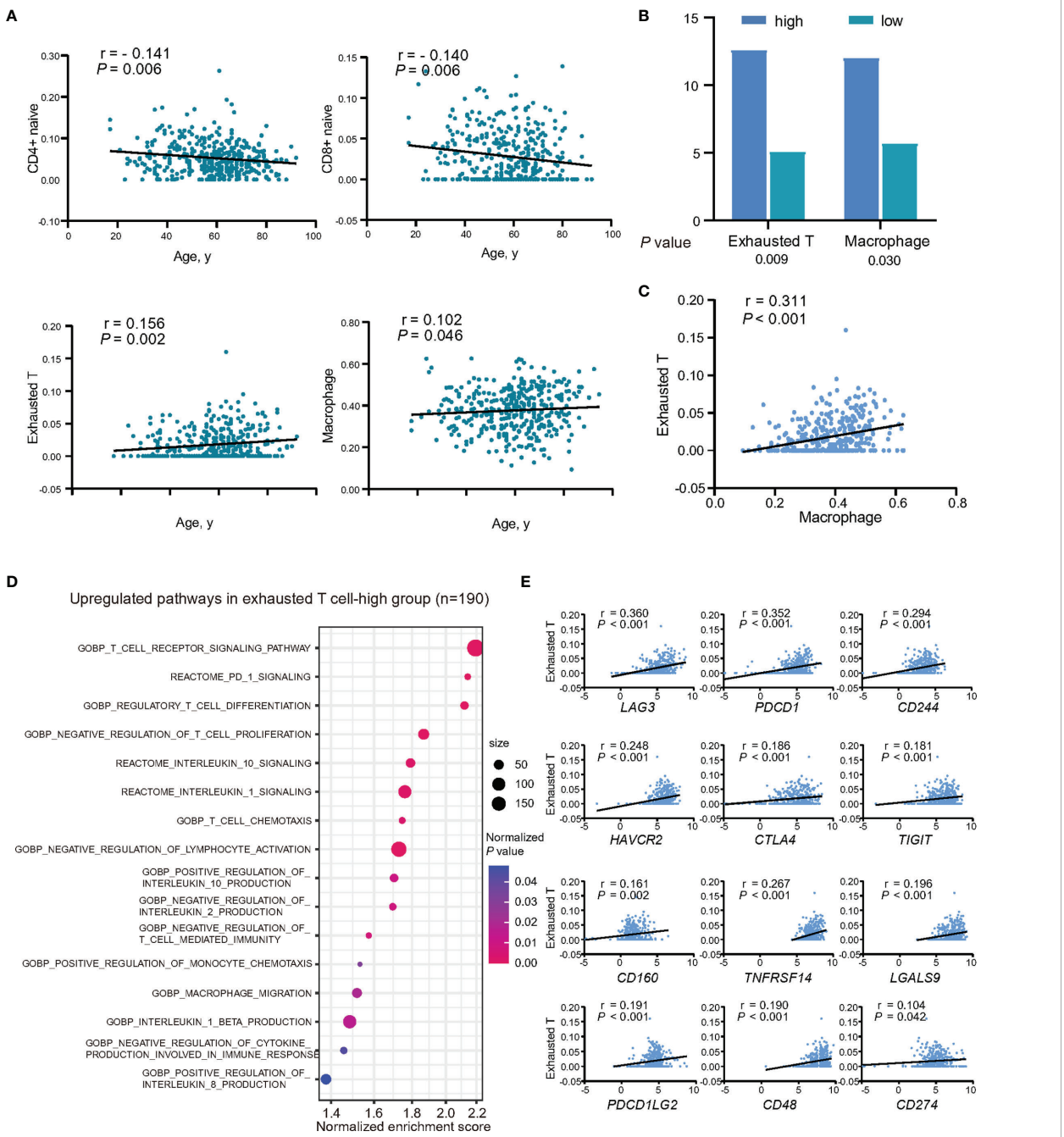

FIGURE 4 | Relationship between intratumor immune cells and age at diagnosis in DLBCL. **(A)** Abundance of immune cell subtypes in patients showing decreased or increased trend with age at diagnosis. **(B)** Mutation rates of *CD79B* between exhausted T-high group and exhausted T-low group, and also between macrophage-high group and macrophage-low group. Lower graph indicates *P*-values. **(C)** Correlation between the abundance of exhausted T cells and macrophages. *P*-value and r-value were indicated in the plot. **(D)** Pathway enrichment analysis in exhausted T-high group (n = 190), as compared to exhausted T-low group (n = 195, *P* <0.05). Color of points indicates normalized *P*-value of upregulated pathways in two groups. Size of points indicates number of genes included in each gene set. **(E)** Correlations between the expression of inhibitory receptors, ligands, and the abundance of exhausted T cells. *P*-values and r-values were indicated in each plot.

DISCUSSION

Age at diagnosis is one of the major risk factors in DLBCL, resulting in poor response to R-CHOP-based immunochemotherapy and adverse clinical outcomes, particularly in patients diagnosed over 75 years. In our cohort, older DLBCL presented advanced disease stage, elevated serum LDH, poor performance status, multiple extranodal involvement, high percentage of double expressor

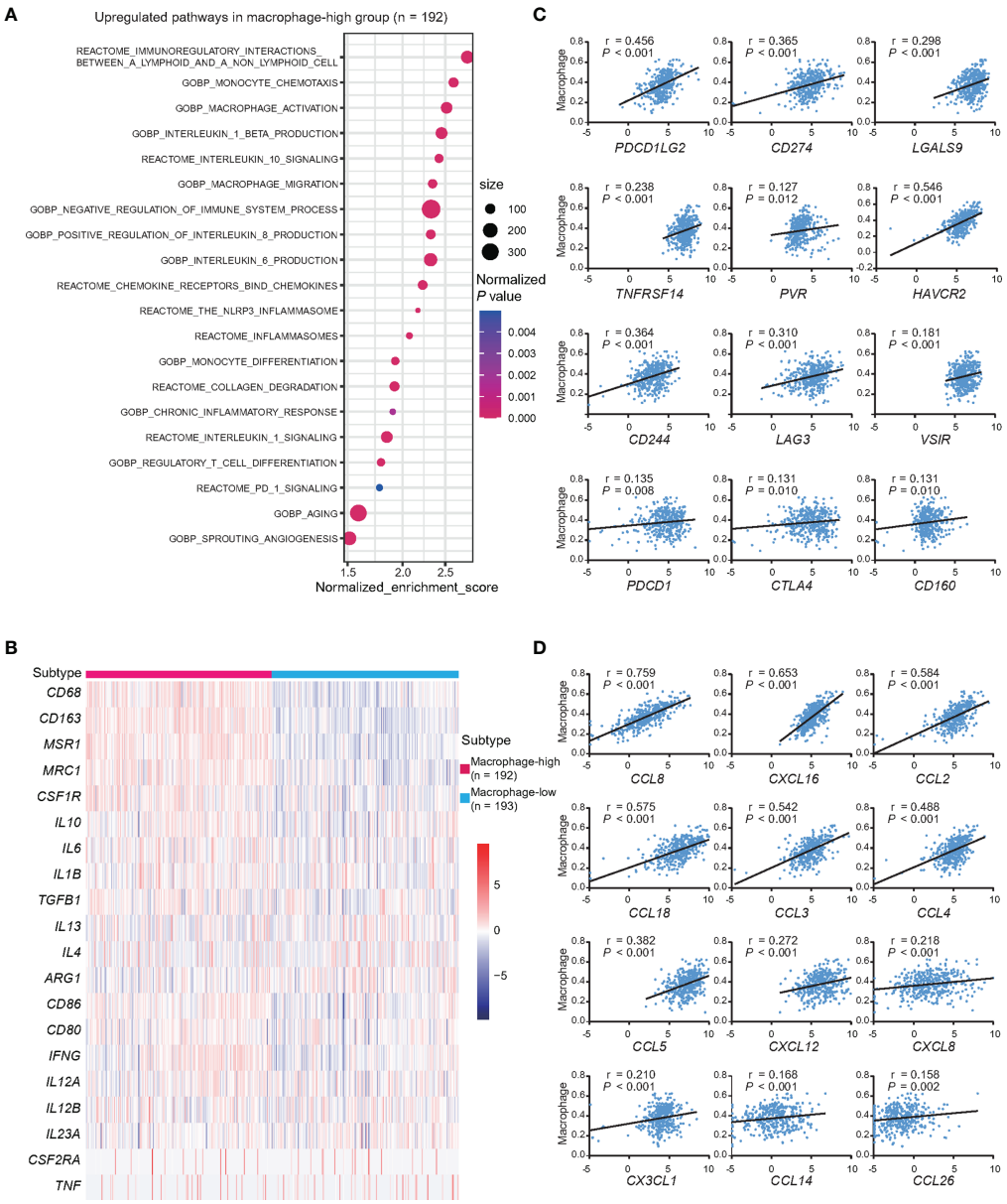

FIGURE 5 | Dysfunctions of macrophages and age at diagnosis in DLBCL. **(A)** Pathway enrichment analysis in macrophage-high group (n = 192), as compared to macrophages-low group (n = 193, *P* <0.05). Color of points indicates normalized *P*-value of upregulated pathways in two groups. Size of points indicates number of genes included in each gene set. **(B)** Heatmap of genes associated with the markers of macrophage M2 and M1 in macrophage-high group (n = 192), as compared to macrophages-low group (n = 193). **(C)** Correlations between the expression of inhibitory receptors, ligands, and the abundance of macrophages. *P*-values and r-values were indicated in each plot. **(D)** Correlations between the expression of chemokines and the abundance of macrophages. *P*-values and r-values were indicated in each plot.

subtype, and poor prognosis, which may be resulted from specific biological features.

Based on the genomic data of a large cohort, we observed overall enhanced mutagenesis in the coding region as the age at diagnosis increased in DLBCL, probably due to spontaneous deamination (22). Among oncogenic mutations, eight genes manifested positive association with age at diagnosis. *PIM1*, *MYD88*, and *CD79B* mutations are frequent mutations related to MYD88 genetic subtype and activated B cell-like DLBCL dependent on BCR signaling and constitutive activation of NF-κB pathway, which were found to be enriched in patients that experienced inferior survival and early progression upon R-CHOP treatment (23–26). *BTG2* and *BTG1* were considered as anti-proliferation genes and frequently deleted or mutated in hematological malignancies with aggressive cell behavior and treatment resistance (27). *TET2* mutations impaired enhancer

H3K27 acetylation and disrupted transit of B cells through germinal centers, leading to lymphomagenesis (28). *CREBBP* mutations resulted in reduced histone H3 acetylation, enhanced cell proliferation and low expression of MHC II, provoking immune evasion and disease progression (29, 30). *TBL1XR1* mutations co-opted SMRT/HDAC3 repressor complexes toward binding the memory B-cell transcription factor BACH2 and disrupted the differentiation into plasma cells, leading to a striking extranodal immunoblastic lymphoma phenotype (31). Moreover, based on biological functions, mutations involving BCR/NF-κB signaling, B-cell differentiation, and histone acetylation were positively associated with age at diagnosis, which provides potential therapeutic targets, such as BTK inhibitors and epigenetic regulators (32, 33). Together, distinct oncogenic mutations function as important determinators for disease progression in older DLBCL patients and older DLBCL might be considered as a specific entity associated with genetic subtyping.

Tumor microenvironment is also implicated in DLBCL progression. Decreased $CD4^+$ naïve T and $CD8^+$ naïve T cells were age-related, due to declined production of new T cells from involuted and nonfunctional thymus and results in reduced richness of the TCR repertoire in aging populations (34). Exhausted T cells and macrophages were increased in older patients and related to age-related mutations, particularly *CD79B*. As mechanism of action, *CD79B* mutations contributed to activation of BCR signaling and resulted in upregulated expression of *IL10*, a key immunosuppressive cytokine linked to T-cell exhaustion and macrophage M2 polarization (35, 36). Higher abundance of exhausted T cells presented the suppression of T-cell immunity and upregulation of PD-1 signaling, related to recruitment of immunosuppressive cells and production of immunosuppressive cytokines. The positive correlation between the expression of *IL10* and the abundance of exhausted T cells pointed out that IL10 might be involved in T-cell exhaustion in DLBCL (37). Meanwhile, several inhibitory receptors and ligands were positively correlated to the abundance of exhausted T cells, among which *CD244* and *PDCD1* showed correlation to age (10, 38). Indeed, the inhibitory receptors co-expressed at high levels on T cells and synergistically mediated T-cell exhaustion and dysfunction with the ligands on tumor cells and antigen presenting cells, which implies combinations of agents blocking inhibitory receptors may function in older DLBCL patients to overcome T-cell exhaustion and to restore anti-tumor immunity.

Macrophages constitute a major component of tumor microenvironment and are involved in cancer progression, metastasis and immune evasion, creating an immunosuppressive microenvironment through secretion of anti-inflammatory cytokines, expression of PD-L1, and recruitment of Th2 and Treg cells (39, 40). This was in keeping with the results by pathway analysis that higher abundance of macrophages was associated with the enrichment pathways of negative regulation of immune, chronic inflammatory response, collagen degradation, angiogenesis, and PD-1 signaling in macrophage-high DLBCL. Importantly, higher abundance of macrophages also manifested increased expression of markers of immunosuppressive macrophage M2, namely, *CD163*, *MSR1*, and *MRC1* (41–43). The positive correlation between the expression of cytokines of M2 polarization and the abundance of macrophages suggested that *IL10*, *CSF1*, *IL1B*, *IL6*, and *TGFB1* could involve in M2 polarization in DLBCL (44–48). As macrophages was a major source of immunosuppressive cytokines and showed positive correlation to inhibitory receptors and ligands, the abundance of macrophages was in positive correlation with exhausted T cells and could contribute to age-related immunosuppression in DLBCL (40, 49). Several chemokines related to macrophage chemotaxis and immunosuppressive function increased with macrophage, and among them, *CCL3* and *CCL5* are secreted factors of senescence-associated secretory phenotype and increased with age and age-associated macrophage recruitment (50). Macrophage infiltrations were linked to poor prognosis in DLBCL, suggesting inhibition of macrophages may also be alternative immunomodulatory strategy in DLBCL (14).

However, there was a difference in distribution of clinical features between western and Chinese DLBCL populations according to previous reports and our cohort, namely, age at diagnosis (median age: 62–66 years vs. 53–59 years), Ann Arbor stage (III–IV: 54.1–62.8% vs. 35.2–57.4%), and performance status (Eastern Cooperative Oncology Group score ≥2: 16.7–37.3% vs. 13.0–19.9%) (21, 51–60). Future epidemiology studies are necessary to elucidate the different characteristics between western and eastern countries, which may provide better understanding of targeted therapeutic approaches in DLBCL.

In conclusion, older DLBCL could be a specific entity with unfavorable clinical and molecular features, represented by accumulation of oncogenic mutations and immunosuppressive tumor microenvironment alterations. Thus, clinical studies on immunotherapies warrant further investigation on future mechanism-based treatment in older DLBCL.

DATA AVAILABILITY STATEMENT

The datasets including WGS, WES and RNA sequencing data were deposited on The National Omics Data Encyclopedia (https://www.biosino.org/node) in project OEP001143 and OEP001040.

ETHICS STATEMENT

The studies involving human participants were reviewed and approved by the Shanghai Rui Jin Hospital Review Board. Written informed consent to participate in this study was provided by the participants.

AUTHOR CONTRIBUTIONS

WLZ, PPX, QT, LW, and SC designed and supervised the study. YZ collected and analyzed the data, and wrote the manuscript. DF, QS, and ZYS recruited patients, collected study data, and

prepared biological samples. LD and HMY reviewed the histopathologic diagnoses. ZHL acquired the biological samples. YF, QL and HF provided technical support for bioinformatic analysis. All authors listed have made a substantial, direct, and intellectual contribution to the work and approved it for publication.

ACKNOWLEDGMENTS

We sincerely appreciate the efforts of the doctors for enrolling patients and all the patients enrolled for allowing us to analyze their clinical data. Meanwhile, we thank the fundings supported by the National Natural Science Foundation of China (82130004, 81830007 and 82070204), Shanghai Municipal Education Commission Gaofeng Clinical Medicine (20152206 and 20152208), Multicenter Clinical Research Project by Shanghai Jiao Tong University School of Medicine (DLY201601), Clinical Research Plan of Shanghai Hospital Development Center (SHDC2020CR1032B), Chang Jiang Scholars Program, Samuel Waxman Cancer Research Foundation, and the Foundation of National Facility for Translational Medicine (Shanghai, TMSK-2020-115).

SUPPLEMENTARY MATERIAL

The Supplementary Material for this article can be found online at: https://www.frontiersin.org/articles/10.3389/fimmu.2022.842439/full#supplementary-material

REFERENCES

1. Project INHsLPF. A Predictive Model for Aggressive non-Hodgkin's Lymphoma. *N Engl J Med* (1993) 329(14):987–94. doi: 10.1056/NEJM199309303291402
2. Zhou Z, Sehn LH, Rademaker AW, Gordon LI, Lacasce AS, Crosby-Thompson A, et al. An Enhanced International Prognostic Index (NCCN-IPI) for Patients With Diffuse Large B-Cell Lymphoma Treated in the Rituximab Era. *Blood* (2014) 123(6):837–42. doi: 10.1182/blood-2013-09-524108
3. Vijg J, Dong X. Pathogenic Mechanisms of Somatic Mutation and Genome Mosaicism in Aging. *Cell* (2020) 182(1):12–23. doi: 10.1016/j.cell.2020.06.024
4. Di M, Huntington SF, Olszewski AJ. Challenges and Opportunities in the Management of Diffuse Large B-Cell Lymphoma in Older Patients. *Oncologist* (2021) 26(2):120–32. doi: 10.1002/onco.13610
5. Kim Y, Ju H, Kim DH, Yoo HY, Kim SJ, Kim WS, et al. CD79B and MYD88 Mutations in Diffuse Large B-Cell Lymphoma. *Hum Pathol* (2014) 45(3):556–64. doi: 10.1016/j.humpath.2013.10.023
6. Xie M, Lu C, Wang J, McLellan MD, Johnson KJ, Wendl MC, et al. Age-Related Mutations Associated With Clonal Hematopoietic Expansion and Malignancies. *Nat Med* (2014) 20(12):1472–8. doi: 10.1038/nm.3733
7. Niroula A, Sekar A, Murakami MA, Trinder M, Agrawal M, Wong WJ, et al. Distinction of Lymphoid and Myeloid Clonal Hematopoiesis. *Nat Med* (2021) 27(11):1921–7. doi: 10.1038/s41591-021-01521-4
8. Lian J, Yue Y, Yu W, Zhang Y. Immunosenescence: A Key Player in Cancer Development. *J Hematol Oncol* (2020) 13(1):151. doi: 10.1186/s13045-020-00986-z
9. Kasakovski D, Xu L, Li Y. T Cell Senescence and CAR-T Cell Exhaustion in Hematological Malignancies. *J Hematol Oncol* (2018) 11(1):91. doi: 10.1186/s13045-018-0629-x
10. Wherry EJ, Kurachi M. Molecular and Cellular Insights Into T Cell Exhaustion. *Nat Rev Immunol* (2015) 15(8):486–99. doi: 10.1038/nri3862
11. Jackaman C, Nelson DJ. Are Macrophages, Myeloid Derived Suppressor Cells and Neutrophils Mediators of Local Suppression in Healthy and Cancerous Tissues in Aging Hosts? *Exp Gerontol* (2014) 54:53–7. doi: 10.1016/j.exger.2013.11.009
12. Swerdlow SH, Campo E, Pileri SA, Harris NL, Stein H, Siebert R, et al. The 2016 Revision of the World Health Organization Classification of Lymphoid Neoplasms. *Blood* (2016) 127(20):2375–90. doi: 10.1182/blood-2016-01-643569
13. Shen R, Xu PP, Wang N, Yi HM, Dong L, Fu D, et al. Influence of Oncogenic Mutations and Tumor Microenvironment Alterations on Extranodal Invasion in Diffuse Large B-Cell Lymphoma. *Clin Transl Med* (2020) 10(7):e221. doi: 10.1002/ctm2.221
14. Huang YH, Cai K, Xu PP, Wang L, Huang CX, Fang Y, et al. CREBBP/EP300 Mutations Promoted Tumor Progression in Diffuse Large B-Cell Lymphoma Through Altering Tumor-Associated Macrophage Polarization *via* FBXW7-NOTCH-CCL2/CSF1 Axis. *Signal Transduct Target Ther* (2021) 6(1):10. doi: 10.1038/s41392-020-00437-8
15. Qin W, Fu D, Shi Q, Dong L, Yi H, Huang H, et al. Molecular Heterogeneity in Localized Diffuse Large B-Cell Lymphoma. *Front Oncol* (2021) 11:638757. doi: 10.3389/fonc.2021.638757
16. Li MM, Datto M, Duncavage EJ, Kulkarni S, Lindeman NI, Roy S, et al. Standards and Guidelines for the Interpretation and Reporting of Sequence Variants in Cancer: A Joint Consensus Recommendation of the Association for Molecular Pathology, American Society of Clinical Oncology, and College of American Pathologists. *J Mol Diagn* (2017) 19(1):4–23. doi: 10.1016/j.jmoldx.2016.10.002
17. Anders S, Pyl PT, Huber W. HTSeq–a Python Framework to Work With High-Throughput Sequencing Data. *Bioinformatics* (2015) 31(2):166–9. doi: 10.1093/bioinformatics/btu638
18. Scott DW, Wright GW, Williams PM, Lih CJ, Walsh W, Jaffe ES, et al. Determining Cell-of-Origin Subtypes of Diffuse Large B-Cell Lymphoma Using Gene Expression in Formalin-Fixed Paraffin-Embedded Tissue. *Blood* (2014) 123(8):1214–7. doi: 10.1182/blood-2013-11-536433
19. Miao YR, Zhang Q, Lei Q, Luo M, Xie GY, Wang H, et al. ImmuCellAI: A Unique Method for Comprehensive T-Cell Subsets Abundance Prediction and its Application in Cancer Immunotherapy. *Adv Sci (Weinh)* (2020) 7 (7):1902880. doi: 10.1002/advs.201902880
20. Hans CP, Weisenburger DD, Greiner TC, Gascoyne RD, Delabie J, Ott G, et al. Confirmation of the Molecular Classification of Diffuse Large B-Cell Lymphoma by Immunohistochemistry Using a Tissue Microarray. *Blood* (2004) 103(1):275–82. doi: 10.1182/blood-2003-05-1545
21. Lacy SE, Barrans SL, Beer PA, Painter D, Smith AG, Roman E, et al. Targeted Sequencing in DLBCL, Molecular Subtypes, and Outcomes: A Haematological Malignancy Research Network Report. *Blood* (2020) 135(20):1759–71. doi: 10.1182/blood.2019003535
22. Chapuy B, Stewart C, Dunford AJ, Kim J, Kamburov A, Redd RA, et al. Molecular Subtypes of Diffuse Large B Cell Lymphoma are Associated With Distinct Pathogenic Mechanisms and Outcomes. *Nat Med* (2018) 24(5):679–90. doi: 10.1038/s41591-018-0016-8
23. Hartert KT, Wenzl K, Krull JE, Manske M, Sarangi V, Asmann Y, et al. Targeting of Inflammatory Pathways With R2CHOP in High-Risk DLBCL. *Leukemia* (2021) 35(2):522–33. doi: 10.1038/s41375-020-0766-4
24. Wilson WH, Young RM, Schmitz R, Yang Y, Pittaluga S, Wright G, et al. Targeting B Cell Receptor Signaling With Ibrutinib in Diffuse Large B Cell Lymphoma. *Nat Med* (2015) 21(8):922–6. doi: 10.1038/nm.3884
25. Ma J, Yan Z, Zhang J, Zhou W, Yao Z, Wang H, et al. A Genetic Predictive Model for Precision Treatment of Diffuse Large B-Cell Lymphoma With Early Progression. *Biomark Res* (2020) 8:33. doi: 10.1186/s40364-020-00214-3
26. Pedrosa L, Fernandez-Miranda I, Perez-Callejo D, Quero C, Rodriguez M, Martin-Acosta P, et al. Proposal and Validation of a Method to Classify Genetic Subtypes of Diffuse Large B Cell Lymphoma. *Sci Rep* (2021) 11 (1):1886. doi: 10.1038/s41598-020-80376-0

27. Yuniati L, Scheijen B, van der Meer LT, van Leeuwen FN. Tumor Suppressors BTG1 and BTG2: Beyond Growth Control. *J Cell Physiol* (2019) 234(5):5379–89. doi: 10.1002/jcp.27407
28. Dominguez PM, Ghamlouch H, Rosikiewicz W, Kumar P, Beguelin W, Fontan L, et al. TET2 Deficiency Causes Germinal Center Hyperplasia, Impairs Plasma Cell Differentiation, and Promotes B-Cell Lymphomagenesis. *Cancer Discov* (2018) 8(12):1632–53. doi: 10.1158/2159-8290.CD-18-0657
29. Hashwah H, Schmid CA, Kasser S, Bertram K, Stelling A, Manz MG, et al. Inactivation of CREBBP Expands the Germinal Center B Cell Compartment, Down-Regulates MHCII Expression and Promotes DLBCL Growth. *Proc Natl Acad Sci USA* (2017) 114(36):9701–6. doi: 10.1073/pnas.1619555114
30. Mondello P, Tadros S, Teater M, Fontan L, Chang AY, Jain N, et al. Selective Inhibition of HDAC3 Targets Synthetic Vulnerabilities and Activates Immune Surveillance in Lymphoma. *Cancer Discov* (2020) 10(3):440–59. doi: 10.1158/2159-8290.CD-19-0116
31. Venturutti L, Teater M, Zhai A, Chadburn A, Babiker L, Kim D, et al. TBL1XR1 Mutations Drive Extranodal Lymphoma by Inducing a Pro-Tumorigenic Memory Fate. *Cell* (2020) 182(2):297–316.e27. doi: 10.1016/j.cell.2020.05.049
32. Dunleavy K, Erdmann T, Lenz G. Targeting the B-Cell Receptor Pathway in Diffuse Large B-Cell Lymphoma. *Cancer Treat Rev* (2018) 65:41–6. doi: 10.1016/j.ctrv.2018.01.002
33. Hogg SJ, Beavis PA, Dawson MA, Johnstone RW. Targeting the Epigenetic Regulation of Antitumour Immunity. *Nat Rev Drug Discov* (2020) 19 (11):776–800. doi: 10.1038/s41573-020-0077-5
34. Cunha LL, Perazzio SF, Azzi J, Cravedi P, Riella LV. Remodeling of the Immune Response With Aging: Immunosenescence and Its Potential Impact on COVID-19 Immune Response. *Front Immunol* (2020) 11:1748. doi: 10.3389/fimmu.2020.01748
35. Li L, Zhang J, Chen J, Xu-Monette ZY, Miao Y, Xiao M, et al. B-Cell Receptor-Mediated NFATc1 Activation Induces IL-10/STAT3/PD-L1 Signaling in Diffuse Large B-Cell Lymphoma. *Blood* (2018) 132(17):1805–17. doi: 10.1182/blood-2018-03-841015
36. Davis RE, Ngo VN, Lenz G, Tolar P, Young RM, Romesser PB, et al. Chronic Active B-Cell-Receptor Signalling in Diffuse Large B-Cell Lymphoma. *Nature* (2010) 463(7277):88–92. doi: 10.1038/nature08638
37. Brooks DG, Trifilo MJ, Edelmann KH, Teyton L, McGavern DB, Oldstone MB. Interleukin-10 Determines Viral Clearance or Persistence In Vivo. *Nat Med* (2006) 12(11):1301–9. doi: 10.1038/nm1492
38. Blackburn SD, Shin H, Haining WN, Zou T, Workman CJ, Polley A, et al. Coregulation of CD8+ T Cell Exhaustion by Multiple Inhibitory Receptors During Chronic Viral Infection. *Nat Immunol* (2009) 10(1):29–37. doi: 10.1038/ni.1679
39. DeNardo DG, Ruffell B. Macrophages as Regulators of Tumour Immunity and Immunotherapy. *Nat Rev Immunol* (2019) 19(6):369–82. doi: 10.1038/s41577-019-0127-6
40. Jackaman C, Tomay F, Duong L, Abdol Razak NB, Pixley FJ, Metharom P, et al. Aging and Cancer: The Role of Macrophages and Neutrophils. *Ageing Res Rev* (2017) 36:105–16. doi: 10.1016/j.arr.2017.03.008
41. Gundra UM, Girgis NM, Ruckerl D, Jenkins S, Ward LN, Kurtz ZD, et al. Alternatively Activated Macrophages Derived From Monocytes and Tissue Macrophages are Phenotypically and Functionally Distinct. *Blood* (2014) 123 (20):e110-22. doi: 10.1182/blood-2013-08-520619
42. Mantovani A, Sozzani S, Locati M, Allavena P, Sica A. Macrophage Polarization: Tumor-Associated Macrophages as a Paradigm for Polarized M2 Mononuclear Phagocytes. *Trends Immunol* (2002) 23(11):549–55. doi: 10.1016/S1471-4906(02)02302-5
43. Song Q, Hawkins GA, Wudel L, Chou PC, Forbes E, Pullikuth AK, et al. Dissecting Intratumoral Myeloid Cell Plasticity by Single Cell RNA-Seq. *Cancer Med* (2019) 8(6):3072–85. doi: 10.1002/cam4.2113
44. Jung M, Ma Y, Iyer RP, DeLeon-Pennell KY, Yabluchanskiy A, Garrett MR, et al. IL-10 Improves Cardiac Remodeling After Myocardial Infarction by Stimulating M2 Macrophage Polarization and Fibroblast Activation. *Basic Res Cardiol* (2017) 112(3):33. doi: 10.1007/s00395-017-0622-5
45. Pyonteck SM, Akkari L, Schuhmacher AJ, Bowman RL, Sevenich L, Quail DF, et al. CSF-1R Inhibition Alters Macrophage Polarization and Blocks Glioma Progression. *Nat Med* (2013) 19(10):1264–72. doi: 10.1038/nm.3337
46. Das S, Shapiro B, Vucic EA, Vogt S, Bar-Sagi D. Tumor Cell-Derived IL1beta Promotes Desmoplasia and Immune Suppression in Pancreatic Cancer. *Cancer Res* (2020) 80(5):1088–101. doi: 10.1158/0008-5472.CAN-19-2080
47. Weng YS, Tseng HY, Chen YA, Shen PC, Al Haq AT, Chen LM, et al. MCT-1/miR-34a/IL-6/IL-6R Signaling Axis Promotes EMT Progression, Cancer Stemness and M2 Macrophage Polarization in Triple-Negative Breast Cancer. *Mol Cancer* (2019) 18(1):42. doi: 10.1186/s12943-019-0988-0
48. Liu F, Qiu H, Xue M, Zhang S, Zhang X, Xu J, et al. MSC-Secreted TGF-Beta Regulates Lipopolysaccharide-Stimulated Macrophage M2-Like Polarization *via* the Akt/FoxO1 Pathway. *Stem Cell Res Ther* (2019) 10(1):345. doi: 10.1186/s13287-019-1447-y
49. Farhood B, Najafi M, Mortezaee K. CD8(+) Cytotoxic T Lymphocytes in Cancer Immunotherapy: A Review. *J Cell Physiol* (2019) 234(6):8509–21. doi: 10.1002/jcp.27782
50. Schafer MJ, Zhang X, Kumar A, Atkinson EJ, Zhu Y, Jachim S, et al. The Senescence-Associated Secretome as an Indicator of Age and Medical Risk. *JCI Insight* (2020) 5(12):e133668. doi: 10.1172/jci.insight.133668
51. El-Galaly TC, Villa D, Alzahrani M, Hansen JW, Sehn LH, Wilson D, et al. Outcome Prediction by Extranodal Involvement, IPI, R-IPI, and NCCN-IPI in the PET/CT and Rituximab Era: A Danish-Canadian Study of 443 Patients With Diffuse-Large B-Cell Lymphoma. *Am J Hematol* (2015) 90(11):1041–6. doi: 10.1002/ajh.24169
52. Ennishi D, Mottok A, Ben-Neriah S, Shulha HP, Farinha P, Chan FC, et al. Genetic Profiling of MYC and BCL2 in Diffuse Large B-Cell Lymphoma Determines Cell-of-Origin-Specific Clinical Impact. *Blood* (2017) 129 (20):2760–70. doi: 10.1182/blood-2016-11-747022
53. Keane C, Gill D, Vari F, Cross D, Griffiths L, Gandhi M. CD4(+) Tumor Infiltrating Lymphocytes are Prognostic and Independent of R-IPI in Patients With DLBCL Receiving R-CHOP Chemo-Immunotherapy. *Am J Hematol* (2013) 88(4):273–6. doi: 10.1002/ajh.23398
54. Montalban C, Diaz-Lopez A, Dlouhy I, Rovira J, Lopez-Guillermo A, Alonso S, et al. Validation of the NCCN-IPI for Diffuse Large B-Cell Lymphoma (DLBCL): The Addition of Beta2 -Microglobulin Yields a More Accurate GELTAMO-IPI. *Br J Haematol* (2017) 176(6):918–28. doi: 10.1111/bjh.14489
55. Scott DW, Mottok A, Ennishi D, Wright GW, Farinha P, Ben-Neriah S, et al. Prognostic Significance of Diffuse Large B-Cell Lymphoma Cell of Origin Determined by Digital Gene Expression in Formalin-Fixed Paraffin-Embedded Tissue Biopsies. *J Clin Oncol* (2015) 33(26):2848–56. doi: 10.1200/JCO.2014.60.2383
56. Han Y, Yang J, Liu P, He X, Zhang C, Zhou S, et al. Prognostic Nomogram for Overall Survival in Patients With Diffuse Large B-Cell Lymphoma. *Oncologist* (2019) 24(11):e1251–e61. doi: 10.1634/theoncologist.2018-0361
57. Li M, Liu CL, Yin WJ, He YX, Xue XM, Duan ZJ, et al. The Clinical Significance of a New Classification Algorithm in Chinese DLBCL Cases. *Zhonghua Xue Ye Xue Za Zhi* (2012) 33(10):801–4. doi: 10.3760/cma.j.issn.0253-2727.2012.10.003
58. Liu Y, Wang X, Ding N, Mi L, Ping L, Jin X, et al. TP53 Arg72 as a Favorable Prognostic Factor for Chinese Diffuse Large B-Cell Lymphoma Patients Treated With CHOP. *BMC Cancer* (2017) 17(1):743. doi: 10.1186/s12885-017-3760-0
59. Ren W, Ye X, Su H, Li W, Liu D, Pirmoradian M, et al. Genetic Landscape of Hepatitis B Virus-Associated Diffuse Large B-Cell Lymphoma. *Blood* (2018) 131(24):2670–81. doi: 10.1182/blood-2017-11-817601
60. Shi Y, Han Y, Yang J, Liu P, He X, Zhang C, et al. Clinical Features and Outcomes of Diffuse Large B-Cell Lymphoma Based on Nodal or Extranodal Primary Sites of Origin: Analysis of 1,085 WHO Classified Cases in a Single Institution in China. *Chin J Cancer Res* (2019) 31(1):152–61. doi: 10.21147/j.issn.1000-9604.2019.01.10

Conflict of Interest: The authors declare that the research was conducted in the absence of any commercial or financial relationships that could be construed as a potential conflict of interest.

frontiers | Frontiers in Immunology

ORIGINAL RESEARCH
published: 01 April 2022
doi: 10.3389/fimmu.2022.858021

Anti-PD-1 Therapy Enhances the Efficacy of CD30-Directed Chimeric Antigen Receptor T Cell Therapy in Patients With Relapsed/Refractory CD30+ Lymphoma

Wei Sang[1,2,3†], *Xiangmin Wang*[1,2,3†], *Hongzhi Geng*[4†], *Tianci Li*[1,2,3], *Dashan Li*[1,2,3], *Bingpei Zhang*[1,2,3], *Yi Zhou*[1,2,3], *Xuguang Song*[1,2,3], *Cai Sun*[1,2,3], *Dongmei Yan*[1,2,3], *Depeng Li*[1,2,3], *Zhenyu Li*[1,2,3], *Caixia Li*[4*] and *Kailin Xu*[1,2,3*]

[1] Department of Hematology, The Affiliated Hospital of Xuzhou Medical University, Xuzhou, China, [2] Blood Diseases Institute, Xuzhou Medical University, Xuzhou, China, [3] Key Laboratory of Bone Marrow Stem Cell, Xuzhou, China, [4] Department of Hematology, The First Affiliated Hospital of Soochow University, Suzhou, China

Anti-CD30 CAR-T is a potent candidate therapy for relapsed/refractory (r/r) CD30+ lymphomas with therapy limitations, and the efficacy needed to be further improved. Herein a multi-center phase II clinical trial (NCT03196830) of anti-CD30 CAR-T treatment combined with PD-1 inhibitor in r/r CD30+ lymphoma was conducted. After a lymphocyte-depleting chemotherapy with fludarabine and cyclophosphamide, 4 patients in cohort 1 and 3 patients in cohort 2 received 10^6/kg and 10^7/kg CAR-T cells, respectively, and 5 patients in cohort 3 received 10^7/kg CAR-T cells combined with anti-PD-1 antibody. The safety and the efficacy of CAR-T cell therapy were analyzed. Cytokine release syndrome (CRS) was observed in 4 of 12 patients, and only 1 patient (patient 9) experienced grade 3 CRS and was treated with glucocorticoid and tocilizumab. No CAR-T-related encephalopathy syndrome was observed. Only two patients in cohorts 2 and 3 experienced obviously high plasma levels of IL-6 and ferritin after CD30 CAR-T cell infusion. The overall response rate (ORR) was 91.7% (11/12), with 6 patients achieving complete remission (CR) (50%). In cohorts 1 and 2, 6 patients got a response (85.7%), with 2 patients achieving CR (28.6%). In cohort 3, 100% ORR and 80% CR were obtained in 5 patients without ≥3 grade CRS. With a median follow-up of 21.5 months (range: 3_50 months), the progression-free survival and the overall survival rates were 45 and 70%, respectively. Of the 11 patients who got a response after CAR-T therapy, 7 patients (63.6%) maintained their response until the end of follow-up. Three patients died last because of disease progression. Taken together, the combination of anti-PD-1 antibody showed an enhancement effect on CD30 CAR-T therapy in r/r CD30+ lymphoma patients with minimal toxicities.

Keywords: PD-1, chimeric antigen receptor, CD30, efficacy, relapsed/refractory CD30+ lymphoma

OPEN ACCESS

Edited by:
Catherine Sautes-Fridman, INSERM U1138 Centre de Recherche des Cordeliers (CRC), France

Reviewed by:
Zheng Wei, Fudan University, China
Guangxun Gao, Fourth Military Medical University, China
Ting Yang, Fujian Medical University, China

***Correspondence:**
Kailin Xu
lihmd@163.com
Caixia Li
licaixia@suda.edu.cn

†These authors have contributed equally to this work and share first authorship

Specialty section:
This article was submitted to Cancer Immunity and Immunotherapy, a section of the journal Frontiers in Immunology

Received: *19 January 2022*
Accepted: *10 March 2022*
Published: *01 April 2022*

Citation:
Sang W, Wang X, Geng H, Li T, Li D, Zhang B, Zhou Y, Song X, Sun C, Yan D, Li D, Li Z, Li C and Xu K (2022) Anti-PD-1 Therapy Enhances the Efficacy of CD30-Directed Chimeric Antigen Receptor T Cell Therapy in Patients With Relapsed/Refractory CD30+ Lymphoma. Front. Immunol. 13:858021. doi: 10.3389/fimmu.2022.858021

INTRODUCTION

Chimeric antigen receptor (CAR) T-cell therapy offers an effective therapeutic option for patients with lymphoid malignancies (1–3). CD19 antigen was commonly selected in CAR-T treatment of B cell hematologic malignancies and got a response of 80% overall response rate (ORR) in lymphomas (2, 4) and higher than 90% ORR in B acute lymphocytic leukemia (B-ALL) patients (5) with controllable toxicities. However, most patients do not have a durable response, and there remains a room for improvement (6). The use of combinatorial approaches, including immunomodulatory drugs, checkpoint inhibitors, BTK inhibitor, *etc.*, have been tried in CAR-T cell therapy and showed a synergetic anti-tumor effect with endurable toxicities (7).

CD30 is a target universally expressed in virtually all classical Hodgkin lymphomas (cHL), anaplastic large cell lymphomas (ALCL), and in a proportion of other lymphoma types (8). Intensive chemotherapy followed by hematopoietic stem cell transplantation (HSCT) is commonly used in those r/r lymphoma patients, but a considerable proportion of patients eventually relapse after treatment (9). The CD30-specific antibody drug conjugate brentuximab vedotin treatment is an important immunotherapy option at present, with promising anti-tumor activity and manageable toxicity in cHL and CD30-positive peripheral T-cell lymphoma (10), but the long-term disease control capacity really needed to be improved. More than half of patients will eventually relapse (11), so it is imperative to develop novel effective therapeutics to improve the prognosis for patients of those lymphoma subtypes.

CD30-directed CAR-T cell therapy offers a remarkable opportunity to these r/r CD30+ lymphoma patients. However, although well tolerated, the anti-tumor activity of CD30 CAR-Ts in r/r cHL or ALCL needed to be further improved (12, 13). In a previous phase I study, the anti-CD30 CART cell infusion just yielded a 39% ORR (12). Strategies to enhance the curative effect of CD30 CAR-T cells, including lymphodepleting chemotherapy regimen optimization (14) and combination of PD-1 inhibitor (15), have emerged as new foci on research in recent years. PD-1 was shown to be upregulated by nearly 40% in activated CAR-T cells (16). Besides this, following activation, CAR-T cells could upregulate programmed death ligand-1 (PD-L1) expression on cancer cells, which leads to the lack of clinical efficacy of CAR-T cells (17). Furthermore, PD-1 blockade was shown to improve the expansion and persistence of CAR-T cells through interrupting the PD-1/PD-L1 pathway (18). Based on the critical role of the PD-1/PD-L1 axis in the anti-CD30 CAR-T cell therapies, the combination treatment with PD-1-blocking antibody has become a work worthy of exploration in the future.

Herein, in this study, we performed a combinatorial strategy with anti-PD-1 and anti-CD30 CAR-T cell treatment in patients with r/r CD30+ lymphomas and showed a synergetic anti-tumor activity of immune checkpoint inhibitor with minimal toxicities.

PATIENTS AND METHODS

Patients

A multi-center phase II clinical trial (ClinicalTrials.gov identifiifiers: NCT03196830) was conducted in the Affiliated Hospital of Xuzhou Medical University and the First Affiliated Hospital of Soochow University. The inclusion criteria were as follows: (1), All the recruited relapsed or refractory lymphoma patients in this study must be confirmed CD30-positive through immunohistochemistry staining by at least two pathologists (2), Eastern Cooperative Oncology Group performance status of 2 or less (3), have ≥1 cm of measurable lesion, and (4) experienced disease progression after at least 1 line of systemic chemotherapy regimen concluded at least 1 month prior. The exclusion criteria include (1) severe organ dysfunction (2), a history of active systemic autoimmune or immunodeficiency disease, and (3) treatment history of immunosuppressive agents or glucocorticoids within the last month. All patients provided written informed consent in accordance with the Declaration of Helsinki before enrolling in the study. The study protocol and the consent forms were approved by the ethics committee of the Affiliated Hospital of Xuzhou Medical University and the First Affiliated Hospital of Soochow University.

Treatment Protocol

CD30 CAR-Ts were generated *via* a lentiviral vector. After a lymphocyte-depleting chemotherapy with (FC regimen (three daily doses of fludarabine, 30 mg/m², -5–3 days before infusion; one dose of cyclophosphamide, 750 mg/m², -5 days), the patients received a single dose of autologous CD30 CAR-T cell infusion intravenously (**Figure 1**).

The patients enrolled in this study were divided into 3 cohorts. The patients of cohort 1 and cohort 2 received 10^6/kg and 10^7/kg of CAR-T cells, respectively. The patients of cohort 3 received additional anti-PD-1 antibody at 14 days after 10^7/kg CAR-T cell infusion, and this continued every 3 weeks (**Figure 1**). Sequential auto-HSCT was done in part of patients. A second infusion of CD30 CAR-Ts was allowed in patients who had progressive disease (PD) after the first treatment or after auto-HSCT.

Outcomes

The priority of this study was to assess the safety and feasibility of CD30 CAR-Ts. Cytokine release syndrome (CRS) was graded according to the ASBMT consensus (19). Grade 3 or higher CRS was considered to be severe. Neurotoxic effects were assessed according to the National Cancer Institute Common Terminology Criteria for Adverse Events, version 4.03. The anti-tumor activity of anti-CD30 CAR-T cells was assessed and shown as ORR, complete remission (CR), partial remission (PR), overall survival (OS), and progression-free survival (PFS). OS was defined as the time from infusion to the date of death from any cause. PFS was defined as days from CD30 CAR-T cell infusion to relapse, progression, or death.

Statistical Analysis

The sample size was based on clinical considerations. This is an exploratory study, and all analyses are descriptive in nature. Frequencies or percentages for categorical variables were used to analyze the safety and efficacy of CAR-T therapy. Follow-up time was estimated using the Kaplan–Meier method, whereas OS and PFS were estimated using the Kaplan–Meier method. Data were analyzed using Graphpad Prism version 8.

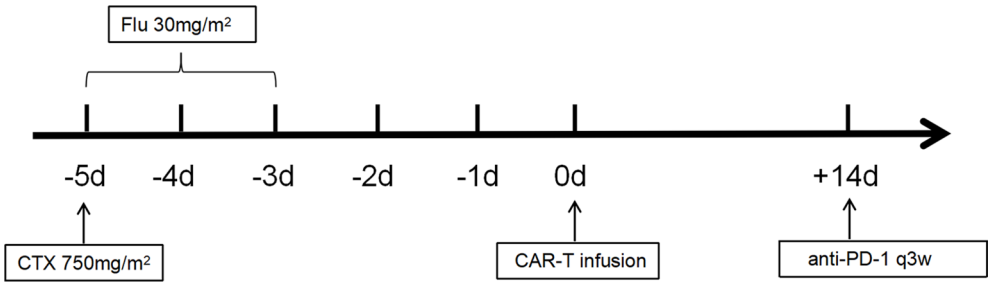

FIGURE 1 | Flowchart for anti-CD30 CAR-T trials.

RESULTS

Patient Characteristics

From July 1, 2017 to July 31, 2021, 13 patients including 9 cHL, 2 angioimmunoblastic T-cell lymphoma (AITL), and 2 gray zone lymphoma patients were enrolled. Finally, a total of 12 patients were evaluated for response because 1 AITL patient was lost to follow-up. The patient characteristics are summarized in **Table 1**. The median age was 25 years old (range: 19–64 years), and 7 patients were male patients. Most of them have complex pretreatment histories, including chemotherapy, radiotherapy, anti-PD-1 antibody, or even HSCT. At the time of enrollment into the CD30 CAR-T cell protocol, 9 of the 12 patients have extranodal invasion, including lung, bone, liver, muscle, *etc.* The disease status of all patients was PD before CD30 CAR-T infusion. Three patients received two cycles of CD30 CAR-T treatment. All the patients received FC lympho-depleting chemotherapy prior to CD30 CAR-T infusion. Sequential auto-HSCT and allo-HSCT were conducted in 5 and 1 patient, respectively. In total, in cohort 1, 4 patients received 10^6/kg CAR-T cells; in cohort 2, 3 patients received 10^7/kg CAR-T cells; and in cohort 3, 5 patients received 10^7/kg CAR-T cells combined with anti-PD-1 antibody (**Figure 2**).

Safety

The CD30 CAR-T infusions were well tolerated, and no treatment-related deaths occurred during the study. CRS was the most common non-hematological adverse event after CD30 CAR-T infusion. In total, 4 patients (33.3%) experienced CRS, and severe CRS occurred in one patient (patient 5). Fever occurred in all the 4 CRS patients, hypoxia occurred in 1 patient (patient 9), and hypotension occurred in 1 patient (patient 5) (**Table 2**). Only patient 9 was treated with glucocorticoid and tocilizumab. Patient 5 experienced obviously elevated plasma levels of IL-6 and ferritin immediately after CD30 CAR-T cell infusion. Intriguingly, delayed IL-6 peak occurred at 1 month after cell infusion in patient 9 and was sustained for 1 week (**Figure 3**). Six patients (50%) experienced cytopenias, including neutropenia, thrombocytopenia, or anemia, among which grade 3 or higher hematological toxicities happened in 5 cases (41.7%). Transient elevation of ALT/AST was observed in 3 patients (25%). Fatigue, nausea/vomiting, diarrhea, and skin rash were observed in 4 patients (33.3%), 2 patients (16.7%), 1 patient (8.3%), and 1 patient (8.3%), respectively. No neurotoxicity was observed during this study (**Table 2**).

Efficacy

Of the 12 evaluable patients, 6 patients had CR and 5 patients had PR after infusion, with 91.7% ORR and 50% CR rate (**Figure 2**, **Table 1**). In cohort 1, 3 of 4 patients achieved PR. In cohort 2, 2 of 3 patients achieved CR and 1 achieved PR, while in cohort 3, 100% ORR and 80% CR rate were achieved. Among 3 patients receiving a second CAR-T cell infusion, 2 patients achieved CR and 1 patient achieved PR. In the 11 patients responding to CAR-T treatment, 7 patients (7/11) continued to have responses until October 31, 2021. Of the 6 patients achieving CR, 4 patients continued to sustain a CR status until now. Among the 9 patients with cHL, 8 patients had response and 5 patients achieved CR (55.6%). Five of six (83.3%) cHL patients receiving 10^7/kg CAR-T cells ± PD-1-blocking antibody achieved CR, while no CR was obtained in patients receiving 10^6/kg CAR-T cells (cohort 1). Of 5 patients receiving HSCT after CAR-T cell infusion, 4 had CR and 1 had PR, with 100% ORR and 80% CR rate (**Figure 2**, **Table 1**). In particular, patient 8 in cohort 3, who received auto-HSCT and secondary CD30 CAR-T treatment immediately after achieving PR of the first CD30 CAR-Ts infusion, finally obtained CR and sustained remission until now (**Figure 4**). At a median follow-up of 21.5 months (range: 3–50 months), the PFS and OS were 45 and 70%, respectively (**Figure 5**). In total, 3 patients died lastly because of PD. Patient 1 (cohort 1) did not benefit from CAR-T and died 11 months after cell infusion. Patient 5 (cohort 2) and patient 9 (cohort 3) had PR and CR and died at 8 and 12 months post-CAR-T cell infusion, respectively.

DISCUSSION

CD30 CAR-T is an important treatment option for r/r CD30+ lymphoma, but the efficacy requires further improvement. In our multi-center study, based on the strategy of combinatorial treatment, anti-PD-1 antibody combined with CD30 CAR-T achieved encouraging results of 100% ORR and 80% CR rate with minimal toxicities.

TABLE 1 | Baseline characteristics of patients.

Patient number	Age (years)	SeX	Diagnosis/ stage	Status of pre-CAR-T	Extranodal sites	Chemotherapy regimens	RT	ASCT	CAR-T infuse X1	Bridge anti- PD-1	CRSgrade	Best response	Current status
	21	M	HLIIIIA	PD	Lung	ABVD*4, GDP*2, BGB-A317, PD-1*8	N	N	06fkg 8.5	N	0	NR	Death
2	19	M	HLIIVB	PD	Bone, spleen	ABVD*6	N	N	7.6	N	0	PR	Relapsed
3	25	M	HLIIIIB	PD	N	ABVD*6, PD-1+ABVD*4, ABVD*1, RT*1	y	N	6.2	N	0	PR	PR
4	27	M	GZLIIIB	PD	N	R-EPOCH*6, R-ESHAP*4, PD-1*1	N	y	5	N		PR	PR
5	27	F	GZLI IVB	PD	Lung, mediastinal mass	R-CHOP*4, ABVD*4, GDP*2	N	Allo-HSCT	25	N	3	PR	Death
6	52	F	AITLIIV B	PD	N	CHOP*8, DICE+ chidamide*2	N	Y	15.4/10.2	N	111	CR	Relapsed
7	29	F	HLIIVB	PD	Bone marrow, adnexa uteri	ABVD*6,1GEV*6, HD-MTX*1	N	Y	12.6	N	0	CR	CR
8	24	M	HLIIVB	PD	Liver, muscle, bone	VAMP*2, COPDAC*3, ABVD*2, EDAP*1, COPDAC*1, GDP*2, Gemcitabine+VP-16*1, GEMOX*1, GDP*1, PD-1 *16, RT, DHAP + lenalidomide	y	Y	12.9/14.8	Y	0/0	CR	CR
9	64	F	HLIIVB	PD	Bone	CHOP*1, CHOPE*6, GCD*4, ICE*4, PD-1*13, lenalidomide	y	N	14.2/12.6	Y	2	CR	Death
10	25	M	HLIIVA	PD	Bone, nasopharynx	*2, RT*15 Chemo *3, ABVD*5, PDL-1*4, PD-1*7	N	N	12.2	Y	0/0	PR	PR
11	19	F	HLIIVB	PD	Bone, lung	ABVD*2, PD-1+AVD·*4	N	Y	13.6	Y	0	CR	CR
12	19	M	HLIIVB	PD	Mediastinal mass	ABVD*6, RT, ESHAP*3, PD-1*4, ASCT*1	y	N	20	Y	0	CR	CR

M, male; F, female; HL, Hodgkin lymphoma; GZL, gray zone lymphoma; AITL, angioimmunoblastic T-cell lymphoma; RT, radiation therapy; ASCT, autologous stem cell transplantation; CRS, cytokine release syndrome; PD, progressive disease; CR, complete remission; PR, partial remission; NR, no response.

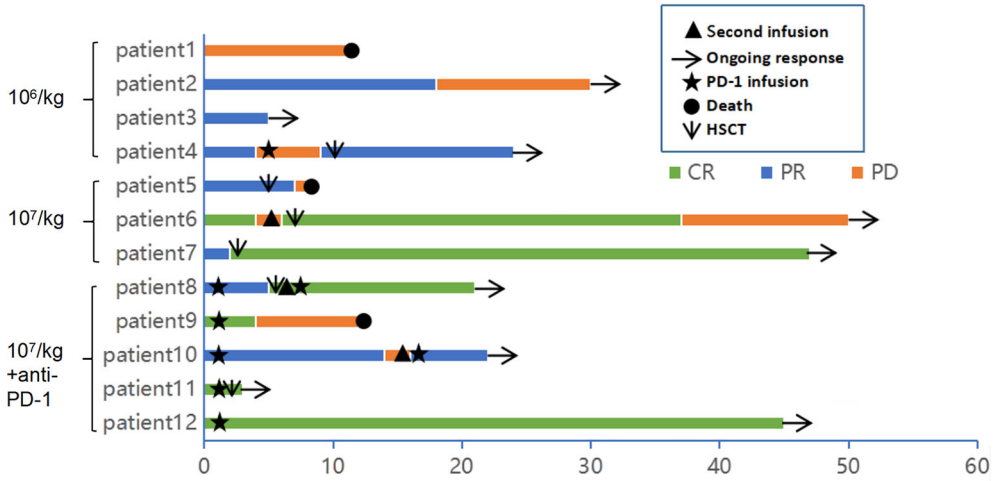

FIGURE 2 | Clinical response and duration for patients after anti-CD30 CAR-T cell infusion. The color and the length of each bar indicate the response to the anti-CD30 CART treatment and the duration of response, respectively. CR, complete remission; PR, partial remission; PD, progressive disease. The black triangle indicates the start time of the second cycle of CAR-T cell infusion. The arrow indicates a sustained response. The star indicates the start time of anti-PD-1 antibody therapy. The original point and the downward pointing arrow represent the death and the start time of hematopoietic stem cell transplantation.

For CD19 CAR-T, nearly 1/3 B-ALL patients and up to 13% of B-cell lymphoma patients were shown to undergo grade 3 or higher CRS (20, 21). While CAR-T targeting CD30 was shown to be well tolerated clinically, with rare cases of CRS and neurological toxicity (12, 13). In this study, based on the dosage explorations of CAR-T cells and the combinatorial strategy of PD-1 blockade, 3 cohorts of patients were conducted. In total, 8.3% severe CRS reaction was observed, and no neurotoxicity was found, and only 2 patients had significantly high plasma levels of IL-6 and ferritin after CAR-T treatment, which was consistent with the previous CD30 CAR-T studies of low toxicity characteristics (12, 13). Notably, our study showed that both 10^7/kg dose level of CAR-Ts and the combinatorial treatment of anti-PD-1 antibody were safe with acceptable toxicities. The most probable related adverse event was hematologic events, which happened in about 50% of patients and may be partly attributed to lymphodepletion. Severe cytopenia was common (41.7%) but recoverable with proper management. Other toxicities, including nausea, rash, and diarrhea, were transient and endurable in our study.

TABLE 2 | Adverse events of patients after anti-CD30 CAR-T cell infusion.

	Number of patients (%, *n* = 12)	
Adverse events	**All grades**	**Grades 2–3**
CRS	4 (33.3)	1 (8.3)
Fever	4 (33.3)	
Hypoxia	1 (8.3)	
Hypotension	1 (8.3)	
ICANS	0 (0)	0 (0)
Fatigue	4 (33.3)	2 (16.7)
Nausea/vomit	2 (16.7)	0 (0)
Diarrhea	1 (8.3)	0 (0)
Hematologic events	6 (50)	5 (41.7)
ALT/AST elevation	3 (25.0)	2 (16.7)
Rash	1 (8.3)	0 (0)

CRS, cytokine release syndrome; ICANS, immune effector cell-associated neurotoxicity syndrome.

It was hard for CD30 CAR-Ts alone to get a satisfactory clinical response in the previous studies (12, 13). The strategy of combining with PD-1 inhibitor to refuel the CAR-T cells was being tried, and this obtained a gratifying initial result (18). In our study of evaluable patients, CD30 CAR-Ts have a significant clinical activity in heavily pretreated r/r CD30+ lymphoma patients with ORR of 91.7% and CR rate of 50%. However, the clinical efficacy of 10^6/kg CAR-T is not exciting because no patient obtained CR in cohort 1. In cohorts 2 and 3, a high dose of CAR-T and a combinatorial strategy of anti-PD-1 antibody significantly improved the therapeutic response of CAR-T, especially in cohort 3, of which 80% CR and 100% ORR was achieved. Furthermore, bridging HSCT after CAR-T treatment was done in 6 patients and got responses of 100% ORR and 66.7% CR rate, indicating a potential beneficial role of HSCT in improving the efficacy of CAR-T therapy. Notably, at a median follow-up of 21.5 months, nearly two-thirds of patients maintained their response until the end of follow-up.

After encountering a tumor-specific antigen *in vivo*, CARs could transmit an activation signal to T cells through the intracellular domain and cause T cell activation and expansion, which is dependent on the antigen density of tumor cells (22). For B-ALL, a dose of 10^5/kg CAR-T cells is enough to obtain a satisfactory curative effect (23), while at least 10^6/kg of CAR-T cells is needed in multiple myeloma (MM) and lymphoma (21, 24). Moreover, under the condition of 10^6/kg CAR-T cell treatment, B-ALL showed significantly more severe adverse events than MM and B-cell lymphoma (20, 21, 24). In our study, 10^6/kg of CD30 CAR-T

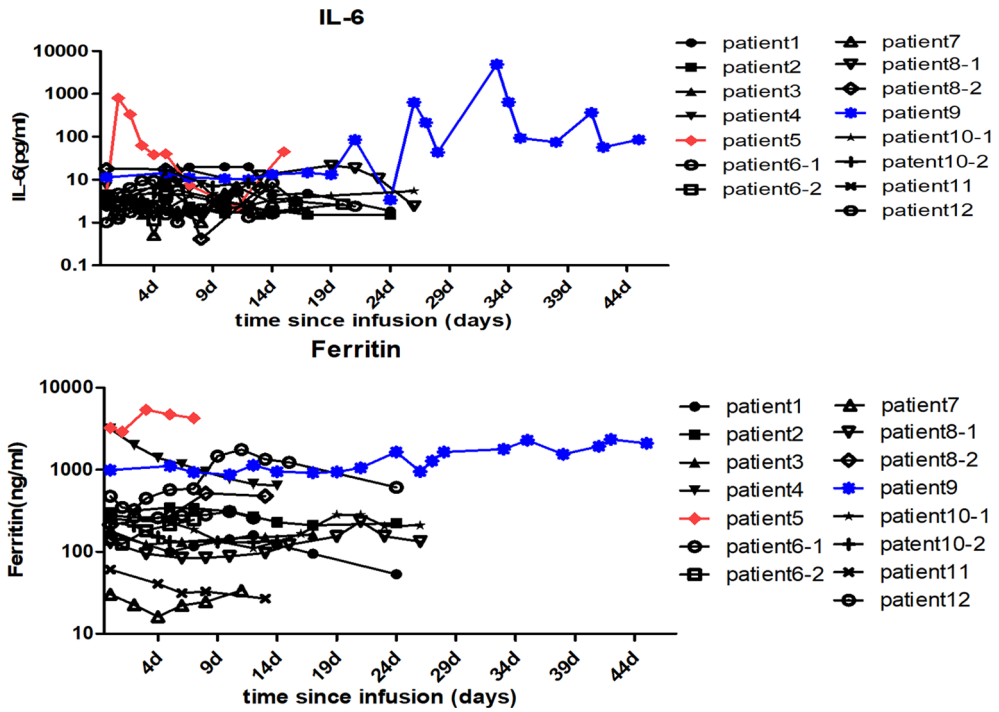

FIGURE 3 | Changes in the patients' serum cytokine levels after anti-CD30 CAR-T cell infusion. The serum IL-6 and ferritin levels of each patient were assessed before and at serial time points after anti-CD30 CAR-T cell infusion. The red and the blue lines, respectively, represent patient 5 and patient 9 with higher IL-6 and ferritin levels than the others.

cells failed to obtain a satisfactory response, which may be related to the special pathological characteristics of cHL. cHL is characterized by small numbers of large CD30+ Reed–Sternberg cells surrounded by a mixed infiltration of inflammatory and immune cells, which will show a low antigen density of CD30+ tumor cells. Therefore, CAR-T cell of a larger order of magnitude was tried in this study, and an exciting effect was obtained. The above-mentioned studies show that tumor load may be the key factor determining the dose level of CAR-T cell infusion, which will be further explored in the follow-up study.

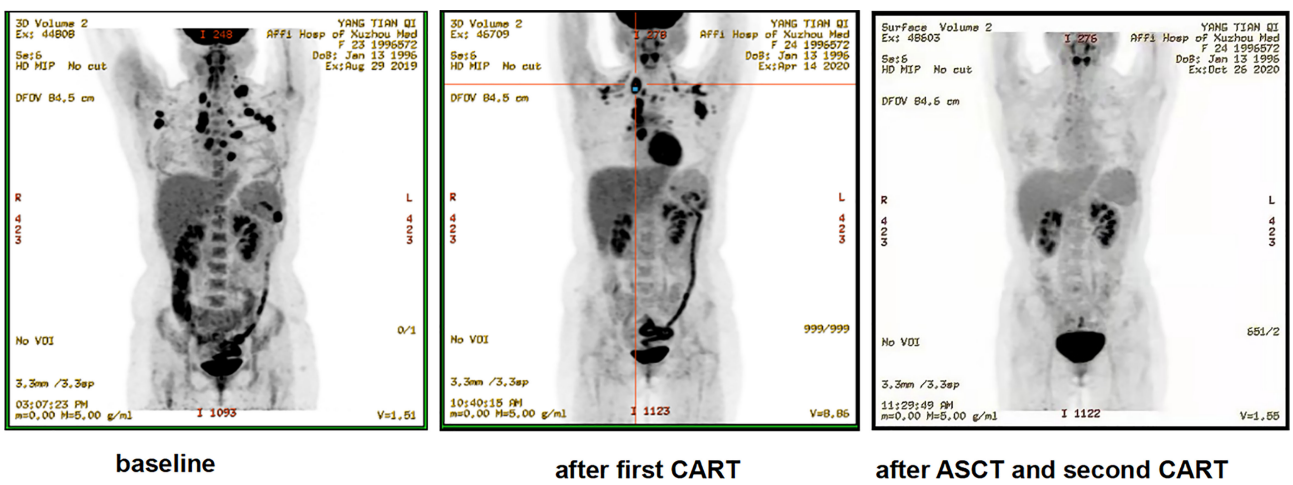

FIGURE 4 | Representative clinical response images of the patient after anti-CD30 CAR-T cell infusion (patient 8). The second cycle of anti-CD30 CAR-T cells was infused 2 weeks after the autologous stem cell transplantation (ASCT). Positron emission tomography–computed tomography scans demonstrated a significant shrinkage of masses after the first cycle of anti-CD30 CAR-T cell infusion and complete disappearance of abnormal lymph nodes after ASCT and the second cycle of anti-CD30 CAR-T treatment.

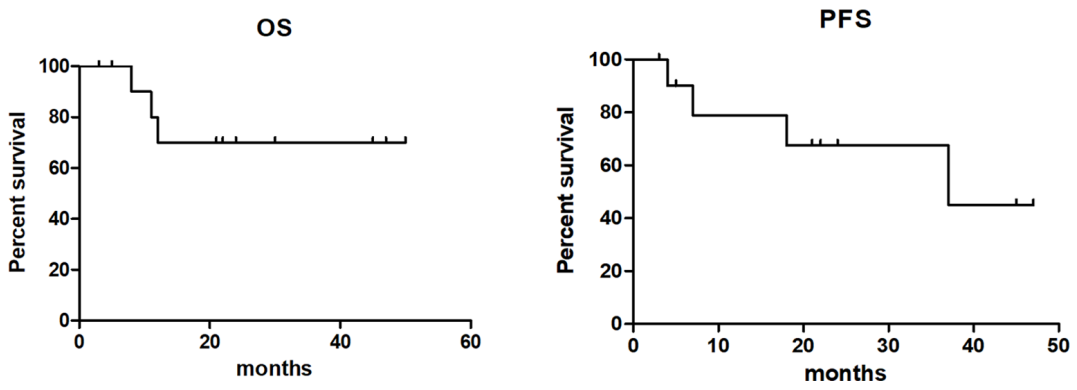

FIGURE 5 | Overall survival and progression-free survival of patients after anti-CD30 CAR-T cell infusion.

PD-1 is an important negative costimulatory regulatory molecule to maintain T cell immune tolerance, and its ligand is commonly detected on cHL and NK/T lymphoma, *etc.* (8). Furthermore, upregulation of PD-1 could be seen in activated CAR-T cells (16). PD-1 blockade seems to be an ideal partner for CAR-T cell therapies. Therefore, immune checkpoint blockade in overcoming T cell exhaustion, including PD-1 gene knockout in CAR-T cells, engineering CAR-T cells to secrete anti-PD-1 and combinatorial treatment of anti-PD-1, *etc.*, is continuously tried to be applied to CD30 CAR- T cells (15, 25, 26). Studies of PD-1 blockade enhancing the eradication of tumor cells of CAR-Ts revealed the potentially critical role of the PD-1/PD-L1 pathway in CAR-T cell immunotherapy (18). Similarly, our combinatorial treatment of PD-1 inhibitor also showed an encouraging result of 100% ORR. Moreover, in four CR patients in cohort 3, all of whom were previously resistant to the checkpoint inhibitor, the combinatorial treatment of anti-PD-1 antibody was still shown to be effective. CAR-T cell expansion improvement and activity enhancement by PD-1 blockade may be the potential reasons (17, 18). The above-mentioned study suggests that the synergistic effect of PD-1 blockade seems to be unaffected by the previous PD-1 resistance status. The anti-PD-1 antibody was added with the aim of improving the expansion and reducing the exhaustion of CAR-T cells and also have the potential risk of triggering or exacerbating a CRS reaction. Acute and severe CRS mostly occurred within 2 weeks after CAR-T cell infusion. Therefore, we add anti-PD-1 antibody at 14 days after CAR-T cell infusion and continued such every 3 weeks in our study. Further optimization of the administration time of the anti-PD-1 antibody needs to be further explored.

In summary, our study suggested that PD-1 blockade yields a high clinical benefit to some extent for r/r CD30 lymphoma patients receiving anti-CD30 CAR-T therapy, and minimal toxicities were observed. These results are exciting and further support the combination of PD-1 inhibitor with anti-CD30 CAR-T therapy. In view of the small cohort in this study, larger clinical studies with more participants are required in the future to further confirm the critical role of the PD-1/PD-L1 axis in anti-CD30 CAR-T cell therapies.

DATA AVAILABILITY STATEMENT

The original contributions presented in the study are included in the article material. Further inquiries can be directed to the corresponding author.

ETHICS STATEMENT

The studies involving human participants were reviewed and approved by the ethics committee of the Affiliated Hospital of Xuzhou Medical University and the First Affiliated Hospital of Soochow University. The patients/participants provided their written informed consent to participate in this study.

AUTHOR CONTRIBUTIONS

KX, CL, and WS designed the research. XW, HG, TL, DL, BZ, YZ, XS, CS, DY, DL, and ZL collected the data. XW, WS, HG, and TL analyzed and interpreted the results. XW and WS wrote the manuscript. All authors contributed to the article and approved the submitted version.

FUNDING

This work was supported by the Natural Science Foundation of Jiangsu Province (BK20190985), the National Natural Science Foundation of China (81900177), and the Key Young Medical Talents of Jiangsu Province (QNRC2016791).

ACKNOWLEDGMENTS

We thank the numerous individuals who participated in this study.

REFERENCES

1. Barrett DM, Singh N, Porter DL, Grupp SA, June CH. Chimeric Antigen Receptor Therapy for Cancer. *Annu Rev Med* (2014) 65:333–47. doi: 10.1146/annurev-med-060512-150254
2. Abramson JS. Anti-CD19 CAR T-Cell Therapy for B-Cell Non-Hodgkin Lymphoma. *Transfus Med Rev* (2020) 34:29–33. doi: 10.1016/j.tmrv.2019.08.003
3. Wang M, Munoz J, Goy A, Locke FL, Jacobson CA, Hill BT, et al. KTE-X19 CAR T-Cell Therapy in Relapsed or Refractory Mantle-Cell Lymphoma. *N Engl J Med* (2020) 382:1331–42. doi: 10.1056/NEJMoa1914347
4. Locke FL, Ghobadi A, Jacobson CA, Miklos DB, Lekakis LJ, Oluwole OO, et al. Long-Term Safety and Activity of Axicabtagene Ciloleucel in Refractory Large B-Cell Lymphoma (ZUMA-1): A Single-Arm, Multicentre, Phase 1-2 Trial. *Lancet Oncol* (2019) 20:31–42. doi: 10.1016/S1470-2045(18)30864-7
5. Chen W, Ma Y, Shen Z, Chen H, Ma R, Yan D, et al. Humanized Anti-CD19 CAR-T Cell Therapy and Sequential Allogeneic Hematopoietic Stem Cell Transplantation Achieved Long-Term Survival in Refractory and Relapsed B Lymphocytic Leukemia: A Retrospective Study of CAR-T Cell Therapy. *Front Immunol* (2021) 12:755549. doi: 10.3389/fimmu.2021.755549
6. Anagnostou T, Riaz IB, Hashmi SK, Murad MH, Kenderian SS. Anti-CD19 Chimeric Antigen Receptor T-Cell Therapy in Acute Lymphocytic Leukaemia: A Systematic Review and Meta-Analysis. *Lancet Haematol* (2020) 7:e816–e26. doi: 10.1016/S2352-3026(20)30277-5
7. Bansal R, Reshef R. Revving the CAR - Combination Strategies to Enhance CAR T Cell Effectiveness. *Blood Rev* (2021) 45:100695. doi: 10.1016/j.blre.2020.100695
8. Grover NS, Savoldo B. Challenges of Driving CD30-Directed CAR-T Cells to the Clinic. *BMC Cancer* (2019) 19:203. doi: 10.1186/s12885-019-5415-9
9. Schmitz N, Pfistner B, Sextro M, Sieber M, Carella AM, Haenel M, et al. Aggressive Conventional Chemotherapy Compared With High-Dose Chemotherapy With Autologous Haemopoietic Stem-Cell Transplantation for Relapsed Chemosensitive Hodgkin's Disease: A Randomised Trial. *Lancet* (2002) 359:2065–71. doi: 10.1016/S0140-6736(02)08938-9
10. Younes A, Gopal AK, Smith SE, Ansell SM, Rosenblatt JD, Savage KJ, et al. Results of a Pivotal Phase II Study of Brentuximab Vedotin for Patients With Relapsed or Refractory Hodgkin's Lymphoma. *J Clin Oncol* (2012) 30:2183–9. doi: 10.1200/JCO.2011.38.0410
11. Chen R, Gopal AK, Smith SE, Ansell SM, Rosenblatt JD, Savage KJ, et al. Five-Year Survival and Durability Results of Brentuximab Vedotin in Patients With Relapsed or Refractory Hodgkin Lymphoma. *Blood* (2016) 128:1562–6. doi: 10.1182/blood-2016-02-699850
12. Wang CM, Wu ZQ, Wang Y, Guo YL, Dai HR, Wang XH, et al. Autologous T Cells Expressing CD30 Chimeric Antigen Receptors for Relapsed or Refractory Hodgkin Lymphoma: An Open-Label Phase I Trial. *Clin Cancer Res* (2017) 23:1156–66. doi: 10.1158/1078-0432.CCR-16-1365
13. Ramos CA, Ballard B, Zhang H, Dakhova O, Gee AP, Mei Z, et al. Clinical and Immunological Responses After CD30-Specific Chimeric Antigen Receptor-Redirected Lymphocytes. *J Clin Invest* (2017) 127:3462–71. doi: 10.1172/JCI94306
14. Ramos CA, Grover NS, Beaven AW, Lulla PD, Wu MF, Ivanova A, et al. Anti-CD30 CAR-T Cell Therapy in Relapsed and Refractory Hodgkin Lymphoma. *J Clin Oncol* (2020) 38:3794–804. doi: 10.1200/JCO.20.01342
15. Wang D, Zeng C, Xu B, Xu JH, Wang J, Jiang LJ, et al. Anti-CD30 Chimeric Antigen Receptor T Cell Therapy for Relapsed/Refractory CD30(+) Lymphoma Patients. *Blood Cancer J* (2020) 10:8. doi: 10.1038/s41408-020-0274-9
16. Li F, Zhang Z, Xuan Y, Zhang D, Liu J, Li A, et al. PD-1 Abrogates the Prolonged Persistence of CD8(+) CAR-T Cells With 4-1BB Co-Stimulation. *Signal Transduct Target Ther* (2020) 5:164. doi: 10.1038/s41392-020-00277-6
17. Rafiq S, Yeku OO, Jackson HJ, Purdon TJ, van Leeuwen DG, Drakes DJ, et al. Targeted Delivery of a PD-1-Blocking scFv by CAR-T Cells Enhances Anti-Tumor Efficacy. *vivo Nat Biotechnol* (2018) 36:847–56. doi: 10.1038/nbt.4195
18. Chong EA, Melenhorst JJ, Lacey SF, Ambrose DE, Gonzalez V, Levine BL, et al. PD-1 Blockade Modulates Chimeric Antigen Receptor (CAR)-Modified T Cells: Refueling the CAR. *Blood* (2017) 129:1039–41. doi: 10.1182/blood-2016-09-738245
19. Lee DW, Santomasso BD, Locke FL, Ghobadi A, Turtle CJ, Brudno JN, et al. ASTCT Consensus Grading for Cytokine Release Syndrome and Neurologic Toxicity Associated With Immune Effector Cells. *Biol Blood Marrow Transplant* (2019) 25:625–38. doi: 10.1016/j.bbmt.2018.12.758
20. Lee DW, Kochenderfer JN, Stetler-Stevenson M, Cui YK, Delbrook C, Feldman SA, et al. T Cells Expressing CD19 Chimeric Antigen Receptors for Acute Lymphoblastic Leukaemia in Children and Young Adults: A Phase 1 Dose-Escalation Trial. *Lancet* (2015) 385:517–28. doi: 10.1016/S0140-6736(14)61403-3
21. Neelapu SS, Locke FL, Bartlett NL, Lekakis LJ, Miklos DB, Jacobson CA, et al. Axicabtagene Ciloleucel CAR T-Cell Therapy in Refractory Large B-Cell Lymphoma. *N Engl J Med* (2017) 377:2531–44. doi: 10.1056/NEJMoa1707447
22. Gudipati V, Rydzek J, Doel-Perez I, Goncalves VDR, Scharf L, Konigsberger S, et al. Inefficient CAR-Proximal Signaling Blunts Antigen Sensitivity. *Nat Immunol* (2020) 21:848–56. doi: 10.1038/s41590-020-0719-0
23. Liu S, Deng B, Yin Z, Lin Y, An L, Liu D, et al. Combination of CD19 and CD22 CAR-T Cell Therapy in Relapsed B-Cell Acute Lymphoblastic Leukemia After Allogeneic Transplantation. *Am J Hematol* (2021) 96:671–9. doi: 10.1002/ajh.26160
24. Yan Z, Cao J, Cheng H, Qiao J, Zhang H, Wang Y, et al. A Combination of Humanised Anti-CD19 and Anti-BCMA CAR T Cells in Patients With Relapsed or Refractory Multiple Myeloma: A Single-Arm, Phase 2 Trial. *Lancet Haematol* (2019) 6:e521–e9. doi: 10.1016/S2352-3026(19)30115-2
25. Rupp LJ, Schumann K, Roybal KT, Gate RE, Ye CJ, Lim WA, et al. CRISPR/Cas9-Mediated PD-1 Disruption Enhances Anti-Tumor Efficacy of Human Chimeric Antigen Receptor T Cells. *Sci Rep* (2017) 7:737. doi: 10.1038/s41598-017-00462-8
26. Li S, Siriwon N, Zhang X, Yang S, Jin T, He F, et al. Enhanced Cancer Immunotherapy by Chimeric Antigen Receptor-Modified T Cells Engineered to Secrete Checkpoint Inhibitors. *Clin Cancer Res* (2017) 23:6982–92. doi: 10.1158/1078-0432.CCR-17-0867

Conflict of Interest: The authors declare that the research was conducted in the absence of any commercial or financial relationships that could be construed as a potential conflict of interest.

frontiers | Frontiers in Immunology

ORIGINAL RESEARCH
published: 11 April 2022
doi: 10.3389/fimmu.2022.882589

Epstein-Barr Virus-Positive Lymphoma-Associated Hemophagocytic Syndrome: A Retrospective, Single-Center Study of 51 Patients

*Ailin Zhao†, Jinrong Yang†, Meng Li, Linfeng Li, Xinai Gan, Jie Wang, He Li, Kai Shen, Yunfan Yang and Ting Niu**

Department of Hematology, West China Hospital, Sichuan University, Chengdu, Sichuan, China

OPEN ACCESS

Edited by:
Wei Sang,
The Affiliated Hospital of Xuzhou Medical University, China

Reviewed by:
Robert Gale,
Imperial College London, United Kingdom
Jun Peng,
Shandong University, China
Weili Zhao,
Shanghai Jiao Tong University, China

***Correspondence:**
Ting Niu
niuting@wchscu.cn

†These authors have contributed equally to this work and share first authorship

Specialty section:
This article was submitted to Cancer Immunity and Immunotherapy, a section of the journal Frontiers in Immunology

Received: *24 February 2022*
Accepted: *18 March 2022*
Published: *11 April 2022*

Citation:
Zhao A, Yang J, Li M, Li L, Gan X, Wang J, Li H, Shen K, Yang Y and Niu T (2022) Epstein-Barr Virus-Positive Lymphoma-Associated Hemophagocytic Syndrome: A Retrospective, Single-Center Study of 51 Patients. Front. Immunol. 13:882589. doi: 10.3389/fimmu.2022.882589

Purpose: To investigate clinical characteristics, management, and prognosis of Epstein-Barr virus (EBV)-positive lymphoma-associated hemophagocytic syndrome (LAHS) patients in real-world practice.

Methods: This was a retrospective, single-center cohort study. EBV-positive LAHS patients diagnosed from January 2010 to December 2021 in our center were enrolled. Clinical characteristics, treatment, overall response rate (ORR), and overall survival (OS) were investigated. Univariate and multivariate analysis of potential factors were conducted.

Results: Of the 51 patients, 44 were T/NK cell lymphoma; five were B cell lymphoma; two were Hodgkin lymphoma. EBV-positive T/NK cell LAHS patients were significantly younger and showed lower fibrinogen levels and C-reactive protein levels than EBV-positive B cell LAHS patients (P=0.033, P=0.000, and P=0.004, respectively). Combined treatment of anti-hemophagocytic lymphohistiocytosis (HLH) and anti-lymphoma treatment was conducted in 24 patients; anti-HLH treatment was conducted in 18 patients; anti-lymphoma treatment was conducted in three patients; glucocorticoid treatment was conducted in one patient. ORR was 47.8%, and the median OS was 61 (95% confidence interval 47.9-74.1) days for overall patients. Patients who received anti-HLH treatment and turned to anti-lymphoma treatment early displayed higher ORR and OS than those of anti-HLH patients (P=0.103, and P=0.003, respectively). Elevated alanine aminotransferase level was the independent risk factor of EBV-positive LAHS prognosis.

Conclusions: Prognosis of EBV-positive LAHS patients was poor. Anti-lymphoma treatment should be initiated as soon as HLH was rapidly controlled.

Keywords: epstein-barr virus, lymphoma, hemophagocytic syndrome, overall response rate, overall survival

INTRODUCTION

Epstein-Barr virus (EBV) is a double-stranded DNA herpesvirus, whose infection is prevalent in 95% of the world's population (1). EBV mainly infects B lymphocytes due to interaction between viral glycoprotein gp350 and CD21 receptor, with memory B cells serving as EBV reservoir (2). Besides B cells, EBV can also infect T and NK cells. EBV-associated lymphoproliferative disorders (LPDs) include various diseases, ranging from reactive disorders to lymphoma. The majority of EBV-associated lymphoma displays type II EBV latency, which expresses five nuclear antigens (EBNA1, 3A–C and LP) and three membrane proteins (LMP1, LMP2A and LMP2B), except EBNA2, one of the dominant transforming proteins. A minority of EBV-associated lymphoma, for example, Burkitt lymphoma, shows type I EBV latency, which only expresses EBNA1, regulating episomal EBV genome replication (3). Immune escape and immunodeficiency are essential to EBV-associated lymphomagenesis, depending on different subtypes of lymphoma and immune status of patients. In EBV^+ Hodgkin lymphoma (HL) and EBV^+ nodal diffuse large B cell lymphoma (DLBCL) young patients, immune escape plays an important part in pathogenesis, as evidenced by recurrent alterations in *PD-L1* and *PD-L2* (4, 5). The extent of PD-L1 expression was significantly related to EBV positivity (6). However, in EBV^+ peripheral T cell lymphoma (PTCL), immunodeficiency leads to gradual impairment of T-cell antigenic repertoire, and the chronic inflammatory environment brings free radicals triggering lymphomagenesis (7, 8).

Hemophagocytic syndrome, also named hemophagocytic lymphohistiocytosis (HLH), is a rare but lethal hyperinflammatory syndrome. Aberrant activation of lymphocytes, monocytes, and macrophages leads to substantial release of inflammatory cytokines. HLH typically manifests itself as fever, hepatosplenomegaly, and multiple organ dysfunction syndrome (MODS). HLH can be categorized into primary HLH and secondary HLH. Primary HLH is characterized by early onset and cytotoxicity-related gene mutations. Secondary HLH mainly attacks adult patients secondary to malignancy, infection, autoimmune disease, pregnancy, and other triggers, with the incidence of 0.125 per 100,000 per year (9). Lymphoma-associated hemophagocytic syndrome (LAHS) is the most common type of secondary HLH. An epidemiological investigation of all HLH cases in China was conducted in 2019. In the general Chinese population, the incidence of LAHS was 0.014/100,000 per year (10). HLH can occur not only upon lymphoma onset, but also during relapse or advanced stage of lymphoma. Clinical features of LAHS largely overlap with those of other types of HLH, sepsis, and MODS, which could impede in-time diagnosis and treatment. Prognosis of LAHS patients is poor, with a median overall survival (OS) of 28 to 36 days (11, 12). Though EBV-positive LAHS has been described in case reports (13–15), comprehensive investigation of clinical characteristics and outcome of the EBV-positive LAHS cohort is rare. Thus, this study is a single-center, retrospective, cohort study to explore clinical features and prognosis of EBV-positive LAHS patients.

MATERIALS AND METHODS

Participants and Treatment

Patients consecutively diagnosed as EBV-positive LAHS from January, 2010 to December, 2021 at West China Hospital, Sichuan University were enrolled (16, 17). EBV positivity was assessed by EBER *in situ* hybridization. Besides antiviral treatment, induction treatment was divided into anti-HLH treatment, anti-lymphoma treatment, and the combination of both. Anti-HLH treatment consisted of HLH-1994 regimen, HLH-2004 regimen, and GED regimen (gemcitabine-etoposide-dexamethasone). Anti-lymphoma treatment was chemotherapy depending on different subtypes of lymphoma. Treatment response was evaluated according to the following conditions. Complete response (CR) required disappearance of all HLH-related symptoms, and HLH-related lab findings returning to normal range, including ferritin, soluble CD25 (sCD25), complete blood count, triglyceride, alanine aminotransferase (ALT), etc. Consciousness should recover to normal if central nervous system was involved. Partial response (PR) required normal body temperature and improvement by over 25% in at least two symptoms or lab findings, including sCD25 decrease by at least one third, ferritin and triglyceride decrease by at least 25%, ALT decrease by at least 50% if formerly over 400U/L, and neutrophil increase by 100% without transfusion. If neutrophil counts were formerly less than 0.5×10^9/L, they should exceed 0.5×10^9/L after treatment. If neutrophil counts were formerly over 0.5×10^9/L but less than 2×10^9/L, they should exceed 2×10^9/L after treatment. No response (NR) was defined as being unable to reach CR or PR. Overall response rate (ORR) was calculated as (CR+PR)/total patients × 100%. OS was defined as the interval between HLH diagnosis and all-cause death. The patients were followed up until December, 2021. This study was conducted with the approval of the West China Hospital ethics committee, according to Declaration of Helsinki.

Statistical Analysis

Statistical analysis was conducted with SPSS 23.0 and GraphPad Prism 7.0 software. Measurable data with normal distribution and skewed distribution were evaluated with *t* test and *U* test, respectively. Enumeration data were evaluated with χ^2 test. Survival analysis was assessed with Kaplan-Meier methods, and compared with Log rank test. Univariate and multivariate analysis of prognostic predictors was conducted with Cox proportional hazard model. It was regarded as statistically significant with $P<0.05$.

RESULTS

Baseline Characteristics

Fifty-one EBV-positive LAHS patients were enrolled in this study, including 35 (68.6%) male patients and 16 (31.4%) female patients. Median age at HLH diagnosis was 37 (13-64) years. Three (5.9%) patients were newly diagnosed as lymphoma, while 48 (94.1%)

patients were relapsed/refractory lymphoma cases. Clinical characteristics of these patients at baseline were listed in **Table 1**. The total cohort consisted of 44 (86.3%) T/NK cell lymphoma cases, five (9.8%) B cell lymphoma cases, and two (3.9%) HL cases. Regarding T/NK cell lymphoma, extranodal NK/T-cell lymphoma (ENKL), nasal type (22/51, 43.1%) and aggressive natural killer cell leukemia (ANKL) (13/51, 25.5%) were the dominant subtypes. Besides, PTCL, not otherwise specified (PTCL, NOS) (4/51, 7.8%), angioimmunoblastic T cell lymphoma (AITL) (3/51, 5.9%), anaplastic large cell lymphoma (ALCL) (1/51, 2.0%), and systemic EBV-positive T-cell lymphoma of childhood (1/51, 2.0%) were also discovered. B cell lymphoma group included four (7.8%) DLBCL cases and one (2.0%) lymphoplasmacytic lymphoma (LPL) case. The majority of (94.1%) EBV-positive LAHS patients were at Ann Arbor stage III-IV. In terms of clinical manifestations, fever was present in all patients. Splenomegaly, serous effusion, hepatomegaly, edema, and jaundice were seen in 42 (82.4%), 28 (54.9%), 22 (43.1%), 12 (23.5%), and 10 (19.6%) patients, respectively. Hemophagocytosis phenomena were discovered in 24 (47.1%) patients.

TABLE 1 | Clinical characteristics of EBV-positive LAHS patients at baseline.

Characteristics	n (%)
Sex	
Male	35 (68.6)
Female	16 (31.4)
Age at HLH diagnosis, median (range)	37 (13-64)
Lymphoma subtype	
T/NK cell lymphoma	44 (86.3)
Extranodal NK/T-cell lymphoma, nasal type	22 (43.1)
Aggressive natural killer cell leukemia	13 (25.5)
Peripheral T cell lymphoma, not otherwise specified	4 (7.8)
Angioimmunoblastic T cell lymphoma	3 (5.9)
Anaplastic large cell lymphoma	1 (2.0)
Systemic EBV-positive T-cell lymphoma of childhood	1 (2.0)
B cell lymphoma	5 (9.8)
Diffuse large B cell lymphoma	4 (7.8)
Lymphoplasmacytic lymphoma	1(2.0)
Hodgkin lymphoma	2 (3.9)
Lymphoma stage	
I-II stage	3 (5.9)
III-IV stage	48 (94.1)
Clinical manifestations	
Fever	51 (100)
Splenomegaly	42 (82.4)
Serous effusion	28 (54.9)
Hepatomegaly	22 (43.1)
Edema	12 (23.5)
Jaundice	10 (19.6)
Lab test, median (range)	
Hemoglobin (g/L)	96 (44-132)
Neutrophil ($\times10^9$/L)	1.53 (0.03-12.58)
Platelet ($\times10^9$/L)	45 (7-264)
Alanine aminotransferase (U/L)	87 (10-597)
Aspartate aminotransferase (U/L)	108 (15-936)
Total bilirubin (μmol/L)	20.55 (5.20-178.90)
Albumin (g/L)	30.55 (19.0-55.0)
Lactate dehydrogenase (U/L)	758.5 (108-3346)
Triglyceride (mmol/L)	2.885 (0.90-7.66)
Fibrinogen (g/L)	1.60 (0.50-6.57)
Ferritin (ng/mL), n=47	2799 (314-161681)
sCD25 (pg/mL), n=38	8547.5 (1455-36685)
Hemophagocytosis phenomenon	24 (47.1)
Plasma EBV-DNA (copies/mL)	145000 (647-744000000)

LAHS, lymphoma-associated hemophagocytic syndrome.

Baseline characteristics of EBV-positive T/NK cell LAHS patients were compared to those of EBV-positive B cell LAHS patients. T/NK cell LAHS patients were significantly younger than B cell LAHS patients upon HLH diagnosis (34 v.s. 47 years, *P*=0.033). Fibrinogen level and C-reactive protein (CRP) level were significantly lower in T/NK cell LAHS patients than B cell LAHS patients (*P*=0.000 and *P*=0.004, respectively). Plasma EBV DNA level tended to be higher in B cell LAHS patients than in T/NK cell LAHS patients, but the difference was not significant. There was no significant difference in sex, IPI score, ECOG score, clinical manifestations, complete blood count, liver and kidney function, triglyceride, ferritin, sCD25, hemophagocytosis phenomenon, and the occurrence order of lymphoma and HLH between EBV-positive T/NK cell LAHS patients and EBV-positive B cell LAHS patients (**Table 2**).

We also compared EBV-positive LAHS patients and EBV-negative LAHS patients who were consecutively diagnosed in our department during the same period of time. EBV-positive LAHS patients (median 37 years, range 13-64 years) were significantly younger at HLH diagnosis than EBV-negative LAHS patients (median 42 years, range 13-90 years, *P*=0.049). EBV-positive LAHS patients displayed significantly higher hemoglobin and triglyceride levels at baseline than EBV-negative LAHS patients (*P*=0.008, and *P*=0.007, respectively). T/NK-cell lymphoma tended to account for a higher proportion of EBV-positive LAHS patients (86.3%) than EBV-negative LAHS patients (69.8%), but the difference was insignificant (**Table S1**).

Treatment and Response

Of the 51 patients, three patients only received antiviral treatment in our department, and two patients initiated HLH-1994 regimen but died in three days. After excluding these five patients, the remaining 46 patients were evaluable for treatment response. Treatment was divided into combined treatment group, anti-HLH treatment group, anti-lymphoma treatment group, and glucocorticoid treatment group (**Figure 1**). Combined treatment of anti-HLH regimen and anti-lymphoma chemotherapy was conducted in 24 (52.2%) patients. Nineteen (41.3%) patients first underwent anti-HLH treatment of 3 (1-9) weeks, and then turned to anti-lymphoma chemotherapy. HLH-1994 regimen was conducted in 12 (26.1) patients. GED regimen was given to four (8.7%) patients, and HLH-2004 regimen was performed in three (6.5%) patients. Median number of chemotherapy cycles was 2 (1-8). The detailed anti-lymphoma chemotherapy was listed in **Table 3**. Another five (10.9%) patients first received anti-lymphoma chemotherapy and turned to HLH-1994 regimen subsequently. These patients were all ENKL patients, and the detailed chemotherapy was also listed in **Table 3**. The median number of chemotherapy cycles was 1 (1-3). The median weeks of HLH-1994 treatment was 4 (2-4).

In the 18 (39.1%) patients who only received anti-HLH treatment, the median weeks of induction treatment was

TABLE 2 | Comparison of baseline characteristics between EBV-positive T/NK cell LAHS patients and EBV-positive B cell LAHS patients.

Characteristics, n (%)	T/NK cell LAHS (n=44)	B cell LAHS (n=5)	*P*
Sex			1.000
Male	30 (68.2)	3 (60.0)	
Female	14 (31.8)	2 (40.0)	
Age at HLH diagnosis, y, median (range)	34 (13-64)	47 (44-63)	0.033
IPI score			0.117
0-1	0	0	
2-3	23 (52.3)	5 (100)	
4-5	21 (47.7)	0	
ECOG score			0.540
0-2	24 (54.5)	4 (80.0)	
3-5	20 (45.5)	1 (20.0)	
Manifestations			
Splenomegaly	36 (81.8)	4 (80.0)	1.000
Serous effusion	24 (54.5)	3 (60.0)	1.000
Hepatomegaly	19 (43.2)	2 (40.0)	1.000
Edema	12 (27.3)	0	0.427
Jaundice	10 (22.7)	0	0.542
Lab tests, median (range)			
Hemoglobin (g/L)	97.5 (44-132)	101 (74-117)	0.870
Neutrophil ($\times10^9$/L)	1.30 (0.03-12.58)	1.89 (0.83-4.72)	0.714
Platelet ($\times10^9$/L)	45 (7-264)	44 (35-128)	0.682
Alanine aminotransferase (U/L)	93 (13-597)	81 (10-146)	0.428
Aspartate aminotransferase (U/L)	111 (17-936)	97 (15-297)	0.561
Total bilirubin (μmol/L)	22.5 (5.2-178.9)	19.8 (16.6-67)	0.714
Albumin (g/L)	30.55 (19.0-55.0)	31.3 (20.6-35.4)	0.665
Lactate dehydrogenase (U/L)	771 (108-3346)	577 (399-1167)	0.409
Triglyceride (mmol/L)	3.37 (0.93-7.66)	2.08 (0.90-3.87)	0.131
Fibrinogen (g/L)	1.32 (0.5-6.2)	4.15 (2.36-6.57)	0.000
Ferritin (ng/mL), n=47	2861.5 (314-161681)	2431.8 (863.7-20063)	0.578
sCD25 (pg/mL), n=38	7699 (1455-36685)	8714 (5396-21578)	0.758
C-reactive protein (mg/L)	35.05 (2.32-167)	122 (86.2-228)	0.004
Hemophagocytosis phenomenon	20 (45.5)	2 (40.0)	1.000
Plasma EBV-DNA (copies/mL)	142000(654-3200000)	278000(7610-744000000)	0.375
Occurrence order of lymphoma and HLH			0.632
HLH prior to lymphoma	4 (9.1)	0	
lymphoma prior to HLH	7 (15.9)	1 (20.0)	
Simultaneous occurrence	33 (75.0)	4 (80.0)	

HLH, hemophagocytic lymphohistiocytosis; LAHS, lymphoma-associated hemophagocytic syndrome.

4 (1-8). The majority of (12/18, 66.7%) patients received HLH-1994 regimen. HLH-2004 regimen (3/18, 16.7%) and GED regimen (3/18, 16.7%) were conducted in three patients each. Three (6.5%) patients only received anti-lymphoma chemotherapy. One ENKL patient and one ANKL patient received GLIDE regimen, and one DLBCL patient received chidamide-RCHOP regimen. Median number of chemotherapy cycles was 3 (2-8). One (2.2%) patient only received glucocorticoid treatment.

For patients who were at higher risk or failed to achieve CR with a poor control of EBV infection, consolidation treatment was conducted, which included PD-1 monoclonal antibody treatment, chidamide treatment, and autologous or allogenic stem cell transplantation. For patients whose biopsy revealed positive PD-L1 staining of tumor cells, especially HL patients and DLBCL patients, PD-1 monoclonal antibody treatment was conducted. For patients who displayed aberrant epigenetic alterations, especially PTCL patients and double expression DLBCL patients, chidamide treatment was conducted. For young, fit, and high-risk patients with sufficient stem cells collected who were willing to receive transplantation, autologous or allogenic stem cell transplantation was conducted. Overall, seven (15.2%) patients underwent consolidation therapy. Three (6.5%) patients (one HL case, one DLBCL case, and one ENKL case) received PD-1 monoclonal antibody treatment, of whom the DLBCL patient also received autologous stem cell transplantation after PD-1 monoclonal antibody treatment. Two (4.3%) patients (one ENKL case and the DLBCL patient who received PD-1 monoclonal antibody treatment) received autologous stem cell transplantation. One (2.2%) ANKL patient received allogenic stem cell transplantation. Two (4.3%) AITL patients received chidamide treatment.

Of the 46 evaluable patients, CR was achieved in four (8.7%) patients, and PR was achieved in 18 (39.1%) patients. Twenty-four (52.2%) patients remained NR. ORR was 47.8%. In the combined treatment group, CR was reached in two (8.3%) patients, and PR was reached in 12 (50%) patients. NR was present in 10 (41.7%) patients. ORR was 58.3%. For patients who first received anti-HLH treatment and turned to anti-lymphoma chemotherapy subsequently, CR was achieved in two (10.5%)

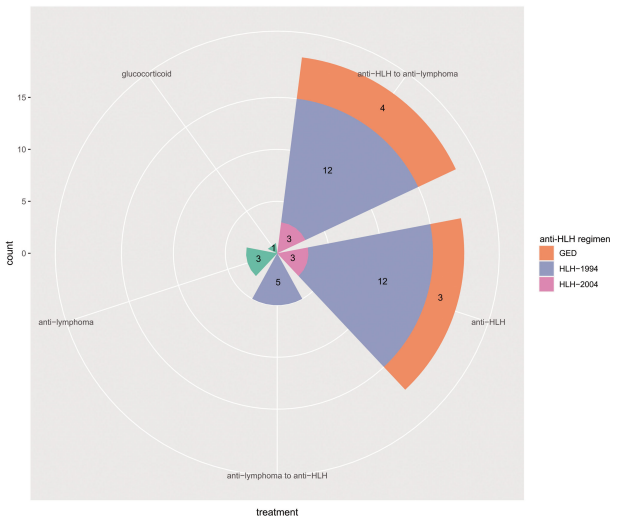

FIGURE 1 | Treatment of EBV-positive lymphoma-associated hemophagocytic syndrome patients.

patients, and PR was achieved in 10 (52.6%) patients. Seven (36.8%) patients remained NR. ORR was 63.2%. For those who first received anti-lymphoma chemotherapy and turned to anti-HLH treatment subsequently, PR was achieved in two (40%) patients, and three (60%) patients remained NR. ORR was 40%. In anti-HLH treatment group, six (33.3%) patients achieved PR and twelve (66.7%) patients remained NR. ORR was 33.3% for the total anti-HLH treatment group, the HLH-1994 regimen subgroup, the HLH-2004 regimen subgroup, and the GED regimen subgroup. In anti-lymphoma treatment group, CR was achieved in two (66.7%) patients while one (33.3%) patient remained NR. ORR was 66.7%. One patient only received glucocorticoid treatment but remained NR. Patients who first received anti-HLH treatment and turned to anti-lymphoma treatment subsequently tended to show a higher ORR than those who received anti-HLH treatment only, but the difference was not significant (63.2% v.s. 33.3%, P=0.103). There was no significant difference in ORR among different treatment groups (**Figure 2**).

At baseline, plasma EBV-DNA of all patients was positive (median 145000 copies/mL, range 647-744000000 copies/mL). After induction treatment, plasma EBV-DNA decreased significantly in all patients but one, who was a ANKL patient only receiving anti-HLH treatment but remaining NR (median 643.5 copies/mL, range 0-88800 copies/mL). Plasma EBV-DNA of ten patients after treatment was negative. Another three patients had a plasma EBV-DNA level lower than 50 copies/mL after treatment. There was no significant difference in plasma EBV-DNA after treatment between T/NK-cell LAHS (median 623 copies/mL, range 0-88800 copies/mL) and B-cell LAHS patients (median 14835 copies/mL, range 0-32300 copies/mL, P=0.540). In terms of treatment group, median plasma EBV-DNA of patients after treatment in combined treatment group and anti-HLH group was 272.5 copies/mL (range 0-64800 copies/mL), and 3130 copies/mL (range 0-33800 copies/mL), respectively. For the three patients in anti-lymphoma group, median plasma EBV-DNA of patients after treatment was 0 copies/mL (range 0-50 copies/mL). For the only patient in glucocorticoid group, his plasma EBV-DNA level decreased from 158000 copies/mL to 88800 copies/mL after treatment. There was no significant difference in plasma EBV-DNA level after treatment among treatment groups.

TABLE 3 | Combined treatment of anti-HLH and anti-lymphoma regimen in EBV-positive LAHS patients.

Anti-HLH regimen prior to anti-lymphoma chemotherapy	n (%)
ENKL, n=8	
GLIDE	6 (75%)
SMILE	1 (12.5%)
ECHOP	1 (12.5%)
ANKL, n=5	
GLIDE	4 (80%)
L-GIFoX	1 (20%)
PTCL, NOS, n=2	
CHOP	2 (100%)
AITL, n=1	
Chi-CHOP	1 (100%)
DLBCL, n=1	
RCHOP	1 (100%)
HL, n=2	
ABVD	2 (100%)
Anti-lymphoma chemotherapy prior to anti-HLH regimen	
ENKL, n=5	
GLIDE	2 (40%)
VDLP	2 (40%)
VLP	1 (20%)

AITL, angioimmunoblastic T cell lymphoma; ANKL, aggressive natural killer cell leukemia; DLBCL, diffuse large B cell lymphoma; ENKL, extranodal NK/T-cell lymphoma, nasal type; HL, Hodgkin lymphoma; HLH, hemophagocytic lymphohistiocytosis; LAHS, lymphoma-associated hemophagocytic syndrome; PTCL, Peripheral T cell lymphoma.

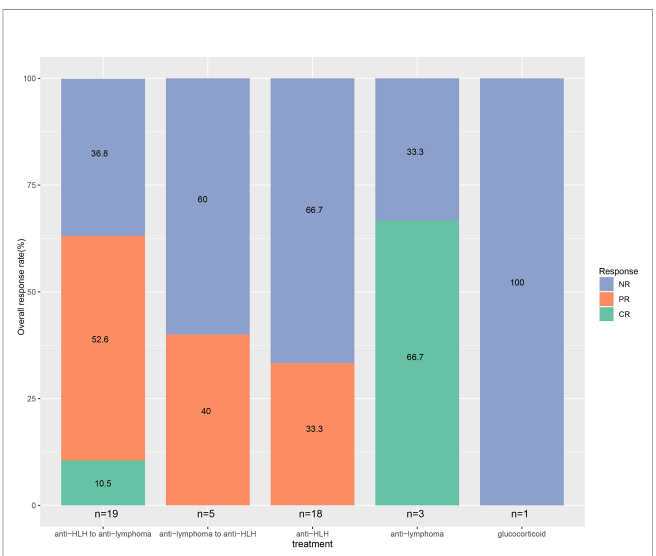

FIGURE 2 | Response rate of EBV-positive lymphoma-associated hemophagocytic syndrome patients.

Regarding EBV-positive T/NK cell LAHS patients, three patients only received antiviral treatment in our department, and one patient initiated HLH-1994 regimen but died in three days. After excluding these patients, 40 patients were evaluable for treatment response. Twenty-one (52.5%) patients received combined treatment. Sixteen (40%) patients first underwent anti-HLH treatment of 3.5 (1-9) weeks, and then turned to anti-lymphoma chemotherapy. Median number of chemotherapy cycles was 1 (1-8). Another five (12.5%) patients first received anti-lymphoma chemotherapy and turned to HLH-1994 regimen subsequently. The median number of chemotherapy cycles was 1 (1-3). The median weeks of HLH-1994 treatment was 4 (2-4). In the 16 (40%) patients who only received anti-HLH treatment, the median weeks of induction treatment was 4 (1-8). Two (5%) patients only received anti-lymphoma chemotherapy. Median number of chemotherapy cycles was 2.5 (2-3). One (2.5%) patient only received glucocorticoid treatment.

Of the 40 evaluable EBV-positive T/NK cell LAHS patients, CR was achieved in three (7.5%) patients, and PR was achieved in 14 (35%) patients. Twenty-three (57.5%) patients remained NR. ORR was 42.5%. In the combined treatment group, CR was reached in two (9.5%) patients, and PR was reached in nine (42.9%) patients. NR was present in 10 (47.6%) patients. ORR was 52.4%. For patients who first received anti-HLH treatment and turned to anti-lymphoma chemotherapy subsequently, CR was achieved in two (12.5%) patients, and PR was achieved in seven (43.75%) patients. Seven (43.75%) patients remained NR. ORR was 56.25%. For those who first received anti-lymphoma chemotherapy and turned to anti-HLH treatment subsequently, PR was achieved in two (40%) patients, and three (60%) patients remained NR. ORR was 40%. In anti-HLH treatment group, five (31.25%) patients achieved PR and 11 (68.75%) patients remained NR. ORR was 31.25%. In anti-lymphoma treatment group, CR was achieved in one (50%) patient while one (50%) patient remained NR. ORR was 50%. One patient only received glucocorticoid treatment but remained NR. There was no significant difference in ORR among different treatment groups.

We also compared treatment and response of EBV-positive LAHS patients and EBV-negative LAHS patients in our department. Treatment choice for these patients was significantly different, with a higher proportion of EBV-positive LAHS patients (52.2%) receiving combined treatment than EBV-negative LAHS patients (31.4%, P=0.033, **Table S2**). The ORR of EBV-positive LAHS patients (47.8%) was similar to that of EBV-negative LAHS patients (51.4%). The ORR of EBV-negative LAHS patients who received combined treatment (72.7%) tended to be higher than that of EBV-positive LAHS patients (58.3%), especially for those who first underwent anti-HLH treatment and turned to anti-lymphoma treatment subsequently (80% v.s. 63.2%), but the difference was insignificant (**Table S3**).

Survival Outcome

With a median follow-up of 79.5 (10-605) days, the median OS of the total cohort was 61 (95% CI 47.9-74.1) days. The median OS of EBV-positive NK/T cell LAHS patients was 65 (95% CI 52.7-77.3) days, while that of EBV-positive B cell LAHS or EBV-positive HL LAHS was not evaluable due to limited sample size. Patients whose baseline plasma EBV DNA exceeded 10^5 copies/mL (median 51 days, 95%CI 30.6-71.4 days) tended to display worse OS compared to patients whose plasma EBV DNA was no more than 10^5 copies/mL (median 188 days, 95%CI 151.0-225.0 days), but the difference was not significant (P=0.159) (**Figure 3A**). ENKL or ANKL patients (median 56 days, 95%CI 42.8-69.2 days) tended to have a poorer OS than patients with other subtypes of lymphoma (not reached), but the difference was not significant (P=0.060) (**Figure 3B**). Patients whose baseline ALT exceeded 80 U/L (median 42 days, 95%CI 17.6-66.4 days) had a significantly worse OS than patients with baseline ALT no more than 80 U/L (median 305 days, 95%CI 95.1-514.9 days, P=0.041) (**Figure 3C**). EBV-positive LAHS patients who received combined treatment (median 78 days, 95%CI 0.1-230.5 days) had a significantly improved OS compared to patients who only received anti-HLH treatment (median 31 days, 95%CI 18.1-43.9 days) (P=0.003) (**Figure 3D**). Specifically, for patients who received combined treatment, those who first received anti-HLH treatment and turned to anti-lymphoma treatment subsequently (median 174 days, 95%CI 0.1-371.9 days) displayed a significantly better OS than patients who only received anti-HLH treatment (median 31 days, 95%CI 18.1-43.9 days, P=0.003) (**Figure 3E**). Regarding treatment response, EBV-positive LAHS patients who achieved PR or above (median 305 days, 95%CI 54.2-555.8 days) had a significantly improved OS compared to those who remained NR (median 41 days, 95%CI 31.1-50.9 days, P=0.006) (**Figure 3F**). There was no significant influence of other baseline characteristics on OS. For patients who did not receive consolidation treatment, median OS was 56 days (95%CI 28.9-83.1 days). For patients who underwent consolidation treatment, median OS was not reached. Patients who underwent consolidation treatment had a significantly better OS than those without consolidation treatment (HR 0.203, 95%CI 0.048-0.865, P=0.031, **Figure S1**). Of the three patients who received PD-1 monoclonal antibody consolidation treatment, one ENKL patient died at 55 days after HLH diagnosis. A DLBCL patient and a HL patient were still alive after a follow-up of 673 days and 1484 days, respectively.

In univariate analysis, lower baseline ALT level, combined treatment of first anti-HLH regimen and subsequent anti-lymphoma regimen, achieving CR or PR were significantly related to improved OS (P=0.001, P=0.004, and P=0.009, respectively). ENKL or ANKL tended to associate with worse OS (P=0.069). There was no significant association between plasma EBV-DNA level after treatment and OS. There was no significant relationship between other baseline characteristics and OS. When combining baseline ALT level, combined treatment of first anti-HLH regimen and subsequent anti-lymphoma regimen, treatment response, and ENKL or ANKL subtype in multivariate analysis, elevated baseline ALT level was the independent risk factor of OS (P=0.025). Combined treatment of first anti-HLH regimen and subsequent anti-lymphoma regimen and achieving CR or PR were independent protective factors of OS (P=0.001, and P=0.025, respectively) (**Table 4**).

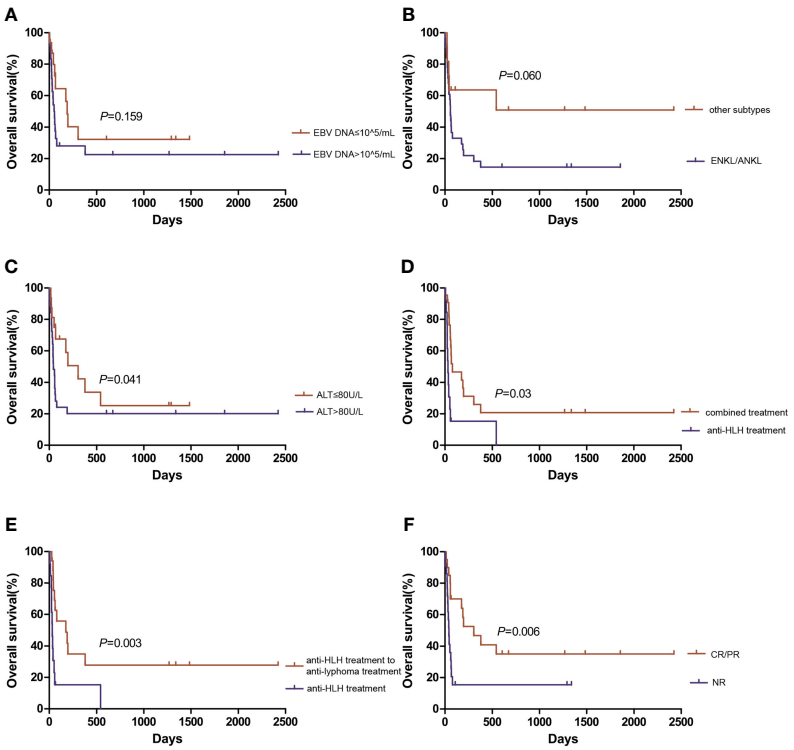

FIGURE 3 | Overall survival of EBV-positive lymphoma-associated hemophagocytic syndrome patients. Comparison of overall survival based on **(A)** plasma EBV DNA level, **(B)** lymphoma subtype, and **(C)** alanine aminotransferase level. **(D)** Comparison of overall survival between combined treatment and anti-HLH treatment. **(E)** Comparison of overall survival between anti-HLH to anti-lymphoma treatment and anti-HLH treatment. **(F)** Comparison of overall survival based on treatment response. ALT, alanine aminotransferase; ANKL, aggressive natural killer cell leukemia; CR, complete response; ENKL, extranodal NK/T-cell lymphoma, nasal type; HLH, hemophagocytic lymphohistiocytosis; NR, no response; PR, partial response.

Regarding EBV-positive T/NK cell LAHS patients, univariate analysis revealed lower ALT level, lower IL6 level, higher PT level, combined treatment of first anti-HLH regimen and subsequent anti-lymphoma regimen, achieving CR or PR were significantly related to improved OS (P=0.001, P=0.016, P=0.044, P=0.017, and P=0.013, respectively). When combining these factors in multivariate analysis, lower ALT level, combined treatment of first anti-HLH regimen and subsequent anti-lymphoma regimen,

TABLE 4 | Univariate analysis and multivariate analysis of risk factors in EBV-positive LAHS patients.

Factors	Univariate analysis			Multivariate analysis		
	HR	95% CI	*P*	HR	95% CI	*P*
HGB	0.989	0.971-1.006	0.204			
NEUT	0.897	0.763-1.055	0.190			
PLT	0.996	0.987-1.004	0.331			
ALT	1.005	1.002-1.009	0.001	1.007	1.001-1.012	0.025
TG	1.003	0.779-1.290	0.984			
FIB	0.952	0.733-1.234	0.708			
IL6	1.003	1.000-1.006	0.073			
EBV DNA>10^5 copies/mL	1.769	0.791-3.958	0.165			
ENKL or ANKL	2.458	0.933-2.476	0.069	1.263	0.369-4.326	0.710
anti-HLH to anti-lymphoma v.s. anti-HLH treatment	0.290	0.124-0.676	0.004	0.210	0.081-0.549	0.001
CR or PR v.s. NR	0.358	0.166-0.769	0.009	0.295	0.102-0.857	0.025

ALT, alanine aminotransferase; ANKL, aggressive natural killer cell leukemia; CI, confidence interval; CR, complete response; ENKL, extranodal NK/T-cell lymphoma, nasal type; FIB, fibrinogen; HGB, hemoglobin; HLH, hemophagocytic lymphohistiocytosis; HR, hazard ratio; IL6, interleukin 6; LAHS, lymphoma-associated hemophagocytic syndrome. NEUT, neutrophil; NR, no response; PLT, platelet; PR, partial response; TG, triglyceride.

and achieving CR or PR were independent protective factors of OS (*P*=0.038, *P*=0.040, and *P*=0.041, respectively).

We also compared prognosis of EBV-positive LAHS patients and EBV-negative LAHS patients in our department. OS of EBV-positive LAHS patients was similar to that of EBV-negative LAHS patients (61 v.s. 42 days, *P*=0.997, **Figure S2**). In univariate analysis of EBV-negative LAHS patients, baseline ferritin more than 2000 ng/mL (*HR*=4.222, 95%CI 1.423-12.528, *P*=0.009), and achieving CR or PR were significantly related to improved OS (*HR*=0.168, 95%CI 0.053-0.536, *P*=0.003). When combining both factors in multivariate analysis, only achieving CR or PR remained significantly related to improved OS (HR=0.228, 95%CI 0.057-0.917, *P*=0.037), serving as protective factor of prognosis.

DISCUSSION

EBV-positive LPD ranges from reactive proliferation of lymphocytes to lymphoma, and most cases have been reported in East Asia. Due to the tropism of EBV to B cells, EBV-positive LPDs mostly arise from B cell lineage. EBV-positive B-cell lymphoma consist of Burkitt lymphoma, EBV-positive DLBCL in immunocompetent patients, and non-Hodgkin lymphoma associated with human immunodeficiency virus infection in immunodeficient patients. The latent proteins expressed by EBV can immortalize B cell, and the recurrent PD-L1 expression on lymphoma cells indicates an important role of immune evasion in B-cell lymphomagenesis (18, 19). EBV-positive T and NK-cell lymphoma mainly include ENKL, ANKL, systemic EBV-positive T-cell lymphoma of childhood, and primary EBV-positive nodal T and NK-cell lymphoma. The recurrent deletion of LMP1 gene of EBV impairs immune recognition, leading to T and NK-cell lymphomagenesis (20, 21). HLH is a rare hyperinflammatory syndrome triggered by various factors, frequently stimulated by lymphoma or EBV infection. Though some case reports of EBV-positive LAHS have been published, deeper investigation of the disease with a larger sample size is required due to the overlapping clinical manifestations and the poor prognosis. Thus, this study is one of the first and largest cohorts of EBV-positive LAHS patients, aiming at revealing clinical characteristics, management, and prognosis of the disease.

In our study of EBV-positive LAHS patients, T/NK cell lymphoma accounted for 86.3%, while B cell lymphoma only accounted for 9.8%. The proportion of T/NK cell lineage in EBV-positive LAHS was noticeably higher than that in LAHS cohorts of western countries (22), and slightly higher than that in other LAHS cohorts of East Asia (23). This phenomenon could be explained by the following hypothesis. First, ENKL and EBV infection were more prevalent in East Asia than otherwhere. Second, HLH was more commonly triggered by T/NK cell lymphoma than B cell lymphoma. Additionally, it was found in our study that EBV-positive T/NK cell LAHS patients were significantly younger than EBV-positive B cell LAHS patients, similar to the finding of Chang et al. (24). Besides, EBV-positive T/NK cell LAHS patients were found to display significantly lower fibrinogen levels than EBV-positive B cell LAHS patients. We hypothesized that the hyperactivation of T cells in T/NK cell lymphoma might upregulate tissue factors on macrophage surface by generating interferon-gamma, leading to abnormal coagulation activity and fibrinogen consumption (25). Moreover, EBV-positive T/NK cell LAHS patients had significantly lower CRP levels than EBV-positive B cell LAHS patients, which might be attributable to different activation mechanism of monocyte/macrophage lineage in T/NK cell LAHS and B cell LAHS (26).

EBV-associated HLH and EBV-positive LAHS share overlapping clinical manifestations and lab tests, making differential diagnosis thorny and the lymphoma background underestimated. Previous studies have reported that the majority of LAHS manifested itself as HLH upon disease onset, without definite history or evidence of lymphoma (27). In our study, HLH occurred prior to or at the same time of lymphoma in 84.3% of EBV-positive LAHS patients. Thus, for secondary HLH patients, a thorough screening of the potential lymphoma background is needed, even if EBV infection has been confirmed. PET/CT can serve as a sensitive tool to screen lymphoma. It was reported that FDG uptake in LAHS patients was significantly higher than that in other subtypes of HLH patients, and that the level of FDG uptake was related to the extent of cytokine release storm, rendering FDG uptake as a potential predictor of LAHS prognosis (28). Consequently, PET/CT is recommended as a useful tool to search for underlying triggers of secondary HLH.

Due to lack of prospective studies in LAHS treatment, whether initial induction treatment should first focus on HLH or lymphoma has been controversial. Some experts claimed that controlling inflammation should be the priority, because LAHS patients mostly died of MODS caused by cytokine storm. The anti-lymphoma treatment brought about immunosuppression, which might aggravate infection, activate lymphocytes, and amplify cytokine storm (29, 30). Others believed that anti-lymphoma treatment should be initiated immediately with proper anti-inflammatory treatment. Otherwise, HLH might aggravate or relapse rapidly (31). In our study, all EBV-positive LAHS patients received anti-viral treatment immediately. For induction treatment, patients who first underwent anti-HLH treatment for a median time of three weeks and turned to anti-lymphoma treatment subsequently had a significantly better OS and tended to show a higher ORR than patients who only received anti-HLH treatment. This finding indicates that anti-lymphoma therapy should be initiated immediately after cytokine storm is rapidly controlled. Furthermore, diagnosis of lymphoma relies on tissue biopsy. For HLH patients, time should not be wasted on waiting for verification of pathological diagnosis. HLH-1994 regimen and other anti-cytokine storm treatment should be initiated immediately. Individualized lymphoma treatment could be conducted after pathological diagnosis is confirmed. Some studies also claimed that adding doxorubicin or liposomal doxorubicin to the HLH-1994 regimen could control both cytokine storm and lymphoma in the

meantime. R-DED (ruxolitinib-doxorubicin-etoposide-dexamethasone) regimen and DEP (liposomal doxorubicin-etoposide-methylprednisolone) regimen yielded significantly higher ORR than the traditional HLH-1994 regimen (23, 32). Thus, it is recommended that anti-HLH treatment should be initiated first and anti-lymphoma treatment should be conducted immediately after cytokine storm is controlled. Prospective studies with larger sample size are still required to explore the optimal induction regimen and strategy. On the other hand, immune evasion has been reported to participate in pathogenesis of EBV-positive HL and EBV-positive DLBCL (33). For consolidation therapy, the EBV-positive HL patient and the EBV-positive DLBCL patient received PD-1 monoclonal antibody consolidation treatment and remained alive until now in our study, indicating the potential application of PD-1 immunotherapy to EBV-positive LAHS treatment.

The prognosis of LAHS is poor. Zhou et al. reported that median OS of LAHS patients on HLH-1994 treatment was only 1.5 months (23). Bigenwald et al. also discovered that median OS of NK/T cell LAHS patients was only 40 days (34). In our study, the median OS of EBV-positive LAHS patients was 61 days, similar to the LAHS study of Ishii et al. (30). Studies investigating prognosis predictors of LAHS patients are rare. Higher ECOG score, skin involvement, lower fibrinogen level, jaundice have been reported as risk factors of LAHS prognosis (24, 35, 36). Studies exploring risk factors of EBV-positive LAHS are lacking. Our study revealed that higher ALT level was an independent risk factor of the disease. Patients who received combined treatment and those who achieved CR or PR had a better prognosis.

With the high prevalence of EBV infection and EBV-associated LPD in East Asia, our study is one of the largest cohort studies to explore clinical features, management, and prognosis of the rare but devastating EBV-positive LAHS. Regarding limitations, this is a single-center, retrospective study, which might bring about selection bias and confounders. Second, the follow-up is relatively short, restricting the observation of clinical outcome. Prospective, multi-center studies with larger sample size and longer follow-up is needed to further investigate optimal management and prognosis predictors of the disease in the future.

DATA AVAILABILITY STATEMENT

The original contributions presented in the study are included in the article/**Supplementary Material**. Further inquiries can be directed to the corresponding author.

ETHICS STATEMENT

The studies involving human participants were reviewed and approved by West China Hospital, Sichuan University. Written informed consent to participate in this study was provided by the participants' legal guardian/next of kin.

AUTHOR CONTRIBUTIONS

Study conception and design: AZ and TN. Acquisition of data: AZ, JY, ML, LL, XG, JW, HL, KS, and YY. Analysis and interpretation of data: AZ, JY, JW, HL, KS, YY, and TN. Statistical analysis: AZ, JY, ML, LL, and XG. Drafting the article: AZ, JY, ML, LL, and XG. Critical revision of the article: JW, HL, KS, YY, and TN. All authors contributed to the article and approved the submitted version.

FUNDING

This work was supported by Incubation Program for Clinical Trials (No. 19HXFH030), Achievement Transformation Project (No. CGZH21001), 1.3.5 Project for Disciplines of Excellence, West China Hospital, Sichuan University (No. ZYJC21007), Translational Research Grant of NCRCH (No. 2021WWB03), and China Postdoctoral Science Foundation (No. 2021M692310).

SUPPLEMENTARY MATERIAL

The Supplementary Material for this article can be found online at: https://www.frontiersin.org/articles/10.3389/fimmu.2022.882589/full#supplementary-material

REFERENCES

1. Kim WY, Montes-Mojarro IA, Fend F, Quintanilla-Martinez L. Epstein-Barr Virus-Associated T and Nk-Cell Lymphoproliferative Diseases. *Front Pediatr* (2019) 7:71. doi: 10.3389/fped.2019.00071
2. Nemerow GR, Mold C, Schwend VK, Tollefson V, Cooper NR. Identification of Gp350 as the Viral Glycoprotein Mediating Attachment of Epstein-Barr Virus (Ebv) to the Ebv/C3d Receptor of B Cells: Sequence Homology of Gp350 and C3 Complement Fragment C3d. *J Virol* (1987) 61(5):1416–20. doi: 10.1128/jvi.61.5.1416-1420.1987
3. Dojcinov SD, Fend F, Quintanilla-Martinez L. Ebv-Positive Lymphoproliferations of B- T- and Nk-Cell Derivation in Non-Immunocompromised Hosts. *Pathogens* (2018) 7(1):28. doi: 10.3390/pathogens7010028
4. Kataoka K, Miyoshi H, Sakata S, Dobashi A, Couronné L, Kogure Y, et al. Frequent Structural Variations Involving Programmed Death Ligands in Epstein-Barr Virus-Associated Lymphomas. *Leukemia* (2019) 33(7):1687–99. doi: 10.1038/s41375-019-0380-5
5. Roemer MG, Advani RH, Ligon AH, Natkunam Y, Redd RA, Homer H, et al. Pd-L1 and Pd-L2 Genetic Alterations Define Classical Hodgkin Lymphoma and Predict Outcome. *J Clin Oncol* (2016) 34(23):2690–7. doi: 10.1200/jco.2016.66.4482
6. Kiyasu J, Miyoshi H, Hirata A, Arakawa F, Ichikawa A, Niino D, et al. Expression of Programmed Cell Death Ligand 1 Is Associated With Poor Overall Survival in Patients With Diffuse Large B-Cell Lymphoma. *Blood* (2015) 126(19):2193–201. doi: 10.1182/blood-2015-02-629600
7. Satou A, Nakamura S. Ebv-Positive B-Cell Lymphomas and Lymphoproliferative Disorders: Review From the Perspective of Immune Escape and Immunodeficiency. *Cancer Med* (2021) 10(19):6777–85. doi: 10.1002/cam4.4198
8. Sakakibara A, Kohno K, Ishikawa E, Suzuki Y, Shimada S, Eladl AE, et al. Age-Related Ebv-Associated B-Cell Lymphoproliferative Disorders and Other Ebv + Lymphoproliferative Diseases: New Insights Into Immune Escape and Immunodeficiency Through Staining With Anti-Pd-L1 Antibody Clone Sp142. *Pathol Int* (2020) 70(8):481–92. doi: 10.1111/pin.12946

9. Ramos-Casals M, Brito-Zerón P, López-Guillermo A, Khamashta MA, Bosch X. Adult Haemophagocytic Syndrome. *Lancet* (2014) 383(9927):1503–16. doi: 10.1016/s0140-6736(13)61048-x
10. Yao S, Wang Y, Sun Y, Liu L, Zhang R, Fang J, et al. Epidemiological Investigation of Hemophagocytic Lymphohistiocytosis in China. *Orphanet J Rare Dis* (2021) 16(1):342. doi: 10.1186/s13023-021-01976-1
11. Han L, Li L, Wu J, Li X, Zhang L, Wang X, et al. Clinical Features and Treatment of Natural Killer/T Cell Lymphoma Associated With Hemophagocytic Syndrome: Comparison With Other T Cell Lymphoma Associated With Hemophagocytic Syndrome. *Leuk Lymphoma* (2014) 55 (9):2048–55. doi: 10.3109/10428194.2013.876629
12. Han AR, Lee HR, Park BB, Hwang IG, Park S, Lee SC, et al. Lymphoma-Associated Hemophagocytic Syndrome: Clinical Features and Treatment Outcome. *Ann Hematol* (2007) 86(7):493–8. doi: 10.1007/s00277-007-0278-6
13. Iizuka H, Mori Y, Iwao N, Koike M, Noguchi M. Hemophagocytic Lymphohistiocytosis Associated With Epstein-Barr Virus-Positive Diffuse Large B-Cell Lymphoma, Nos of Bone Marrow-Liver-Spleen Type: An Autopsy Case Report. *J Clin Exp Hematop* (2021) 61(2):102–8. doi: 10.3960/jslrt.20053
14. Ricard JA, Charles R, Tommee CG, Yohe S, Bell WR, Flanagan ME. Epstein Virus Barr-Positive Diffuse Large B-Cell Lymphoma Associated With Hemophagocytic Lymphohistiocytosis. *J Neuropathol Exp Neurol* (2020) 79 (8):915–20. doi: 10.1093/jnen/nlaa061
15. Iardino A, Amar Z, Ahmed Y. Epstein-Barr-Positive Classical Hodgkin Lymphoma-Associated Haemophagocytic Lymphohistocytiosis: A Rare Case. *BMJ Case Rep* (2018) 2018:1–4. doi: 10.1136/bcr-2018-225262
16. Swerdlow SH, Campo E, Pileri SA, Harris NL, Stein H, Siebert R, et al. The 2016 Revision of the World Health Organization Classification of Lymphoid Neoplasms. *Blood* (2016) 127(20):2375–90. doi: 10.1182/blood-2016-01-643569
17. Henter JI, Horne A, Aricó M, Egeler RM, Filipovich AH, Imashuku S, et al. Hlh-2004: Diagnostic and Therapeutic Guidelines for Hemophagocytic Lymphohistiocytosis. *Pediatr Blood Cancer* (2007) 48(2):124–31. doi: 10.1002/pbc.21039
18. Nicolae A, Pittaluga S, Abdullah S, Steinberg SM, Pham TA, Davies-Hill T, et al. Ebv-Positive Large B-Cell Lymphomas in Young Patients: A Nodal Lymphoma With Evidence for a Tolerogenic Immune Environment. *Blood* (2015) 126(7):863–72. doi: 10.1182/blood-2015-02-630632
19. Kelly GL, Milner AE, Baldwin GS, Bell AI, Rickinson AB. Three Restricted Forms of Epstein-Barr Virus Latency Counteracting Apoptosis in C-Myc-Expressing Burkitt Lymphoma Cells. *Proc Natl Acad Sci USA* (2006) 103 (40):14935–40. doi: 10.1073/pnas.0509988103
20. Nagamine M, Takahara M, Kishibe K, Nagato T, Ishii H, Bandoh N, et al. Sequence Variations of Epstein-Barr Virus Lmp1 Gene in Nasal Nk/T-Cell Lymphoma. *Virus Genes* (2007) 34(1):47–54. doi: 10.1007/s11262-006-0008-5
21. Kim JE, Kim YA, Jeon YK, Park SS, Heo DS, Kim CW. Comparative Analysis of Nk/T-Cell Lymphoma and Peripheral T-Cell Lymphoma in Korea: Clinicopathological Correlations and Analysis of Ebv Strain Type and 30-Bp Deletion Variant Lmp1. *Pathol Int* (2003) 53(11):735–43. doi: 10.1046/j.1320-5463.2003.01552.x
22. Parikh SA, Kapoor P, Letendre L, Kumar S, Wolanskyj AP. Prognostic Factors and Outcomes of Adults With Hemophagocytic Lymphohistiocytosis. *Mayo Clin Proc* (2014) 89(4):484–92. doi: 10.1016/j.mayocp.2013.12.012
23. Zhou L, Liu Y, Wen Z, Yang S, Li M, Zhu Q, et al. Ruxolitinib Combined With Doxorubicin, Etoposide, and Dexamethasone for the Treatment of the Lymphoma-Associated Hemophagocytic Syndrome. *J Cancer Res Clin Oncol* (2020) 146(11):3063–74. doi: 10.1007/s00432-020-03301-y
24. Chang Y, Cui M, Fu X, Han L, Zhang L, Li L, et al. Lymphoma Associated Hemophagocytic Syndrome: A Single-Center Retrospective Study. *Oncol Lett* (2018) 16(1):1275–84. doi: 10.3892/ol.2018.8783
25. Valade S, Mariotte E, Azoulay E. Coagulation Disorders in Hemophagocytic Lymphohistiocytosis/Macrophage Activation Syndrome. *Crit Care Clin* (2020) 36(2):415–26. doi: 10.1016/j.ccc.2019.12.004
26. Mortensen RF, Zhong W. Regulation of Phagocytic Leukocyte Activities by C-Reactive Protein. *J Leukoc Biol* (2000) 67(4):495–500. doi: 10.1002/jlb.67.4.495
27. Lehmberg K, Sprekels B, Nichols KE, Woessmann W, Müller I, Suttorp M, et al. Malignancy-Associated Haemophagocytic Lymphohistiocytosis in Children and Adolescents. *Br J Haematol* (2015) 170(4):539–49. doi: 10.1111/bjh.13462
28. Yang YQ, Ding CY, Xu J, Fan L, Wang L, Tian T, et al. Exploring the Role of Bone Marrow Increased Fdg Uptake on Pet/Ct in Patients With Lymphoma-Associated Hemophagocytic Lymphohistiocytosis: A Reflection of Bone Marrow Involvement or Cytokine Storm? *Leuk Lymphoma* (2016) 57 (2):291–8. doi: 10.3109/10428194.2015.1048442
29. Jordan MB, Allen CE, Weitzman S, Filipovich AH, McClain KL. How I Treat Hemophagocytic Lymphohistiocytosis. *Blood* (2011) 118(15):4041–52. doi: 10.1182/blood-2011-03-278127
30. Ishii E, Ohga S, Imashuku S, Yasukawa M, Tsuda H, Miura I, et al. Nationwide Survey of Hemophagocytic Lymphohistiocytosis in Japan. *Int J Hematol* (2007) 86(1):58–65. doi: 10.1532/ijh97.07012
31. Liang JH, Wang L, Zhu HY, Qian J, Liao H, Wu JZ, et al. Dose-Adjusted Epoch Regimen as First-Line Treatment for Non-Hodgkin Lymphoma-Associated Hemophagocytic Lymphohistiocytosis: A Single-Arm, Open-Label, Phase Ii Trial. *Haematologica* (2020) 105(1):e29–32. doi: 10.3324/haematol.2019.220301
32. Meng G, Wang Y, Wang J, Wang Z. The Dep Regimen Is Superior to the Hlh-1994 Regimen as First-Line Therapy for Lymphoma-Associated Haemophagocytic Lymphohistiocytosis. *Leuk Lymphoma* (2021) 62(4):854–60. doi: 10.1080/10428194.2020.1849671
33. Marques-Piubelli ML, Salas YI, Pachas C, Becker-Hecker R, Vega F, Miranda RN. Epstein-Barr Virus-Associated B-Cell Lymphoproliferative Disorders and Lymphomas: A Review. *Pathology* (2020) 52(1):40–52. doi: 10.1016/j.pathol.2019.09.006
34. Bigenwald C, Fardet L, Coppo P, Meignin V, Lazure T, Fabiani B, et al. A Comprehensive Analysis of Lymphoma-Associated Haemophagocytic Syndrome in a Large French Multicentre Cohort Detects Some Clues to Improve Prognosis. *Br J Haematol* (2018) 183(1):68–75. doi: 10.1111/bjh.15506
35. Lin CH, Shih YH, Chen TC, Chou CW, Hsu CY, Teng CJ. A Decade of Lymphoma-Associated Hemophagocytic Lymphohistiocytosis: Does the Outcome Improve? *J Clin Med* (2021) 10(21):5114. doi: 10.3390/jcm10215114
36. Liu YZ, Bi LQ, Chang GL, Guo Y, Sun S. Clinical Characteristics of Extranodal Nk/T-Cell Lymphoma-Associated Hemophagocytic Lymphohistiocytosis. *Cancer Manag Res* (2019) 11:997–1002. doi: 10.2147/cmar.S183784

Conflict of Interest: The authors declare that the research was conducted in the absence of any commercial or financial relationships that could be construed as a potential conflict of interest.

frontiers | Frontiers in Immunology

ORIGINAL RESEARCH
published: 27 April 2022
doi: 10.3389/fimmu.2022.873789

T Cell Defects: New Insights Into the Primary Resistance Factor to CD19/CD22 Cocktail CAR T-Cell Immunotherapy in Diffuse Large B-Cell Lymphoma

Jiachen Wang[1,2], Kefeng Shen[1,2], Wei Mu[1,2], Weigang Li[3], Meilan Zhang[1,2], Wei Zhang[1,2], Zhe Li[1,2], Tong Ge[1,2], Zhoujie Zhu[4], Shangkun Zhang[5], Caixia Chen[1,2], Shugang Xing[1,2], Li Zhu[1,2], Liting Chen[1,2], Na Wang[1,2], Liang Huang[1,2], Dengju Li[1,2], Min Xiao[1,2] and Jianfeng Zhou[1,2]**

[1] Department of Hematology, Tongji Hospital, Tongji Medical College, Huazhong University of Science and Technology, Wuhan, China, [2] Immunotherapy Research Center for Hematologic Diseases of Hubei Province, Wuhan, China, [3] Department of Pediatric Surgery, Tongji Hospital, Tongji Medical College, Huazhong University of Science and Technology, Wuhan, China, [4] Perfectgen Diagnostics, Ezhou, China, [5] Wuhan Bio-Raid Biotechnology Co., Ltd., Wuhan, China

Despite impressive progress, a significant portion of patients still experience primary or secondary resistance to chimeric antigen receptor (CAR) T-cell immunotherapy for relapsed/refractory diffuse large B-cell lymphoma (r/r DLBCL). The mechanism of primary resistance involves T-cell extrinsic and intrinsic dysfunction. In the present study, a total of 135 patients of DLBCL treated with murine CD19/CD22 cocktail CAR T-therapy were assessed retrospectively. Based on four criteria (maximal expansion of the transgene/CAR-positive T-cell levels post-infusion [C_{max}], initial persistence of the transgene by the CAR transgene level at +3 months [T_{last}], CD19+ B-cell levels [B-cell recovery], and the initial response to CAR T-cell therapy), 48 patients were included in the research and divided into two groups (a T-normal group [n=22] and a T-defect [n=26] group). According to univariate and multivariate regression analyses, higher lactate dehydrogenase (LDH) levels before leukapheresis (hazard ratio (HR) = 1.922; p = 0.045) and lower cytokine release syndrome (CRS) grade after CAR T-cell infusion (HR = 0.150; p = 0.026) were independent risk factors of T-cell dysfunction. Moreover, using whole-exon sequencing, we found that germline variants in 47 genes were significantly enriched in the T-defect group compared to the T-normal group (96% vs. 41%; p<0.0001), these genes consisted of CAR structure genes (n=3), T-cell signal 1 to signal 3 genes (n=13), T cell immune regulation- and checkpoint-related genes (n=9), cytokine- and chemokine-related genes (n=13), and T-cell metabolism-related genes (n=9). Heterozygous germline *UNC13D* mutations had the highest intergroup differences (26.9% vs. 0%; p=0.008). Compound heterozygous *CX3CR1*$^{I249/M280}$ variants, referred to as pathogenic and risk factors according to the ClinVar database, were enriched in the T-defect group (3 of 26). In summary, the clinical characteristics and T-cell immunodeficiency genetic features may help explain the

Edited by:
Wei Sang,
The Affiliated Hospital of Xuzhou Medical University, China

Reviewed by:
Xudong Zhang,
First Affiliated Hospital of Zhengzhou University, China
Zijun Y. Xu-Monette,
Duke University Medical Center, United States

***Correspondence:**
Min Xiao
xiaomin@tjh.tjmu.edu.cn
Jianfeng Zhou
jfzhou@tjh.tjmu.edu.cn

Specialty section:
This article was submitted to Cancer Immunity and Immunotherapy, a section of the journal Frontiers in Immunology

Received: *11 February 2022*
Accepted: *21 March 2022*
Published: *27 April 2022*

Citation:
Wang J, Shen K, Mu W, Li W, Zhang M, Zhang W, Li Z, Ge T, Zhu Z, Zhang S, Chen C, Xing S, Zhu L, Chen L, Wang N, Huang L, Li D, Xiao M and Zhou J (2022) T Cell Defects: New Insights Into the Primary Resistance Factor to CD19/CD22 Cocktail CAR T-Cell Immunotherapy in Diffuse Large B-Cell Lymphoma. Front. Immunol. 13:873789. doi: 10.3389/fimmu.2022.873789

underlying mechanism of treatment primary resistance and provide novel insights into CAR T-cell immunotherapy.

Keywords: CAR-T cell immunotherapy, immune resistance, primary immunodeficiencies, T cell dysfunction, germline alterations, LDH – lactate dehydrogenase, cytokine release syndrome (CRS), DLBCL - diffuse large B cell lymphoma

INTRODUCTION

CAR T- cell immunotherapy has demonstrated unprecedented efficacy in relapsed/refractory large B-cell lymphoma (1). Previously, we reported the remarkable safety and efficacy of CD19/22 CAR T-cell cocktail immunotherapy alone and following autologous stem cell transplantation (ASCT) in the treatment of adult patients with r/r B-cell malignancies (2–7). However, a substantial number of patients treated with CAR T cells may experience primary (no response, NR) or secondary (initial response followed by relapse/escape) resistance.

Primary resistance occurs at significantly higher rates in diffuse large B-cell lymphoma (DLBCL) (27% to 48%) than in B-cell precursor acute lymphoblastic leukemia (B-ALL) (19%), follicular lymphoma (14%), and mantle cell lymphoma (16%) with tisagenlecleucel and lisocabtagene maraleucel (8). Several studies reported that primary resistance was correlated with weaker expansion (maximal expansion of transgene/CAR-positive T-cell levels post-infusion [C_{max}]) and shorter persistence (CAR transgene level at +3 months [T_{last}]) of CAR T cells in r/r non-Hodgkin lymphoma (NHL) (9–11). In addition, the potent antitumor activity of CD19 CAR T cells in patients is associated with long-term B-cell aplasia (BCA) (12). In this study, T-cell dysfunction-related primary resistance was assessed by the expansion (C_{max}) and the persistence (T_{last}) of the CAR transgene, $CD19^+$B cell aplasia, and initial response after CAR T-cell infusion. In contrast, the mechanisms of T-cell dysfunction-related primary resistance remain poorly understood, in which extrinsic and intrinsic factors might play roles.

Abbreviations: 95%CI, 95% confidence interval; AE, adverse events; ASCT, autologous stem cell transplantation; B-ALL, B-cell precursor acute lymphoblastic leukemia; BEAM, bis-carmustine, etoposide, cytarabine, melphalan; BCA, B-cell aplasia; CAR, chimeric antigen receptor; C_{max}, maximal expansion of transgene; COO, cell of origin; CR, complete remission; CRS, cytokine release syndrome; CTCAE, Common Terminology Criteria for Adverse Events; ddPCR, droplet digital PCR; DLBCL, diffuse large B-cell lymphoma; FISH, fluorescence *in situ* hybridization; GO, gene ontology; HLH, hemophagocytic lymphohistiocytosis; HR, hazard ratio; IL, interleukin; IPI, international prognostic index; IQRs, interquartile ranges; IUIS, International Union of Immunological Societies; KEGG, kyoto encyclopedia of genes and genomes; LDH, lactate dehydrogenase; MAF, minor allele frequency; MTD, maximal tumor diameter; NGS, next-generation sequencing; NHL, non-Hodgkin Lymphoma; NK, natural killer; NR, no response; OS, overall survival; PBMCs, peripheral blood mononuclear cells; PD, progressive disease; PET/CT, positron emission tomography/computed tomography; PFS, progression-free survival; PIDs, primary immunodeficiencies PR, partial remission; r/r, relapsed/refractory; SD, stable disease; SNPs, single-nucleotide polymorphisms; TCR, T cell receptors; T_{last}, persistence of CAR transgene; TME, tumor microenvironment; ULN, upper limit of normal; WES, whole exon sequencing; WT, wild type.

Extrinsic factors might influence CAR T-cell function. It has been reported that an immunosuppressive tumor microenvironment (TME), such as $CD4^+CD25^+$ regulatory T cells and myeloid-derived suppressor cells and their respective proinflammatory factors, may generate resistance to CAR T cell treatment (13). Disease burden can positively affect the degree of cell expansion in B-ALL, which in turn might increase the risk and severity of cytokine release syndrome (CRS) (14, 15). In addition, a high tumor burden might trigger an aberrant immune microenvironment and T cell exhaustion (16). However, Liu et al. reported that no explicit significance was found in the relationship between tumor burden and CAR T-cell expansions and persistence in r/r DLBCL (17). Other risk factors, including cytokines, inhibitory receptors, and competition for nutrients within the TME, also contribute to CAR T cell dysfunction (18). Moreover, the influence of meditation, such as corticosteroids, tocilizumab, and bendamustine, is still controversial and needs to be further studied.

T-cell dysfunction can also be driven by T cell-intrinsic factors. The relevant studies have focused on three fields. First, the inherent T cell memory phenotype abnormalities revealed by flow cytometry showed that an elevated frequency of $CD27^+CD45RO^-CD8^+$ T cells was associated with sustained remission (11). Second, characteristic transcriptomic profiling indicated by RNA sequencing showed that T cell clusters with higher expression of cytotoxicity (PRF1, GZMB, and GZMK) and proliferation genes were corrected with good ability in expansion and persistence (19). Third, next-generation sequencing (NGS) studies suggested that transgenes integrated into the *TET2* locus may also occur in CAR T-cell therapy (20). In addition to these alterations, inborn errors of immunity, referred to as primary immunodeficiencies (PIDs), also participate in the mechanism of intrinsic T-cell defects. PID is caused by monogenic germline mutations that result in loss of function (hypomorphic), or gain-of-function (hypermorphic) of encoded protein (21). Currently studies on germline alterations are limited in CAR T-cell immunotherapy.

Germline genetic aberrations may have indications for targeted agents. For example, in the field of targeted immunotherapy, microsatellite instability and mismatch repair deficiency, which may arise from *MLH1*, *MSH2*, *MSH6*, and *PMS2* mutations, suggests potential vulnerability to PD-1 inhibitors (22). Olaparib, a poly polymerase inhibitor, is approved as maintenance therapy for patients with advanced pancreatic cancer and a germline *BRCA1* or *BRCA2* pathogenic ovarian cancer (23). Genetic studies of DLBCLs in humans have revealed an increasing number of potentially relevant germline alterations (24). However, in the field of CAR T-cell immunotherapy, it remains unclear whether germline

mutations affect cellular kinetic T-cell function. T cell germline defects add another layer of complexity in understanding the CAR T-cell therapy resistance mechanism and provide novel insight into targeted drug developments.

In this study, we analyzed the clinical and genetic characteristics of 48 r/r DLBCL patients receiving CD19/CD22 cocktail CAR T-cell therapy, aiming to characterize the prognostic factors of T cell dysfunction related to the primary resistance mechanism. This work may help explain the underlying mechanisms of primary resistance to treatment and provide novel insights into CAR T-cell immunotherapy.

MATERIALS AND METHODS

Patient Population

In our study, patients with DLBCL treated with murine CAR T-cell cocktail therapy at Tongji Hospital between January 2019 and August 2020 were enrolled according to a previous report (2, 7). Two clinical trials (Trial A and Trial B) were included in the analysis. Trial A involves a murine CAR19/22 T-cell "cocktail" therapy, and Trial B involves an ASCT followed by CAR19/22 T-cell "cocktail" therapy. The timeline of leukapheresis, leukodepletion, chimeric antigen receptor therapy T-cell (CAR-T) infusion, and the follow-up period are described in **Figure S1**.

All the patients were followed up until they died, lost to follow-up, or withdrew consent. A series of screening conditions were set up to select patients with typical T-cell characteristics (**Figure 1**). Patients were divided into 2 groups: a T-normal group (n=22) and a T-defect group (n=26). Grouping was based on four criteria (maximal expansion of transgene/CAR-positive T-cell levels post-infusion [C_{max}], initial persistence of transgene by CAR transgene level at +3 months [T_{last}], $CD19^+$ B-cell levels [B-cell recovery], and initial response assessment after CAR-T cell infusion). Patient characteristics and outcomes were collected retrospectively. The raw data are shown in **Table S1**.

Further details regarding the study procedures are described in the **Supplementary Methods**. This study was carried out following the Declaration of Helsinki and approved by the Medical Ethics Committee of the Department of Hematology, Tongji Hospital, Tongji Medical College, Huazhong University of Science and Technology (ChiCTR-OPN-16009847, ChiCTR-OPN-16008526). Because of the retrospective nature of the study and that the specimens used were the remaining samples of clinical testing retrospectively, free of additional harm to the patients, the need for informed consent was waived.

Bioanalytical Methods

Peripheral blood was collected from patients to evaluate post-infusion CAR transgene levels *via* droplet digital PCR (ddPCR).

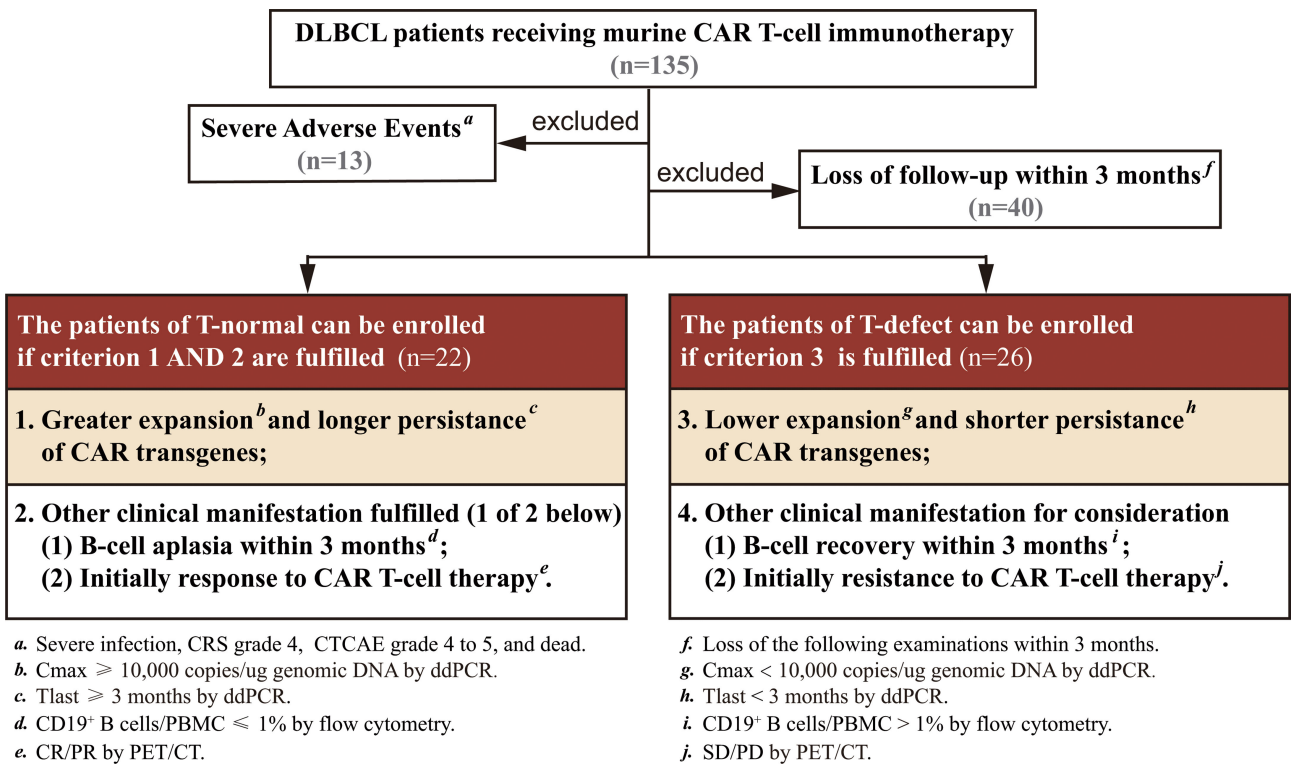

FIGURE 1 | Flow diagram summarizing patient recruitment, exclusion criteria, and patient groups. Patients were divided into a T-normal group (n=22) and T-defect group (n=26) according to the criteria of CAR transgene expansion, persistence, BCA, and initial response to CAR T-cell therapy. BCA, B-cell aplasia; CR, complete remission; CRS, cytokine release syndrome; CTCAE, common terminology criteria adverse events; ddPCR, droplet digital PCR; PET/CT, positron emission tomography-computed tomography; PR, partial remission; SD, stable disease; PD, disease progression.

The details related to the analytical methods have been previously published (2). CAR transgene was detected by ddPCR measurements before lymphodepletion chemotherapy; just after infusion; on days 4, 7, 11, 14, 17, 21, and 28; and at months 2 and 3. Bone marrow collection occurred at screening, day 28 if the patient was in complete response (CR), and at month 3. Partitioning of the CAR transgene was assessed by the ratio of bone marrow concentrations to peripheral blood levels. Cellular kinetics exposure parameters included maximal expansion of transgene/CAR-positive T-cell levels post-infusion (C_{max}) and persistence (duration transgene/CAR-T cells are present in peripheral blood and tissues [T_{last}]). The results are reported as transgene copies/micrograms of genomic DNA for ddPCR. $CD19^+$ B-cell levels were evaluated pre-/post-infusion to monitor B-cell aplasia *via* flow cytometry (25).

Staging and response assessments were defined according to the National Comprehensive Cancer Network guidelines and Lugano Treatment Response Criteria (26). CRS was graded according to the scale proposed by Lee et al. (27). Risk factors for the CRS grade included high marrow tumor burden, lymphodepletion *via* cyclophosphamide and fludarabine, higher CAR-T cell dose, thrombocytopenia before lymphodepletion, and manufacturing of CAR-T cells without selection of $CD8^+$ central memory T cells (28). CAR T cell-related encephalopathy syndrome and other adverse events (AEs) were evaluated according to Common Terminology Criteria for Adverse Events (CTCAE) v.4.03 (29).

Tumor burden was approximated using lactate dehydrogenase (LDH) levels before leukapheresis or CAR-T cell infusion, and maximum tumor diameter (MTD) was measured on CT or positron emission tomography/computed tomography (PET/CT) scans (30). Interphase fluorescence *in situ* hybridization (FISH) was performed using commercially available probes (Abbott Molecular, Downers, Grove, IL, USA). LSI IGH/IGHV (14q32), LSI MYC (8q24) Dual Color, break-apart rearrangement probes were used to detect the rearrangement of *BCL2*, *BCL6*, and *C-MYC*, respectively. A 17p13.1 (P53) probe (Vysis, Downers, Grove, IL) was used to detect 17p deletions. Sample preparations and hybridizations were conducted following the manufacturer's recommendations, and 200 cells were analyzed for each probe as previously reported (31).

Targeted Sequencing Analysis

Targeted high-throughput sequencing was applied for somatic alterations. A total of 57 genes were selected in this study (listed in **Table S2**). Most genes were frequently altered in DLBCL, according to data from several previously published large-scale DLBCL group studies (32–34). Using genome build hg19/GRCh37 as a reference, a sequencing panel covering the coding sequences within five intronic base pairs around exons in 57 genes was designed online (Designstudio Sequencing, Illumina, San Diego, USA). Sequencing libraries were prepared with AmpliSeq™ Library PLUS for Illumina, using 20 ng of input genomic DNA per sample. Library sequencing was performed to 2000X coverage on a NextSeq™ 550 system using an Illumina NextSeq™ 500/550 High Output v2 Kit (Illumina, San Diego, USA). The alignment and variant calling were performed using a DNA Amplicon workflow with default parameters on BaseSpace Sequence Hub (Illumina). The generated variants were further annotated using ANNOVAR (35). Further details are described in the **Supplementary Methods**.

Whole-Exome Sequencing (WES) Analysis

We performed WES for germline alteration analysis. The T cell-related gene panel included ten categories of CAR-T and T-cell biology (I=CAR structure; II=TCR signal; III=T cell co-stimulation signal; IV= interleukin 2 (IL-2) signal; V=Immune dysregulation; VI=JAK-STAT signal; VII=Immune checkpoints; VIII=cytokines; IX=chemokines; and X=Metabolism). A total of 124 genes were enrolled in the panel (listed in **Table S3**). In addition, the gene panel of Human Inborn Errors of Immunity was set up according to the 2019 update on the classification from the International Union of Immunological Societies (IUIS) Expert Committee, the gene number of which was 403 (listed in **Table S4**) (21). Forty-nine genes (e.g., *CD19*, *CD3D*, *TNFRSF9*, *UNC13D*, *JAK3*, *IFNAR1*, *CSF3R*, *IL10*) overlapped in the two panels.

Genomic DNA was extracted from PBMCs with a QIAmp DNA Blood Mini kit (Qiagen, Germany) according to the manufacturer's instructions. An Agilent SureSelect Human All ExonV6 Kit (Agilent Technologies, Santa Clara, CA, USA) was used for exome capture. The genomic DNA was sequenced by Illumina NovaSeq following the manufacturer's protocols. BWA software aligned the raw data to the human genome (hg37). Public databases (1000G_EAS, ExAC_EAS, and GenomAD_EAS) were used to filter and remove common single-nucleotide polymorphisms (SNPs). Rare variants with minor allele frequency (MAF) ≤ 0.03 were included. The study strategies of germline and somatic mutations are displayed in **Figure S2**. Further details regarding the study procedures are described in the **Supplementary Methods**.

Statistical Analysis

Patients' baseline and clinical characteristics were described in **Tables 1**, **2**, using the means ± standard deviations for normally distributed continuous variables (e.g., age), medians and interquartile ranges (IQRs) for nonnormally distributed continuous variables (e.g., lines prior to CAR-T, cycles prior to CAR-T), and counts and percentages for categorical variables (e.g., male sex, disease stage). Student's t test, the Mann-Whitney U test, and Pearson's Chi-Squared test were applied to compare the above results. After assigned values for statistically significant variables (**Table 3**), the values included in the regression model were: score of maximal tumor diameter (MTD), score of LDH/upper limit of normal level before leukapheresis, score of CRS grade. Univariate and multivariate forward stepwise regression analyses were performed to identify the significant risk factors for the T-cell dysfunction related to primary resistance in **Table 4**. Statistical analysis was performed using GraphPad Prism 8 and SPSS version 19 software. $P < 0.05$ (2-sided) was considered statistically significant.

TABLE 1 | Baseline characteristics of patients with and without T-cell defects after CAR-T therapy.

	All Patients (n=48)	T-normal (n=22)	T-defect (n=26)	*P*
Age in years	46.40 ± 11.52	49.52 ± 13.08	42.95 ± 8.57	0.081
Male sex	27 (56.3%)	12 (54.4%)	15 (57.7%)	0.827
IPI score				0.978
< 2 risk factors	13 (27.1%)	6 (27.3%)	7 (26.9%)	
≥ 2 risk factors	35 (72.9%)	16 (72.7%)	19 (73.1%)	
Disease stage				0.861
Stages I and II	4 (8.3%)	2 (9.1%)	2 (7.7%)	
Stages III and IV	44 (91.7%)	20 (90.9%)	24 (92.3%)	
B symptom				0.312
Yes	10 (20.8%)	6 (27.3%)	4 (15.4%)	
No	38 (79.2%)	16 (72.7%)	22 (84.6%)	
Cell of origin of cancer				0.165
Germinal center B-cell type	15 (31.3%)	10 (45.5%)	5 (19.2%)	
Nongerminal center B-cell type	25 (52.1%)	11 (50.0%)	14 (53.8%)	
Missing	8 (16.7%)	1 (4.5%)	7 (26.9%)	
Lines prior to CAR-T	3 (3-4)	3 (3-4)	3 (2-4)	0.815
Cycles prior to CAR-T	8 (7-11)	8 (7.5-11)	7 (6-12)	0.354
CAR T-cell infusion regimen				0.422
Murine CAR-T	21 (43.7%)	11 (50.0%)	10 (38.5%)	
Murine CAR-T following auto-HSCT	27 (56.3%)	11 (50.0%)	16 (61.5%)	
Average dose of CAR T cells				0.675
≤ 4 x 10^6/kg	29 (60.4%)	14 (63.6%)	15 (57.7%)	
> 4 x 10^6/kg	19 (39.6%)	8 (36.4%)	11 (42.3%)	

The values are presented as the means ± standard deviations or counts (percentages). IPI, International Prognostic Index; auto-HSCT, autologous hematopoietic stem cell transplantation.

RESULTS

Baseline Characteristics

From January 2019 to August 2020, 135 patients with r/r DLBCL were screened for eligibility, and all received murine CD19/CD22 CAR T-cell cocktail therapy. Forty-eight patients were retrospectively enrolled in the present study (**Figure 1**): 21 patients who received CAR T-cell infusion and 27 patients who received CAR T-cell therapy following ASCT. The detailed timeline and process of CAR T-cell infusion are shown in **Figure S1**.

The baseline characteristics are summarized in **Tables 1** and **S1**. There was no significant difference in age (median 49 vs. 43 years; p=0.081), international prognostic index (IPI) score (≥2 risk factors: 72.7% vs. 73.1%; p=0.978), disease stage (stage II, IV: 90.9% vs. 92.3%, p=0.312), or cell of origin (COO) (germinal center B-cell type: 45.5% vs. 19.2%, p=0.165) (36). In addition, the data in the two groups for lines (median 3 vs. 3; p=0.815) and cycles (median 8 vs. 7; p=0.815) prior to CAR-T were not significantly different. Besides, there was no difference in bridging treatment between two groups (ASCT: 50.0% vs. 61.50%; p=0.422). Furthermore, the average dose of CAR-T cells (>4 x 10^6/kg: 36.4% vs. 42.3%; p=0.675) also did not significantly differ.

T-Cell Functionality-Related Characteristics

Four T-cell functionality-related primary resistance factors were analyzed between the two groups. The C_{max} of CAR transgene DNA (p<0.0001) and T_{last} of transgene level at three months (p<0.0001) were significantly lower in the T-defect group than in the T-normal group (**Figures 2A, B**). Within three months after CAR T-cell infusion, B-cell recovery rates differed considerably between the two groups (0% in the T-normal; 37.5% in the T-defect; p=*0.002*) (**Figure 2C**). Moreover, the T-defect group had a lower response (CR/PR at initial assessment after CAR T-cell infusion) rate (33.3% vs. 100%, p<*0.0001*) than the T-normal group did (**Figure 2C**). In summary, T-cell functionality differed markedly between the two groups, which was the basis for subsequent statistical analysis.

Univariate Analysis

Factors related to disease characteristics, leukapheresis, and CAR T-cell infusion were explored (**Table 2**). The *p53* deletion incidence was 50.0% in the T-normal group and 43.8% in the T-defect group (p=0.703). Although not statistically significant, the bone marrow infection rate (40.0% vs. 18.2%; p=0.103), double hit/triple-hit lymphoma incidence (21.1% vs. 0%; p=0.163), *TP53* mutation rates (50% vs. 26.3%; p= 0.129), and bendamustine usage before leukapheresis (7.7% vs. 0%; p=0.189) were higher in the T-defect group than in the T-normal group. However, there was no significant difference in platinum-based, cyclophosphamide, or lenalidomide drug use within three months before leukapheresis (p>0.05). The median value of MTD (4.90 vs. 3.40; p=0.010; **Figure 2D**) and the LDH level before leukapheresis (307.0 vs. 222.0; p=0.020; **Figure 2E**) were higher in the T-defect group than in the T-normal group. In contrast, instant LDH (median: 472.0 vs. 244.0; p=0.153) and maximum LDH levels (median: 795.0 vs. 365.0; p=0.102) before CAR T-cell infusion were not significantly different between the two groups. Moreover, the CRS grade was significantly lower in the T-defect group (p=0.013) (**Figure 2F**).

TABLE 2 | Univariate analysis of outcomes in patients treated with CAR-T cells.

	All Patients (n=48)	T-normal (n=22)	T-defect (n=26)	*P*
Characteristics of patients				
HBV/HCV infection	18 (37.5%)	10 (45.5%)	8 (30.8%)	0.295
Bone marrow involvement	14 (29.8%)	4 (18.2%)	10 (40.0%)	0.103
***P53* deletion detected by FISH**	14 (46.7%)	7 (50.0%)	7 (43.8%)	0.703
Double-hit/triple-hit lymphoma	4 (21.1%)	0 (0.0%)	4 (21.1%)	0.164
***TP53* mutation**	15 (38.5%)	5 (26.3%)	10 (50.0%)	0.129
Tumor maximum diameter (cm)	4.30 (2.10-6.75)	3.40 (1.65-4.50)	4.90 (4.10-9.20)	**0.010**
Bendamustine	2 (4.2%)	0 (0.0%)	2 (7.7%)	0.189
Leukapheresis related factors				
Days from initial diagnosis to leukapheresis	456.0 (295.5-770.75)	537.0 (327.5-827.0)	400.0 (221.0-683.0)	0.175
LDH level before leukapheresis	240.50 (198.5-787.3)	222.0 (190.0-329.5)	307.0 (210.00-559.0)	**0.020**
Platinum-based drugs (3 months)	22 (45.8%)	10 (45.5%)	11 (42.3%)	0.827
CTX (3 months)	15 (31.3%)	5 (22.7%)	10 (38.4%)	0.241
Lenalidomide (3 months)	3 (6.3%)	2 (9.1%)	1 (3.8%)	0.454
CAR T-cell infusion-related factors				
Days from initial diagnosis to CAR T-cell infusion	463.0 (298.0-787.3)	554.0 (309.5-841.0)	420.0 (236.0-694.0)	0.247
LDH level before CAR T-cell infusion (IU/L)	356.0 (195.8-414.8)	244.0 (186.0-557.5)	472.0 (255.0-685.0)	0.153
Maximum LDH level prior to CAR T-cell infusion (IU/L)	520.0 (274.5-1208.0)	365.0 (243.0-1012.5)	795.0 (414.0-1590.0)	0.102
CRS				**0.013**
Grade 0	14.9 (29.2%)	2 (9.1%)	12 (46.2%)	
Grade 1	19 (41.3%)	9 (40.9%)	10 (38.5%)	
Grade 2	13 (28.3%)	9 (40.9%)	4 (15.4%)	
Grade 3	2 (4.3%)	2 (9.1%)	0 (0.0%)	
Grade 4	0 (0.0%)	0 (0.0%)	0 (0.0%)	
Dexamethasone	12 (25%)	6 (27.3%)	6 (23.1%)	0.738

Values in bold refer to P-value <0.05. CRS, cytokine release syndrome; CTX, cyclophosphamide; FISH, fluorescence in situ hybridization; HBV, hepatitis B virus; HCV, hepatitis C virus; LDH, lactate dehydrogenase.

Univariate and Multivariate Logistic Regression Analysis

Uni- and multivariate logistic regression analyses of overall survival (OS) were performed by including broad groupings of patient characteristics to define the clinical factors correlated with T-cell dysfunction. The three risk factors above, namely, MTD, LDH level before leukapheresis, and CRS grade after CAR T-cell infusion, were included in the regression analysis. First, values were assigned for these variables, as listed in **Table 3**. Second, univariate logistic regression analysis revealed that these factors were statistically significant risks (**Table 4**). Furthermore, in the multivariable regression analysis, compared to T-normal group, patients with T-cell dysfunction (T-defect group) were associated with a significantly higher risk of LDH/ULN prior to leukapheresis (hazard ratio (HR) =1.922, 95% confidence interval (95% CI) 1.015-3.641, p=0.045) and decreased risk of CRS grade (HR=0.150, 95%CI 0.028-0.795, p=0.026) but no increased risk in MTD (HR=1.346; 95% CI=0.737-2.456; p=0.334). In summary, LDH/ULN before leukapheresis was associated with a significantly higher risk of T-cell dysfunction, and CRS grade was the only independent favorable factor.

TABLE 3 | Scores of factors that are significant in the univariate analysis.

Variable	Value	Score
MTD (cm)	<3	0
	3-5	1
	5-7.5	2
	7.5-10	3
	≥10	4
LDH level before leukapheresis	N times higher than ULN	N
CRS grade	0	0
	1, 2	1
	≥3	2

CRS, cytokine release syndrome; LDH, lactate dehydrogenase; MTD, maximal tumor diameter; ULN, upper limit of normal.

Somatic Features of the Genetics of the Two Groups

Targeted NGS was performed to investigate the somatic genetic alterations. Among the 48 patients, 36 samples were obtained from initial diagnosed formalin-fixed paraffin-embedded tissue (n=29) or peripheral blood circulating tumor DNA (n=7), and performed targeted NGS. A total of 259 somatic mutations (MAF ≤ 0.01) in 57 genes were identified, namely, 13 splice-site mutations, 176 missense mutations, 24 truncated mutations, 27 frameshift insertions/deletions, and 19 non-frameshift insertions/deletions (**Table S5**), exclusively in tumor cells compared to peripheral blood mononuclear cells (PBMCs). Forty-seven mutated genes were detected in the 36 "screened" cases. The most frequently mutated genes included the tumor suppressor factor gene *TP53* (42%, 16 of 36), immunoglobulin variable gene *IGLL5* (36%, 13 of 36), and epigenetic regulator gene *KMT2D* (28%, 10 of 36) (37). There was no significant difference in somatic mutations between the two groups (p>0.05) (**Figure 2G**). Somatic clonal evolution of three patients in the T-defect group (**Figure S3**).

TABLE 4 | Univariate and multivariate forward stepwise regression analysis.

Variable	Univariate analysis		Multivariable analysis	
	HR (95% CI)	P- Value	HR (95% CI)	P-Value
***Score of* MTD**	1.878 (1.117-3.159)	**0.017**	1.346 (0.737-2.456)	0.334
***Score of* LDH/ULN prior to leukapheresis**	2.141 (1.224-3.744)	**0.008**	1.922 (1.015-3.641)	**0.045**
***Score of* CRS grade**	0.113 (0.023-0.555)	**0.007**	0.150 (0.028-0.795)	**0.026**

Values in bold refer to P-value <0.05. 95% CI, 95% confidence interval; CRS, cytokine release syndrome; HR, hazard ratio; LDH, lactate dehydrogenase; MTD, maximal tumor diameter; ULN, upper limit of normal.

Germline Features of the Genetics of the Two Groups

The inherent T cell phenotype of CAR T cells can affect post-infusion CAR T-cell behavior (38). Intrinsic T-cell dysfunction was linked to inborn T cell biology-related genes (21). Therefore, WES of patient PBMCs was performed to explore germline genetic features. A T-cell-related gene panel containing 124 genes was constructed (**Figure 3A**). Patients in the T-defect group (counts average: 6; IQR: 4-8) harbored significantly more germline variants of the T-cell-related genes (counts average: 3; IQR: 2-6) than those in the T-normal group (**Table S6**). Forty-seven genes were presented in the factorized mutational heatmap by groups in the order of the T cell-related gene panel (**Figure 3A**) that met one of the following conditions: 1) the variants were presented only in the T-defect group, 2) the percentage in the T-defect group was more than two times than that in the T-normal group. The top 47 mutated genes that differed between the two groups were selected for the waterfall plot (96% vs. 41%; $p<0.0001$). Genes were arranged according to the order of the T cell-related gene panel (**Figure 3B**). The chi-square tests indicated that gene variants of CAR structure ($p=0.016$), T cell receptors (TCR) signaling ($p=0.036$), co-stimulation signaling ($p=0.020$), immune dysregulation ($p=0.004$), JAK/STAT signaling ($p=0.016$), chemokines ($p=0.036$), and T-cell metabolism ($p=0.002$) were higher in the T-defect group than in the T-normal group. The IL-2 signal ($p=0.184$), immune checkpoint ($p=0.100$), and cytokines ($p=0.054$) were not different between the two groups. Gene Ontology (GO) and Kyoto Encyclopedia of Genes and Genomes (KEGG) analyses of the 47 differentially expressed genes enriched in the T-defect group indicated enrichment in several T cell-related immunodeficiency pathways and JAK/STAT, NF-κB, and HIF-1 signaling pathways (**Figures 4A, B**).

Heterozygous germline *UNC13D* mutations presented the highest intergroup differences (26.9% vs. 0%; $p=0.008$). Six heterozygous mutants were found in *UNC13D*. P11 and P39 shared the same missense mutation [c.1228A>C(p.Ile410Leu)]. P31 and P38 shared another frameshift deletion [c.3229_3235del; p.Arg1077SerfsTer48]. **Figure 4C** shows the protein structure of wild-type (WT) and heterozygous mutants in *UNC13D* with PyMOL software, which included the following variants: c.1228A>C(p.Ile410Leu), c.1280G>A(p.Arg427Gln), c.2240G>A(p.Ser747Asn), and c.2588G>A(p.Gly863Asp). Except for the five variants below, P11 harbored a missense mutation [c.175G>A(p.Ala59Thr)] that was beyond the modeling scope of PyMOL software. Compound heterozygous *CX3CR1* variants [c.841G>A(p.Val281Ile), and c.935C>T (p.Thr312Met)], were enriched in the T-defect group (3 of 26). The ClinVar database indicated that these two compound heterozygous mutations were *CX3CR1* (dbSNP:rs3732378, and dbSNP:rs3732379, https://www.ncbi.nlm.nih.gov/clinvar/variation/8152/), whose clinical significance was defined as pathogenic to human immunodeficiency virus type 1 infection and as a risk factor for age-related macular degeneration 12. Variants of WT and $CX3CR1^{I249/M280}$ structures were analyzed and displayed using PyMOL in **Figure 4D**.

DISCUSSION

The clinical characteristics and germline genetic framework for DLBCL that we present here provide a new and evolving understanding of the primary resistance of CAR T-cell immunotherapy and the molecular attributes that may influence therapeutic response. One key idea of this study is that T-cell dysfunction-related primary resistance could be measured by four parameters: CD19 CAR transgene expansion, persistence, $CD19^+$ B cell recovery, and therapeutic response in CAR T-cell immunotherapy. Unlike previous investigations showing that T-cell dysfunction-related primary resistance to CART19 mainly focused on the T cell memory phenotype, exhausted transcriptomic profiling, and acquired T cell destruction (11, 19, 20, 39), our study revealed a novel model that contributed to weak CAR T-cell expansion and persistence. There are three overarching phases and implications of these findings as follows: an intrinsic resistance response to T-cell related heterozygous germline alterations (e.g., *UNC13D*, *CX3CR1* mutations), followed by an extrinsic high antigen-driven T cell dysfunction measured by higher LDH level before leukapheresis, finally with the manifestation of low CRS severity (**Figure 5**).

A higher LDH level before leukapheresis was an independent risk factor for T-cell dysfunction in this study. Elevated LDH at the time of pre-infusion or pre-lymphodepletion was associated with early therapeutic response, early relapse, shorter progression-free survival (PFS), and shorter OS in B-NHL patients receiving murine CD19 CAR T-cell therapies (40–43). The presence of high lactate levels in the TME is usually associated with an acidic extracellular pH (6.5) and a lower number and activity of $CD8^+$ T cells and natural killer (NK) cells both *in vitro* and *in vivo*. High LDH levels have been shown to suppress T-cell functions, including IL-2 secretion and TCR activation (44). Together, these observations suggest that

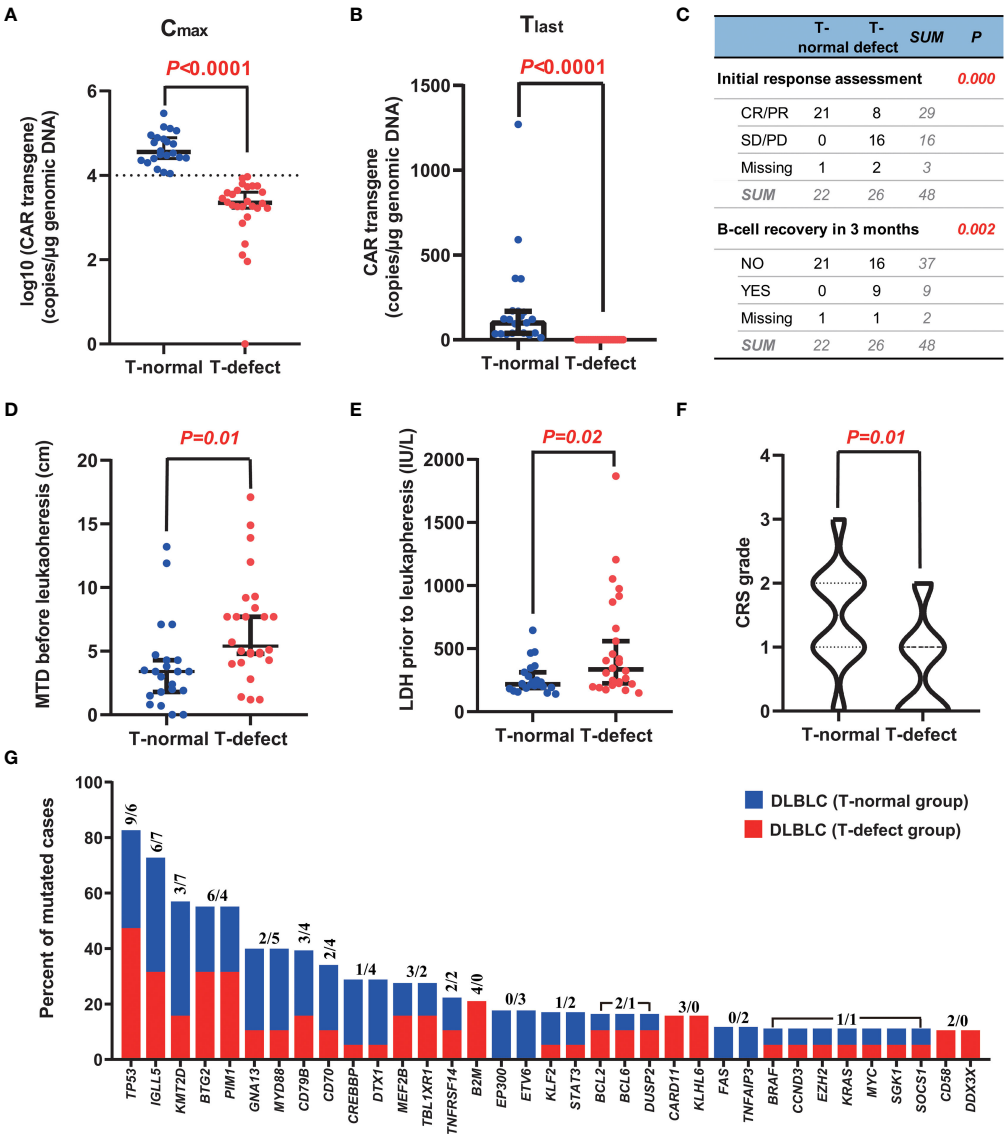

FIGURE 2 | Typical characteristics of the two groups. **(A, B)** CAR T-cell expansion (C_{max}) and persistence (T_{last} at +3 months) in peripheral blood were greater in the T-normal group than in the T-defect group (p<0.0001). **(C)** The initial response to CAR-T cell therapy was also considerably better in patients with T-normal function than in those with T-defect function (p<0.0001). In addition, there were significant differences in B-cell recovery in the T-normal group compared with the T-defect group (p=0.002). **(D, E)** MTD and LDH level in the T-normal and T-defect groups before leukapheresis demonstrate significant differences (p=0.01, and 0.02, respectively) according to the Mann-Whitney Test. **(F)** The T-normal group showed higher CRS grades than the T-defect group according to a Pearson chi-square test (p=0.01). **(G)** Recurrent somatic mutations in DLBCL. Shown is the prevalence of the indicated genetic abnormalities in 57 genes in the T-normal group (in blue) and T-defect group (in red). The two numbers for each mutation represent the counts of individuals carrying the genetic alterations in the T-defect and T-normal groups, respectively. The somatic origin of the mutations was confirmed by analysis of paired PBMC germline DNA. CAR, chimeric antigen receptor; CR, complete remission; CRS, cytokine release syndrome; PD, disease progression; PR, partial remission; SD, stable disease; SNP, single nucleotide polymorphism; MTD, maximal tumor diameter.

proceeding with leukapheresis earlier when the TMB is low in treatment may benefit patients more from CAR T-cell therapy.

CRS, the most common toxicity of cellular immunotherapy, is triggered by the activation of T cells upon the engagement of their TCRs or CARs with cognate antigens expressed by tumor cells (29). Expansion of the CAR transgene was associated with CRS severity in B-ALL and DLBCL, in accordance with our research (45). We suspect that CRS symptoms manifest T cell cytotoxicity *in vitro* and help doctors estimate patients' T-cell function early and quickly. Since severe AEs were excluded from our study, the influence of life-threatening CRS on cellular kinetics warrants future research.

Pathogenic germline alterations provide evolving insights into primary resistance mechanisms. Previously, our therapeutic

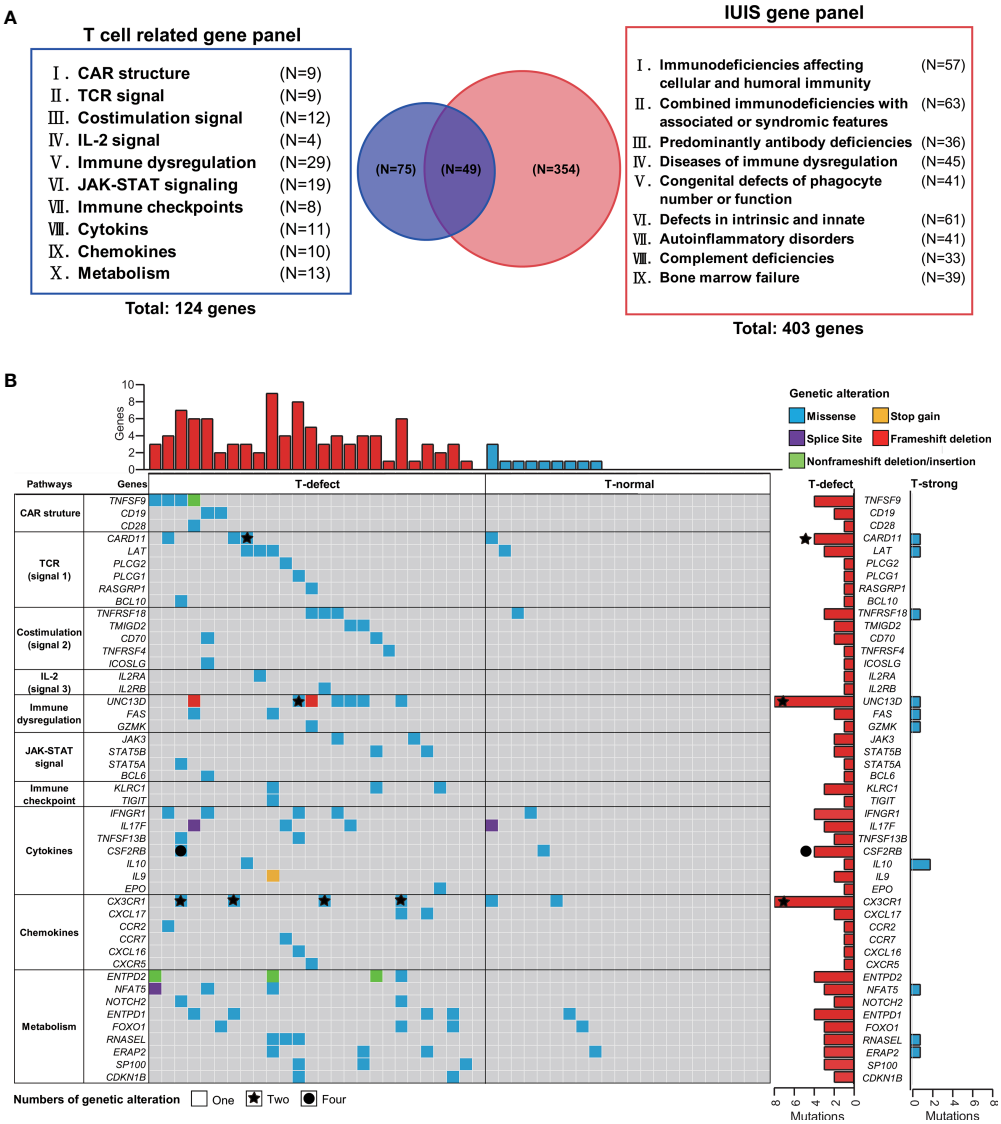

FIGURE 3 | Targeted gene panel of T-cell functions and waterfall plot of germline mutations. **(A)** One hundred and twenty-six target genes, including ten T-cell and CAR-T cell biology categories, were selected for the waterfall plot with T-cell grading information. Fifty genes were identical to primary genetic defects reported by the IUIS/WHO committee. **(B)** The top 47 mutated genes that differed between the two groups, such as *TNFSF9*, *CD19*, *CARD11*, *UNC13D*, and *CX3CR1*, were selected for the waterfall plot with T-cell group information. The genes were arranged according to the T cell-related gene panel in **(A)**. Each column corresponds to a sample, and cases are ordered by the lymphoma with T-defect on the left (red bar) and with T-normal (blue bar) on the right. The types of genetic alterations are shown as different colors as shown in the legend in the upper-right corner. The counts of genetic alterations are shown as none, stars, and circles, representing once, twice, and four times person-times, respectively. CAR, chimeric antigen receptor; JAK-STAT, Janus kinase-signal transducer and activator of transcription; IL-2, interleukin-2; IUIS, International Union of Immunological Societies; TCR, T-cell receptor; WHO, World Health Organization.

center reported two patients who harbored germline mutations and received murine monoclonal anti-CD19 and anti-CD22 CAR T-cell "cocktail" therapy (5, 46). A pathogenic *PIM1* mutation (c.403G>A, p.Glu135Lys, heterozygous) was detected in a MYC/BCL2/BCL6 triple-hit DLBCL patient, and a pathogenic *TP53* germline mutation (c.818G>A, p.R273H, heterozygous) was found in another DLBCL patient (5, 46). These two patients had weak C_{max} and T_{last} values (C_{max} < 10,000 copies/μg, T_{last} < 3 months), and the disease progressed, which met the criteria of "T-defect" group. So these two patients were suspected of having T-cell dysfunction in CAR T-cell immunotherapy. In the present study, the polygenic inheritance pattern may play a role in T-cell dysfunction.

Some germline variants are too damaging to be compatible with normal organism function, leading to monogenic inherence disease. In contrast, some germline variants may also remain asymptomatic or lead to milder disease. Compared with healthy people, patients who harbor germline mutations may be more prone to severe

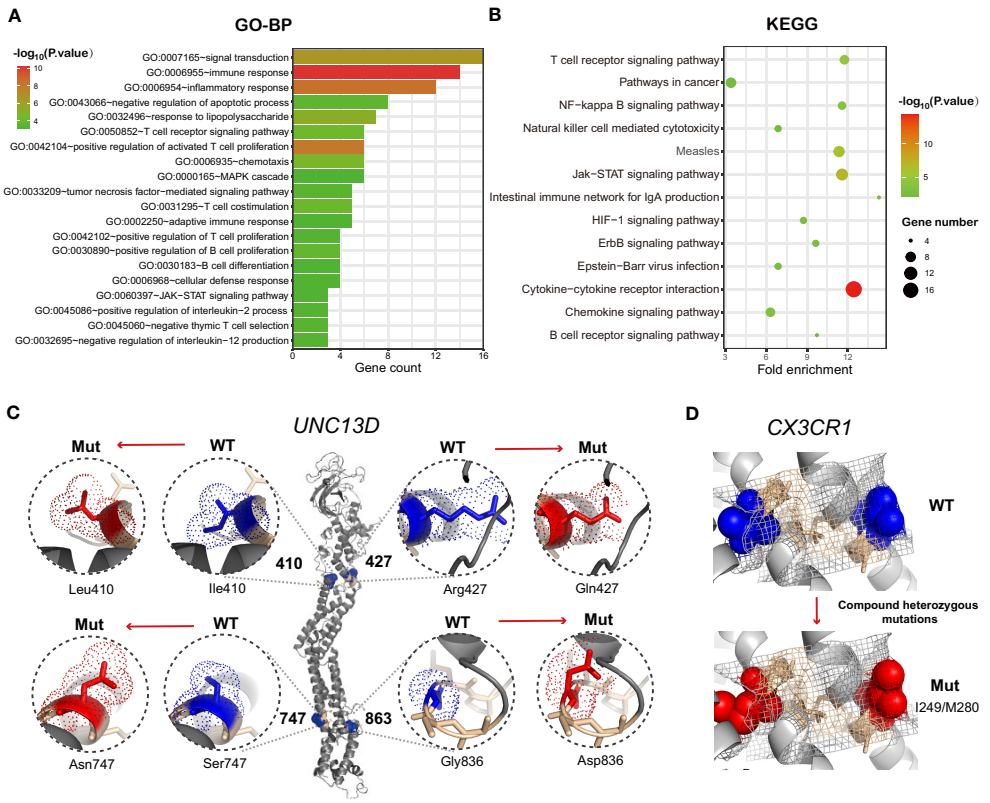

FIGURE 4 | **(A)** Histograms showing the top 20 GO-BP enrichment results of 47 differentially mutated genes between the T-defect and T-normal groups in **Figure 3B**. The x-axis represents the enriched gene count, and the intensities of the different colors represent the p values. **(B)** Bubble diagram showing the top 13 KEGG enrichment items of differentially expressed genes between the patient and two healthy donors. The x-axis represents the gene ratio, and the intensities of the different colors represent the p-values. **(C, D)** *UNC13D* mutations and *CX3CR1* compound heterozygous mutations were the most frequent germline alterations in the patients. Shown is a ribbon cartoon indicating the locations of WT and mutants in the UNC13D and CX3CR1 proteins. The figures were prepared *via* PyMOL (www.pymol.org). Four *UNC13D* alterations are reported in ClinVar (rs766652119, rs117221419, rs140184929, rs9904366). Most variants in *UNC13D* were frameshift and missense variants. The UNC13D$^{p.Arg1077SerfsTer48}$ variant [NM_199242.3(UNC13D):c.3229_3235del (p.Arg1077fs)] is defined as pathogenic by the American College of Medical Genetics and Genomics (ACMG) and is suspected for for pathogenicity for familial hemophagocytic lymphohistiocytosis (HLH). GO-BP, Gene Ontology-Biological Process; KEGG, Kyoto Encyclopedia of Genes and Genomes; WT, wild type; Mut, mutant.

symptoms (47). A multistep pathogenesis for immune diseases has been suggested, in which multiple variants, both inherited and somatic ones, contribute to the emergence of disease (48). For example, secondary hemophagocytic lymphohistiocytosis (HLH) is a life-threatening hyperinflammatory disease that may have a polygenic inheritance model. Heterozygous variants in the various "polygenic" dual gene combinations were found in various analyses (49). Not surprisingly, the genes implicated in single-gene disorders have also been linked to polygenic disorders. Polygenic inheritance patterns are likely to account for more common systemic autoimmune diseases (50).

T cell biology- and CAR-T cell structure-relevant genes were included in our analysis (n=124). Interestingly, there was considerable overlap with PID genes (n=50). An effective T cell response requires both signal one (TCR/CD3-ζ) and signal two (costimulatory signals, such as CD28 or 4-1BB). In addition, IL-2 and JAK/STAT signals are also essential for T cell activation and persistence through the activation of the JAK kinase and STAT3/5 transcription factor signaling pathways. Given the increased understanding of CAR-T cells, it is known that CAR T cells have been modified to become fifth-generation CAR T cells. The fifth-generation CAR contained a TCR signal-transduction moiety, costimulatory domains (CD), an additional cytoplasmic domain derived from IL-2Rβ and a STAT3/5 binding motif, providing antigen-dependent cytokine signaling (51). The role of immunomodulatory genes, including *UNC13D, LYST, PRF1*, *DNMT3A*, etc., is increasingly being recognized. Ishii et al. reported that one patient who developed severe CRS associated with HLH following CD19 CAR therapy for ALL was found to carry a mutation in the perforin (*PRF1*) gene, which predisposes to HLH (52). The HLH-phenotype in PRF1-deficient patients included late expansion and/or persistence of activated CAR-T cells. Deleting DNMT3A in CAR T cells prevents exhaustion and enhances antitumor activity (53). Moreover, chemokines enhance tumor T cell infiltration to enable cancer immunotherapy. Finally, T-cell metabolism-related genes were included in the analysis panel.

In this study, based on previous research methods on tumor somatic mutations, we focused on germline mutations in patients

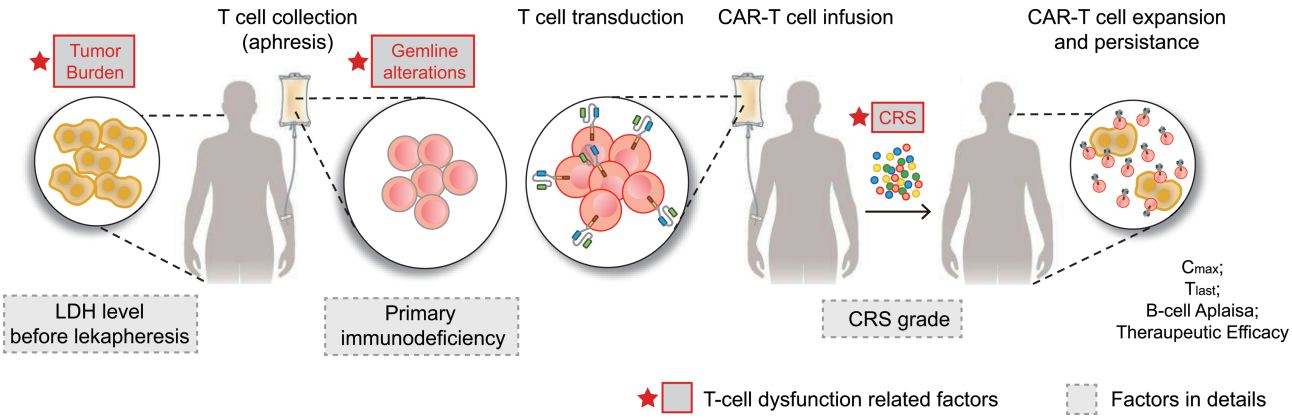

FIGURE 5 | CAR-T cell therapy and T-cell dysfunction-related factors. CAR-T therapy involves separating a patient's T cells *via* apheresis and then genetically engineering the cells to produce receptors on their surfaces, called CARs. CARs are fusion proteins of an antigen-recognition domain from a monoclonal antibody and one or more T-cell receptors. They allow T cells to recognize and attach to specific proteins, namely tumor antigens. T cells counts are expanded to hundreds of millions, after which the cells are then infused back into the patient, selectively destroying chemotherapy-resistant cancer cells. Patients receiving CAR-T are at risk for developing CRS, an inflammatory response that occurs secondary to cytokine release by infused CAR-T cells. CRS is characterized by fevers, hypotension, tachycardia, elevated inflammatory marker levels, and end-organ damage, including acute kidney injury and neurotoxicity. In summary, tumor burden (LDH level before leukapheresis), germline alterations (T cell-related PIDs), and CRS (CRS grade) were factors associated with CAR T-cell function. CAR, chimeric antigen receptor; CRS, cytokine release syndrome; LDH, lactate dehydrogenase.

(33, 54). The differential germline mutation analysis of the two groups found that the enrichment of T cell-related germline gene mutations appeared in patients with T cell defects during CAR-T therapy (**Figure 4B**). Apart from universal CAR T-cell therapy, autogenous CAR-T cells were harvested from patients' lymphocytes for modification. T cell-related germline alterations might lead to T-cell defects, which means a virtual lack of functional T cells and immune function. Patients with T-cell PID are generally categorized into the absence of T cells, the presence of B cells (T^-, B^+), or the absence of both T and B cells (T^-, B^-). However, normal T-cell numbers do not exclude the possibility of T-cell defects. These findings suggest that further investigations of T-cell function-related PID in CAR T-cell immunotherapy are warranted.

We speculate that for patients with inborn errors of immunity, autologous CAR-T cells may have expansion and persistence barriers, weakening CAR-T cell efficacy and leading to a poor prognosis. This new mechanism complements the conventional CAR-T resistance mechanism. Germline genetic characteristics remind us to consider germline mutation screening before choosing CAR-T products. Universal CAR-T cells, or fully or half-matched CAR-T cells from healthy relatives, may give rise to improved therapeutic effects for patients with T-cell immunodeficiency. Allogeneic hematopoietic stem cell transplantation might be a curative method for PID (55). Moreover, the recurrent differential mutations between the two groups might explain the mechanism of T cell defects and provide a new insight for future CAR-T transformation. Significantly, alterations in the *UNC13D* and *CX3CR1* genes were enriched in the T cell defect group.

UNC13D, which encodes the Munc13-4 protein, was the most frequently differentially mutated gene between the two groups. Activation of the TCR signaling pathway induces Munc13-4 expression in $CD8^+$ T cells (56). Munc13-4 expression is obligatory for exocytosis of lytic granules, facilitating cytotoxicity by T cells and NK cells. To date, all reported pathogenic *UNC13D* mutations evaluated for protein expression cause a marked reduction in munc13-4 protein expression (57). Germline mutations of *UNC13D* are associated with familial hemophagocytic lymphohistiocytosis type 3 (FHL3, MIM 608898). *UNC13D* deficiency-induced significantly less CD107a surface expression in $CD8^+$T cells and NK cells, resulting in T cell dysfunction in degranulation (58). Lack of cytotoxicity and antigen stimulation may be responsible for CAR-T cell defects in therapy.

The compound heterozygous $CX3CR1^{I249/M280}$ variant had specific intergroup differences, which led to the suppression of CX3CR1 protein expression. Both missenses were defined as pathogenic and risk factors by the ClinVar database. In addition, various studies indicated that in CX3CR1-deficient $CD8^+$T cells, the coinhibitory tumor receptors such as PD-1, TIM3, LAG3, and TIGIT exhibited significantly lower levels, production of effector cytokines such as IL-2 demonstrated significantly higher levels, and they also exhibited substantially lower cytotoxicity than their CX3CR1-high counterparts did both *in vivo* and *in vitro* (59, 60). The specific high expression of the chemokine CX3CL1 in DLBCL was revealed by The Cancer Genome Atlas data, which provided a solid foundation for increasing the homing ability of $CX3CR1^+$ cells. Moreover, recent studies revealed that $CX3CR1^+CD8^+$T cell subsets not only precisely predicted early response in anti-PD1 therapy, but also enhanced the anti-tumor efficacy *in vitro* (60, 61). These results strongly suggest that the deficiency of CX3CR1 targeted on the CX3CR1/CX3CL1 axis may impair the CAR-T therapeutic effect by inducing immune cell infiltration and CAR-T cell homing in DLBCL. Furthermore, more works are needed in

the future to explore the underlying mechanism and to ultimately improve the curative effect of immunotherapies for lymphoma.

Notably, though limited by sample size and the single-center nature of our high-throughput sequencing study, the current study lacks external data to support our theories further. However, we aimed to validate our model in a larger-scale multicentered study in future explorations. Considering the PID genetic diversities among different human races, we believe future research including multiple populations would provide more consolidated evidence. Further validation of these new findings and frequently mutated genes (e.g., *UNC13D*, *CX3CR1*) is helpful for determining the pathogenesis of T cell dysfunction and developing novel therapeutic strategies for CAR modification in r/r DLBCL.

The results of our studies suggest that, in CD19 CAR T-cell therapy, targeted characteristics in r/r DLBCL could be used to evaluate the prognosis of T cell dysfunction related primary resistance. First, higher LDH before leukapheresis is correlated with poorer T-cell functionality. Freezing hemopoietic stem cells in the state of low LDH burden will benefit patients. Second, those who experienced high-grade CRS were more likely to have more significant CAR transgene expansion and better T-cell functionality. Third, inborn immunity errors of polygenic heterozygous variants (e.g., T-cell signaling, T-cell cytotoxicity, T-cell regulation) potentially offer clinically meaningful strata for the early identification of high-risk individuals. Allogeneic or universal CAR-T products might be an optimal treatment and overcome this situation.

In summary, our analysis builds on the clinical examination of primary resistance in cellular immunotherapy by the addition of a T-cell-related germline genetic nosology that may inform resistance mechanisms. Our investigation revealed a new interrelationship between pathogenic germline alterations and the dynamic characteristics of the CAR transgene. This work may help explain the underlying mechanism of primary resistance to treatment and provide novel insights into CAR T-cell immunotherapy.

DATA AVAILABILITY STATEMENT

The datasets presented in this study can be found in online repositories. The names of the repository/repositories and accession number(s) can be found below: NCBI, BioProject: PRJNA804958, https://dataview.ncbi.nlm.nih.gov/.

ETHICS STATEMENT

This study was carried out following the Declaration of Helsinki and approved by the Medical Ethics Committee of the Department of Hematology, Tongji Hospital, Tongji Medical College, Huazhong University of Science and Technology (ChiCTR-OPN-16009847, ChiCTR-OPN-16008526). The ethics committee waived the requirement of written informed consent for participation.

AUTHOR CONTRIBUTIONS

JW analyzed the data and wrote the manuscript. KS and WM analyzed the data. WL, MZ, WZ, and ZL revised the manuscript and were in charge of the manuscript's final approval. TG, ZZ, SZ, CC, SX, LZ, and LC performed the experiments. NW and LH provided clinical information. DL, MX, and JZ directed the research. All authors contributed to the article and approved the submitted version.

FUNDING

This work was supported by the National Natural Science Foundation of China (No. 81770211 to MX) and the National Natural Science Foundation of China (No. 81630006 and No.81830008 to JZ).

ACKNOWLEDGMENTS

The authors would like to thank all the study team members, the patient, and his family. We would also like to thank the Bio-RAID Company for preparing CAR T cells, PerfectGen for providing DNA sequencing service, and Novogene Company for providing RNA sequencing service.

SUPPLEMENTARY MATERIAL

The Supplementary Material for this article can be found online at: https://www.frontiersin.org/articles/10.3389/fimmu.2022.873789/full#supplementary-material

Supplementary Figure 1 | Two clinical trials (Trial A and Trial B) were included in the analysis. Trial A involves a murine CAR19/22 T cell "cocktail" therapy, and Trial B involves an ASCT followed by CAR19/2 T cell "cocktail" therapy. Timeline of leukapheresis, leukodepletion, chimeric antigen receptor therapy T-cell (CAR-T) infusion, and follow-up period. CAR-T therapy involves separating a patient's T cells *via* apheresis and then genetically engineering the cells to produce receptors on their surfaces, called CARs. CARs are fusion proteins of an antigen-binding domain from a monoclonal antibody and one or more T-cell receptors. T cell counts are expanded to hundreds of millions, after which the cells are then infused back into the patient, selectively destroying chemotherapy-resistant cancer cells. Before CAR-T infusion, patients in Trial A received lymphodepleting chemotherapy in the form of cyclophosphamide and fludarabine (usually 2-4 days before CAR-T therapy), and the patients in Trial B were given a standard dose of the BEAM regimen (300 mg/m^2 bis-carmustine, –6 days; 200 mg/m^2 etoposide, –5 to –2 days; 400mg/m^2 cytarabine, –5 to –2days; and 140mg/m^2 melphalan, –1 day) as myeloablative chemotherapy, which promotes *in vivo* expansion of CAR-T cells and improves their efficacy. ASCT, autologous hematopoietic stem cell transplantation; CAR, chimeric antigen receptor (CAR)-T cell (CAR-T) therapy and its complications.

Supplementary Figure 2 | Study strategies of germline variants and somatic mutations. WES, whole-exome sequencing; VAF, variant allele frequency; MAF, minor allele frequency; 1000G_EAS,1000 Genome Project_East Asian; ExAC_EAS, Exome Aggregation Consortium_East Asian; gnomeAD_EAS, genome Aggregation Database_East Asian; dbsnp142, the database of SNP human build 14.

Supplementary Figure 3 | Somatic clonal evolution of three patients in the T-defect group. Schematic models of evolutionary progression before and after CAR T cell

infusion in three patients in the T-defect group. Primary dominant clones, secondary dominant clones, and subclones are represented in blue, red, and yellow shapes. References and VAFs of germline and somatic mutations investigated by NGS. NGS, next-generation sequencing; VAFs, variant allele frequency.

REFERENCES

1. Lin JK, Muffly LS, Spinner MA, Barnes JI, Owens DK, Goldhaber-Fiebert JD. Cost Effectiveness of Chimeric Antigen Receptor T-Cell Therapy in Multiply Relapsed or Refractory Adult Large B-Cell Lymphoma. *J Clin Oncol* (2019) 37 (24):2105–19. doi: 10.1200/JCO.18.02079
2. Wang N, Hu X, Cao W, Li C, Xiao Y, Cao Y, et al. Efficacy and Safety of CAR19/22 T-Cell Cocktail Therapy in Patients With Refractory/Relapsed B-Cell Malignancies. *Blood* (2020) 135(1):17–27. doi: 10.1182/blood.2019000017
3. Cao W, Wei J, Wang N, Xu H, Xiao M, Huang L, et al. Entecavir Prophylaxis for Hepatitis B Virus Reactivation in Patients With CAR T-Cell Therapy. *Blood* (2020) 136(4):516–9. doi: 10.1182/blood.2020004907
4. Wei J, Zhu X, Mao X, Huang L, Meng F, Zhou J. Severe Early Hepatitis B Reactivation in a Patient Receiving Anti-CD19 and Anti-CD22 CAR T Cells for the Treatment of Diffuse Large B-Cell Lymphoma. *J Immunother Cancer* (2019) 7(1):315. doi: 10.1186/s40425-019-0790-y
5. Chen L, Xu B, Long X, Gu J, Lou Y, Wang D, et al. CAR T-Cell Therapy for a Relapsed/Refractory Acute B-Cell Lymphoblastic Lymphoma Patient in the Context of Li-Fraumeni Syndrome. *J Immunother Cancer* (2020) 8(1): e000364. doi: 10.1136/jitc-2019-000364
6. Wei J, Mao Z, Wang N, Huang L, Cao Y, Sun W, et al. Long-Term Outcomes of Relapsed/Refractory Double-Hit Lymphoma (R/R DHL) Treated With CD19/22 CAR T-Cell Cocktail Therapy. *Clin Transl Med* (2020) 10(5):e176. doi: 10.1002/ctm2.176
7. Cao Y, Xiao Y, Wang N, Wang G, Huang L, Hong Z, et al. CD19/CD22 Chimeric Antigen Receptor T Cell Cocktail Therapy Following Autologous Transplantation in Patients With Relapsed/Refractory Aggressive B Cell Lymphomas. *Transplant Cell Ther* (2021) 27(11):910.e1–e11. doi: 10.1016/j.jtct.2021.08.012
8. Lemoine J, Vic S, Houot R. Disease-Specific Outcomes After Chimeric Antigen Receptor T-Cell Therapy. *Eur J Cancer* (2022) 160:235–42. doi: 10.1016/j.ejca.2021.10.022
9. Neelapu SS, Locke FL, Bartlett NL, Lekakis LJ, Miklos DB, Jacobson CA, et al. Axicabtagene Ciloleucel CAR T-Cell Therapy in Refractory Large B-Cell Lymphoma. *N Engl J Med* (2017) 377(26):2531–44. doi: 10.1056/NEJMoa1707447
10. Majzner RG, Mackall CL. Clinical Lessons Learned From the First Leg of the CAR T Cell Journey. *Nat Med* (2019) 25(9):1341–55. doi: 10.1038/s41591-019-0564-6
11. Fraietta JA, Lacey SF, Orlando EJ, Pruteanu-Malinici I, Gohil M, Lundh S, et al. Determinants of Response and Resistance to CD19 Chimeric Antigen Receptor (CAR) T Cell Therapy of Chronic Lymphocytic Leukemia. *Nat Med* (2018) 24(5):563–71. doi: 10.1038/s41591-018-0010-1
12. Paszkiewicz PJ, Frassle SP, Srivastava S, Sommermeyer D, Hudecek M, Drexler I, et al. Targeted Antibody-Mediated Depletion of Murine CD19 CAR T Cells Permanently Reverses B Cell Aplasia. *J Clin Invest* (2016) 126 (11):4262–72. doi: 10.1172/JCI84813
13. Larson RC, Maus MV. Recent Advances and Discoveries in the Mechanisms and Functions of CAR T Cells. *Nat Rev Cancer* (2021) 21(3):145–61. doi: 10.1038/s41568-020-00323-z
14. Lee DW, Kochenderfer JN, Stetler-Stevenson M, Cui YK, Delbrook C, Feldman SA, et al. T Cells Expressing CD19 Chimeric Antigen Receptors for Acute Lymphoblastic Leukaemia in Children and Young Adults: A Phase 1 Dose-Escalation Trial. *Lancet* (2015) 385(9967):517–28. doi: 10.1016/S0140-6736(14)61403-3
15. Gardner RA, Finney O, Annesley C, Brakke H, Summers C, Leger K, et al. Intent-to-Treat Leukemia Remission by CD19 CAR T Cells of Defined Formulation and Dose in Children and Young Adults. *Blood* (2017) 129 (25):3322–31. doi: 10.1182/blood-2017-02-769208
16. Long AH, Haso WM, Shern JF, Wanhainen KM, Murgai M, Ingaramo M, et al. 4-1BB Costimulation Ameliorates T Cell Exhaustion Induced by Tonic Signaling of Chimeric Antigen Receptors. *Nat Med* (2015) 21(6):581–90. doi: 10.1038/nm.3838
17. Liu C, Ayyar VS, Zheng X, Chen W, Zheng S, Mody H, et al. Model-Based Cellular Kinetic Analysis of Chimeric Antigen Receptor-T Cells in Humans. *Clin Pharmacol Ther* (2021) 109(3):716–27. doi: 10.1002/cpt.2040
18. Kloss CC, Lee J, Zhang A, Chen F, Melenhorst JJ, Lacey SF, et al. Dominant-Negative TGF-Beta Receptor Enhances PSMA-Targeted Human CAR T Cell Proliferation and Augments Prostate Cancer Eradication. *Mol Ther* (2018) 26 (7):1855–66. doi: 10.1016/j.ymthe.2018.05.003
19. Sheih A, Voillet V, Hanafi LA, DeBerg HA, Yajima M, Hawkins R, et al. Clonal Kinetics and Single-Cell Transcriptional Profiling of CAR-T Cells in Patients Undergoing CD19 CAR-T Immunotherapy. *Nat Commun* (2020) 11 (1):219. doi: 10.1038/s41467-019-13880-1
20. Fraietta JA, Nobles CL, Sammons MA, Lundh S, Carty SA, Reich TJ, et al. Disruption of TET2 Promotes the Therapeutic Efficacy of CD19-Targeted T Cells. *Nature* (2018) 558(7709):307–12. doi: 10.1038/s41586-018-0178-z
21. Tangye SG, Al-Herz W, Bousfiha A, Chatila T, Cunningham-Rundles C, Etzioni A, et al. Human Inborn Errors of Immunity: 2019 Update on the Classification From the International Union of Immunological Societies Expert Committee. *J Clin Immunol* (2020) 40(1):24–64. doi: 10.1007/s10875-019-00737-x
22. Cheng HH, Sokolova AO, Schaeffer EM, Small EJ, Higano CS. Germline and Somatic Mutations in Prostate Cancer for the Clinician. *J Natl Compr Canc Netw* (2019) 17(5):515–21. doi: 10.6004/jnccn.2019.7307
23. Reiss KA, Mick R, O'Hara MH, Teitelbaum U, Karasic TB, Schneider C, et al. Phase II Study of Maintenance Rucaparib in Patients With Platinum-Sensitive Advanced Pancreatic Cancer and a Pathogenic Germline or Somatic Variant in BRCA1, BRCA2, or PALB2. *J Clin Oncol* (2021) 39(22):2497–505. doi: 10.1200/JCO.21.00003
24. Leeksma OC, de Miranda NF, Veelken H. Germline Mutations Predisposing to Diffuse Large B-Cell Lymphoma. *Blood Cancer J* (2017) 7(2):e532. doi: 10.1038/bcj.2017.15
25. Maude SL, Frey N, Shaw PA, Aplenc R, Barrett DM, Bunin NJ, et al. Chimeric Antigen Receptor T Cells for Sustained Remissions in Leukemia. *N Engl J Med* (2014) 371(16):1507–17. doi: 10.1056/NEJMoa1407222
26. Cheson BD, Fisher RI, Barrington SF, Cavalli F, Schwartz LH, Zucca E, et al. Recommendations for Initial Evaluation, Staging, and Response Assessment of Hodgkin and Non-Hodgkin Lymphoma: The Lugano Classification. *J Clin Oncol* (2014) 32(27):3059–68. doi: 10.1200/JCO.2013.54.8800
27. Lee DW, Gardner R, Porter DL, Louis CU, Ahmed N, Jensen M, et al. Current Concepts in the Diagnosis and Management of Cytokine Release Syndrome. *Blood* (2014) 124(2):188–95. doi: 10.1182/blood-2014-05-552729
28. Hay KA, Hanafi LA, Li D, Gust J, Liles WC, Wurfel MM, et al. Kinetics and Biomarkers of Severe Cytokine Release Syndrome After CD19 Chimeric Antigen Receptor-Modified T-Cell Therapy. *Blood* (2017) 130(21):2295–306. doi: 10.1182/blood-2017-06-793141
29. Neelapu SS, Tummala S, Kebriaei P, Wierda W, Gutierrez C, Locke FL, et al. Chimeric Antigen Receptor T-Cell Therapy - Assessment and Management of Toxicities. *Nat Rev Clin Oncol* (2018) 15(1):47–62. doi: 10.1038/nrclinonc.2017.148
30. Allen SD, Wallis MG, Cooke R, Swerdlow AJ. Radiologic Features of Breast Cancer After Mantle Radiation Therapy for Hodgkin Disease: A Study of 230 Cases. *Radiology* (2014) 272(1):73–8. doi: 10.1148/radiol.14131789
31. Zhang W, Yang L, Guan YQ, Shen KF, Zhang ML, Cai HD, et al. Novel Bioinformatic Classification System for Genetic Signatures Identification in Diffuse Large B-Cell Lymphoma. *BMC Cancer* (2020) 20(1):714. doi: 10.1186/s12885-020-07198-1
32. Reddy A, Zhang J, Davis NS, Moffitt AB, Love CL, Waldrop A, et al. Genetic and Functional Drivers of Diffuse Large B Cell Lymphoma. *Cell* (2017) 171 (2):481–94.e15. doi: 10.1016/j.cell.2017.09.027
33. Schmitz R, Wright GW, Huang DW, Johnson CA, Phelan JD, Wang JQ, et al. Genetics and Pathogenesis of Diffuse Large B-Cell Lymphoma. *N Engl J Med* (2018) 378(15):1396–407. doi: 10.1056/NEJMoa1801445

34. Chapuy B, Stewart C, Dunford AJ, Kim J, Kamburov A, Redd RA, et al. Molecular Subtypes of Diffuse Large B Cell Lymphoma are Associated With Distinct Pathogenic Mechanisms and Outcomes. *Nat Med* (2018) 24(5):679–90. doi: 10.1038/s41591-018-0016-8
35. Wang K, Li M, Hakonarson H. ANNOVAR: Functional Annotation of Genetic Variants From High-Throughput Sequencing Data. *Nucleic Acids Res* (2010) 38(16):e164. doi: 10.1093/nar/gkq603
36. Hans CP, Weisenburger DD, Greiner TC, Gascoyne RD, Delabie J, Ott G, et al. Confirmation of the Molecular Classification of Diffuse Large B-Cell Lymphoma by Immunohistochemistry Using a Tissue Microarray. *Blood* (2004) 103(1):275–82. doi: 10.1182/blood-2003-05-1545
37. Xu-Monette ZY, Medeiros LJ, Li Y, Orlowski RZ, Andreeff M, Bueso-Ramos CE, et al. Dysfunction of the TP53 Tumor Suppressor Gene in Lymphoid Malignancies. *Blood* (2012) 119(16):3668–83. doi: 10.1182/blood-2011-11-366062
38. Shah NN, Fry TJ. Mechanisms of Resistance to CAR T Cell Therapy. *Nat Rev Clin Oncol* (2019) 16(6):372–85. doi: 10.1038/s41571-019-0184-6
39. Finney OC, Brakke HM, Rawlings-Rhea S, Hicks R, Doolittle D, Lopez M, et al. CD19 CAR T Cell Product and Disease Attributes Predict Leukemia Remission Durability. *J Clin Invest* (2019) 129(5):2123–32. doi: 10.1172/JCI125423
40. Ram R, Grisariu S, Shargian-Alon L, Amit O, Bar-On Y, Stepensky P, et al. Toxicity and Efficacy of Chimeric Antigen Receptor T-Cell in Patients With Diffuse Large B Cell Lymphoma Above the Age of 70 Years Compare to Younger Patients - A Matched Control Multi-Center Cohort Study. *Haematologica* (2021). doi: 10.3324/haematol.2021.278288
41. Vercellino L, Di Blasi R, Kanoun S, Tessoulin B, Rossi C, D'Aveni-Piney M, et al. Predictive Factors of Early Progression After CAR T-Cell Therapy in Relapsed/Refractory Diffuse Large B-Cell Lymphoma. *Blood Adv* (2020) 4 (22):5607–15. doi: 10.1182/bloodadvances.2020003001
42. Hirayama AV, Gauthier J, Hay KA, Voutsinas JM, Wu Q, Gooley T, et al. The Response to Lymphodepletion Impacts PFS in Patients With Aggressive Non-Hodgkin Lymphoma Treated With CD19 CAR T Cells. *Blood* (2019) 133 (17):1876–87. doi: 10.1182/blood-2018-11-887067
43. Nastoupil LJ, Jain MD, Feng L, Spiegel JY, Ghobadi A, Lin Y, et al. Standard-of-Care Axicabtagene Ciloleucel for Relapsed or Refractory Large B-Cell Lymphoma: Results From the US Lymphoma CAR T Consortium. *J Clin Oncol* (2020) 38(27):3119–28. doi: 10.1200/JCO.19.02104
44. Calcinotto A, Filipazzi P, Grioni M, Iero M, De Milito A, Ricupito A, et al. Modulation of Microenvironment Acidity Reverses Anergy in Human and Murine Tumor-Infiltrating T Lymphocytes. *Cancer Res* (2012) 72(11):2746–56. doi: 10.1158/0008-5472.CAN-11-1272
45. Awasthi R, Pacaud L, Waldron E, Tam CS, Jager U, Borchmann P, et al. Tisagenlecleucel Cellular Kinetics, Dose, and Immunogenicity in Relation to Clinical Factors in Relapsed/Refractory DLBCL. *Blood Adv* (2020) 4(3):560–72. doi: 10.1182/bloodadvances.2019000525
46. Wang J, Shang Z, Wang J, Xu J, Li W, Guan Y, et al. MYC/BCL2/BCL6 Triple Hit and TP53 Deletion in a Case of High-Grade B Cell Lymphoma Receiving CAR T Cell Immunotherapy. *J Immunother Cancer* (2021) 9(6):e002029. doi: 10.1136/jitc-2020-002029
47. Mensa-Vilaro A, Bravo Garcia-Morato M, de la Calle-Martin O, Franco-Jarava C, Martinez-Saavedra MT, Gonzalez-Granado LI, et al. Unexpected Relevant Role of Gene Mosaicism in Patients With Primary Immunodeficiency Diseases. *J Allergy Clin Immunol* (2019) 143(1):359–68. doi: 10.1016/j.jaci.2018.09.009
48. Goodnow CC. Multistep Pathogenesis of Autoimmune Disease. *Cell* (2007) 130(1):25–35. doi: 10.1016/j.cell.2007.06.033
49. Chinn IK, Eckstein OS, Peckham-Gregory EC, Goldberg BR, Forbes LR, Nicholas SK, et al. Genetic and Mechanistic Diversity in Pediatric Hemophagocytic Lymphohistiocytosis. *Blood* (2018) 132(1):89–100. doi: 10.1182/blood-2017-11-814244
50. Grimbacher B, Warnatz K, Yong PFK, Korganow AS, Peter HH. The Crossroads of Autoimmunity and Immunodeficiency: Lessons From Polygenic Traits and Monogenic Defects. *J Allergy Clin Immunol* (2016) 137(1):3–17. doi: 10.1016/j.jaci.2015.11.004
51. Abreu TR, Fonseca NA, Goncalves N, Moreira JN. Current Challenges and Emerging Opportunities of CAR-T Cell Therapies. *J Control Release* (2020) 319:246–61. doi: 10.1016/j.jconrel.2019.12.047
52. Ishii K, Pouzolles M, Chien CD, Erwin-Cohen RA, Kohler ME, Qin H, et al. Perforin-Deficient CAR T Cells Recapitulate Late-Onset Inflammatory Toxicities Observed in Patients. *J Clin Invest* (2020) 130(10):5425–43. doi: 10.1172/JCI130059
53. Prinzing B, Zebley CC, Petersen CT, Fan Y, Anido AA, Yi Z, et al. Deleting DNMT3A in CAR T Cells Prevents Exhaustion and Enhances Antitumor Activity. *Sci Transl Med* (2021) 13(620):eabh0272. doi: 10.1126/scitranslmed.abh0272
54. Wright GW, Huang DW, Phelan JD, Coulibaly ZA, Roulland S, Young RM, et al. A Probabilistic Classification Tool for Genetic Subtypes of Diffuse Large B Cell Lymphoma With Therapeutic Implications. *Cancer Cell* (2020) 37 (4):551–68.e14. doi: 10.1016/j.ccell.2020.03.015
55. McCusker C, Upton J, Warrington R. Primary Immunodeficiency. *Allergy Asthma Clin Immunol* (2018) 14(Suppl 2):61. doi: 10.1186/s13223-018-0290-5
56. Cichocki F, Schlums H, Li H, Stache V, Holmes T, Lenvik TR, et al. Transcriptional Regulation of Munc13-4 Expression in Cytotoxic Lymphocytes is Disrupted by an Intronic Mutation Associated With a Primary Immunodeficiency. *J Exp Med* (2014) 211(6):1079–91. doi: 10.1084/jem.20131131
57. Shibata H, Yasumi T, Shimodera S, Hiejima E, Izawa K, Kawai T, et al. Human CTL-Based Functional Analysis Shows the Reliability of a Munc13-4 Protein Expression Assay for FHL3 Diagnosis. *Blood* (2018) 131(18):2016–25. doi: 10.1182/blood-2017-10-812503
58. Bryceson YT, Rudd E, Zheng C, Edner J, Ma D, Wood SM, et al. Defective Cytotoxic Lymphocyte Degranulation in Syntaxin-11 Deficient Familial Hemophagocytic Lymphohistiocytosis 4 (FHL4) Patients. *Blood* (2007) 110 (6):1906–15. doi: 10.1182/blood-2007-02-074468
59. Yamauchi T, Hoki T, Oba T, Saito H, Attwood K, Sabel MS, et al. CX3CR1-CD8+ T Cells are Critical in Antitumor Efficacy But Functionally Suppressed in the Tumor Microenvironment. *JCI Insight* (2020) 5(8):e133920. doi: 10.1172/jci.insight.133920
60. Yan Y, Cao S, Liu X, Harrington SM, Bindeman WE, Adjei AA, et al. CX3CR1 Identifies PD-1 Therapy-Responsive CD8+ T Cells That Withstand Chemotherapy During Cancer Chemoimmunotherapy. *JCI Insight* (2018) 3 (8):e97828. doi: 10.1172/jci.insight.97828
61. Yamauchi T, Hoki T, Oba T, Jain V, Chen H, Attwood K, et al. T-Cell CX3CR1 Expression as a Dynamic Blood-Based Biomarker of Response to Immune Checkpoint Inhibitors. *Nat Commun* (2021) 12(1):1402. doi: 10.1038/s41467-021-21619-0

Conflict of Interest: Author SZ was employed by Wuhan Bio-Raid Biotechnology Co., Ltd.

The remaining authors declare that the research was conducted in the absence of any commercial or financial relationships that could be construed as a potential conflict of interest.

frontiers | Frontiers in Immunology

ORIGINAL RESEARCH
published: 03 May 2022
doi: 10.3389/fimmu.2022.888250

Aberrantly Activated APOBEC3B Is Associated With Mutant p53-Driven Refractory/Relapsed Diffuse Large B-Cell Lymphoma

Xuzhao Zhang[1,2,3†], Zhaoxing Wu[1†], Yuanyuan Hao[1†], Teng Yu[1], Xian Li[1], Yun Liang[1], Jinfan Li[4], Liansheng Huang[1], Yang Xu[1], Xiuzhen Li[4], Xiaohua Xu[1], Weiqin Wang[1], Genbo Xu[1], Xiaohong Zhang[1], Qinghua Lv[2], Yongming Fang[2], Rongzhen Xu[1,2] and Wenbin Qian[1*]*

[1] Department of Hematology, The Second Affiliated Hospital of Zhejiang University School of Medicine, Hangzhou, China, [2] Cancer Institute (Key Laboratory of Cancer Prevention and Intervention, China National Ministry of Education), The Second Affiliated Hospital of Zhejiang University School of Medicine, Hangzhou, China, [3] Zhejiang Provincial Key Laboratory for Cancer Molecular Cell Biology, Zhejiang University, Hangzhou, China, [4] Department of Pathology, The Second Affiliated Hospital of Zhejiang University School of Medicine, Zhejiang University, Hangzhou, China

Tumor protein 53 (*TP53*) mutation predicts an unfavorable prognosis in diffuse large B-cell lymphoma (DLBCL), but the molecular basis for this association remains unclear. In several malignancies, the cytidine deaminase apolipoprotein B mRNA editing enzyme catalytic subunit 3B (APOBEC3B) has been reported to be associated with the *TP53* G/C-to-A/T mutation. Here, we show that the frequency of this mutation was significantly higher in relapsed/refractory (R/R) than in non-R/R DLBCL, which was positively associated with the *APOBEC3B* expression level. APOBEC3B overexpression induced the *TP53* G/C-to-A/T mutation *in vitro*, resulting in a phenotype similar to that of DLBCL specimens. Additionally, APOBEC3B-induced p53 mutants promoted the growth of DLBCL cells and enhanced drug resistance. These results suggest that APOBEC3B is a critical factor in mutant p53-driven R/R DLBCL and is therefore a potential therapeutic target.

Keywords: ***TP53*** **mutation, APOBEC3B, DLBCL, refractory, relapse**

OPEN ACCESS

Edited by:
Wei Sang,
The Affiliated Hospital of Xuzhou Medical University, China

Reviewed by:
Ken Young,
Duke University, United States
Zhiming Li,
Sun Yat-sen University Cancer Center (SYSUCC), China

***Correspondence:**
Wenbin Qian
qianwb@zju.edu.cn
Xuzhao Zhang
zxzzju@zju.edu.cn

†These authors have contributed equally to this work and share first authorship

Specialty section:
This article was submitted to Cancer Immunity and Immunotherapy, a section of the journal Frontiers in Immunology

Received: *02 March 2022*
Accepted: *04 April 2022*
Published: *03 May 2022*

Citation:
Zhang X, Wu Z, Hao Y, Yu T, Li X, Liang Y, Li J, Huang L, Xu Y, Li X, Xu X, Wang W, Xu G, Zhang X, Lv Q, Fang Y, Xu R and Qian W (2022) Aberrantly Activated APOBEC3B Is Associated With Mutant p53-Driven Refractory/Relapsed Diffuse Large B-Cell Lymphoma. Front. Immunol. 13:888250. doi: 10.3389/fimmu.2022.888250

INTRODUCTION

Diffuse large B-cell lymphoma (DLBCL) is the most common type of lymphoid malignancy in adults and has a heterogeneous clinical course. The combination immunotherapy regimen of rituximab, cyclophosphamide, doxorubicin, vincristine, and prednisone (R-CHOP)—the current standard of care for DLBCL—has greatly improved the outcome of patients, with durable remission achieved in 50% of cases (1). However, approximately one-third of patients do not respond to this regimen (2), highlighting a need for different therapies against novel targets.

Tumor protein 53 (*TP53*) encodes the tumor suppressor p53, which participates in the regulation of the cell cycle, DNA repair, apoptosis, and senescence. Approximately 50% of human cancers have alterations in the *TP53* gene (3, 4). About 80% of *TP53* mutations are missense mutations and are located in the DNA-binding domain (DBD); 8 of these (R175, V157F, Y220C, G245, R248, R249, R273, and R282) account for ~28% of the total mutations in *TP53* (5). The *TP53* mutation is present in about 20%

of patients with DLBCL (6) and is associated with a low treatment response rate (7, 8). Importantly, several hotspot mutations including those at residues 283, 248, 273, 175, 176, and 213—which are mainly located in the DBD, and specifically in the loop–sheet–helix and L3 motifs—are independent predictors of poor DLBCL outcome (9, 10). However, the mechanistic basis thereof is not fully understood. G/C-to-A/T mutations in *TP53* are considered high-risk hotspot mutations (11) and are similar to those induced by apolipoprotein B mRNA editing enzyme catalytic subunit 3s (APOBEC3s) family proteins (12).

Based on the above evidence, we speculated that APOBEC3 is responsible for *TP53* G/C-to-A/T mutations in DLBCL. To test this hypothesis, we analyzed the association between the *TP53* G/C-to-A/T mutation and APOBEC3B expression in clinical specimens from relapsed/refractory (R/R) DLBCL patients. Our results provide insight into the mechanistic basis for the *TP53* G/C-to-A/T mutation in DLBCL and reveal a new potential therapeutic target in the treatment of this disease.

MATERIALS AND METHODS

Patients

A total of 61 patients (33 female and 28 male patients) diagnosed with *de novo* DLBCL by surgical biopsy of tumor tissue and treated with R-CHOP at the Second Affiliated Hospital of Zhejiang University School of Medicine and treated with R_CHOP from November 2016 to July 2018 were included in this study. The diagnosis of DLBCL was made independently by 2 experienced pathologists according to the 2016 World Health Organization classification; 19 cases were R/R DLBCL according to the criteria of Cheson et al. (13). This study was approved by the ethics committee of the hospital and was conducted in accordance with the principles of the Declaration of Helsinki. All patients provided written informed consent at enrollment.

Detection of the *TP53* G/C-to-A/T Mutation in R/R DLBCL Clinical Specimens

Formalin-fixed, paraffin-embedded (FFPE) tumor tissue blocks were collected for each patient, and tumor tissue genomic DNA was extracted using the QIAamp DNA FFPE Tissue Kit (Qiagen) according to the manufacturer's instructions. Peripheral blood samples were collected as matched normal samples. Total DNA of peripheral blood mononuclear cells (PBMCs) were extracted using the QIAamp DNA Blood Mini Kit (Qiagen) according to the manufacturer's instructions. G/C-to-A/T mutations in *TP53* exon 8 were detected by differential DNA denaturation PCR (3D-PCR)-based Sanger sequencing as previously described (14), with some modifications (**Supplementary Material**).

Cellular Localization of APOBEC3s

Immunofluorescence labeling of APOBEC3s-HA was performed as previously described (15). APOBEC3s-pEGFP detection is described in the **Supplementary Material**.

DLBCL Database Analysis of APOBEC3A and APOBEC3B Expression

Oncomine DLBCL Database Analysis

As APOBEC3A and APOBEC3B were reported to potentially induce the *TP53* G/C-to-T/A mutation in several human cancers, we analyzed the expression status of APOBEC3A (12, 14) and APOBEC3B in DLBCL using the Oncomine database (http://www.oncomine.org) based on existing cancer microarray datasets. APOBEC3A and APOBEC3B expression data of 2 lymphoma groups, Brune lymphoma, and Compagno lymphoma, were extracted from GSE12453 and GSE12195 gene chips in the Gene Expression Omnibus (GEO) database (https://www.ncbi.nlm.nih.gov/geo/). Expression levels of APBOEC3A and APOBEC3B were compared between DLBCL and different types of normal cells as well as in DLBCL samples.

Gene Expression Profiling Interactive Analysis DLBCL Database Analysis

We searched the Gene Expression Profiling Interactive Analysis (GEPIA) database (http://gepia.cancer-pku.cn) to obtain expression data for *APOBEC3A* and *APOBEC3B* in DLBCL on box plots *via* Single Gene Analysis.

GEO DLBCL Database Analysis

DLBCL gene expression profiles and *APOBEC3A* and *APOBEC3B* expression data were obtained from the GEO database. Search results were sorted by the number of samples. Because the *APOBEC3A* and *APOBEC3B* expression data were derived from different sample types including frozen tumor tissue and FFPE tumor tissue, they were compared to frozen tissue and FFPE samples in GSE19246 to determine whether the sample source influenced the results.

Detection of APOBEC3B in Refractory/Relapse DLBCL Samples

FFPE tumor tissue blocks were collected for each patient and APOBEC3B was detected by immunohistochemistry. Anti-APOBEC3B antibody was purchased from Abcam (Cambridge, MA, USA; cat. no. ab191695). The DAKO Envision+ System (Dako, Glostrup, Denmark; code K4002) was used for diaminobenzidine detection according to the manufacturer's instructions.

Construction of Plasmids and APOBEC3A/APOBEC3B-Inducible Cell Lines

Cell lines

Pfeiffer and OCI-LY10 DLBCL cell lines were purchased from the American Type Culture Collection (ATCC; Manassas, VA, USA) and cultured in RPMI1640 medium supplemented with 10% fetal bovine serum and penicillin/streptomycin. Human embryonic kidney (HEK)293 and 293T cell lines were purchased from ATCC and cultured in Dulbecco's modified Eagle's medium supplemented with 10% fetal bovine serum and penicillin/streptomycin. Cell lines were maintained in a humidified atmosphere of 5% CO_2 at 37°C.

APOBEC3A/APOBEC3B-Inducible DLBCL Cell Lines

APOBEC3A/APOBEC3B-flag cDNA was cloned into the pLV-Ptight-puro vector (Clontech/Takara Bio, Dalian, China) to construct the inducible APOBEC3A/APOBEC3B-flag/pLV-Ptight-puro plasmid. Pfeiffer, OCI-LY10, 293T, and HEK293 cells were transfected using Polyjet *In Vitro* DNA Transfection Reagent (SignaGen, Frederick, MD, USA) according to the manufacturer's protocol. The 293T cells were transfected with APOBEC3A/APOBEC3B-flag/pLV-ptight-puro vector along with PCL and 10A1. At 72 h after transfection, the supernatant containing viral particles was collected and purified by centrifugation and passed through a 0.45-μm filter. Then, the virus supernatant was stored at −80°C for the subsequent experiments. Pfeiffer, OCI-LY10, and HEK293 cells were seeded in a 6-well culture plate; after 24 h, the medium was replaced with fresh medium and culture supernatant with virus was added along with 8 μg/ml polybrene (Qiagen). After 12 h, the medium was replaced with fresh medium, and 48 h later, 3 μg/ml puromycin (Qiagen) was added to the medium to select infected clones. Inducible expression of APOBEC3A/APOBEC3B-flag was confirmed by Western blotting using an anti-flag antibody (Medical and Biological Laboratories, Nagoya, Japan; cat. no. M185-3L).

After puromycin selection for 14 days, the remaining cells were seeded at a concentration of 1 cell/well in a 96-well plate and cultured with a medium containing 4 μg/ml doxycycline (Sigma-Aldrich, St. Louis, MO, USA). Positive clones were used in the following steps.

Detection of APOBEC3A/APOBEC3B-Induced G/C-to-A/T Mutations in *TP53* exon 8

After 14 days of induction with doxycycline, APOBEC3A/APOBEC3B-flag-inducible and pLV-pTight-puro cells were collected and total DNA was extracted using the QIAamp DNA mini kit (Qiagen). G/C-to-T/A mutations were detected and analyzed by 3D-PCR-based Sanger sequencing as described above.

Analysis of Proliferation and Drug Sensitivity of p53-Mutant-derived DLBCL Cells

Colony Formation Assay

The colony formation assay was performed as previously described (16). Briefly, APOBEC3B-inducible DLBCL cells were induced with 4 μg/ml doxycycline for 14 days, after which the doxycycline was removed and the cells were cultured for another 24 h until APOBEC3B-Flag expression disappeared. APOBEC3B expression and control cells were seeded in 6-well culture plates containing semi-soft agarose at a concentration of 200 cells/well. The cells were cultured for another 14 days and colonies were subjected to Giemsa staining and counted under a microscope.

Construction of p53 Mutants (R273C and R282Q) and Doxorubicin Sensitivity Analysis in DLBCL

The PCW-CAS9 vector was modified to express wild-type and mutant p53. The mutant constructs (R273C and R282Q) were generated using the MutanBEST Kit (Takara, Dalian, China) according to the manufacturer's instructions and transfected into Ly10 cells. Expression of wild-type and mutant p53 was induced with doxycycline and confirmed by Western blotting. Doxorubicin sensitivity was measured with the MTT assay (17).

Statistical Analysis

Statistical analyses were performed with SPSS Statistics v20 (IBM, Armonk, NY, USA). Frequency tables and descriptive statistics (mean, median, minimum, and maximum) were used to summarize patient characteristics. The significance of differences between groups of patients was evaluated with the maximum likelihood chi-squared test and Fisher's exact test for categorical variables and with the Mann–Whitney *U* test for continuous variables. Progression-free survival (PFS) was defined as time to disease progression, relapse, or death, and was estimated using the Kaplan–Meier method and compared using the log-rank test. The Kaplan–Meier method was used for univariate survival analysis. The multivariate Cox proportional hazard model was used to evaluate whether *TP53* mutation was an independent prognostic factor for PFS and overall survival. Colony formation data are reported as mean values ± SEM and were analyzed with the independent *t*-test. *APOBEC3A* and *APOBEC3B* gene expression data were compared and doxorubicin 50% inhibitor concentration (IC_{50}) was analyzed using Prism 5 software (GraphPad, San Diego, CA, USA). *p*-values <0.05 were considered statistically significant.

RESULTS

TP53 exon 8 G/C-to-A/T Mutations Increased in R/R DLBCL Samples

Using the 3D-PCR-based direct sequencing method, G/C-to-A/T mutations were detected in clinical specimens of R/R DLBCL patients (**Figure 1** and **Supplementary Figure S1**). In most cases, the mutation resulted in changes in the amino acid sequence of the p53 protein (**Figure 2A** and **Supplementary Table S1**). Several mutations including R273C, R282W, R282Q, R283C, and R290H (**Figure 2B**) occurred more frequently than others; most of these (R273C, R282Q, R282W, and R283C) are previously reported hotspot mutations. *TP53* exon 8 G/C-to-A/T mutations were more frequent in R/R DLBCL samples (83.33%, 15/18) than in non-R/R DLBCL (23.26%, 10/43) samples (χ^2 = 18.93, p < 0.001) (**Figure 2C**). Hotspot mutations were detected in 14 of 18 R/R DLBCL patients, but only 5/43 non-R/R DLBCL patients (χ^2 = 25.89, p < 0.001) (**Figure 2D**).

The complete response (CR) rates of different groups based on *TP53* exon 8 status were calculated and compared at the 12-month follow-up. The overall CR rate for the study population was 68.90%, which was similar to a previously reported value (2). However, CR rates differed according to *TP53* mutation status. Among patients with wild-type *TP53* exon 8, the CR rate was 81.08% (30/37) (**Figure 3A**); by comparison, those with *TP53* exon 8 mutation had a CR rate of 28.57% (8/28) (χ^2 = 18.1, p < 0.01; data not shown).

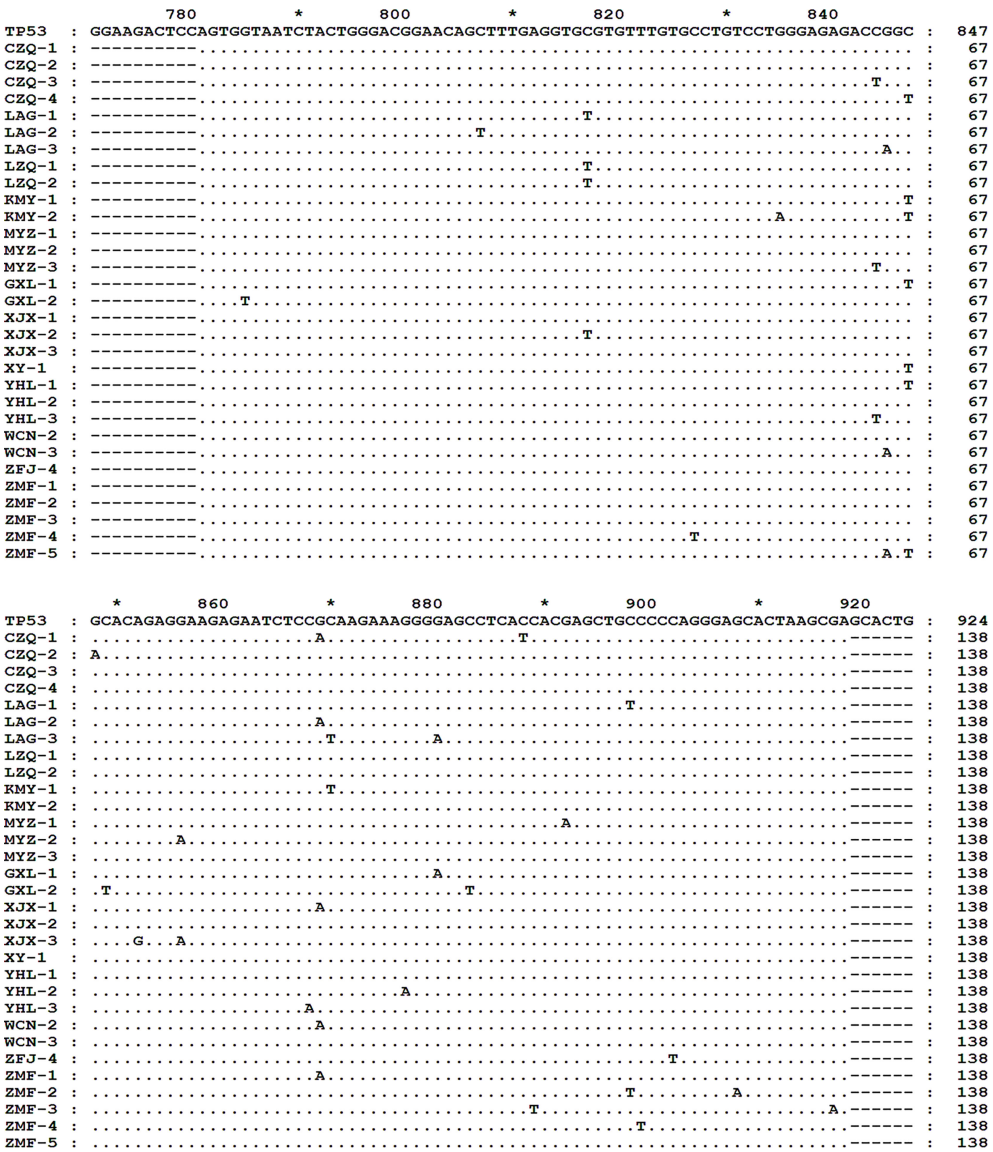

FIGURE 1 | *TP53* exon 8 G/C-to-A/T mutations in R/R DLBCL. *TP53* exon 8 G/C-to-A/T mutation was detected in R/R DLBCL. Total DNA were extracted from FFPE DLBCL tissues and *TP53* exon 8 was amplified by 3D-PCR and sequenced by Sanger sequencing. Sequences were aligned and analyzed with the Clustal and Genedoc software. * indicates the number in the middle of the two numbers before and after

Patients harboring a hotspot mutation had the lowest CR rate (21.05% [4/19] vs. wild type, $\chi^2 = 18.97$, $p < 0.01$; **Figure 3A**), whereas those with a non-hotspot mutation had a CR rate of 80% (4/5) ($p = 0.028$ vs. hotspot group [Fisher's exact test] and $\chi^2 = 0$, $p = 1$ vs. wild-type group; **Figure 3A**). Thus, the *TP53* wild-type and non-hotspot mutation groups combined had a higher CR rate than the *TP53* hotspot mutation group ($\chi^2 = 23.203$, $p < 0.01$; data not shown). The hotspot mutation group had a median PFS of 6 months (95% confidence interval [CI]: 3.245–8.755; **Figure 3B**); meanwhile, PFS was not reached for the non-hotspot mutation and wild-type groups at the 12-month follow-up (**Figure 3B**). These 2 groups had similar demographic and clinical profiles except for sex ratio and B symptoms (**Table 1**).

The *TP53* hotspot group had a greater proportion of patients with International Prognostic Index (IPI) >2 (high-intermediate and high risk) than the *TP53* wild-type and non-hotspot groups. We therefore examined the relationship between *TP53* mutation status and IPI and found that in the IPI >2 (high-intermediate and high risk) group, *TP53* mutation status also had a predictive value for PFS (**Figure 3C**, $p = 0.04$). Meanwhile, the PFS of *TP53* wild-type and non-hotspot mutation and the IPI > 2 group was similar to that of the IPI 0–2 group ($p = 0.08$; **Figure 3D**). These results indicate that *TP53* mutation status has a prognostic value that is not captured by the IPI for DLBCL.

To assess whether *TP53* mutation was an independent prognostic factor for shorter PFS, risk factors were first

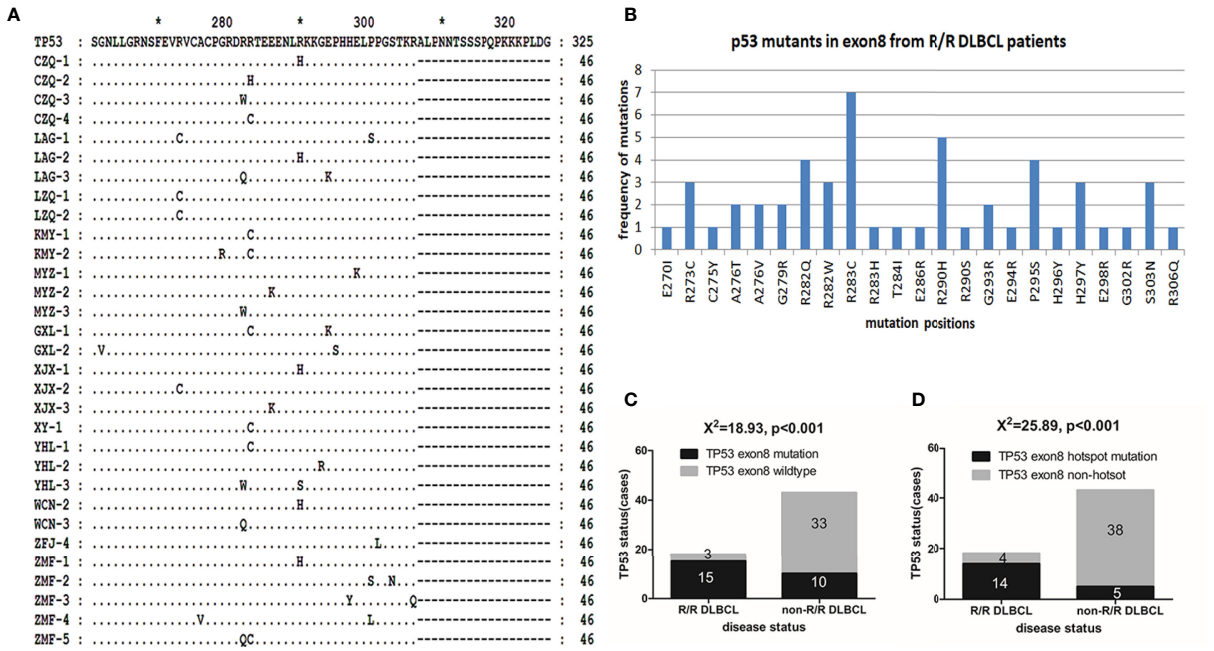

FIGURE 2 | p53 mutants in R/R DLBCL. **(A)** p53 mutants were detected in R/R DLBCL. p53 protein sequences were translated with the Genedoc software based on DNA sequences and aligned with the Clustal and Genedoc software. **(B)** Distribution of p53 point mutants in R/R DLBCL. Numbers are the total number of patients in which a mutation was detected. **(C, D)** *TP53* mutation rates in R/R and non-R/R DLBCL. Frequencies were calculated as a percentage. Differences between groups of patients were assessed with the maximum likelihood chi-squared test.

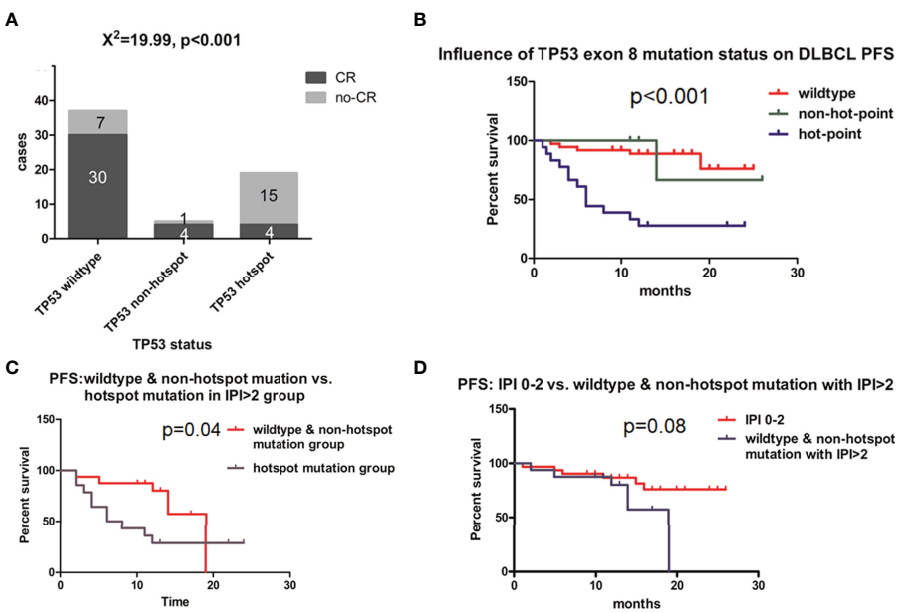

FIGURE 3 | Effect of *TP53* exon 8 mutation on the clinical outcome of DLBCL patients. **(A)** CR rates in different groups based on *TP53* status. CR status was evaluated by positron emission tomography–computed tomography scanning according to Lugano response criteria for non-Hodgkin's lymphoma. Differences between groups of patients were assessed with the maximum likelihood chi-squared test. **(B)** PFS of different *TP53* status groups. **(C)** PFS of IPI >2 group; patients with *TP53* hotspot mutations, wild-type *TP53*, and non-hotspot *TP53* mutations were compared. **(D)** Comparison of PFS between IPI 0–2 and IPI >2 groups with wild-type *TP53* and non-hotspot *TP53* mutations. Patients were followed up for 12 months until disease progression, relapse, or end of observation. PFS was defined as time to disease progression, relapse, or death, and was estimated with the Kaplan–Meier method and compared with the log-rank test.

TABLE 1 | Clinical characteristics of patients in the *TP53* mutation groups.

Characteristic	*TP53* wild type and non-hotspot mutation group (*N* = 42)	*TP53* hotspot mutation group (*N* = 19)	*p*-value
Age, years			0.915
≤60	21 (50.0)	9 (47.4)	
61–70	12 (28.6)	7 (36.8)	
71–80	6 (14.3)	2 (10.5)	
>80	3 (7.1)	1 (5.3)	
Median (range)	60.5 (18–88)	61 (34–83)	
Sex			0.036
Male	15 (35.7)	13 (68.4)	
Female	27 (64.3)	6 (31.6)	
DLBCL subtype			0.803
GCB	14 (33.3)	5 (26.3)	
Non-GCB	28 (66.7)	14 (73.7)	
Stage			0.201
I	9 (21.4)	2 (10.5)	
II	9 (21.4)	1 (5.3)	
III	4 (9.5)	1 (5.3)	
IV	19 (45.2)	15 (78.9)	
B symptoms			0.029
Present	14 (33.3)	12 (63.2)	
Absent	28 (66.7)	7 (36.8)	
IPI			0.268
0	4 (9.5)	1 (5.3)	
1	11 (26.2)	2 (10.5)	
2	10 (23.8)	2 (10.5)	
3	7 (16.7)	7 (36.8)	
4	4 (9.5)	3 (15.8)	
5	5 (11.9)	4 (21.1)	

Values represent n (%) unless otherwise indicated.
Differences between groups were evaluated with the maximum likelihood chi-squared test and Fisher's exact test for categorical variables and the Mann–Whitney U test for continuous variables.
DLBCL, diffuse large B-cell lymphoma; GCB, germinal center B-like; IPI, International Prognostic Index.

evaluated by univariate survival analysis with the Kaplan–Meier method (**Supplementary Table S2**). IPI, *TP53* mutation status, lactate dehydrogenase (LDH) activity, tumor stage, and sex were included in the multivariate Cox model. *TP53* hotspot mutation was the strongest independent predictor of PFS (hazard ratio [HR] = 5.146, 95% CI: 2.134–12.409; $p < 0.0003$), followed by *TP53* mutation (HR = 3.616, 95% CI: 1.49–8.773; $p = 0.004$). These data suggest that *TP53* mutation—especially in the hotspot—contributes to the poor outcome of DLBCL patients treated with R-CHOP.

APOBEC3B but Not APOBEC3A Is Upregulated in DLBCL Compared to Normal Tissue

APOBEC3A, APOBEC3B, APOBEC3F, and APOBEC3G of the APOBEC3s family exhibit cytidine deaminase activity that induces G/C-to-A/T mutation in a single DNA strand. APOBEC3F and APOBEC3G cause hypermutation in the human immunodeficiency virus (HIV) genome but are localized in the cytoplasm (**Supplementary Figure S2**). APOBEC3A is localized in both the cytoplasm and the nucleus, whereas APOBEC3B is predominantly localized in the nucleus (**Supplementary Figure S2**) with access to genomic DNA. Previous studies have shown that APOBEC3A and APOBEC3B may contribute to host DNA mutation. Analysis of the Brune lymphoma dataset in the Oncomine database revealed that the *APOBEC3A* mRNA level in DLBCL was similar to (**Figure 4A**) whereas the *APOBEC3B* mRNA level was higher than (**Figure 4B**) that in normal tissue. Similar trends in *APOBEC3B* and *APOBEC3A* expression in DLBCL were observed in The Cancer Genome Atlas (TCGA)-based GEPIA database (data not shown), but not in the Compagno lymphoma DLBCL dataset of TCGA (**Figures 4D, E**). We also found that APOBEC3B was more highly expressed than APOBEC3A in DLBCL tissues in both the Brune and Compagno lymphoma datasets (**Figures 4C, F**).

APOBEC3A and *APOBEC3B* expression levels in DLBCL were further compared in the GEO database. The results were sorted by the number of samples from highest to lowest, and the top 13 results were analyzed. The *APOBEC3A* expression level was higher than that of *APOBEC3B* in 3/13 datasets including the largest one (**Supplementary Figures S3A, D, I**), whereas in 10/13 datasets, the *APOBEC3B* expression level was higher (**Supplementary Figure S3**). In the dataset with the largest number of samples (GSE117556), RNA was extracted from FFPE tumor tissue; therefore, *APOBEC3A* and *APOBEC3B* expression levels were analyzed in different samples in GSE19246, which contains both frozen and FFPE tumor tissue. *APOBEC3A* expression level was similar between the 2 sample sources (**Supplementary Figure S4A**), but the *APOBEC3B* expression level was higher in frozen tumor tissue than in the FFPE sample (**Supplementary Figure S4B**). These results indicate that analyzing the *APOBEC3B* expression level in FFPE tumor tissue sample may result in an underestimate. Additionally, the *APOBEC3B* expression level was higher than that of *APOBEC3A* in most frozen tumor tissue samples. In summary, the analysis of online databases showed that *APOBEC3B* was more highly expressed than *APOBEC3A* in DLBCL.

APOBEC3B Level Is Higher in R/R DLBCL Than in Non-R/R DLBCL

Given that APOBEC3B induces G/C-to-A/T mutation in human cancers including breast cancer and is upregulated in DLBCL, we compared the level of APOBEC3B protein in R/R and non-R/R DLBCL samples by immunohistochemistry. Interestingly, APOBEC3B protein level was higher in R/R DLBCL (**Figures 5A–F**) than in non-R/R DLBCL (**Figures 5G–L**) samples. As expected, APOBEC3B protein was predominantly localized in the nucleus. Based on the analysis of the APOBEC3B expression level stratified by *TP53* mutation status using a cutoff value for an APOBEC3B positive rate of 20%, we found that the APOBEC3B protein level was higher in the *TP53* mutation group (58.33%) than in the *TP53* wild-type group (27.03%) ($\chi^2 = 4.657$ $p = 0.038$) (**Supplementary Table S3**). Moreover, the APOBEC3B positive rate was higher in the *TP53* hotspot mutation group (68.42%) than in the *TP53* wild-type and non-hotspot groups (26.19%) ($\chi^2 = 9.776$, $p = 0.004$) (**Supplementary Table S4**). These data suggest that APOBEC3B overexpression is associated with *TP53* mutation—especially those in the hotspot—in R/R DLBCL.

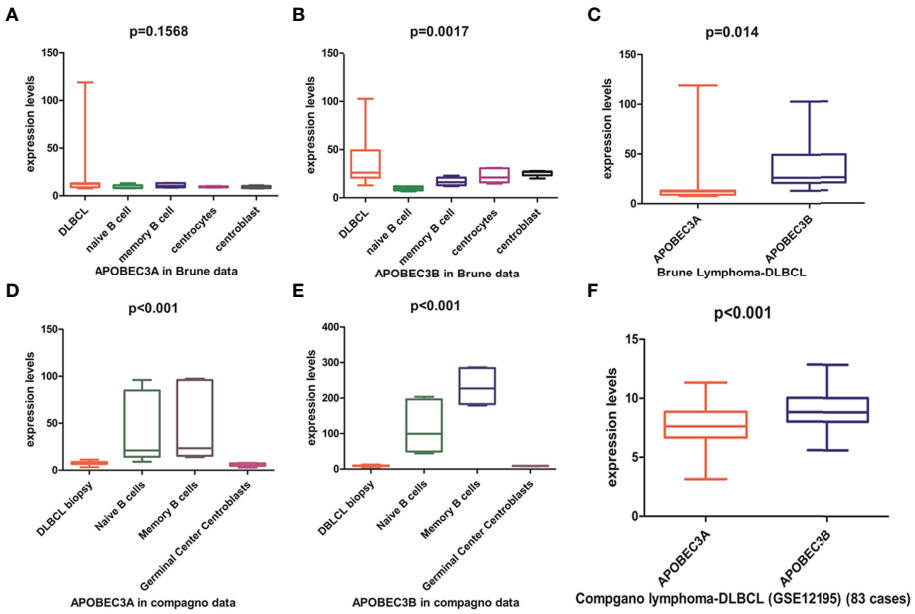

FIGURE 4 | APOBEC3A and APOBEC3B expression in DLBCL based on the Oncomine online database. **(A, B)** APOBEC3A **(A)** and APOBEC3B **(B)** expression in the Brune lymphoma dataset including DLBCL, naïve B cells, memory B cells, centrocytes, and centroblasts. **(C)** Comparison of APOBEC3A and APOBEC3B expression in the Brune lymphoma dataset. **(D, E)** APOBEC3A **(D)** and APOBEC3B **(E)** expression in the Compagno lymphoma dataset including DLBCL, naïve B cell, memory B cell, and germinal center centroblasts. **(F)** Comparison of APOBEC3A and APOBEC3B expression in the Compagno lymphoma dataset.

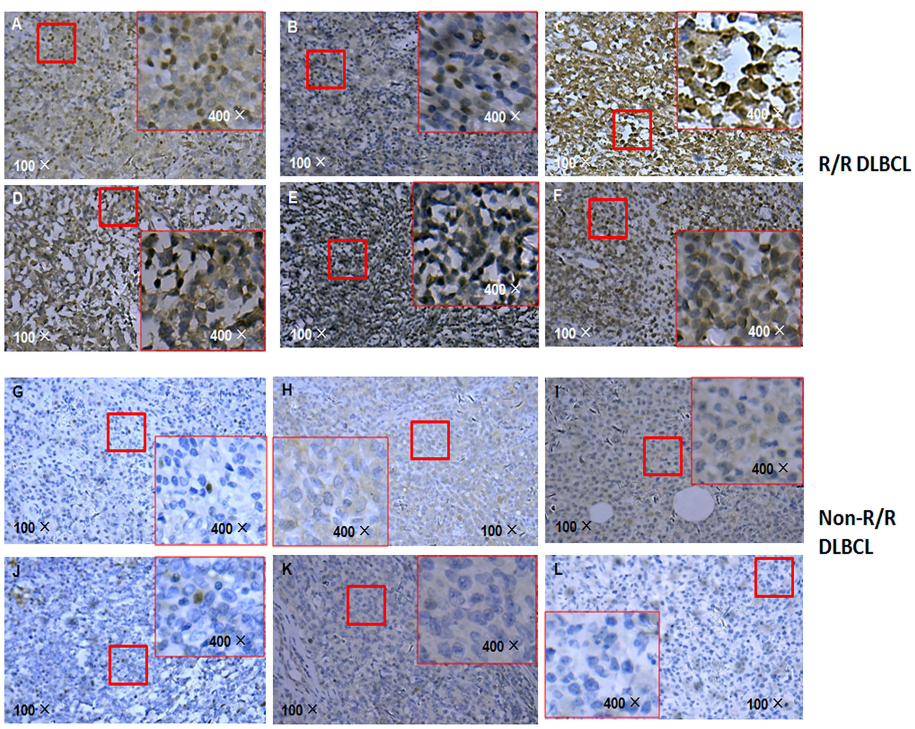

FIGURE 5 | APOBEC3B expression in R/R DLBCL and non-R/R DLBCL samples detected by immunohistochemistry. **(A–F)** R/R samples. **(G–L)** Non-R/R samples.

APOBEC3B Induces G/C-to-A/T Mutation in DLBCL Cell Lines

To further investigate whether overexpressed APOBEC3B can induce *TP53* mutation in DLBCL, we performed an *in vitro* assay using DLBCL cell clones with inducible APOBEC3B expression. APOBEC3B-flag expression was confirmed by Western blotting following induction with doxycycline (**Figure 6C**). *TP53* exon 8 was amplified by 3D-PCR and c-MYC exon 2, which is less frequently mutated in DLBCL (18, 19), and was also amplified as a control. As the denaturing temperature was decreased from 94°C to 87°C, the *TP53* exon 8 fragment was detected at 88°C and 87°C in APOBEC3B-inducible cells but not in control cells (**Figure 6A**). Meanwhile, the *MYC* exon 2 fragment was not detected at denaturing temperatures <94°C (**Figure 6B**). Additionally, in DLBCL cells overexpressing APOBEC3A, the *TP53* exon 8 fragment was not detected by 3D-PCR at a denaturing temperature of 89°C (**Supplementary Figure S5**). Single-clone sequencing of *TP53* exon 8 PCR products at 87°C revealed that >20% of clones harbored >1 G/C-to-A/T mutation compared to the control and the 94°C PCR products. The major mutation patterns were TG and GC; the mutation pattern and sites were similar to that of DLBC samples (**Figure 6D**). Further analysis showed that there were several known hotspot amino acid mutations including R273C, R282Q, R282W, and R283W (**Figure 6D**). These data suggest that APOBEC3B can induce the *TP53* G/C-to-A/T mutation—including in the hotspot—in DLBCL cells.

APOBEC3B-Induced p53 Mutation Promotes Cell Proliferation and Doxorubicin Resistance

Given our finding that APOBEC3B induced *TP53* mutation, we examined the effect of this mutation on proliferation and drug sensitivity of APOBEC3B-expressing Pfeiffer DLBCL cells. The results of the semi-soft agar colony formation assay showed that after the induction of APOBEC3B expression for 14 days, cells generated more colonies than the control group despite APOBEC3B expression being restored (**Figures 7A, B**). APOBEC3B-expressing cells showed resistance to doxorubicin, with a 4.65-fold increase in IC_{50} compared to the control (6.484 vs. 1.395 μg/ml) (**Figure 7C**). The results of the *in vitro* doxorubicin sensitivity assay using Ly10 cells (wild-type *TP53* DLBCL cell line) expressing mutant p53 showed that the R273C and R282Q mutants had reduced sensitivity to doxorubicin, with 2.28- and 2.23-fold increases in IC_{50}, respectively (**Figure 8**). These data suggest that APOBEC3B-induced

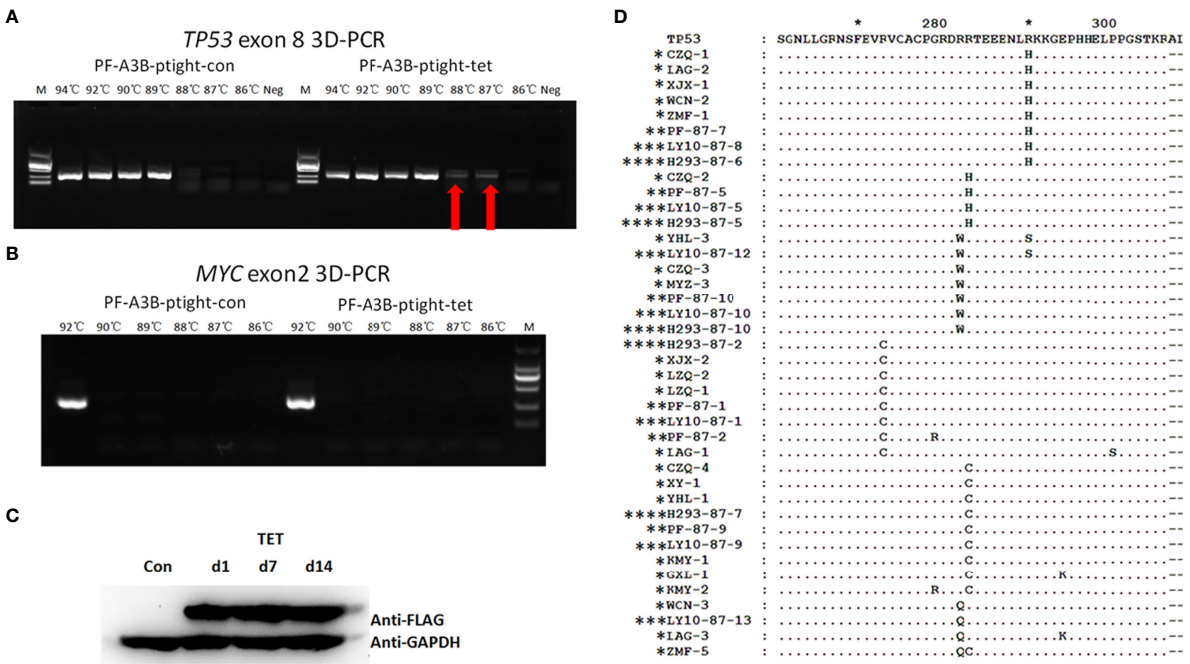

FIGURE 6 | APOBEC3B induces *TP53* exon 8 mutations *in vitro*. **(A)** 3D-PCR amplification of *TP53* exon 8 in APOBEC3B-inducible Pfeiffer cells (right) and control cells (left). Red arrows indicate DNA fragments that amplified at a denaturing temperature of 88°C and 87°C. PCR products were separated by agarose gel electrophoresis (top). APOBEC3B-flag expression was confirmed by Western blotting using an anti-flag antibody (bottom). Con, cell lysis before induction with doxycycline; d1, cell lysis after induction with doxycycline for 1 day; d7, cell lysis after induction with doxycycline for 7 days; d14, cell lysis after induction with doxycycline for 14 days; M, DNA ladder marker; Neg, negative control; PF, Pfeiffer. Denaturation temperatures in 3D-PCR ranged from 92°C to 87°C. **(B)** 3D-PCR amplification of MYC exon 2 in APOBEC3B-inducible Pfeiffer cells. PCR products were separated by agarose gel electrophoresis (top). Expression of APOBEC3B-flag was confirmed by Western blotting using an anti-flag antibody (bottom). **(C)** Detection of APOBEC3B-flag by Western blotting in APOBEC3B-inducible cells. **(D)** Comparison of *in vitro* APOBEC3B-induced p53 mutants with R/R DLBCL samples. P53 sequences were analyzed using Clustal and Genedoc software. *DLBCL patients. **APOBEC3B-inducible Pfeiffer cells. ***APOBEC3B-inducible OCI-LY10 cells. **** APOBEC3B-inducible HEK293 cells.

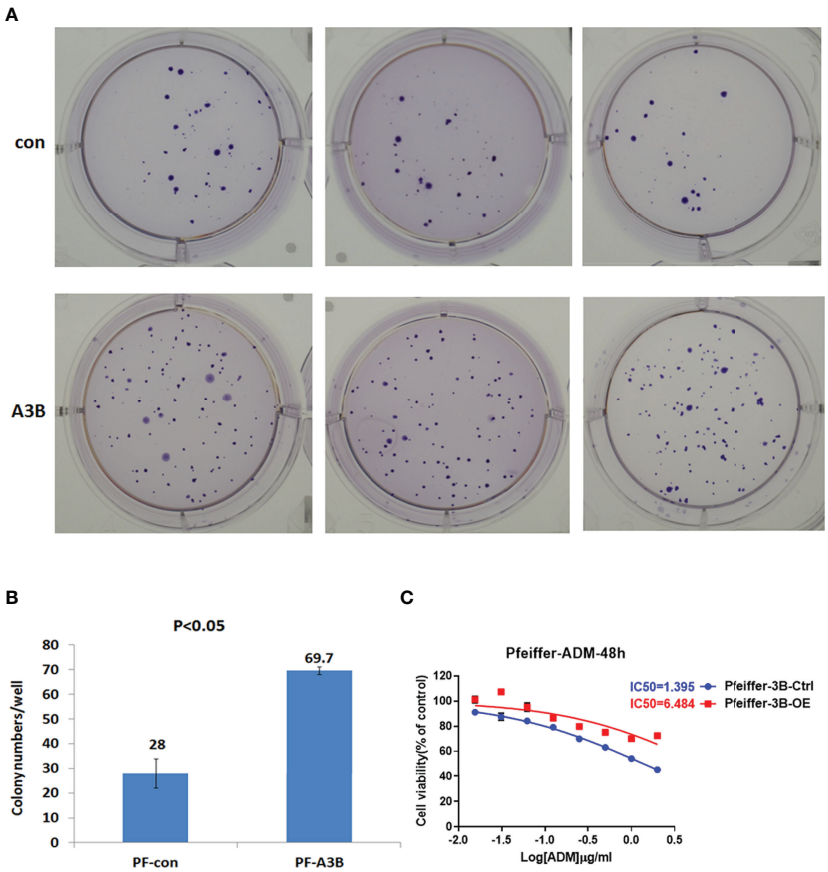

FIGURE 7 | APOBEC3B-induced proliferation and drug resistance in DLBCL cells. **(A, B)** Colony formation after induction of APOBEC3B expression. A3B inducible, APOBEC3B-Flag/pLV-Ptight-puro vector-transfected Pfeiffer cells; Con, pLV-Ptight-puro vector-transfected Pfeiffer cells; PF-A3B, APOBEC3B-Flag/pLV-Ptight-puro vector-transfected Pfeiffer cells; PF-con, pLV-Ptight-puro vector-transfected Pfeiffer cells. **(C)** Doxorubicin resistance after induction of APOBEC3B expression. ADM, doxorubicin; Pfeiffer-3B-Ctrl, pLV-Ptight-puro vector-transfected Pfeiffer cells; Pfeiffer-3B-OE, APOBEC3B-Flag/pLV-Ptight-puro vector-transfected Pfeiffer cells.

mutant p53 promotes proliferation and confers drug resistance in DLBCL cells.

DISCUSSION

The results of this study demonstrate that APOBEC3B induces p53 mutation and may confer drug resistance in DLBCL. The rate of *TP53* mutation in DLBCL is 20%–30%, with similar frequencies of the germinal center B-cell and activated B-cell subtypes (7–9). In the present study, 3D-PCR-based sequencing identified *TP53* exon 8 mutations in 35.9% of the cohort, which is higher than in previous reports. Even in non-R/R DLBCL cases, the TP53 exon 8 mutation rate was 23.26%. This may be explained by selective amplification of DNA fragments containing the G/C-to-A/T mutation (20). Thus, 3D-PCR detected the G/C-to-A/T mutation with higher sensitivity than standard PCR. A shortcoming of this method is that it misses other mutation types; however, as G/C to A/T is the main *TP53* mutation and accounts for most hotspot mutations (10), 3D-PCR is a valuable method for *TP53* mutation detection in DLBCL.

Given its function as a tumor suppressor, mutations in *TP53* predict poor prognosis in acute myelogenous leukemia and chronic lymphocytic leukemia in National Comprehensive Cancer Network guidelines and in multiple myeloma in the Mayo Clinic Stratification for Myeloma and Risk-Adapted Therapy system. It has been reported that *TP53* mutation is also a prognostic factor for a poor outcome in DLBCL (7–9). However, other studies failed to demonstrate a correlation between *TP53* mutation and prognosis (21, 22). In the present study, we found that *TP53* exon 8 G/C-to-A/T mutation frequency was higher in R/R DLBCL patients than in non-R/R DLBCL patients. Most were missense mutations that caused an amino acid change. Patients with *TP53* mutation had a lower CR rate than those with wild-type *TP53* when treated with the R-CHOP regimen. *TP53* hotspot mutations were able to distinguish patients with IPI > 2, who had a worse outcome than patients with high-risk IPI but wild-type and non-hotspot *TP53*, who had an outcome similar to the IPI 0–2 group. The multivariate Cox model showed that *TP53* hotpot mutation was a stronger

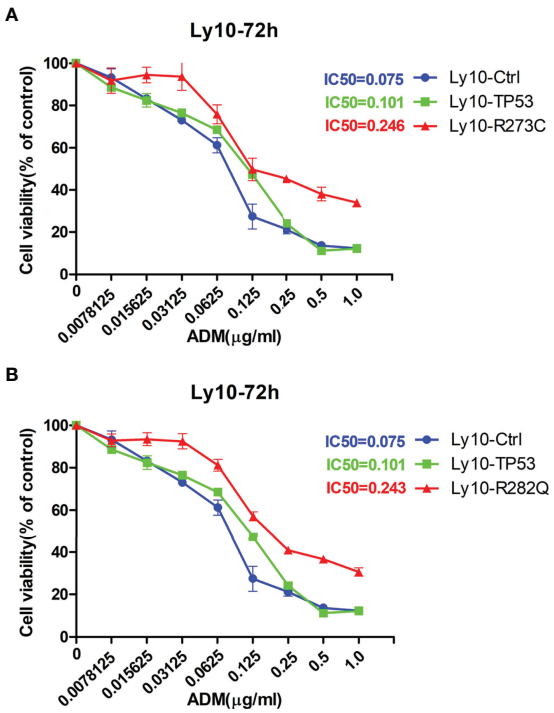

FIGURE 8 | p53 mutants (R273C and R282Q) induce doxorubicin resistance. **(A, B)** Effect of R273C **(A)** and R282Q **(B)** mutation on doxorubicin sensitivity in Ly10 cells. ADM, doxorubicin; Ly10-Ctrl, empty vector-transfected Ly10 cell; Ly10-R273C, p53 R273C mutant-transfected Ly10 cells; Ly10-R282Q, p53 R282Q mutant-transfected Ly10 cells; Ly10-TP53, wild-type p53-transfected Ly10 cells.

prognostic factor for PFS than IPI, LDH activity, tumor stage, and sex. Consistent with previous reports, our data showed that *TP53* mutation was an independent prognostic factor for poor outcome in DLBCL. However, as we only sequenced and analyzed exon 8, the *TP53* mutation rate may have been underestimated; *TP53* mutations in other exons need to be examined to confirm this association.

About one-third of *TP53* mutations were clustered in 5 hotspot residues—namely, p.R175, p.G245, p.R248, p.R273, and p.R282 (23). Most previous studies did not evaluate the differential prognostic value of *TP53* mutation at different positions in DLBCL. Mutations in the DBD—especially in the loop–sheet–helix motif and L3 regions—were shown to be associated with worse survival (8). Codons 248, 273, 175, 176, and 213 of the p53 protein have the highest mutation frequency, which is associated with poor prognosis (9). Thus, hotspot mutations may be more important for p53 activity and have greater prognostic value than non-hotspot mutations. We found that some hotspot mutations including those in codons 273, 282, and 283 were higher in R/R DLBCL than in non-R/R DLBCL. Patients with non-hotspot mutations had a CR rate and PFS similar to patients with wild-type *TP53*; however, this requires confirmation in a larger cohort. Hotspot mutations but not non-hotspot mutations were strongly associated with lower CR rate and shorter PFS in DLBCL patients, and were previously shown to affect the DNA-binding activity of the p53 protein, thereby impairing the regulation of target genes (24, 25). Some of these hotspot p53 mutants were also responsible for gain of function in carcinogenesis and drug resistance (26, 27). For example, the R273C and R273H mutants conferred cancer cells with a more aggressive phenotype and enhanced resistance to DNA-damaging drugs (28). The *TP53* missense mutations R273H and R282W were also reported to exert a dominant-negative effect and caused drug resistance in AML cells (29). We found that hotspot mutations rather than all *TP53* mutation sites were associated with worse survival in DLBCL patients. Which of these mutations have a greater prognostic value and how they influence the role of p53 in tumorigenesis and drug resistance remain to be determined.

TP53 mutation may confer resistance to chemotherapy agents such as doxorubicin (29) and cisplatin (30, 31), which are typically used to treat DLBCL. However, the underlying mechanism is not well understood, which has prevented the development of therapeutic strategies to overcome mutant p53-mediated drug resistance. G/C to A/T is the most common *TP53* mutation type, especially at mutation hotspots. Most known carcinogens such as polycyclic aromatic hydrocarbons (benzo[a]pyrene), aristolochic acid, aflatoxin B1, vinyl chloride, and 3-nitrobenzanthrone do not induce G/C-to-A/T mutation (32), although ultraviolet radiation was reported to induce CC-to-TT mutation in skin cancer (33). However, the mechanism through which most *TP53* G/C-to-A/T mutations arise is unclear. Our group and others previously demonstrated that some APOBEC3 family members could induce the G/C-to-A/T mutation in the genome of viruses including HIV (34, 35), HTLV-1 (36), and HBV (15, 37, 38). APOBEC3B is among the most widely studied factors related to G/C-to-A/T mutations in various human cancers (14, 39, 40). APOBEC3s were shown to be upregulated by interferon (41), which is an important cytokine involved in inflammation; chronic inflammation may contribute to lymphoma carcinogenesis. Based on our findings, we propose that APOBEC3s—especially APOBEC3B—are responsible for the *TP53* G/C-to-A/T mutation.

Among the APOBEC3 family members, APOBEC3B is mainly localized in the nucleus; APOBEC3G, APOBEC3F, and APOBEC3DE are present in the cytoplasm; and APOBEC3A and APOBEC3C are localized in both compartments (15, 37). A bioinformatic analysis of APOBEC3 expression in DLBCL revealed that APOBEC3B but not APOBEC3A was upregulated in DLBCL in several lymphoma databases, suggesting that it is responsible for *TP53* mutations in DLBCL.

Using an inducible expression system, we overexpressed APOBEC3B in DLBCL cells and found that the G/C-to-A/T mutation was induced in *TP53* exon 8. These *in vitro* APOBEC3B-induced mutation patterns including hotspot

mutants were the same as those observed in clinical R/R DLBCL samples. Overexpression of APOBEC3A did not induce the G/C-to-A/T mutation in *TP53*. Thus, APOBEC3B and not APOBEC3A may be responsible for the *TP53* G/C-to-A/T mutation in DLBCL, although the molecular details remain to be elucidated. The APOBEC3B-induced mutants enhanced the proliferation of DLBCL cells and conferred resistance to the CHOP component doxorubicin, which has been previously reported (29). Thus, APOBEC3B-induced p53 mutants may be responsible for R/R DLBCL. As APOBEC3B targets different DNA sequences in different cells, additional research is needed to determine the sequence and associated factors in R/R DLBCL. Recently, the p53 protein was shown to regulate APOBEC3B3 expression, which increased APOBEC signature mutations in p53-defective cells (42). Thus, the crosstalk between p53 and APOBEC3B in carcinogenesis and drug resistance warrants further study.

As APOBEC3B has been shown to be associated with mutations in genomic DNA, tumorigenesis, and drug resistance, it is a potential therapeutic target for cancer treatment. Inhibiting APOBEC3B *via* modified single-stranded DNA and thereby reducing the risk of genomic mutations (43–45) and targeting uracil DNA glycosylases to selectively inhibit tumor cells with high APOBEC3B expression (46) have been described as possible strategies. However, it is unclear whether the former can reduce the frequency of *TP53* mutations in DLBCL and the latter can prevent R/R in DLBCL.

CONCLUSION

In this study, we demonstrated that aberrantly activated APOBEC3B can induce *TP53* G/C-to-A/T mutations in DLBCL, which may lead to proliferation and drug resistance and may contribute to R/R DLBCL. As a DNA mutator, APOBEC3B is a potential therapeutic target to reduce the rate of *TP53* mutation and improve the prognosis of DLBCL patients. *TP53* mutants—especially those in hotspots—have a prognostic value for DLBCL treated with R-CHOP. We also provided a more sensitive method for detecting *TP53* mutation in tumor tissue DNA, which may be helpful for further study of *TP53* mutations in malignancies beyond DLBCL. In conclusion, our findings provide insight into the mechanism underlying *TP53* mutation in DLBCL as well as a potential target for overcoming drug resistance in this disease.

DATA AVAILABILITY STATEMENT

The datasets presented in this study can be found in online repositories. The names of the repository/repositories and accession number(s) can be found in the article/**Supplementary Material**.

ETHICS STATEMENT

The studies involving human participants were reviewed and approved by the Ethics Committee of the Second Affiliated Hospital of Zhejiang University School of Medicine. The patients/participants provided their written informed consent to participate in this study.

AUTHOR CONTRIBUTIONS

XZZ and RX designed the experiments. XZZ, ZW, TY, XiaL, and YL performed the experiments. JL and XiuL contributed to the analysis of pathological data. YX, LH, XH, WW, GX, and XHZ collected the clinical data. QL and YF contributed to the collection of patient material. XZZ and ZW contributed to the analysis of the data. YH contributed to the data analysis and revision. XZZ, RX, and WQ contributed to the writing of the manuscript. All authors contributed to the article and approved the submitted version.

FUNDING

This work was supported by a grant from the National Natural Science Foundation of China (81000895 to XZZ), a grant from the Zhejiang Provincial Natural Science Foundation of China (LY14H160032 to XZZ), and a grant from the Leukemia Research Innovative Team of Zhejiang Province (2011R50015 to XZZ). This work was also partly supported by a grant from the Zhejiang Provincial Natural Science Foundation of China (LQ22H080007 to ZW).

SUPPLEMENTARY MATERIAL

The Supplementary Material for this article can be found online at: https://www.frontiersin.org/articles/10.3389/fimmu.2022.888250/full#supplementary-material

REFERENCES

1. Roschewski M, Staudt LM, Wilson WH. Diffuse Large B-Cell Lymphoma-Treatment Approaches in the Molecular Era. *Nat Rev Clin Oncol* (2014) 11:12–23. doi: 10.1038/nrclinonc.2013.197
2. Coiffier B, Lepage E, Briere J, Herbrecht R, Tilly H, Bouabdallah R, et al. CHOP Chemotherapy Plus Rituximab Compared With CHOP Alone in Elderly Patients With Diffuse Large-B-Cell Lymphoma. *N Engl J Med* (2002) 346:235–42. doi: 10.1056/NEJMoa011795
3. Hollstein M, Sidransky D, Vogelstein B, Harris CC. P53 Mutations in Human Cancers. *Sci* (1991) 253:49–53. doi: 10.1126/science.1905840
4. Ciriello G, Miller ML, Aksoy BA, Senbabaoglu Y, Schultz N, Sander C. Emerging Landscape of Oncogenic Signatures Across Human Cancers. *Nat Genet* (2013) 45:1127–33. doi: 10.1038/ng.2762

5. Baugh EH, Ke H, Levine AJ, Bonneau RA, Chan CS. Why are There Hotspot Mutations in the TP53 Gene in Human Cancers? *Cell Death Differ* (2018) 25:154–60. doi: 10.1038/cdd.2017.180
6. Flynt E, Bisht K, Sridharan V, Ortiz M, Towfic F, Thakurta A. Prognosis, Biology, and Targeting of TP53 Dysregulation in Multiple Myeloma. *Cells* (2020) 9:287–310. doi: 10.3390/cells9020287
7. Tessoulin B, Eveillard M, Lok A, Chiron D, Moreau P, Amiot M, et al. P53 Dysregulation in B-Cell Malignancies: More Than a Single Gene in the Pathway to Hell. *Blood Rev* (2017) 31:251–59. doi: 10.1016/j.blre.2017.03.001
8. Zenz T, Kreuz M, Fuge M, Klapper W, Horn H, Staiger AM, et al. TP53 Mutation and Survival in Aggressive B Cell Lymphoma. *Int J Cancer* (2017) 141:1381–8. doi: 10.1002/ijc.30838
9. Young KH, Leroy K, Møller MB, Colleoni GW, Sánchez-Beato M, Kerbauy FR, et al. Structural Profiles of *TP53* Gene Mutations Predict Clinical Outcome in Diffuse Large B-Cell Lymphoma: An International Collaborative Study. *Blood* (2008) 112:3088–98. doi: 10.1182/blood-2008-01-129783
10. Xu-Monette ZY, Wu L, Visco C, Tai YC, Tzankov A, Liu WM, et al. Mutational Profile and Prognostic Significance of *TP53* in Diffuse Large B-Cell Lymphoma Patients Treated With R-CHOP: Report From an International DLBCL Rituximab-CHOP Consortium Program Study. *Blood* (2012) 120:3986–96. doi: 10.1182/blood-2012-05-433334
11. Zhang J, Grubor V, Love CL, Banerjee A, Richards KL, Mieczkowski PA, et al. Genetic Heterogeneity of Diffuse Large B-Cell Lymphoma. *Proc Natl Acad Sci USA* (2013) 110(4):1398–403. doi: 10.1073/pnas.1205299110
12. Roberts SA, Lawrence MS, Klimczak LJ, Grimm SA, Fargo D, Stojanov P, et al. An APOBEC Cytidine Deaminase Mutagenesis Pattern is Widespread in Human Cancers. *Nat Genet* (2013) 45:970–6. doi: 10.1038/ng.2702
13. Cheson BD, Pfistner B, Juweid ME, Gascoyne RD, Specht L, Horning SJ, et al. International Harmonization Project on Lymphoma. Revised Response Criteria for Malignant Lymphoma. *J Clin Oncol* (2007) 25:579–86. doi: 10.1200/JCO.2006.09.2403
14. Burns MB, Lackey L, Carpenter MA, Rathore A, Land AM, Leonard B, et al. APOBEC3B is an Enzymatic Source of Mutation in Breast Cancer. *Nat* (2013) 494:366–70. doi: 10.1038/nature11881
15. Xu R, Zhang X, Zhang W, Fang Y, Zheng S, Yu XF. Association of Human APOBEC3 Cytidine Deaminases With the Generation of Hepatitis Virus B X Antigen Mutants and Hepatocellular Carcinoma. *Hepatol* (2007) 46(6):1810–20. doi: 10.1002/hep.21893
16. Chen T, Meng Z, Gan Y, Wang X, Xu F, Gu Y, et al. The Viral Oncogene Np9 Acts as a Critical Molecular Switch for Co-Activating β-Catenin, ERK, Akt and Notch1 and Promoting the Growth of Human Leukemia Stem/Progenitor Cells. *Leukemia* (2013) 27(7):1469–78. doi: 10.1038/leu.2013.8
17. Gu Y, Chen T, Meng Z, Gan Y, Xu X, Lou G, et al. CaMKII γ, A Critical Regulator of CML Stem/Progenitor Cells, Is a Target of the Natural Product Berbamine. *Blood* (2012) 120(24):4829–39. doi: 10.1182/blood-2012-06-434894
18. Mareschal S, Dubois S, Viailly PJ, Bertrand P, Bohers E, Maingonnat C, et al. Whole Exome Sequencing of Relapsed/Refractory Patients Expands the Repertoire of Somatic Mutations in Diffuse Large B-Cell Lymphoma. *Genes Chromosomes Cancer* (2016) 55(3):251–67. doi: 10.1002/gcc.22328
19. Morin RD, Assouline S, Alcaide M, Mohajeri A, Johnston RL, Chong L, et al. Genetic Landscapes of Relapsed and Refractory Diffuse Large B-Cell Lymphomas. *Clin Cancer Res* (2016) 22(9):2290–300. doi: 10.1158/1078-0432.CCR-15-2123
20. Suspene R, Henry M, Guillot S, Wain-Hobson S, Vartanian JP. Recovery of APOBEC3-Edited Human Immunodeficiency Virus G-A Hypermutants by Differential DNA Denaturation PCR. *J Gen Virolo* (2005) 86(Pt 1):125–9. doi: 10.1099/vir.0.80426-0
21. Osada M, Ishioka C, Ichinohasama R, Kadowaki I, Murakawa Y, Watanabe M, et al. Influence of P53 Mutation on Pathological Grade, But Not Prognosis of non-Hodgkin's Lymphoma. *Anticancer Drug Des* (1999) 14(2):107–14.
22. Barrans SL, Carter I, Owen RG, Owen RG, Davies FE, Patmore RD, et al. Germinal Center Phenotype and Bcl-2 Expression Combined With the International Prognostic Index Improves Patient Risk Stratification in Diffuse Large B-Cell Lymphoma. *Blood* (2002) 99(4):1136–43. doi: 10.1182/blood.v99.4.1136
23. Brosh R, Rotter V. When Mutants Gain New Powers: News From the Mutant P53 Field. *Nat Rev Cancer* (2009) 9(10):701–13. doi: 10.1038/nrc2693
24. Frebourg T, Kassel J, Lam KT, Gryka MA, Barbier N, Andersen TI, et al. Germ-Line Mutations of the P53 Tumor Suppressor Gene in Patients With High Risk for Cancer Inactivate the P53 Protein. *Proc Natl Acad Sci USA* (1992) 89(14):6413–7. doi: 10.1073/pnas.89.14.6413
25. Quesnel S, Verselis S, Portwine C, Garber J, White M, Feunteun J, et al. P53 Compound Heterozygosity in a Severely Affected Child With Li-Fraumeni Syndrome. *Oncogene* (1999) 18(27):3970–8. doi: 10.1038/sj.onc.1202783
26. Lang GA, Iwakuma T, Suh YA, Liu G, Rao VA, Parant JM, et al. Gain of Function of a P53 Hot Spot Mutation in a Mouse Model of Li-Fraumeni Syndrome. *Cell* (2004) 119(6):861–72. doi: 10.1016/j.cell.2004.11.006
27. Stambolsky P, Tabach Y, Fontemaggi G, Weisz L, Maor-Aloni R, Siegfried Z, et al. Modulation of the Vitamin D3 Response by Cancer-Associated Mutant P53. *Cancer Cell* (2010) 17(3):273–85. doi: 10.1016/j.ccr.2009.11.025
28. Li J, Yang L, Gaur S, Zhang K, Wu X, Yuan YC, et al. Mutants TP53 P.R273H and P.R273C But Not P.R273G Enhance Cancer Cell Malignancy. *Hum Mutation* (2014) 35(5):575–84. doi: 10.1002/humu.22528
29. Boettcher S, Miller PG, Sharma R, McConkey M, Leventhal M, Krivtsov AV, et al. A Dominant-Negative Effect Drives Selection of *TP53* Missense Mutations in Myeloid Malignancies. *Sci* (2019) 365(6453):599–604. doi: 10.1126/science.aax3649
30. Reles A, Wen WH, Schmider A, Gee C, Runnebaum IB, Kilian U, et al. Correlation of P53 Mutations With Resistance to Platinum-Based Chemotherapy and Shortened Survival in Ovarian Cancer. *Clin Cancer Res* (2001) 7(10):2984–97.
31. Alexandrova EM, Yallowitz AR, Li D, Xu S, Schulz R, Proia DA, et al. Improving Survival by Exploiting Tumor Dependence on Stabilized Mutant P53 for Treatment. *Nat* (2015) 523(7560):352–56. doi: 10.1038/nature14430
32. Olivier M, Hollstein M, Hainaut P. *TP53* Mutations in Human Cancers: Origins, Consequences, and Clinical Use. *Cold Spring Harb Perspect Biol* (2010) 2(1):a001008. doi: 10.1101/cshperspect.a001008
33. Giglia-Mari G, Sarasin A. *TP53* Mutations in Human Skin Cancers. *Hum Mutat* (2003) 21(3):217–28. doi: 10.1002/humu.10179
34. Harris RS, Bishop KN, Sheehy AM, Craig HM, Petersen-Mahrt SK, Watt IN, et al. DNA Deamination Mediates Innate Immunity to Retroviral Infection. *Cell* (2003) 113(6):803–9. doi: 10.1016/s0092-8674(03)00423-9
35. Lecossier D, Bouchonnet F, Clavel F, Hance AJ. Hypermutation of HIV-1 DNA in the Absence of the Vif Protein. *Sci* (2003) 300(5622):1112. doi: 10.1126/science.1083338
36. Mahieux R, Suspène R, Delebecque F, Henry M, Schwartz O, Wain-Hobson S, et al. Extensive Editing of a Small Fraction of Human T-Cell Leukemia Virus Type 1 Genomes by Four APOBEC3 Cytidine Deaminases. *J Gen Virol* (2005) 86(Pt 9):2489–94. doi: 10.1099/vir.0.80973-0
37. Suspène R, Guétard D, Henry M, Sommer P, Wain-Hobson S, Vartanian JP. Extensive Editing of Both Hepatitis B Virus DNA Strands by APOBEC3 Cytidine Deaminases *In Vitro* and *In Vivo*. *Proc Natl Acad Sci USA* (2005) 102 (23):8321–6. doi: 10.1073/pnas.0408223102
38. Bonvin M, Achermann F, Greeve I, Stroka D, Keogh A, Inderbitzin D, et al. Interferon-Inducible Expression of APOBEC3 Editing Enzymes in Human Hepatocytes and Inhibition of Hepatitis B Virus Replication. *Hepatol* (2006) 43(6):1364–74. doi: 10.1002/hep.21187
39. Burns MB, Temiz NA, Harris RS. Evidence for APOBEC3B Mutagenesis in Multiple Human Cancers. *Nat Genet* (2013) 45(9):977–83. doi: 10.1038/ng.2701
40. Yamazaki H, Shirakawa K, Matsumoto T, Hirabayashi S, Murakawa Y, Kobayashi M, et al. Endogenous APOBEC3B Overexpression Constitutively Generates DNA Substitutions and Deletions in Myeloma Cells. *Sci Rep* (2019) 9(1):7122. doi: 10.1038/s41598-019-43575-y
41. Peng G, Lei KJ, Jin W, Greenwell-Wild T, Wahl SM. Induction of APOBEC3 Family Proteins, A Defensive Maneuver Underlying Interferon-Induced Anti-HIV-1 Activity. *J Exp Med* (2006) 203(1):41–6. doi: 10.1084/jem.20051512
42. Periyasamy M, Singh AK, Gemma C, Kranjec C, Farzan R, Leach DA, et al. P53 Controls Expression of the DNA Deaminase APOBEC3B to Limit Its Potential Mutagenic Activity in Cancer Cells. *Nucleic Acids Res* (2017) 45 (19):11056–69. doi: 10.1093/nar/gkx721

43. Kvach MV, Barzak FM, Harjes S, Schares HAM, Jameson GB, Ayoub AM, et al. Inhibiting APOBEC3 Activity With Single-Stranded DNA Containing 2'-Deoxyzebularine Analogues. *Biochem* (2019) 58(5):391–400. doi: 10.1021/acs.biochem.8b00858
44. Barzak FM, Harjes S, Kvach MV, Kurup HM, Jameson GB, Filichev VV, et al. Selective Inhibition of APOBEC3 Enzymes by Single-Stranded DNAs Containing 2'-Deoxyzebularine. *Org Biomol Chem* (2019) 17(43):9435–41. doi: 10.1039/c9ob01781j
45. Kvach MV, Barzak FM, Harjes S, Schares HAM, Kurup HM, Jones KF, et al. Differential Inhibition of APOBEC3 DNA-Mutator Isozymes by Fluoro- and Non-Fluoro-Substituted 2'-Deoxyzebularine Embedded in Single-Stranded DNA. *Chembiochem* (2020) 21(7):1028–35. doi: 10.1002/cbic.201900505
46. Serebrenik AA, Starrett GJ, Leenen S, Jarvis MC, Shaban NM, Salamango DJ, et al. The Deaminase APOBEC3B Triggers the Death of Cells Lacking Uracil DNA Glycosylase. *Proc Natl Acad Sci USA* (2019) 116(44):22158–63. doi: 10.1073/pnas.1904024116

Conflict of Interest: The authors declare that the research was conducted in the absence of any commercial or financial relationships that could be construed as a potential conflict of interest.

Publisher's Note: All claims expressed in this article are solely those of the authors and do not necessarily represent those of their affiliated organizations, or those of the publisher, the editors and the reviewers. Any product that may be evaluated in this article, or claim that may be made by its manufacturer, is not guaranteed or endorsed by the publisher.

frontiers | Frontiers in Immunology

ORIGINAL RESEARCH
published: 17 May 2022
doi: 10.3389/fimmu.2022.899073

Clinical and Molecular Characteristics of 60 Patients With Human Immunodeficiency Virus-Negative Castleman Disease

Siyu Qian[1], Mengjie Ding[1], Huting Hou[1], Zeyuan Wang[1], Jieming Zhang[1], Yue Zhang[1], Meng Dong[1], Linan Zhu[1], Guannan Wang[2], Wencai Li[2] and Xudong Zhang[1]**

[1] Department of Oncology, The First Affiliated Hospital, Zhengzhou University, Zhengzhou, China, [2] Department of Pathology, The First Affiliated Hospital of Zhengzhou University, Zhengzhou, China

OPEN ACCESS

Edited by:
Jo Caers,
University of Liège, Belgium

Reviewed by:
Jingwei Liu,
University of Texas MD Anderson Cancer Center, United States
Liang Wang,
Capital Medical University, China
Shujuan Wen,
Xinjiang Medical University, China

***Correspondence:**
Xudong Zhang
fcczhangxd@zzu.edu.cn
Wencai Li
Wencailizzu@126.com

Specialty section:
This article was submitted to Cancer Immunity and Immunotherapy, a section of the journal Frontiers in Immunology

Received: 18 March 2022
Accepted: 19 April 2022
Published: 17 May 2022

Citation:
Qian S, Ding M, Hou H, Wang Z, Zhang J, Zhang Y, Dong M, Zhu L, Wang G, Li W and Zhang X (2022) Clinical and Molecular Characteristics of 60 Patients With Human Immunodeficiency Virus-Negative Castleman Disease. Front. Immunol. 13:899073. doi: 10.3389/fimmu.2022.899073

Castleman disease (CD) is a rare lymphoproliferative disorder. The mechanistic target of rapamycin (mTOR) pathway is a key regulator of various cellular functions, which may be related with the potential mechanisms of CD occurrence. We retrospectively collected the clinical information of 60 CD patients diagnosed in the First Affiliated Hospital of Zhengzhou University. And FFPE biopsy specimens were collected from 31 patients (12 unicentric CD patients and 19 multicentric CD patients) to detect the mTOR pathway protein expression. We are the first to demonstrate that thrombocytopenia and hypoalbuminemia are independent poor prognostic factors for CD. Moreover, mTOR activation was higher in CD compared to reactive lymphoid hyperplasia (used as a control group). This study offers some elucidation for the management and treatment of CD patients.

Keywords: Castleman disease, classifications, prognosis, mTOR pathway, thrombocytopenia

1 INTRODUCTION

Castleman disease (CD), also known as angiofollicular lymph node hyperplasia or giant lymph node hyperplasia, is a rare lymphoproliferative disorder first described by Benjamin Castleman in 1956 (1). According to the distribution of enlarged lymph nodes, it was clinically divided into unicentric CD (UCD) and multicentric CD (MCD). According to human herpes virus-8 (HHV-8) status, MCD was further classified as HHV-8 positive and HHV-8 negative; the latter is referred to as idiopathic MCD (iMCD) (2) (**Figure 1A**). TAFRO syndrome is a newly recognized variant of iMCD that includes a constellation of syndromes: thrombocytopenia, anasarca, fever, reticulin fibrosis, and organomegaly (3).

The clinical and mechanisms of CD remain poorly understood. UCD may involve a process of clonal tumorigenesis (4). The preferred therapy for UCD is complete surgical resection. Complete surgical

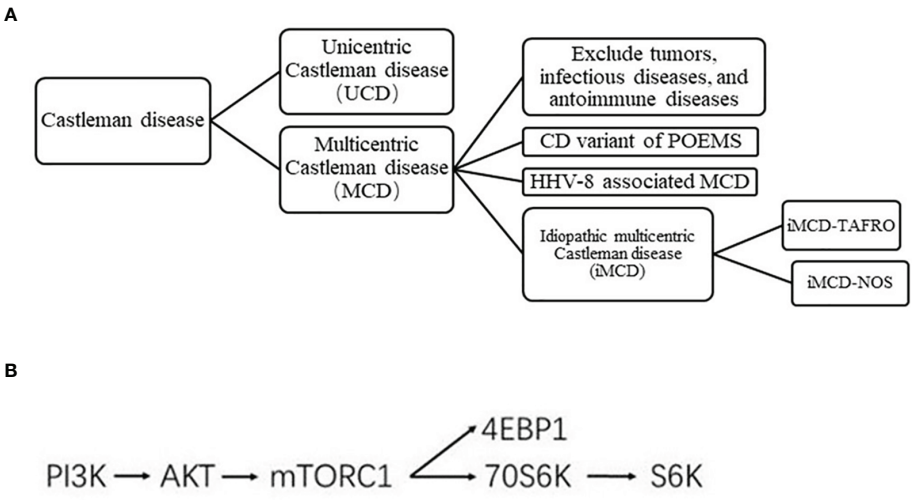

FIGURE 1 | **(A)** Clinical classification of CD. **(B)** Simplified mTOR pathway.

excision usually eliminates all systemic symptomatology and laboratory abnormalities, if present (5). Interleukin 6 (IL-6) is a multifunctional cytokine *in vivo* that can stimulate bone marrow hematopoiesis and plasma cell differentiation, inducing the systemic symptoms of CD (6). HHV-8 encodes a viral IL-6 homolog with a similar structure and function to human IL-6, which leads to the occurrence of HHV-8-associated MCD (7, 8). As for HHV-8 associated MCD, treatment regimen based on rituximab can be used. Asymptomatic MCD patients can be followed up with only observation. There is no standard treatment for iMCD patients. Although iMCD patients tested negative for HHV-8, the level of IL-6 remained high. The role of excessive IL-6 signaling in the pathogenesis of iMCD has led to the development of novel iMCD therapies targeting IL-6. However, 50% to 66% of patients with iMCD remain refractory to therapy with an IL-6 blocker. The mechanistic target of rapamycin (mTOR) pathway is a key regulator of various cellular functions, such as protein synthesis and cell growth, division, and survival, and is a critical event in the development of different hematological malignancies (9). The mTOR inhibitor has been recommended as a second-line treatment for iMCD patients. At present, there is a lack of large number of clinical samples to explore the exact expression of mTOR pathway protein in CD patients. The present study evaluated the clinical characteristics of HIV-negative CD patients and determined the mTOR pathway activity using an immunohistochemical (IHC) approach.

2 MATERIALS AND METHODS

2.1 Patients

From October 2012 to October 2021, 60 patients with CD confirmed through clinical, laboratory and pathological examination, with adequate follow-up data, from the First Affiliated Hospital of Zhengzhou University were recruited in this study. The patients' data were obtained from the medical records and *via* telephone interview, including general information, clinical complaints and symptoms, results of pathological and IHC examinations of biopsy specimens, clinical laboratory tests, imaging performed, and follow-up information. None of the patients developed HIV infection. Follow-up was performed until December 10, 2020. Formalin-fixed paraffin-embedded biopsy specimens from 31 patients with CD (12 with UCD and 19 with MCD) and 10 patients with reactive lymphoid hyperplasia were collected for IHC analysis.

2.2 IHC

All tissues were embedded in paraffin, cut into 5-μm slices, and used for IHC analysis. After heating at 40°C for deparaffinization, the slices were deparaffinized three times (20 min each time) and rehydrated with absolute ethanol for 10 min, 95% ethanol for 5 min, and 80% ethanol for 5 min. The slides were incubated overnight with the primary antibodies against p70S6k, p4EBP1, pS6, S6, and pAKT. Immunostaining was performed by two independent pathologists.

2.3 Grading Criteria

At least 200 positive cells per field of vision were counted. The positive cells appeared yellow to dark brown in color. Based on the shade of positive staining, the sections were graded as follows: 0 points, no color; 1 point, light yellow; 2 points, tawny; and 3 points, dark brown. The amount of staining was graded as follows: 0 point, 0%–10% positive cells; 1 point, 11%–25% positive cells; 2 points, 25%–50% positive cells; and 3 points, >50% positive cells. The scores from the two evaluations were then multiplied. Samples with 0–2 points were classified into the low expression group, while those with ≥3 points were classified into the high expression group.

2.4 Statistical Analysis

The patients' clinical characteristics were summarized using descriptive statistics. The UCD and MCD were compared

using the X^2 test, Fisher's exact test, and t-test. The Kaplan-Meier method was used to analyze the survival curves, and the differences were compared using the log-rank test. All statistical analyses were performed using the SPSS software (Version 21.0). A *P*-value of <0.05 was considered significant.

3 RESULTS

3.1 Clinical Characteristics and Manifestations

A total of 19 patients had UCD, with an average age of 39 years, while 41 had MCD, with an average age of 36 years. Among the MCD patients, two had TAFRO syndrome. The most common pathology type of UCD was hyaline vascular, whereas the plasma cell type and mixed type were highly expressed in MCD (*P*<0.001). No significant difference was observed between the MCD and UCD groups in terms of age and sex. The most common initial symptom of UCD was lymphadenopathy, especially in the neck, which was also observed in the axillary, groin, breast, and other parts, and UCD was more prevalent than MCD (*P*=0.019). Fever (38°C) was the initial symptom of MCD, which was accompanied by night sweats, fatigue, and so on (*P*=0.034). Some patients remained asymptomatic regardless of the CD type, but UCD was more common than MCD (*P*=0.031) (**Table 1**).

3.2 Laboratory Tests and Virus Detection

By analyzing the detailed laboratory test information of patients with CD, we found that MCD patients were more likely to have anemia, hypoproteinemia, abnormal albumin/globulin (A/G) ratio, abnormal platelet count, and elevated lactate dehydrogenase (LDH) and urinary protein levels than UCD patients (*P*<0.05) (**Table 2**). Twenty-seven patients underwent a series of tests for common types of viruses, including Coxsackie virus, measles virus, cytomegalovirus, and herpes simplex virus; meanwhile, 55 patients underwent a series of tests for common infectious diseases. All patients tested negative for HIV serum antibodies. EBV was found in 87.0% of the tested patients with MCD and in 75.0% of patients with UCD (*P*=0.025). Similar proportions of patients tested positive for cytomegalovirus (**Table 3**).

3.3 Imaging Examination

According to the computed tomography (CT) and ultrasound images of patients, the most common region of lymphadenopathy was the neck in both UCD patients (65.0%) and MCD patients (80.5%). In addition, splenomegaly (22.0%) and serous effusion (14.6%) were observed in patients with MCD (**Figure 2**). Positron emission tomography-CT (PET-CT) was performed in 17 patients. Comparing the maximum standard uptake value (SUVmax) according to multicentricity, SUVmax was significantly higher in the MCD group than in the UCD group (6.8 ± 4.2 and 2.8 ± 0.7, respectively; *P*<0.001).

3.4 Immunohistochemistry

3.4.1 Conventional IHC

CD3, CD20, CD21, and Ki-67 were detected in most CD patients. CD3, CD20, and CD21 were detected in all (100%) patients with UCD and in 90% of patients with MCD. Ki-67 was expressed in all patients, and the mean positive rate was approximately 23%. A significant difference was observed in the expression of Bcl-2 between UCD patients and MCD patients (*P*=0.034, **Supplemental Table**).

3.4.2 Expression of mTOR Pathway-Related Proteins

To verify the activity of the mTOR pathway, the phosphorylation levels of AKT, 4EBP1, p70S6K, and S6K, and levels of

TABLE 1 | Clinical characteristics and manifestations of patients with UCD and MCD.

	UCD (n = 19)	MCD (n = 41)	*P* Value
Age(years)	39 ± 15	36 ± 15	0.453
Gender			0.781
Female	9	21	
Male	10	20	
Histopathological subtype			**<0.001**
Plasmacytic variant	0	17	
Hyaline vascular variant	19	13	
Mixed cellular variant	0	11	
No symptoms	4	1	**0.031**
Lymphadenopathy	11	12	**0.019**
Neck	8	6	
Axilla	1	2	
Groin	1	0	
Breast	1	1	
Submandibular	0	2	
Posterior auricular	0	1	
Fever	2	17	**0.034**
Fatigue	0	3	0.546
Edema	1	4	1.000
Mouth ulcer	0	2	1.000
Abdominal pain	1	2	1.000
Cough, chest tightness	0	1	1.000
Foam urine	0	1	1.000

Bold values is statistically meaningful (P < 0.05).

TABLE 2 | Laboratory test information of patients with UCD and MCD.

	UCD (n = 19)	MCD (n = 41)	*P* Value
Anemia	3	22	**0.010**
Abnormal WBC count	3	7	1.000
Abnormal neutrocyte count	1	8	0.249
Abnormal lymphocyte count	4	11	0.755
Abnormal platelet count	4	23	**0.013**
Hypoalbuminemia	1	18	**<0.001**
Elevated globulin	1	4	1.000
Abnormal albumin/globulin(A/G)	6	27	**0.024**
Elevated LDH	0	7	**<0.001**
Elevated β2-MG	1	10	0.086
Elevated alkaline phosphatase	1	6	0.414
Elevated uric acid	3	9	0.735
Elevated creatinine	1	3	1.000
Elevated urinary protein	1	12	**0.045**

Bold values is statistically meaningful (P < 0.05).

TABLE 3 | Virological results in UCD and MCD patient.

Virology	UCD (n=19)		MCD (n=41)		*P* value
	Tested in n patients	Positive (%)	Tested in n patients	Positive (%)	
HIV	18	0	37	0	1.000
HBV	18	0	37	3	0.543
HCV	18	0	37	1	1.000
EBV	4	3	23	20	**0.025**
CoxsackieV	4	0	23	2	1.000
MeaselesV	4	0	23	3	1.000
Cytomegalovirus	4	3	23	20	**0.025**
Herpes SimplexV	4	1	23	0	0.148

Bold values is statistically meaningful (P < 0.05).

unphosphorylated S6k were measured by immunohistochemistry in the tissue samples of 31 patients with CD and 10 patients with reactive lymphoid hyperplasia (**Figure 1B**). IHC results showed that the expression levels of pAKT, p4EBP1, p70S6K, and pS6k in the tissue samples of CD patients was significantly higher than those in patients with reactive lymphoid hyperplasia (*P*=0.001, 0.007, 0.039, and 0.007, respectively) (**Table 4A**, **Figure 3**). We also analyzed the difference in the expression levels of mTOR pathway-related proteins between UCD patients and MCD patients. Expression levels of p4EBP1, p70S6K, and pS6k were higher in MCD patients than in UCD patients (*P*=0.029, <0.001, and <0.001, respectively) (**Table 4B**). Inconsistency was detected in the difference in pAKT expression. Further analysis showed that the expression levels of pAKT in UCD and MCD patients were higher than those in patients with reactive lymphoid hyperplasia (*P*=0.011,0.002 respectively).

3.5 Univariate and Survival Analyses of CD

Using the Kaplan–Meier method, three risk factors were identified among patients with CD: thrombocytopenia, elevated uric acid levels, and hypoalbuminemia (*P*=0.006, 0.001, and 0.002, respectively; **Figures 4A–C**). No significant differences were observed in other investigated factors including LDH, β2-MG, clinical complaint, B symptoms, hepatosplenomegaly, serous cavity effusion, anemia, and A/G ratio. Moreover, no significant differences were observed in the PFS and OS survival curves between UCD patients and MCD patients (*P*=0.189 and *P*=0.737, respectively; **Figures 4D, E**).

4 DISCUSSION

CD is an uncommon lymphoproliferative disorder with remarkably heterogeneous clinicopathologic findings and is included in *First National List of Rare Diseases* issued by the Chinese government (10). Because of the low prevalence, the clinical studies conducted to investigate CD were primarily case reports and small series trials, posing challenges for the diagnosis and management of patients with CD (11). Using the detailed clinical, laboratory, imaging, and virology data of 60 patients with CD, we were able to provide a comprehensive evaluation of CD to improve the clinicians' understanding of this condition. Furthermore, we presented a comprehensive IHC analysis of the mTOR pathway activity in patients with CD to better understand its underlying mechanism and to develop effective therapeutic targets in order to improve patients' survival.

UCD typically involves single lymph nodes or single regional lymph nodes. Patients with UCD are usually asymptomatic; however, the enlargement of lymph nodes can trigger the occurrence of corresponding symptoms (12). MCD involves the enlargement of multiple regional lymph nodes and is often accompanied by inflammatory symptoms, such as fever, night sweats, fatigue, weight loss, and dropsy of the serous cavity (13). The laboratory test results of UCD patients are usually normal, but anemia, increased C-reactive protein (CRP) levels, increased erythrocyte sedimentation rate (ESR), and other abnormalities can be present (14). MCD is often accompanied by a systemic inflammatory response, which is characterized by a variety of laboratory and imaging abnormalities, such as anemia, hypoalbuminemia, elevated

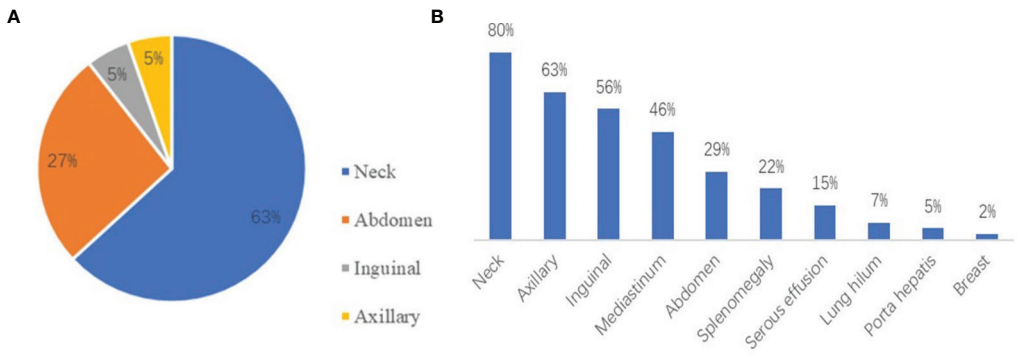

FIGURE 2 | **(A)** The distribution of lymphadenopathy among patients with HIV-negative UCD. **(B)** The locations of coexistent lymphadenopathies and other signs among patients with MCD.

TABLE 4A | Expression differences between Castleman and Reactive lymphoid hyperplasia.

		CD (n=31)	Reactive lypmhoid hyperplasia (n=10)	*P* value
pAKT	High	9	1	**0.001**
	Low	22	9	
P4EBP1	High	16	0	**0.007**
	Low	15	10	
P70S6k	High	20	1	**0.039**
	Low	11	9	
S6k	High	13	3	0.712
	Low	18	7	
pS6K	High	16	0	**0.007**
	Low	15	10	

Bold values is statistically meaningful (P < 0.05).

CRP and ESR levels, abnormal liver and kidney function, and serous effusion (15). In our study, anemia, abnormal platelet count, abnormal A/G, and elevated LDH levels were significantly more common in MCD patients than in UCD patients (all $P<0.05$). EBV and cytomegalovirus were more commonly detected in MCD patients than in UCD patients based on the results virological tests; hence, we cannot confirm the causal relationship between virus infection and the extent of disease. Chih-Hao Chen et al. published their experience of 20 cases of Castleman disease, which indicated that more EBV-positive cells in germinal centers are associated with increased vascularity and smaller tumor size. Anti-vessel growth therapy plays a potential role to control the disease (16). The localization and distribution of UCD and MCD are shown in **Figure 2**. The neck was the most common site of lymphadenopathy in patients with UCD (63%) and those with MCD (80%). PET-CT can be a useful diagnostic imaging modality for assessing the involved lymph nodes in patients with CD. CD demonstrates an increased but variable range of 18F-FDG uptake (17). In several case reports, CD showed as SUV_{max} of over 2.0. In a subgroup of 17 patients, PET-CT scan was performed, and the SUV_{max} was significantly higher in the MCD group than in the UCD group (18). According to multicentricity, SUV_{max} was significantly higher in the MCD group than in the UCD group in our study (6.8 ± 4.2, and 2.8 ± 0.7, respectively; $P<0.001$). Bcl-2 is a key protein that regulates apoptosis. It can promote the growth of tumor cells by cooperating with the ras proto-oncogene (19). Bcl-2 overexpression is observed in various human tumor tissues and cells. The positive rate of Bcl-2 in MCD patients was higher than that in UCD patients ($P=0.040$), which were considered correlated with the high proliferative activity of MCD.

TABLE 4B | Expression differences between UCD and MCD.

		UCD (n=12)	MCD (n=19)	*P* value
pAKT	High	4	5	0.704
	Low	8	14	
P4EBP1	High	3	13	**0.029**
	Low	9	6	
P70S6k	High	3	17	**<0.001**
	Low	9	2	
S6k	High	3	10	0.158
	Low	9	9	
pS6K	High	1	15	**<0.001**
	Low	11	4	

Bold values is statistically meaningful (P < 0.05).

Most CD patients have a good prognosis (20). Furthermore, the survival of patients with UCD was better than that of patients with MCD, but the difference was not significant, which may be due to the small sample size or presence of statistical bias. However, the condition of some patients with CD progresses rapidly, and their prognosis becomes relatively poor (21, 22). Hence, it is crucial to identify the prognostic factors of different classifications to improve treatment decisions and determine the prognosis early (11). Thrombocytopenia, increased uric acid levels, and hypoalbuminemia were identified as poor prognostic factors of CD.

Megakaryocytes usually produce more platelets when IL-6 is boosted, which contradicts the occurrence of thrombocytopenia (23). TAFRO syndrome, which is characterized by thrombocytopenia, anasarca, fever, reticulin fibrosis, and organomegaly, is a subtype with the worst prognosis (24, 25). Thrombocytopenia occurred in four patients, while only two patients were diagnosed with TAFRO syndrome. The other two patients had no other relevant anomalies except thrombocytopenia. Therefore, we confirmed that thrombocytopenia is a poor diagnostic factor for CD, not just putting down to TAFRO syndrome. However, the reason for this remains unclear. The increase in uric acid level is related to worsening of renal function, which has been identified as a possible risk factor in previous large-scale studies (26, 27). Hypoalbuminemia was also proven to be a poor diagnosis factor as it was associated with other conditions, including renal function deterioration, splenomegaly, effusion, and so on, which was brought forth in a previous study (11).

Surgical resection is the first line of treatment for UCD, and the cure rate of surgical resection is approximately 90% (28). There is no standard treatment for relapse or refractory UCD patients. As for iMCD patients, IL-6 blockers can decrease symptoms and lymphadenopathy (29, 30). Approximate 66% of the patients in a randomized controlled trial did not respond to the therapy, and mTOR has been recommended as a second-line treatment for iMCD patients (31). This is a follow-up study to previous work in the CD field related to mTOR pathway. For further analysis of the mTOR pathway in CD, we analyzed the related proteins, including pAKT, p4EBP1, p70S6K, S6K, and pS6k. The results indicated that the activity of the mTOR pathway was higher than that of reactive lymphoid hyperplasia, and some UCD specimens were tested positive. We suspected that the increasing IL-6 may activate the mTOR pathway causing CD to a certain extent. The mTOR inhibitors may be effective in all types of CD, both UCD and MCD.

Because of the low prevalence, the types of clinical studies that have investigated CD are primarily case reports and small series trials, posing challenges for the diagnosis and management of patients with CD. There is no established standardized treatment protocol, and clinicians lack sufficient knowledge to

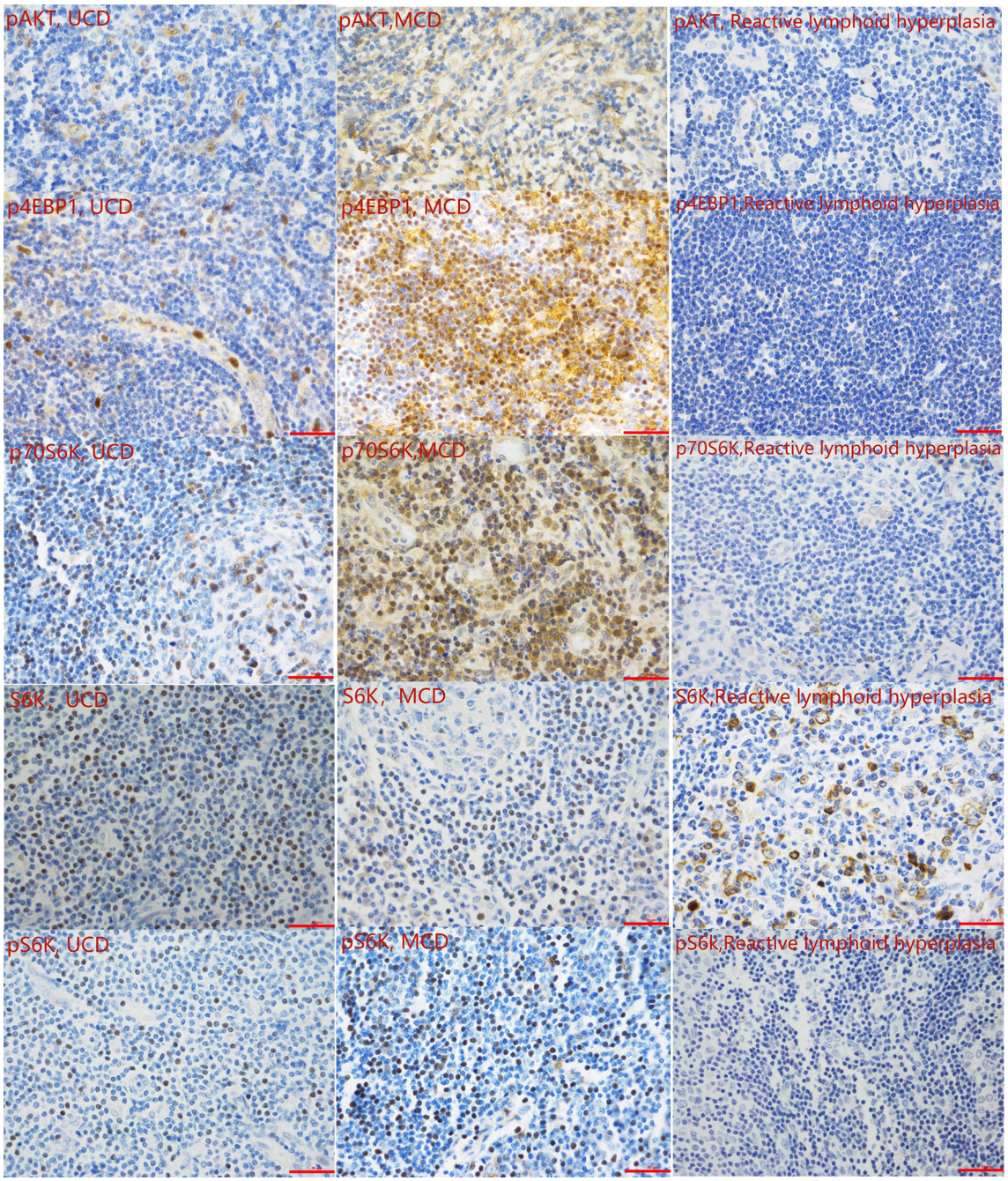

FIGURE 3 | Representative immunohistochemistry images of the mTOR pathway activity analysis (400 magnification).

manage patients rationally. The present study increases our understanding of CD and contributes to more detailed clinical information on this rare disease. We initially put forward that thrombocytopenia is a poor diagnostic factor for CD, which serves as a basis when making appropriate clinical decisions. We also explored the mTOR pathway activity in CD patients, offering some elucidation for the management and treatment of CD patients. Larger studies are required to clarify the molecular abnormalities and potential therapeutic targets of this uncommon condition.

CONCLUSION

Thrombocytopenia was the independent poor prognostic factor for CD was first proposed, as well as elevated uric

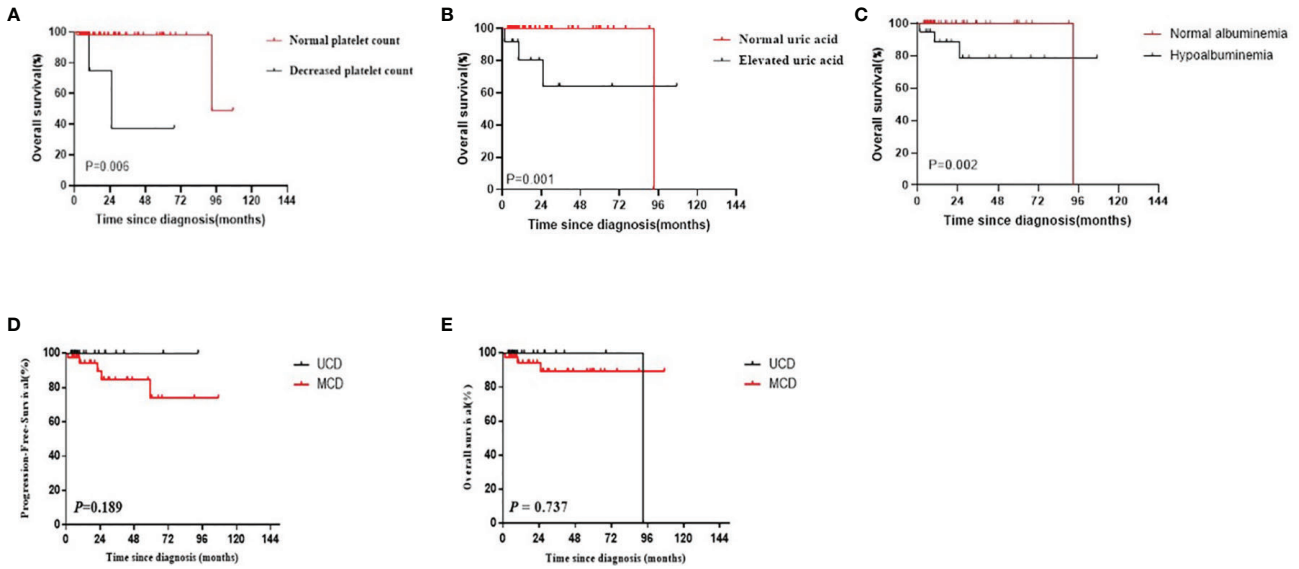

FIGURE 4 | **(A–C)** The survival curves of different risk factors among patients with CD **(A)** Platelet count; **(B)** Uric acid; **(C)** Hypoalbuminemia). **(D, E)** PFS and OS curves of patients with CD by multicentricity (**D**: PFS, **E**: OS).

acid levels, hypoalbuminemia. And the activity of the mTOR pathway was higher than reactive lymphoid hyperplasia which served as control group, and some UCD specimens were tested positive.

DATA AVAILABILITY STATEMENT

The raw data supporting the conclusions of this article will be made available by the authors, without undue reservation.

AUTHOR CONTRIBUTIONS

SQ, MJD, and XZ designed the research. All investigators and their respective research teams recruited and followed up the patient. HH, YZ, MD, MJD, and LZ collected and analyzed research data. SQ and ZW wrote and edited the manuscript. GW and WL are pathologists who interprets the immunohistochemical results. All authors were involved at each stage of manuscript preparation and approved the final version. All authors contributed to the article and approved the submitted version.

FUNDING

The authors would like to thank the financial support provided by National Natural Science Foundation of China (82070210) and Major Medicine Scientific and Technology Project of Henan Province (NO.SBG 202001008).

SUPPLEMENTARY MATERIAL

The Supplementary Material for this article can be found online at: https://www.frontiersin.org/articles/10.3389/fimmu.2022.899073/full#supplementary-material

Supplementary Table 1 | Conventional IHC difference between UCD and MCD.

REFERENCES

1. Inada K, Hamazaki M. Localized Mediastinal Lymph-Node Hyperplasia Resembling Thymoma; A Case Report. *Ann Surg* (1958) 147(3):409–13. doi: 10.1097/00000658-195803000-00018
2. González-García A, Patier de la Peña JL, García-Cosio M, García-Cosio M, Sarhane Y, Sánchez Díaz C, et al. Clinical and Pathological Characteristics of Castleman Disease: An Observational Study in a Spanish Tertiary Hospital. *Leuk Lymphoma* (2019) 60(14):3442–8. doi: 10.1080/10428194.2019.1639168
3. Hawkins JM, Pillai V. Tafro Syndrome or Castleman-Kojima Syndrome: A Variant of Multicentric Castleman Disease. *Blood* (2015) 126(18):2163. doi: 10.1182/blood-2015-07-662122
4. Li Z, Lan X, Li C, Zhang Y, Wang Y, Xue W, et al. Recurrent PDGFRB Mutations in Unicentric Castleman Disease. *Leukemia* (2019) 33(4):1035–8. doi: 10.1038/s41375-018-0323-6
5. Boutboul D, Fadlallah J, Chawki S, Fieschi C, Malphettes M, Dossier A, et al. Treatment and Outcome of Unicentric Castleman Disease: A Retrospective Analysis of 71 Cases. *Br J Haematol* (2019) 186(2):269–73. doi: 10.1111/bjh.15921
6. Ara T, DeClerck YA. Interleukin-6 in Bone Metastasis and Cancer Progression. *Eur J Cancer.* (2010) 46(7):1223–31. doi: 10.1016/j.ejca.2010.02.026
7. El-Osta HE, Kurzrock R. Castleman's Disease: From Basic Mechanisms to Molecular Therapeutics. *Oncologist.* (2011) 16(4):497–511. doi: 10.1634/theoncologist.2010-0212

8. Yu L, Tu M, Cortes J, Xu-Monette ZY, Miranda RN, Zhang J, et al. Clinical and Pathological Characteristics of HIV-And HHV-8-Negative Castleman Disease. *Blood*. (2017) 129(12):1658–68. doi: 10.1182/blood-2016-11-748855
9. Van Rhee F, Wong RS, Munshi N, Rossi J-F, Ke X-Y, Fossså A, et al. Siltuximab for Multicentric Castleman's Disease: A Randomised, Double-Blind, Placebo-Controlled Trial. *Lancet Oncol* (2014) 15(9):966–74. doi: 10.1016/S1470-2045(14)70319-5
10. Lan X, Li Z, Zhang M. Analysis of Clinical Characteristics and Prognosis Factors of 71 Cases With HIV-Negative Castleman's Disease: Hypoproteinemia Is an Unfavorable Prognostic Factor Which Should be Treated Appropriately. *J Cancer Res Clin Oncol* (2018) 144(7):1265–77. doi: 10.1007/s00432-018-2647-z
11. van Rhee F, Oksenhendler E, Srkalovic G, Voorhees P, Lim M, Dispenzieri A, et al. International Evidence-Based Consensus Diagnostic and Treatment Guidelines for Unicentric Castleman Disease. *Blood Adv* (2020) 4(23):6039–50. doi: 10.1182/bloodadvances.2020003334
12. Van Rhee F, Voorhees P, Dispenzieri A, Fossså A, Srkalovic G, Ide M, et al. International, Evidence-Based Consensus Treatment Guidelines for Idiopathic Multicentric Castleman Disease. *Blood* (2018) 132(20):2115–24. doi: 10.1182/blood-2018-07-862334
13. Oksenhendler E, Boutboul D, Fajgenbaum D, Mirouse A, Fieschi C, Malphettes M, et al. The Full Spectrum of Castleman Disease: 273 Patients Studied Over 20 Years. *Br J Haematol* (2018) 180(2):206–16. doi: 10.1111/bjh.15019
14. Dispenzieri A, Armitage JO, Loe MJ, Geyer SM, Allred J, Camoriano JK, et al. The Clinical Spectrum of Castleman's Disease. *Am J Hematol* (2012) 87(11):997–1002. doi: 10.1002/ajh.23291
15. Chen CH, Liu HC, Hung TT, Liu TP. Possible Roles of Epstein-Barr Virus in Castleman Disease. *J Cardiothorac Surg* (2009) 4:1–5. doi: 10.1186/1749-8090-4-31
16. Barker R, Kazmi F, Stebbing J, Ngan S, Chinn R, Nelson M, et al. FDG-PET/CT Imaging in the Management of HIV-Associated Multicentric Castleman's Disease. *Eur J Nucl Med Mol Imaging*. (2009) 36(4):648–52. doi: 10.1007/s00259-008-0998-4
17. Lee ES, Paeng JC, Park CM, Chang W, Lee WW, Kang KW, et al. Metabolic Characteristics of Castleman Disease on 18f-FDG PET in Relation to Clinical Implication. *Clin Nucl Med* (2013) 38(5):339–42. doi: 10.1097/RLU.0b013e3182816730
18. Freedman A. Follicular Lymphoma: 2018 Update on Diagnosis and Management. *Am J Hematol* (2018) 93(2):296–305. doi: 10.1002/ajh.24937
19. Bowne WB, Lewis JJ, Filippa DA, Niesvizky R, Brooks AD, Burt ME, et al. The Management of Unicentric and Multicentric Castleman's Disease: A Report of 16 Cases and a Review of the Literature. *Cancer*. (1999) 85(3):706–17. doi: 10.1002/(SICI)1097-0142(19990201)85:3<706::AID-CNCR21>3.0.CO;2-7
20. Zhou N, Huang CW, Huang C, Liao W. The Characterization and Management of Castleman's Disease. *J Int Med Res* (2012) 40(4):1580–8. doi: 10.1177/147323001204000438
21. Liu AY, Nabel CS, Finkelman BS, Ruth JR, Kurzrock R, van Rhee F, et al. Idiopathic Multicentric Castleman's Disease: A Systematic Literature Review. *Lancet Haematol* (2016) 3(4):e163–75. doi: 10.1016/S2352-3026(16)00006-5
22. Williams SCP. First IL-6–Blocking Drug Nears Approval for Rare Blood Disorder. *Nat Med* (2013) 19(10):1193. doi: 10.1038/nm1013-1193
23. Lunning MA, Armitage JO. Do You Know TAFRO? *Blood* (2018) 132(20):2109–10. doi: 10.1182/blood-2018-09-875112
24. Sakashita K, Murata K, Takamori M. TAFRO Syndrome: Current Perspectives. *J Blood Med* (2018) 9:15–23. doi: 10.2147/JBM.S127822
25. Dong Y, Wang M, Nong L, Wang L, Cen X, Liu W, et al. Clinical and Laboratory Characterization of 114 Cases of Castleman Disease Patients From a Single Centre: Paraneoplastic Pemphigus Is an Unfavourable Prognostic Factor. *Br J Haematol* (2015) 169(6):834–42. doi: 10.1111/bjh.13378
26. Zhang L, Li Z, Cao X, Feng J, Zhong D, Wang S, et al. Clinical Spectrum and Survival Analysis of 145 Cases of HIV-Negative Castleman's Disease: Renal Function is an Important Prognostic Factor. *Sci Rep* (2016) 2015:2–7.
27. Mitsos S, Stamatopoulos A, Patrini D, George RS, Lawrence DR, Panagiotopoulos N. The Role of Surgical Resection in Unicentric Castleman's Disease: A Systematic Review. *Adv Respir Med* (2018) 86(1):36–43. doi: 10.5603/ARM.2018.0008
28. Dispenzieri A. POEMS Syndrome: 2019 Update on Diagnosis, Risk-Stratification, and Management. *Am J Hematol* (2019) 94(7):812–27. doi: 10.1002/ajh.25495
29. Ostrowska B, Szymczyk A, Olszewska-Szopa M, Romejko-Jarosińska J, Domańska-Czyż K, Dąbrowska-Iwanicka A, et al. Efficacy of Siltuximab in the Treatment of Idiopathic Multicentric Castleman Disease, the First Polish, Real-World Experience With Long-Term Observation. *Leuk Lymphoma* (2021) 62(12):3031–34. doi: 10.1080/10428194.2021.1941926
30. Arenas DJ, Floess K, Kobrin D, Pai R-AL, Srkalovic MB, Tamakloe M-A, et al. Increased mTOR Activation in Idiopathic Multicentric Castleman Disease. *Blood* (2020) 135(19):1673–84. doi: 10.1182/blood.2019002792
31. Jiang Q, Huang X, Yu W, Huang R, Zhao X. mTOR Signaling in the Regulation of CD4+ T Cell Subsets in Periodontal Diseases. *Immunol CCJFi* (2022) 13:827461. doi: 10.3389/fimmu.2022.827461

Conflict of Interest: The authors declare that the research was conducted in the absence of any commercial or financial relationships that could be construed as a potential conflict of interest.

Publisher's Note: All claims expressed in this article are solely those of the authors and do not necessarily represent those of their affiliated organizations, or those of the publisher, the editors and the reviewers. Any product that may be evaluated in this article, or claim that may be made by its manufacturer, is not guaranteed or endorsed by the publisher.

frontiers | Frontiers in Immunology

ORIGINAL RESEARCH
published: 24 May 2022
doi: 10.3389/fimmu.2022.919012

Machine Learning Models for the Diagnosis and Prognosis Prediction of High-Grade B-Cell Lymphoma

Hui Kong[1†], Haojie Zhu[1†], Xiaoyun Zheng[1†], Meichen Jiang[2], Lushan Chen[2], Lingqiong Lan[3], Jinhua Ren[1], Xiaofeng Luo[1], Jing Zheng[1], Zhihong Zheng[1], Zhizhe Chen[1], Jianda Hu[1] and Ting Yang[1*]*

[1] Department of Hematology, Fujian Institute of Hematology, Fujian Provincial Key Laboratory of Hematology, Fujian Medical University Union Hospital, Fuzhou, China, [2] Department of Pathology, Fujian Medical University Union Hospital, Fuzhou, China, [3] Department of Hematology, The Second Hospital of Longyan, Longyan, China

OPEN ACCESS

Edited by:
Wei Sang,
The Affiliated Hospital of Xuzhou Medical University, China

Reviewed by:
David Horne,
City of Hope National Medical Center, United States
Liang Wang,
Capital Medical University, China

***Correspondence:**
Ting Yang
yang.hopeting@gmail.com
Jianda Hu
drjiandahu@163.com

†These authors have contributed equally to this work and share first authorship

Specialty section:
This article was submitted to Cancer Immunity and Immunotherapy, a section of the journal Frontiers in Immunology

Received: *13 April 2022*
Accepted: *25 April 2022*
Published: *24 May 2022*

Citation:
Kong H, Zhu H, Zheng X, Jiang M, Chen L, Lan L, Ren J, Luo X, Zheng J, Zheng Z, Chen Z, Hu J and Yang T (2022) Machine Learning Models for the Diagnosis and Prognosis Prediction of High-Grade B-Cell Lymphoma. Front. Immunol. 13:919012. doi: 10.3389/fimmu.2022.919012

High-grade B-cell lymphoma (HGBL) is a newly introduced category of rare and heterogeneous invasive B-cell lymphoma (BCL), which is diagnosed depending on fluorescence *in situ* hybridization (FISH), an expensive and laborious analysis. In order to identify HGBL with minimal workup and costs, a total of 187 newly diagnosed BCL patients were enrolled in a cohort study. As a result, the overall survival (OS) and progression-free survival (PFS) of the HGBL group were inferior to those of the non-HGBL group. HGBL (n = 35) was more likely to have a high-grade histomorphology appearance, extranodal involvement, bone marrow involvement, and whole-body maximum standardized uptake (SUVmax). The machine learning classification models indicated that histomorphology appearance, Ann Arbor stage, lactate dehydrogenase (LDH), and International Prognostic Index (IPI) risk group were independent risk factors for diagnosing HGBL. Patients in the high IPI risk group, who are CD10 positive, and who have extranodal involvement, high LDH, high white blood cell (WBC), bone marrow involvement, old age, advanced Ann Arbor stage, and high SUVmax had a higher risk of death within 1 year. In addition, these models prompt the clinical features with which the patients should be recommended to undergo a FISH test. Furthermore, this study supports that first-line treatment with R-CHOP has dismal efficacy in HGBL. A novel induction therapeutic regimen is still urgently needed to ameliorate the poor outcome of HGBL patients.

Keywords: high-grade B-cell lymphoma, clinical characteristics, diagnostic predictor, machine learning, classification models

INTRODUCTION

Diffuse large B-cell lymphoma (DLBCL) is an aggressive, highly heterogeneous type of lymphoma characterized by various clinical features and outcomes. Among DLBCL patients, some harbor not only morphological features of DLBCL but also MYC, Bcl-2, and/or Bcl-6 rearrangements. Based on the 2016 revision of the WHO classification of lymphoid neoplasms (1), these patients are classified as having high-grade B-cell lymphoma (HGBL), an extra-aggressive disease with complex karyotype

and a series of pathomorphological features. Currently, HGBL is subgrouped as HGBL with MYC and Bcl-2 and/or Bcl-6 rearrangements, so-called double- or triple-hit lymphoma (HGBL-DH or HGBL-TH, respectively) (2) and as HGBL, not otherwise specified (HGBL-NOS), which lacks MYC and Bcl-2 and/or Bcl-6 rearrangements. HGBL is diagnosed using immunohistochemistry (IHC) and cytogenetic fluorescence *in situ* hybridization (FISH) of excised pathological tissues (3) such as the lymph node, bone marrow, and spleen (4). In addition, another entity, called "double-expressor lymphoma" (DEL) (5, 6), has been identified based on MYC and Bcl-2 protein overexpression by IHC without gene aberrations (MYC and Bcl-2 and/or Bcl-6 rearrangements) by FISH, with positive cut-off values for MYC+ of ≥40% and Bcl-2+ of ≥50% in most studies (7, 8). Although not as malignant as HGBL-DH, DEL is generally invasive, more common, and likely to have a better prognosis than HGBL-DH (5, 9, 10).

These new entities, defined by biological and histological peculiarities, have a well-known worse outcome, especially HGBL-DH/TH, and indicate a diagnostic and therapeutic difficulty for pathologists and clinicians.

Nevertheless, due to limited research, a uniform international consensus on which DLBCL should be detected with FISH, the only diagnostic method for HGBL-DH or HGBL-TH, has not yet been reached. Furthermore, predictive markers are lacking, and it is controversial to regard DEL as a predictor of HGBL-DH or HGBL-TH, although there is a certain degree of overlap between them (7, 8, 10). Considering the difficulties of routinely screening HGBL using FISH and the dismal prognosis of HGBL-DH or-TH, this retrospective study herein aims to compare and analyze the data from patients identified as HGBL and non-HGBL based on FISH analysis and to define valuable diagnostic predictors to build a diagnosis prediction model, setting the stage for further molecular genetic analysis of B-cell lymphoma patients with high-risk factors.

MATERIALS AND METHODS

Patients

Data from 187 patients with aggressive mature B-cell lymphomas (including 152 cases with DLBCL and 35 cases with HGBL-DH/TH/NOS) followed up at the Fujian Medical University Union Hospital between April 1, 2018, and April 1, 2022, were retrospectively collected.

Specimen Processing, Fluorescence *In Situ* Hybridization, and Immunohistochemistry

The pathological specimens from all cases were excised, stored as fresh-frozen or formalin-fixed paraffin-embedded (FFPE) tissues, and later analyzed by FISH and IHC. MYC, Bcl-2, or Bcl-6 translocation was detected by FISH using DNA probes annealing to specific sequences of the target genes and the ThermoBrite FISH slide processing system, strictly following the manufacturer's instruction. The dual-color Break Apart rearrangement probes, namely, Vysis LSI MYC (8q24.21) (Cat# 05J91-001), Vysis LSI Bcl-2 (18q21.33) (Cat# 07J75-001), and Vysis LSI Bcl-6 (3q27.3) (Cat# 01N23-020) (ASR), and the ThermoBrite system were purchased from Abbott Laboratories (Chicago, IL, USA). For IHC staining, samples were probed with primary monoclonal antibodies against CD10 (clone SP67; Cat# 790-4506, Roche Tissue Diagnostics, Oro Valley, AZ, USA), MUM-1 (clone MRQ-43; Cat# 760-4529, Roche Tissue Diagnostics), Bcl-2 (clone SP66; Cat# 790-4604, Roche Tissue Diagnostics), c-MYC (clone Y69; Cat# 790-4628, Roche Tissue Diagnostics), Bcl-6 (RTU clone GI191E/A8; Cat# 760-4241, Roche Tissue Diagnostics), and Ki67 (clone 30-9; Cat# 790-4286, Roche Confirm); the primary antibodies were probed with the anti-rabbit or mouse secondary antibodies labeled with horseradish peroxidase (HRP). All staining was performed using the Ventana Benchmark ULTRA IHC staining module (Ventana, Tucson, AZ, USA). Each pathology report included H&E-stained sections and FISH, reviewed by the senior lymphoma pathologists in the Pathology Department based on the 2016 WHO lymphohematopoietic system tumor classification.

Diagnosis, Staging, and Prognostic Index Score

All DLBCL cases with MYC and Bcl-2 and/or Bcl-6 rearrangements were diagnosed as HGBL-DH or HGBL-TH. Cases that appear blastoid or intermediate between DLBCL and Burkitt's lymphoma (BL) that lacked MYC and Bcl-2 and/or Bcl-6 rearrangements were classified as HGBL-NOS. The cell of origin (COO) was defined according to the Hans algorithm (11), which is used to classify cases as germinal center B cell (GCB) or non-GCB depending on the expression of CD10, Bcl-6, and MUM-1 assessed by IHC. Patients were divided into DEL and non-DEL based on overexpression positivity cutoff for Bcl-2 or MYC of ≥50% or ≥40% of stained cells, respectively (6, 12). The Ann Arbor staging classification system (13), revised by Cotswold et al. in 1989 (14) (**Table S1**), for the risk group converted by the International Prognostic Index (IPI) (15) was used to evaluate the staging and prognosis of all patients (**Table S2**).

Assessment of Clinical Features

Patient clinical characteristics included gender, age, white blood cell (WBC) count, serum lactate dehydrogenase (LDH) level, β2 microglobulin, Ann Arbor staging, A or B symptoms, IPI score, risk group, extranodal involvement sites (especially bone marrow), histomorphology, chromosome karyotype, immunophenotype (such as CD10, MYC, Bcl-2, Bcl-6, and MUM-1), DEL, Ki-67 proliferation index, baseline whole-body maximum standardized uptake (SUVmax), and the Epstein–Barr virus-encoded small nuclear RNA (EBER). Among the above characteristics, the Ann Arbor staging (13) and IPI score (15) were previously described. For cases in which the chromosome karyotype was available, a cytogenetic complexity score was calculated. Any numerical or structural abnormality, except for the translocations involving 3q27, 8q24, or 18q21, was counted as 1 event each. Cases with a cytogenetic complexity score >2 were considered to have a complex karyotype (16, 17). SUVmax

before first induction was used to evaluate the functional metabolisms of tumors when diagnosing.

Chemotherapeutic Regimens

The first-line chemotherapy treatment used was mainly the R-CHOP regimen (rituximab, cyclophosphamide, doxorubicin, vincristine, and prednisone). The second-line regimens included R-CHOP + X (X being lenalidomide, chidamide, zanubrutinib, or others), R-DA-EPOCH (rituximab, dose-adjusted etoposide, prednisone, vincristine, cyclophosphamide, and doxorubicin), R-DA-EDOCH (rituximab, dose-adjusted etoposide, dexamethasone, vincristine, cyclophosphamide, and doxorubicin), and R-HyperCVAD (rituximab, hyper-fractionated cyclophosphamide, vincristine, doxorubicin, and dexamethasone).

Efficacy and Follow-Up

According to the Lugano Lymphoma Efficacy Criteria (18, 19), ^{18}F-fluorodeoxyglucose (FDG) PET/CT or enhanced CT was used to evaluate disease status based on the Deauville score (20). Imaging evaluation was performed before the first induction chemotherapy and after every four courses of chemotherapy until the end of follow-up on April 1, 2022.

Efficacy was divided into complete remission (CR), partial remission (PR), stable disease (SD), and progressive disease (PD). The objective response rate (ORR) was calculated according to the percentage of CR+PR patients among all patients. Duration of remission (DOR) was defined as the period from the occurrence of the first CR to disease relapse or death due to any cause.

Statistical Analysis

The data were analyzed with the SPSS V.26.0, Python V.3.9.0, and R 4.1.1 statistical software. A $p < 0.05$ was considered statistically significant. Student's t-test was used for metric variables conforming to the normal distribution, while the Mann–Whitney U test was used for fitting non-normal distribution. The disorderly classification variables between two groups were analyzed by Pearson's chi-square test (Fisher's exact probability method was used when necessary). Survival rates including overall survival (OS) and progression-free survival (PFS) were estimated using the Kaplan–Meier method. The least absolute shrinkage and selection operator (LASSO) method (21) for high-dimensional data reduction is used to select the best predictive features of risk factors from HGBL patients (22). Machine learning algorithms, including Gradient Boosting Classifier, CatBoost Classifier, Random Forest Classifier, Extra Trees Classifier, Extreme Gradient Boosting, Logistic Regression, Decision Tree Classifier, Ridge Classifier, Ada Boost Classifier, K Neighbors Classifier, SVM-Linear Kernel, Naive Bayes, and Quadratic Discriminant Analysis, were used to establish prediction models. The 187 cases were split into a training set containing 70% of the observations and a test set containing the remaining 30%. For several models, the area under the curve (AUC), confusion matrix, precision, recall, and F1 value were used to evaluate the models (see details in the **Supplementary Material**).

RESULT

General Clinical Features

A total of 187 patients were included in this study, with 105 men (56.1%) and 82 women (43.9%) and an average age of 55.50 (± 15.02) years. All had high-risk factors, including but not limited to advanced Ann Arbor stage, extranodal involvement, double expressor, high intermediate, and high IPI risk group. Thirty-five cases out of 187 tumors had been classified as HGBL. Among them, HGBL-DH was the most common, with 3 cases of MYC/Bcl-2 HGBL-DH (8.6%, including 2 cases complicated with follicular lymphoma) and 21 cases of MYC/Bcl-6 HGBL-DH (60.0%, including 1 case complicated with the hemophagocytic syndrome). Four cases were HGBL-TH (11.4%), and 7 were HGBL-NOS (20%). Among the 187 patients, 135 were in the advanced Ann Arbor stage (29 of them were HGBL), 123 cases had extranodal involvement (28 cases were HGBL), 91 cases were with double expressor (20 cases were HGBL), and 112 cases were with high intermediate and high IPI risk group (26 cases were HGBL). Other essential features and IHC phenotypes are detailed in **Table 1**. Karyotypes were available for 18 out of 35 HGBL patients and 69 out of 152 non-HGBL patients. Among them, 2 cases in the former and 7 cases in the latter showed complex chromosomal aberrations (**Table S3**).

Compared with the non-HGBL group, the HGBL group was more likely to have a high-grade histopathological appearance, including necrosis, massive mitoses, or a "starry sky" appearance ($p = 0.009$). Other statistically significant differences between the HGBL and non-HGBL patients were bone marrow involvement (28.6% vs. 11.8%; $p = 0.012$) and extranodal involvement >1 (42.9% vs. 23%; $p = 0.017$). The SUVmax of HGBL patients was higher than that of non-HGBL patients ($p = 0.045$), which means that the functional metabolism of tumors in HGBL is far more active than in non-HGBL. The IHC analysis of MUM-1 expression level was negatively correlated with HGBL, with the expression level in the HGBL group significantly lower than that of the non-HGBL group (**Table 2**). As for the HGBL subcategory, bone marrow involvement was significantly associated with HGBL-DH/TH compared with non-HGBL-DH/TH. Also, the high-grade histomorphology appearance was significantly different between patients with HGBL and non-HGBL. In addition, we found that the protein expression level of c-MYC was superior with HGBL-DH/TH than that with non-HGBL-DH/TH by IHC analysis, but the MUM-1 protein expression level of the HGBL-DH/TH group was inferior to that of the non-HGBL-DH/TH group (**Table S4**).

Survival Prognosis

The outcome of HGBL and non-HGBL patients undergoing induction chemotherapy is shown in **Figure 1**. Two patients harboring two types of tumors, one patient with HIV antibody positive, and two patients without survival data were excluded from the survival analysis. The Kaplan–Meier curves of OS revealed significant statistical differences between patients with HGBL and non-HGBL ($p = 0.015$). Compared with non-HGBL

TABLE 1 | Clinical characteristics of all patients.

Characteristics	HGBL (n = 35)			Non-HGBL (n = 152)	p-Value
	HGBL-DH (n = 24)	HGBL-TH (n = 4)	HGBL-NOS (n = 7)		
Gender					0.316
Male	13 (37.1%)	0 (0%)	4 (11.4%)	88 (57.9%)	
Female	11 (31.5%)	4 (11.4%)	3 (8.6%)	64 (42.1%)	
Age					0.182
>60	9 (25.7%)	0 (0%)	3 (8.6%)	71 (46.7%)	
≤60	15 (42.9%)	4 (11.4%)	4 (11.4%)	81 (53.3%)	
Ann Arbor stage					0.118
I–II	1 (2.9%)	3 (8.6%)	2 (5.7%)	46 (30.3%)	
III–IV	23 (65.6%)	1 (2.9%)	5 (14.3%)	106 (69.7%)	
B symptom					0.436
Yes	7 (20.0%)	1 (2.9%)	3 (8.6%)	38 (25.0%)	
No	17 (48.5%)	3 (8.6%)	4 (11.4%)	114 (75.0%)	
IPI score					0.054
<2	2 (5.7%)	3 (8.6%)	4 (11.4%)	66 (43.4%)	
≥2	22 (62.8%)	1 (2.9%)	3 (8.6%)	86 (56.6%)	
Double expressor					0.227
Yes	15 (42.9%)	2 (5.7%)	3 (8.6%)	72 (47.4%)	
No	9 (25.7%)	2 (5.7%)	4 (11.4%)	80 (52.6%)	
COO					0.013
GCB	11 (31.4%)	3 (8.6%)	5 (14.3%)	50 (32.9%)	
Non-GCB	12 (34.2%)	1 (2.9%)	2 (5.7%)	101 (66.5%)	
NA	1 (2.9%)	0 (0%)	0 (0%)	1 (0.6%)	

IPI, International Prognostic Index score; COO, cell of origin; GCB, germinal center B cell; HGBL-DH, double-hit high-grade B-cell lymphoma; HGBL-TH, triple-hit high-grade B-cell lymphoma; HGBL-NOS, high-grade B-cell lymphoma, not otherwise specified.

TABLE 2 | Comparison of clinical features between HGBL and non-HGBL.

Features	HGBL (n = 35)	Non-HGBL (n = 152)	p-Value
High-grade histomorphology			0.009
Yes	6	7	
No	29	145	
WBC > ULN			0.398
Yes	6	18	
No	29	134	
β2 microglobulin > ULN			0.771
Yes	14/28	51/96*	
No	14/28	45/96	
Extranodal involvement			0.057
Yes	28	96	
No	7	56	
E > 1			0.017
Yes	15	35	
No	20	117	
BM involvement			0.012
Yes	10	18	
No	25	134	
Gastrointestinal involvement			0.056
Yes	13	33	
No	22	119	
CNS involvement			0.876
Yes	4	16	
No	31	136	
CD10			0.070
Positive	14/34	39/152	
Negative	20/34	113/152	
Ki67 ≥ 90%			0.351
Yes	17/34	61/148	
No	17/34	87/148	

(Continued)

TABLE 2 | Continued

Features	HGBL (n = 35)	Non-HGBL (n = 152)	p-Value
EBER			0.569
Positive	2/31	6/146	
Negative	29/31	140/146	
Serum LDH	650.63 ± 172.292	502.26 ± 48.685	0.587
Bcl-2	0.7265 ± 0.297	0.7733 ± 0.320	0.082
Bcl-6	0.9412 ± 0.239	0.9603 ± 0.196	0.622
c-MYC	0.4955 ± 0.043	0.4101 ± 0.224	0.052
MUM-1	0.6964 ± 0.416	0.8264 ± 0.341	0.019
SUVmax	16 ± 14.30	26 ± 20.73	0.045

WBC, white blood cell count; ULN, upper limit of normal; E, Extranodal involvemen; BM, bone marrow; CNS, central nervous system; EBER, the Epstein–Barr virus-encoded small nuclear RNA; LDH, serum lactate dehydrogenase; SUVmax, baseline whole-body maximum standardized uptake; HGBL, high-grade B-cell lymphoma.
**Some patients' data were not available.*

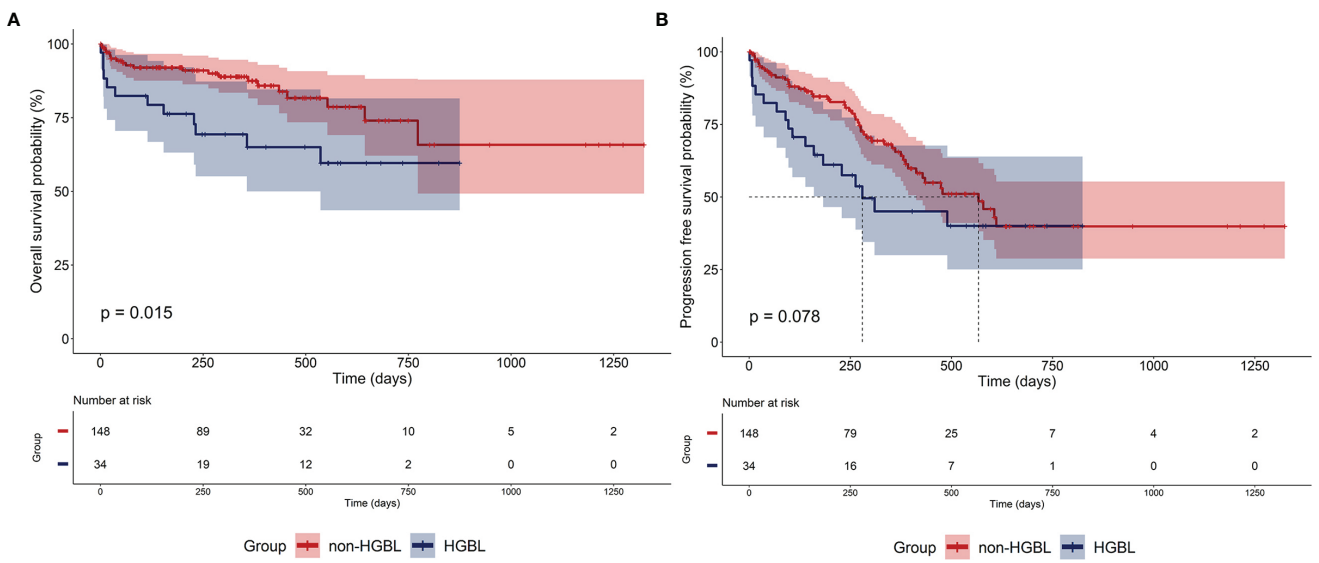

FIGURE 1 | Outcomes of patients. **(A)** Overall survival (OS) and **(B)** progression-free survival (PFS) of high-grade B-cell lymphoma (HGBL) and non-HGBL patients.

patients, HGBL patients had a more dismal prognosis and a trend toward superior median PFS. The median OS was not reached in all patients, while the median PFS in HGBL, non-HGBL, and all patients were 280, 567, and 490 days, respectively.

Seventeen patients in the HGBL group and 79 in the non-HGBL group were given the R-CHOP regimen as the first-line treatment, of which 10 and 63 patients, respectively, achieved CR or PR after completing standard induction chemotherapy. The ORR of HGBL and non-HGBL patients treated with the R-CHOP regimen was 64.7% and 83.5%, respectively (p = 0.077, **Figure 2A**). Among 72 out of the 187 patients who achieved first CR, six cases with HGBL (including 4 cases of MYC-Bcl-6 HGBL-DH, one case of HGBL-TH, and one case of HGBL-NOS) and 17 cases with non-HGBL relapsed during maintenance treatment after the first remission. The DOR was significantly shorter in the HGBL group than in the non-HGBL group, with a median time of 121 vs. 258 days, respectively (p = 0.007; **Figure 2B**).

Establishment of the Classification Model

Thirty-seven general clinical features collected were reduced to eight potential predictors with non-zero coefficients in the LASSO regression model (**Figure 3**). These potential predictors and other clinically significant factors in related studies were incorporated into the machine learning classification algorithm. After a comparison of the results of various models, a logistic binary regression model for predicting HGBL was established. The model showed high-grade histomorphology appearance (p = 0.012), advanced Ann Arbor stage (p = 0.007), LDH > upper limit of normal (ULN) (p = 0.045), and IPI risk group 3 or 4 (p = 0.003) as independent risk factors for HGBL (see **Table 3** for detailed equations). Evaluating the model's effectiveness in the test set, the micro-average and macro-average AUC values of the ROC curve were 0.85 and 0.53, respectively. This model had high prediction efficiency for non-HGBL but was not excellent enough for HGBL (**Figure 4**).

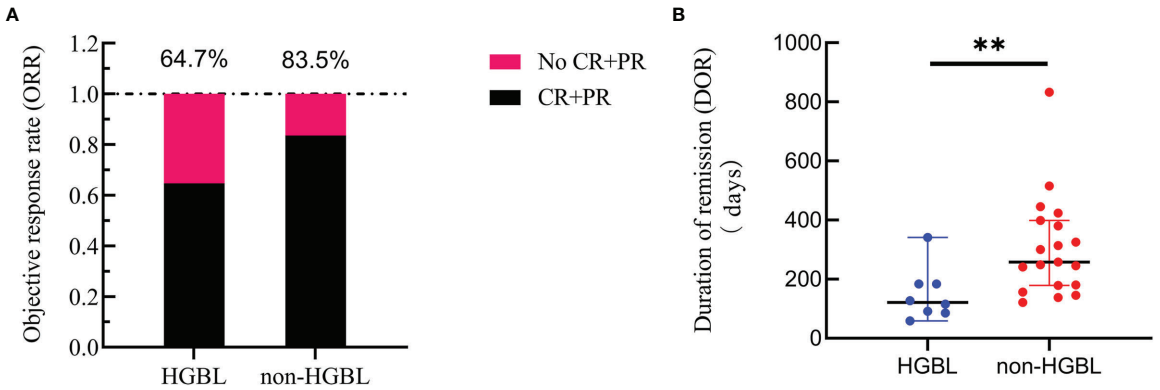

FIGURE 2 | Curative effect. **(A)** Comparison of the objective response rate (ORR) between high-grade B-cell lymphoma (HGBL) patients and non-HGBL patients after induction chemotherapy with the R-CHOP regimen ($p = 0.105$). **(B)** Duration of remission (DOR) comparison of HGBL and non-HGBL patients from complete remission to relapse or death (**, $p < 0.01$).

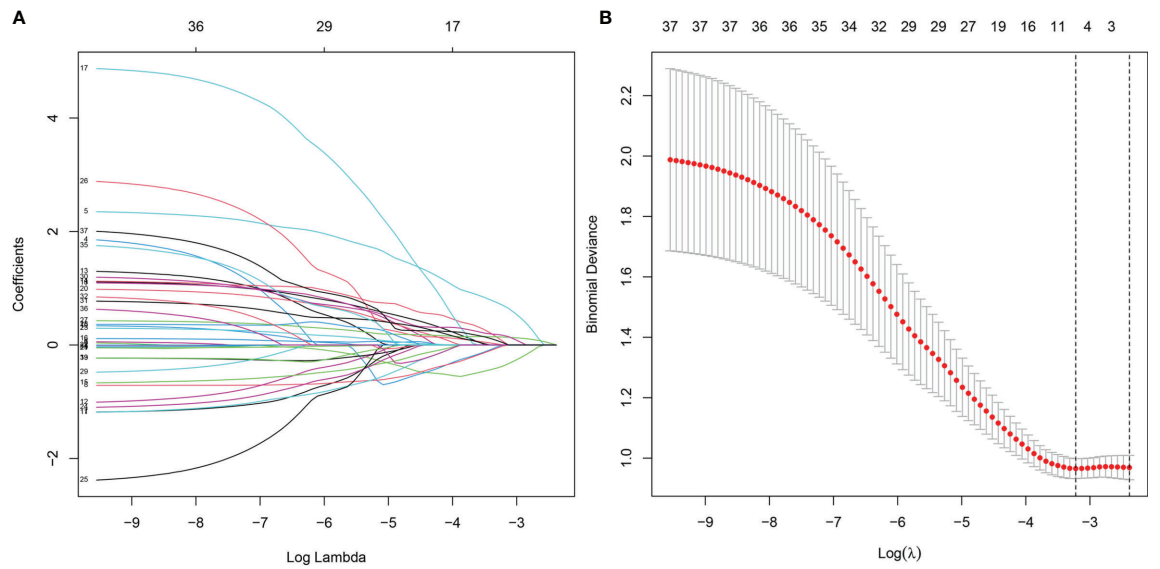

FIGURE 3 | Clinical feature selection using the LASSO binary logistic regression model. **(A)** LASSO coefficient profiles of the 37 features. A coefficient profile plot was produced against the log(lambda) sequence. **(B)** Optimal parameter (lambda) selection in the LASSO model used eightfold cross-validation *via* minimum criteria. The partial likelihood deviance (binomial deviance) curve was plotted versus log(lambda). Dotted vertical lines were drawn at the optimal values by using the minimum criteria and the 1 SE of the minimum criteria (the 1 – SE criteria). LASSO, least absolute shrinkage and selection operator.

Likewise, a logistic binary regression model was established to predict HGBL-DH. Patients with high-grade histomorphology, SUVmax > 25.25, IPI risk group 3 or 4, c-MYC > 0.575, extranodal involvement >1, WBC > ULN, and LDH > ULN were more likely HGBL-DH. In the evaluation of the model's effectiveness in the test set, the micro-average and macro-average AUC values of the ROC curve were 0.61 and 0.86, respectively (**Figure 5**). In view of the adverse impact of MYC rearrangement on prognosis, we also constructed a model to predict MYC rearrangement. After comparing with other models, we found that the Extreme Gradient Boosting classification model had the best AUC, precision, and recall rate, with the micro-average and macro-average AUC values being 0.81 and 0.70, respectively. In the feature importance plot, the variables according to the descending order in importance were high-grade histomorphology, c-MYC > 0.575, extranodal involvement >1, WBC > ULN, SUVmax > 25.25, IPI risk group 3 or 4, male, age > 60, LDH > ULN, and Bcl-6 overexpression positive (**Figure S2**).

TABLE 3 | Logistic regression model for HGBL prediction.

Features	B	Wald	p	Exp (B)
Gender	0.608	0.772	0.380	1.836
Age > 60	0.012	0.133	0.715	1.012
High-grade histomorphology	2.693	6.302	0.012	14.774
Ki67 ≥ 90%	8.262	3.467	0.063	3874.165
Bcl-2	−2.279	3.650	0.056	0.102
Bcl-6	1.913	2.166	0.141	6.773
c-MYC	0.018	0.000	0.993	1.018
Advanced Ann Arbor stage	−1.375	7.161	0.007	0.253
WBC > ULN	0.064	0.599	0.439	1.067
LDH > ULN	−0.002	4.013	0.040	0.998
β2 microglobulin	0.158	0.984	0.321	1.171
IPI score	−1.456	2.646	0.104	0.233
IPI risk group	3.341	8.592	0.003	28.239
Extranodal involvements	0.398	3.738	0.053	1.489
BM involvement	1.710	2.673	0.102	5.531
Constant	−12.526	4.755	0.029	0.000

ULN, upper limit of normal; WBC, white blood cell count; LDH, serum lactate dehydrogenase; IPI, International Prognostic Index score; BM, bone marrow; HGBL, high-grade B-cell lymphoma.

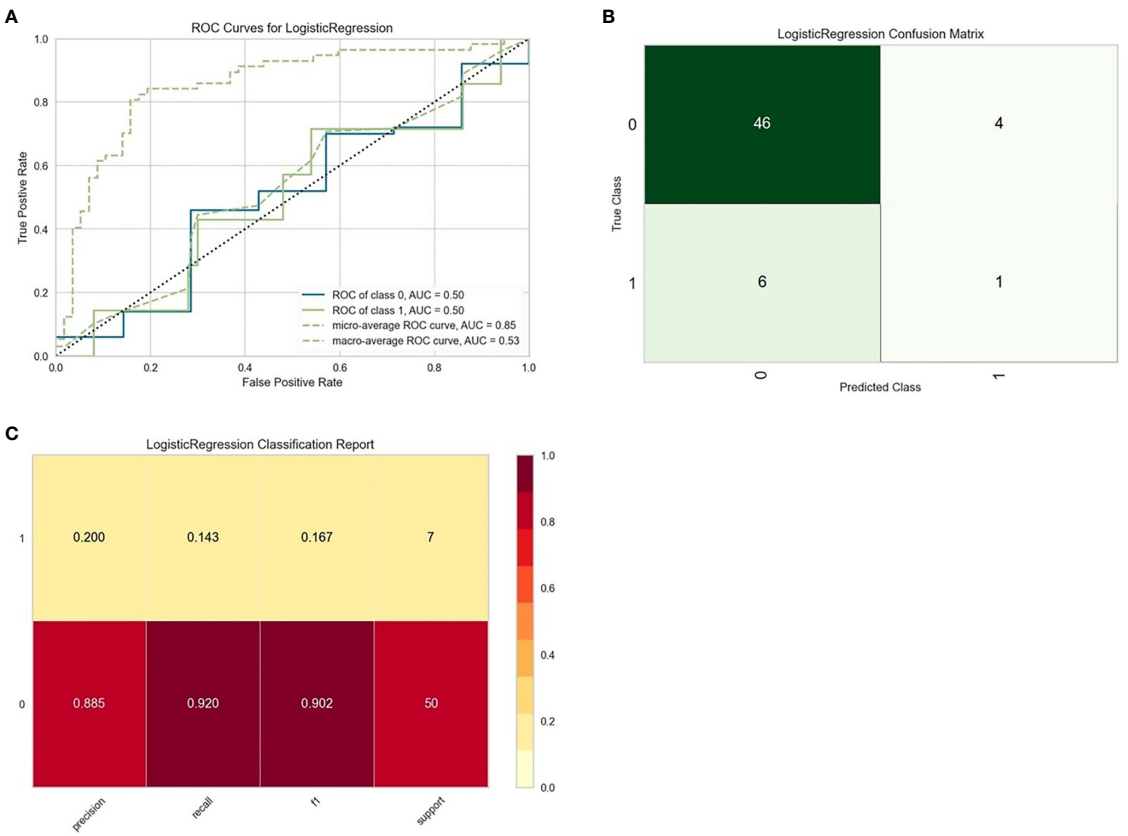

FIGURE 4 | Evaluation of logistic regression models for predicting high-grade B-cell lymphoma (HGBL) in the test set. "Class 1" refers to the HGBL group, and "class 0" refers to the non-HGBL group. **(A)** The receiver operating characteristic (ROC) curves of the model. **(B)** The confusion matrix represents whether the classifier prediction is correct. **(C)** The precision, recall, F1 value, and support of the model.

Furthermore, the logistic binary regression model was chosen for the 1-year survival prediction. In the test set, the macro-average and micro-average AUC values of the ROC curve were 0.82 and 0.73, respectively. The validity of the model predicting death within 1 year was high, and the precision, the recall rate, and the F1 value of the test set were 0.714, 0.833, and 0.769, respectively. Patients with IPI risk group 3 or 4, CD10 positive, extranodal involvement, LDH > ULN, WBC > ULN, bone

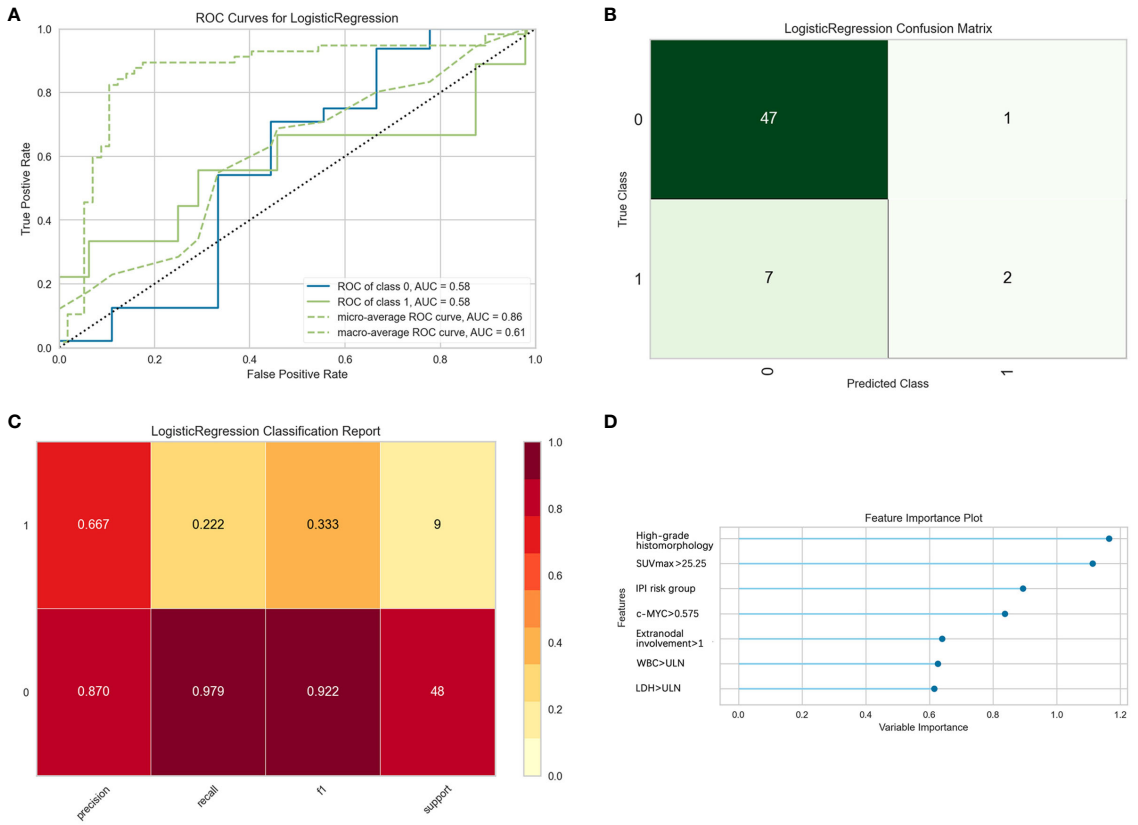

FIGURE 5 | Evaluation of logistic regression models for predicting double-hit high-grade B-cell lymphoma (HGBL-DH) in the test set. "Class 1" refers to the HGBL-DH group, and "class 0" refers to the non-HGBL-DH group. **(A)** The receiver operating characteristic (ROC) curves of the model. **(B)** The confusion matrix represents whether the classifier prediction is correct. **(C)** The precision, recall, F1 value, and support of the model. **(D)** The bar plot represents the importance of clinical variables enrolled by the machine.

marrow involvement, age > 60, advanced Ann Arbor stage, and SUVmax > 25.25 had a higher risk of death within 1 year (**Figure 6**).

DISCUSSION

In the 2016 revision of the WHO classification of lymphoid neoplasms, HGBL is a newly introduced category of rare and heterogeneous invasive B-cell lymphoma that has recently received increasing attention clinically and in the literature. HGBL is comprised of two types, i.e., HGBL with MYC and Bcl-2 and/or Bcl-6 rearrangements (HGBL-DH or HGBL-TH) and HGBL-NOS, which replaced the category of B-cell lymphoma, unclassifiable, with features intermediate between DLBCL and BL (BCLU). Neither Ki-67 proliferation indices (23) nor double expressor is independently sensitive enough to distinguish the HGBL-DH or HGBL-TH cases. Some pathologists and clinicians have suggested that additional molecular genetic analysis should only be done in cases with the GCB phenotype or high-grade histomorphology features and those with MYC overexpression (4). Admittedly, using this protocol could save time and cost and may identify more HGBL patients. Nevertheless, it would inevitably miss some cases. For clinicians, accurate, widely available, and affordable methods are urgently needed.

Eleven of the 21 MYC/Bcl-6 HGBL-DH cases in our study were considered non-GCB phenotypes by the Hans classification. Furthermore, previous studies (24, 25) showed that MYC/Bcl-6 HGBL-DH was still observed in a large proportion of non-GCB phenotypes. Thus, it appears inappropriate to perform the FISH analysis only in cases with the GCB phenotype. At the same time, it is not advisable to perform a FISH test for all DLBCL cases. Hence, to explore which clinical characteristics can be regarded as diagnostic predictors and better understand this type of lymphomas, we analyze their clinical and pathologic features and establish a classification model.

Among the 24 HGBL-DH cases in our study, 21 patients had MYC and Bcl-6 rearrangements, and only 3 cases were MYC/Bcl-2 HGBL-DH. Interestingly, we found that MYC/Bcl-2 HGBL-DH constitutes the majority of HGBL-DH in most European and American studies (16, 26–29), such as in the United States, France, and Canada. In contrast, some studies

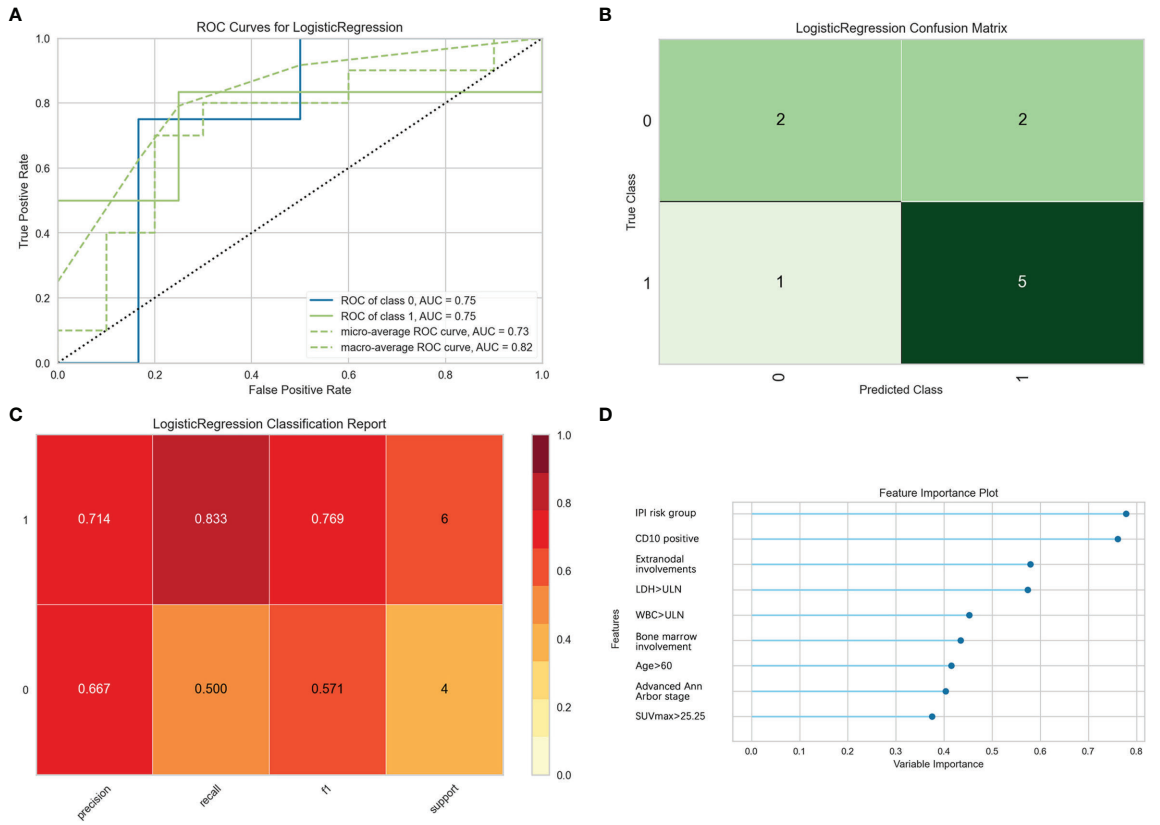

FIGURE 6 | Evaluation of logistic regression model for predicting 1-year survival. "Class 1" refers to the death group, and "class 0" refers to the survival group. **(A)** The receiver operating characteristic (ROC) curves of the model. **(B)** The confusion matrix represents whether the classifier prediction in the test set is correct. **(C)** The precision, recall, F1 value, and support were used to evaluate the model's prediction effectiveness. **(D)** The bar plot represents the importance of clinical variables enrolled by the machine.

from China's southern regions like the Guangdong and Taiwan Provinces (30, 31) showed that MYC/Bcl-6 HGBL-DH is the most common. We consider that it may be due to geographical differences or the relatively small number of specimens. All 3 cases with MYC/Bcl-2 HGBL-DH had the GCB phenotype, which shows similarity to HGBL-TH in terms of COO and immunophenotype, in agreement with those earlier studies in the literature (32, 33). In our study, almost every HGBL-TH case had CD10 overexpression, while it also often was observed in MYC/Bcl-2 HGBL-DH, which was consistent with those reported results (33, 34).

For HGBL, the standard treatment was not yet established, and R-CHOP remains the basis of therapy. Some reports (35, 36) showed that higher-intensity chemotherapy such as R-DA-EPOCH can prolong PFS and OS than R-CHOP in HGBL-DH patients. Still, the retrospective analysis of Landsburg et al. (27) showed no differences in OS between R-DA-EPOCH and R-CHOP. Moreover, due to insufficient data on HGBL-TH and HGBL-NOS patients, it is still necessary to develop new treatments to improve the prognosis of these patients. In our study, the HGBL group also showed a dismal prognosis, and the classical R-CHOP regimen has also been shown to have lower efficacy. In addition, patients treated with R-CHOP combined with lenalidomide, ibrutinib, or chidamide (R-CHOP + X) regimens exhibited initial curative effects. However, this approach will need to be tested in more patients.

Classification models were established to predict the diagnosis and prognosis of HGBL by machine learning algorithms in this study. The Extreme Gradient Boosting approach had the highest AUC, while the random forest classification model had the highest accuracy. However, in case of the good interpretability of the logistic regression model, whose AUC and precision are also reliable, we chose to build the logistic binary regression model to predict HGBL. Some models showed high effective predictive ability, including HGBL-DH and MYC rearrangement. They indicated that we should focus on SUVmax, IPI risk group, c-MYC overexpression, Bcl-6 overexpression, extranodal involvement, WBC, and LDH as references when considering whether FISH screening was recommended. It is noteworthy that the 1-year survival prediction model had a high AUC, precision, and recall rate. This model could be a helpful prognosis evaluation method for clinicians. However, because of the complexity of diagnosis of

HGBL and the limited number of cases in a single research center, the bias of these models was hard to certify. Multicenter studies need to be carried out in the future to improve the accuracy of the models further.

In summary, HGBL is a new category of highly aggressive B-cell malignancies characterized by laborious diagnosis and poor effects of therapy. Our study identified several independent risk factors for the diagnosis of HGBL. Prediction models contribute to clinicians making a comprehensive diagnosis and evaluating the prognosis more accurately. Otherwise, R-CHOP, as the most frequently used first-line treatment, was considered to have dismal efficacy for HGBL in our study. A standard induction therapeutic regimen is urgently needed to ameliorate the poor outcome.

DATA AVAILABILITY STATEMENT

The original contributions presented in the study are included in the article/**Supplementary Material**. Further inquiries can be directed to the corresponding authors.

ETHICS STATEMENT

The studies involving human participants were reviewed and approved by Fujian Medical University Union Hospital Ethics Committee. The patients/participants provided their written informed consent to participate in this study.

AUTHOR CONTRIBUTIONS

TY and JH designed and performed the study. HK, HZ, and XZ collected the data. HK, JR, and XL collected the pathological specimens. MJ and LC performed the IHC and FISH analyses. HK, HZ, and LL performed the statistical analyses. HZ, JR, and TY interpreted the results and developed the initial manuscript draft. JZ, ZZ, XZ, and ZC contributed to patient management. All authors contributed to manuscript revisions and approved the final version for publication. TY and JH had full access to all the data and had final responsibility for the decision to submit it for publication.

FUNDING

This work was funded by the National Natural Science Foundation of China (81870138, U2005204), Startup Fund for Scientific Research Project of Fujian Medical University (2020QH2021), National Key Clinical Specialty Discipline Construction Program (2021-76), and Clinical Research Center for Hematological Malignancies of Fujian Province (2020Y2006).

SUPPLEMENTARY MATERIAL

The Supplementary Material for this article can be found online at: https://www.frontiersin.org/articles/10.3389/fimmu.2022.919012/full#supplementary-material

REFERENCES

1. Swerdlow SH, Campo E, Pileri SA, Harris NL, Stein H, Siebert R, et al. The 2016 Revision of the World Health Organization Classification of Lymphoid Neoplasms. *Blood* (2016) 127(20):2375–90. doi: 10.1182/blood-2016-01-643569
2. Aukema SM, Siebert R, Schuuring E, van Imhoff GW, Kluin-Nelemans HC, Boerma EJ, et al. Double-Hit B-Cell Lymphomas. *Blood* (2011) 117(8):2319–31. doi: 10.1182/blood-2010-09-297879
3. Foot NJ, Dunn RG, Geoghegan H, Wilkins BS, Neat MJ. Fluorescence *in Situ* Hybridisation Analysis of Formalin-Fixed Paraffin-Embedded Tissue Sections in the Diagnostic Work-Up of Non-Burkitt High Grade B-Cell Non-Hodgkin's Lymphoma: A Single Centre's Experience. *J Clin Pathol* (2011) 64(9):802–8. doi: 10.1136/jclinpath-2011-200015
4. Novo M, Castellino A, Nicolosi M, Santambrogio E, Vassallo F, Chiappella A, et al. High-Grade B-Cell Lymphoma: How to Diagnose and Treat. *Expert Rev Hematol* (2019) 12(7):497–506. doi: 10.1080/17474086.2019.1624157
5. Hu S, Xu-Monette ZY, Tzankov A, Green T, Wu L, Balasubramanyam A, et al. Myc/Bcl2 Protein Coexpression Contributes to the Inferior Survival of Activated B-Cell Subtype of Diffuse Large B-Cell Lymphoma and Demonstrates High-Risk Gene Expression Signatures: A Report From the International Dlbcl Rituximab-Chop Consortium Program. *Blood* (2013) 121 (20):4021–31. doi: 10.1182/blood-2012-10-460063
6. Steven H. Swerdlow. Diagnosis of 'Double Hit' Diffuse Large B-Cell Lymphoma and B-Cell Lymphoma, Unclassifiable, With Features Intermediate Between Dlbcl and Burkitt Lymphoma When and How, Fish Versus Ihc. *Hematol Am Soc Hematol Educ Program* (2014) 2014(1):90–9. doi: 10.1182/asheducation-2014.1.90
7. Green TM, Young KH, Visco C, Xu-Monette ZY, Orazi A, Go RS, et al. Immunohistochemical Double-Hit Score Is a Strong Predictor of Outcome in Patients With Diffuse Large B-Cell Lymphoma Treated With Rituximab Plus Cyclophosphamide, Doxorubicin, Vincristine, and Prednisone. *J Clin Oncol* (2012) 30(28):3460–7. doi: 10.1200/JCO.2011.41.4342
8. Johnson NA, Slack GW, Savage KJ, Connors JM, Ben-Neriah S, Rogic S, et al. Concurrent Expression of Myc and Bcl2 in Diffuse Large B-Cell Lymphoma Treated With Rituximab Plus Cyclophosphamide, Doxorubicin, Vincristine, and Prednisone. *J Clin Oncol* (2012) 30(28):3452–9. doi: 10.1200/JCO.2011.41.0985
9. Perry AM, Alvarado-Bernal Y, Laurini JA, Smith LM, Slack GW, Tan KL, et al. Myc and Bcl2 Protein Expression Predicts Survival in Patients With Diffuse Large B-Cell Lymphoma Treated With Rituximab. *Br J Haematol* (2014) 165(3):382–91. doi: 10.1111/bjh.12763
10. Horn H, Ziepert M, Becher C, Barth TF, Bernd HW, Feller AC, et al. Myc Status in Concert With Bcl2 and Bcl6 Expression Predicts Outcome in Diffuse Large B-Cell Lymphoma. *Blood* (2013) 121(12):2253–63. doi: 10.1182/blood-2012-06-435842
11. Hans CP, Weisenburger DD, Greiner TC, Gascoyne RD, Delabie J, Ott G, et al. Confirmation of the Molecular Classification of Diffuse Large B-Cell Lymphoma by Immunohistochemistry Using a Tissue Microarray. *Blood* (2004) 103(1):275–82. doi: 10.1182/blood-2003-05-1545
12. Hilton Laura K, Tang J, Ben-Neriah S, Alcaide M, Jiang A, Grande BM, et al. The Double-Hit Signature Identifies Double-Hit Diffuse Large B-Cell Lymphoma With Genetic Events Cryptic to Fish. *Blood* (2019) 134 (18):1528–32. doi: 10.1182/blood.2019002600
13. Carbone PP, Kaplan HS, Musshoff K, Smithers DW, Tubiana M. Report of the Committee on Hodgkin's Disease Staging Classification. *Cancer Res* (1971) 31 (11):1860–1.
14. Lister TA, Crowther D, Sutcliffe SB, Glatstein E, Canellos GP, Young RC, et al. Report of a Committee Convened to Discuss the Evaluation and Staging of Patients With Hodgkin's Disease: Cotswolds Meeting. *J Clin Oncol* (1989) 7 (11):1630–6. doi: 10.1200/JCO.1989.7.11.1630

15. Project TIN-H'sLPF. A Predictive Model for Aggressive Non-Hodgkin's Lymphoma. *N Engl J Med* (1993) 329(14):987–94. doi: 10.1056/NEJM199309303291402
16. Pillai RK, Sathanoori M, Van Oss SB, Swerdlow SH. Double-Hit B-Cell Lymphomas With Bcl6 and Myc Translocations Are Aggressive, Frequently Extranodal Lymphomas Distinct From Bcl2 Double-Hit B-Cell Lymphomas. *Am J Surg Pathol* (2013) 37:323–32. doi: 10.1097/PAS.0b013e31826cebad
17. Seegmiller AC, Garcia R, Huang R, Maleki A, Karandikar NJ, Chen W. Simple Karyotype and Bcl-6 Expression Predict a Diagnosis of Burkitt Lymphoma and Better Survival in Ig-Myc Rearranged High-Grade B-Cell Lymphomas. *Mod Pathol* (2010) 23(7):909–20. doi: 10.1038/modpathol.2010.76
18. Cheson BD, Fisher RI, Barrington SF, Cavalli F, Schwartz LH, Zucca E, et al. Recommendations for Initial Evaluation, Staging, and Response Assessment of Hodgkin and Non-Hodgkin Lymphoma: The Lugano Classification. *J Clin Oncol* (2014) 32(27):3059–68. doi: 10.1200/JCO.2013.54.8800
19. Cheson BD, Pfistner B, Juweid ME, Gascoyne RD, Specht L, Horning SJ, et al. Revised Response Criteria for Malignant Lymphoma. *J Clin Oncol* (2007) 25(5):579–86. doi: 10.1200/JCO.2006.09.2403
20. Xie W, Jiang X, Zhao W, L W. Prognostic Evaluation of Different Pet/Ct Reading Methods in Hodgkin Lymphoma and Diffused Large B-Cell Lymphoma. *J Shanghai Jiaotong Univ (Medical Edition)* (2018) 38(8):955–9. doi: 10.3969/j.issn.1674-8115.2018.08.016
21. Sauerbrei W, Royston P, Binder H. Selection of Important Variables and Determination of Functional Form for Continuous Predictors in Multivariable Model Building. *Stat Med* (2007) 26(30):5512–28. doi: 10.1002/sim.3148
22. Kidd AC, McGettrick M, Tsim S, Halligan DL, Bylesjo M, Blyth KG. Survival Prediction in Mesothelioma Using a Scalable Lasso Regression Model: Instructions for Use and Initial Performance Using Clinical Predictors. *BMJ Open Respir Res* (2018) 5(1):e000240. doi: 10.1136/bmjresp-2017-000240
23. Mationg-Kalaw E, Tan LH, Tay K, Lim ST, Tang T, Lee YY, et al. Does the Proliferation Fraction Help Identify Mature B Cell Lymphomas With Double- and Triple-Hit Translocations? *Histopathology* (2012) 61(6):1214–8. doi: 10.1111/j.1365-2559.2012.04351.x
24. Scott DW, King RL, Staiger AM, Ben-Neriah S, Jiang A, Horn H, et al. High-Grade B-Cell Lymphoma With Myc and Bcl2 and/or Bcl6 Rearrangements With Diffuse Large B-Cell Lymphoma Morphology. *Blood* (2018) 131(18):2060–4. doi: 10.1182/blood-2017-12-820605
25. Valera A, Lopez-Guillermo A, Cardesa-Salzmann T, Climent F, Gonzalez-Barca E, Mercadal S, et al. Myc Protein Expression and Genetic Alterations Have Prognostic Impact in Patients With Diffuse Large B-Cell Lymphoma Treated With Immunochemotherapy. *Haematologica* (2013) 98(10):1554–62. doi: 10.3324/haematol.2013.086173
26. Laude MC, Lebras L, Sesques P, Ghesquieres H, Favre S, Bouabdallah K, et al. First-Line Treatment of Double-Hit and Triple-Hit Lymphomas: Survival and Tolerance Data From a Retrospective Multicenter French Study. *Am J Hematol* (2021) 96(3):302–11. doi: 10.1002/ajh.26068
27. Landsburg DJ, Falkiewicz MK, Maly J, Blum KA, Howlett C, Feldman T, et al. Tatyana FeldmanOutcomes of Patients With Double-Hit Lymphoma Who Achieve First Complete Remission. *J Clin Oncol* (2017) 35:2260–7. doi: 10.1200/JCO.2017
28. Landsburg DJ, Petrich AM, Abramson JS, Sohani AR, Press O, Cassaday R, et al. Impact of Oncogene Rearrangement Patterns on Outcomes in Patients With Double-Hit Non-Hodgkin Lymphoma. *Cancer* (2016) 122(4):559–64. doi: 10.1002/cncr.29781
29. Petrich AM, Gandhi M, Jovanovic B, Castillo JJ, Rajguru S, Yang DT, et al. Impact of Induction Regimen and Stem Cell Transplantation on Outcomes in Double-Hit Lymphoma: A Multicenter Retrospective Analysis. *Blood* (2014) 124(15):2354–61. doi: 10.1182/blood-2014-05-578963
30. Zhang JJ, Weng ZP, Huang YH, Li M, Wang F, Wang Y, et al. High-Grade B-Cell Lymphoma With myc, bcl2, and/Or Bcl6 Translocations/Rearrangements Clinicopathologic Features of 51 Cases in a Single Institution of South China. *Am J Surg Pathol* (2020) 44(12):1602–11. doi: 10.1097/PAS.0000000000001577
31. Tsai CC, Su YC, Bamodu OA, Chen BJ, Tsai WC, Cheng WH, et al. High-Grade B-Cell Lymphoma (Hgbl) With Myc and Bcl2 and/or Bcl6 Rearrangements Is Predominantly Bcl6-Rearranged and Bcl6-Expressing in Taiwan. *Cancers (Basel)* (2021) 13(7):1620. doi: 10.3390/cancers13071620
32. Li S, Lin P, Medeiros LJ. Advances in Pathological Understanding of High-Grade B Cell Lymphomas. *Expert Rev Hematol* (2018) 11(8):637–48. doi: 10.1080/17474086.2018.1494567
33. Wang W, Hu SM, Lu XY, Young KH, Medeiros LJ. Triple-Hit B-Cell Lymphoma With Myc, Bcl2, and Bcl6 Ranslocations/Rearrangements Clinicopathologic Features of 11 Cases. *Am J Surg Pathol* (2015) 39(8):1132–9. doi: 10.1097/PAS.0000000000000434
34. Li SY, Lin P, Young KH, Rashmi K-S, Yin CC, Medeiros LJ. Myc/Bcl2 Double-Hit High-Grade B-Cell Lymphoma. *Adv Anat Pathol* (2013) 20(5):315–26. doi: 10.1097/PAP.0b013e3182a289f2
35. Zhang XY, Liang JH, Wang L, Zhu HY, Wu W, Cao L, et al. Da-Epoch-R Improves the Outcome Over That of R-Chop Regimen for Dlbcl Patients Below 60 Years, Gcb Phenotype, and Those With High-Risk Ipi, But Not for Double Expressor Lymphoma. *J Cancer Res Clin Oncol* (2019) 145(1):117–27. doi: 10.1007/s00432-018-2771-9
36. Dunleavy K. Double-Hit Lymphomas: Current Paradigms and Novel Treatment Approaches. *Hematol Am Soc Hematol Educ Program* (2014) 2014(1):107–12. doi: 10.1182/asheducation-2014.1.107

Conflict of Interest: The authors declare that the research was conducted in the absence of any commercial or financial relationships that could be construed as a potential conflict of interest.

frontiers | Frontiers in Immunology

ORIGINAL RESEARCH
published: 06 June 2022
doi: 10.3389/fimmu.2022.922471

m6A-Regulator Expression Signatures Identify a Subset of Follicular Lymphoma Harboring an Exhausted Tumor Microenvironment

Tingting Zhang[1,2†], Hengqi Liu[1,2†], Fenghua Gao[1,2†], Wenchen Gong[3†], Yaoli Cui[1,2†], Jin He[1,2], Lanfang Li[1,2], Lihua Qiu[1,2], Zhengzi Qian[1,2], Shiyong Zhou[1,2], Bin Meng[3], Xiubao Ren[4], Huilai Zhang[1,2] and Xianhuo Wang[1,2*]*

[1] Department of Lymphoma, Tianjin Medical University Cancer Institute and Hospital, National Clinical Research Center for Cancer, Tianjin, China, [2] Key Laboratory of Cancer Prevention and Therapy, Tianjin's Clinical Research Center for Cancer, The Sino-US Center for Lymphoma and Leukemia Research, Tianjin, China, [3] Department of Pathology, Tianjin Medical University Cancer Institute and Hospital, Tianjin, China, [4] Department of Immunology/Biotherapy, Tianjin Medical University Cancer Institute and Hospital, Tianjin, China

The role of N6-methyladenosine (m6A) modification in tumor microenvironment has rarely been explored in follicular lymphoma (FL). To examine the role of m6A modification in biological behavior, especially the immune landscape of FL, we utilized the Gene Expression Omnibus database to determine the expression signatures of m6A-regulators by unsupervised clustering, and then condense into a risk score, which was validated in an external cohort from the Tianjin Medical University Cancer Institute and Hospital. Finally, 16 m6A-regulators in 351 FL patients were evaluated and two m6A clusters were identified, characterized by differences in prognosis and biological behaviors. The m6A score was further developed based on 20-genes to quantify the m6A-regulator expression signature in each patient with FL. The low m6A score was associated with inferior prognosis of patients, with a median survival time of 8.84 (95% confidence interval [CI]: 7.251-10.429) years, which was remarkably shorter than that of patients with high m6A scores (15.73 years, 95% CI: 11.729-19.731; p<0.0001). Genes like TNFRSF14, CREBBP, and CARD11 were shown to be more often mutated in the low m6A group. This group was enriched with immune/inflammatory response but along with the abundant infiltration of exhausted T cells and the upregulated PD-1 and PD-L1 expression. Finally, we verified the m6A score could predict the response to anti-PD-L1 antibodies in an immunotherapy cohort. To conclude, the m6A score recognizes a section of FL patients harboring an exhausted tumor microenvironment and may help guide more effective immunotherapy strategies for patients with FL.

Keywords: m6A, tumor microenvironment, immunotherapy, follicular lymphoma, exhaustion

OPEN ACCESS

Edited by:
Wei Sang,
The Affiliated Hospital of Xuzhou Medical University, China

Reviewed by:
Zhaoming Li,
First Affiliated Hospital of Zhengzhou University, China
Aiping Tong,
Sichuan University, China
Chengfeng Bi,
University of Nebraska Medical Center, United States

***Correspondence:**
Huilai Zhang
zhlwgq@126.com
Xianhuo Wang
tjzlyy_xianhuow@163.com

†These authors have contributed equally to this work

Specialty section:
This article was submitted to Cancer Immunity and Immunotherapy, a section of the journal Frontiers in Immunology

Received: *18 April 2022*
Accepted: *13 May 2022*
Published: *06 June 2022*

Citation:
Zhang T, Liu H, Gao F, Gong W, Cui Y, He J, Li L, Qiu L, Qian Z, Zhou S, Meng B, Ren X, Zhang H and Wang X (2022) m6A-Regulator Expression Signatures Identify a Subset of Follicular Lymphoma Harboring an Exhausted Tumor Microenvironment. Front. Immunol. 13:922471. doi: 10.3389/fimmu.2022.922471

INTRODUCTION

Follicular lymphoma (FL), the most common type of indolent B cell non-Hodgkin lymphoma, is a highly heterogeneous disease with variable biological and clinical behaviors (1). Despite therapeutic advances during the past decades and median overall survival (OS) duration of more than 10 years, 20-30% of patients will experience early disease progression, and subsets of individuals suffering from FL are more prone to mortality from this disease (2, 3). Still, the basic molecular processes that lead to the pathological development of FL are not clearly understood. Hence, a deep understanding of FL oncogenesis and development is important to facilitate a more personalized approach to the management of FL.

Epigenetic dysregulation is crucial for the pathological development of FL (4, 5). Recently, N6-methyladenosine (m6A), the most common posttranscriptional modification of mRNA, has attracted great attention in the cancer research field. m6A modification influences a series of biological functions, including RNA stabilization, splicing, export, translation, and degradation (6–10). Accumulating evidence indicates that m6A modification is extensively involved in the development and progression of multiple non-hematological and hematological cancers (11). Research has revealed that m6A modification could increase the self-renewal ability of acute myeloid leukemia cells and contribute to the pathogenesis of acute myeloid leukemia (12–14). The function of m6A modification in lymphoma has also been reported. For example, WTAP, an m6A methyltransferase, was markedly upregulated in nasal-type natural killer/T-cell lymphoma, and WTAP-guided m6A methylation contributed to tumor cell proliferation and chemotherapy resistance (15). Cheng Y and colleagues found that the m6A methylation level was upregulated in diffuse large B-cell lymphoma (DLBCL) and that METTL3 promoted disease progression (16). However, the role of m6A modification in FL is largely unknown.

Extensive studies have suggested that m6A modification is important for both innate and adaptive immune modulation, and also to shape the tumor microenvironment (TME) (17, 18). In solid tumors, such as gastric cancer and clear cell renal carcinoma, m6A modification is closely connected to distinct immune subtypes and cell infiltration characteristics (19, 20). FL is characterized by the infiltration of a substantial number of T cells in TME, which has a significant impact on the FL biology and outcome (5). However, the role of m6A modification in the formation of TME diversity and complexity in FL, is poorly understood.

m6A modification, a reversible and dynamic process, is mainly regulated by three categories of proteins: "writers" (methyltransferases), "readers" (effector proteins), and "erasers" (demethylases). The measuring techniques of m6A modification level includes MeRIP-seq, miCLIP-seq, SCARLET, LC-MS/MS and so on (21). All those detection methods have their own limitations and their application in clinical practice remains challenge. Nevertheless, the m6A modification level is closely related to the expression level of writers, readers, and erasers. Hence, we evaluated the interaction role of m6A-regulators instead directly determining the m6A modification level for the convenience of practical application. In this study, we comprehensively evaluated the expression of 16 m6A-regulators in 351 FL patients from three cohorts, examined different m6A-regulator expression signatures and further identified a subset of patients prone to therapeutic effects of immune therapy.

METHODS

Data Collection and Processing

The Gene Expression Omnibus (GEO) database was thoroughly searched for all eligible FL datasets. Then, three datasets, GSE16131 (N=184), GSE119214 (N=137), and GSE66166 (N=138), were enrolled. Gene expression data and related clinical details from the three datasets were downloaded from the GEO database (https://www.ncbi.nlm.nih.gov/geo/). Notably, the samples in both GSE119214 and GSE66166 were obtained from the BC Cancer Agency cohort. Hence, only 30 samples in GSE66166 were subjected to further analysis after removing the 108 duplicated samples in GSE119214. Finally, in this research, total 351 patients were recruited, of whom 317 had available survival data. Detailed clinical information of each dataset is provided in **Table S1**. The batch effect was removed using ComBat from the R package sva (version 3.40.0) (22).

Fresh frozen tumor biopsies from 77 FL patients were acquired from the Tianjin Medical University Cancer Institute and Hospital. After excluding patients with grade 3b, histologic transformed FL, FL with concurrent DLBCL and with incomplete follow-up data, 41 patients being provided with standard first-line therapy were recruited for the validation cohort. For these patients, sufficient amount of quality genomic RNA (n=41) and DNA (n=38) from tumor biopsies were extracted for high-throughput sequencing. The Tianjin Medical University Cancer Institute and Hospital's Clinical Research Ethics Board provided the approval for this study. Informed written consents were acquired. The flow diagram of our study is briefed in **Figure S1**.

Unsupervised Clustering of 16 m6A-Regulators

Total 16 m6A-regulators were isolated from the integrated GEO database, including eight writers (WTAP, RBM15, RBM15B, ZC3H13, METTL3, METTL14, KIAA1429, and CBLL1), seven readers (HNRNPC, HNRNPA2B1, YTHDC1, YTHDF2, IGF2BP1, ELAVL1, and LRPPRC) and one eraser (ALKBH5). The STRING database (http://www.db.org/) was utilized to analyse the interactive network of these m6A-regulators. Unsupervised clustering analysis was conducted using the ConsensusClusterPlus package (version 1.56.0) (23) based on the k-means algorithm to evaluate the distinct expression signatures of m6A-regulators. The Euclidean distance was utilized as the distance measure, and 1000 bootstrap replications were performed.

Gene Set Annotation Enrichment Analysis

Gene set variation analysis (GSVA) was performed to identify the distinct biological processes between the expression signatures of m6A-regulators using GSVA R package (version 1.40.1) (24). The 'c2. cp. kegg. v6.2. symbols' gene set, obtained from Molecular Signatures Database, was used for GSVA. A statistical significance of adjusted $p<0.05$ was used in the analysis. Gene set enrichment analysis (GSEA) was performed using the Java desktop software (version 4.1.0) (25, 26). The significance threshold was established at |normalized enrichment score|>1, nominal p-value < 0.05.

Identification of Differentially Expressed Genes (DEGs)

Patients were grouped into distinct m6A clusters based on m6A regulator expression to identify genes that correlated with m6A-regulator expression signature. DEGs between m6A clusters were determined using the limma package (version 3.48.3) (27). Genes with an adjusted $p<0.01$ were identified as differentially expressed.

Generation of the m6A-Related Cluster and m6A Score

To better characterize the underlying biological differences between m6A clusters, we identified m6A-related clusters based on the DEGs identified from m6A clusters by unsupervised clustering analysis. On top of that, we developed a scoring model to quantify the m6A-regulator expression signature in each patient. Briefly, we utilized the random forest approach to remove redundant DEGs obtained in the previous step. The remaining genes' predictive significance was assessed *via* Univariate Cox regression analysis. Genes with statistical significance of $p<0.05$ were subjected to further analysis. Then, principal component analysis (PCA) was conducted and both principal components 1 and 2 were plotted to quantify the m6A-regulator expression signature, termed the m6A score. The calculation formula was as follows:

$$m6\text{A score} = \sum \text{PC1}i + \sum \text{PC2}i$$

where i is the expression of DEGs with significant prognostic value between the m6A clusters.

RNA Sequencing and Gene Expression Analysis

RNeasy Kit (Qiagen, Hilden, Germany) was utilized to isolate RNA. RNAs libraries were created *via* NEBNext® UltraTM RNA Library Prep Kit and sequenced based on Illumina NovaSeq 6000 platform (San Diego, CA, USA) with 150 bp paired-end reads. Subsequently, reads were aligned to the Human Genome Reference Consortium build 37(GRCh37/hg19). Fragments per kilobase per million (FPKM) were utilized to standardize the expression values of each gene. Then, m6A score was calculated to measure the m6A-regulator expression signature in each patient.

Whole Exome Sequencing and Identification of Somatic Single Nucleotide Variations and Indels

DNeasy Tissue and Blood Kit (Qiagen, Venlo, Netherlands) were utilized to isolate DNA. Libraries were created *via* Agilent SureSelect Human All Exon kit V6 (Agilent Technologies, CA, USA) and sequenced on an Illumina NovaSeq 6000 platform with 150 bp paired-end reads. Valid sequencing data were then aligned to the GRCh37/hg19 by BWA (v0.7.12) (28). Then, SAM tools (29), Picard (v1.87) and Genome Analysis Toolkit (GATK) (30) were used to sort BAM files and performing repeated marking, local realignment, and base quality recalibration. Single nucleotide variants (SNVs) were identified using the GATK Unified Genotyper and indels were determined using VarScan. ANNOVAR package (31) were used for annotation of all substitutions and indels. Recurrent mutated genes in FL reported in previous literature were selected and further analysed (5).

Estimation of Infiltrating Immune Cells

The relative abundance of six immune cell subtypes was evaluated by TIMER (https://cistrome.shinyapps.io/timer/) (32). Immune Cell Abundance Identifier (ImmuCellAI) was further utilized to specifically evaluate the abundance of 18 comprehensive T-cell subpopulations (http://bioinfo.life.hust.edu.cn/web/ImmuCellAI/) (33).

Prediction of the Response to Anti-PD-L1 Therapy

An immunotherapeutic cohort of patients with advanced urothelial cancer administered with atezolizumab, an anti-PD-L1 antibody (IMvigor210 cohort, N=354), was enrolled in this study to predict the response to immunotherapy (34). The expression data and corresponding clinical information were downloaded from http://research-pub.Gene.com/imvigor210corebiologies. The FPKM value was converted from the raw count value and m6A score was calculated. Then, receiver operating characteristic (ROC) curve analysis was conducted to compare the performance of m6A score with other predictive biomarkers in predicting the response of anti-PD-L1 therapy, such as PD-L1 expression on tumor cells, tumor immune dysfunction and exclusion (TIDE) (35), and tumor inflammation signature (TIS) (36). PD-L1 expression data was downloaded from https://research-pub.Gene.com/imvigor210corebiologies. After the expression data quantile normalized, TIDE score was calculated using the web application (HTTPS://tide.dfci.harvard.edu/) and TIS score was calculated as an average value of 18 signature gene expression after log10 transformed.

Statistical Analysis

The Wilcoxon two-tailed test was utilized for comparing two groups. Correlations were evaluated by Spearman analysis. Comparison for the survival curves was dawn *via* the Kaplan-Meier log-rank test. $p<0.05$ was of statistical significance. The optimal cutoff point of the m6A score was calculated using the "survminer" package (version 0.4.9) for the survival analysis.

ROC curves with the "pROC" package (version 1.18.0) and time-dependent ROC curves with "survivalROC" package (version 1.0.3) were used to compare the performance of the m6A score. All the analysis was performed *via* R (version 4.1.0).

RESULTS

Landscape of m6A-Regulators in FL

A total of 16 m6A-regulators were ultimately identified in this study: eight writers, seven readers, and one eraser. **Figure S2A** showed the locations of the m6A-regulators on chromosomes. As m6A methylation is involved in the interaction of writers, erasers, and readers, we then analyzed the correlation of m6A-regulator expression. We found that these regulators had complex and interlaced correlations with each other (**Figures S2B, C**; **Table S2**), highlighting the need to identify potential expression signatures to elucidate the clinical significance of these m6A-regulators.

m6A Clusters Mediated by 16 m6A-Regulators

FL patients were classified based on the expression data of 16 m6A-regulators using unsupervised clustering. As per the similarities shown by 16 m6A-regulators expression, k-means clustering was carried out numerous times for different values of k (k = 2-10), and k = 2 was found as having the best clustering stability. (**Figures 1A**, **S3**). Ultimately, two different m6A-regulator expression signatures were identified, termed m6A clusters A and B. Prognostic analysis revealed that m6A cluster A was significantly associated with poorer outcomes as compared to m6A cluster B (p=0.0085; **Figure 1B**). To explore differences in biological behaviors between the two m6A clusters, we performed GSVA. Significantly differentially activated pathways (adjusted p<0.05) between the two groups were summarized in **Table S3**. Specifically, m6A cluster A showed enrichment in the DNA replication, RNA degradation and cell cycle. However, m6A cluster B had a significant enrichment in oncogenic pathways such as the MAPK signaling pathway and hedgehog signaling pathway (**Figure 1C**). Particularly, immune pathways, such as the cytokine-cytokine receptor interaction and T-cell receptor signaling, were activated in m6A cluster B (**Figure 1C**), suggesting that m6A modifications play certain roles in the TME of FL.

Construction of the m6A-Related Cluster

To comprehensively characterize the underlying biological differences between m6A clusters, we identified DEGs between the two groups. Total 2429 DEGs were identified (adjusted p<0.01, **Table S4**). Unsupervised analysis was performed again to divide patients into distinct subgroups based on the 2429 DEGs, named m6A-related clusters A and B (**Figure 2A**). Patients with m6A-related cluster A experienced worse outcomes as compared to the ones with m6A-related cluster B (p=0.0096; **Figure 2B**). The expression level of 16 m6A-regulators was clearly different between the two m6A-related clusters (**Figure 2C**). These findings suggest the existence of m6A-regulator expression signature that plays an important role in FL.

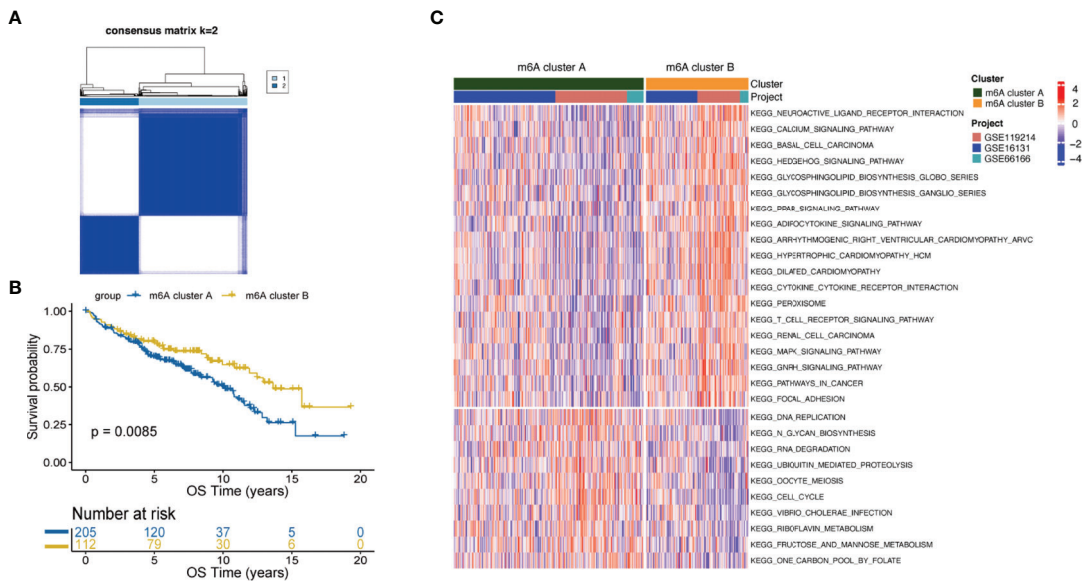

FIGURE 1 | m6A clusters mediated by m6A-regulators and the biological features of each cluster. **(A)** Unsupervised clustering based on m6A-regulator expression and consensus matrices for k = 2. **(B)** Survival analysis between m6A clusters by the log-rank test. **(C)** GSVA showing the activation status of biological pathways in m6A cluster A vs. m6A cluster B. An adjusted p-value<0.05 was considered significantly significant. Biological pathways with adjusted p<0.05 and p<0.0001 were shown in the figure.

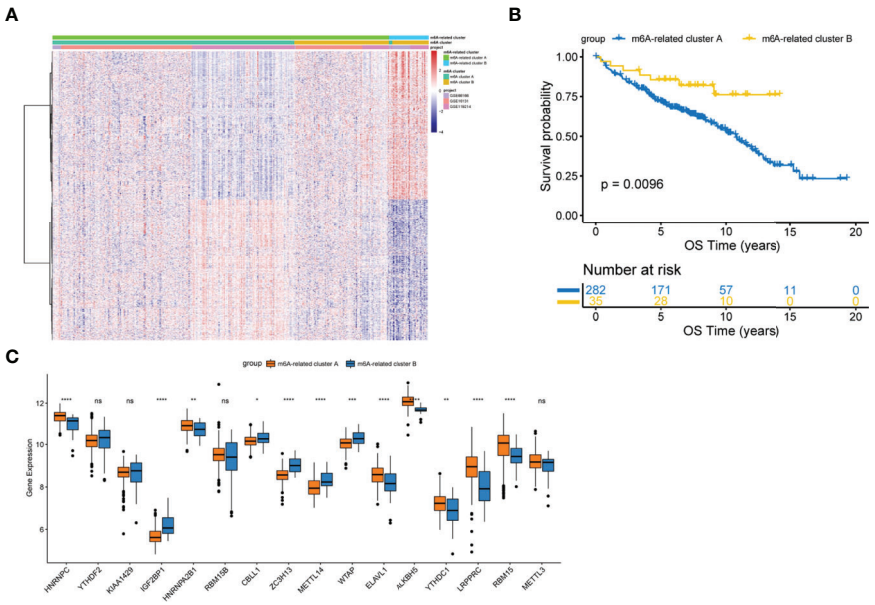

FIGURE 2 | Construction of the m6A-related clusters. **(A)** Patients were classified into m6A-related cluster A and B groups by unsupervised clustering based on the differentially expressed genes between m6A clusters. **(B)** Survival differences according to m6A-related clusters by the log-rank test. **(C)** Differential expression of 16 m6A-regulators between the m6A-related cluster A and B groups. NS, not significant; *p < 0.05; **p <0.01; ***p < 0.001; ****p < 0.0001.

Generation of the m6A Score

To facilitate practical application, a scoring model was developed to quantify the m6A-regulator expression signature in FL patients, termed the m6A score. By using a random forest approach and univariate Cox regression analysis, twenty genes that were most relevant to m6A clusters and with significant prognostic value were isolated to construct the m6A scoring model (**Table S5** and **Figure S4**). Patients were classified into high and low m6A score groups according to the optimal threshold value calculated by the survminer package (cutoff= -0.03). **Figure 3A** shows the attribute changes in m6A-regulator expression signatures in individual patients. m6A cluster A and m6A-related cluster A had significantly low m6A scores (**Figure S5**). Moreover, patients with low m6A scores showed markedly shorter survival as compared to the ones with high m6A scores (p<0.0001; **Figures 3B** and **S6**). Patients with low and high m6A scores had median survival durations of 8.84 (95% confidence interval [CI]: 7.251-10.429) and 15.73 (95% CI: 11.729-19.731) years, respectively. Among the 20 genes used to construct the m6A scoring model, genes such as ARAP1, RNF219 and SCFD1 were inclined to be expressed in patients with low m6A scores, while genes such as MCM6, PCNT and SNX2 were enriched in patients with high m6A scores (**Figure S6**). The survival prediction according to the m6A score was evaluated by time-dependent ROC curve analysis. The area under the ROC curve for 5, 10 and 15-year survival was 0.63, 0.67 and 0.68, respectively (**Figure 3C**). In addition, it was found that age older than 60 years, advanced disease and a high LDH level were greatly linked to a low m6A score (**Figure 3D**). Multivariate Cox regression analysis demonstrated that the m6A score is an independent element of risk for FL (hazard ratio=2.757, 95% CI: 1.338-5.682, p=0.006; **Table S6**). When the cohort GSE16131 and GSE119214 were analyzed separately, we found that the m6A score still had strong potency for predicting prognosis regardless of the application of rituximab in FL (**Figure S7**).

Validation of the m6A Score in an External Cohort

The prognostic value of m6A score was further validated in an external cohort from the Tianjin Medical University Cancer Institute and Hospital. As shown in **Figure 3E**, patients with low m6A scores showed significantly poorer survival compared to the ones with high m6A scores (p=0.0026). We then compared the genetic mutations of patients with low and high m6A scores in our own cohort. Genes such as CREBBP, TNFRSF14 and CARD11 were more frequently altered in the low m6A score group, while genes such as BCL2, ARID1A and ATP6V1B2 were greatly and often times mutated in the high m6A score group (**Figure 3F**). In addition, BCL6, ATP6AP1 and GNAI2 carried much frequent mutations in patients with low m6A scores, but in none of the patients with high m6A scores. Genes such as DTX1, RRAGC, MEF2B, EP300, NOTCH2, BCL7A, FOXO1, KMT2C and NOTCH3 were exclusively mutated in the high m6A score group (**Figure 3F**). Of note, research studies have shown that CREBBP is a key transcriptional regulator of Treg differentiation (37) and HVEM delivers a co-inhibitory signal to T cells through binding to BTLA (38), both these suggesting frequently mutated

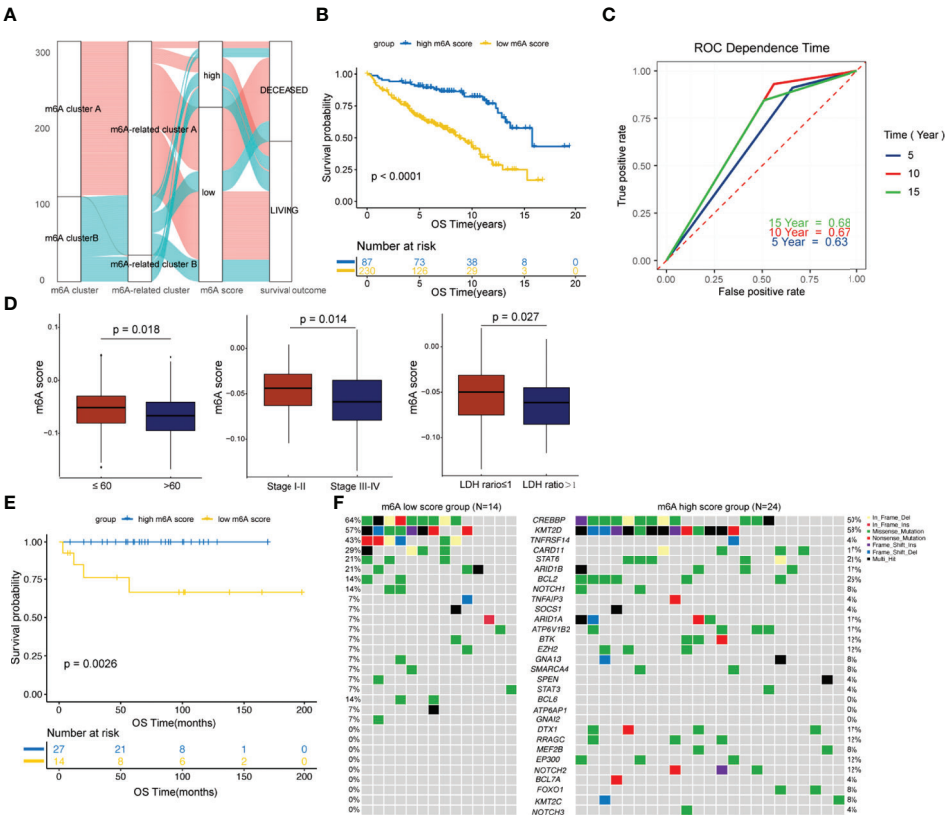

FIGURE 3 | Development and validation of the m6A score. **(A)** Alluvial diagram showing the changes in m6A clusters, m6A-related clusters and m6A scores. **(B)** Comparison of survival curves between the high and low m6A score groups by the log-rank test. **(C)** The predictive value of the m6A score for survival evaluated by time-dependent ROC curves. **(D)** Differences in the m6A score among distinct clinical subgroups. **(E)** Validation of the prognostic value of the m6A score in an external cohort. **(F)** The waterfall plot depicted tumor somatic mutations of patients with low and high m6A scores in the external cohort.

genes in the low m6A score group may mediate negatively regulate immune response.

Differences in Infiltrating Immune Cells Between the m6A Score Groups

Previous studies have demonstrated that m6A modification plays important roles in the TME (18–20). We then specifically examined the connection between the m6A score and the immune cells' infiltrating levels. The relative abundance of six main immune cell subtypes was evaluated by TIMER (32). We found that the m6A scores were proportional to the extent of infiltration of macrophages (p=0.002) and $CD4^+$ T cells (p<0.001) (**Figure 4A**). However, the m6A scores displayed a markedly inverse correlation with the infiltrationin levels of myeloid dendritic cells (p<0.001) and $CD8^+$ T cells (p<0.001) (**Figure 4A**). Furthermore, the high m6A score group was observably enriched in infiltrating macrophages and $CD4^+$ T cells, while the low m6A score group was prominently enriched in infiltrating myeloid dendritic cells and $CD8^+$ T cells (**Figure 4B**). These findings suggested that the m6A score could be used to differentiate between groups with different immune cell infiltration patterns.

The m6A Score Identified a Subset of Patients Harboring an Exhausted Immune Microenvironment

The observation that patients with low m6A scores presented high infiltration of $CD8^+$ T cells but had inferior OS was particularly intriguing, as increased infiltration levels of $CD8^+$ T cells are usually linked to good survival. We hypothesized that these $CD8^+$ T cells were exhausted T cells. The expression of PD-1 is the hallmark of exhausted T cells (39). Considering the lack of PD-1 expression data in the GSE16131 cohort, we chose the GSE119214 cohort to further analyze the immune characteristics. First, we evaluated the differences in immune responses between the high and low m6A score groups. GSVA showed that immune-associated biological processes, including T-cell receptor signaling, B-cell receptor signaling and FC gamma R-mediated phagocytosis, were significantly enhanced in patients with low m6A scores (adjusted p<0.05; **Figure 5A**). CD8A, GZMB, IFNG, TBX2 and TNF were considered to be involved in the immune/inflammatory responses according to published literature (19). A significantly upregulated expression of these genes was observed in the low m6A score group (**Figure 5B**). T cells constitute an important component of the

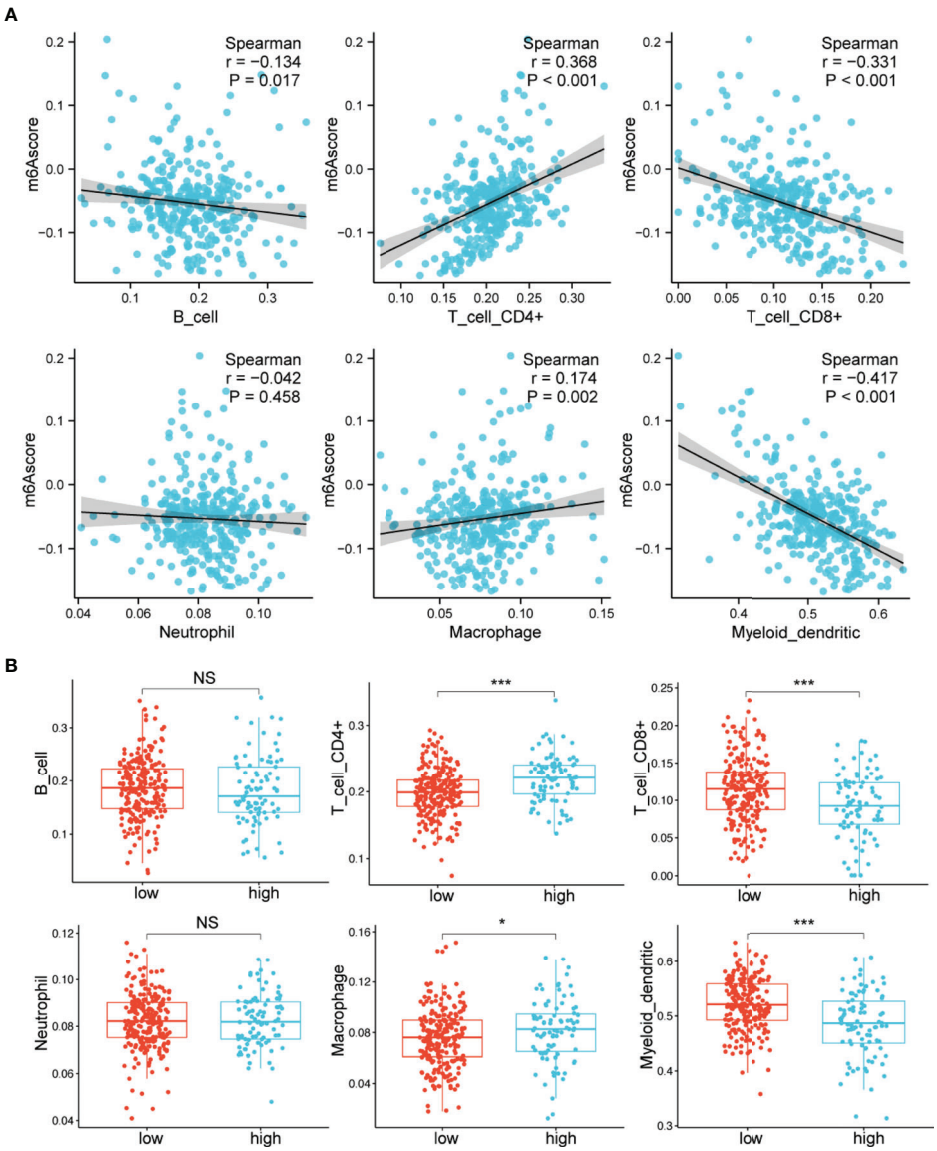

FIGURE 4 | Relationships between the m6A score and infiltrating immune cells. **(A)** Correlations between the m6A score and the degree of immune cell infiltration by Spearman analysis. **(B)** Comparison of the relative abundance of infiltrating immune cells between the high and low m6A score groups. NS, not significant; *p < 0.05; ***p < 0.001.

antitumor immune cell brigade. We then used ImmuCellAI (33) to evaluate the infiltration degree of distinct T cell subtypes. As expected, we found that exhausted T cells were markedly enriched in the low m6A score group (**Figure 5C**). Moreover, the expression of PD-1 and PD-L1 in the low m6A score group was significantly increased than that in the high m6A score group (**Figures 5D, E**). In addition, GSEA demonstrates that the low m6A score group showed an enhanced IFN-γ response (**Figure 5F**). Persistent activation of IFN-γ signaling can directly upregulate the expression of PD-L1 and activate the PD-1/PD-L1 signaling axis (40). Considered as a whole, the above results indicate that the immune and inflammatory responses were enhanced in the low m6A score group. However, the expression of PD-1 and PD-L1 was also upregulated in this group and induced an exhausted immune microenvironment, ultimately leading to a poor prognosis in FL patients.

Predicting the Response to Anti-PD-L1 Therapy Using the m6A Score

Immunotherapies with anti-PD-L1 antibodies have shown great success in many types of cancer. Patients with abundant $CD8^+$ T

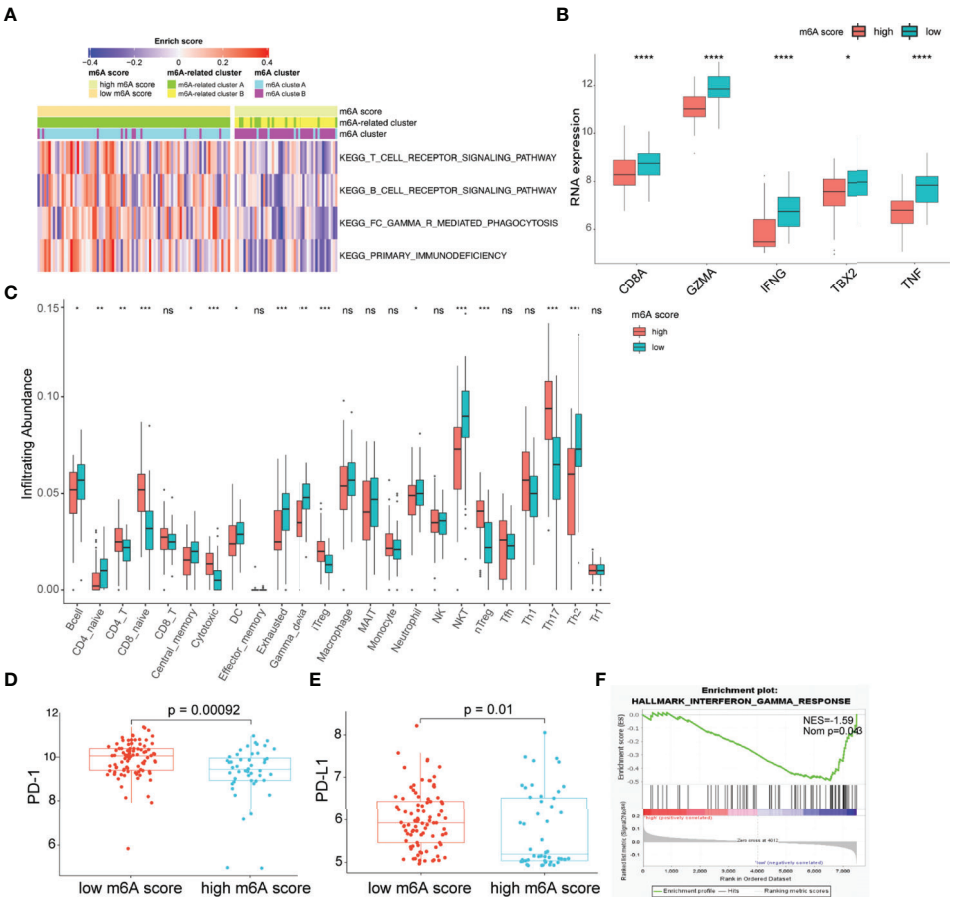

FIGURE 5 | Characteristics of the TME between the high and low m6A score groups. **(A)** Heatmap showing differences in the immune-associated biological pathways between m6A score groups (adjusted p-value<0.05). **(B)** Differences in inflammatory/immune response-associated genes between m6A score groups. **(C)** Differences in the relative abundance of infiltrating immune cells between m6A score groups. **(D, E)** Differences in the expression of PD-1 **(D)** and PD-L1 **(E)** between m6A score groups. **(F)** The interferon-gamma response is enriched in the low m6A score group by GSEA. TME, tumor microenvironment; NES, normalized enrichment score; NOM p, nominal p-value; NS, not significant; *p < 0.05; **p < 0.01; ***p < 0.001; ****p < 0.0001.

cell infiltration as well as high PD-1/PD-L1 expression are more likely to benefit from anti-PD-L1 therapy. Herein, we hypothesized that the m6A score may predict a patient's response to anti-PD-L1 therapy. Given the lack of available data on FL patients receiving anti-PD-L1 therapy, we chose an external anti-PD-L1 cohort (IMvigor210) to explore the potential predictive value of the m6A score. Of the 354 patients, 298 were evaluated for an objective response. The detailed clinical information of patients and m6A scores calculated were showed in **Table S7**. We found that the m6A score presented a significant negative correlation with tumor neoantigen burden (p=0.001, **Figure 6A**). Moreover, low m6A score group displayed significantly clinical and survival benefits than high m6A score group (**Figures 6B–D**). Finally, we compared the performance of m6A score with other predictive biomarkers. We found that the m6A score has a slight advantage over TIS and TIDE. The area under the ROC curve for m6A score, TIDE, TIS and PD-L1 expression on tumor cells was 0.60, 0.58, 0.58 and 0.49 respectively (**Figure 6E**).

DISCUSSION

Epigenetic deregulation is critical to the tumorigenesis of FL (4, 5). Genetic alterations involved in the posttranslational modification of histones, such as the histone methyltransferases KMT2D and KMT2C and the histone acetyltransferases CREBBP and EP300, frequently occur in FL (4). However, the role of m6A methylation, as the most frequent posttranscriptional mRNA modification, is less known in FL.

Specific m6A-regulators have specific carcinogenic properties that vary in various tumors. Some serve as tumor inhibitors, but others serve as tumor promoters. Hence, an integrated and comprehensive analysis of m6A-regulators is needed. In this study, we identified two m6A clusters, which was significantly associated with distinct carcinogenic processes and could be used to predict the prognosis of FL patients. Moreover, m6A-related clusters were constructed to comprehensively characterize the underlying biological differences between m6A clusters. The m6A score, a quantification model, was further developed to

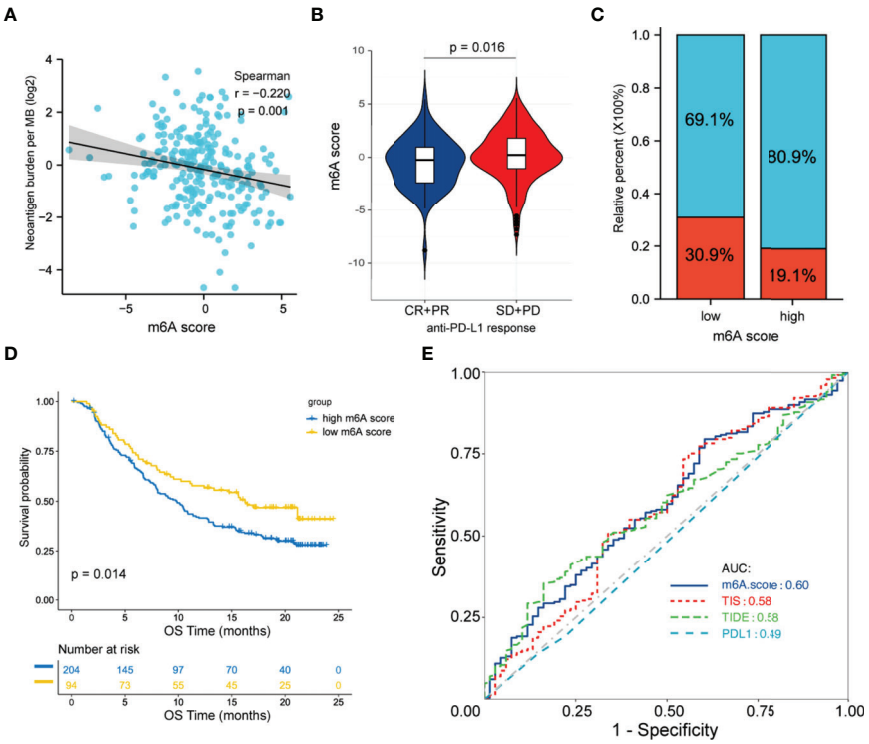

FIGURE 6 | Predictive value of the m6A score for anti-PD-L1 therapy in the IMvigor210CoreBiologies cohort. **(A)** Correlation between the m6A score and tumor neoantigen burden by Spearman analysis. **(B)** Differences in the m6A score between patients with different clinical responses. **(C)** Proportion of patients with clinical response in the low and high m6A score groups. **(D)** Survival analysis between m6A score groups by the log-rank test. **(E)** ROC curve analysis for m6A score, TIDE, TIS and PD-L1 expression on tumor cells in predicting the response to anti-PD-L1 therapy. ROC, receiver operating characteristic; TIDE, tumor immune dysfunction and exclusion; TIS, tumor inflammation signature.

reflect the synthetic cross-talk of m6A modification. Low m6A scores were significantly associated with poorer patient survival than high m6A scores.

The role of m6A modification in the TME has been largely investigated (18–20). m6A-regulators showed either a positive or negative correlation with the level of immune cell infiltration regardless of their categorization as a "writer", "reader", or "eraser" (19). The TME usually represents a major obstacle that restricts the anti-tumor immune responses and limits the efficacy of immunotherapeutic agents. FL is characterized by high infiltration of T-cell subpopulations (5). Here, we observed that patients with high m6A scores had enhanced $CD4^+$ T cell infiltration, and those with low m6A scores had enhanced $CD8^+$ T cell infiltration. Moreover, the low m6A score group harbored enriched immune and inflammatory responses. Nevertheless, PD-1/PD-L1 signaling was also activated and subverted the antitumor response of cytotoxic $CD8^+$ T cells, which promoted immune escape. Ultimately, this exhausted TME led to an inferior prognosis in patients with low m6A scores.

PD-1/PD-L1 signaling blockade reverses local immunosuppression. Clinical responses to PD-1/PD-L1 inhibitors occur most often in patients with rich but exhausted immune cell infiltration (41–43). Patients with low m6A scores represent a subset of candidates who might benefit from anti-PD-1/PD-L1 immunotherapy. Anti-PD-1 antibody response rates in unselected FL patients have been lower than expected (44). Our study first uncovered the prediction of immunotherapy response that could be attributed to m6A modification in FL. What is worth mentioning is that the m6A score shows effective predictive ability in immune response in a solid tumor cohort, although it was developed from FL patients. Hence, the application of m6A score in predicting immune efficacy may be extended to pan-cancers. More studies are urgently needed to validate this finding.

m6A modification is a reversible and dynamic process; targeting m6A-regulators to change m6A modification patterns and further reshaping the adverse cell infiltration characteristics in TME may enhance the efficacy of immunotherapy. A preclinical study by Han D and colleagues showed that Ythdf1-deficient mice presented an elevated $CD8^+$ T cell antitumor immune response, and the effectiveness of PD-L1 inhibition therapy was improved in these mice. This result indicates that YTHDF1 is a potential treatment target and that combination therapies can increase immunotherapy efficacy (45). A variety of small-molecule drugs targeting m6A-regulators have been studied, although the clinical applications of these drugs still need further development (46–48). Our study provides a new

insight into the combination therapy strategies targeting m6A modification and immunotherapy to improve FL patients' clinical responses.

In conclusion, our study demonstrated that m6A-regulator expression signatures were characterized by significant differences in the immune landscape of FL. The m6A score identified a subset of FL harboring an exhausted tumor microenvironment and may contribute to personalized immunotherapy strategies making in patients with FL.

DATA AVAILABILITY STATEMENT

The original contributions presented in the study are publicly available. This data can be found here: https://db.cngb.org/search/project/CNP0002472/ and https://db.cngb.org/search/project/CNP0002473/.

ETHICS STATEMENT

The studies involving human participants were reviewed and approved by the Clinical Research Ethics Board of the Tianjin Medical University Cancer Institute and Hospital. The patients/participants provided their written informed consent to participate in this study.

AUTHOR CONTRIBUTIONS

XW conceived and designed the study. XW and HZ supervised all aspects of the research project and interpreted the data. TZ and HL performed the research and statistical and bioinformatics analyses. TZ, FG, and YC collected data and prepared the images. JH, LL, LQ, ZQ, and SZ analyzed clinical information. WG and BM provided some suggestions about FL classifications. XR provided technical support. TZ wrote the manuscript and finalized the figures. XW and HZ reviewed the manuscript. All authors contributed to the article and approved the submitted version.

FUNDING

This study was supported by grants from the Natural Science Foundation of Tianjin (19JCYBJC26500), the National Natural Science Foundation of China (81770213), the Clinical Oncology Research Fund of CSCO (Y-XD2019-162, Y-Roche20192-0097), and the National Human Genetic Resources Sharing Service Platform/Cancer Biobank of Tianjin Medical University Cancer Institute and Hospital grant (2005DKA21300).

ACKNOWLEDGMENTS

The authors thank Beijing Gap Technology Co., Ltd for providing technical assistance and insightful suggestions for this study.

SUPPLEMENTARY MATERIAL

The Supplementary Material for this article can be found online at: https://www.frontiersin.org/articles/10.3389/fimmu.2022.922471/full#supplementary-material

Supplementary Figure 1 | Flowchart of the study design. FL, follicular lymphoma; DLBCL, diffuse large B cell lymphoma; OS, overall survival; TMUCH, Tianjin Medical University Cancer Institute and Hospital.

Supplementary Figure 2 | The interactions among 16 m6A-regulators in follicular lymphoma. **(A)** Chromosomal distribution of 16 m6A-regulator genes. **(B)** Pairwise correlation of 16 m6A-regulators by Spearman analysis. Red (blue) indicates positive (negative) correlations. *p < 0.05; **p < 0.01; ***p < 0.001. **(C)** Protein-protein interaction among the 16 m6A-regulators.

Supplementary Figure 3 | Identification of consensus clusters by 16 m6A-regulators. **(A)** Consensus clustering matrices for k = 3 to 10. **(B)** Relative change in the area under the cumulative distribution function curve.

Supplementary Figure 4 | Forest plot shows the 20 prognostic genes used to construct the m6A scoring model.

Supplementary Figure 5 | Distribution of the m6A score between the m6A clusters and m6A-related clusters. ****p < 0.0001.

Supplementary Figure 6 | Distribution of the m6A score, overall survival, overall survival status and heatmap of the 20 prognostic genes used to construct the m6A scoring model.

Supplementary Figure 7 | The prognostic value of the m6A score in the cohort GES16131 **(A)** and GSE119214 **(B)**.

REFERENCES

1. Guidelines for the Diagnosis and Treatment of Follicular Lymphoma in China. *Cancer Biol Med* (2013) 10(1):36–42. doi: 10.7497/j.issn.2095-3941.2013.01.006
2. Casulo C, Byrtek M, Dawson KL, Zhou X, Farber CM, Flowers CR, et al. Early Relapse of Follicular Lymphoma After Rituximab Plus Cyclophosphamide, Doxorubicin, Vincristine, and Prednisone Defines Patients at High Risk for Death: An Analysis From the National LymphoCare Study. *J Clin Oncol* (2015) 33(23):2516–22. doi: 10.1200/JCO.2014.59.7534
3. Maurer MJ, Ghesquieres H, Ansell SM, Thompson CA, Nowakowski GS, Inwards DJ, et al. Event-Free Survival at 12 Months (EFS12) From Diagnosis Is a Robust Endpoint for Disease-Related Survival in Patients With Follicular Lymphoma in the Immunochemotherapy Era. *Blood* (2014) 124(21):1664–4. doi: 10.1182/blood.V124.21.1664.1664
4. Green MR. Chromatin Modifying Gene Mutations in Follicular Lymphoma. *Blood* (2018) 131(6):595–604. doi: 10.1182/blood-2017-08-737361
5. Huet S, Sujobert P, Salles G. From Genetics to the Clinic: A Translational Perspective on Follicular Lymphoma. *Nat Rev Cancer* (2018) 18(4):224–39. doi: 10.1038/nrc.2017.127
6. Lee M, Kim B, Kim VN. Emerging Roles of RNA Modification: M(6)A and U-Tail. *Cell* (2014) 158(5):980–7. doi: 10.1016/j.cell.2014.08.005
7. Wang X, Lu Z, Gomez A, Hon GC, Yue Y, Han D, et al. N6-Methyladenosine-Dependent Regulation of Messenger RNA Stability. *Nature* (2014) 505(7481):117–20. doi: 10.1038/nature12730

8. Wang X, Zhao BS, Roundtree IA, Lu Z, Han D, Ma H, et al. N(6)-Methyladenosine Modulates Messenger RNA Translation Efficiency. *Cell* (2015) 161(6):1388–99. doi: 10.1016/j.cell.2015.05.014
9. Xiao W, Adhikari S, Dahal U, Chen YS, Hao YJ, Sun BF, et al. Nuclear M(6)A Reader YTHDC1 Regulates mRNA Splicing. *Mol Cell* (2016) 61(4):507–19. doi: 10.1016/j.molcel.2016.01.012
10. Roundtree IA, Luo GZ, Zhang Z, Wang X, Zhou T, Cui Y, et al. YTHDC1 Mediates Nuclear Export of N(6)-Methyladenosine Methylated mRNAs. *Elife* (2017) 6:e31311. doi: 10.7554/eLife.31311
11. Wei W, Ji X, Guo X, Ji. S. Regulatory Role of N(6) -Methyladenosine (M(6) A) Methylation in RNA Processing and Human Diseases. *J Cell Biochem* (2017) 118(9):2534–43. doi: 10.1002/jcb.25967
12. Vu LP, Pickering BF, Cheng Y, Zaccara S, Nguyen D, Minuesa G, et al. The N (6)-Methyladenosine (M(6)A)-Forming Enzyme METTL3 Controls Myeloid Differentiation of Normal Hematopoietic and Leukemia Cells. *Nat Med* (2017) 23(11):1369–76. doi: 10.1038/nm.4416
13. Weng H, Huang H, Wu H, Qin X, Zhao BS, Dong L, et al. METTL14 Inhibits Hematopoietic Stem/Progenitor Differentiation and Promotes Leukemogenesis *via* mRNA M(6)A Modification. *Cell Stem Cell* (2018) 22 (2):191–205.e199. doi: 10.1016/j.stem.2017.11.016
14. Barbieri I, Tzelepis K, Pandolfini L, Shi J, Millán-Zambrano G, Robson SC, et al. Promoter-Bound METTL3 Maintains Myeloid Leukaemia by M(6)A-Dependent Translation Control. *Nature* (2017) 552(7683):126–31. doi: 10.1038/nature24678
15. Ma H, Shen L, Yang H, Gong H, Du X, Li J. M6a Methyltransferase Wilms' Tumor 1-Associated Protein Facilitates Cell Proliferation and Cisplatin Resistance in NK/T Cell Lymphoma by Regulating Dual-Specificity Phosphatases 6 Expression *via* M6a RNA Methylation. *IUBMB Life* (2021) 73(1):108–17. doi: 10.1002/iub.2410
16. Cheng Y, Fu Y, Wang Y, Wang J. The M6a Methyltransferase METTL3 Is Functionally Implicated in DLBCL Development by Regulating M6a Modification in PEDF. *Front Genet* (2020) 11:955. doi: 10.3389/fgene.2020.00955
17. Shulman Z, Stern-Ginossar N. The RNA Modification N(6)-Methyladenosine as a Novel Regulator of the Immune System. *Nat Immunol* (2020) 21(5):501–12. doi: 10.1038/s41590-020-0650-4
18. Wang YN, Yu CY, Jin HZ. RNA N(6)-Methyladenosine Modifications and the Immune Response. *J Immunol Res* (2020) 2020:6327614. doi: 10.1155/2020/6327614
19. Zhang B, Wu Q, Li B, Wang D, Wang L, Zhou YL. M(6)A Regulator-Mediated Methylation Modification Patterns and Tumor Microenvironment Infiltration Characterization in Gastric Cancer. *Mol Cancer* (2020) 19(1):53. doi: 10.1186/s12943-020-01170-0
20. Zhong J, Liu Z, Cai C, Duan X, Deng T, Zeng G. M(6)A Modification Patterns and Tumor Immune Landscape in Clear Cell Renal Carcinoma. *J Immunother Cancer* (2021) 9(2):e001646. doi: 10.1136/jitc-2020-001646
21. Zaccara S, Ries RJ, Jaffrey. Reading SR. Writing and Erasing mRNA Methylation. *Nat Rev Mol Cell Biol* (2019) 20(10):608–24. doi: 10.1038/s41580-019-0168-5
22. Johnson WE, Li C, Rabinovic A. Adjusting Batch Effects in Microarray Expression Data Using Empirical Bayes Methods. *Biostatistics* (2007) 8 (1):118–27. doi: 10.1093/biostatistics/kxj037
23. Wilkerson MD, Hayes DN. ConsensusClusterPlus: A Class Discovery Tool With Confidence Assessments and Item Tracking. *Bioinformatics* (2010) 26 (12):1572–3. doi: 10.1093/bioinformatics/btq170
24. Hänzelmann S, Castelo R, Guinney J. GSVA: Gene Set Variation Analysis for Microarray and RNA-Seq Data. *BMC Bioinf* (2013) 14:7. doi: 10.1186/1471-2105-14-7
25. Subramanian A, Tamayo P, Mootha VK, Mukherjee S, Ebert BL, Gillette MA, et al. Gene Set Enrichment Analysis: A Knowledge-Based Approach for Interpreting Genome-Wide Expression Profiles. *Proc Natl Acad Sci USA* (2005) 102(43):15545–50. doi: 10.1073/pnas.0506580102
26. Mootha VK, Lindgren CM, Eriksson KF, Subramanian A, Sihag S, Lehar J, et al. PGC-1alpha-Responsive Genes Involved in Oxidative Phosphorylation Are Coordinately Downregulated in Human Diabetes. *Nat Genet* (2003) 34 (3):267–73. doi: 10.1038/ng1180
27. Ritchie ME, Phipson B, Wu D, Hu Y, Law CW, Shi W, et al. Limma Powers Differential Expression Analyses for RNA-Sequencing and Microarray Studies. *Nucleic Acids Res* (2015) 43(7):e47. doi: 10.1093/nar/gkv007
28. Li H, Durbin. Fast R. And Accurate Long-Read Alignment With Burrows-Wheeler Transform. *Bioinformatics* (2010) 26(5):589–95. doi: 10.1093/bioinformatics/btp698
29. Danecek P, Bonfield JK, Liddle J, Marshall J, Ohan V, Pollard MO, et al. Twelve Years of SAMtools and BCFtools. *Gigascience* (2021) 10(2):giab008. doi: 10.1093/gigascience/giab008
30. McKenna A, Hanna M, Banks E, Sivachenko A, Cibulskis K, Kernytsky A, et al. The Genome Analysis Toolkit: A MapReduce Framework for Analyzing Next-Generation DNA Sequencing Data. *Genome Res* (2010) 20(9):1297–303. doi: 10.1101/gr.107524.110
31. Wang K, Li M, H Hakonarson. ANNOVAR: Functional Annotation of Genetic Variants From High-Throughput Sequencing Data. *Nucleic Acids Res* (2010) 38(16):e164. doi: 10.1093/nar/gkq603
32. Becht E, Giraldo NA, Lacroix L, Buttard B, Elarouci N, Petitprez F, et al. Estimating the Population Abundance of Tissue-Infiltrating Immune and Stromal Cell Populations Using Gene Expression. *Genome Biol* (2016) 17 (1):218. doi: 10.1186/s13059-016-1070-5
33. Miao YR, Zhang Q, Lei Q, Luo M, Xie GY, Wang H, et al. ImmuCellAI: A Unique Method for Comprehensive T-Cell Subsets Abundance Prediction and Its Application in Cancer Immunotherapy. *Adv Sci (Weinh)* (2020) 7 (7):1902880. doi: 10.1002/advs.201902880
34. Mariathasan S, Turley SJ, Nickles D, Castiglioni A, Yuen K, Wang Y, et al. Tgfβ Attenuates Tumour Response to PD-L1 Blockade by Contributing to Exclusion of T Cells. *Nature* (2018) 554(7693):544–8. doi: 10.1038/nature25501
35. Jiang P, Gu S, Pan D, Fu J, Sahu A, Hu X, et al. Signatures of T Cell Dysfunction and Exclusion Predict Cancer Immunotherapy Response. *Nat Med* (2018) 24(10):1550–8. doi: 10.1038/s41591-018-0136-1
36. Ayers M, Lunceford J, Nebozhyn M, Murphy E, Loboda A, Kaufman DR, et al. IFN-Gamma-Related mRNA Profile Predicts Clinical Response to PD-1 Blockade. *J Clin Invest* (2017) 127(8):2930–40. doi: 10.1172/JCI91190
37. Castillo J, Wu E, Lowe C, Srinivasan S, McCord R, Wagle MC, et al. CBP/p300 Drives the Differentiation of Regulatory T Cells Through Transcriptional and Non-Transcriptional Mechanisms. *Cancer Res* (2019) 79(15):3916–27. doi: 10.1158/0008-5472.CAN-18-3622
38. Murphy KM, Nelson CA, Sedý JR. Balancing Co-Stimulation and Inhibition With BTLA and HVEM. *Nat Rev Immunol* (2006) 6(9):671–81. doi: 10.1038/nri1917
39. Wherry EJ, Kurachi M. Molecular and Cellular Insights Into T Cell Exhaustion. *Nat Rev Immunol* (2015) 15(8):486–99. doi: 10.1038/nri3862
40. Abiko K, Matsumura N, Hamanishi J, Horikawa N, Murakami R, Yamaguchi K, et al. IFN-γ From Lymphocytes Induces PD-L1 Expression and Promotes Progression of Ovarian Cancer. *Br J Cancer* (2015) 112(9):1501–9. doi: 10.1038/bjc.2015.101
41. Binnewies M, Roberts EW, Kersten K, Chan V, Fearon DF, Merad M, et al. Understanding the Tumor Immune Microenvironment (TIME) for Effective Therapy. *Nat Med* (2018) 24(5):541–50. doi: 10.1038/s41591-018-0014-x
42. Galon J, Bruni D. Approaches to Treat Immune Hot, Altered and Cold Tumours With Combination Immunotherapies. *Nat Rev Drug Discov* (2019) 18(3):197–218. doi: 10.1038/s41573-018-0007-y
43. Gajewski TF, Corrales L, Williams J, Horton B, Sivan A, Spranger S. Cancer Immunotherapy Targets Based on Understanding the T Cell-Inflamed Versus Non-T Cell-Inflamed Tumor Microenvironment. *Adv Exp Med Biol* (2017) 1036:19–31. doi: 10.1007/978-3-319-67577-0_2
44. Lesokhin AM, Ansell SM, Armand P, Scott EC, Halwani A, Gutierrez M, et al. Nivolumab in Patients With Relapsed or Refractory Hematologic Malignancy: Preliminary Results of a Phase Ib Study. *J Clin Oncol* (2016) 34(23):2698–704. doi: 10.1200/JCO.2015.65.9789
45. Han D, Liu J, Chen C, Dong L, Liu Y, Chang R, et al. Anti-Tumour Immunity Controlled Through mRNA M(6)A Methylation and YTHDF1 in Dendritic Cells. *Nature* (2019) 566(7743):270–4. doi: 10.1038/s41586-019-0916-x
46. Qiao Y, Zhou B, Zhang M, Liu W, Han Z, Song C, et al. A Novel Inhibitor of the Obesity-Related Protein FTO. *Biochemistry* (2016) 55(10):1516–22. doi: 10.1021/acs.biochem.6b00023
47. Xu C, Liu K, Tempel W, Demetriades M, Aik W, Schofield CJ, et al. Structures of Human ALKBH5 Demethylase Reveal a Unique Binding Mode for Specific Single-Stranded N6-Methyladenosine RNA Demethylation. *J Biol Chem* (2014) 289(25):17299–311. doi: 10.1074/jbc.M114.550350

48. Chen B, Ye F, Yu L, Jia G, Huang X, Zhang X, et al. Development of Cell-Active N6-Methyladenosine RNA Demethylase FTO Inhibitor. *J Am Chem Soc* (2012) 134(43):17963–71. doi: 10.1021/ja3064149

Conflict of Interest: The authors declare that the research was conducted in the absence of any commercial or financial relationships that could be construed as a potential conflict of interest.

Publisher's Note: All claims expressed in this article are solely those of the authors and do not necessarily represent those of their affiliated organizations, or those of the publisher, the editors and the reviewers. Any product that may be evaluated in this article, or claim that may be made by its manufacturer, is not guaranteed or endorsed by the publisher.

frontiers | Frontiers in Immunology

ORIGINAL RESEARCH
published: 15 June 2022
doi: 10.3389/fimmu.2022.904693

Fucosylation Promotes Cytolytic Function and Accumulation of NK Cells in B Cell Lymphoma

Xing Tong[1,2,3,4†], Yuhua Ru[1,2,3†], Jianhong Fu[1,2,3†], Ying Wang[1,2,3†], Jinjin Zhu[1,2,3], Yiyang Ding[1,2,3], Fulian Lv[1,2,3], Menglu Yang[1,2,3], Xiya Wei[1,2,3], Chenchen Liu[1,2,3], Xin Liu[1,2,3], Lei Lei[1,2,3], Xiaojin Wu[1,2,3], Lingchuan Guo[4], Yang Xu[1,2,3], Jie Li[5], Peng Wu[5], Huanle Gong[1,2,3*], Jia Chen[1,2,3*] and Depei Wu[1,2,3*]*

[1] National Clinical Research Center for Hematologic Diseases, Jiangsu Institute of Hematology, The First Affiliated Hospital of Soochow University, Suzhou, China, [2] Institute of Blood and Marrow Transplantation, Collaborative Innovation Center of Hematology, Soochow University, Suzhou, China, [3] Key Laboratory of Stem Cells and Biomedical Materials of Jiangsu Province and Chinese Ministry of Science and Technology, Suzhou, China, [4] Department of Pathology, The First Affiliated Hospital of Soochow University, Suzhou, China, [5] Department of Molecular Medicine, The Scripps Research Institute, La Jolla, CA, United States

Natural killer (NK) cells have been demonstrated as a promising cellular therapy as they exert potent anti-tumor immune responses. However, applications of NK cells to tumor immunotherapy, especially in the treatment of advanced hematopoietic and solid malignancies, are still limited due to the compromised survival and short persistence of the transferred NK cells *in vivo*. Here, we observed that fucosyltransferase (FUT) 7 and 8 were highly expressed on NK cells, and the expression of CLA was positively correlated with the accumulation of NK cells in clinical B cell lymphoma development. *Via* enzyme-mediated *ex vivo* cell-surface fucosylation, the cytolytic effect of NK cells against B cell lymphoma was significantly augmented. Fucosylation also promoted NK cell accumulation in B cell lymphoma-targeted tissues by enhancing their binding to E-selectin. Moreover, fucosylation of NK cells also facilitated stronger T cell anti-tumor immune responses. These findings suggest that *ex vivo* fucosylation contributes to enhancing the effector functions of NK cells and may serve as a novel strategy for tumor immunotherapy.

Keywords: fucosylation, NK cells, lymphoma, tumor immunotherapy, graft-versus-tumor effect

OPEN ACCESS

Edited by:
Wei Sang,
The Affiliated Hospital of Xuzhou Medical University, China

Reviewed by:
Jianhua Yu,
City of Hope National Medical Center, United States
Wenbin Qian,
Zhejiang University, China
Shimin Zhang,
Joint Pathology Center (JPC), United States

****Correspondence:***
Peng Wu
pengwu@scripps.edu
Huanle Gong
happy_kung@163.com
Jia Chen
drchenjia@163.com
Depei Wu
drwudepei@163.com

†These authors have contributed equally to this work

Specialty section:
This article was submitted to Cancer Immunity and Immunotherapy, a section of the journal Frontiers in Immunology

Received: *25 March 2022*
Accepted: *11 May 2022*
Published: *15 June 2022*

Citation:
Tong X, Ru Y, Fu J, Wang Y, Zhu J, Ding Y, Lv F, Yang M, Wei X, Liu C, Liu X, Lei L, Wu X, Guo L, Xu Y, Li J, Wu P, Gong H, Chen J and Wu D (2022) Fucosylation Promotes Cytolytic Function and Accumulation of NK Cells in B Cell Lymphoma. Front. Immunol. 13:904693. doi: 10.3389/fimmu.2022.904693

INTRODUCTION

Allogeneic hematopoietic stem cell transplantation (allo-HSCT) is one of the most curative therapies for malignant hematological diseases, predominantly in lymphoma and leukemia, for their potent graft-versus-tumor (GVT) effects. B cell acute lymphoblastic leukemia (B-ALL), an advanced B-cell malignancy, has a high relapse rate and poor prognosis after allo-HSCT (1). Subsequently, second transplantation provides long-term overall survival for 10%-40% of patients (2). Donor-derived T cells exhibit anti-tumor activities, whilst they can also induce graft-versus-host disease (GVHD), which has a significant impact on patients' morbidity and mortality. New therapeutic strategies are needed to separate GVT and GVHD. Natural killer (NK) cells preserve

critical GVT effects without aggravating GVHD (3). NK cells not only play a direct role in killing viruses and tumors but also act as a regulatory cell to mediate adaptive immune response by interacting with T cells, macrophages, dendritic cells (DCs), and endothelial cells (4). Although NK cell infusion has emerged as a promising immunotherapy for the treatment of hematologic malignancies, it is still limited due to their short lifespan and poor infiltration in solid tumors (5). The ability of immune cells to traffic to the tumor site usually relies on their robust binding to selectin, especially E-selectin (CD62E) expressed on activated endothelial cells (6). E-selection ligand, cutaneous lymphocyte antigen (CLA) must be sialofucosylated and presents the sialyl Lewis X (sLe^X) epitope (7, 8). A straightforward glycan engineering approach based on exploiting α1,3-fucosyltransferase to transfer fucose residues from the guanosine diphosphate-fucose (GDP-fucose) donor onto the cell-surface α-2,3-sialyllactosamine acceptor substrate has been demonstrated effective and efficient to enforce sLe^X display in cell surface (9, 10). On the other hand, *ex vivo* cytokines pre-activation and genetically modification have been proven for promoting NK cell activity and infiltration (11, 12). Efforts are enforced to exploit the proliferation and migration of NK cells to generate potent anti-tumor properties.

Recent studies revealed that fucosylation play critical roles in the regulation of the development, functions, and trafficking of immune cells (13–15). For example, Diego et al. reported that *ex vivo* enforced sialofucosylation enhanced E-selectin binding of the modified CD19-CAR T cells, as well as their activity and homing to bone marrow (16). Likewise, Wu and coworkers also demonstrated that *ex vivo* fucosylation of NK-92MI cells to create the E-selectin ligand sLe^X on the cell surface promoted NK trafficking to bone marrow (17). However, the specific role and mechanism of fucosylation in modulating the NK cell-mediated anti-tumor immune response remains largely unexplored.

In this study, we discovered that NK cells were highly fucosylated and fucosylation was positively correlated with the infiltration of NK cells into the tumor microenvironment in B cell lymphomas. Fucosylation significantly promoted the cytolytic effect and the accumulation of NK cells. These findings suggest that *ex vivo* fucosylation contributes to enhanced effector functions of NK cells, which could be a novel strategy for tumor immunotherapy.

MATERIALS AND METHODS

Animals

Female BALB/c (H2-Kd) and C57BL/6 CD45.2 (H2-Kb) mice were purchased from Shanghai Laboratory Animal Center (Shanghai, China). C57BL/6 CD45.1 (H2-Kb) mice were obtained from Beijing Vital River Laboratory Animal Technology Co. Ltd (Beijing, China). All mice used were aged 6-8 weeks and housed in a specific-pathogen-free environment and received acidified autoclaved water at Animal Facilities of Soochow University. All animal experiments were performed in accordance with the guidelines and approved by the Animal Care and Use Committee of Soochow University.

Cell Line

A20 cells line (BALB/c B cell lymphoma, H2-Kd) was purchased from American Type Culture Collection (Manassas, VA, USA). Luciferase-expressing A20 cells were generated by lentiviral system and sorted by flow cytometry (BD FACS Aria III, BD Bioscience, San Jose, CA, USA). Both of these cells were cultured with RPMI 1640 medium with 10% FBS at 37°C in a 5% CO_2 incubator.

GVT Model

Murine GVT model was established as previously described (18). Briefly, BALB/c recipients received lethal irradiation of 650cGy (X-Ray, 325cGy per dose with 4h interval) and were injected intravenously with 5×10^6 bone marrow (BM) cells from C57BL/6 mice together with 1×10^6 A20 lymphoma cells or 5×10^6 A20-*luc*$^+$/*yfp* cells, respectively. Survival of recipients were monitored daily.

Fucosylation and Generation of NK Cells

NK cells were generated from bone marrow of CD45.2 C57BL/6 mice or CD45.1 C57BL/6 mice as described previously (19). T cells in BM components were depleted by EasySep™ Mouse CD90.2 Positive Selection Kit (STEMCELL Technologies, Vancouver, BC, Canada). T cell depleted (TCD)-BM cells were incubated in fucosylation solution (40ug/ml α-1,3-fucosyltransferase and 100 μM GDP-fucose in phosphate-buffered saline with 0.5% FBS) for 30 min at room temperature and then cultured for 7 days in the presence of IL-2 and Indomethacin. The success of cell-surface fucosylation was characterized by the increased expression of sLe^X residues, as assessed by flow cytometry, using CLA, recognized by the monoclonal antibody HECA-452 (20). Purity of $CD3^-$ $NK1.1^+$ NK cells was >95%. NK cells were washed three times with PBS before transfer.

CFSE Labeling and *In Vivo* Proliferation Analysis

Donor NK cells were labeled with 5 mM CellTrace™ Violet Cell Proliferation kit (Invitrogen, Waltham, MA, USA) as described previously (19) and then transferred into tumor-bearing recipients. Four days post adoptive transfer, the proliferation of donor NK cells was analyzed by individual CTV generations.

Cytotoxicity Assay

Control or fucosylated NK cells and A20-*luc*$^+$/*yfp* cells were co-cultured in 96-well plates at different effector/target (E: T) ratios. After co-cultured for 6h, apoptosis of *yfp*$^+$ lymphoma cells were detected by Annexin V/PI Apoptosis Detection Kit (Vazyme, China). The cytotoxic activities of NK cells were represented by the apoptotic rates.

Flow Cytometric Analysis

Single cell suspensions from the spleen and liver were acquired according to the methods previously described (21) and analyzed using flow cytometry. Antibodies used for flow cytometry staining including Percp-Cy5.5-anti-mouse-CD45.1, APC-Cy7-anti-mouse-CD11b, Percp-Cy5.5-anti-mouse-NK1.1, BV650-

anti-mouse-H2-Kb were purchased from BD Bioscience (SanDiego, CA, USA); purified anti-mouse-CD16/32, APC-anti-mouseCD43, PE-anti-mouse-NKp46, APC-anti-mouse-CD107, FITC-anti-mouse-NKG2D, PE-anti-mouse-IFN-γ, PE/Cy7-anti-mouse-TNF-α, FITC-anti-mouse-CD62E, PE-anti-mouse-CD4, PE/Cy7-anti-mouse-CD44, APC/Cy7-anti-mouse-CD62L, Pacific Blue-anti-mouse-CD8a, FITC-anti-mouse-CD69 were purchased from Biolegend (San Diego, CA, USA); PE-Cy7-anti-mouse-Granzyme B, APC-anti-mouse-Perforin were purchased from eBioscience (San Diego, CA, USA). Recombinant Mouse E-Selectin, P-Selectin, and L-Selectin chimera were purchased from Biolegend (San Diego, CA, USA) for detecting the binding abilities. Samples were detected on a NovoCyte Flow Cytometer (ACEA Biosciences, San Diego, CA, USA) and data were analyzed by using Flowjo software (Flowjo, Ashland, OR, USA).

Single Cell RNA Sequencing Analysis

Single cell RNA sequencing (scRNA-seq) data were available in a previous study that deposited in the GEO database (NCBI) repository, accession number GSE182434 and normalized by R package "Seurat". After filtering cells with low numbers of total UMI counts, detected genes and low proportion of mitochondrial gene counts per cell, poor-quality cells were removed. Differential gene expression (DEG) testing was performed using the "FindMarkers" function in Seurat with a Wilcoxon test, and *p*-values were adjusted using Bonferroni correction. DEGs were filtered using a maximum adjusted *p*-value of 0.05. Enrichment analysis for the functions of the DEGs was conducted using the clusterProfiler (v3.12.0) R package and GSEApy (0.10.2) in Python3. Metascape (http://metascape.org/gp/index.html#/main/step1) was used to create gene ontology and cell type enrichment barplots using DGE of relevant groups. The gene sets were based on Gene Ontology terms in MSigDB, and all the gene sets with NESscores higher than 1 and a *p*-value less than 0.05 were included. scRNA-seq plots were generated using ggplot2 (v3.3.5). Cell interactions were performed by Cellphone DB.

Morphology and Immunohistochemistry

The tissue wax obtained from the Department of Pathology, The First Affiliated Hospital of Soochow University. Formalin-fixed, paraffin-embedded (FFPE) tissues was used for morphological examination *via* hematoxylin-eosin (H&E) staining. The following antibodies were applied on BenchMark XT automated immunostainer (Ventana Medical Systems, Tucson, AZ, USA) with Cell Conditioning 1 heat retrieval solution (Ventana Medical Systems, Tucson, AZ, USA): CD56 antibody (clone number: 123C3, Gene Tech, China; Ready-to-use), CD8 antibody (clone number: SP16, Gene Tech, China; Ready-to-use) and CLA (clone number: HECA-452, BioLegend, USA). IHC results of CD8, CD56 and CLA were calculated as IHC score by multiplying the percentage of positive cells (0 to 100, recorded in the increment by 5%) with mean intensity (0, no staining; 1, weak staining; 2, moderate staining; 3, strong staining), and given a range from 0 to 300. Two pathologists (Xing Tong and Lingchuan Guo) were independently responsible for evaluating the morphological and immunohistochemistry (IHC) results. The use of human samples was approved by the Ethical Committee of The First Affiliated Hospital of Soochow University and all patients provided signed informed consents.

Statistical Analysis

Data were analyzed using GraphPad Prism 9 software for Mac (GraphPad Software, San Diego, CA, USA). Unpaired Student's *t*-test was used to investigate statistical significance. The Kaplan-Meier curve was used to analyze the survival of allo-HSCT. $p < 0.05$ was considered statistically significant (*), less than 0.01 or 0.001 was shown as ** or ***, respectively. Data are presented as means ± SD.

RESULTS

Fucosylation Promoted Effector Functions of NK Cells in B Cell Lymphoma

To explore the role of immune cell fucosylation in B cell lymphomas pathophysiology, we first analyzed the expressions of individual fucosyltransferases in publicly available scRNA-seq database of 14 patients with diffuse large B cell lymphoma (DLBCL) and follicular lymphoma (FL) (22). We found that fucosyltransferases, including *FUT1, 2, 3, 5, 6, 9*, and *10* had extremely low expression levels on different immune cell subsets. *FUT4* was restrictedly expressed on monocytes and macrophages. Notably, *FUT7* was predominantly expressed on NK cells and plasma cells, which was responsible for α1,3 fucosylation to produce sLe^X. Similarly, we observed *FUT8*, a specific fucosyltransferase for α-1,6 core fucose, was highly expressed on NK cells (**Figure 1A**). These results indicated that fucosylation may have a potential function in anti-tumor immune responses regulated by NK cells during the pathogenesis of B cell lymphoma. We next performed gene-set enrichment analysis (GSEA) with KEGG (Kyoto Encyclopedia of Genes and Genomes) pathway analysis to investigate the functions of fucosylated NK cells. Interestingly, the expression patterns of genes known to be involved in 'nature killer cell mediated cytotoxicity' and 'regulation of leukocyte mediated immunity' were increased with fucosylation of NK cells (**Figure 1B**). Cell type analysis further enriched NK cell signatures (**Figure 1C**). Moreover, we also observed an elevated expression of NK effector genes including *KLRC1*, *KLRC3*, *KLRK1*, *BHLHE40*, *CD27* and down regulation of inhibitory molecules including *KLRB*, *KLRG1*, and *TIGIT* (**Figure 1D**). Interactions between different cell subsets played critical roles in anti-tumor responses. Given that NK cells and $CD8^+$ T cells are fundamental in anti-tumor immunity, we then performed cell-cell interaction analysis and calculated the numbers of receptor-ligand parings based on Cellphone DB to elucidate the redistribution of each kind of ligand-receptor interactions of fucosylated NK cells and T cells in B cell lymphoma (23). We observed interactions of cytokine receptors, immune checkpoints, and adhesion molecules between fucosylated NK cells and $CD8^+$ T cells in B cell lymphoma (**Figure 1E**). Thus, these results suggest that

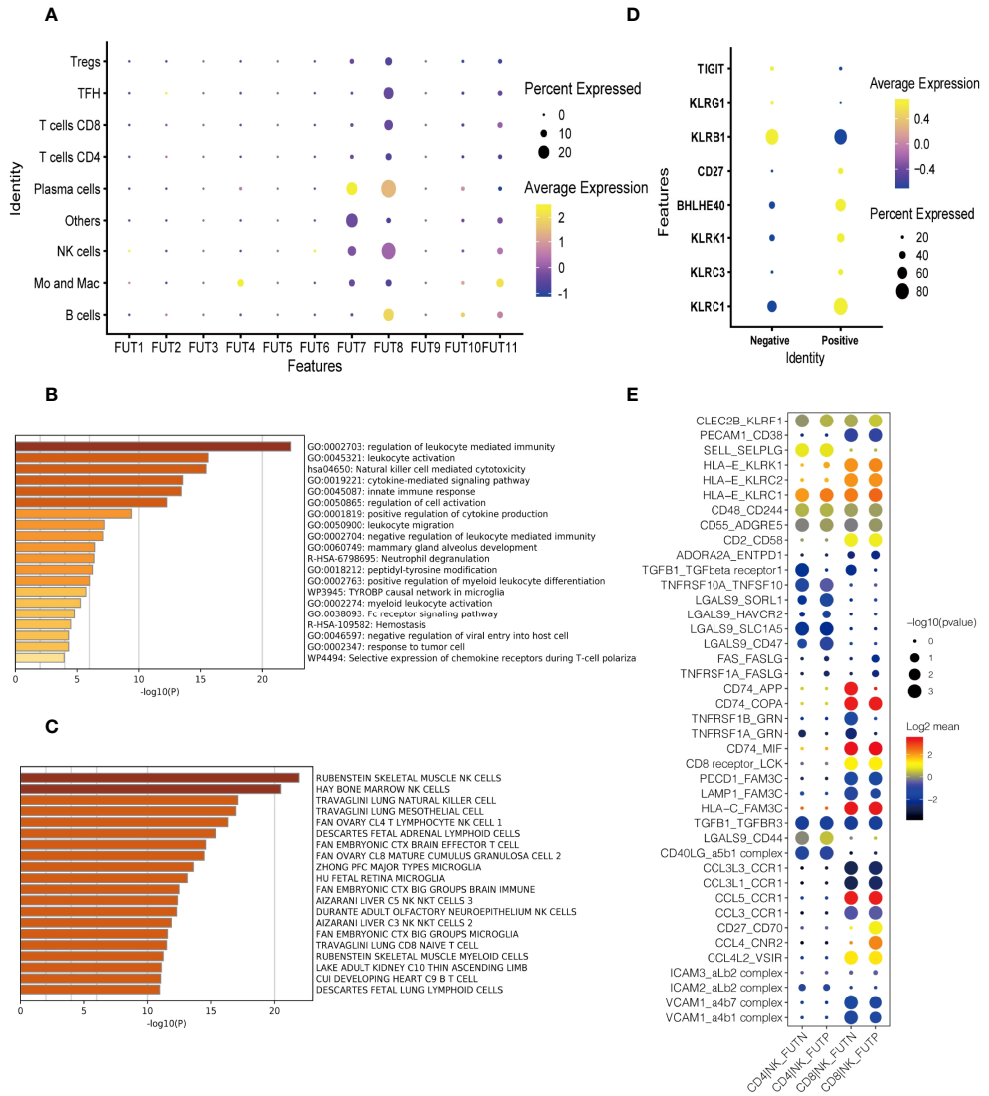

FIGURE 1 | Fucosylation promoted effector functions of NK cells in B cell lymphoma. **(A)** Heatmap of relative expressions of different fucosyltransferases in each cluster defined by scRNA-seq analysis. The dot size represented the relative percentage of expressions. The color scale represented the expression level. **(B)** GSEA of the upregulated gene set in fucosylated NK cells versus normal NK cells. **(C)** Enrichment of cell type signatures in fucosylated NK cells versus normal NK cells. **(D)** Heatmap of relative expressions of NK effector genes. The dot size represented the relative percentage of expressions. The color scale represented the expression level. **(E)** The GO annotation of ligand-receptor pairs between NK cells and T cells. The dot size represented the adjusted *p*-value. The color scale represented number of genes.

fucosylation promotes NK cell effector functions and may have a potential regulatory role in facilitating T cell anti-tumor responses.

Fucosylation Was Relevant to Infiltration of NK Cells in DLBCL

It is reported that CLA is mainly expressed on memory/effector T cells and NK cells (24). With H&E staining, we observed that tumor cells were numerous on moderate to large lymphocytes proliferating diffusely, featured with marked heteromorphy, and large and deeply stained nuclei which distinguished from those small lymphocytes in backgrounds in DLBCL (**Figure 2A**). To further investigate the role of fucosylation in B cell lymphoma, we performed immunohistochemical staining to detect the correlations between fucosylation and CD8 or CD56. Our results showed that compared to normal control, CD8 expression in DLBCL remained strong and diffuse positive (**Figure 2B**), while CD56 expression decreased significantly amidst reactive backgrounds (**Figure 2C**). Moreover, weak and scattered expression of CLA was observed only on small lymphocytes in normal control, and further decreased in DLBCL (**Figure 2A**), which was in accordance with CD56 expression (**Figure 2E**). By contrast, there existed no correlations between the expression of CD8 and CLA (**Figure 2D**). These results implied the role of NK cells in DLBCL, which was potentially related to fucosylation.

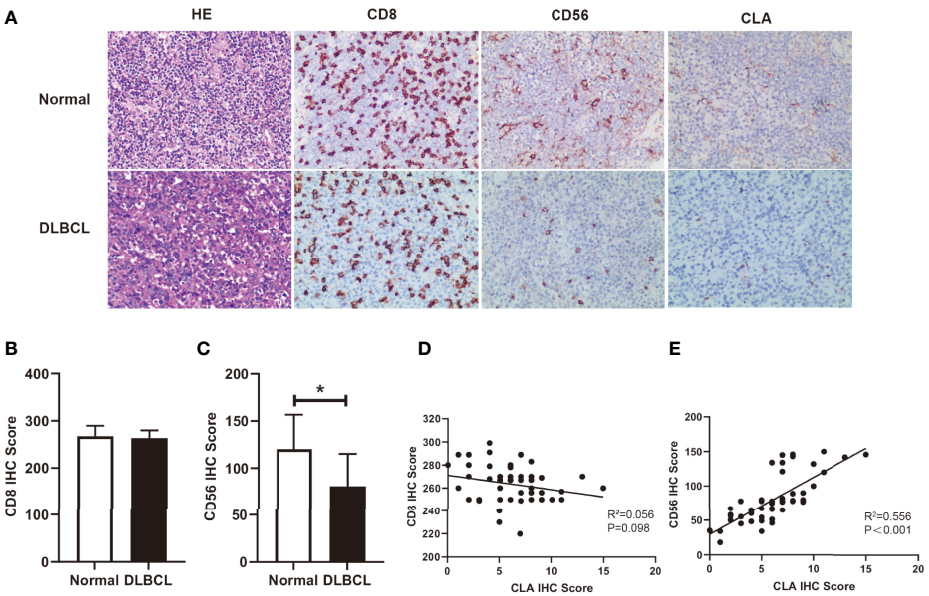

FIGURE 2 | Fucosylation was relevant to infiltration of NK cells in DLBCL. **(A)** Representative images of morphology with H&E staining and immunohistochemical staining of CD8, CD56, and CLA between normal and DLBCL cases (magnification×200). **(B, C)** Statistics were based on the expression of $CD8^+$ T cells and $CD56^+$ NK cells in DLBCL(n = 50) and normal lymph node (n = 4) biopsies per field of each group. **(D)** Correlations of CLA positive cells and $CD8^+$ T cells in DLBCL ($p = 0.098$, $r^2 = 0.056$, n = 50) **(E)** Correlations of CLA positive cells and $CD56^+$ NK cells in DLBCL ($p < 0.001$, $r^2 = 0.56$, n = 50). Data are presented as mean ± SD. *$p < 0.05$.

Ex Vivo Fucosylation Augmented Cytotoxic Activities of NK Cells

Fucosylation is regulated by fucosyltransferases and GDP-fucose as the substrate (25). In order to investigate the function of fucosylation of NK cells, we incubated TCD-BM progenitors with H. pylori α-1,3-fucosyltransferases (26) and GDP-fucose for 30 min at room temperature. BM progenitors only expressed a relatively low level of fucosylation. *Ex vivo* fucosylation significantly promoted the CLA expression on cell surface as increased from 5.27% to 87.71% (**Figure 3A**). The purity of generated NK cells was high (more than 95%) (**Figure 3B**). There was no significant difference of CD11b and CD43 expression between the fucosylated and untreated groups, suggesting that fucosylation had no impact on the maturation of NK cells. Likewise, the activation markers NKG2D and NKp46 were not substantially altered by fucosylation (**Figure 3C**). However, production of IFN-γ, granzyme B as well as perforin were markedly increased in fucosylated NK cells as compared to those of the untreated controls (**Figures 3D-F**). We also observed an elevated IFN-γ secretion in the supernatant of fucosylated NK cells (**Figure 3G**). Collectively, these results demonstrated that *ex vivo* fucosylation promoted the cytotoxic abilities of NK cells.

Fucosylated Donor NK Cells Enhanced GVT Effect Against B Cell Lymphoma

To evaluate the potential GVT effect of fucosylation on NK cells, we performed cytotoxicity assay to detect the direct killing abilities of NK cells against B cell lymphoma cells (A20 cells). We found that fucosylation significantly promoted the cytotoxic activities of NK cells at different E: T ratios compared to control NK cells (**Figure 4A**). Results of murine GVT model showed that compared to recipients without NK cells infusion, recipients receiving control NK cells have a trend of prolonged survival, but without statistical significance. By contrast, recipients that received the transfer of fucosylated NK cells exhibited prolonged survival and profound therapeutic effects compared to recipients receiving control NK cells (**Figure 4B**). The proportions of A20 cells were significantly decreased both in the spleen and liver in mice infused fucosylated NK cells compared with those in controls (**Figures 4C, D**). Thus, our results demonstrated that fucosylation of NK cells displayed enhanced anti-tumor responses both *in vitro* and *in vivo*.

Fucosylation Promoted Donor NK Cells Accumulation After Allo-HSCT

To investigate the mechanisms of promoting GVT effect with *ex vivo* fucosylation of NK cells, we assessed the properties of NK cells 7 days post transplantation. We found that neither the expressions of maturation markers (CD11b and CD43) nor the expressions of activation markers (NKG2D and NKp46) differed between the fucosylated and the control NK cells isolated from the recipient mice (**Figure 5A**). In addition, we also found similar levels of CD107a expressed on NK cells between these two groups. Consistent with our *in vitro* results, the production of IFN-γ and perforin was elevated in the fucosylated NK cells (**Figures 5B, C**). Significantly, we found the frequency of NK cells in the spleen and the liver was substantially increased in the recipient mice that received fucosylated NK cells when compared

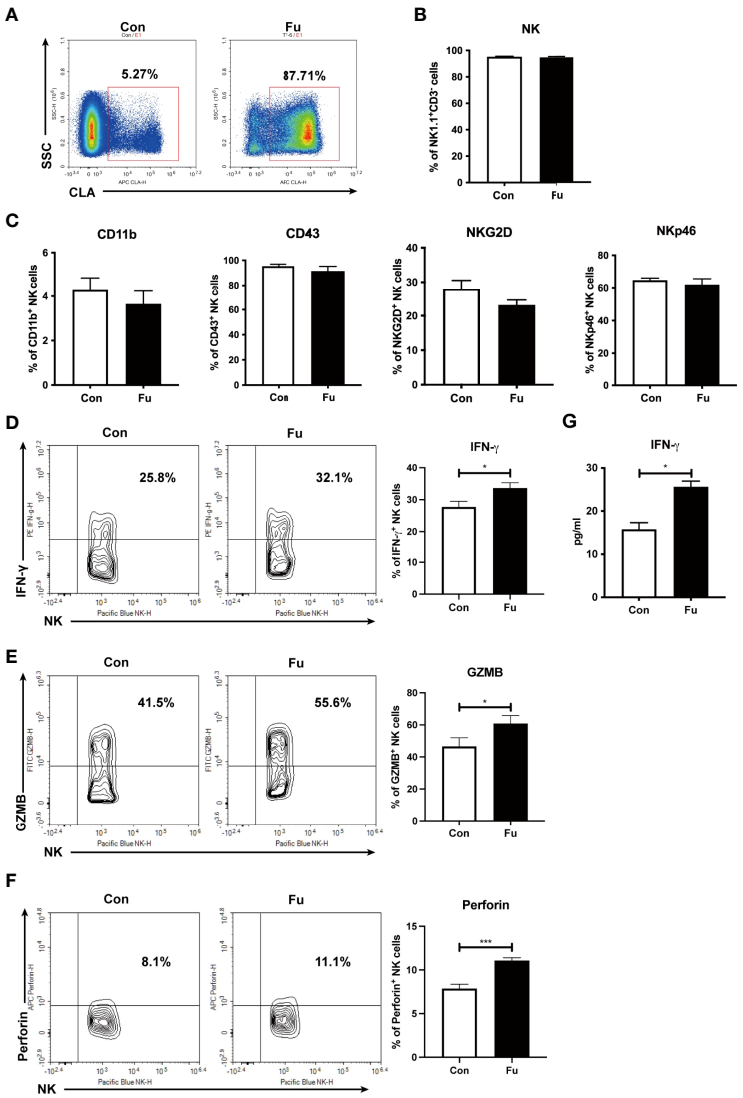

FIGURE 3 | *Ex vivo* fucosylation augmented cytotoxic activities of NK cells. **(A)** Representative flow cytometry plots of control and fucosylated BM progenitor cells. **(B)** The percentage of NK1.1$^+$CD3$^-$ cells in the generated control and fucosylated NK cells. **(C)** Expressions of CD11b, CD43, NKG2D, NKp46 in control and fucosylated NK cells are shown. **(D, F, G)** Representative flow cytometry plots and statistics of the proportions of IFN-γ, GZMB and perforin productions in control and fucosylated NK cells are shown, respectively. **(E)** IFN-γ production in the superannuants of control and fucosylated NK cells were detected by ELISA (n = 4 per group). Data are representative of three independent experiments and shown as mean ± SD. *$p < 0.05$; ***$p < 0.001$.

to those receiving control NK cells (**Figure 5D**). To determine the origin of NK cells increased in these organs, we then labeled donor NK cells with CTV before transfer. The fucosylated NK cells exhibited a similar rate of apoptosis and proliferation to that of the control NK cells (**Figures 5E, F**). However, the fucosylated NK cells had increased affinity to E-selectin rather than P-selectin or L-selectin, which hinted at superior accumulation ability of the fucosylated NK cells compared to the controls (**Figure 5G**). These results suggested that, instead of enhanced proliferation or hindered apoptosis, fucosylation promoted the accumulation of NK cells in lymphoma-involved organs by enhanced binding to E-selectin *in vivo*.

Fucosylation of NK Cells Triggered T Cell Anti-Tumor Immune Responses

Results of scRNA-seq indicated that engagements of fucosylated NK cells and T cells might facilitate the anti-tumor immunity. Hereby, we assessed the early T cell response 7 days post adoptive transfer. We found that the percentage of CD8$^+$ T cells was significantly increased in recipients with fucosylated NK cells, whereas the population of CD4$^+$ T cells was not altered (**Figures 6A, B**). Compared to mice with control NK cells, CD8$^+$ T cells of mice with fucosylated NK cells also exhibited a more activated phenotype with elevated expression of CD69 (**Figures 6C–E**). Accordingly, we observed a decrease of naïve

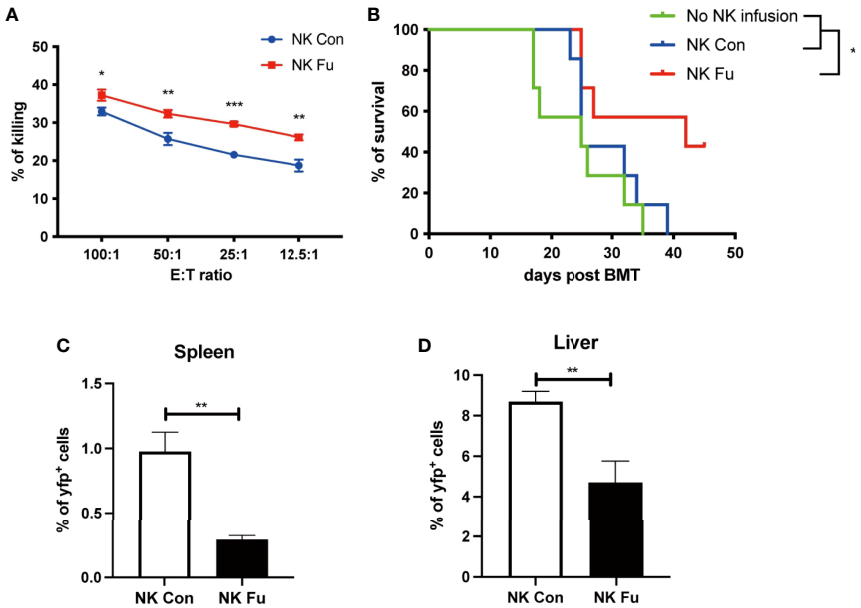

FIGURE 4 | Fucosylated donor NK cells have enhanced GVT effect against B cell lymphoma. **(A)** Fucosylated NK cells and control NK cells were cocultured with A20 lymphoma cells at different ratios for 6 hours, respectively. Cytotoxicity of NK cells were evaluated by the apoptosis of yfp$^+$ lymphoma cells as detected by flow cytometry. **(B)** BALB/c recipients were lethally irradiated and transplanted of 5x10^6 BM cells together with 5×10^6 A20-*luc*$^{+/}$*yfp* cells. Recipients were transferred with or without 1x10^6 control NK cells or fucosylaed NK cells, respectively. Survival of recipients were monitored (n = 7-9 mice per group). **(C, D)** Proportions of *yfp* positive lymphoma cells in the spleen and liver were detected by flow cytometry 7 days post transplantation. Data are representative of three independent experiments and presented as mean ± SD. *$p < 0.05$; **$p < 0.01$; ***$p < 0.001$.

CD8$^+$ T cells and an increase of effector memory CD8$^+$ T cells in recipient mice that received fucosylated NK cells compared with those receiving control NK cells (**Figure 6F**). However, similar alterations were not observed in CD4$^+$ T cells. Thus, fucosylation of NK cells probably contributed to the activation of CD8$^+$ T cells, which further promoted the anti-tumor immune response.

DISCUSSION

NK cells were defined as a distinct lymphocyte subset in 1975, which are capable of directly recognizing and killing tumor cells without previous sensitization (27). It has been demonstrated that NK cells play critical roles in GVT responses without aggravating GVHD (3, 28). NK cells can directly eliminate tumor cells by cytotoxic effect through releasing perforin and granzymes. In addition, by producing IFN-γ, NK cells also facilitate the activation and differentiation of cytotoxic T lymphocytes to restrict tumor growth (29). Apart from these direct manners, NK cells can assist in indirect regulation of T cell responses, such as interactions with B cells, triggering DC maturation and antigen cross presentation (30). Indeed, we observed an increased activation of CD8$^+$ T cells in recipient mice infused with fucosylated NK cells as compared with those infused with the control, untreated NK cells. However, clinical applications of NK cells infusion in tumor immunotherapy, especially in the treatment of advanced hematopoietic and solid malignancies, are still challenging due to their limited ability for survival or accumulation. It is supposed that *ex vivo* modification may provide potentials to ameliorate their ability and enhance their anti-tumor properties.

Fucose is a natural 6-deoxy hexose, characterized by the form of L-configuration and lacks a hydroxyl group on the carbon at the 6-position (C-6). There exists a variety of fucose types in mammal tissues, including skin and nervous system. Fucose can be incorporated into the terminal portions of N-, O-, or lipid-linked oligosaccharide chains as a terminal modification of glycan structures (31). Besides, levels of L-fucose in serum and urine can be a valuable biomarker of alcoholic liver disease, hepatocarcinoma, cirrhosis, and gastric ulcers (32, 33). Fucosylation is an enzymatic process catalyzed by fucosyltransferase (FUTs). FUT family, including FUT1 to FUT11, are fucosylation synthases which are responsible for forming glycosidic linkages between saccharides and other saccharides, peptides, and lipids (34). They are involved in proliferating cancer cells and play an important role in tumor metastasis (35, 36). It was reported that expression of FUT3/6/7 was a poor prognostic indicator, but higher FUT4 expression was a favorable prognostic factor in AML patients who received chemotherapy alone (37). FUT7 promoted the proliferation, migration, invasion, and EMT of bladder cancer cells, and positively correlated with immune cell infiltration levels (CD8$^+$ T cells, CD4$^+$T cells, macrophage, neutrophil, and DCs) (38). In our study, we found that FUT genes wereassociated with immune infiltration in B cell lymphoma. FUT4 was restrictedly expressed on monocytes and macrophages, while FUT7 and FUT8 were predominantly expressed on NK cells through scRNA-seq analysis.

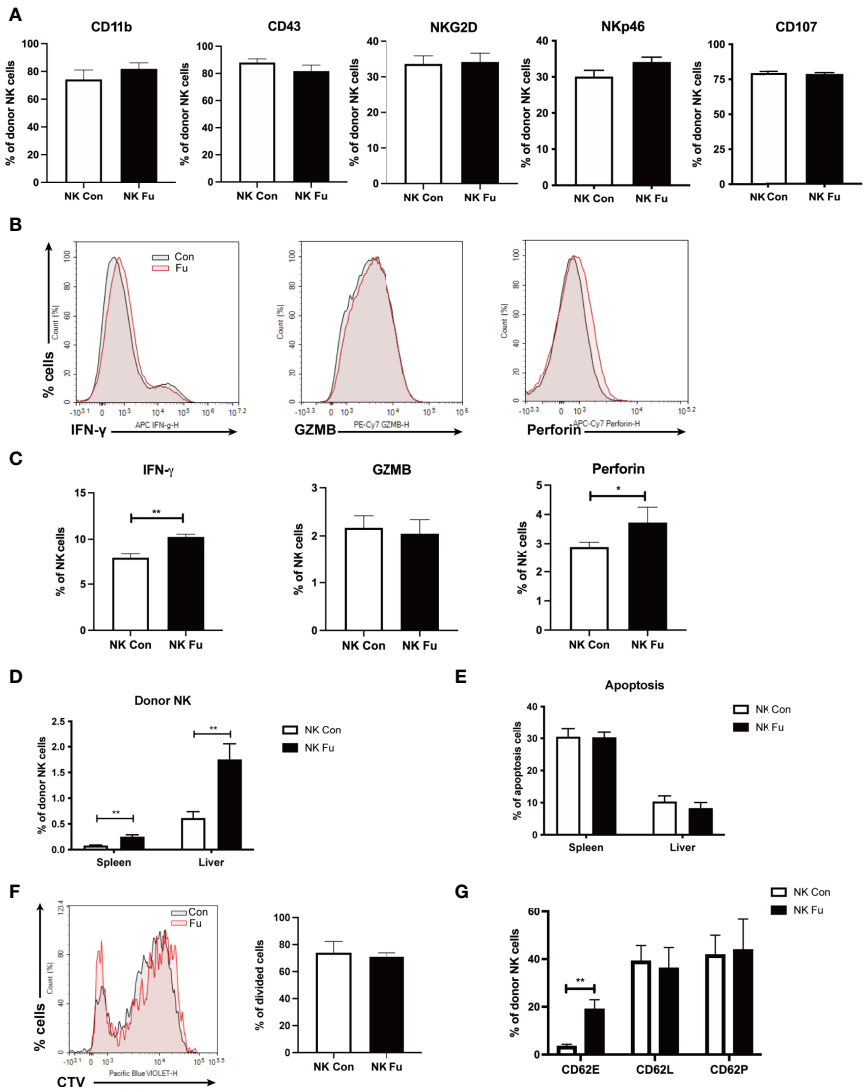

FIGURE 5 | Fucosylation promoted donor NK cells accumulation after allo-HSCT. BALB/c recipients were lethally irradiated and transplanted of 5x10^6 BM cells together with 5×10^6 A20-*luc*$^+$/*yfp* cells. Recipients were transferred with 1x10^6 control NK cells or fucosylaed NK cells, respectively. **(A)** Expressions of CD11b, CD43, NKG2D, NKp46, and CD107 of NK cells in the spleen from mice infused with control or fucosylated NK cells (n = 5-6 per group). **(B, C)** Representative flow cytometry plots and summary data of the frequencies of IFN-γ, GZMB and perforin of NK cells from mice infused with control or fucosylated NK cells (n = 5-6 per group). **(D)** Percentages of donor NK cells in the spleen and liver in recipients were detected by flow cytometry 7 days after allo-HSCT (n = 5-6 per group). **(E)** Percentages of apoptosis of control and fucosylated NK cells in spleen and liver are depicted. **(F)** Control and fucosylated NK cells were labeled with CTV. The proliferation of CTV labeled control and fucosylated NK cells were detected by flow cytometry 4 days post transfer (n = 4-6 per group). **(G)** Binding abilities of control and fucosylated NK cells to CD62E, CD62L and CD62P *in vivo* was detected by flow cytometry (n = 3-6 per group). Data are representative of three independent experiments and shown as mean ± SD. *$p < 0.05$; **$p < 0.01$.

Interestingly, we found that there was scarcely any expression of CLA on the lymphoma cells by immunohistochemical staining.

Fucosylation is involved in the formation of ABO blood group H antigen, Lewis blood group antigen, selectin-mediated leukocyte extravasation or homing, host pathogen interaction, and signal pathway modification (39). *Ex vivo* fucosylation has emerged as an enabling way to facilitate the trafficking and tumor infiltration of adoptively transferred immune cells. In the pioneering work of Xia, Shpall, and coworkers, cord blood hematopoietic cells fucosylation mediated fucosyltransferase-VI effectively accelerated neutrophil and platelet engraftment after transplantation both in animal models and clinic trials. Likewise, Sackstein applied similar strategies to create sLe^X on human multipotent mesenchymal stromal cells to enhance their trafficking and bone marrow engraftment. In the scenarios of adoptive T cell transfer, *ex vivo* fucosylation was effective to enhance anti-GVHD potency of human regulatory T cells (13, 14, 40, 41). It also reported that fucosylated CD19-CAR T-cell acquired improved activity and prolonged persistence *in vivo* (16). However, little is known about fucosylation in NK cell immunity.

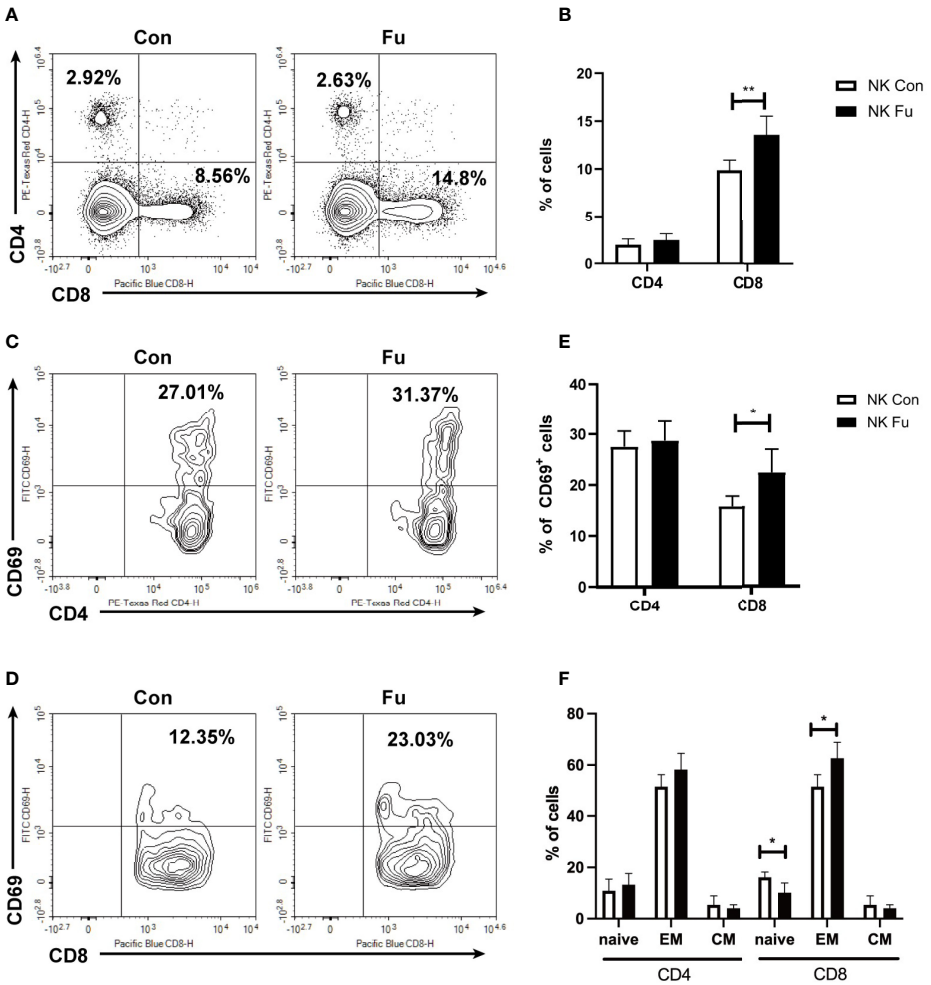

FIGURE 6 | Fucosylation of NK cells triggered T cell anti-tumor T cell responses. BALB/c recipients were lethally irradiated and transplanted of 5x10^6 BM cells together with 5×10^6 A20-*luc*$^+$/*yfp* cells. Recipients were transferred with 1x10^6 control NK cells or fucosylaed NK cells, respectively. **(A, B)** Representative flow cytometry plots and summary data of the proportions of CD4$^+$ and CD8$^+$ T cells in recipients 7 days post allo-HCST were shown (n = 5-7 per group). **(C–E)** Representative figures and summary data of the proportions of CD69$^+$CD4$^+$ T cells and CD69$^+$CD8$^+$ T cells are depicted (n = 5-7 per group). **(F)** Populations of naïve, effector memory and central memory CD4$^+$ and CD8$^+$ T cells were detected by flow cytometry in recipients received control and fucosylated NK cells 7 days post allo-HCST (n = 5-7 per group). Data are representative of three independent experiments and shown as mean ± SD. *$p < 0.05$; **$p < 0.01$.

In the current study, we discovered that in clinical B cell lymphoma FUT7 responsible for creating sLeX was highly expressed on NK cells and CLA that presented sLeX was positively correlated with the accumulation of NK cells in tumor bed. By employing recombinant H. pylori α1,3-fucosyltransferase for *ex vivo* fucosylation, we successfully introduced sLeX onto murine NK cells. *Ex vivo* fucosylation significantly enhanced the cytolytic activity of the treated NK cells as well as their infiltration into lymphoma-involved organs such as the spleen and the liver. Moreover, fucosylated NK cells exhibited superior activities to restrict tumor growth by facilitating CD8$^+$ T cell activation. However, we observed that fucosylation on the cell surface persisted less than 2 weeks in our study (data not shown). How to prolong the persistence of fucosylation needs to be explored in further studies. Besides, the molecular mechanism through which cell-surface fucosylation enhances NK effector function remains to be explored. There is a possibility that fucosylation enforces stronger interactions between NK cells and target cells, which results in the formation of a stronger immunological synapse and thereby better tumor cell killing. Because H. pylori α1,3-fucosyltransferase possesses unprecedented donor substrate promiscuity–even fucose residues conjugated with antibodies can be transferred onto the cell surface (42) - it is also possible to use this enzyme to incorporate other functional molecules, e.g., cytokines and growth factors, onto NK cells to further boost their *in vivo* properties. Recently, PDGFD-PDGFRβ signal was proven to promote IL-15 mediated NK cell survival (43). We observed no significant change of PDGFRB-PDGFD interactions in scRNA-seq analysis by Cellphone DB, which was consistent

with our results that fucosylation would not affect the apoptosis and proliferation of NK cells in GVT model. In conclusion, one of the key factors that govern the success of NK cell-based cancer immunotherapy is achieving efficient early trafficking of an adequate number of activated NK cells into the tumor microenvironment for mounting an effective immune response. *Ex vivo* cell-surface fucosylation certainly serves as a promising strategy to realize this goal.

DATA AVAILABILITY STATEMENT

The scRNA-seq data presented in the study are deposited in the GEO database (NCBI) repository, accession number GSE182434.

ETHICS STATEMENT

The animal study was reviewed and approved by the Animal Care and Use Committee of Soochow University.

AUTHOR CONTRIBUTIONS

PW, HG, JC, and DW designed the study; XT, YR, JF, and YW performed the research; JZ, YD, FL, MY, XiyW, CL, XL, LL, XiaW, LG, and YX contributed to the experiments; XT and HG analyzed the data; XT, HG, JC, and DW wrote the manuscript. PW revised the manuscript critically for important intellectual content.

FUNDING

This work was supported by the National Natural Science Foundation of China (No. 81730003, 81700173, 81974001, 81900180, 81974001 and 82170222), National Science and Technology Major Project (2017ZX09304021), National Key R&D Program of China (2019YFC0840604 and 2017YFA0104502), Key R&D Program of Jiangsu Province (BE2019798), Priority Academic Program Development of Jiangsu Higher Education Institutions (PAPD), Jiangsu Medical Outstanding Talents Project (JCRCA2016002), Jiangsu Provincial Key Medical Center (YXZXA2016002), the Jiangsu "333" Talent Project (BRA2015497), the Jiangsu Social Development Program (BE2018651), the Jiangsu Summit Six Top Talent Person project, Jiangsu Medical Junior Talent Person award (QNRC2016707), the Applied Basic Research Programs of Suzhou City (SYS2018027), Suzhou Science and Technology Program Project (SLT201911), the Jiangsu Natural Science Foundation (BK20211070), the Key Disease Program of Suzhou (LCZX202101), China Postdoctoral Science Foundation (2019M661938), Jiangsu Planned Projects for Postdoctoral Research Funds (2019K098), The Natural Science Foundation of Jiangsu Higher Education Institutions of China (20KJD320001), and Translational Research Grant of NCRCH (2021ZKQC01). PW is supported by the NIH (R35GM139643).

ACKNOWLEDGMENTS

We thank Dr. Hongjian Sun from Qilu University of Technology for excellent transcriptomic data analysis.

REFERENCES

1. Sun W, Malvar J, Sposto R, Verma A, Wilkes JJ, Dennis R, et al. Outcome of Children With Multiply Relapsed B-Cell Acute Lymphoblastic Leukemia: A Therapeutic Advances in Childhood Leukemia & Lymphoma Study. *Leukemia* (2018) 32(11):2316–25. doi: 10.1038/s41375-018-0094-0
2. Poon LM, Bassett RJr., Rondon G, Hamdi A, Qazilbash M, Hosing C, et al. Outcomes of Second Allogeneic Hematopoietic Stem Cell Transplantation for Patients With Acute Lymphoblastic Leukemia. *Bone Marrow Transplant* (2013) 48(5):666–70. doi: 10.1038/bmt.2012.195
3. Bachanova V, Cooley S, Defor TE, Verneris MR, Zhang B, McKenna DH, et al. Clearance of Acute Myeloid Leukemia by Haploidentical Natural Killer Cells Is Improved Using Il-2 Diphtheria Toxin Fusion Protein. *Blood* (2014) 123(25):3855–63. doi: 10.1182/blood-2013-10-532531
4. Vivier E, Tomasello E, Baratin M, Walzer T, Ugolini S. Functions of Natural Killer Cells. *Nat Immunol* (2008) 9(5):503–10. doi: 10.1038/ni1582
5. Habif G, Crinier A, Andre P, Vivier E, Narni-Mancinelli E. Targeting Natural Killer Cells in Solid Tumors. *Cell Mol Immunol* (2019) 16(5):415–22. doi: 10.1038/s41423-019-0224-2
6. McEver RP. Selectins: Lectins That Initiate Cell Adhesion Under Flow. *Curr Opin Cell Biol* (2002) 14(5):581–6. doi: 10.1016/s0955-0674(02)00367-8
7. Sarkar AK, Rostand KS, Jain RK, Matta KL, Esko JD. Fucosylation of Disaccharide Precursors of Sialyl Lewisx Inhibit Selectin-Mediated Cell Adhesion. *J Biol Chem* (1997) 272(41):25608–16. doi: 10.1074/jbc.272.41.25608
8. Merzaban JS, Burdick MM, Gadhoum SZ, Dagia NM, Chu JT, Fuhlbrigge RC, et al. Analysis of Glycoprotein E-Selectin Ligands on Human and Mouse Marrow Cells Enriched for Hematopoietic Stem/Progenitor Cells. *Blood* (2011) 118(7):1774–83. doi: 10.1182/blood-2010-11-320705
9. Wan X, Sato H, Miyaji H, McDaniel JM, Wang Y, Kaneko E, et al. Fucosyltransferase Vii Improves the Function of Selectin Ligands on Cord Blood Hematopoietic Stem Cells. *Glycobiology* (2013) 23(10):1184–91. doi: 10.1093/glycob/cwt055
10. Robinson SN, Thomas MW, Simmons PJ, Lu J, Yang H, Parmar S, et al. Fucosylation With Fucosyltransferase Vi or Fucosyltransferase Vii Improves Cord Blood Engraftment. *Cytotherapy* (2014) 16(1):84–9. doi: 10.1016/j.jcyt.2013.07.003
11. Huber CM, Doisne JM, Colucci F. Il-12/15/18-Preactivated Nk Cells Suppress Gvhd in a Mouse Model of Mismatched Hematopoietic Cell Transplantation. *Eur J Immunol* (2015) 45(6):1727–35. doi: 10.1002/eji.201445200
12. Abicht JM, Sfriso R, Reichart B, Langin M, Gahle K, Puga Yung GL, et al. Multiple Genetically Modified Gtko/Hcd46/Hla-E/Hbeta2-Mg Porcine Hearts Are Protected From Complement Activation and Natural Killer Cell Infiltration During *Ex Vivo* Perfusion With Human Blood. *Xenotransplantation* (2018) 25(5):e12390. doi: 10.1111/xen.12390
13. Parmar S, Liu X, Najjar A, Shah N, Yang H, Yvon E, et al. *Ex Vivo* Fucosylation of Third-Party Human Regulatory T Cells Enhances Anti-Graft-Versus-Host Disease Potency *in Vivo*. *Blood* (2015) 125(9):1502–6. doi: 10.1182/blood-2014-10-603449
14. Xia L, McDaniel JM, Yago T, Doeden A, McEver RP. Surface Fucosylation of Human Cord Blood Cells Augments Binding to P-Selectin and E-Selectin and Enhances Engraftment in Bone Marrow. *Blood* (2004) 104(10):3091–6. doi: 10.1182/blood-2004-02-0650
15. Li J, Hsu HC, Mountz JD, Allen JG. Unmasking Fucosylation: From Cell Adhesion to Immune System Regulation and Diseases. *Cell Chem Biol* (2018) 25(5):499–512. doi: 10.1016/j.chembiol.2018.02.005
16. Sanchez-Martinez D, Gutierrez-Aguera F, Romecin P, Vinyoles M, Palomo M, Tirado N, et al. Enforced Sialyl-Lewis-X (Slex) Display in E-Selectin Ligands

by Exofucosylation Is Dispensable for Cd19-Car T-Cell Activity and Bone Marrow Homing. *Clin Transl Med* (2021) 11(2):e280. doi: 10.1002/ctm2.280
17. Hong S, Yu C, Wang P, Shi Y, Cao W, Cheng B, et al. Glycoengineering of Nk Cells With Glycan Ligands of Cd22 and Selectins for B-Cell Lymphoma Therapy. *Angew Chem Int Ed Engl* (2021) 60(7):3603–10. doi: 10.1002/anie.202005934
18. Song Y, Hu B, Liu Y, Jin Z, Zhang Y, Lin D, et al. Il-12/Il-18-Preactivated Donor Nk Cells Enhance Gvl Effects and Mitigate Gvhd After Allogeneic Hematopoietic Stem Cell Transplantation. *Eur J Immunol* (2018) 48(4):670–82. doi: 10.1002/eji.201747177
19. Hu B, Bao G, Zhang Y, Lin D, Wu Y, Wu D, et al. Donor Nk Cells and Il-15 Promoted Engraftment in Nonmyeloablative Allogeneic Bone Marrow Transplantation. *J Immunol* (2012) 189(4):1661–70. doi: 10.4049/jimmunol.1103199
20. Hunger RE, Yawalkar N, Braathen LR, Brand CU. The Heca-452 Epitope Is Highly Expressed on Lymph Cells Derived From Human Skin. *Br J Dermatol* (1999) 141(3):565–9. doi: 10.1046/j.1365-2133.1999.03031.x
21. Liu Y, Wu Y, Wang Y, Cai Y, Hu B, Bao G, et al. Il-35 Mitigates Murine Acute Graft-Versus-Host Disease With Retention of Graft-Versus-Leukemia Effects. *Leukemia* (2015) 29(4):939–46. doi: 10.1038/leu.2014.310
22. Steen CB, Luca BA, Esfahani MS, Azizi A, Sworder BJ, Nabet BY, et al. The Landscape of Tumor Cell States and Ecosystems in Diffuse Large B Cell Lymphoma. *Cancer Cell* (2021) 39(10):1422–37.e10. doi: 10.1016/j.ccell.2021.08.011
23. Efremova M, Vento-Tormo M, Teichmann SA, Vento-Tormo R. Cellphonedb: Inferring Cell-Cell Communication From Combined Expression of Multi-Subunit Ligand-Receptor Complexes. *Nat Protoc* (2020) 15(4):1484–506. doi: 10.1038/s41596-020-0292-x
24. Tsuchiyama J, Yoshino T, Toba K, Harada N, Nishiuchi R, Akagi T, et al. Induction and Characterization of Cutaneous Lymphocyte Antigen on Natural Killer Cells. *Br J Haematol* (2002) 118(2):654–62. doi: 10.1046/j.1365-2141.2002.03608.x
25. Kawamoto S, Moriwaki K, Nakagawa T, Terao M, Shinzaki S, Yamane-Ohnuki N, et al. Overexpression of Alpha1,6-Fucosyltransferase in Hepatoma Enhances Expression of Golgi Phosphoprotein 2 in a Fucosylation-Independent Manner. *Int J Oncol* (2011) 39(1):203–8. doi: 10.3892/ijo.2011.1005
26. Wang W, Hu T, Frantom PA, Zheng T, Gerwe B, Del Amo DS, et al. Chemoenzymatic Synthesis of Gdp-L-Fucose and the Lewis X Glycan Derivatives. *Proc Natl Acad Sci USA* (2009) 106(38):16096–101. doi: 10.1073/pnas.0908248106
27. Terren I, Orrantia A, Vitalle J, Zenarruzabeitia O, Borrego F. Nk Cell Metabolism and Tumor Microenvironment. *Front Immunol* (2019) 10:2278. doi: 10.3389/fimmu.2019.02278
28. Freud AG, Mundy-Bosse BL, Yu J, Caligiuri MA. The Broad Spectrum of Human Natural Killer Cell Diversity. *Immunity* (2017) 47(5):820–33. doi: 10.1016/j.immuni.2017.10.008
29. Martin-Fontecha A, Thomsen LL, Brett S, Gerard C, Lipp M, Lanzavecchia A, et al. Induced Recruitment of Nk Cells to Lymph Nodes Provides Ifn-Gamma for T(H)1 Priming. *Nat Immunol* (2004) 5(12):1260–5. doi: 10.1038/ni1138
30. Crouse J, Xu HC, Lang PA, Oxenius A. Nk Cells Regulating T Cell Responses: Mechanisms and Outcome. *Trends Immunol* (2015) 36(1):49–58. doi: 10.1016/j.it.2014.11.001
31. Schneider M, Al-Shareffi E, Haltiwanger RS. Biological Functions of Fucose in Mammals. *Glycobiology* (2017) 27(7):601–18. doi: 10.1093/glycob/cwx034
32. Sakai T, Yamamoto K, Yokota H, Hakozaki-Usui K, Hino F, Kato I. Rapid, Simple Enzymatic Assay of Free L-Fucose in Serum and Urine, and Its Use as a Marker for Cancer, Cirrhosis, and Gastric Ulcers. *Clin Chem* (1990) 36(3):474–6. doi: 10.1093/clinchem/36.3.474
33. Yamauchi M, Kimura K, Maezawa Y, Ohata M, Mizuhara Y, Hirakawa J, et al. Urinary Level of L-Fucose as a Marker of Alcoholic Liver Disease. *Alcohol Clin Exp Res* (1993) 17(2):268–71. doi: 10.1111/j.1530-0277.1993.tb00761.x
34. Ma B, Simala-Grant JL, Taylor DE. Fucosylation in Prokaryotes and Eukaryotes. *Glycobiology* (2006) 16(12):158R–84R. doi: 10.1093/glycob/cwl040
35. Liang L, Gao C, Li Y, Sun M, Xu J, Li H, et al. Mir-125a-3p/Fut5-Fut6 Axis Mediates Colorectal Cancer Cell Proliferation, Migration, Invasion and Pathological Angiogenesis *Via* Pi3k-Akt Pathway. *Cell Death Dis* (2017) 8(8):e2968. doi: 10.1038/cddis.2017.352
36. Weston BW, Hiller KM, Mayben JP, Manousos GA, Bendt KM, Liu R, et al. Expression of Human Alpha(1,3)Fucosyltransferase Antisense Sequences Inhibits Selectin-Mediated Adhesion and Liver Metastasis of Colon Carcinoma Cells. *Cancer Res* (1999) 59(9):2127–35.
37. Dai Y, Cheng Z, Pang Y, Jiao Y, Qian T, Quan L, et al. Prognostic Value of the Fut Family in Acute Myeloid Leukemia. *Cancer Gene Ther* (2020) 27(1-2):70–80. doi: 10.1038/s41417-019-0115-9
38. Liu M, Zheng Q, Chen S, Liu J, Li S. Fut7 Promotes the Epithelial-Mesenchymal Transition and Immune Infiltration in Bladder Urothelial Carcinoma. *J Inflammation Res* (2021) 14:1069–84. doi: 10.2147/JIR.S296597
39. Miyoshi E, Moriwaki K, Nakagawa T. Biological Function of Fucosylation in Cancer Biology. *J Biochem* (2008) 143(6):725–9. doi: 10.1093/jb/mvn011
40. Sackstein R, Merzaban JS, Cain DW, Dagia NM, Spencer JA, Lin CP, et al. *Ex Vivo* Glycan Engineering of Cd44 Programs Human Multipotent Mesenchymal Stromal Cell Trafficking to Bone. *Nat Med* (2008) 14(2):181–7. doi: 10.1038/nm1703
41. Popat U, Mehta RS, Rezvani K, Fox P, Kondo K, Marin D, et al. Enforced Fucosylation of Cord Blood Hematopoietic Cells Accelerates Neutrophil and Platelet Engraftment After Transplantation. *Blood* (2015) 125(19):2885–92. doi: 10.1182/blood-2015-01-607366
42. Li J, Chen M, Liu Z, Zhang L, Felding BH, Moremen KW, et al. A Single-Step Chemoenzymatic Reaction for the Construction of Antibody-Cell Conjugates. *ACS Cent Sci* (2018) 4(12):1633–41. doi: 10.1021/acscentsci.8b00552
43. Ma S, Tang T, Wu X, Mansour AG, Lu T, Zhang J, et al. Pdgf-D-Pdgfrbeta Signaling Enhances Il-15-Mediated Human Natural Killer Cell Survival. *Proc Natl Acad Sci USA* (2022) 119(3). doi: 10.1073/pnas.2114134119

Conflict of Interest: The authors declare that the research was conducted in the absence of any commercial or financial relationships that could be construed as a potential conflict of interest.

Publisher's Note: All claims expressed in this article are solely those of the authors and do not necessarily represent those of their affiliated organizations, or those of the publisher, the editors and the reviewers. Any product that may be evaluated in this article, or claim that may be made by its manufacturer, is not guaranteed or endorsed by the publisher.

frontiers | Frontiers in Immunology

CASE REPORT
published: 16 June 2022
doi: 10.3389/fimmu.2022.890059

Case Report: Primary Cardiac T-Cell Lymphoma With Complete Atrio-Ventricular Block Diagnosed by Endomyocardial Biopsy

Panpan Chen[1,2†], *Yuanyuan Hao*[1,2†], *Xi Qiu*[1,2], *Xibin Xiao*[1,2], *Wei Zhu*[3,4], *Yang Xu*[1,2] *and Wenbin Qian*[1,2*]

[1] Department of Hematology, The Second Affiliated Hospital, College of Medicine, Zhejiang University, Hangzhou, China,
[2] Key Laboratory for Cancer Molecular Cell Biology, Life Sciences Institute, Zhejiang University, Hangzhou, China,
[3] Department of Cardiology, The Second Affiliated Hospital, College of Medicine, Zhejiang University, Hangzhou, China,
[4] Provincial Key Laboratory of Cardiovascular Research, Hangzhou, China

OPEN ACCESS

Edited by:
Ken H. Young,
University of Texas MD Anderson Cancer Center, United States

Reviewed by:
Konstantinos Melissaropoulos, Agios Andreas Hospital, Greece
Zijun Y. Xu-Monette, Duke University Medical Center, United States

***Correspondence:**
Wenbin Qian
qianwb@zju.edu.cn

[†]These authors have contributed equally to this work and share first authorship

Specialty section:
This article was submitted to Cancer Immunity and Immunotherapy, a section of the journal Frontiers in Immunology

Received: 05 March 2022
Accepted: 18 May 2022
Published: 16 June 2022

Citation:
Chen P, Hao Y, Qiu X, Xiao X, Zhu W, Xu Y and Qian W (2022) Case Report: Primary Cardiac T-Cell Lymphoma With Complete Atrio-Ventricular Block Diagnosed by Endomyocardial Biopsy. Front. Immunol. 13:890059. doi: 10.3389/fimmu.2022.890059

Primary cardiac lymphoma (PCL) is a rare disease, the definite diagnosis of which is sometimes difficult and mainly relies on endomyocardial biopsy. Primary cardiac T-cell lymphoma (PCTL) is an extremely rare sub-type of PCL. Here, we report on a 47-year-old female with PCTL who presented with fever, syncope, palpitations, and a third-degree atrioventricular block (AVB) on electrocardiogram. Chemotherapy was administered with two courses of methotrexate, cyclophosphamide, liposomal doxorubicin, vincristine, and dexamethasone (MTX-CHOP). As the tumor vanished, AVB changed from third degree to second degree and finally to sinus rhythm. In conclusion, endomyocardial biopsy is valuable in the diagnosis of primary cardiac lymphoma. It is worth noting that alterations in the electrocardiogram may indicate an attack on the heart by PCTL.

Keywords: primary cardiac lymphoma, T-cell lymphoma, complete atrioventricular block, immunotherapy, case report

INTRODUCTION

Primary cardiac lymphoma is defined as a malignant lymphoma located in the myocardium and pericardium with cardiac symptoms due to myocardial infiltration of the lymphoma as the main manifestation (1). Due to its rarity and difficulty in confirming the diagnosis, it is largely reported as an isolated case. In 2016, Gordon et al. reviewed, in Pubmed, 94 cases between 1990 and 2015 of non-hodgkin lymphoma (NHL) involvement with biopsy evidence (2). Of these cases, only 51 were diagnosed as primary cardiac lymphoma and 43 were diagnosed as secondary. Primary diffuse large B-cell lymphoma was the most common histological subtype (58%), followed by T- cell lymphoma (16%), Burkitt lymphoma (9%), and small lymphocyte lymphoma (6%) (2).

Here, we report a case of primary cardiac peripheral T-cell lymphoma with third-degree atrioventricular block that was successfully treated and reversed to first-degree AVB. Wang et al. also reported a primary heart T-cell lymphoma with third-degree atrioventricular block before treatment, which turned into first-degree atrioventricular block one week later, similar to our case (3).

CASE PRESENTATION

A 47-year-old female patient visited the emergency department of our hospital on 30 May 2020 reporting an episode of syncope lasting 1-2 minutes. Three hours ago, the patient experienced syncope without convulsions, incontinence, vertigo, tinnitus, nausea or vomiting, chest pain, or chest tightness. About three months ago, she started to have a fever up to 38.6°C, accompanied with dizziness and weakness. She was diagnosed with an infection of unknown etiology at another clinic and was prescribed anti-infective therapy. The medication taken included antibiotics and methylprednisolone. However, the anti-infection therapy was ineffective and the fever persisted.

She was then admitted into the Department of Cardiology in our hospital, on physical examination, her heart rate was 59 beats/min, the blood pressure was 100/56mmHg, and respiratory rate was 19/min. The thorax was symmetrical, with no deformities on inspection, both lungs had clear breathing sounds, and neither dry nor wet rales were heard on auscultation. The heart rate was normal rhythm and no pathological murmur was detected in each valve auscultation area. The abdomen was soft, without pain from pressure, and there was no swelling of either lower limbs.

PET-CT examination suggested a thickening of the posterior and bilateral walls of the paranasal nasopharynx and soft tissues, enlarged shape of the left atrium, bilateral pulmonary valves and mediastinum, enlarged multiple lymph nodes in the left clavicular region with increased FDG metabolism, enlarged spleen, and increasingly diffused, uneven FDG metabolism in the bone marrow cavity. Positive infectious disease or possible hematologic lymphoma was considered.

Cranial MRI combined with 3D enhancement and diffusion imaging (3.0T) showed abnormal enhancing shadow in the posterior wall of the nasopharyngeal apex and both walls extending across the middle and posterior skull base to the right temporal and pontocerebellar regions, involving the right temporal and right cerebellar hemisphere meninges, all of which indicated infectious lesions.

The initial electrocardiogram (ECG) showed a complete atrioventricular block (AVB) with a junctional rhythm (**Figure 1A**). Blood examination showed troponin levels within normal range and the brain natriuretic peptide precursor level was 1388 pg/ml. Transthoracic echocardiography (**Figure 2**) shows a homogeneous isoechoic layer thickening of the endocardial surface of the left atrium across the entire left atrial wall with a thickness of approximately 1.06 cm, and the same changes were observed in the left auricle. The rest of the structures were indistinguishable. Left cardiac ultrasonography suggested a homogeneous isoechoic filling of the left atrial wall and left auricle with no perfusion in the imaging.

A cardiac magnetic resonance (CMR) examination was then carried out for the patient (**Figure 3**), confirming a significant thickening of the left atrial wall with no enlargement of the left and right atrial chambers and a triple inversion recovery (IR) sequence showing a more homogeneous high signal with significant inhomogeneous enhancement on the delayed scan. There was no hypertrophy of the ventricle, no dilatation or stenosis of the aorta or pulmonary arteries, and the left ventricular ejection fraction was 66%.

Based on the medical history of ineffective anti-infective therapy with homogeneous isoechoic thickening of the endocardial layer across the whole left atrium and auricle, which involved the AV conduction system, an amyloid or tumorgenic abnormality should be suspected. From an etiologic standpoint, a further examination is required to make a clear diagnosis for the patient

To clarify the diagnosis, an endomyocardial biopsy (EMB) examination and temporary pacemaker implantation were performed in the catheterization laboratory with the guidance of fluoroscope, with ethical consent from the patient's family. A histological examination of samples taken from the left atrium suggested (**Figure 4**) hyperplasia of myocardial and fibrous tissue with localized irregular lymphoid-like cells. Immunohistochemical staining showed the tumor cells were diffusely positive for CD3, CD5 and CD8, scattered positive for CD2, CD7, CD4 and Granzyme B, ki-67 proliferation index reached 30%. However, the tumor cells were negative for CD20, CD56, CD10, BCL6, PD-1, CD21, CXCL13, CD30, ALK, CD99 and P53. T-cell-related markers CD3+, CD5+, CD7 individual+, CD2 individual+, B cell-related markers CD20 and CD21 negative, cell proliferation-related markers ki-67 30%+, CD4 individual+/CD8+. Differentiating from angioimmunoblast T-cell lymphoma, this case was negative for CD10, BCL6, PD-1, and CXCL13, and negative for the markers CD30 and ALK associated with anaplastic large cell lymphoma. The above markers demonstrated that the pathological immunophenotype of this case was non-specific peripheral T-cell lymphoma and not other types of lymphoma. Thus, *in situ* hybridization detected tumors negative for Epstein-Barr virus encoded with small mRNA. In combination with immunohistochemistry and *in situ* hybridization of lymph node pathology, this patient was diagnosed with peripheral T-cell lymphoma. The patient was subsequently transferred to the hematology department for chemotherapy.

The patient was treated with MTX+CHOP chemotherapy (methotrexate 1.52g day1, cyclophosphamide 750mg/m^2 day1, liposomal doxorubicin 30mg/m^2 day1, vinorelbine 30mg/m^2 day1, dexamethasone 15mg day1-5). After 2 courses of chemotherapy, efficacy was assessed as complete remission of the patient. ECG showed the atrioventricular block changed from third degree to second degree (**Figure 1B, C**) and finally to sinus rhythm cardiac (**Figure 1D**). Additionally, the ultrasonography showed no significant abnormalities in size, morphology, structure, and functional blood flow of the heart. Electrocardiogram suggested sinus rhythm. No further atrioventricular dissociation was observed and the pacemaker was removed.

DISCUSSION

The case presented here is a rare case of peripheral T-cell lymphoma of the heart and was diagnosed by EMB. The patient was well-treated and had a remarkable result at the end of the first course of treatment. The patient went from third

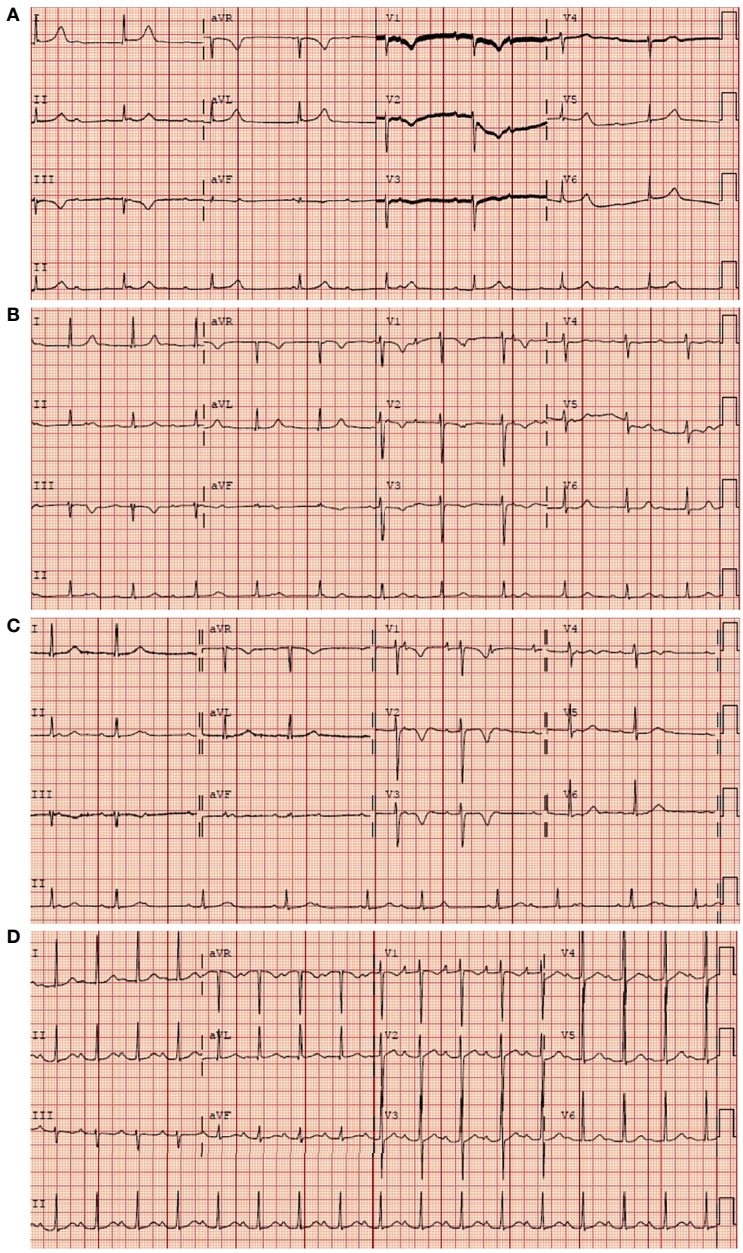

FIGURE 1 | Serial electrocardiographic strips upon patient admission. **(A)** Complete AVB before chemotherapy. **(B)** Still complete AVB on the second day after chemotherapy. **(C)** The complete AVB converted to second degree type 2 AVB on the sixth day after chemotherapy. **(D)** A first degree AVB on the eighteenth day. The initial electrocardiogram (ECG) of the patient during the chemotherapy.

degree AV block to second degree AV block and finally converted to sinus rhythm. Echocardiographic evaluation at the end of the two courses showed no significant abnormalities in the left atrium.

Primary cardiac tumors are rare, with incident rates ranging from 1.38 to 30 per 100,000 people per year (4). Among primary cardiac tumors, 80% are benign and 20% are malignant (5). Malignancies are classified by tissue type as mesenchymal (sarcoma), lymphoma (lymphoma), and mesothelial (mesothelioma), of which sarcoma is the most common (6). Although 16%-28% of patients with diffuse lymphoma have cardiac involvement, primary cardiac lymphoma is very rare. Among the cardiac malignancies found, cardiac lymphomas are quite common and may involve the heart diffusely (6). Among lymphomas with cardiac involvement, the most common type of pathology is diffuse large B-cell lymphoma (58%), whereas T-cell lymphoma is quite rare (16%) (2) And 62% of patients with peripheral T-cell lymphoma present with extranodal diseases (7).

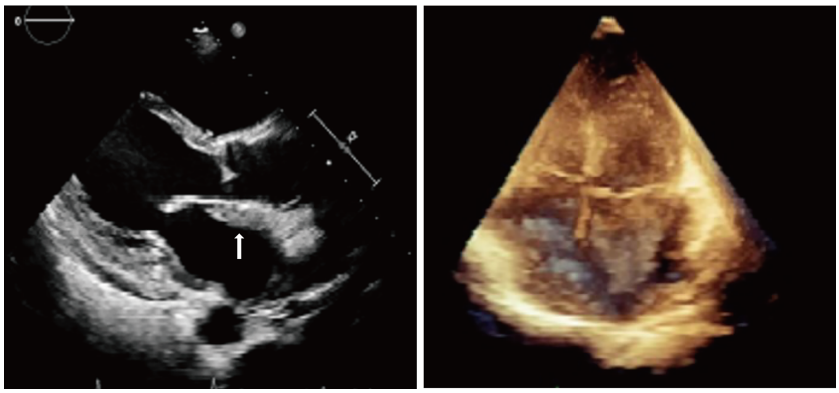

FIGURE 2 | Transthoracic echocardiography showed a homogeneous isoechoic layer thickening of the endocardial surface of the left atrium across the entire left atrial wall.

T-cell lymphoma has been reported to involve the skin (8), heart (9), central nervous system (CNS) (10), intestine, and lungs (11). Also, 23% of primary cardiac lymphomas are presented with arrhythmias and AVB is even more rare at 8% (12). The common clinical manifestations of cardiac lymphoma are dyspnea (64%) and pericardial effusion (58%) (13). However, in the present case, the main manifestation encountered was AVB, which emphasizes the value of electrocardiographic changes in the diagnosis of sudden cardiac disease. In fact, the patient was implanted with a temporary pacemaker. As the tumor vanished, so did the AVB, implying that the electrocardiographic changes caused by the lymphoma were reversible.

The CHOP regimen is recommended as a first-line chemotherapeutic regimen for cardiac lymphoma (14). The CHOP regimen has resulted in an overall response rate of about 60% (15) and a median progression-free survival is around 13 months in T-cell lymphoma (16). Although T-cell lymphoma is less common in the CNS, CNS involvement cannot be excluded since biopsy cannot be performed in nasopharyngeal area. Therefore, as there was a concern of CNS involvement, the patient was treated with CHOP regimen accompanied by MTX for the first 2 courses.

EMB is indicated for the diagnosis of intracardiac masses (17) and arrhythmogenic cardiomyopathy (18). In those patients with refractory arrhythmias, it is clinically relevant to perform EMB to evaluate cardiac T-cell lymphoma. Most cardiac lymphomas are of B-cell lineage presenting B-cell markers, such as CD19, CD20, and CD22. In our case, the biopsy of this patient showed CD3+ and CD5+, which were considered typical characteristics of T-

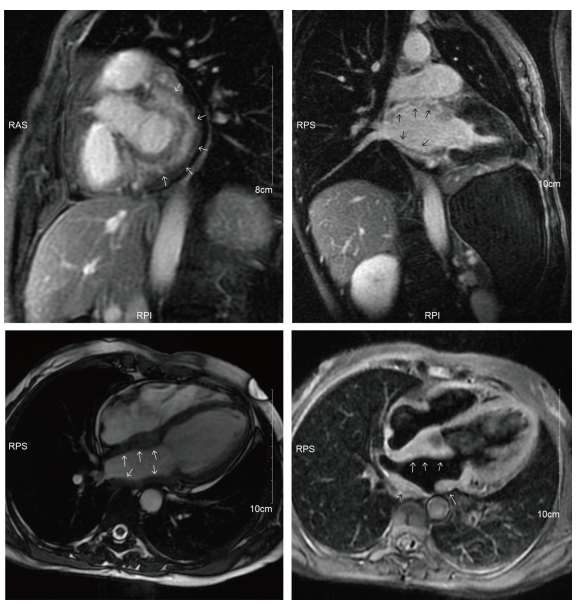

FIGURE 3 | CMR showed a significant thickening of the left atrial wall.

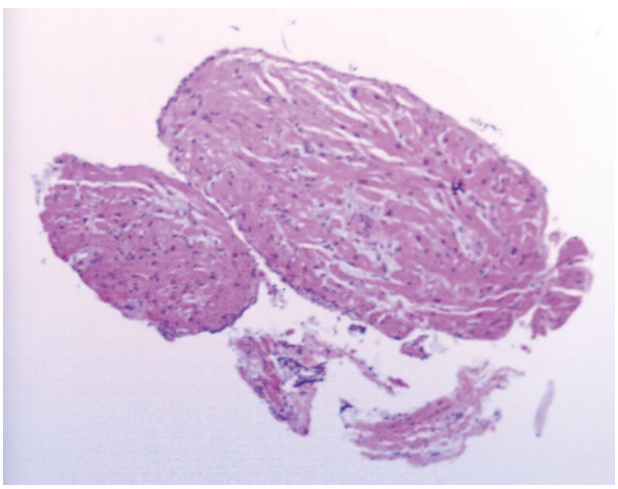

FIGURE 4 | EMB taken from the left atrium showed hyperplasia of myocardial and fibrous tissue with localized irregular lymphoid-like cells.

cell lymphoma. With help of EMB, this patient was diagnosed and treated properly without delay.

CONCLUSION

In this case, we reported a rare case of cardiac T-cell lymphoma, in which EMB was of valuable in diagnose of cardiac lymphoma. Of note, electrocardiography alteration may imply the cardiac assault in T-cell lymphoma.

DATA AVAILABILITY STATEMENT

The original contributions presented in the study are included in the article/supplementary material. Further inquiries can be directed to the corresponding author.

ETHICS STATEMENT

Written informed consent was obtained from the individual(s) for the publication of any potentially identifiable images or data included in this article.

AUTHOR CONTRIBUTIONS

PC and YH collected the data and performed the literature. WQ and YX revised the work. XQ, XX and WZ support-ed the study and reviewed the manuscript. All authors contributed to the article and approved the submitted version.

REFERENCES

1. Giunta R, Cravero RG, Granata G, Sellitto A, Romano C, De Fanis U, et al. Primary Cardiac T-Cell Lymphoma. *Ann Hematol* (2004) 83:450–4. doi: 10.1007/s00277-003-0824-9
2. Gordon MJ, Danilova O, Spurgeon S, Danilov AV. Cardiac non-Hodgkin's Lymphoma: Clinical Characteristics and Trends in Survival. *Eur J Haematol* (2016) 97:445–52. doi: 10.1111/ejh.12751
3. Wang TL, Lai CH, Liou JY, Lo HM, Shyu KG. Complete AV Block and Torsades De Pointes in a Case of Primary Cardiac T-Cell Lymphoma. *Acta Cardiol Sin* (2015) 31:245–8. doi: 10.6515/acs20141117a
4. Lestuzzi C. Primary Tumors of the Heart. *Curr Opin Cardiol* (2016) 31 (6):593–8. doi: 10.1097/HCO.0000000000000335
5. Poterucha TJ, Kochav J, O'Connor DS, Rosner GF. Cardiac Tumors: Clinical Presentation, Diagnosis, and Management. *Curr Treat Options Oncol* (2019) 20(8):66. doi: 10.1007/s11864-019-0662-1
6. Grebenc ML, Rosado DCM, Burke AP, Green CE, Galvin JR. Primary Cardiac and Pericardial Neoplasms: Radiologic-Pathologic Correlation. *Radiographics* (2000) 20:1073–103. doi: 10.1148/radiographics.20.4.g00jl081073
7. Weisenburger DD, Savage KJ, Harris NL, Gascoyne RD, Jaffe ES, MacLennan KA, et al. Peripheral T-Cell Lymphoma, Not Otherwise Specified: A Report of 340 Cases From the International Peripheral T-Cell Lymphoma Project. *Blood* (2011) 117:3402–8. doi: 10.1182/blood-2010-09-310342
8. Geskin LJ, Bagot M, Hodak E, Kim EJ. Chlormethine Gel for the Treatment of Skin Lesions in All Stages of Mycosis Fungoides Cutaneous T-Cell Lymphoma: A Narrative Review and International Experience. *Dermatol Ther (Heidelb)* (2021) 11:1085–106. doi: 10.1007/s13555-021-00539-3
9. Sherkat R, Sabri MR, Dehghan B, Bigdelian H, Reisi N, Afsharmoghadam N, et al. EBV Lymphoproliferative-Associated Disease and Primary Cardiac T-Cell Lymphoma in a STK4 Deficient Patient: A Case Report. *Med (Baltimore)* (2017) 96:e8852. doi: 10.1097/MD.0000000000008852
10. Imataki O, Uchida S, Yokokura S, Uemura M, Kadowaki N. Central Nervous System Peripheral T Cell Lymphoma Manifesting as Lymphomatosis Cerebri That Was Misdiagnosed as Neuro-Behçet's Disease: A Case Report. *Case Rep Oncol* (2018) 11:806–13. doi: 10.1159/000495033
11. Suzuki Y, Minemura H, Tomita H, Saito M, Watanabe N, Umeda T, et al. Monomorphic Epitheliotropic Intestinal T-Cell Lymphoma Involving the Lung and Brain: A Rare Case Study. *Intern Med* (2020) 59:2559–63. doi: 10.2169/internalmedicine.4710-20
12. Carras S, Berger F, Chalabreysse L, Callet-Bauchut E, Cordier JF, Salles G, et al. Primary Cardiac Lymphoma: Diagnosis, Treatment and Outcome in a Modern Series. *Hematol Oncol* (2017) 35:510–9. doi: 10.1002/hon.2301
13. Petrich A, Cho SI, Billett H. Primary Cardiac Lymphoma: An Analysis of Presentation, Treatment, and Outcome Patterns. *Cancer-Am Cancer Soc* (2011) 117:581–9. doi: 10.1002/cncr.25444
14. Avella A, Giordano C, Buffa V, De Girolamo P, Uguccioni M. Diagnosis of Primary Cardiac T-Cell Lymphoma: Feasibility and Safety of Endomyocardial Biopsy Guided by Pre-Acquired Cardiovascular Magnetic Resonance. *Eur J Case Rep Intern Med* (2021) 8:2427. doi: 10.12890/2021_002427
15. Schmitz N, Trümper L, Ziepert M, Nickelsen M, Ho AD, Metzner B, et al. Treatment and Prognosis of Mature T-Cell and NK-Cell Lymphoma: An Analysis of Patients With T-Cell Lymphoma Treated in Studies of the German High-Grade Non-Hodgkin Lymphoma Study Group. *blood* (2010) 116:3418–25. doi: 10.1182/blood-2010-02-270785
16. Vose J, Armitage J, Weisenburger D. International Peripheral T-Cell and Natural Killer/T-Cell Lymphoma Study: Pathology Findings and Clinical Outcomes. *J Clin Oncol* (2008) 26:4124–30. doi: 10.1200/JCO.2008.16.4558
17. Zanobini M, Dello RA, Saccocci M, Conti S, De Camilli E, Vettor G, et al. Endomyocardial Biopsy Guided by Intracardiac Echocardiography as a Key Step in Intracardiac Mass Diagnosis. *BMC Cardiovasc Disord* (2018) 18:15. doi: 10.1186/s12872-018-0749-9
18. Asimaki A, Saffitz JE. The Role of Endomyocardial Biopsy in ARVC: Looking Beyond Histology in Search of New Diagnostic Markers. *J Cardiovasc Electrophysiol* (2011) 22:111–7. doi: 10.1111/j.1540-8167.2010.01960.x

Conflict of Interest: The authors declare that the research was conducted in the absence of any commercial or financial relationships that could be construed as a potential conflict of interest.

frontiers | Frontiers in Immunology

CLINICAL TRIAL
published: 21 June 2022
doi: 10.3389/fimmu.2022.914959

Timing of Tocilizumab Administration Under the Guidance of IL-6 in CAR-T Therapy for R/R Acute Lymphoblastic Leukemia

Yinqiang Zhang[1,2†], *Fen Zhou*[2,3†], *Zhuolin Wu*[1,2], *Yingnan Li*[1,2], *Chenggong Li*[1,2], *Mengyi Du*[1,2], *Wenjing Luo*[1,2], *Haiming Kou*[1,2], *Cong Lu*[1,2] *and Heng Mei*[1,2*]

[1] Institute of Hematology, Union Hospital, Tongji Medical College, Huazhong University of Science and Technology, Wuhan, China, [2] Hubei Clinical Medical Center of Cell Therapy for Neoplastic Disease, Wuhan, China, [3] Department of Pediatrics, Union Hospital, Tongji Medical College, Huazhong University of Science and Technology, Wuhan, China

OPEN ACCESS

Edited by:
Wei Sang,
The Affiliated Hospital of Xuzhou Medical University, China

Reviewed by:
Chunrui Li,
Huazhong University of Science and Technology, China
Xiang Zhou,
University Hospital Würzburg, Germany

***Correspondence:**
Heng Mei
hmei@hust.edu.cn

[†]*These authors share first authorship*

Specialty section:
This article was submitted to Cancer Immunity and Immunotherapy, a section of the journal Frontiers in Immunology

Received: *07 April 2022*
Accepted: *02 May 2022*
Published: *21 June 2022*

Citation:
Zhang Y, Zhou F, Wu Z, Li Y, Li C, Du M, Luo W, Kou H, Lu C and Mei H (2022) Timing of Tocilizumab Administration Under the Guidance of IL-6 in CAR-T Therapy for R/R Acute Lymphoblastic Leukemia. Front. Immunol. 13:914959. doi: 10.3389/fimmu.2022.914959

Chimeric antigen receptor T (CAR-T) cells targeting CD19 have achieved great clinical responses in patients with relapsed or refractory (R/R) acute B lymphoblastic leukemia. However, severe adverse events such as cytokine release syndrome (CRS) and immune effector cell-associated neurotoxicity syndrome restrict it to further application. Tocilizumab is the corner stone for the treatment of severe CRS. It has been used to treat mild CRS in recent years, whereas some statistical supports clarifying the suitable timing of its administration are lacking. Sixty-seven patients with B-cell acute lymphoblastic leukemia (B-ALL) were treated with CD19-CART and enrolled in the study, of which 33 patients received Tocilizumab. Application of Tocilizumab in patients with grade 2 CRS in American Society for Transplantation and Cellular Therapy (ASTCT) criteria can significantly shorten the duration of CRS without affecting side effects and long-term efficacy. However, a number of patients still developed severe CRS with early use of Tocilizumab, indicating the significance of the introduction of clinical laboratories to assist medications. Statistically, patients with less than fourfold increase in IL-6 levels had a higher incidence of severe CRS after receiving Tocilizumab (37.5% versus. 0%, p=0.0125), which provided a basis for refining CRS intervention strategies under the guidance of IL-6.

Clinical Trial Registration: www.clinicaltrials.gov, NCT02965092 and NCT04008251

Keywords: chimeric antigen receptor T cell, cytokine release syndrome, acute lymphoblastic leukemia, tocilizumab, interleukin-6

INTRODUCTION

Chimeric antigen receptor T cell (CAR-T cell) is an emerging and promising therapy for hematologic malignancies. Up to now, five commercialized CAR-T products have been approved by the Food and Drug Administration. CAR-T cells targeting CD19, which is broadly expressed by B-cell malignancies, had shown amazing results in several clinical trials (1–4) with a complete remission rate up to 90% (3). Although excellent efficacy of CAR-T cell has been presented, lethal side effects represented by cytokine

release syndrome (CRS) and immune effector cell-associated neurotoxicity syndrome (ICANS) could not be overlooked.

CRS is the most common toxicity of CAR-T therapy with classic symptoms of pyrexia, fatigue, hypotension, and hypoxicemia. There are several grading systems (5–7) for the classification of CRS associated with CAR-T therapy, among which the American Society for Transplantation and Cellular Therapy (ASTCT) grading system is now adopted in most research and clinical management due to its simplicity and ease of implementation. The mechanism of CRS is still not fully understood, but what is certain is that in the complex inflammatory cascade, immune cells such as macrophages and the various inflammatory factors they release play a major role. The guideline (8) recommends the use of Tocilizumab, corticosteroids, and life-support treatments for CRS, but the ideal timing for the launch of these treatments is still under debate. In recent years, there have been numerous studies exploring the effects of corticosteroids on CAR-T therapy. Several studies (9–11) have demonstrated that the early use of corticosteroids did not affect the amplification of CAR-T, and the long-term efficacy of immunotherapy in lymphoma and leukemia. However, Strati et al. (12) found that higher a cumulative dose and prolonged and early use of corticosteroids were all associated with significantly shorter overall survival.

Tocilizumab is an IL-6 antagonist that can precisely block interleukin-6 (IL-6), which has been shown to be associated with severe CRS (1, 13). It is used in rheumatologic diseases and was approved by FDA to treat CAR-T-associated CRS in patients older than 2 years old (14). Tocilizumab did not influence the proliferation, persistence, and efficacy of CAR-T and did not present severe side effects (2), so there are few studies on the safety and efficacy of Tocilizumab in early administration. Caimi et al. and Banerjee et al. reported that prophylactic Tocilizumab administered 1 h before CAR-T cell infusion or early Tocilizumab given ≤12 h after CRS onset was beneficial for the domination of CRS in non-Hodgkin lymphoma and multiple myeloma patients, respectively (15, 16). However, one preliminary result suggested that the prophylactic use of Tocilizumab did not inhibit or even increase the incidence of ICANS in NHL (17). Studies aiming for the early treatment of Tocilizumab are lacking in patients with leukemia. In the published papers, the onset of Tocilizumab mainly depends on the grading systems. Whether to introduce the quantitative biomarkers into management strategy and optimize the window period of Tocilizumab have certain significance for further improving the safety of CAR-T therapy.

For the purposes described above, we conducted a retrospective analysis of 67 patients with B-ALL to determine the timing for treatment according to patients' symptoms and serum biomarkers and established a flow chart of early intervention strategies for patients with CRS.

METHODS

Patients and Infusion of CAR-T Cells

Complying with the inclusion and exclusion criteria in two clinical trials (NCT02965092, NCT04008251), 75 patients with R/R B-ALL were enrolled in this study. Patients received lymphodepleting chemotherapies following the infusion of murine or humanized CD19 CAR-T cells. The manufacturing and infusion of CAR-T cells were in accordance with a previous article (18). Informed consent in accordance with the Declaration of Helsinki were provided by every patient before participation. Apart from the eight patients not meeting the inclusion criteria, 67 patients were included in this study.

Definitions and Management of CRS

CRS was graded according to the ASTCT consensus, which has a concise interpretation with the following symptoms: grade 1, temperature ≥38°C; grade 2, fever with hypotension or/and hypoxia, not requiring vasopressors or high-flow nasal cannula; grade 3, administration of one vasopressors or/and supplemental oxygen like high-flow nasal cannula and facemask with fever; and grade 4, administration of more than one vasopressor or/and positive pressure respiratory support system.

We further defined grade 1–2 as mild CRS and grade 3–4 as severe CRS. Fever unattributable to any other cause was the onset of CRS. Since temperature can be influenced by administration of corticosteroids, the end of CRS was associated with disappearance of fever and declined cytokines.

Apart from symptomatic treatments such as antipyretic actions, oxygen therapy, and vasopressors, Tocilizumab and corticosteroids are common drugs in the treatment of CRS. Patients who developed persistent fever unrelated to infection and did not respond to antipyretic drugs received Tocilizumab. If symptoms persisted or progressed after two doses of Tocilizumab, corticosteroids such as dexamethasone and methylprednisolone were considered.

Assessment of ICANS and Infections

Neurological symptoms were evaluated and graded according to ASTCT consensus. Headache as a separate symptom was not considered neurotoxic. Corticosteroids were used as first-line agents for neurotoxicity. The diagnosis of infection was based on clinical symptoms and etiological examinations. The classification criteria were in accordance with Common Terminology Criteria for Adverse Events v4.0.3 (CTCAEv4). Severe infection was defined as grade 3–4 infection in which intravenous fluids were required.

Assessment of Response and Prognosis

Response to therapy was assessed using morphological analysis, flow cytometry, and genetic testing. CR was defined as <5% bone marrow blasts in morphology regardless of cell count recovery, negative MRD, and negative high-risk genotype if existing. Bone marrow aspiration detection was performed every month for half a year and every 3 months in 2 years after CAR-T therapy. Relapsed disease was defined as the reappearance of blasts in the blood or bone marrow or in an extramedullary site after CR. Overall survival (OS) was defined as the time from infusion to the date of death or the last follow-up. Progression-free survival (PFS) was calculated from the date of CR to the date of relapse, death, or the last follow-up.

Collection of Clinical Laboratories

Peripheral blood was collected for concentrations of inflammatory factors. The baselines of inflammatory factors were defined as concentrations at day 0 when CAR-T cell was infused. Peak levels were regarded as the maximum concentration before the administration of Tocilizumab or 1 month after CAR-T infusion in patients receiving Tocilizumab or not, respectively. Fold change was defined as the ratio of peak to baseline. Inflammatory factors that changed significantly during the process of CAR-T therapy included interleukin (IL)-2, IL-4, IL-6, IL-10, tumor necrosis factor alpha (TNF-α), interferon gamma (IFN-γ), C-reactive protein (CRP), and ferritin (FER), which were evaluated in the study.

Statistical Analyses

All measurement data were described using median and range and compared using Mann–Whitney tests. Enumeration data were presented as frequency (%) and compared using chi-square tests or Fisher's exact test. Follow-up time, OS, and LFS were estimated using the Kaplan–Meier method, whereas differences between groups were evaluated using log-rank test. Cutoffs were calculated by establishing ROC curves. All tests were two-sided, and $p < 0.05$ was considered statistically significant. Data were analyzed and presented using GraphPad Prism version 9.

RESULTS

Patient Characteristics and Management Post-infusion

From May 2018 to September 2021, a total of 75 patients with R/R B-ALL in our phrase I/II clinical trials received CAR-T cells. Excluding five patients receiving secondary infusion after murine CAR-T therapy and three patients losing examination data, 67 patients were enrolled in our retrospective study. Baseline characteristics of all 67 patients and the subgroup analysis of the toci and non-toci groups were summarized (**Table 1**). As shown, two groups were similar with regard to normal demographics and previous therapies. However, tumor burdens were higher in the toci group with significant statistical difference.

Patients receiving murine or humanized CD19 CAR-T cells accounted for 49.3% and 50.3%, respectively. After infusion, CRS occurred in 43 patients with 27 patients in grade 1, 11 patients in grade 2, 4 patients in grade 3, 1 patient in grade 4, and 1 patient in grade 5. The median onset and duration of CRS was 6 days (range, 2–11) and 5 days (range, 2–21), respectively. Tocilizumab was administrated in 33 patients including 17 patients with grade 1, 9 patients with grade 2, 5 patients with grade 3–5 CRS, and one patient with headache and elevated IL-6 in peripheral blood and cerebrospinal fluid instead of symptoms of CRS. One to four doses of Tocilizumab were used to suppress CRS with median dose of 480 mg (range, 160–800). The dosing interval of tocilizumab was 24–48 h. Corticosteroids were used in 23 patients, and the cumulative dexamethasone-equivalent corticosteroid dose was 62.5 mg (range, 7.5–302.5). Continuous dosing of corticosteroids was administrated until the patients' symptoms improved. Significantly higher usage of corticosteroids appeared in the toci group. Of the total 67 patients, 86.6% (N=58) responded and 85% (N=57) achieved complete remission with MRD and genotype negativity.

Usage of Tocilizumab Can Be Advanced to Grade 2 CRS

Patients' clinical symptoms including pyrexia, hypotension, and hypoxemia were the main basis for CRS grading according to ASTCT criteria. The toci and non-toci groups had similar duration of CRS in grade 1, grade 3–5, and total patients. However, in patients developing grade 2 CRS, those treated with Tocilizumab had significantly shorter duration of CRS than those without Tocilizumab (p=0.0004, **Figure 1A**). Although the non-toci group experienced less severe infections or ICANS when comparing to the toci group, Tocilizumab did

TABLE 1 | Characteristics and treatment of patients and comparison of subgroups.

CHARACTERISTIC	Total (N = 67)	Toci (N = 32)	Non-toci (N = 35)	p
Median age (range), years	29 (13–65)	28 (14–58)	30 (18–65)	0.918
Male, No. (%)	35 (52.2)	13 (40.6)	22 (62.9)	0.068
Previous therapies				
Median lines of therapy (range)	3 (1–10)	3 (1–10)	3 (1–10)	0.088
Allogeneic SCT, No (%)	12 (18.9)	7 (21.9)	5 (14.3)	0.418
Primary refractory disease, No (%)	29 (43.3)	12 (37.5)	17 (48.5)	0.361
Baseline disease burden				
Bone marrow blasts, %				
>50	14 (20.9)	12 (37.5)	2 (5.7)	
25–50	13 (19.4)	8 (25)	5 (14.3)	
5–25	14 (20.9)	4 (12.5)	10 (28.6)	
<5	26 (38.8)	8 (25)	18 (51.4)	
Median blasts, range	16.53 (0–95.18)	30.60 (0–95.18)	4.83 (0–90)	0.001
High-risk phenotype or genotypes	23 (34.3)	8 (25)	15 (42.9)	0.124
Infusion of humanized CAR-T, No (%)	34 (50.7)	19 (59.4)	15 (42.9)	0.177
Doses of CAR-T, range (*10^6/kg)	4 (2-6)	4 (2-4)	4 (2-6)	>0.999
Corticosteroids, No (%)	23 (34.3)	17 (53.1)	6 (17.4)	0.002

SCT, stem cell transplantation.

not amplify the incidence of these adverse events in the subgroup grade 2 (p=0.4545, **Figure 1C**; p>0.9999, **Figure 1D**). There was no difference between the toci and non-toci groups in terms of complete remission rate at 1 month (**Figure 1B**) and long-term efficacy including overall survival (grade 1, p=0.1893; grade 3–5, p=0.6547, **Supplementary Figure 2**; grade 2, p=0.3977, **Figure 1E**) and progression-free survival (grade 1, p=0.1309; grade 3–5, p=0.2743, **Supplementary Figure 2**; grade 2, p=0.9186, **Figure 1F**) regardless of CRS grading.

Two Patients Progressed to Severe CRS After Early Treatment of Tocilizumab

Patient A received CAR-T cells on September 2020 and had a fever with hypoxemia on day 5 post-infusion, which was defined as grade 2 CRS. He was given Tocilizumab twice on days 7 and 9 when the conventional antipyretic therapy was ineffective. However, the condition progressed rapidly right after the second infusion of Tocilizumab and respiratory support system, and vasopressors were required because CRS had upgraded to grade 4. After effective application of corticosteroids and supportive therapies, the patient gradually recovered and achieved complete remission within 21 days.

Patient B who received CAR-T cells on September 2018 seemed to have similar progression of CRS. She experienced prolonged mild CRS during days 3–13. Tocilizumab had been administrated twice when the patient was in grade 2 CRS. However, the intervention did not restrain the progression of CRS, and unfortunately, the patient died of respiratory failure related to severe CRS on day 20 (**Figure 2**).

Cytokines Related to CRS and the Cutoffs

Laboratory biomarkers of inflammation were evaluated in all treated subjects from the time of CAR-T cell infusion to 1 month after infusion. There was no difference between cytokine and inflammation indicator levels of patients before or after treatment of Tocilizumab except for IL-6 (**Supplementary Figure 3**). Thus, Tocilizumab could increase the level of IL-6 in peripheral blood exponentially; we defined peak level of IL-6 in the toci group as the maximum before administration of Tocilizumab.

Both peak amount and fold change of IL-6, IL-10, CRP, and FER had significant statistical differences between patients with or without CRS (**Supplementary Figure 4**), which indicated that these laboratory markers presented a positive correlation with the occurrence of CRS. Therefore, we grouped the patients into low and high levels of IL-6, IL-10, CRP, or FRE, respectively, on the basis of the cutoffs of ROC curve (**Figure 3**).

Fold Change of IL-6 and CRP Back the Use of Tocilizumab

The efficacy of Tocilizumab on CRS, the influence on other adverse events, and the effect on short- or long-term anti-leukemia capacity were evaluated in high- and low-level groups, respectively. In patients with less than fourfold

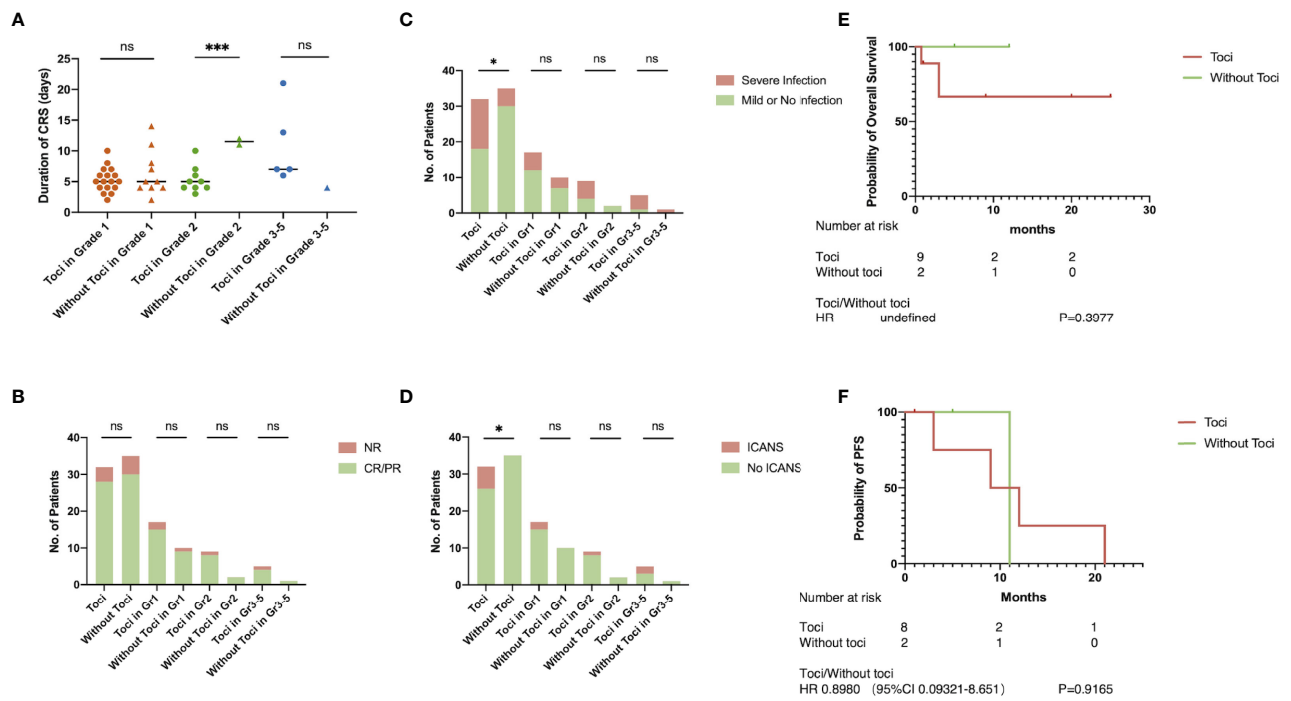

FIGURE 1 | Tocilizumab shortened the duration of CRS. The grading of CRS and whether to use Tocilizumab were the basis for grouping. **(A)** Duration of CRS; **(B)** objective response rate; **(C)** incidence of severe infection; **(D)** incidence of ICANS; **(E)** overall survival rate in patients with grade 2 CRS; **(F)** progression-free survival in patients with grade 2 CRS. *p < 0.05; ***p < 0.001.

increase in IL-6, severe CRS was more likely to take place in patients treated with Tocilizumab (37.5% versus 0%, **Figure 4B**). A shorter duration of CRS could be observed when treatment was given at a remarkably elevated IL-6 (median, 5; range, 3–13 days versus median, 8; range, 2–14 days, p=0.0575, **Figure 4A**), but without statistical difference. When patients were divided according to the level of CRP, it was worth noting that patients with elevated CRP had an additional chance of developing serious infections after receiving Tocilizumab (47.8% versus 11.8%, p=0.0204, **Supplementary Figure 6A**). There was no significantly difference between the two groups parted by IL-10 or FER in all aspects (**Supplementary Figures 7, 8**).

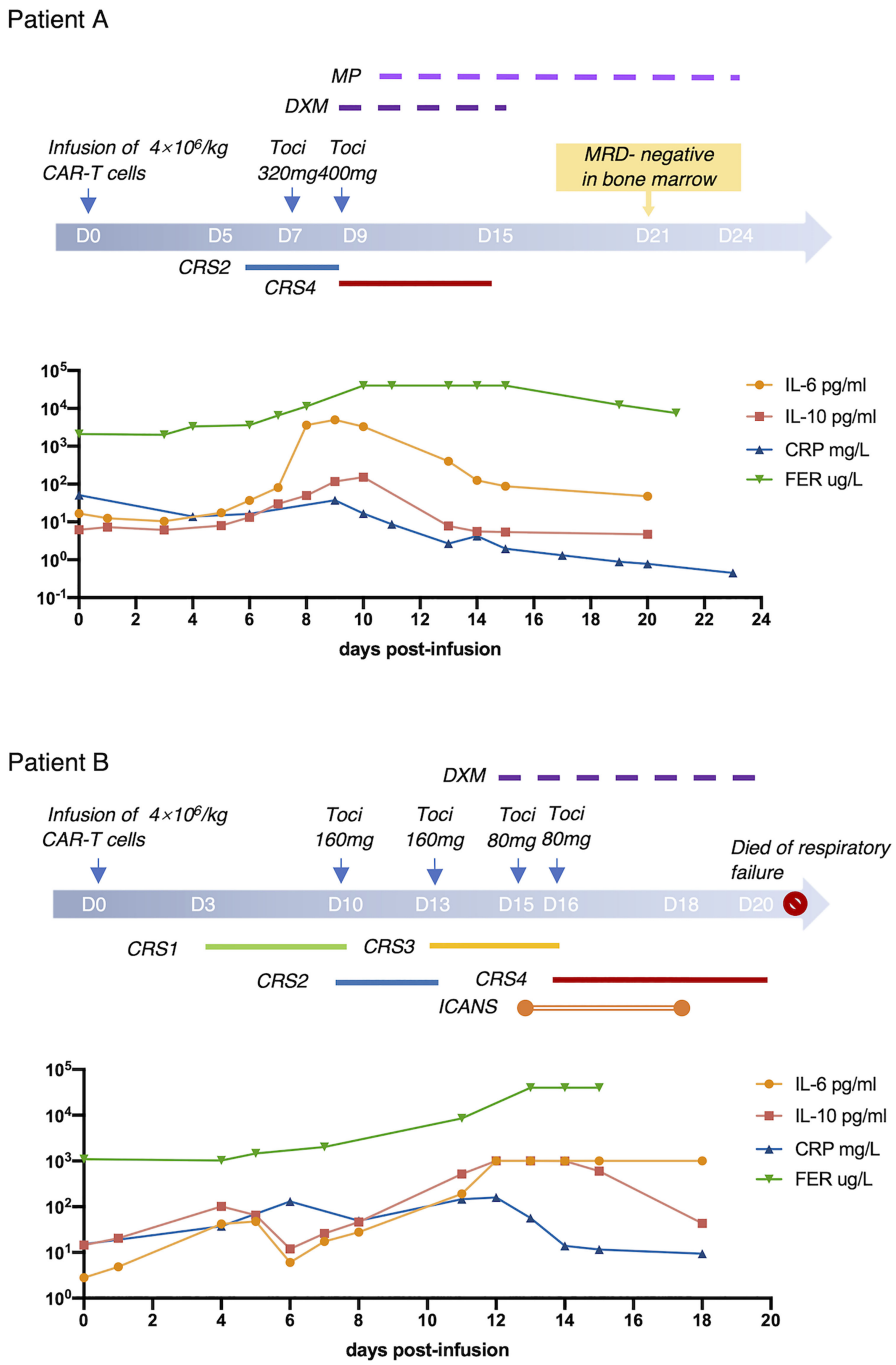

FIGURE 2 | Two Cases With Severe CRS. Progression and treatment of two typical patients with severe CRS. MP, methylprednisolone; DXM, dexamethasone.

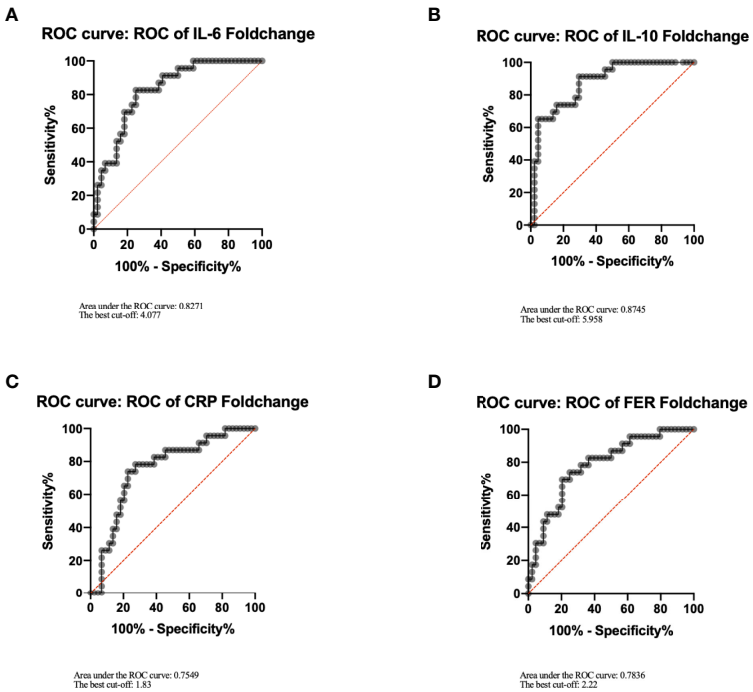

FIGURE 3 | Cutoffs of IL-6, IL-10, CRP, FER. IL-6 **(A)**, IL-10 **(B)**, CRP **(C)**, FER **(D)** were analyzed by ROC curve using GraphPad Prism, and the best cutoffs were determined according to the coordinates of the ROC curve. Youden index=sensitivity+specificity−1. Its maximum value corresponds to the optimal cutoff.

DISCUSSION

CAR-T cell therapy, as a promising novel immunotherapy, resulted in unprecedented remission rates in patients with B-ALL. However, frequent, even potentially life-threatening adverse events represented by CRS limited patients' survival and quality of life after treatment. By binding to IL-6R, Tocilizumab accurately inhibits the downward transmission of IL-6 signaling pathways and effectively reduces the secretion of various acute inflammatory proteins such as CRP, and is considered to be a safe drug that suppresses CRS without affecting CAR-T cell expansion and long-term remission (2, 4, 19). The US Food and Drug Administration had approved Tocilizumab for the treatment of severe CRS, but several studies (15, 16) showed that preemptive usage of Tocilizumab might facilitate the better control of CRS. NCCN (8) had also formulated different timings for infusing Tocilizumab in each commercial CAR-T products, especially the immediate administration of Tocilizumab when CRS occurred within 72 h after infusion of axicabtagene ciloleucel or brexucabtagene autoleucel regardless of grading. However, the ideal timing of the use of Tocilizumab that is universal to different kinds of CAR-T cells has not yet been determined.

Before discussing the effect of tocilizumab on CRS, the influence of other factors on the development of CRS should be excluded. The state of T cells used to manufacture CAR-T cells can affect the proliferation and cytotoxicity of CAR-T cells *in vivo* and, therefore, contributes to CRS. The state of T cells is determined by the baseline characteristics of patients including age, disease, chronic infections, tumor burden, and previous treatments, especially SCT (20). In our study, all participants were patients with ALL, and their baseline conditions are presented in **Table 1** and analyzed between subgroups. Patients in the toci group had a significantly higher tumor load, which would be discussed later, but there was no statistic difference in other aspects.

On the basis of clinical symptoms, the ASTCT grading system proved to be easily applicable, and its accuracy was confirmed in the incidence of adverse reactions in previous clinical trials (7). These clinical symptoms, including fever, hypotension, and hypoxemia, can be used as factors in determining whether to take interventions or not. In our clinical trials, patients who developed grade 2 CRS and received Tocilizumab terminated inflammation responses earlier than those without Tocilizumab, revealing that patients with persistent fever and mild hypotension or hypoxemia should be considered for Tocilizumab intervention. In the whole, the use of Tocilizumab made a statistically significant difference in the occurrence of adverse events such as ICANS and severe infection. In our study, all patients who developed ICANS had used Tocilizumab, but 50% (n=3) of the patients had neurological symptoms such as impaired consciousness before intervention. Besides, the incidence of ICANS in patients using Tocilizumab was not significantly increased in each grade of CRS. To our knowledge, no previous studies have found a relationship among CRS, Tocilizumab, and severe infection. It could cause

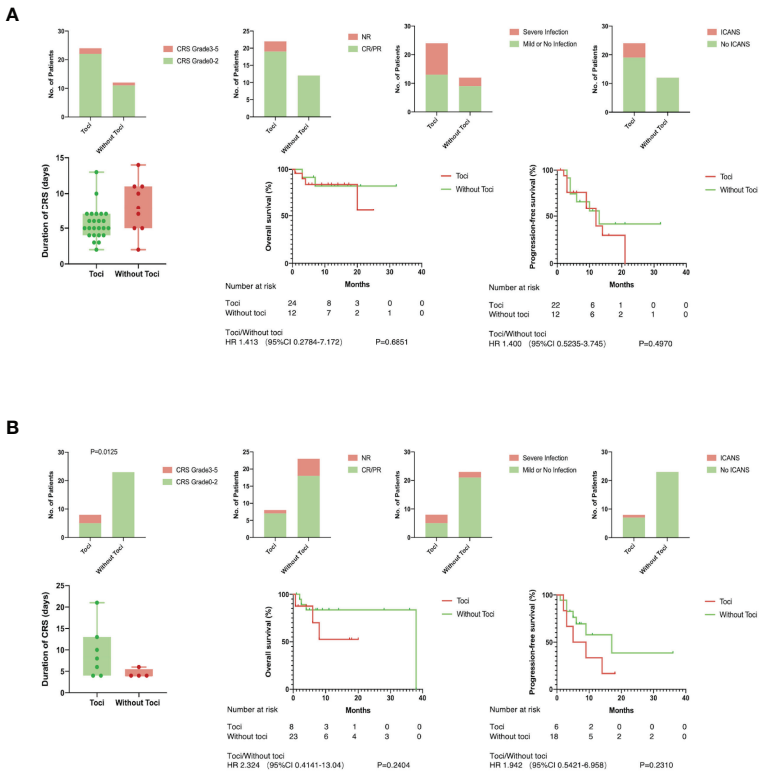

FIGURE 4 | Tocilizumab induced severe CRS in low level group. There was no significantly difference between patients with toci and without toci except for one. **(A)** Duration of CRS, incidence of severe infection and ICANS, objective response rate in short-term, overall survival and progression-free survival in long term were compared between patients with or without toci in high level group of IL-6; **(B)** Duration of CRS, incidence of severe infection and ICANS, objective response rate in short-term, overall survival, and progression-free survival in the long term were compared between patients with or without toci in low level group of IL-6.

a mild reduction in neutrophil count among healthy people (14) and increased susceptibility to bacterial infections in patients with rheumatologic diseases. However, when it comes to CAR-T therapy, the use of Tocilizumab is unlikely to be a direct element in infection due to multiple factors such as the lymphodepleting chemotherapy and hematological toxicity of the CAR-T cells. Similarly, the incidence of severe infections did not increase in patients receiving Tocilizumab in each grade of CRS.

Statistically, the use of Tocilizumab at grade 2 CRS can effectively inhibit the continuous progression of CRS without affecting the efficacy and safety of CAR-T therapies. However, the progression and treatment process of two patients provided us with a new orientation for evaluating intervention. Both of these two patients received Tocilizumab at grade 2 CRS and progressed to grade 4 with mildly elevated IL-6 before treatment of Tocilizumab. A study had proven that elevated levels of IL-6 could predict the use of invasive mechanical ventilation in patients with severe COVID-19 after administration of Tocilizumab (21). Analysis of two cases and the previous study have demonstrated that apart from clinical symptoms, laboratory biomarkers, especially IL-6, may also be able to guide medications.

Given the large differences in baseline levels among patients, we considered that laboratory biomarkers of which both the absolute and the fold change made statistical differences can be included in the following discussion. Patients with IL-6 elevating below four times are more likely to develop severe CRS after receiving Tocilizumab. This phenomenon can be caused by a variety of factors, including precise antagonism of Tocilizumab to IL-6 and delayed treatment such as corticosteroids or plasmapheresis. The blockade of IL-6 pathway would effectively reduce the production of CRP and control the patients temperature. However, at the same time, it may conceal the apparent signs of the ongoing inflammatory storm inside the patients, and other treatments could not be applied in a timely manner. In the group with remarkable elevated IL-6, the use of Tocilizumab did not significantly inhibit the development of CRS and cause changes in safety and efficacy, which is inconsistent with our hypothesis. It is widely acknowledged that the occurrence of inflammation is positively correlated with the tumor burden before treatment. Thus, it is reasonable to speculate that the inconspicuous inhibition of Tocilizumab in CRS may be due to a significant difference in tumor burden between the toci and non-toci groups.

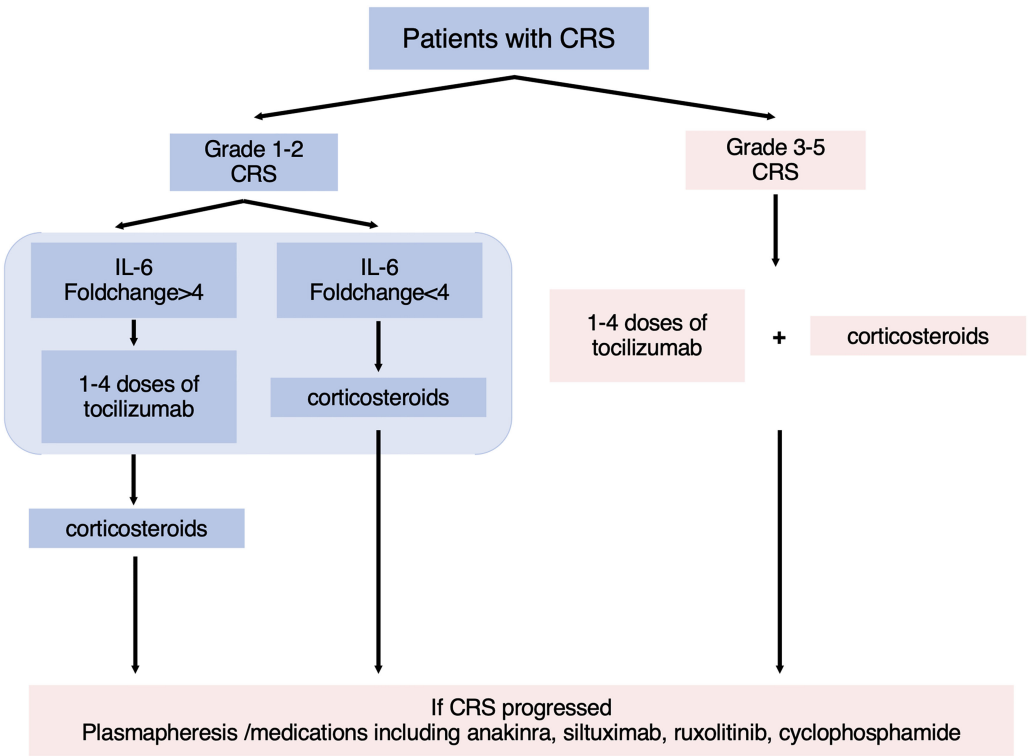

FIGURE 5 | The flowchart of guidelines for the treatment of CRS. According to the ASTCT grading system and level of IL-6, patients were recommended for different treatment options.

Due to the block of receptors using Tocilizumab, dissociative IL-6 in the peripheral blood rose rapidly. It has been reported that cytokines accelerated the activation of endothelial cells, which results in the injury of blood–brain barrier (22, 23). An experiment *in vivo* had proved that IL-6 contributed to blood–brain barrier dysfunction *via* JAK-STAT signaling pathway in tumor microenvironment (24). On the one hand, significantly increased pro-inflammation cytokines diffused to the central nervous system. On the other hand, impaired blood–brain barrier could not inhibit the entry of CAR-T cells, which might targeted mural cells expressing CD19 (25). Both sides contributed to the occurrence of ICANS. Several studies (17, 26, 27) disclosed that Tocilizumab given prophylactically would not benefit or even increase the rates of neurotoxicity. In our study, there was no significant difference between two groups in the incidence of ICANS when the level of IL-6 lifted over four times. If we had a sufficient number of ICANS, it would be reasonable to set up a maximum level of IL-6 beyond which measures were demanded to prevent ICNAS after using Tocilizumab. Severe CRS has been demonstrated to be associated with infections (28, 29) which may be related to liver secreting acute inflammatory proteins induced by IL-6 and pancytopenia caused by severe CRS (28). In our study, patients with elevated CRP over 1.83 times were more likely to develop severe infections after receiving Tocilizumab, which suggested that we should pay more attention to the patients' infection progression after administration of Tocilizumab and intervene as soon as possible.

In summary, we validated the guiding significance of the grading system for the early application of Tocilizumab while introducing level of IL-6 to consummate individualized treatment for patients with different inflammatory responses. Through a retrospective study of 67 patients with B-ALL in our center, Tocilizumab was recommended for patients whose clinical symptoms had meet the standard of ASTCT grade 2 and whose concentration of IL-6 had increased by more than four times (**Figure 5**). For patients whose clinical symptoms had up to standard with IL-6 rising inconspicuously, they were recommended to receive corticosteroids in advance to inhibit the progression of CRS. For patients with CRP increasing >1.83 times, signs and indicators of infection should be strictly monitored after treatment of Tocilizumab to avoid the occurrence of fatal infection. This study still has some limitations. Due to the relatively aggressive treatment regimen for CRS in our center, few patients did not use tocilizumab after the onset of CRS. Although based on the available data, we presented a statistical difference in the duration of CRS between the two groups in grade 2 CRS, a larger sample size is needed to further validate this conclusion. Moreover, 15% of patients lost contact 1 month after CAR-T therapies so the follow-ups were terminated. Nonetheless, our conclusion can guide clinical medication to some extent and improve the safety of CAR-T cell infusion.

DATA AVAILABILITY STATEMENT

The original contributions presented in the study are included in the article/**Supplementary Material**. Further inquiries can be directed to the corresponding author/s.

ETHICS STATEMENT

The studies involving human participants were reviewed and approved by the Medical Ethics Committee of Union Hospital, Tongji Medical College, Huazhong University of Science and Technology. Written informed consent to participate in this study was provided by the participants' legal guardian/next of kin.

AUTHOR CONTRIBUTIONS

HM designed the study. YL, MD, YZ, and FZ contributed to clinical data collection and analysis. YZ, ZW, and FZ wrote the first version of the manuscript. CLi, MD, WL, FZ, and HM revised the manuscript. HK, CLu, and HM performed the clinical trial and provided patient care. All authors read the final manuscript and have agreed to be co-authors.

FUNDING

This work was supported by the National Key Research and Development Program of China (No. 2019YFC1316203), National Natural Science Foundation of China (No. 82070124) and Natural Science Foundation of Hubei Province (No. 2020CFA065).

ACKNOWLEDGMENTS

CAR-T product was provided by Wuhan Sian Medical Technology Co., Ltd. The authors thank the patients who participated in the study and their families and caregivers, the physicians and nurses who cared for patients and supported this clinical trial and the staff members at the study sites.

SUPPLEMENTARY MATERIAL

The Supplementary Material for this article can be found online at: https://www.frontiersin.org/articles/10.3389/fimmu.2022.914959/full#supplementary-material

REFERENCES

1. Lee DW, Kochenderfer JN, Stetler-Stevenson M, Cui YK, Delbrook C, Feldman SA, et al. T Cells Expressing Cd19 Chimeric Antigen Receptors for Acute Lymphoblastic Leukaemia in Children and Young Adults: A Phase 1 Dose-Escalation Trial. *Lancet* (2015) 385(9967):517–28. doi: 10.1016/S0140-6736(14)61403-3
2. Maude SL, Frey N, Shaw PA, Aplenc R, Barrett DM, Bunin NJ, et al. Chimeric Antigen Receptor T Cells for Sustained Remissions in Leukemia. *N Engl J Med* (2014) 371(16):1507–17. doi: 10.1056/NEJMoa1407222
3. Gardner RA, Finney O, Annesley C, Brakke H, Summers C, Leger K, et al. Intent-To-Treat Leukemia Remission by Cd19 Car T Cells of Defined Formulation and Dose in Children and Young Adults. *Blood* (2017) 129(25):3322–31. doi: 10.1182/blood-2017-02-769208
4. Maude SL, Laetsch TW, Buechner J, Rives S, Boyer M, Bittencourt H, et al. Tisagenlecleucel in Children and Young Adults With B-Cell Lymphoblastic Leukemia. *N Engl J Med* (2018) 378(5):439–48. doi: 10.1056/NEJMoa1709866
5. Lee DW, Gardner R, Porter DL, Louis CU, Ahmed N, Jensen M, et al. Current Concepts in the Diagnosis and Management of Cytokine Release Syndrome. *Blood* (2014) 124(2):188–95. doi: 10.1182/blood-2014-05-552729
6. Lee DW, Santomasso BD, Locke FL, Ghobadi A, Turtle CJ, Brudno JN, et al. Astct Consensus Grading for Cytokine Release Syndrome and Neurologic Toxicity Associated With Immune Effector Cells. *Biol Blood Marrow Transplant* (2019) 25(4):625–38. doi: 10.1016/j.bbmt.2018.12.758
7. Pennisi M, Jain T, Santomasso BD, Mead E, Wudhikarn K, Silverberg ML, et al. Comparing Car T-Cell Toxicity Grading Systems: Application of the Astct Grading System and Implications for Management. *Blood Adv* (2020) 4(4):676–86. doi: 10.1182/bloodadvances.2019000952
8. Thompson JA, Schneider BJ, Brahmer J, Andrews S, Armand P, Bhatia S, et al. Nccn Guidelines Insights: Management of Immunotherapy-Related Toxicities, Version 1.2020. *J Natl Compr Canc Netw* (2020) 18(3):230–41. doi: 10.6004/jnccn.2020.0012
9. Liu S, Deng B, Yin Z, Pan J, Lin Y, Ling Z, et al. Corticosteroids Do Not Influence the Efficacy and Kinetics of Car-T Cells for B-Cell Acute Lymphoblastic Leukemia. *Blood Cancer J* (2020) 10(2):15. doi: 10.1038/s41408-020-0280-y
10. Topp MS, van Meerten T, Houot R, Minnema MC, Bouabdallah K, Lugtenburg PJ, et al. Earlier Corticosteroid Use for Adverse Event Management in Patients Receiving Axicabtagene Ciloleucel for Large B-Cell Lymphoma. *Br J Haematol* (2021) 195(3):388–98. doi: 10.1111/bjh.17673
11. Oluwole OO, Bouabdallah K, Muñoz J, De Guibert S, Vose JM, Bartlett NL, et al. Prophylactic Corticosteroid Use in Patients Receiving Axicabtagene Ciloleucel for Large B-Cell Lymphoma. *Br J Haematol* (2021) 194(4):690–700. doi: 10.1111/bjh.17527
12. Strati P, Ahmed S, Furqan F, Fayad LE, Lee HJ, Iyer SP, et al. Prognostic Impact of Corticosteroids on Efficacy of Chimeric Antigen Receptor T-Cell Therapy in Large B-Cell Lymphoma. *Blood* (2021) 137(23):3272–6. doi: 10.1182/blood.2020008865
13. Norelli M, Camisa B, Barbiera G, Falcone L, Purevdorj A, Genua M, et al. Monocyte-Derived Il-1 and Il-6 Are Differentially Required for Cytokine-Release Syndrome and Neurotoxicity Due to Car T Cells. *Nat Med* (2018) 24(6):739–48. doi: 10.1038/s41591-018-0036-4
14. Le RQ, Li L, Yuan W, Shord SS, Nie L, Habtemariam BA, et al. Fda Approval Summary: Tocilizumab for Treatment of Chimeric Antigen Receptor T Cell-Induced Severe or Life-Threatening Cytokine Release Syndrome. *Oncologist* (2018) 23(8):943–7. doi: 10.1634/theoncologist.2018-0028
15. Caimi PF, Pacheco Sanchez G, Sharma A, Otegbeye F, Ahmed N, Rojas P, et al. Prophylactic Tocilizumab Prior to Anti-Cd19 Car-T Cell Therapy for Non-Hodgkin Lymphoma. *Front Immunol* (2021) 12:745320. doi: 10.3389/fimmu.2021.745320
16. Banerjee R, Marsal J, Huang C-Y, Lo M, Kambhampati S, Kennedy VE, et al. Early Time-To-Tocilizumab After B Cell Maturation Antigen-Directed Chimeric Antigen Receptor T Cell Therapy in Myeloma. *Transplant Cell Ther* (2021) 27(6):477.e1–.e7. doi: 10.1016/j.jtct.2021.03.004
17. Locke FL, Neelapu SS, Bartlett NL, Lekakis LJ, Jacobson CA, Braunschweig I, et al. Preliminary Results of Prophylactic Tocilizumab After Axicabtageneciloleucel (Axi-Cel; Kte-C19) Treatment for Patients With Refractory, Aggressive Non-Hodgkin Lymphoma (Nhl). *Blood* (2017) 130(Supplement 1):1547. doi: 10.1182/blood.V130.Suppl_1.1547.1547
18. Jiang H, Liu L, Guo T, Wu Y, Ai L, Deng J, et al. Improving the Safety of Car-T Cell Therapy by Controlling Crs-Related Coagulopathy. *Ann Hematol* (2019) 98(7):1721–32. doi: 10.1007/s00277-019-03685-z

19. Park JH, Rivière I, Gonen M, Wang X, Sénéchal B, Curran KJ, et al. Long-Term Follow-Up of Cd19 Car Therapy in Acute Lymphoblastic Leukemia. *N Engl J Med* (2018) 378(5):449–59. doi: 10.1056/NEJMoa1709919
20. Mehta PH, Fiorenza S, Koldej RM, Jaworowski A, Ritchie DS, Quinn KM. T Cell Fitness and Autologous Car T Cell Therapy in Haematologic Malignancy. *Front Immunol* (2021) 12:780442. doi: 10.3389/fimmu.2021.780442
21. Galván-Román JM, Rodríguez-García SC, Roy-Vallejo E, Marcos-Jiménez A, Sánchez-Alonso S, Fernández-Díaz C, et al. Il-6 Serum Levels Predict Severity and Response to Tocilizumab in Covid-19: An Observational Study. *J Allergy Clin Immunol* (2021) 147(1):72–80.e8. doi: 10.1016/j.jaci.2020.09.018
22. Gust J, Hay KA, Hanafi L-A, Li D, Myerson D, Gonzalez-Cuyar LF, et al. Endothelial Activation and Blood-Brain Barrier Disruption in Neurotoxicity After Adoptive Immunotherapy With Cd19 Car-T Cells. *Cancer Discovery* (2017) 7(12):1404–19. doi: 10.1158/2159-8290.CD-17-0698
23. Santomasso BD, Park JH, Salloum D, Riviere I, Flynn J, Mead E, et al. Clinical and Biological Correlates of Neurotoxicity Associated With Car T-Cell Therapy in Patients With B-Cell Acute Lymphoblastic Leukemia. *Cancer Discovery* (2018) 8(8):958–71. doi: 10.1158/2159-8290.CD-17-1319
24. Kim J, Chuang H-C, Wolf NK, Nicolai CJ, Raulet DH, Saijo K, et al. Tumor-Induced Disruption of the Blood-Brain Barrier Promotes Host Death. *Dev Cell* (2021) 56(19):2712–21.e4. doi: 10.1016/j.devcel.2021.08.010
25. Parker KR, Migliorini D, Perkey E, Yost KE, Bhaduri A, Bagga P, et al. Single-Cell Analyses Identify Brain Mural Cells Expressing Cd19 as Potential Off-Tumor Targets for Car-T Immunotherapies. *Cell* (2020) 183(1):126–42.e17. doi: 10.1016/j.cell.2020.08.022
26. Gardner RA, Ceppi F, Rivers J, Annesley C, Summers C, Taraseviciute A, et al. Preemptive Mitigation of Cd19 Car T-Cell Cytokine Release Syndrome Without Attenuation of Antileukemic Efficacy. *Blood* (2019) 134(24):2149–58. doi: 10.1182/blood.2019001463
27. Gust J, Finney OC, Li D, Brakke HM, Hicks RM, Futrell RB, et al. Glial Injury in Neurotoxicity After Pediatric Cd19-Directed Chimeric Antigen Receptor T Cell Therapy. *Ann Neurol* (2019) 86(1):42–54. doi: 10.1002/ana.25502
28. Juluri KR, Wu V, Voutsinas JM, Hou J, Hirayama AV, Mullane E, et al. Severe Cytokine Release Syndrome Is Associated With Hematologic Toxicity Following Cd19 Car T-Cell Therapy. *Blood Adv* (2021) 6(7):2055–68. doi: 10.1182/bloodadvances.2020004142
29. Korell F, Schubert M-L, Sauer T, Schmitt A, Derigs P, Weber TF, et al. Infection Complications After Lymphodepletion and Dosing of Chimeric Antigen Receptor T (Car-T) Cell Therapy in Patients With Relapsed/Refractory Acute Lymphoblastic Leukemia or B Cell Non-Hodgkin Lymphoma. *Cancers (Basel)* (2021) 13(7):1684. doi: 10.3390/cancers13071684

Conflict of Interest: The authors declare that the research was conducted in the absence of any commercial or financial relationships that could be construed as a potential conflict of interest.

The reviewer CL declared a shared parent affiliation with the authors to the handling editor at the time of review.

frontiers | Frontiers in Immunology

ORIGINAL RESEARCH
published: 04 July 2022
doi: 10.3389/fimmu.2022.876415

The Outcome of Induction Therapy for EBV-Related Hemophagocytic Lymphohistiocytosis: A Model for Risk Stratification

*Tingting Cui, Jingshi Wang and Zhao Wang**

Department of Hematology, Beijing Friendship Hospital, Capital Medical University, Beijing, China

OPEN ACCESS

Edited by:
Weili Zhao,
Shanghai Jiao Tong University, China

Reviewed by:
Tadashi Ariga,
Hokkaido University, Japan
Hirokazu Kanegane,
Tokyo Medical and Dental University, Japan

***Correspondence:**
Zhao Wang
wangzhao@ccmu.edu.cn

Specialty section:
This article was submitted to Cancer Immunity and Immunotherapy, a section of the journal Frontiers in Immunology

Received: *15 February 2022*
Accepted: *30 May 2022*
Published: *04 July 2022*

Citation:
Cui T, Wang J and Wang Z (2022) The Outcome of Induction Therapy for EBV-Related Hemophagocytic Lymphohistiocytosis: A Model for Risk Stratification. Front. Immunol. 13:876415. doi: 10.3389/fimmu.2022.876415

Background: Epstein–Barr virus (EBV)–related hemophagocytic lymphohistiocytosis (HLH) is an abnormal inflammation caused by EBV infection, which has high mortality during induction therapy.

Objectives: This study is aimed to build a model to predict the risk of death during induction therapy.

Methods: The patients with EBV-HLH admitted from January 2015 to December 2018 were retrospectively reviewed. The primary outcome was death during induction therapy. The interval from receiving therapy to death or the end of induction therapy was the observing time. The patients admitted from January 2015 to December 2017 were assigned to the primary group, and the patients admitted from January to December 2018 were assigned to the validation group.

Results: We included 234 patients with EBV-HLH, of whom 65 (27.4%) died during induction therapy. The middle observing time was 25 days. On the basis of the primary group, the multivariate Cox analysis demonstrated age >18 years, blood urea nitrogen, procalcitonin >2 μg/L, serum CD25, and EBV-DNA in peripheral blood mononuclear cell as the risk factors of death during induction therapy. We developed a nomogram integrating the above factors with high predictive accuracy (c-statistic, 0.86) and stratified all patients into the high-risk and the low-risk groups. On the basis of the validation group, the high-risk patients had a higher risk of death (hazard ratio, 4.93; P = 0.012). In the subgroup analysis based on patients receiving etoposide-based strategy, the mortality in high-risk and low-risk patients was 43.9 and 3.1 per 100 person-weeks, respectively.

Conclusion: We developed a nomogram for risk stratification of patients with EBV-HLH receiving induction therapy.

Keywords: hemophagocytic lymphohistiocytosis, Epstein–Barr virus, outcome, induction therapy, predicting model

INTRODUCTION

Epstein–Barr virus (EBV)–related hemophagocytic lymphohistiocytosis (HLH) has been found as an abnormal inflammation, characterized by the overactivity of immune cells caused by EBV infection. Without appropriate therapy, patients with EBV-HLH have a mortality up to 20%–95.7% (1–3). Although the allogenic haemopoietic stem cell transplantation has been found as an effective method to treat EBV-HLH, about two-thirds of patients will die during induction therapy, especially in the sixth to the eighth week after they receive standard therapy (2). To identify the patients with a high risk of death during induction therapy is conducive to managing the patients with EBV-HLH and predicting the outcome.

There have been few reliable models and factors to predict the risk of death of patients with EBV-HLH after they receive induction therapy. Moreover, the factors of the death of patients with EBV-HLH during induction therapy were also unclear. Some studies found that age, serum CD25 (sCD25), and EBV loading were the factors of poor outcome (4–6). However, the correlation between these factors and death during induction therapy has been unknown.

In this study, we reviewed the clinical characteristics and therapy strategy of patients with EBV-HLH admitted to our medical institution. This study is aimed to investigate the risk factors of the death during induction therapy and build a model to predict this event.

METHODS AND MATERIALS

Population and Study Design

The study was approved by the institutional review board of Beijing Friendship Hospital (2020-P2-096-01). Written informed consents were obtained, and the privacy of patients was effectively protected.

In this study, the patients with EBV-HLH admitted to our medical institution between January 2015 and December 2018 were retrospectively reviewed. The inclusion criteria of patients with EBV-HLH included the following (1): patients were diagnosed with HLH in accordance with HLH-2004 diagnostic criteria; (2) the EBV-DNA was positive (>500 copies/ml) in plasma or peripheral blood mononuclear cell (PBMC); and (3) complete or traceable clinical record. A total of 270 eligible patients were included. Moreover, 30 patients diagnosed with lymphoma by pathological examinations and (2) six patients diagnosed with primary HLH by gene examination were excluded [We excluded four patients with familial hemophagocytic lymphocytosis 2 (compound heterozygote). One patient with familial hemophagocytic lymphocytosis 3 and one patient with X-linked lymphoproliferative disease were excluded. No primary immunodeficiency]. Last, we included 234 appropriate patients with EBV-HLH.

Among the included patients with EBV-HLH, the patients admitted from January 2015 to December 2017 were assigned to the primary group (184 patients with EBV-HLH) to build a predictive model, and the patients admitted from January to December 2018 were assigned to the validation group (50 patients with EBV-HLH). The ratio of the primary group to the validation group was about 3.5:1 (**Figure 1**).

Procedures

We acquired the information according to the electronic medical records, including demographic information (e.g., gender, age, the history of infection, the history of tuberculous infection and bleeding history, brain involvement, and liver/spleen involvement), laboratory findings at admission [i.e., white blood cell (WBC) count, hemoglobin, platelet count, glutamic-pyruvic transaminase (ALT), glutamic oxalacetic transaminase (AST), gamma-glutamyl transpeptidase (GGT), alkaline phosphatase (ALP), total bilirubin (Tbi), direct bilirubin (Dbi), indirect bilirubin (Ibi), albumin (ALB), creatinine (Cr), blood urea nitrogen (Bun), K^+, Ca^{2+}, Na^+, fibrinogen, procalcitonin (PCT), and erythrocyte sedimentation rate (ESR)], and specific findings [hemophagocytosis, serum ferritin, sCD25, the activity of nature killer cells (NK cells), EBV-DNA in plasma and PBMC, the CD107a in NK cell (NK-CD107a), and the CD107a in cytotoxic T lymphocyte (CTL-CD107a)].

We divided all the patients into the group with the age >18 years and the group ≤18 years. For the history of tuberculous infection correlated with poor outcome in HLH, patients were categorized as the group of history of tuberculous infection and the group of other infections. According to liver and spleen involvement, patients were classified as splenomegaly, hepatomegaly, and hepatosplenomegaly groups. PCT >2 μg/L indicated a severe inflammation, so we classified patients into PCT >2 μg/L and PCT ≤2 μg/L groups.

Management and Induction Therapy

In accordance with HLH therapy guideline, the therapy strategy for patients with EBV-HLH included etoposide-based protocol (e.g., HLH-1994, HLH-2004, doxorubicin-etoposide-methylprednisolone (DEP), and PEG aspargase-DEP (LDEP)) instead of etoposide-based protocol (e.g., corticosteroids and corticosteroids + rituximab) (7).

In general, the interval from standard induction therapy to transplantation is at least 8 weeks. Moreover, death occurred mostly in the sixth to the eighth week (2). For the above reasons, we observed patients and recorded the outcome at weeks 4 and 8 after standard therapy began.

Outcomes

The primary outcome was death during induction therapy (in 8 weeks after the patients received standard therapy). We set the interval from receiving standard therapy to death or the end of induction therapy (8 weeks) as the observing time for further

Abbreviation: HLH, hemophagocytic lymphohistiocytosis; EBV, Epstein–Barr virus; sCD25, serum CD25; PBMC, peripheral blood mononuclear cell; ALT, glutamic-pyruvic transaminase; AST, glutamic oxalacetic transaminase; GGT, gamma-glutamyl transpeptidase; ALP, alkaline phosphatase; Tbi, total bilirubin; Dbi, direct bilirubin; Ibi, indirect bilirubin; ALB, albumin; Cr, creatinine; Bun, blood urea nitrogen; PCT, procalcitonin; ESR, erythrocyte sedimentation rate; NK cells, nature killer cells.

analysis. According to the primary outcome, we divided all patients into the survival group and the death group.

Statistical Analysis

Continuous variables with normal distribution were expressed as means and standard deviation, or medians (m) and inter-quartile range (IQR) if otherwise. Categorical variables were expressed as numbers (no.) and percentage (%). We compared the differences between the death and survival groups in continuous variables through student's t-tests or Wilcoxon rank sum tests, and we compared the differences in categorical variables through chi-square tests or Fisher's exact tests. We conducted univariate Cox regression analyses to detect the factors for the primary outcome. We entered the parameters with statistical significance in univariate Cox regression analyses in multivariate regression models through a backward step-down selection process. The result was expressed as hazard ratios (HR) and 95% confidence intervals (CI).

The nomogram was developed with the package of "rms" in R version 4.1.1. Subsequently, we generated a nomogram to predict the primary outcome (death during induction therapy). In accordance with the result of the multivariate Cox regression analysis, we developed a nomogram model that included the factors for the primary outcome. We calculated the survival probabilities 4 and 8 weeks after the patients received standard therapy. We measured the performance of the nomogram to predict the primary outcome by the c-statistic values in receiver operating the characteristic curve (ROC) analysis. The model with c-statistic >0.8 and P <0.05 was considered to be good clinical utility. The calibration curves were generated to evaluate the calibration of the nomogram. We performed bootstrapping validation for the nomogram (1,000 bootstrap resamples). To identify the breakpoint of nomogram points for the primary outcome, we conducted regression discontinuity analysis using the package of "smoothHR" and "Hmisc" in R version 4.1.1. The restricted cubic splines were used to smooth model and visualize the relation of predicted death risk and actual death risk. The nomogram point value with breaking HR change was recognized as the breakpoint. According to the calculated breakpoint, we separated all patients into the low-risk group and the high-risk group. We conducted the survival analyses using Kaplan–Meier method. Moreover, the mortality was calculated.

The statistical analysis was conducted using SPSS 24.0 (SPSS, Chicago, IL), and two-sided P <0.05 had statistical significance.

RESULTS

Demographic and Clinical Characteristics of Patients in the Primary Group

Among 184 patients with EBV-HLH included in the primary group, 54 died (29.3%) during induction therapy. Twenty-two patients died of multiple organ dysfunction syndrome, 23 patients died of infection, six patients died of gastrointestinal bleeding, and three patients died of central nervous system involved. Among 50 patients with EBV-HLH included in the validation group, 10 died (20%) during induction therapy, three patients died of multiple organ dysfunction syndrome, five patients died of infection, one patient died of gastrointestinal bleeding, and one patient died of central nervous system involved. **Table 1** lists the demographic and clinical information of patients with EBV-HLH in the primary group. One-hundred fifteen patients were male, with a median age of 25.0 (15.5–39.5). One-hundred forty-seven (79.9%) patients were treated with etoposide. More patients with age >18 years (P = 0.007), history of tuberculous infection (P = 0.043), brain involvement (P < 0.001), hepatosplenomegaly (P = 0.049), and PCT >2 μg/L (P = 0.027) died during induction therapy. Moreover, sCD25 level and EBV-DNA in PBMC were higher in the patients ending up dead (P = 0.019 and 0.007, respectively). Moreover, the significance was found in WBC count (P = 0.015), hemoglobin (P = 0.001), platelet count (P = 0.007), GGT (P = 0.007), ALP (P = 0.049), Tbi (P = 0.031), Dbi (P = 0.004), ALB (P < 0.001), Bun (P = 0.038), Ca^{2+} (P = 0.002), Na^{+} (P = 0.013), and fibrinogen (P = 0.018) between the death group and the survival group. However, there was no significant difference in gender, therapy strategy, other infections, splenomegaly, hepatomegaly, ALT, AST, Ibi, Cr, K^{+}, ESR, hemophagocytosis, serum ferritin, the activity of NK cells, EBV-DNA in plasma, and CD107a (all P >0.05).

The Factors of Death During Induction Therapy and Nomogram

On the basis of the primary group, we entered all significant parameters into the univariate analysis and entered the parameters with clinical significance into the univariate Cox regression analysis. As indicated by the result, age >18 years (HR, 1.48; 95% CI, 1.04–2.13; P = 0.031), GGT (HR, 1.00; 95% CI, 1.00–1.00; P = 0.040), Cr (HR, 1.01; 95% CI, 1.00–1.01; P = 0.003), Bun (HR, 1.08; 95% CI, 1.03–1.13; P = 0.003), PCT >2 μg/L (HR, 1.05; 95% CI, 1.01–1.10; P = 0.028), sCD25 (HR, 1.07; 95% CI, 1.02–1.12; P = 0.004), and EBV-DNA in PBMC (HR, 1.09; 95% CI, 1.04–1.14; P < 0.001) were correlated with death during induction therapy (**Figure 2A** and **Supplementary Table 1**). Subsequently, we entered the above parameters into the multivariate Cox regression analysis. The parameters, including age >18 years (HR, 1.24; 95% CI, 1.08–1.42; P = 0.040), Bun (HR, 1.08; 95% CI, 1.02–1.13; P = 0.015), PCT > 2 μg/L (HR, 2.60; 95% CI, 1.49–4.55; P = 0.001), sCD25 (HR, 1.08; 95% CI, 1.02–1.14; P = 0.010), and EBV-DNA in PBMC (HR, 1.10; 95% CI, 1.05–1.16; P < 0.001), were independent risk factors of death during induction therapy (**Table 2**).

We developed a nomogram integrating the above risk factors (**Figure 2B**), which can predict the survival probability of patients with EBV-HLH during induction therapy. In accordance with the result of the regression discontinuity analysis (**Figure 2C**), we identified the breakpoints of the nomogram points as 80. According to **Figure 2D**, we divided all patients into the low-risk group (>80 points) and the high-risk group (≤80 points). The calibration curves indicated that the death predicted by the nomogram was consistent with the actual death (**Figures 3A, B**). The prediction accuracy of the

TABLE 1 | Demographic and clinical information of patients with EBV-HLH in the primary cohort.

Characteristics	Deathn = 54	Survivaln = 130	*P*-value
Male, no. (%)	29 (53.7%)	86 (66.2%)	0.113
Age >18 years, no. (%)	44 (81.4%)	79 (60.8%)	0.007†
Therapy strategy, no. (%)			0.206
Etoposide-based	40 (74.1%)	107 (82.3%)	
No etoposide-based	14 (25.9%)	23 (17.7%)	
Infection history, no. (%)			
Tuberculous	12 (22.2)	14 (10.8%)	0.043†
Other	50 (92.5%)	111 (85.4%)	0.179
Brain involvement, no. (%)	18 (33.3%)	12 (1.5%)	<0.001†
Liver/spleen involvement, no. (%)			
Splenomegaly	18 (33.3%)	60 (46.2%)	0.110
Hepatomegaly	1 (1.9%)	4 (3.1%)	0.643
Hepatosplenomegaly	28 (51.9%)	47 (36.2%)	0.049†
Laboratory findings			
WBC count, m (IQR), $\times10^9$	1.5 (0.9–2.5)	2.1 (1.4–3.6)	0.015†
Hemoglobin (g/l), m (IQR)	87 (77–100)	101.5 (84–119)	0.001†
Platelet count, m (IQR), $\times10^9$	45 (24–68)	60.5 (37–118)	0.007†
ALT (U/L), m (IQR)	91.5 (63.0–183.0)	81.5 (42.0–188.0)	0.455
AST (U/L), m (IQR)	145.2 (52.5–257.0)	84.9 (43.0–193.0)	0.070
GGT (U/L), m (IQR)	202 (111–378)	124 (48–282)	0.007†
ALP (U/L), m (IQR)	290 (129–566)	207 (100–400)	0.049†
Tbi (μmol/L), m (IQR)	32.0 (14.2–62.4)	19.4 (12.3–34.0)	0.031†
Dbi (μmol/L), m (IQR)	17.2 (5.0–58.1)	7.4 (3.5–20.0)	0.004†
Ibi (μmol/L), m (IQR)	12.9 (8.3–27.3)	12.0 (7.1–15.5)	0.055
ALB (g/L), m (IQR)	27.2 (24.0–32.9)	31.7 (27.7–37.4)	<0.001†
Cr (μmol/L), m (IQR)	55.2 (44.0–78.3)	53.7 (44.2–69.4)	0.455
Bun (mmol/L), m (IQR)	5.7 (4.2–7.5)	5.0 (3.7–7.1)	0.038†
K^+ (mmol/L), m (IQR)	3.92 (3.61–4.10)	4.04 (3.72–4.39)	0.052
Ca^{2+} (mmol/L), m (IQR)	1.97 (1.78–2.11)	2.10 (1.93–2.23)	0.002†
Na^+ (mmol/L), m (IQR)	134.0 (132.1–137.8)	136.9 (133.2–139.6)	0.013†
Fibrinogen (g/L), m (IQR)	1.26 (0.77–1.79)	1.61 (1.02–2.47)	0.018†
PCT > 2 μg/L, no. (%)	15	16	0.027†
ESR (mm/H), m (IQR)	27 (10–30)	18 (10–30)	0.845
Specific findings			
Hemophagocytosis, no. (%)	41 (75.9%)	105 (80.8%)	0.461
Serum ferritin (ng/ml), m (IQR), $\times10^3$	2.82 (1.65–15.00)	2.20 (0.95–13.07)	0.078
sCD25 (pg/ml)†, m (IQR), $\times10^4$	2.52 (1.94–4.40)	2.18 (0.31–4.01)	0.019†
The activity of NK cells (%)‡, m (IQR)	14.4 (13.0–14.5)	14.4 (13.5–16.4)	0.085
EBV-DNA (copies/ml), m (IQR), $\times10^5$			
Plasma	3.8 (1.5–17.0)	3.8 (0.3–26.0)	0.530
PBMC	8.7 (4.6–100.0)	6.2 (0.8–21.0)	0.007†
NK-CD107a (%), m (IQR)	12.2 (10.4–12.2)	12.2 (10.7–20.3)	0.198
CTL-CD107a (%), m (IQR)	2.7 (2.7–3.4)	2.7 (2.2–3.3)	0.247

†*The parameter was significant.*

†*The normal range of sCD25 is <6,400.*

‡*The normal range of the activity of NK cells is ≥15.11%.*

WBC, white blood cell; ALT, glutamic-pyruvic transaminase; AST, glutamic oxalacetic transaminase; GGT, gamma-glutamyl transpeptidase; ALP, alkaline phosphatase; Tbi, total bilirubin; Dbi, direct bilirubin; Ibi, indirect bilirubin; ALB, albumin; Cr, creatinine; Bun, blood urea nitrogen; PCT, procalcitonin; ESR, erythrocyte sedimentation rate; serum CD25; NK cells, nature killer cells; EBV, Epstein–Barr virus; DNA, deoxyribonucleic acid; PBMC, peripheral blood mononuclear cell; CTL, cytotoxic T lymphocyte.

nomogram was higher than that of any single parameters for the death during induction therapy (AUC was 0.76 for the 4-week death and was 0.86 for the 8-week death; **Figures 3C, D** and **Table 3**). The proportion of death was significantly different between the high-risk group and the low-risk group (**Figure 3E**). The survival analysis indicated that the high-risk group had a high risk of death during induction therapy (**Figure 3F**).

Validation of the Nomogram and Subgroup Analysis

The prediction accuracy of the nomogram was subsequently validated in validation group. The comparison of characteristics between the primary group and validation group is summarized in **Supplementary Table 2**.

According to the result of the validation group, the high-risk group still had a higher risk of death (HR, 4.93; 95% CI, 1.42–17.11; P = 0.012) during induction therapy (**Figure 4A**). As demonstrated by the multivariate Cox regression analysis, the high-risk group had a higher risk of death (HR, 3.89; 95% CI, 1.02–14.84; P = 0.047; **Figure 4B** and **Supplementary Tables 3, 4**). The nomogram had high performance in the validation group to predict the risk of death during induction therapy (AUC was 0.85 for the death in 4 weeks and was 0.81 for the death in 8 weeks**; Figures 4C, D** and **Table 3**). The

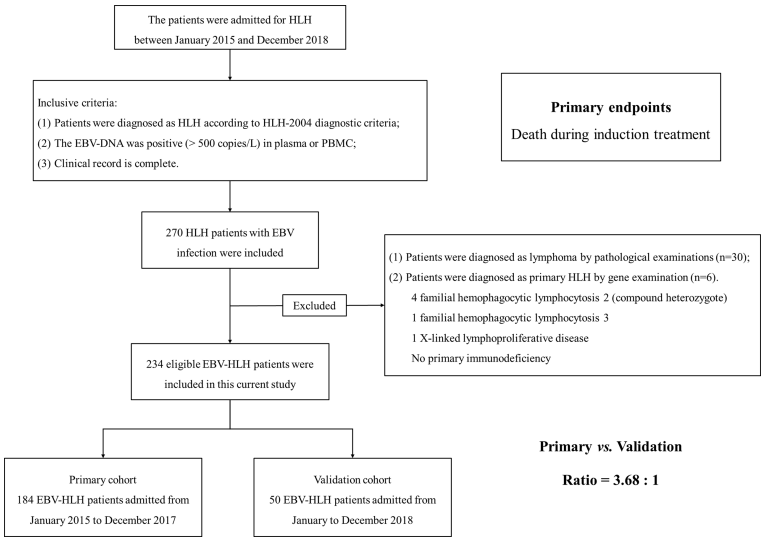

FIGURE 1 | The flow chart of patient enrollment. We retrospectively reviewed the patients admitted to our medical institution from January 2015 to December 2018. Finally, 234 patients were enrolled into this current study. We set patients admitted from January 2015 to December 2017 as primary cohort and patients admitted from January to December 2018 as validation cohort. The ratio of primary cohort to validation cohort was approximately 3.5:1.

calibration curves showed that the death predicted by the nomogram was consistent with the actual death (**Figures 4E, F**).

We further performed the subgroup analysis based on the therapy strategy (**Table 4**). The nomogram was used to categorize all patients of the primary and validation groups into the low-risk group (n = 177) and the high-risk group (n = 57). For those patients treated with etoposide, the mortality was 43.9 per 100 person-weeks for the high-risk patients, significantly higher than the mortality of 3.1 per 100 person-weeks for the low-risk patients. For the therapy without etoposide, the result was similar (34.4 vs. 9.5, per 100 person-weeks). The mortality was higher in the second 4-week period.

DISCUSSION

EBV-HLH is a second type of HLH with high mortality and has a high incidence in Asians (1, 8). Significant mortality in induction therapy has been found as a significant cause for poor outcome (1–3). In this study, we found age, Bun, PCT, sCD25, and EBV-DNA in PBMC as the factors of death during induction therapy. On the basis of the above factors, we built a nomogram model and validated the prediction accuracy of this model for the death in induction therapy. In the subgroup analysis, the high-risk patients had a higher mortality in both patients treated with etoposide and patients not treated with etoposide. High-risk patients treated with etoposide had a lower mortality.

This study found that patients with the age >18 years, increased sCD25, and high EBV-DNA in PBMC had a higher risk of death in induction therapy. For EBV-related diseases, older age was considered a sign of poor outcome (4). As reported in a previous study, the child patients were more likely to have a good outcome (9, 10), and the age ≥50 was a predictor for poor outcome (6), probably because mature immune system of adult patients can cause a severer inflammation response compared with the immature immune system of child patients (11, 12). sCD25 is positively correlated with the systematic inflammation response, which was recognized as a parameter to monitor the

TABLE 2 | Multivariate Cox regression analysis[†] for the risk factors associated with the survival in induction therapy based on primary cohort.

	HR	95% CI	*P*-value
Age >18 years	1.24	1.08–1.42	0.040
GGT		Omitted	
Cr		Omitted	
Bun	1.08	1.02–1.13	0.015
PCT >2 μg/L	2.60	1.49–4.55	0.001
sCD25, $\times 10^4$	1.08	1.02–1.14	0.010
EBV-DNA in PBMC, $\times 10^5$	1.10	1.05–1.16	<0.001

[†]*The multivariate Cox regression analysis was performed using backward method.*

HR, hazard ratio; GGT, gamma-glutamyl transpeptidase; Cr, creatinine; Bun, blood urea nitrogen; PCT, procalcitonin; serum CD25; EBV, Epstein–Barr virus; DNA, deoxyribonucleic acid; PBMC, peripheral blood mononuclear cell.

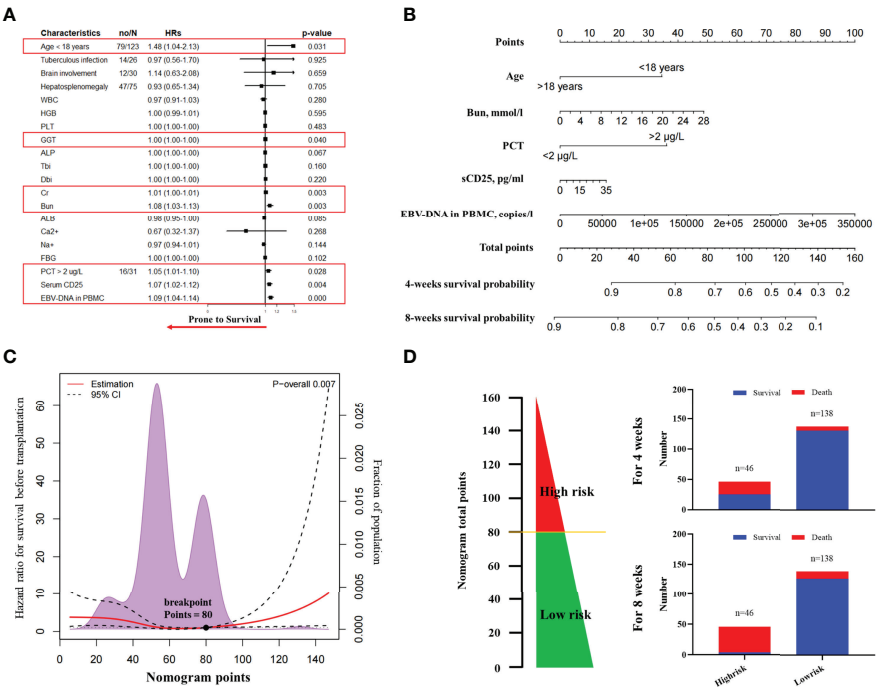

FIGURE 2 | The nomogram to predict the risk of death in induction therapy. **(A)** The forest plot of univariate Cox regression analysis. The result showed that age, GGT, Cr, Bun, PCT, sCD25, and EBV-DNA in PBMC were risk factors associated with the death in induction therapy. **(B)** The nomogram to predict the risk of death in induction therapy. **(C)** The breakpoints of nomogram points for the death in induction therapy. Using the regression discontinuity analysis, we identified the breakpoints of nomogram points as 80. **(D)** We categorized 46 patients as the high-risk group and 138 patients as the low-risk group. The histogram showed the death rate in each group. HR, hazard ratio; WBC, white blood cell; GGT, gamma-glutamyl transpeptidase; ALP, alkaline phosphatase; Tbi, total bilirubin; Dbi, direct bilirubin; ALB, albumin; Cr, creatinine; Bun, blood urea nitrogen; PCT, procalcitonin; EBV, Epstein–Barr virus; PBMC, peripheral blood mononuclear cell; CTL, cytotoxic T lymphocyte.

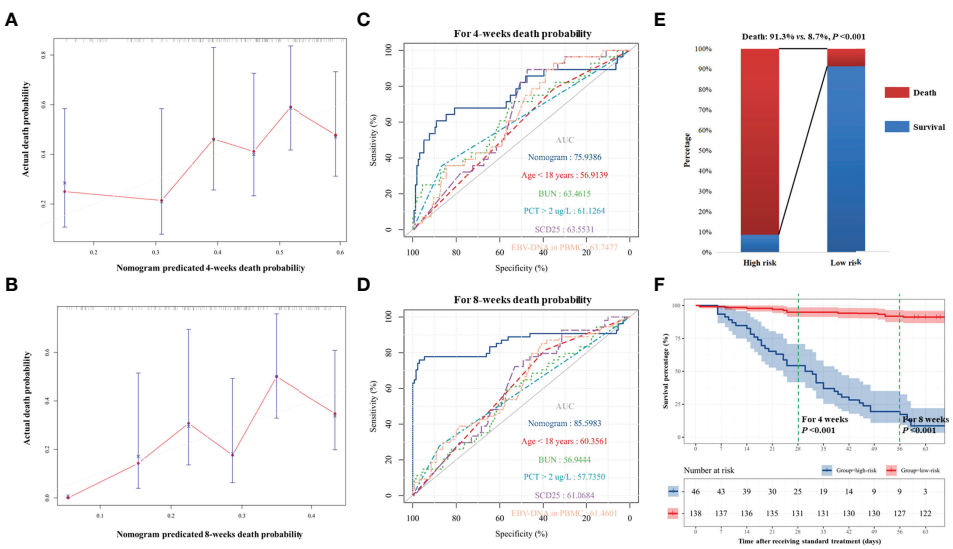

FIGURE 3 | The predicting accuracy of nomogram for death in induction therapy. **(A, B)** For death within 4 and 8 weeks, the nomogram has good consistency with actual death. **(C, D)** The predictive accuracy of nomogram and other risk factors for 4-week death and 8-week death. **(E)** The proportion of death in the high-risk group and the low-risk group. The difference was significant (91.3% vs. 8.7%, $P < 0.001$). **(F)** The survival analysis showed that high-risk patients had higher risk of death. Bun, blood urea nitrogen; PCT, procalcitonin; EBV, Epstein–Barr virus; DNA, deoxyribonucleic acid; PBMC, peripheral blood mononuclear cell.

TABLE 3 | The predicting accuracies of different models for the death after receiving standard therapy.

Models	Survival within 4 weeks				Survival within 8 weeks			
	Primary cohort		Validation cohort		Primary cohort		Validation cohort	
	c-statistic values	*P*-value	c-statistic values	*P*-value	c-statistic values	*P*-value	c-statistic values	*P*-value
Age >18 years	0.57 (0.46–0.68)	0.245	0.62 (0.45–0.81)	0.235	0.60 (0.52–0.69)	0.027	0.63 (0.40–0.84)	0.399
Bun	0.63 (0.52–0.75)	0.023	0.80 (0.59–0.97)	0.016	0.57 (0.48–0.66)	0.138	0.76 (0.61–0.90)	0.032
PCT >2 μg/L	0.61 (0.49–0.73)	0.061	0.82 (0.62–0.95)	0.219	0.58 (0.48–0.67)	0.099	0.63 (0.52–0.74)	0.414
sCD25	0.64 (0.54–0.73)	0.024	0.83 (0.74–0.90)	0.013	0.61 (0.53–0.69)	0.019	0.77 (0.68–0.98)	0.017
EBV-DNA in PBMC	0.64 (0.54–0.74)	0.021	0.56 (0.36–0.72)	0.874	0.61 (0.53–0.70)	0.014	0.51 (0.35–0.72)	0.649
Nomogram	0.76 (0.72–0.87)	<0.001	0.85 (0.72–0.93)	<0.001	0.86 (0.74–0.95)	0.004	0.81 (0.71–0.94)	0.011

Bun, blood urea nitrogen; PCT, procalcitonin; serum CD25; EBV, Epstein–Barr virus; DNA, deoxyribonucleic acid; PBMC, peripheral blood mononuclear cell.

recurrence of HLH (13). Compared with the secondary HLH caused by other factors, patients with EBV-HLH had a higher sCD25 level (14). The 5-year survival possibility of patients with HLH with sCD25 >10,000 IU/ml was 36%, significantly lower than that of patients with sCD25 ≤10,000 IU/ml as 78% (5). Thus, the high sCD25 level indicated that patients with EBV-HLH had a severe condition. Moreover, high EBV-DNA in PBMC was found as the factor of death in induction therapy, which was consistent with existing studies (10, 15). We considered that it might be because high EBV-DNA can induce a severe T cell and NK cell response. The EBV-DNA in PBMC reflects the intracellular EBV load, whereas the EBV-DNA in plasma reflects the leakage virus, which is from cells and tissues necrotic (16). For different EBV-related diseases, the EBV-DNA in plasma and in PBMC had different diagnostic values. For example, like chronic active EBV infection, EBV-DNA in PBMC had a higher predictive value for prognosis (17). However, for EBV-related tumor, like EBV+ NK/T cell lymphoma, EBV-DNA in plasma is meaningful (18). The pathological mechanism of EBV-HLH is close to chronic active EBV infection. For EBV-HLH, EBV-infected cells cannot be eliminated, which will result in an abnormal increase of cytokines (19). More EBV existed in NK/T cells, with no leak into plasma. Thus, for EBV-HLH, EBV-DNA in PBMC had a higher predictive value for prognosis.

Importantly, we found that high Bun and PCT >2 μg/L were correlated with a high risk of death in induction therapy. The increased Bun reflected impaired renal function and multiple organs dysfunctions. Existing studies reported a high incident rate of acute kidney injury in the activity period of HLH, which was mainly caused by acute renal tubular necrosis, renal hypoperfusion, tumor lysis syndrome, and HLH-related glomerulopathy (20). In addition to HLH, chemical therapy can cause renal injury and a multiple-organ failure. In this

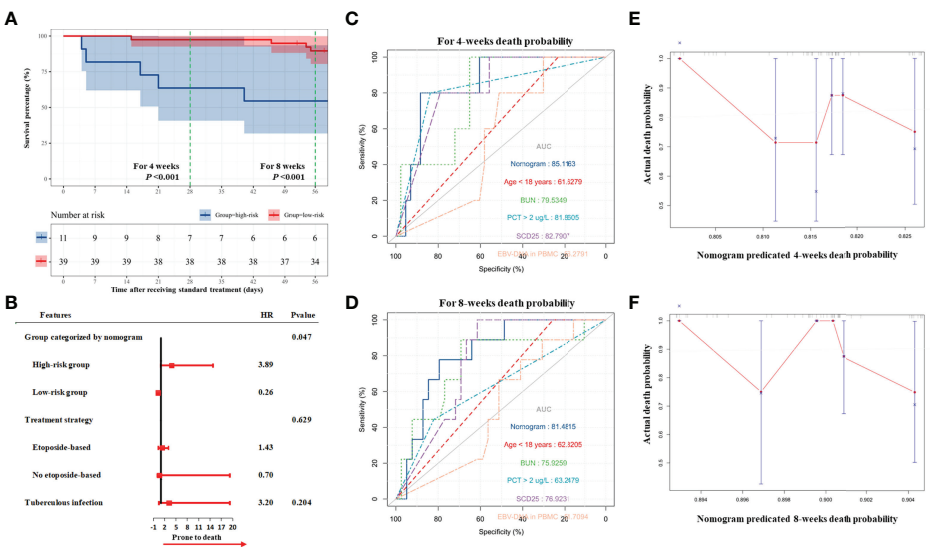

FIGURE 4 | Validation of nomogram for death in induction therapy. **(A)** On the basis of validation cohort, the survival analysis showed that high-risk patients had higher risk of death. **(B)** The result of multivariate Cox analysis. The result showed that the high-risk group categorized by nomogram was related to high risk of death. **(C, D)** The predicted accuracy of nomogram and other risk factors for 4- and 8-week death. **(E, F)** The calibration analyses showed that the death predicted by nomogram was consistent with the actual death. Bun, blood urea nitrogen; PCT, procalcitonin; EBV, Epstein–Barr virus; DNA, deoxyribonucleic acid; PBMC, peripheral blood mononuclear cell.

TABLE 4 | The incident rate of death in patients receiving different therapy strategy.

Groups		Etoposide-basedn = 181		No etoposide-basedn = 53	
		no.†	IR (95% CI)††	no.†	IR (95% CI)††
Low-risk group†††	The first 4 weeks	4	2.9 (0.1–5.7)	4	10.8 (0.3–21.3)
n = 177	The second 4 weeks	6	4.4 (0.9–7.9)	3	9.1 (0.0–19.4)
	Overall	10	3.1 (1.4–5.8)	7	9.5 (2.9–16.1)
High-risk group†††	The first 4 weeks	18	43.9 (28.0–59.8)	7	43.8 (16.4–71.1)
n = 57	The second 4 weeks	18	78.3 (60.0–96.5)	4	44.4 (3.9–85.0)
	Overall	36	43.9 (38.7–49.2)	11	34.4 (21.6–47.2)

†*The accumulative number of deaths.*

††*The incident rate of death per 100 person-weeks.*

††† *The patients with nomogram points > 80 were recognized as low-risk group, otherwise as the high-risk group.*

IR, incident rate.

study, we found that the risk of death would increase 1.08 times if the Bun increased as 1 U/L. Thus, a high Bun level before induction therapy can indicate the risk of death. Interestingly, PCT >2 μg/L was correlated with the high risk of death as well. In patients with the secondary HLH, an increased PCT was found in 77.7% of those patients (21). PCT >2 μg/L is correlated with a severe infection, especially bacterial infection, which is an important cause of death of patients with HLH (22, 23). During induction therapy, the immunological suppression caused by chemotherapy will increase the risk of bacterial infection (24). As indicated by our result, the patients with PCT >2 μg/L had 2.6 times of death compared with the patients with PCT ≤2 μg/L. Of the 19 patients who died with PCT >2 μg/L, 10 patients (52.6%) died of severe infection. Accordingly, PCT is also a parameter to predict the risk of death.

By integrating age, Bun, sCD25, and EBV-DNA in PBMC, we developed a nomogram to more effectively find the high-risk patients. This nomogram transferred patients' characteristics into points and categorized patients into the high-risk group and the low-risk group based on the above points, which is easily accessible to physicians. As indicated by our result, this nomogram had higher prediction accuracy compared with single parameters. If a patient has the nomogram points >80, then this patient will be recognized as belonging to the high-risk group, with a death probability in 4 weeks of 30% and a death probability in 8 weeks of more than 50%. We should monitor the apostasies (e.g., multiple organ dysfunction syndrome, severe infection, or gastrointestinal bleeding) once chemical therapy was admitted, especially in the second 4 weeks after patients received therapy. For patients with the nomogram points <80, they were assigned to the low-risk group and had a favorable outcome during induction therapy.

Another notable finding is the different therapeutic responses to different therapy strategies. A good outcome was found in low-risk patients not treated with etoposide and high-risk patients treated with etoposide during induction therapy. The reason for this outcome was considered to be that high-risk patients usually had a severer condition of overactivated immune cells compared with low-risk patients. Etoposide can quickly kill the overactivated immune cells, which is conducive to controlling EBV-HLH (4). However, low-risk patients could be quickly relieved after simple immunosuppressive therapy, e.g., corticosteroids (7). Thus, the therapy with etoposide is urgently recommended for high-risk patients.

This study had some limitations. First, this study was a single-center and retrospective study. Our conclusion might be limited by the cross-sectional study design. Second, we only investigated the risk factors of death in induction therapy and the reliability of the nomogram based on Chinese population. Whether our conclusion is suitable for other populations is unclear. Third, we only included the results of laboratory examination before induction therapy and did not monitor the change of each laboratory parameter during induction therapy. Fourth, we did not discuss the effect of EBV infection cell type on outcome. Although this study had the above limitations, we still developed a useful nomogram model to identify the high-risk patients with EBV-HLH before induction therapy.

CONCLUSION

Age, Bun, PCT, sCD25, and EBV-DNA in PBMC were the factors for death during induction therapy. We developed a nomogram to help identify the patients with a high risk of death during induction therapy. For patients with different risks of death, the therapy strategy could be different to improve the outcome during induction therapy. The therapy with etoposide is recommended for high-risk patients. It is necessary to monitor the apostasies of the mentioned high-risk patients, especially in the second 4 weeks after they receive chemical therapy. Acknowledgments

We thank Dr. Qingyuan Liu (China National Clinical Research Center for Neurological Diseases and Beijing Tiantan Hospital, Beijing, China) for helping in statistical analyses.

DATA AVAILABILITY STATEMENT

The original contributions presented in the study are included in the article/**Supplementary Material**. Further inquiries can be directed to the corresponding author/s.

ETHICS STATEMENT

The studies involving human participants were reviewed and approved by the Institutional Review Board of Beijing Friendship

Hospital. Written informed consent to participate in this study was provided by the participants' legal guardian/next of kin.

AUTHOR CONTRIBUTIONS

Author contributions to the study and manuscript preparation include the following. Conception and design: ZW and JW. Acquisition of data: TC. Analysis and interpretation of data: TC. Drafting the article: TC. Critically revising the article: ZW. Approving the final version of the manuscript on behalf of all authors: ZW. Study supervision: ZW. All authors contributed to the article and approved the submitted version.

FUNDING

This study was supported by the "National Natural Science Foundation of China (Grant No. 81871633 and 82170122)" and "The Capital Health Research and Development of Special (Grant No. 2020-1-2022)".

SUPPLEMENTARY MATERIAL

The Supplementary Material for this article can be found online at: https://www.frontiersin.org/articles/10.3389/fimmu.2022.876415/full#supplementary-material

REFERENCES

1. Ishii E, Ohga S, Imashuku S, Yasukawa M, Tsuda H, Miura I, et al. Nationwide Survey of Hemophagocytic Lymphohistiocytosis in Japan. *Int J Hematol* (2007) 86(1):58–65. doi: 10.1532/IJH97.07012
2. Bergsten E, Horne A, Arico M, Astigarraga I, Egeler RM, Filipovich AH, et al. Confirmed Efficacy of Etoposide and Dexamethasone in HLH Treatment: Long-Term Results of the Cooperative HLH-2004 Study. *Blood* (2017) 130 (25):2728–38. doi: 10.1182/blood-2017-06-788349
3. Lai W, Wang Y, Wang J, Wu L, Jin Z, Wang Z. Epstein-Barr Virus-Associated Hemophagocytic Lymphohistiocytosis in Adults and Adolescents-a Life-Threatening Disease: Analysis of 133 Cases From a Single Center. *Hematology* (2018) 23(10):810–6. doi: 10.1080/10245332.2018.1491093
4. Song Y, Wang Y, Wang Z. Requirement for Etoposide in the Initial Treatment of Epstein-Barr Virus-Associated Haemophagocytic Lymphohistiocytosis. *Br J Haematol* (2019) 186(5):717–23. doi: 10.1111/bjh.15988
5. Imashuku S, Hibi S, Sako M, Ishida Y, Mugishima H, Chen J, et al. Soluble Interleukin-2 Receptor: A Useful Prognostic Factor for Patients With Hemophagocytic Lymphohistiocytosis. *Blood* (1995) 86(12):4706–7. doi: 10.1182/blood.V86.12.4706.bloodjournal86124706
6. Oh EJ, Yoon JH, Park KH, Bae HJ, Yun SJ, Min GJ, et al. Natural-Killer Cell Cytotoxicity as a Diagnostic and Prognostic Marker for Adult Patients With Secondary Hemophagocytic Lymphohistiocytosis: A Prospective Phase II Observational Study. *Ther Adv hematol* (2021) 12:20406207211020544. doi: 10.1177/20406207211020544
7. La Rosee P, Horne A, Hines M, von Bahr Greenwood T, Machowicz R, Berliner N, et al. Recommendations for the Management of Hemophagocytic Lymphohistiocytosis in Adults. *Blood* (2019) 133(23):2465–77. doi: 10.1182/blood.2018894618
8. Ramos-Casals M, Brito-Zeron P, Lopez-Guillermo A, Khamashta MA, Bosch X. Adult Haemophagocytic Syndrome. *Lancet* (2014) 383(9927):1503–16. doi: 10.1016/S0140-6736(13)61048-X
9. Chen S, Wei A, Ma H, Zhang L, Lian H, Zhao Y, et al. Clinical Features and Prognostic Factors of Children With Chronic Active Epstein-Barr Virus Infection: A Retrospective Analysis of a Single-Center. *J Pediatr* (2021) 238:268–74 e2. doi: 10.1016/j.jpeds.2021.07.009
10. Yanagaisawa R, Matsuda K, Ohga S, Kanegane H, Morimoto A, Okamoto Y, et al. Factors Predicting the Recurrence of Epstein-Barr Virus-Associated Hemophagocytic Lymphohistiocytosis in Children After Treatment Using the HLH-2004 Protocol. *Int J Hematol* (2019) 109(5):612–7. doi: 10.1007/s12185-019-02612-2
11. Ahn JS, Rew SY, Shin MG, Kim HR, Yang DH, Cho D, et al. Clinical Significance of Clonality and Epstein-Barr Virus Infection in Adult Patients With Hemophagocytic Lymphohistiocytosis. *Am J hematol* (2010) 85(9):719–22. doi: 10.1002/ajh.21795
12. Shiraishi A, Ohga S, Doi T, Ishimura M, Takimoto T, Takada H, et al. Treatment Choice of Immunotherapy or Further Chemotherapy for Epstein-Barr Virus-Associated Hemophagocytic Lymphohistiocytosis. *Pediatr Blood Cancer* (2012) 59(2):265–70. doi: 10.1002/pbc.24039
13. Lin M, Park S, Hayden A, Giustini D, Trinkaus M, Pudek M, et al. Clinical Utility of Soluble Interleukin-2 Receptor in Hemophagocytic Syndromes: A Systematic Scoping Review. *Ann hematol* (2017) 96(8):1241–51. doi: 10.1007/s00277-017-2993-y
14. Shamriz O, Kumar D, Shim J, Briones M, Quarmyne MO, Chonat S, et al. T Cell-Epstein-Barr Virus-Associated Hemophagocytic Lymphohistiocytosis (HLH) Occurs in Non-Asians and Is Associated With a T Cell Activation State That Is Comparable to Primary HLH. *J Clin Immunol* (2021) 41 (7):1582–96.. doi: 10.1007/s10875-021-01073-9
15. Yu S, Yang Q, Wu J, Zhu M, Ai J, Zhang H, et al. Clinical Application of Epstein-Barr Virus DNA Loads in Epstein-Barr Virus-Associated Diseases: A Cohort Study. *J infect* (2021) 82(1):105–11. doi: 10.1016/j.jinf.2020.11.027
16. Heslop HE. How I Treat EBV Lymphoproliferation. *Blood* (2009) 114 (19):4002–8. doi: 10.1182/blood-2009-07-143545
17. Ito Y, Suzuki M, Kawada J, Kimura H. Diagnostic Values for the Viral Load in Peripheral Blood Mononuclear Cells of Patients With Chronic Active Epstein-Barr Virus Disease. *J Infect Chemother* (2016) 22(4):268–71. doi: 10.1016/j.jiac.2015.11.002
18. Suzuki R, Yamaguchi M, Izutsu K, Yamamoto G, Takada K, Harabuchi Y, et al. Prospective Measurement of Epstein-Barr Virus-DNA in Plasma and Peripheral Blood Mononuclear Cells of Extranodal NK/T-Cell Lymphoma, Nasal Type. *Blood* (2011) 118(23):6018–22. doi: 10.1182/blood-2011-05-354142
19. Imashuku S, Tabata Y, Teramura T, Hibi S. Treatment Strategies for Epstein-Barr Virus-Associated Hemophagocytic Lymphohistiocytosis (EBV-HLH). *Leuk Lymphoma* (2000) 39(1-2):37–49. doi: 10.3109/10428190009053537
20. Aulagnon F, Lapidus N, Canet E, Galicier L, Boutboul D, Peraldi MN, et al. Acute Kidney Injury in Adults With Hemophagocytic Lymphohistiocytosis. *Am J Kidney Dis* (2015) 65(6):851–9. doi: 10.1053/j.ajkd.2014.10.012
21. Strenger V, Merth G, Lackner H, Aberle SW, Kessler HH, Seidel MG, et al. Malignancy and Chemotherapy Induced Haemophagocytic Lymphohistiocytosis in Children and Adolescents-a Single Centre Experience of 20 Years. *Ann hematol* (2018) 97(6):989–98. doi: 10.1007/s00277-018-3254-4
22. Pontrelli G, De Crescenzo F, Buzzetti R, Jenkner A, Balduzzi S, Calo Carducci F, et al. Accuracy of Serum Procalcitonin for the Diagnosis of Sepsis in Neonates and Children With Systemic Inflammatory Syndrome: A Meta-Analysis. *BMC Infect dis* (2017) 17(1):302. doi: 10.1186/s12879-017-2396-7
23. Hu L, Shi Q, Shi M, Liu R, Wang C. Diagnostic Value of PCT and CRP for Detecting Serious Bacterial Infections in Patients With Fever of Unknown Origin: A Systematic Review and Meta-Analysis. *Appl Immunohistochem Mol Morphol* (2017) 25(8):e61–e9. doi: 10.1097/PAI.0000000000000552
24. Atkins S, He F. Chemotherapy and Beyond: Infections in the Era of Old and New Treatments for Hematologic Malignancies. *Infect Dis Clin North Am* (2019) 33(2):289–309. doi: 10.1016/j.idc.2019.01.001

Conflict of Interest: The authors declare that the research was conducted in the absence of any commercial or financial relationships that could be construed as a potential conflict of interest.

this article, or claim that may be made by its manufacturer, is not guaranteed or endorsed by the publisher.

frontiers | Frontiers in Immunology

TYPE Original Research
PUBLISHED 04 August 2022
DOI 10.3389/fimmu.2022.891175

OPEN ACCESS

EDITED BY
Weili Zhao,
Shanghai Jiao Tong University, China

REVIEWED BY
Meng Zhou,
Wenzhou Medical University, China
Aimei Dai,
Sun Yat-sen University, China

*CORRESPONDENCE
Yongzhong Yao
yyz1006@hotmail.com
Meng Cao
caomeng814@njmu.edu.cn

†These authors have contributed equally to this work

SPECIALTY SECTION
This article was submitted to Cancer Immunity and Immunotherapy, a section of the journal Frontiers in Immunology

RECEIVED 07 March 2022
ACCEPTED 28 June 2022
PUBLISHED 04 August 2022

CITATION
Li H, Liu H, Hao Q, Liu X, Yao Y and Cao M (2022) Oncogenic Signaling Pathway-Related Long Non-Coding RNAs for Predicting Prognosis and Immunotherapy Response in Breast Cancer.
Front. Immunol. 13:891175.
doi: 10.3389/fimmu.2022.891175

Oncogenic signaling pathway-related long non-coding RNAs for predicting prognosis and immunotherapy response in breast cancer

Huamei Li[1†], Hongjia Liu[2†], Qiongyu Hao[3†], Xianglin Liu[1], Yongzhong Yao[1*] and Meng Cao[1*]

[1]Department of General Surgery, Nanjing Drum Tower Hospital, the Affiliated Hospital of Nanjing University Medical School, Nanjing, China, [2]State Key Laboratory of Bioelectronics, School of Biological Science & Medical Engineering, Southeast University, Nanjing, China, [3]Division of Cancer Research and Training, Charles R. Drew University of Medicine and Science, Los Angeles, CA, United States

Background: The clinical outcomes of breast cancer (BC) are unpredictable due to the high level of heterogeneity and complex immune status of the tumor microenvironment (TME). When set up, multiple long non-coding RNA (lncRNA) signatures tended to be employed to appraise the prognosis of BC. Nevertheless, predicting immunotherapy responses in BC is still essential. LncRNAs play pivotal roles in cancer development through diverse oncogenic signal pathways. Hence, we attempted to construct an oncogenic signal pathway–based lncRNA signature for forecasting prognosis and immunotherapy response by providing reliable signatures.

Methods: We preliminarily retrieved RNA sequencing (RNA-seq) data from The Cancer Genome Atlas (TCGA) database and extracted lncRNA profiles by matching them with GENCODE. Following this, Gene Set Variation Analysis (GSVA) was used to identify the lncRNAs closely associated with 10 oncogenic signaling pathways from the TCGA-BRCA (breast-invasive carcinoma) cohort and was further screened by the least absolute shrinkage and selection operator Cox regression model. Next, an lncRNA signature (OncoSig) was established through the expression level of the final 29 selected lncRNAs. To examine survival differences in the stratification described by the OncoSig, the Kaplan–Meier (KM) survival curve with the log-rank test was operated on four independent cohorts (n = 936). Subsequently, multiple Cox regression was used to investigate the independence of the OncoSig as a prognostic factor. With the concordance index (C-index), the time-dependent receiver operating characteristic was employed to assess the performance of the OncoSig compared to other publicly available lncRNA signatures for BC. In addition, biological differences between the high- and low-risk groups, as portrayed by the OncoSig, were analyzed on the basis of statistical tests. Immune cell infiltration was investigated using gene set enrichment analysis (GSEA) and deconvolution tools (including CIBERSORT and ESTIMATE). The combined

effect of the Oncosig and immune checkpoint genes on prognosis and immunotherapy was elucidated through the KM survival curve. Ultimately, a pan-cancer analysis was conducted to attest to the prevalence of the OncoSig.

Results: The OncoSig score stratified BC patients into high- and low-risk groups, where the latter manifested a significantly higher survival rate and immune cell infiltration when compared to the former. A multivariate analysis suggested that OncoSig is an independent prognosis predictor for BC patients. In addition, compared to the other four publicly available lncRNA signatures, OncoSig exhibited superior predictive performance (AUC = 0.787, mean C-index = 0.714). The analyses of the OncoSig and immune checkpoint genes clarified that a lower OncoSig score meant significantly longer survival and improved response to immunotherapy. In addition to BC, a high OncoSig score in several other cancers was negatively correlated with survival and immune cell infiltration.

Conclusions: Our study established a trustworthy and discriminable prognostic signature for BC patients with similar clinical profiles, thus providing a new perspective in the evaluation of immunotherapy responses. More importantly, this finding can be generalized to be applicable to the vast majority of human cancers.

KEYWORDS

breast cancer, oncogenic signaling pathway, long non-coding RNA, immune infiltration, risk score, prognosis, immunotherapy

Introduction

Breast cancer (BC) is one of the most common cancers worldwide and is the major cause of cancer-related death in women (1). Based on the differences in historical and molecular levels, BC can be classified into five subtypes: HER2-positive (HER2), triple-negative/basal (Basal), normal-like (Normal), and luminal-A and B (LumA and LumB) (2, 3). So far, a combination of surgery, chemotherapy, hormone therapy, radiation therapy, and targeted therapy has been administered in the treatment of BC (4). Unfortunately, the considerable functional heterogeneity of diverse immune cell types in BC intrinsic subtypes has contributed to variations in the prognosis of BC patients (5, 6). With progress in research, the immune system has been found to play a vital role in tumorigenesis and cancer development (6). Previous reviews have summarized that protumorigenic and pro-inflammatory immune cells in the tumor microenvironment (TME) in BC consist of myeloid-derived suppressor cells (MDSCs), M2 macrophages, neutrophils, Th2 CD4+, Th17 CD4+, and FoxP3+ CD4+ T cells (T-regs) as well as T helper cells of type 1 (Th1) CD4+, CD8+ cytotoxic T lymphocytes (CTLs), M1 macrophages, dendritic cells (DCs), and natural killer (NK) cells, respectively (7, 8). Tumor-infiltrating lymphocytes (TILs) have been considered as predictive (9, 10) and prognostic (11, 12) biomarkers of immunotherapy in patients undergoing TNBC and HER2 BC treatment. However, to our current knowledge, there will be challenges to putting TIL assessment into clinical practice, mainly due to the lack of best TILs, upskilled clinicians, and prospective clinical trials (12). Thus, to obtain precise evidence for setting up an appropriate individual treatment strategy, there still remains an urgent need for credible signatures that provide trustworthy evidence for evaluating prognosis and response to immunotherapy in BC.

Long non-coding RNA (lncRNA) is an abundant type of RNA in the human transcriptome, with a transcript length of over 200 nucleotides, which lacks the capability to code protein (13). LncRNAs participate in 70% of gene expressions by enhancing or inhibiting the effects of DNA, RNA, and protein (14) and are strongly associated with cancer development, progression, and prognosis (15). Furthermore, lncRNAs play essential roles in many oncogenic signal pathways (16). Studies have confirmed that Linc00514 has the ability to regulate tumorigenicity and promote metastasis through the Jagged1-mediated Notch signal pathway in BC (17). While lncRNA *AU021063* promotes BC metastasis by activating the Mek/Erk

signaling pathway (18), the lncRNA *NIKLA* could inhibit NF-κB activation. Effectively, low levels of *NIKLA* in BC may be the underlying mechanism behind BC metastasis and poor prognosis, whilst a rising *NIKLA* level can be stimulated by Nuclear factor kappa-B (NF-κB), thus generating negative feedback (16, 19).

Furthermore, the results from previous research that built an oncogenic lncRNA landscape for BC identified 55 lncRNAs that are primarily involved in the regulation of immune system activation, TGFβ, and Jak-STAT signal pathways (20). Previous studies have affirmed that the prediction of cancer prognosis can be achieved by establishing lncRNA signatures. Hong et al. constructed a predictive landscape for human hepatocellular carcinoma by examining 36 pairs of immune-related lncRNAs (21). An 11-lncRNA prognosis signature that correlates with immune cell infiltration in BC has also been set up (22). Furthermore, a novel upregulated-lncRNA GATA3-AS1 contributing to tumor development and immune evasion by degrading *GATA3* and stabilizing *PD-L1* has been found in TNBC (23), suggesting that lncRNA has a strong association with cancer progression as it affects the immune checkpoint. Currently, the signatures of oncogenic signaling pathways and tumor immune infiltration–associated lncRNAs have been preliminarily explored but without sufficient description. The purpose of our study is to build a novel signature that displays tumor immune infiltration–related lncRNA identification through the analysis of oncogenic signal pathways for implementation in evaluating the immunotherapy responses and clinical outcomes of BC subtypes.

In this study, we identified lncRNAs that are highly related to BC prognosis through 10 critical tumor- signaling pathways, after which we established a novel prognostic signature entitled OncoSig. We demonstrated the OncoSig as a predictor of prognosis and immunotherapy response, which is composed of 29 lncRNAs that are highly correlated with biological characteristics, immune features, overall survival (OS), gene mutation, and so on. Additionally, the pan-cancer analysis revealed that OncoSig is significantly related to the prognosis of 21 cancer types, indicating its reliability and clinical value.

Materials and methods

Data source and preprocessing

The basic clinical and RNA sequencing (RNA-seq) data (RNA SeqV2) of 33 cancers were retrieved from The Cancer Genome Atlas (TCGA) database using the Bioconductor package *TCGAbiolinks* (version: 2.20.0) (24), where expression data were normalized by FPKM (fragments per kilobase of exon model per million mapped fragments) and then transformed using $\log_2$(FPKM + 1). Mutation data for breast-invasive carcinoma (BRCA, also noted as TCGA-BRCA) patients were also obtained from the TCGA using *TCGAbiolinks*. In addition, four microarray datasets of BC were available from the Gene Expression Omnibus [accession numbers: GSE21653 (25), GSE20685 (26), GSE31448 (27), and GSE103091 (28, 29)], and their expression was corrected and normalized using the robust multiarray averaging (*RMA*) procedure (30).

The TCGA-BRCA dataset was used to establish the OncoSig prognostic signature for BC patients, and four independent microarray datasets were employed to assess the performance of this signature. Datasets from TCGA for the other 32 cancers were used to explore the broader prognostic performance of the OncoSig in pan-cancer. The details of these datasets mentioned above can also be found in Supplementary Table S1.

Identification of oncogenic signaling pathway-related long non-coding RNAs

By matching the RNA-seq expression profiles of genes and the annotation file GENCODE (version 25), we extracted genes annotated as "long non-coding RNAs" from the GENCODE project. The lncRNAs starting with "MT-" and "RP" were filtered out, and 3,006 unique lncRNAs were retained. To identify oncogenic signaling pathway–related lncRNAs, we first exclusively wielded the microarray model of the R package *GSVA* (version 3.48.1) (31) to assess the activity [also called the enrichment score (ES)] of 10 oncogenic signaling pathways for each patient in the TCGA-BRCA cohort. These 10 pathways are Receptor Tyrosine Kinase (RTK)-RAS, Notch, Hippo, β-catenin/Wnt (Wnt), PI-3-Kinase/Akt (PI3K), Cell cycle, TGFb Transforning growth factor beta (TGFβ), Myc, P53, and Nrf2; their corresponding genes can be collected from a previous study (32). Then, for each pathway, the correlation between lncRNA expression and the ES for each pathway was calculated, and the top 5% was retained. Finally, 498 unique lncRNAs were obtained (see Figure 1).

Development of oncogenic signaling pathway–related long non-coding RNA signatures

A total of 1,109 BC patients (only tumor samples) were randomly allocated to the training group (n = 554) and testing group (n = 555). For the training group, lncRNAs significantly associated with OS were filtered out from 498 unique lncRNAs through the univariate Cox regression analysis in combination with clinical data. Further, relying on the least absolute shrinkage and selection operator (LASSO) Cox regression model (R package, *glmnet*), resulted in the retention of 29 lncRNAs (see Table S2). Finally, a prognostic signature was proposed as a linear combination between the retained lncRNA expression values and their weights, which were derived using multivariate Cox

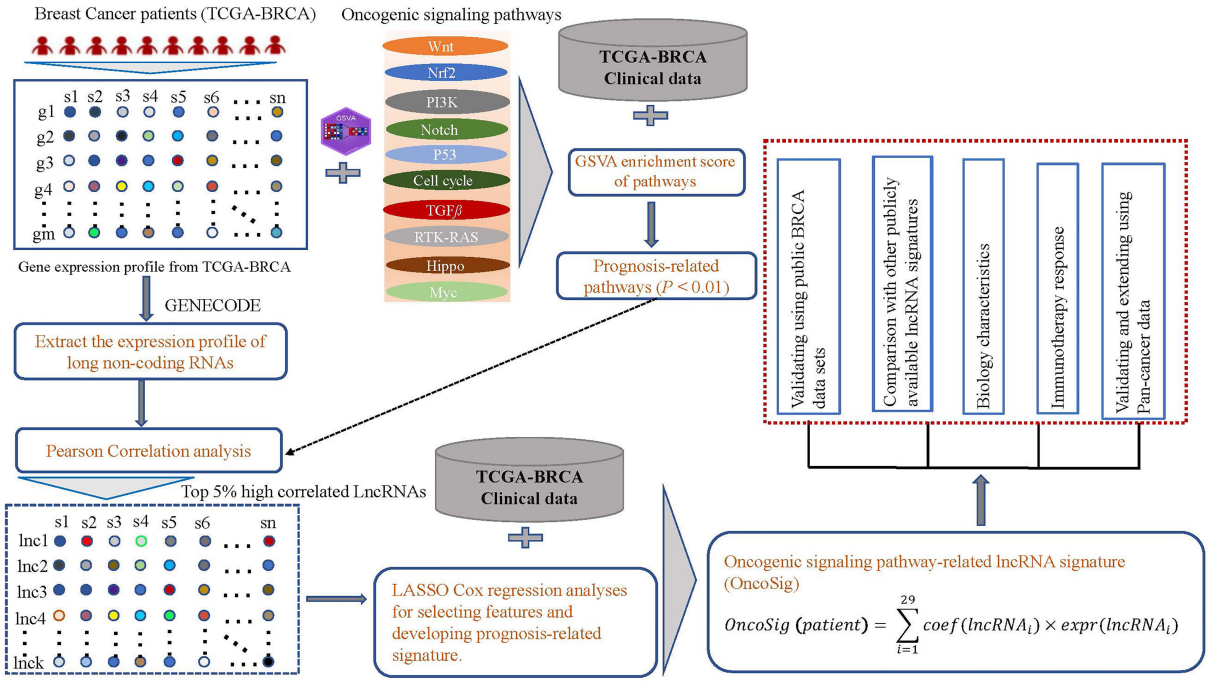

FIGURE 1
Analysis overview. Transcriptomic, mutational, and clinical data for breast cancer (BC) patients were collected from The Cancer Genome Atlas (TCGA) database. The GSVA tool was used to assess the enrichment scores (ESs) of 10 oncogenic signaling pathways in each patient. Long non-coding RNAs (lncRNAs) were extracted based on the annotation information in GENECODE, and the correlation coefficients between the lncRNA levels and ESs of each prognostically relevant pathway were calculated. Only the top 5% of relevant lncRNAs were retained for each oncogenic signaling pathway and further combined with clinical data to screen for lncRNAs significantly associated with prognosis, resulting in the retention of 29 lncRNAs. The weighting coefficients for these lncRNAs were estimated using multivariate Cox regression to generate the OncoSig signature. Lastly, BC and pan-cancer cohorts were used to assess the potential biological characteristics of the signatures as well as their broader clinical value.

regression (see Figure 1 and the following equation). The testing group was initially used to assess the prognostic performance of the signatures generated from these 29 lncRNAs.

$$\text{OncoSig (patient)} = \sum_{i=1}^{29} coef(lncRNA_i) \times expr(lncRNA_i)$$

Additionally, to improve the robustness of the signature, the training and testing groups (i.e., the TCGA-BRCA cohort) were merged to produce the final coefficients of these lncRNAs, as listed in Table S2.

Kaplan–Meier survival curve

KM survival curves were combined with the log-rank tests to assess whether the different risk groups (e.g., high- and low-risk groups determined by the OncoSig) demonstrated significantly different patterns of survival (*surv cutpoint* function, R package *survminer*, version 0.4.2), with their survival curves being considered as having a significant statistical difference when the *p*-value ≤0.05.

Differentially expressed genes associated with groups depicted by the OncoSig

The identification of DEGs between the groups (i.e., high- and low-risk groups) depicted by the OncoSig involved two steps: 1) assessing differences between the groups using the *limma* package (version, 3.48.1) (33) and 2) with |log2FC| ≥ 1 and adjusted *p*-value ≤ 0.01 [Benjamini–Hochberg method (34)] as the filtering conditions. The genes that met both these conditions were considered significantly different.

Functional enrichment analysis and gene set enrichment analysis

The gene annotation enrichment analysis of DEGS between the groups, as depicted by the OncoSig, was used to derive statistically different gene ontology (GO) terms. It was performed using the R Bioconductor package *clusterProfiler* (version 4.0.2) (35), where GO terms with the Benjamini–

Hochberg (27) adjusted at p-value ≤0.01 were considered significantly different.

To evaluate the infiltration of immune cells, a compendium of 782 marker genes related to 28 tumor-infiltrating immune cell types was obtained from the study by Charoentong P et al. (36). Again, gene set enrichment analysis (GSEA) was performed on the marker gene sets of these immune cells using the Bioconductor package *clusterProfiler* (version 4.0.2).

Cellular infiltration estimation

The stromal, immune, and tumor purity scores were assessed for each patient using the ESTIMATE algorithm (R package *estimate*, version 1.0.13) (37).

The relative fraction of 22 immune cell types for each patient was estimated using CIBERSORT (https://cibersort.stanford.edu/), where the signature gene expression profile (also called the base matrix) was LM22 (38).

Immunophenoscore calculation

The immunophenoscore (IPS) quantifies four different immune phenotypes, including antigen presentation, effector cells, suppressor cells, and checkpoint markers, using several immune responses or immune toleration markers provided in a previous study (36). A higher z-score of IPS summarizing these four categories indicates a more immunogenic sample (36, 39).

Performance comparison among different breast cancer prognostic signatures

To compare the performance of the prognostic signatures, a concordance index (C-index)—which reflects the probability of agreement between the predicted results and the actual observed value—was employed. Three steps were adopted: (1) 200 patients were randomly chosen without replacement from the TCGA-BRCA cohort; (2) the C-index corresponding to each BC signature was calculated separately using the *coxph* function (R package, *survival*, version: 3.3-1); and (3) the above steps were repeated 100 times and, subsequently, the distribution of the C-index for each signature was summarized.

Statistical analysis

Hierarchical cluster analyses were performed using Euclidean distances and the complete linkage method, while correlations between the gene expression of lncRNAs were calculated using the *Pearson* method. The significance of differences between the two groups was obtained using the Wilcoxon's test function. Additionally, a linear regression model was used to meet the trend of the scattered points. The time-dependent receiver operating characteristic (ROC) curve evaluated the performance of the OncoSig. Furthermore, a multivariate Cox regression was carried out to assess the independence of the OncoSig from other key clinical factors, including age, PAM50 subtype, and tumor grade. Since the PAM50 typing of BC was not available in the testing microarray datasets (see Table S1), it was predicted using the *genefu* package (40) (version: 2.24.2). To systematically understand the prognostic value of the OncoSig in the different BC cohorts, a prognostic meta-analysis was performed by deploying a fixed effects model that used the R package *meta* (version 5.2-0). All statistical analyses were implemented using the tool R project for statistical computing (version 4.1.0). The *P*-values (Wilcoxon's test, Fisher's exact test, and Student's *t*-test) when comparing the groups were two sided, with $* p \leq 0.05$ considered as statistically significant.

Results

Identification of Oncogenic Signaling Pathway– and Prognosis–Associated Long Non-Coding RNAs

Ten crucial signaling pathways have been identified as influencing cancer progression—Cell cycle, Hippo, Myc, Notch, Nrf2, PI3K, RTK-RAS, TGFβ, P53, and β-catenin/Wnt (Wnt) (32). To characterize the impact of these pathways on BC, we first fetched BC samples from the TCGA database and, subsequently, calculated the activity of each pathway in each BC patient using the single-sample GSEA method encapsulated in the GSVA package (Figure 1, see Materials and Methods) (31). Based on the activity scores and activities of different tumor pathways in the BC cohort, we set up interaction networks between 10 cancer pathways and analyzed their relationship with the survival prognosis. The results showed RKT-RAS, Notch, Hippo, Wnt, and TGFβ as having strong positive correlations that were significantly associated with survival prognosis in BC patients (Figures 1, 2A). Although the MYC pathway was significantly associated with patient prognosis, the positive correlation with the other pathways was weaker (Figure 2A). Interestingly, the Cell cycle pathway was negatively correlated with TGFβ, Nrf2, RKT_RAS, and PI3K, and it served as a protective factor for the prognosis of BC patients (Figure 2A). At the same time, no significant association was observed between Nrf2, PI3K, and the prognosis of BC patients (Figure 2A). Further, we compared the distribution of the activity scores (also called ESs) of each of the 10 pathways across the PAM50 subtypes to identify significant differences in their activities in the different subtypes. On combining the

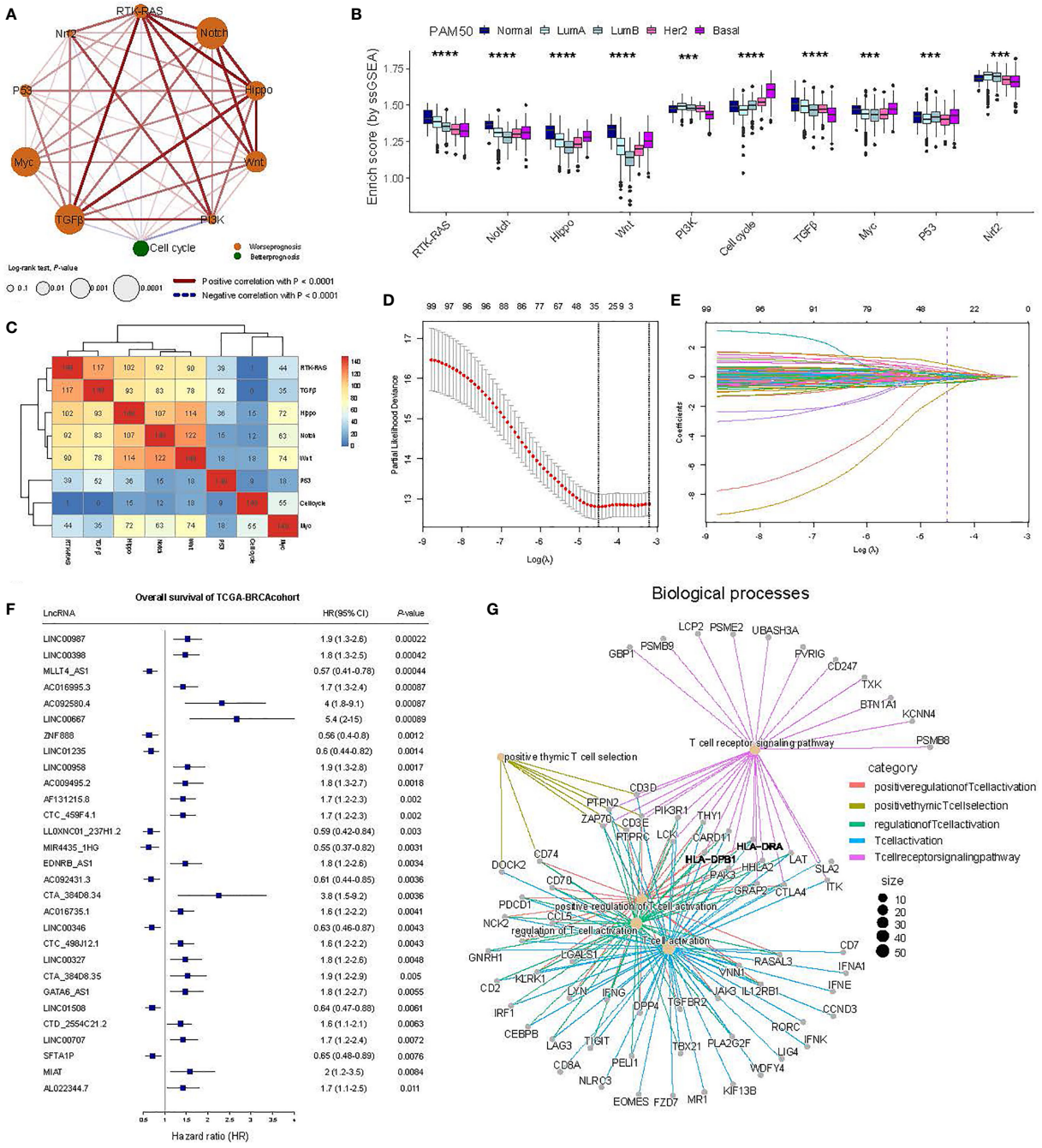

FIGURE 2
Identification of oncogenic signaling pathway-associated lncRNAs using TCGA-BRCA transcriptome data. **(A)** Interaction of 10 oncogenic signaling pathways. The size of the circles represents the prognostic effect of each cell type, while the color of the fill is scaled by the P-value. Red and blue colors indicate positive and negative correlations, respectively. **(B)** A comparison of the ESs of the oncogenic signaling pathways in the PAM50 subtypes. The Wilcoxon rank-sum test was used for statistical analysis. ***$p \leq 0.001$, ****$p \leq 0.0001$. **(C)** Heat map showing the number of overlaps between lncRNAs highly associated with specific oncogenic signaling pathways and other pathways using hierarchical clustering. The top 5% of the lncRNAs associated with specific oncogenic signaling pathways were selected. The upper bound of the color bar is 150. **(D)** The least absolute shrinkage and selection operator (LASSO) regression model revealed partial likelihood deviance in the 10-fold cross-validation. **(E)** The LASSO coefficient profiles of prognosis-related lncRNAs in 10-fold cross-validation. **(F)** The forest plot of 29 candidate prognosis-related lncRNAs associated with OS in the TCGA-BRCA cohort. **(G)** Gene ontology (GO) functional enrichment analysis for mRNAs with coexpressed lncRNAs.

clinical prognosis of PAM50 patients—normal-like over LumA over LumB over HER2 over basal—we observed that the ESs of the RTK-RAS and Cell cycle pathways were most consistent with the PAM50 clinical trend. The RTK-RAS ES was the highest for Normal-like and lowest for Basal. For the Cell cycle pathway, the ESs for LumA activity and Basal were the lowest and the highest, respectively (Figure 2B). These results depict the synergistic or antagonistic relationships between 10 tumor-related pathways and their impact on BC patients' prognoses, revealing that different pathways have different abilities to portray PAM50 subtypes (Figures 2A, B). Since the crosstalk between the signaling pathways and lncRNAs impacts cancer progression (17–19), we annotated the genes from the TCGA-BRCA cohort using GENECODE and correlated the expressions of the annotated lncRNAs (3006) with the ESs of eight pathways that exhibited significant association with the prognosis in BC patients, selecting only the top 5% of correlated lncRNAs in each pathway (149 lncRNAs for each pathway). On analyzing the lncRNAs shared among the different pathways, we found a number of them present in RTK-RAS, TGFβ, Hippo, Notch, and Wnt, whereas P53, Cell cycle, and Myc shared fewer lncRNAs with the other pathways, indicating solid specificity. Following this, the hierarchical clustering also showed that there are two different functional pathway modules, implying that their status and role in tumor progression may be quite different (Figure 2C).

To identify the pivotal lncRNAs that were highly associated with the prognosis of BC patients, we combined the clinical data and screened the lncRNAs mentioned above using LASSO-Cox regression (Figures 1, 2D, E), which yielded 29 lncRNAs (Figure 2F). Furthermore, to analyze the biological processes in which these lncRNAs may be involved, we conducted a coexpression analysis of the lncRNAs with mRNAs. For each lncRNA, only the top 50 mRNAs with the highest coexpression correlation were retained. Annotating the GO of these mRNAs using the R package *clusterProfiler* (35) revealed that they are mainly involved in T-cell activation, regulation, and differentiation processes (Figure 2G). These results suggest that 29 lncRNAs are involved in tumor-associated pathways. Their altered expression may affect normal gene damage repair pathways by disrupting the balance of lncRNA-associated regulatory networks, thereby affecting the stable regulation of important pathways.

Proposing a Novel Long Non-Coding RNA Signature for the Clinical Stratification of Breast Cancer Patients

To explore the potential prognostic roles of the selected 29 lncRNAs associated with oncogenic signaling pathways in clinical diagnosis, we first measured the correlations between their expressions, which showed that only a few of the lncRNAs had a relatively strong positive/negative correlation with each other. This finding indicated that these 29 lncRNAs had a low degree of colinearity and good independence that could help to provide a comprehensive picture of their impact on the prognosis of BC patients (Figure 3A). Next, we divided the TCGA-BRCA cohort into a training set (n = 554) and testing set (n = 555) using random sampling without replacement. For the training set, we coupled the expression data of the lncRNAs with clinical characteristics and used multivariate Cox regression to obtain 29 coefficients that characterize the degree of prognostic impact of the lncRNAs. The linear sum of these coefficients multiplied by the expression of the 29 lncRNAs was indicated as OncoSig. The training and testing sets were split according to their higher and lower OncoSig scores, respectively, using optimal cut points determined by the *surv_cutpoint* method (see Materials and Methods), whereby significant differences (p-value ≤ 0.01) in OS were noted for both groups (Figures 3B, C), indicating that the novel OncoSig signature successfully portrayed the prognosis of BC patients. To adjust for the coefficients obtained previously, we merged the training and testing sets and reused the multivariate Cox regression to acquire a new OncoSig that better described the prognosis of BC patients. The 5-year survival rate for the low-risk score group of BC patients was 64.4%, which is significantly higher than the high-risk group (35.8%) (Figure 3D). For this reason, we used the adjusted OncoSig as the final signature of the 29 lncRNAs (see Table S2).

The area under the curve (AUC) of the signature was used to further analyze the prognostic performance of the OncoSig, presenting 0.787 and 0.784 at 5 and 3 years of OS, respectively (Figure 3E). We also found that a higher-scoring OncoSig group meant shorter survival time and signified more deaths (Figure 3F). In addition, we investigated the composition of the PAM50 patients in both groups stratified by the OncoSig to find that Basal and HER2 patients dominated the high-risk group, while Normal-like and LumA patients were in the low-risk group (Figure 3G). Subsequently, a new question that arises is whether OncoSig can be applied as a valid and independent prognostic indicator in the BC cohort. For this purpose, multivariate Cox regression analysis was employed using covariates such as OncoSig, age, PAM50, and stage. The results demonstrated that OncoSig, age, and stage III and IV were significantly associated with prognosis in BC patients, with OncoSig exhibiting the worst HR value, hinting that it could certainly be the most crucial risk factor compared to these key clinical characteristics (Figure 3H). In summary, this evidence indicates that the higher the OncoSig score, the worse the prognosis and vice versa. This result also establishes OncoSig as an independent prognostic factor that contributes to clinical diagnosis and research.

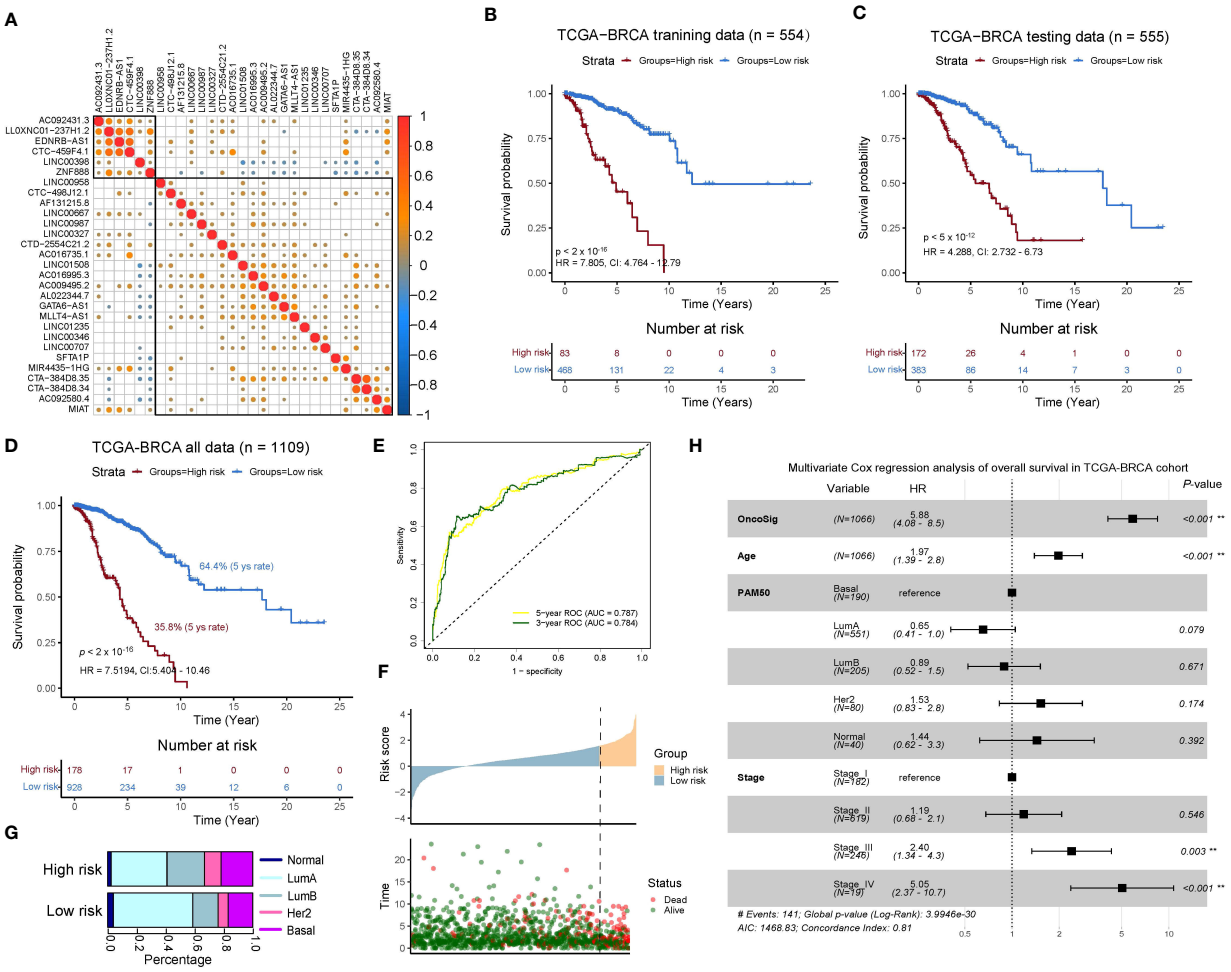

FIGURE 3
Development and validation of an oncogenic signaling pathway–derived lncRNA signature for outcome prediction in the TCGA-BRCA cohort. **(A)** Pearson correlation analysis for 29 lncRNA expressions divided into two submodules based on hierarchical clustering. **(B–D)** Kaplan–Meier (KM) survival analysis for the overall survival (OS) curves of BC patients in training **(B)**, testing **(C)**, and the total set. **(E)** Time-dependent receiver operating characteristic (*ROC*) curve at 3 and 5 years of OS. **(F)** High- and low-risk groups depicted by the OncoSig, ordered according to their scores, presenting the corresponding survival status for the BC patients. **(G)** Composition of patients with the PAM50 subtype in the two groups. **(H)** A multivariate analysis of the OncoSig, age, PAM50, and stage with OS in the TCGA-BRCA cohort.

Evaluating and comparing the prognostic performance of the OncoSig

To estimate the prognostic value of the OncoSig more broadly, we obtained four independent gene expression datasets of BC from the GEO database —GSE21653 (25), GSE20685 (26), GSE31448 (27), and GSE103091 (28, 29)—each with its gene expression signal backgrounds corrected and quantiles normalized using the *RMA* (30) package in R (see Materials and Methods) and then calculated their OncoSig scores. The results demonstrated that both the high- and low-risk groups portrayed by the OncoSig were significantly different in each of these independent test sets ($p \leq 0.05$), consistent with the trend reflected in the TCGA-BRCA cohort (Figure 4A). In addition, we needed to explore whether the OncoSig remained available as an independent prognostic factor in the four testing cohorts. For this purpose, a multiple Cox regression strategy was applied, where the included covariates were age (i.e., ≥ 60 or not), PAM50 typing, and tumor grade. It should be noted that, as the clinical data in the GSE20685 and GSE103091 datasets did not contain the PAM50 subtypes, the *genefu* (40) package in R was used to make separate predictions for each sample in these two datasets. In addition, as the clinical data for GSE103091 did not include the tumor grade, this covariate was omitted in the multiple Cox regression analysis. The results revealed that OncoSig was statistically significant in all the testing cohorts ($p \leq 0.05$) (Figure 4B; Table S1), further suggesting that the signature can be regarded as an independent prognostic factor in

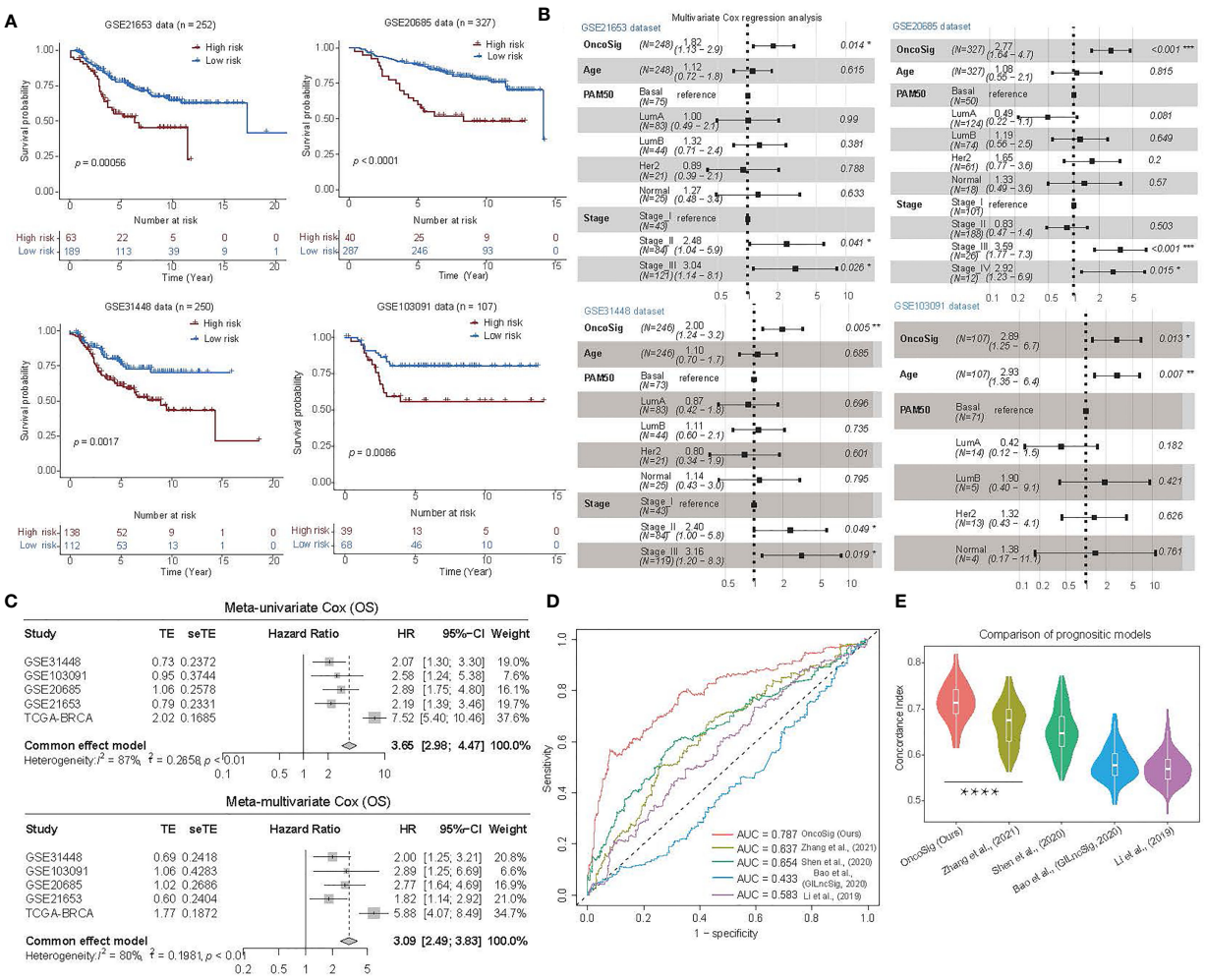

FIGURE 4
Prognostic performance of the OncoSig on four independent BC testing cohorts. **(A)** KM survival analysis for the OS curves of BC patients in GSE21653, GSE20685, GSE31448, and GSE103091, respectively. **(B)** Multivariate analysis of the OncoSig, age, PAM50, and stage with OS using the four testing cohorts, respectively. **(C)** Meta-analysis performed on the prognostic value of the OncoSig for patients in the five cohorts, using a fixed effects model to calculate pooled HR values (top: meta-univariate; bottom: meta-multivariate). **(D)** The ROC analysis of 5-year OS of the OncoSig versus other published prognostic signatures for BC. **(E)** Comparison of the performance of five BC signatures using the concordance index (C-index), randomly permuted 100 times, with 200 patients randomly selected from TCGA-BRCA each time, and the C-index calculated separately for each signature. The Wilcoxon rank-sum test was used for the statistical analysis. ****$p \leq 0.0001$.

BC. Moreover, a prognostic meta-analysis was conducted to examine the comprehensive prognostic value of all five BC cohorts, signifying that a high OncoSig score indicated a significant risk factor for the OS of BC patients (Figure 4C). As a whole, these results denoted that the OncoSig could be a potential attribute of BC patients and may be of great value for clinical prognostic assessment.

To our knowledge, several prognostic signatures for BC constructed using lncRNAs have been reported. These include the five-lncRNA signature proposed by Li et al. (41), the signature GILncSig using lncRNAs highly associated with genomic instability constructed by Bao et al. (42), a signature consisting of 11 lncRNAs identified by Shen et al. (22) on comparing differences between high and low immune infiltration groups in BC cohorts, and a signature constructed on 9 lncRNAs derived from autophagy-associated lncRNAs by Zhang et al. (43). To compare the prognostic performance of the OncoSig with the other lncRNA signatures for BC, we calculated the risk score for each sample in the TCGA-BRCA cohort, utilizing each of the four signatures mentioned above. As shown in Figure 4D, the OncoSig predictions attributed the highest AUC to the five-year OS, followed by the nine-lncRNA signature constructed by Zhang et al., while the lowest AUC was adjudged to the five-lncRNA signature constructed by Li et al. (Figure 4D). Since the C-index responds to the probability that the predicted outcome is consistent with the actual observed, we

further randomly sampled the TCGA-BRCA cohort to calculate the C-index corresponding to the optimal stratification of each signature risk score and repeated this activity 100 times (see Materials and Methods). The results showed that the OncoSig has the highest average C-index and is significantly different from Zhang et al. (Figure 4E). Indeed, these results suggest that the OncoSig has a better prognostic performance compared to the other lncRNA signatures for BC.

Clinical and biological landscape of the two groups, as described by the OncoSig

By comparing the expression levels of 29 lncRNAs in the high- and low-risk groups, we found that all but three—*AF131215.8*, *AL022344.7*, and *GATA6-AS1*—exhibited significant differences (Wilcoxon test, p-value ≤ 0.01) (Figure 5A). The relationship between the OncoSig scores and clinical characteristics, which included age (≥60 or not), stage, PAM50, and Pan-Gyn clusters, were further examined in the TCGA-BRCA cohort to reveal significant differences (Figure 5B). Specifically, Lumina A, the least- aggressive subtype of the PAM50, presented the lowest risk score while the HER2 and Basal types were the most aggressive with the highest risk scores (Figure 5B). We also observed a positive concordance between pathological staging and the OncoSig score in BC patients, with a similar trend in the Pan-Gyn C1 to C5 clusters (Figure 5B). In addition, differences in the ES scores of 10 oncogenic pathways obtained using the *GSVA* (31) tool for the two groups depicted by the OncoSig were investigated, where RTK-RAS, Wnt, and Myc showed significant differences, while the other pathways showed none (Wilcoxon's test, p-value ≤ 0.01) (Figure 5C).

Next, the infiltration of 28 immune cell types gathered from the previous study (36) of the two groups depicted by the OncoSig for BC patients was assessed using the GSEA toolkit. It was observed that these groups revealed distinct patterns of immune infiltration, with patients in the low-risk group enriched by an absolute predominance of immune subpopulations (Figure 5D, see Materials and Methods). ESTIMATE (37) was performed to estimate and compare the stromal, immune, and tumor scores in both risk groups, all of whom showed significant differences, with immune showing the most significant difference (Figure 5E). To refine the differences between immune infiltrations in the high- and low-risk groups, we estimated the relative fraction of 22 immune cells for each patient in both groups by using CIBERSORT coupled with the base matrix "LM22," wherein "B-cell naïve," "T-cell CD8," "macrophage M0," and "macrophage M2" demonstrated the most significant differences (Figure 5F; see Materials and Methods). Further, differentially expressed genes (DEGs) in the high- and low-risk groups were identified. The GO annotation of these DEGs indicated that the high-risk group was enriched in biological processes, such as cell development and differentiation, while the low-risk group was more involved in biological processes, such as immune response and regulation (Figure 5G). Overall, these results adequately revealed a profound association between OncoSig and immune infiltration, with lower OncoSig scores associated with higher levels of immune infiltration and vice versa (Figures 5D–G).

To further investigate the heterogeneity of single-nucleotide polymorphisms in the risk groups depicted by the OncoSig, we retrieved a dataset of mutations corresponding to BC patients from the TCGA database. As revealed in Figure 5H, the top 10 genes with the highest mutation frequencies in each group were presented separately, with alterations occurring in 136 of the 161 samples (84.47%) in the high-risk group and in 688 of the 802 samples (83.9%) in the low-risk group. Notably, *TP53*, *SPTA1*, *FLG*, and *RYR2* accounted for 39%, 9%, 8%, and 8% of the mutation frequency in the high-risk group, respectively, while *PIK3CA* (34%) and *CDH1* (16%) were more prominent in the low-risk group (Figure 5H). The mutational burden was also investigated, showing significant differences between the groups portrayed by the OncoSig (Figure 5I). Lastly, genes with significant mutational differences between the two groups were examined, with *ERBB3*, *FMN2*, *DNAH10*, *MIA3*, and *FOXA1* observed to be the frequently mutating genes in the high-risk group, while *CDH1* was found to be enriched in the low-risk group (Figure 5J). Effectively, the high- and low-risk groups depicted by the OncoSig revealed significant heterogeneity in their clinical characteristics and biological mechanisms, suggesting the potential value of the OncoSig as a clinical signature to predict the prognosis of BC patients.

Potential of the OncoSig as an Indicator of Immunotherapy Response in Breast Cancer

To explore the potential of the OncoSig as an indicator of response to immunotherapy in BC patients, the IPS, which refers to an arbitrary 0–10 score based on the sum of weighted average Z-scores for antigen presentation, effector cell, suppressor cell, and checkpoint markers (see Materials and Methods), was calculated. The results displayed that the IPS was negatively connected with the OncoSig scores and also revealed a substantial difference between the high- and low-risk groups, with the latter being more immunogenic (Figure 6A). A recent study (44) has already elaborated that immune checkpoint inhibitor (ICI) genes are of significant value in depicting tumor progression. To further inquire into the complicated interactions between OncoSig and ICI genes, the expression patterns of ICI genes—including *CD247* (*PD-L1*), *PDCD1*, *CTLA4*, *HAVCR2*, and *LAG3*—in the different patient groups stratified by the OncoSig were analyzed. The results revealed that the OncoSig had a significant negative correlation with the

10.3389/fimmu.2022.891175

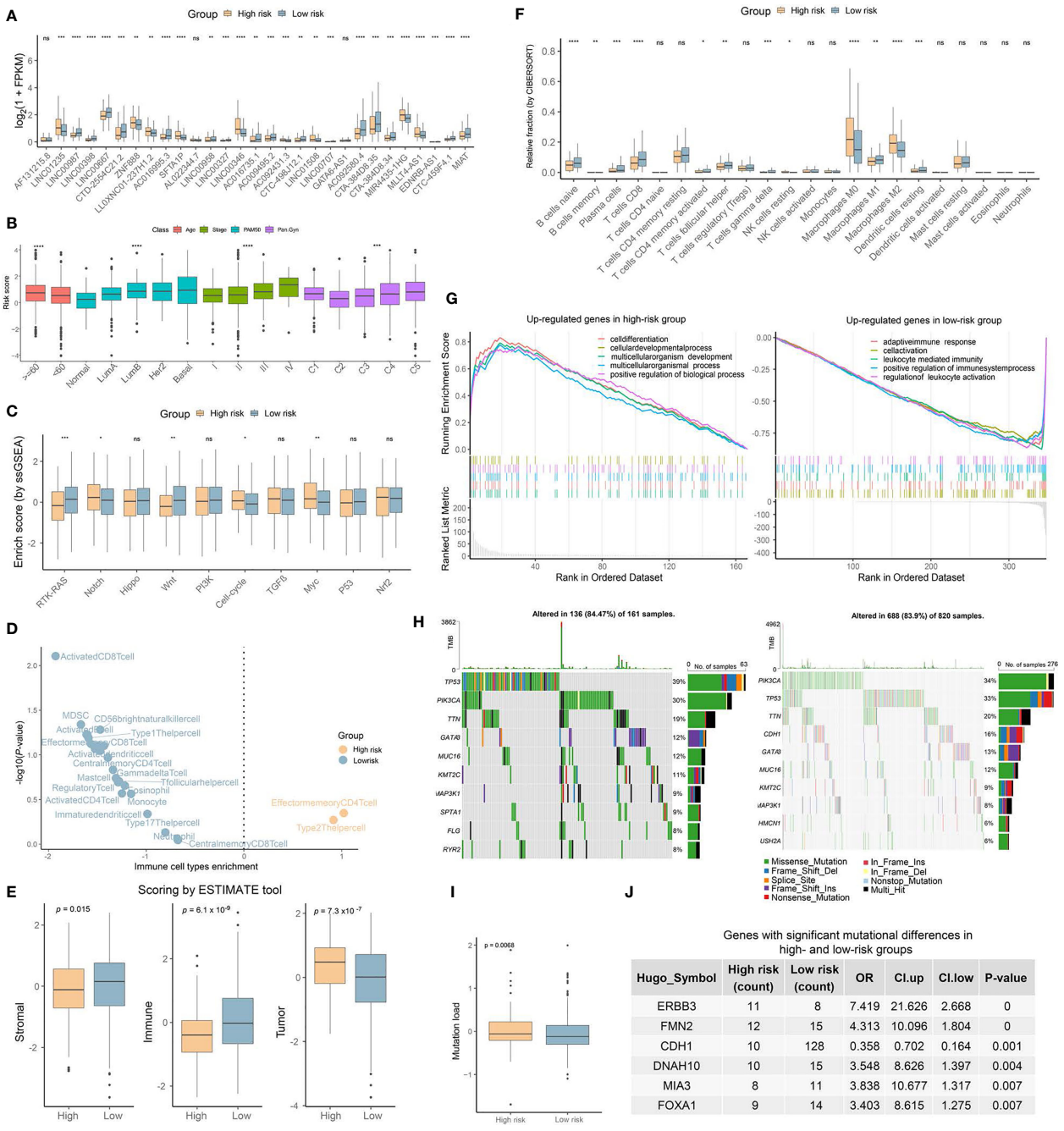

Hugo_Symbol	High risk (count)	Low risk (count)	OR	CI.up	CI.low	P-value
ERBB3	11	8	7.419	21.626	2.668	0
FMN2	12	15	4.313	10.096	1.804	0
CDH1	10	128	0.358	0.702	0.164	0.001
DNAH10	10	15	3.548	8.626	1.397	0.004
MIA3	8	11	3.838	10.677	1.317	0.007
FOXA1	9	14	3.403	8.615	1.275	0.007

FIGURE 5
Clinical and biological characteristics of stratification results of the OncoSig. **(A)** Box plot showing the statistical difference of the 29 lncRNA expressions between high- and low-risk groups. **(B)** Clinical characteristics of the risk score obtained on a stratified analysis of the TCGA-BRCA cohort. **(C)** Box plot showing the statistical difference in the ES of the oncogenic signaling pathways between high- and low-risk groups. **(D)** Volcano plot for the enrichment of immune cell types in tumors with high and low OncoSig scores, calculated based on the normalized enrichment score from the gene set enrichment analysis (GSEA). **(E)** Stromal, immune, and tumor scores from the ESTIMATE tool for the high- and low-risk groups. **(F)** CIBERSORT predictions of the infiltration levels of 22 immune cells in the low- and high-risk groups. The dots represent the immune cell–scaled expression values. **(G)** GSEA showing significantly enriched GO terms in low- and high-risk groups, respectively. **(H)** The tumor mutational burden difference between the low- and high-risk groups. **(I)** Comparison of the relative distribution of the mutation load between the low- and high-risk groups in the TCGA-BRCA cohort. **(J)** Table showing the significantly mutated genes between the low- and high-risk groups. Only genes with more than 10 mutations were included in the Fisher's exact test analysis. Notably, ns: not significant, *$p \leq 0.05$, **$p \leq 0.01$, ***$p \leq 0.001$, ****$p \leq 0.0001$. The Wilcoxon rank-sum test was used for the statistical analysis.

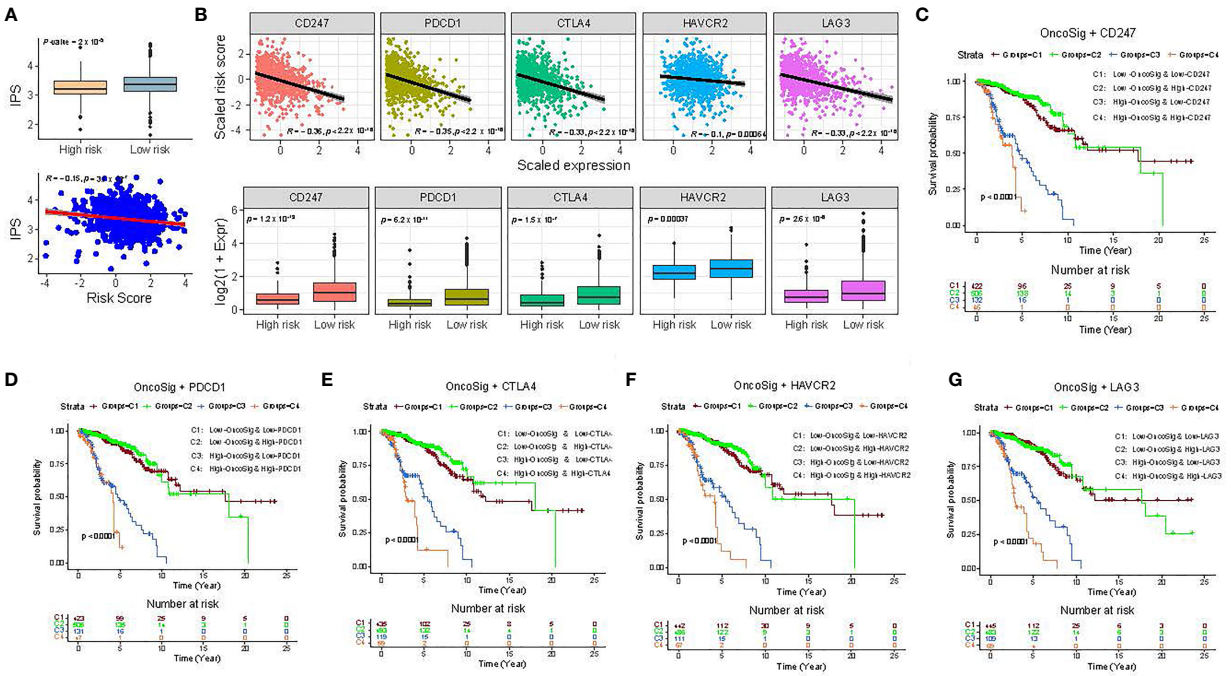

FIGURE 6
Impact of immune checkpoint gene expression and OncoSig on clinical outcome. **(A)** Comparison of the relative distribution of immunophenoscores (IPSs) between low- and high-risk groups in the TCGA-BRCA cohort (top). The scatter plot shows the correlation between the correlated IPS score and the OncoSig score, while *R* indicates the Pearson correlation coefficient (bottom). **(B)** Comparison of the expression pattern of immune checkpoint **(ICI)** genes between patients with higher and lower OncoSig scores in the TCGA-BRCA cohort. **(C-G)** KM OS curves for the four groups stratified by the OncoSig and *CD247* **(C)**, *PDCD1* **(D)**, *CTLA4* **(E)**, *HAVCR2* **(F)**, and *LAG3* **(G)**. The Wilcoxon rank-sum test was used for the statistical analysis.

expression levels of ICI genes (Figure 6B). Additionally, in the TCGA-BRCA cohort, patients with low OncoSig exhibited high levels of ICI gene expression compared to those with high OncoSig (Figure 6B). This trend is consistent with previous observations specifying that a high expression of immune checkpoint genes is associated with a good outcome (45). It is still unclear whether the OncoSig can reflect clinical results more sensitively, with similar expression levels of ICI genes as above. To clarify this confusion, the BC cohort was divided into four groups using the stratification depicted by the OncoSig into high/low (median values as cutoff points) expression levels of each ICI gene. After this, the survival patterns of these four groups were compared. The results demonstrated that patients with low OncoSig and high expression of ICI genes had the best prognostic performance, while those with high OncoSig and low expression of ICI genes had the worst prognosis (log-rank test, p-value ≤ 0.001) (Figures 6C–G). In particular, for high OncoSig patients, stratified ICI gene expressions, that is, C3 and C4, resulted in significant differences in survival. However, on stratifying the cohort using ICI gene expression based on the low OncoSig patients, that is, C1 and C2, no significant survival differences were observed (Figures 6E–G). Accordingly, these results implied that the OncoSig was closely associated with ICI immunotherapy response and, thus, could be a potential predictive signature for BC patients.

Extending the effectiveness and clinical value of the OncoSig using Pan-Cancer RNA-Seq Data

To investigate the effectiveness and clinical values of the OncoSig on other cancers, we obtained transcriptome expression datasets coupled with clinical data from the TCGA database for 32 other cancer types (the full names and abbreviations of these cancers can be found in Table S1) and scored each sample using the OncoSig formula (see Materials and Methods). To assess the prognostic ability of the OncoSig in other cancers, optimal cut points and survival models were used to investigate the survival patterns of the risk groups, with the results showing significant differences between the stratifications depicted by the OncoSig in 21 cancer types (p-value ≤ 0.05), wherein 11 cancer types with a p-value ≤ 0.01 were identified (excluding BRCA, Figures 7A, B). On comparing the immune infiltration, estimated by *ESTIMATE* (37), significant differences were observed between the high- and low-risk groups for each of the 12 cancer types,

10.3389/fimmu.2022.891175

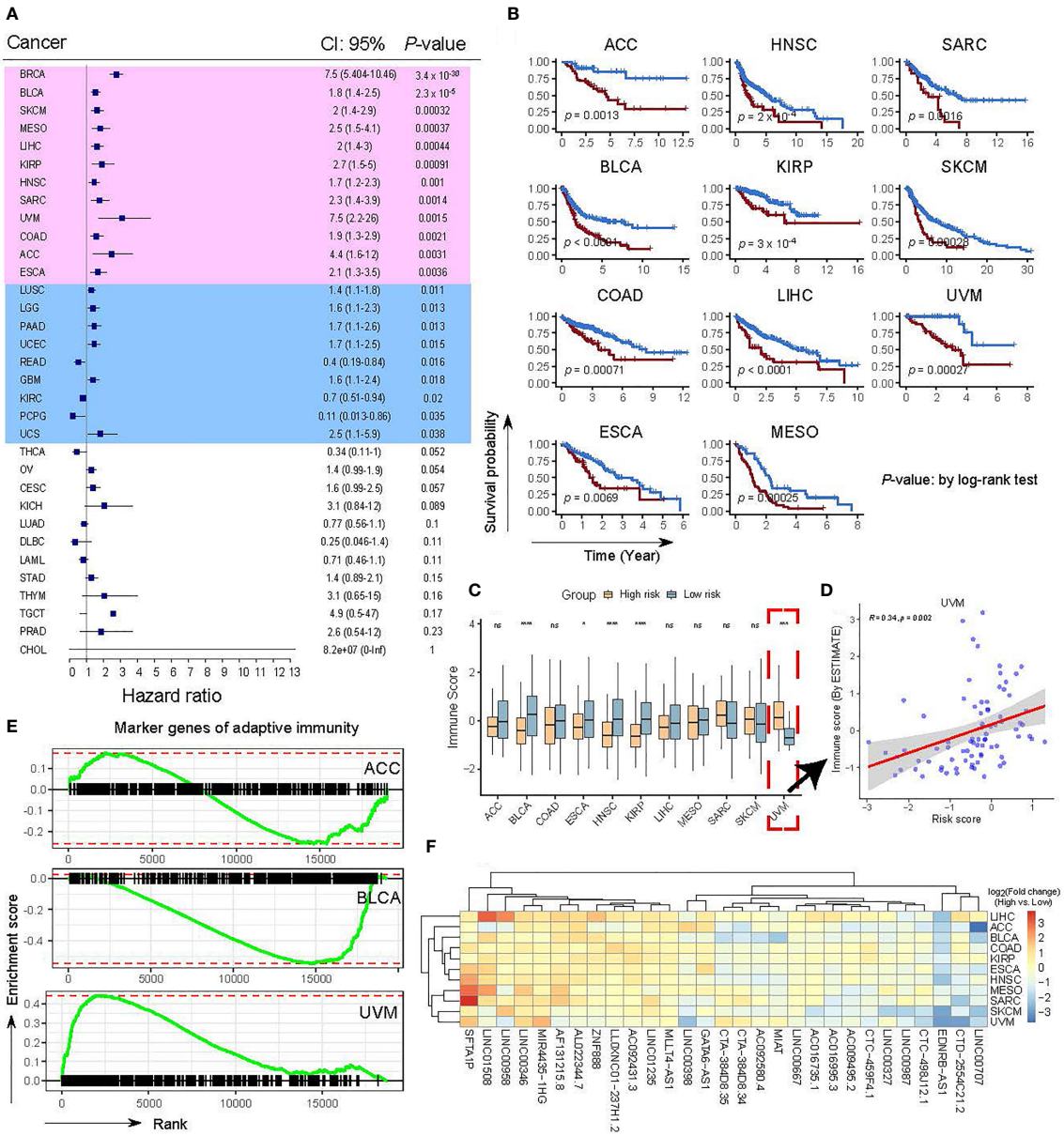

FIGURE 7
Confirmation of the OncoSig using TCGA pan-cancer datasets. **(A)** Validation of the impact of the OncoSig on survival using TCGA pan-cancer datasets. Background colors in pink indicate cancer types with *p*-values less than 0.01, while light blue indicates cancer types with *p*-values less than 0.05. *P*-values were obtained using a log-rank test. **(B)** KM OS curves between patients with a higher and a lower OncoSig score in 11 cancer types. **(C)** Comparison of the relative distribution of immune scores derived from ESTIMATE between high- and low-risk groups in 11 cancer types. **(D)** Scatter plot showing the correlation between the correlated immune score and the OncoSig score. *R* indicates the Pearson correlation coefficient. **(E)** GSEA for 431 marker genes of adaptive immunity reveals the relationship between low- and high-risk score groups in adrenocortical carcinoma, bladder urothelial carcinoma, and uveal melanoma cancer types. **(F)** Heat map with hierarchical clustering showing the expression of 29 lncRNAs between low- and high-risk score groups. Red and blue represent high and low expressions, respectively. The Wilcoxon rank-sum test was used for the statistical analysis. ns: not significant, *$p \leq 0.05$, ***$p \leq 0.001$, ****$p \leq 0.0001$.

including bladder urothelial carcinoma (BLCA), head and neck squamous cell carcinoma (HNSC), and kidney renal papillary cell carcinoma (KIRP), with lower immune infiltration in the high-risk group. This is consistent with the results observed in the BRCA (Figure 7C). Interestingly, there was also a significant difference between the two groups in terms of uterine uveal melanoma (UVM). However, the high-risk group still displayed higher immune infiltration and vice versa. In contrast to the

OncoSig in BRCA, a significant positive correlation was observed when comparing the intrinsic association between the OncoSig score and immune infiltration (Figure 7D). The underlying reason for this may be that UVM belongs to the immune "cold" tumor, that is, a low-density immune infiltrate present both inside and outside the tumor (Figures 7C, D) (46, 47). In addition, no significant difference was observed in the other tumor types (Figure 7C).

Next, to confirm the above results, we shifted our strategy and adopted the GSEA to assess the activity of adaptive immune genes, available from a prior study (36) (see Materials and Methods), in the high- and low-risk groups denoted by the OncoSig. As shown in Figure 7E, no significant enrichment was found between the two groups in adrenocortical carcinoma (ACC); however, considerable enrichment was discovered in the low-risk group in BLCA and in the high-risk group in UVM (>Figure 7E), which corroborates the observations in Figures 7C, D. The above results suggest that the OncoSig still has prognostic potential in a wide range of cancers, but whether this signature is a risk or a protective factor may be profoundly influenced by the immune-hot and -cold feature of the cancer itself. Finally, we examined the panorama of expressions of these 29 lncRNAs in the high- and low-risk groups of 11 cancer types; the hierarchical clustering result revealed that they could be classified into three major categories (Figure 7F)—the comparisons of the low-risk group's highly expressed lncRNAs (such as *SFTA1P* and *LINC00346*), median highly expressed lncRNAs (such as *LINC00398* and *AC009495.2*), and lowly expressed lncRNAs (*EDNRB–AS1* and *LINC00707*) (Figure 7F). Despite this, the expression of these lncRNAs still exhibited heterogeneity across cancers (Figure 7F). Overall, these results demonstrated that the OncoSig can serve as a potential predictive signature of response to BC treatment and has the potential for pan-cancer application.

Discussion

BC is a highly prevalent and heterogeneous malignant disease that occurs almost exclusively in women (1, 3). Immunotherapy for BC has been considered an emerging treatment approach in clinical circumstances. However, an evaluation criterion is extremely necessary due to the uncertainty of the response to immunotherapy and prognosis in BC (6). Li et al. discovered that a new prognostic signature consisting of 24 pairs of differentially expressed immune-related lncRNA (DEirlncRNA) had close connection with tumor-infiltrating immune cells and drug susceptibility (48). An analogous study by Shen et al. identified 36 pairs of DEirlncRNA for appraising the response to immunotherapy and predicting the survival status of invasive BC (49). Along the same lines, our observations highlight the importance of lncRNA signatures pertaining to oncogenic signaling pathways. Previous studies have shown that complex interactions and crosstalk among different signaling pathways are highly relevant to the progression of the disease, making a proper understanding of oncogenic alterations, its detailed mechanisms, and the co-occurrence of these pathways essential for the development of new therapeutic approaches to improve patient care (16, 39). Nonetheless, directly and accurately delineating the roles and alterations among crucial signaling pathways in a clinical setting remains a difficult task. LncRNAs have recently been identified to play fundamental roles in regulating the activation of oncogenic signaling pathways and, thus, can be utilized as specific molecular markers to depict alterations in signaling pathways (16). The current study demonstrated a new 29-lncRNA signature (OncoSig) that is applied as an indicator of immunotherapy response and prognosis in BC from the perspective of interactions between genes and related lncRNAs in oncogene signal pathways.

We originally established interaction networks between 10 cancer pathways and analyzed their relationships with the survival prognosis of BC patients in TCGA. The results showed that the RKT-RAS-, Notch-, Hippo-, Wnt-, and TGFβ- signaling pathways were strongly associated with worse survival prognosis, while the Cell cycle pathway was significantly associated with a better survival prognosis. Surprisingly, there was a contradictory result. As Wang et al. noted, an immune signature named immune-related prognostic score (IRPS), which acted as a tumor suppressor, was appraised by the normalized ES (NES). The results of the IRPS subtypes in the NES values of 10 common oncogenic pathways showed that the Hippo-, Notch-, TGFβ-, and Wnt-related and RAS pathways exhibited pronounced lower NES values in the low IRPS group, while it had a higher value in the high IRPS group, whereas the Cell cycle and PI3K pathways had significantly lower NES in the high IRPS group (45). We speculated on the major reason behind these conflicting findings to conclude that our results reflected the entire TCGA-BRCA data instead of partial data. In the process of data collection, similar to the lncRNA signature of tumor-infiltrating B lymphocytes developed by Zhou et al. in bladder cancer (50), we initially sought RNA-seq data from the TCGA and extracted 3,006 lncRNA expression profiles by matching their lncRNA annotations in GENCODE. Then, based on the critical role of lncRNAs in regulating oncogenic signaling pathways in human cancers (51, 52), we applied association analysis and LASSO feature–selecting strategies to identify 29 lncRNAs that exhibited high correlation with the signaling pathways, thus influencing prognosis considerably. It brought a hepatocellular carcinoma immune-related lncRNA signature into correspondence, which was also screened by deploying LASSO regression analysis (21). Afterward, we equally and randomly allocated the BC patients from the TCGA into the training and testing sets. The high- and low-risk groups were defined according to the optimal cutoff value

of the OncoSig, as determined by the *ROC* curve. Next, the KM survival curve was plotted using the log-rank test, which disclosed that the OS of the high-risk group was worse than that of the low-risk group in both the sets as well as the combined set.

Subsequently, we chose four independent GEO datasets and classified them into two groups according to the best threshold value of the OncoSig. To our astonishment, their KM survival curves wholly displayed a higher OncoSig score and worse OS, similar to the trend in the TCGA-BRCA cohort, implying that it could be developed as a prognostic factor. Additionally, the OncoSig remained an independent risk factor in the multivariate Cox regression model, notwithstanding inequivalently variable factors in five separate datasets and in the prognostic meta-analysis. Above all, we concluded that the newly emerging signature (OncoSig) could be widely applicable. Concurrently, according to our calculations, the OncoSig predicted a five-year OS with the highest AUC for the TCGA-BRCA dataset among the five prognostic signatures. At the same time, it also exhibited the highest average C-index, which estimated whether the predicted probability was consistent with the actual observed value in the above signatures. Evidently, there is no doubt that the OncoSig has better prognostic merit than the other lncRNA signatures for BC.

Similar to our approach, Zhang et al. demonstrated a nine-autophagy-related lncRNA signature for evaluating BC prognosis (43). By using the GSEA, patients in the low-risk group were enriched with 19 immune cell subpopulations; however, only 2 were enriched in patients with high risk. This exhibits the same trend as an existing signature of tumor immune infiltration–related lncRNA in non-small cell lung cancer, which showed 4 immune cell subtypes in the high-risk group and 10 in the low-risk groups (44). Oddly, Zhou et al. obtained the opposite result in the NES, with 11 immune subpopulations mainly concentrated in the high-risk patient group, while only 2 were enriched in the low-risk group (50). GSEA, immune infiltration, and gene function enrichment analysis" need to be corrected as "Immune cells infiltration, immune score and IPS score the high- and low-risk groups stratified by the OncoSig. The TME of diverse cancers comprises three main patterns: immune-desert, immune-excluded, and immune-infiltrated/inflamed (53). We further concluded that the high-risk group appeared to have more immune "cool" tumors with less immune cell infiltration, whereas the low-risk group contained more immune "hot" tumors with stronger immune cell infiltration. This outcome aligns with existing studies, which state that TCGA-BRCA patients have two distinct immune landscapes (54).

Following this, to further ensure the reliability of the OncoSig, we compared the tumor mutation burden (TMB) of the two different risk groups identified by the OncoSig. Our study suggested that *ERBB3*, *FMN2*, *DNAH10*, *MIA3*, and *FOXA1* were the frequently mutating genes in the high-risk group, while *CDH1* predominated in the low-risk group, clearly indicating a higher TMB in the former group when compared to the latter. Karn et al. concluded that lower TMB and less genomic heterogeneity are positively connected with better survival of TIL-rich TNBC (55). Their reviews are consistent with our results, albeit with distinct classification criteria. Our study also disclosed that the Basel, LumB, and HER2 subtypes accounted for larger proportions in the high-risk group than the low-risk group; meanwhile, the LumA subtype showed the opposite trend. Furthermore, Li et al. reported that an altered *CDH1* group involving mutations in the LumA subtype group displayed better survival than a non-altered group (56). This could explain our current result, indicating that a higher *CDH1* mutation rate in the low-risk group is associated with better prognosis in comparison to the high-risk group.

In this study, we focused on how a selected lncRNA affects an oncogenic signaling pathway by altering the expression of related genes and further evaluated the relationships of the PAM50 subtypes. In particular, ICI-based immunotherapy has made tremendous progress in the clinical management of BC patients recently. However, the heterogeneity of tumors has compelled the beneficiary group of this therapeutic strategy to remain a minority. Consequently, it is crucial to select patients who are most likely to profit from ICI by preassessing the predictive signatures of their responses to ICI. Although immune checkpoint genes, such as PD1/PD-L1 and *CTLA4*, are currently available biomarkers used in clinical work, they are insufficient independent predictors of ICI response (57, 58). Meanwhile, despite high expression levels of PD-1/PD-L1, response rates to immune checkpoint blockade therapy have remained variable among BC patients. By comparing the survival distribution of BC patients screened by the OncoSig and immune checkpoint gene expression, we demonstrated that the OncoSig enabled better discrimination between patients with similar levels of gene expression, indicating that patients with low OncoSig and high-level immune checkpoint gene expression may experience greater ICI treatment response. Furthermore, the prognosis of patients with similar OncoSig is, to some extent, influenced by the differential expression of immune checkpoint genes. Therefore, we can conclude that the Oncosig, resembling the immunotherapeutic benefit score developed by Wang et al. (59), has a distinctive characteristic of predicting response to immunotherapy.

To further certify the dependability of the OncoSig, we also obtained transcriptome expression datasets from the TCGA database for 32 other cancer types. We exploited its formula to score each sample of these cancers. Several cancers, including BLCA, HNSC, and KIRP, except for UVM, showed better survival and more immune infiltration cells in the low-risk cohort than its high-risk counterpart. For UVM, the potential cause of this phenomenon could be attributed to the disparity in the immune context of UVM,

since it belongs to the immune desert category, or the heterogeneity of UVM, as it contains the pro-tumorigenic immune cells (MDSCs, M2 macrophages, Th2 CD4+, etc.) of the TME (7, 8, 53).

There are still a few other concepts that can be considered to improve our study. First, the OncoSig requires the conduction of live tissue specimen molecular analysis in the 5 BC subtypes to verify its practicability. Furthermore, our pan-cancer analysis may be a double-edged sword. Although it proved the credibility of the OncoSig to a certain extent by covering multiple types of cancer, it did not cover all the types. In the future, there is certainly a need to design a clinical trial to evaluate the prognosis and immunotherapy response of BC patients by using the OncoSig.

In conclusion, the present study uncovered a robust signature in BC, termed as OncoSig, which acted as an oncogene and relied on the correlations of oncogenic signaling pathways and lncRNAs. We demonstrated a solid implementation of the OncoSig in the evaluation of the prognosis for BC and several other cancers as well as in the detection of immunotherapy responses, proving that it might be helpful in distinguishing clinical outcomes in patients suffering from BC and several other cancers.

Data availability statement

The datasets presented in this study can be found in online repositories. The names of the repository/repositories and accession number(s) can be found in the article/**supplementary material**.

Author contributions

MC and YY designed the study. HL and HL did data analysis. HML and HJL did data analysis. HML, QH, XL, and MC wrote and revised the manuscript.

Funding

This work was supported by NIH/NIMHD Accelerating Excellence in Translational Science Pilot Grants G0814C01 (Q. Hao), and also supported by the 'Jiangsu Province Excellent Postdoctoral Program'.

Conflict of interest

The authors declare that the research was conducted in the absence of any commercial or financial relationships that could be construed as a potential conflict of interest.

Publisher's note

All claims expressed in this article are solely those of the authors and do not necessarily represent those of their affiliated organizations, or those of the publisher, the editors and the reviewers. Any product that may be evaluated in this article, or claim that may be made by its manufacturer, is not guaranteed or endorsed by the publisher.

Supplementary material

The Supplementary Material for this article can be found online at: https://www.frontiersin.org/articles/10.3389/fimmu.2022.891175/full#supplementary-material

SUPPLEMENTARY TABLE 1
Cancer type and sample information.

SUPPLEMENTARY TABLE 2
Coefficients of 29 lncRNAs estimated by multivariate Cox regression model.

References

1. Sung H, Ferlay J, Siegel RL, Laversanne M, Soerjomataram I, Jemal A, et al. Global cancer statistics 2020: GLOBOCAN estimates of incidence and mortality worldwide for 36 cancers in 185 countries. *CA Cancer J Clin* (2021) 71(3):209–49. doi: 10.3322/caac.21660

2. Sorlie T, Tibshirani R, Parker J, Hastie T, Marron JS, Nobel A, et al. Repeated observation of breast tumor subtypes in independent gene expression data sets. *Proc Acad Sci USA* (2003) 100(14):8418–23.

3. Hammerl D, Smid M, Timmermans AM, Sleijfer S, Martens JWM, Debets R, et al. Breast cancer genomics and immuno-oncological markers to guide immune therapies. *Semin Cancer Biol* (2018) 52(Pt 2):178–88. doi: 10.1016/j.semcancer.2017.11.003

4. Esteva FJ, Hubbard-Lucey VM, Tang J, Pusztai L. Immunotherapy and targeted therapy combinations in metastatic breast cancer. *Lancet Oncol* (2019) 20(3):e175–e86. doi: 10.1016/S1470-2045(19)30026-9

5. Denkert C, von Minckwitz G, Darb-Esfahani S, Lederer B, Heppner BI, Weber KE, et al. Tumour-infiltrating lymphocytes and prognosis in different subtypes of breast cancer: A pooled analysis of 3771 patients treated with neoadjuvant therapy. *Lancet Oncol* (2018) 19(1):40–50. doi: 10.1016/S1470-2045(17)30904-X

6. Pruneri G, Vingiani A, Denkert C. Tumor infiltrating lymphocytes in early breast cancer. *Breast* (2018) 37:207–14. doi: 10.1016/j.breast.2017.03.010

7. Emens LA. Breast cancer immunobiology driving immunotherapy: Vaccines and immune checkpoint blockade. *Expert Rev Anticancer Ther* (2012) 12(12):1597–611. doi: 10.1586/era.12.147

8. Spellman A, Tang S-C. Immunotherapy for breast cancer: Past, present, and future. *Cancer Metastasis Rev* (2016) 35(4):525–46. doi: 10.1007/s10555-016-9654-9

9. Dushyanthen S, Teo ZL, Caramia F, Savas P, Mintoff CP, Virassamy B, et al. Agonist immunotherapy restores T cell function following MEK inhibition improving efficacy in breast cancer. *Nat Commun* (2017) 8(1):606. doi: 10.1038/s41467-017-00728-9

10. Gómez-Aleza C, Nguyen B, Yoldi G, Ciscar M, Barranco A, Hernández-Jiménez E, et al. Inhibition of RANK signaling in breast cancer induces an anti-tumor immune response orchestrated by CD8+ T cells. *Nat Commun* (2020) 11(1):6335. doi: 10.1038/s41467-020-20138-8

11. Baxevanis CN, Fortis SP, Perez SA. The balance between breast cancer and the immune system: Challenges for prognosis and clinical benefit from

immunotherapies. *Semin Cancer Biol* (2021) 72:76–89. doi: 10.1016/j.semcancer.2019.12.018

12. El Bairi K, Haynes HR, Blackley E, Fineberg S, Shear J, Turner S, et al. The tale of TILs in breast cancer: A report from the international immuno-oncology biomarker working group. *NPJ Breast Cancer* (2021) 7(1):150. doi: 10.1038/s41523-021-00346-1

13. Wilusz JE, Sunwoo H, Spector DL. Long noncoding RNAs: Functional surprises from the RNA world. *Genes Dev* (2009) 23(13):1494–504. doi: 10.1101/gad.1800909

14. Da Sacco L, Baldassarre A, Masotti A. Bioinformatics tools and novel challenges in long non-coding RNAs (lncRNAs) functional analysis. *Int J Mol Sci* (2012) 13(1):97–114. doi: 10.3390/ijms13010097

15. Huang Q-Y, Liu G-F, Qian X-L, Tang L-B, Huang Q-Y, Xiong L-X. Long non-coding RNA: Dual effects on breast cancer metastasis and clinical applications. *Cancers* (2019) 11(11). doi: 10.3390/cancers11111802

16. Peng WX, Koirala P, Mo YY. LncRNA-mediated regulation of cell signaling in cancer. *Oncogene* (2017) 36(41):5661–7. doi: 10.1038/onc.2017.184

17. Tao S, Chen Q, Lin C, Dong H. Linc00514 promotes breast cancer metastasis and M2 polarization of tumor-associated macrophages *via* Jagged1-mediated notch signaling pathway. *J Exp Clin Cancer Res CR* (2020) 39(1):191. doi: 10.1186/s13046-020-01676-x

18. Nyati KK, Hashimoto S, Singh SK, Tekguc M, Metwally H, Liu Y-C, et al. The novel long noncoding RNA AU021063, induced by IL-6/Arid5a signaling, exacerbates breast cancer invasion and metastasis by stabilizing Trib3 and activating the Mek/Erk pathway. *Cancer Lett* (2021) 520:295–306. doi: 10.1016/j.canlet.2021.08.004

19. Liu B, Sun L, Liu Q, Gong C, Yao Y, Lv X, et al. A cytoplasmic NF-κb interacting long noncoding RNA blocks iκb phosphorylation and suppresses breast cancer metastasis. *Cancer Cell* (2015) 27(3):370–81. doi: 10.1016/j.ccell.2015.02.004

20. Xu S, Kong D, Chen Q, Ping Y, Pang D. Oncogenic long noncoding RNA landscape in breast cancer. *Mol Cancer* (2017) 16(1):129. doi: 10.1186/s12943-017-0696-6

21. Hong W, Liang L, Gu Y, Qi Z, Qiu H, Yang X, et al. Immune-related lncRNA to construct novel signature and predict the immune landscape of human hepatocellular carcinoma. *Mol Ther Nucleic Acids* (2020) 22:937–47. doi: 10.1016/j.omtn.2020.10.002

22. Shen Y, Peng X, Shen C. Identification and validation of immune-related lncRNA prognostic signature for breast cancer. *Genomics* (2020) 112(3):2640–6. doi: 10.1016/j.ygeno.2020.02.015

23. Zhang M, Wang N, Song P, Fu Y, Ren Y, Li Z, et al. LncRNA GATA3-AS1 facilitates tumour progression and immune escape in triple-negative breast cancer through destabilization of GATA3 but stabilization of PD-L1. *Cell Prolif* (2020) 53(9):e12855. doi: 10.1111/cpr.12855

24. Colaprico A, Silva TC, Olsen C, Garofano L, Cava C, Garolini D, et al. TCGAbiolinks: An R/Bioconductor package for integrative analysis of TCGA data. *Nucleic Acids Res* (2016) 44(8):e71–e. doi: 10.1093/nar/gkv1507

25. Sabatier R, Finetti P, Cervera N, Lambaudie E, Esterni B, Mamessier E, et al. A gene expression signature identifies two prognostic subgroups of basal breast cancer. *Breast Cancer Res Treat* (2011) 126(2):407–20. doi: 10.1007/s10549-010-0897-9

26. Kao K-J, Chang K-M, Hsu H-C, Huang AT. Correlation of microarray-based breast cancer molecular subtypes and clinical outcomes: Implications for treatment optimization. *BMC Cancer* (2011) 11(1):1–15. doi: 10.1186/1471-2407-11-143

27. Sabatier R, Finetti P, Adelaide J, Guille A, Borg J-P, Chaffanet M, et al. Down-regulation of ECRG4, a candidate tumor suppressor gene, in human breast cancer. *PLoS One* (2011) 6(11):e27656. doi: 10.1371/journal.pone.0027656

28. Jézéquel P, Loussouarn D, Guérin-Charbonnel C, Campion L, Vanier A, Gouraud W, et al. Gene-expression molecular subtyping of triple-negative breast cancer tumours: Importance of immune response. *Breast Cancer Res* (2015) 17(1):1–16. doi: 10.1186/s13058-015-0550-y

29. Jézéquel P, Kerdraon O, Hondermarck H, Guérin-Charbonnel C, Lasla H, Gouraud W, et al. Identification of three subtypes of triple-negative breast cancer with potential therapeutic implications. *Breast Cancer Res* (2019) 21(1):1–14. doi: 10.1186/s13058-019-1148-6

30. Hubbell E, Liu W-M, Mei R. Robust estimators for expression analysis. *Bioinformatics* (2002) 18(12):1585–92. doi: 10.1093/bioinformatics/18.12.1585

31. Hanzelmann S, Castelo R, Guinney J. GSVA: Gene set variation analysis for microarray and RNA-seq data. *BMC Bioinf* (2013) 14:7. doi: 10.1186/1471-2105-14-7

32. Sanchez-Vega F, Mina M, Armenia J, Chatila WK, Luna A, La KC, et al. Oncogenic signaling pathways in the cancer genome atlas. *Cell* (2018) 173(2):321–37.e10. doi: 10.1016/j.cell.2018.03.035

33. Love MI, Huber W, Anders S. Moderated estimation of fold change and dispersion for RNA-seq data with Deseq2. *Genome Biol* (2014) 15(12):550. doi: 10.1186/s13059-014-0550-8

34. Benjamini Y, Hochberg Y. Controlling the false discovery rate - a practical and powerful approach to multiple testing. *J R Stat Soc B* (1995) 57(1):289–300. doi: 10.1111/j.2517-6161.1995.tb02031.x

35. Yu G, Wang L-G, Han Y, He Q-Y. Clusterprofiler: An r package for comparing biological themes among gene clusters. *OMICS* (2012) 16(5):284–7. doi: 10.1089/omi.2011.0118

36. Charoentong P, Finotello F, Angelova M, Mayer C, Efremova M, Rieder D, et al. Pan-cancer immunogenomic analyses reveal genotype-immunophenotype relationships and predictors of response to checkpoint blockade. *Cell Rep* (2017) 18(1):248–62. doi: 10.1016/j.celrep.2016.12.019

37. Yoshihara K, Shahmoradgoli M, Martínez E, Vegesna R, Kim H, Torres-Garcia W, et al. Inferring tumour purity and stromal and immune cell admixture from expression data. *Nat Commun* (2013) 4:2612. doi: 10.1038/ncomms3612

38. Newman AM, Liu CL, Green MR, Gentles AJ, Feng W, Xu Y, et al. Robust enumeration of cell subsets from tissue expression profiles. *Nat Methods* (2015) 12(5):453–7. doi: 10.1038/nmeth.3337

39. Garcia-Mulero S, Alonso MH, Pardo J, Santos C, Sanjuan X, Salazar R, et al. Lung metastases share common immune features regardless of primary tumor origin. *J Immunother Cancer* (2020) 8(1). doi: 10.1136/jitc-2019-000491

40. Gendoo DM, Ratanasirigulchai N, Schröder MS, Paré L, Parker JS, Prat A, et al. Genefu: An R/Bioconductor package for computation of gene expression-based signatures in breast cancer. *Bioinformatics* (2016) 32(7):1097–9. doi: 10.1093/bioinformatics/btv693

41. Li J, Wang W, Xia P, Wan L, Zhang L, Yu L, et al. Identification of a five-lncRNA signature for predicting the risk of tumor recurrence in patients with breast cancer. *Int J Cancer* (2018) 143(9):2150–60. doi: 10.1002/ijc.31573

42. Bao S, Zhao H, Yuan J, Fan D, Zhang Z, Su J, et al. Computational identification of mutator-derived lncRNA signatures of genome instability for improving the clinical outcome of cancers: A case study in breast cancer. *Briefings Bioinf* (2020) 21(5):1742–55. doi: 10.1093/bib/bbz118

43. Zhang R, Zhu Q, Yin D, Yang Z, Guo J, Zhang J, et al. Identification and validation of an autophagy-related lncRNA signature for patients with breast cancer. *Front Oncol* (2021) 10:3283. doi: 10.3389/fonc.2020.597569

44. Sun J, Zhang Z, Bao S, Yan C, Hou P, Wu N, et al. Identification of tumor immune infiltration-associated lncRNAs for improving prognosis and immunotherapy response of patients with non-small cell lung cancer. *J Immunother Cancer* (2020) 8(1). doi: 10.1136/jitc-2019-000110

45. Wang S, Zhang Q, Yu C, Cao Y, Zuo Y, Yang L. Immune cell infiltration-based signature for prognosis and immunogenomic analysis in breast cancer. *Briefings Bioinf* (2021) 22(2):2020–31. doi: 10.1093/bib/bbaa026

46. Hu F-F, Liu C-J, Liu L-L, Zhang Q, Guo A-Y. Expression profile of immune checkpoint genes and their roles in predicting immunotherapy response. *Briefings Bioinf* (2021) 22(3):bbaa176. doi: 10.1093/bib/bbaa176

47. Zhao H, Chen Y, Shen P, Gong L. Identification of immune cell infiltration landscape and their prognostic significance in uveal melanoma. *Front Cell Dev Biol* (2021) 9. doi: 10.3389/fcell.2021.713569

48. Li S, Sun X, Li J, Zheng A, Cao Y, Guo Y, et al. A novel prognostic signature of immune-related long noncoding RNA pairs for tumor-infiltrating immune cells and drug susceptibility in breast cancer. *DNA Cell Biol* (2022) 41(2):103–15. doi: 10.1089/dna.2021.0489

49. Shen S, Chen X, Hu X, Huo J, Luo L, Zhou X. Predicting the immune landscape of invasive breast carcinoma based on the novel signature of immune-related lncRNA. *Cancer Med* (2021) 10(18):6561–75. doi: 10.1002/cam4.4189

50. Zhou M, Zhang Z, Bao S, Hou P, Yan C, Su J, et al. Computational recognition of lncRNA signature of tumor-infiltrating b lymphocytes with potential implications in prognosis and immunotherapy of bladder cancer. *Briefings Bioinf* (2021) 22(3). doi: 10.1093/bib/bbaa047

51. Li W, Chen Y, Nie XQ. Regulatory mechanisms of lncRNAs and their target gene signaling pathways in laryngeal squamous cell carcinoma. *Front Pharmacol* (2020) 11. doi: 10.3389/fphar.2020.01140

52. Fu P-F, Zheng X, Fan X, Lin A-F. Role of cytoplasmic lncRNAs in regulating cancer signaling pathways. *J Zhejiang Univ Sci B* (2019) 20(1):1–8.

53. Chen DS, Mellman I. Elements of cancer immunity and the cancer-immune set point. *Nature* (2017) 541(7637):321–30. doi: 10.1038/nature21349

54. Wang S, Xiong Y, Zhang Q, Su D, Yu C, Cao Y, et al. Clinical significance and immunogenomic landscape analyses of the immune cell signature based prognostic model for patients with breast cancer. *Briefings Bioinf* (2021) 22(4). doi: 10.1093/bib/bbaa311

55. Karn T, Jiang T, Hatzis C, Sänger N, El-Balat A, Rody A, et al. Association between genomic metrics and immune infiltration in triple-negative breast cancer. *JAMA Oncol* (2017) 3(12):1707–11. doi: 10.1001/jamaoncol.2017.2140

56. Li X, Zhou J, Xiao M, Zhao L, Zhao Y, Wang S, et al. Uncovering the subtype-specific molecular characteristics of breast cancer by multiomics analysis of prognosis-associated genes, driver genes, signaling pathways, and immune activity. *Front Cell Dev Biol* (2021) 9:689028. doi: 10.3389/fcell.2021.689028

57. Bassez A, Vos H, Van Dyck L, Floris G, Arijs I, Desmedt C, et al. A single-cell map of intratumoral changes during anti-PD1 treatment of patients with breast cancer. *Nat Med* (2021) 27(5):820–32. doi: 10.1038/s41591-021-01323-8

58. Hammerl D, Martens JWM, Timmermans M, Smid M, Trapman-Jansen AM, Foekens R, et al. Spatial immunophenotypes predict response to anti-PD1 treatment and capture distinct paths of T cell evasion in triple negative breast cancer. *Nat Commun* (2021) 12(1):5668. doi: 10.1038/s41467-021-25962-0

59. Wang T, Li T, Li B, Zhao J, Li Z, Sun M, et al. Immunogenomic landscape in breast cancer reveals immunotherapeutically relevant gene signatures. *Front Immunol* (2022) 13:805184. doi: 10.3389/fimmu.2022.805184

Frontiers in Immunology

Explores novel approaches and diagnoses to treat immune disorders.

The official journal of the International Union of Immunological Societies (IUIS) and the most cited in its field, leading the way for research across basic, translational and clinical immunology.

Discover the latest Research Topics

See more →

Frontiers

Avenue du Tribunal-Fédéral 34
1005 Lausanne, Switzerland
frontiersin.org

Contact us

+41 (0)21 510 17 00
frontiersin.org/about/contact